

Valentina Emilia Balas
Lakhmi C. Jain
Branko Kovačević *Editors*

Soft Computing Applications

Proceedings of the 6th International
Workshop Soft Computing
Applications (SOFA 2014), Volume 1

Advances in Intelligent Systems and Computing

Volume 356

Series editor

Janusz Kacprzyk, Polish Academy of Sciences, Warsaw, Poland
e-mail: kacprzyk@ibspan.waw.pl

About this Series

The series “Advances in Intelligent Systems and Computing” contains publications on theory, applications, and design methods of Intelligent Systems and Intelligent Computing. Virtually all disciplines such as engineering, natural sciences, computer and information science, ICT, economics, business, e-commerce, environment, healthcare, life science are covered. The list of topics spans all the areas of modern intelligent systems and computing.

The publications within “Advances in Intelligent Systems and Computing” are primarily textbooks and proceedings of important conferences, symposia and congresses. They cover significant recent developments in the field, both of a foundational and applicable character. An important characteristic feature of the series is the short publication time and world-wide distribution. This permits a rapid and broad dissemination of research results.

Advisory Board

Chairman

Nikhil R. Pal, Indian Statistical Institute, Kolkata, India
e-mail: nikhil@isical.ac.in

Members

Rafael Bello, Universidad Central “Marta Abreu” de Las Villas, Santa Clara, Cuba
e-mail: rbellop@uclv.edu.cu

Emilio S. Corchado, University of Salamanca, Salamanca, Spain
e-mail: escorchado@usal.es

Hani Hagrass, University of Essex, Colchester, UK
e-mail: hani@essex.ac.uk

László T. Kóczy, Széchenyi István University, Győr, Hungary
e-mail: koczy@sze.hu

Vladik Kreinovich, University of Texas at El Paso, El Paso, USA
e-mail: vladik@utep.edu

Chin-Teng Lin, National Chiao Tung University, Hsinchu, Taiwan
e-mail: ctlin@mail.nctu.edu.tw

Jie Lu, University of Technology, Sydney, Australia
e-mail: Jie.Lu@uts.edu.au

Patricia Melin, Tijuana Institute of Technology, Tijuana, Mexico
e-mail: epmelin@hafsamx.org

Nadia Nedjah, State University of Rio de Janeiro, Rio de Janeiro, Brazil
e-mail: nadia@eng.uerj.br

Ngoc Thanh Nguyen, Wroclaw University of Technology, Wroclaw, Poland
e-mail: Ngoc-Thanh.Nguyen@pwr.edu.pl

Jun Wang, The Chinese University of Hong Kong, Shatin, Hong Kong
e-mail: jwang@mae.cuhk.edu.hk

More information about this series at <http://www.springer.com/series/11156>

Valentina Emilia Balas · Lakhmi C. Jain
Branko Kovačević
Editors

Soft Computing Applications

Proceedings of the 6th International
Workshop Soft Computing Applications
(SOFA 2014), Volume 1

 Springer

Editors

Valentina Emilia Balas
Faculty of Engineering, Department of
Automation and Applied Informatics
Aurel Vlaicu University of Arad
Arad
Romania

Branko Kovačević
University of Belgrade
Belgrade
Serbia

Lakhmi C. Jain
Faculty of Science and Technology
Data Science Institute, Bournemouth
University
Poole
UK

ISSN 2194-5357 ISSN 2194-5365 (electronic)
Advances in Intelligent Systems and Computing
ISBN 978-3-319-18295-7 ISBN 978-3-319-18296-4 (eBook)
DOI 10.1007/978-3-319-18296-4

Library of Congress Control Number: 2015948723

Springer Cham Heidelberg New York Dordrecht London
© Springer International Publishing Switzerland 2016

This work is subject to copyright. All rights are reserved by the Publisher, whether the whole or part of the material is concerned, specifically the rights of translation, reprinting, reuse of illustrations, recitation, broadcasting, reproduction on microfilms or in any other physical way, and transmission or information storage and retrieval, electronic adaptation, computer software, or by similar or dissimilar methodology now known or hereafter developed.

The use of general descriptive names, registered names, trademarks, service marks, etc. in this publication does not imply, even in the absence of a specific statement, that such names are exempt from the relevant protective laws and regulations and therefore free for general use.

The publisher, the authors and the editors are safe to assume that the advice and information in this book are believed to be true and accurate at the date of publication. Neither the publisher nor the authors or the editors give a warranty, express or implied, with respect to the material contained herein or for any errors or omissions that may have been made.

Printed on acid-free paper

Springer International Publishing AG Switzerland is part of Springer Science+Business Media
(www.springer.com)

Preface

These volumes constitute the Proceedings of the 6th International Workshop on Soft Computing Applications, or SOFA 2014, held during 24–26 July 2014 in Timisoara, Romania. This edition was organized by the University of Belgrade, Serbia in conjunction with the Romanian Society of Control Engineering and Technical Informatics (SRAIT)—Arad Section, The General Association of Engineers in Romania—Arad Section, Institute of Computer Science, Iasi Branch of the Romanian Academy, and IEEE Romanian Section.

Soft Computing concept was introduced by Lotfi Zadeh in 1991 and serves to highlight the emergence of computing methodologies in which the accent is on exploiting the tolerance for imprecision and uncertainty to achieve tractability, robustness, and low solution cost. Soft computing facilitates the use of fuzzy logic, neurocomputing, evolutionary computing, and probabilistic computing in combination, leading to the concept of hybrid intelligent systems.

The combination of such intelligent systems tools and a large number of applications introduces a need for a synergy of scientific and technological disciplines in order to show the great potential of Soft Computing in all domains.

The book covers a broad spectrum of soft computing techniques, theoretical, and practical applications employing knowledge and intelligence to find solutions for world's industrial, economic, and medical problems.

The conference papers included in these proceedings, published post conference, were grouped into the following areas of research:

- Image, Text and Signal Processing
- Intelligent Transportation
- Modeling and Applications
- Biomedical Applications
- Neural Network and Applications
- Knowledge-Based Technologies for Web Applications, Cloud Computing, Security, Algorithms and Computer Networks
- Knowledge-Based Technologies
- Soft Computing Techniques for Time Series Analysis

- Soft Computing and Fuzzy Logic in Biometrics
- Fuzzy Applications Theory and Fuzzy Control
- Business Process Management
- Methods and Applications in Electrical Engineering

In SOFA 2014 we had six eminent keynote speakers: Prof. Lakhmi C. Jain (Australia), Prof. Kay Chen Tan (Singapore), Prof. Ioan Dumitrache (Romania), Prof. Dan Ionescu (Canada), Prof. Sheryl Brahnam (USA) and Prof. Margarita Favorkaya (Russian Federation), and an interesting tutorial of Dr. Jakob Salom (Serbia). Their summarized talks are included in this book.

We especially thank the honorary chair of SOFA 2014, Prof. Lotfi A. Zadeh, who encouraged and motivated us.

We would like to thank the authors of the submitted papers for keeping the quality of the SOFA 2014 conference at high levels. The editors of this book acknowledge all the authors for their contributions and also the reviewers. We have received invaluable help from the members of the International Program Committee and the chairs responsible for different aspects of the workshop. We appreciate also the role of the Special Sessions organizers. Thanks to all of them we were able to collect many papers on interesting topics and had very interesting presentations and stimulating discussions during the workshop.

For their help with organizational issues of all SOFA editions, we express our thanks to TRIVENT Company, Mónica Jetzin, and Teodora Artimon for having customized the software Conference Manager, registration of conference participants, and all local arrangements.

Special thanks go to Janus Kacprzyk (Editor-in-Chief, Springer, Advances in Intelligent Systems and Computing Series) for the opportunity to organize this guest edited volume.

We are grateful to Springer, especially to Dr. Thomas Ditzinger (Senior Editor, Applied Sciences & Engineering Springer-Verlag) for the excellent collaboration, patience, and help during the evolution of this volume.

We hope that the volumes will provide useful information to professors, researchers, and graduate students in the area of soft computing techniques and applications and all will find this collection of papers inspiring, informative, and useful. We also hope to see you at a future SOFA event.

Romania
UK
Serbia

Valentina Emilia Balas
Lakhmi C. Jain
Branko Kovačević

Contents

Part I Image, Text and Signal Processing

A Comparative Study of Text-to-Speech Systems in LabVIEW	3
Manuela Panoiu, Cezara-Liliana Rat and Caius Panoiu	
Parallel Neural Fuzzy-Based Joint Classifier Model for Grading Autistic Disorder	13
Anju Pratap, C.S. Kanimozhiselvi, R. Vijayakumar and K.V. Pramod	
Image Processing with Android Steganography	27
Dominic Bucerzan and Crina Rațiu	

Part II Intelligent Transportation

Social Cities: Redistribution of Traffic Flow in Cities Using a Social Network Approach	39
Alexandru Topirceanu, Alexandru Iovanovici, Cristian Cosariu, Mihai Udrescu, Lucian Prodan and Mircea Vladutiu	
The Computer Assisted Parking of a Bluetooth Controlled Car Using Fuzzy Logic	51
Caius Panoiu, Manuela Panoiu, Cezara-Liliana Rat and Raluca Rob	
A Location-Aware Solution for Predicting Driver’s Destination in Intelligent Traffic Systems	67
Emilian Neclau	
Advances in Urban Video-Based Surveillance Systems: A Survey	87
M. Favorskaya	

Traffic and Pedestrian Risk Inference Using Harmonic Systems	103
I. Acuña Barrios, E. García, Daniela López De Luise, C. Paredes, A. Celayeta, M. Sandillú and W. Bel	

Part III Modeling and Applications

The Electronic Verification of the Weight and the Amount of Food Consumed by Animals in a Farm	115
Doru Anastasiu Popescu and Nicolae Bold	

FEM Modeling of Some Raising Effects of the Magnetic Liquids Around Vertical Conductors with a Current Flow	125
D. Vesa, M. Greconici and I. Tatai	

Hard as a Rock or Deformation Controlled?	135
Gheorghe Sima, Glavan Dan, Popa Alexandru and E. Muncut	

Cast-Resin Dry-Type Transformer Thermal Modeling Based on Particle Swarm Optimization	141
Davood Azizian and Mehdi Bigdeli	

Geometric Model of a Railway Wheel with Irregular Contour	155
T. Mazilu	

Grafting, Locations, and Ordinal Dispersion	167
Tiberiu Spiricu	

Software Solution for Reliability Analysis Based on Interpolative Boolean Algebra	185
Nemanja Lilić, Bratislav Petrović and Pavle Milošević	

Local Search Algorithms for Solving the Combinatorial Optimization and Constraint Satisfaction Problems	199
Y. Kilani, A. Alsarhan, M. Bsoul and A.F. Otoom	

Remote Tuning of Magnetron Frequency in an RF Linac	213
Vijay Sharma, V.K. Madan, S.N. Acharya and K.C. Mittal	

Part IV Biomedical Applications

Using Modern Technologies to Facilitate Translating Logical Observation Identifiers Names and Codes	219
Daniel-Alexandru Jurcau, Vasile Stoicu-Tivadar and Alexandru Serban	

Data Analysis for Patients with Sleep Apnea Syndrome: A Complex Network Approach	231
Alexandru Topirceanu, Mihai Udrescu, Razvan Avram and Stefan Mihaicuta	

Mobile Applications Supporting Healthy Lifestyle 241
 Oana-Sorina Lupșe, Adrian Căprioru and Lăcrămioara Stoicu-Tivadar

Fuzzy Expert System Prediction of Lumbar Spine Subchondral Sclerosis and Lumbar Disk Hernia 249
 Norbert Gal, Diana Andrei, Vasile Stoicu-Tivadar, Dan Ion Nemeș and Emanuela Nădășan

Server-Side Image Segmentation and Patient-Related Data Storage 259
 Ioan Virag, Lăcrămioara Stoicu-Tivadar, Mihaela Crișan-Vida and Elena Amăricăi

Dedicated BSN for Personal Indoor Monitoring 267
 Ștefan Mocanu

Romanian Sign Language Oral Health Corpus in Video and Animated Avatar Technology 279
 Ionut Adrian Chiriac, Lăcrămioara Stoicu-Tivadar and Elena Podoleanu

Hybrid Neuro-Fuzzy Approaches for Abnormality Detection in Retinal Images 295
 D. Jude Hemanth, Valentina E. Balas and J. Anitha

Optimistic Multi-granulation Rough Set-Based Classification for Neonatal Jaundice Diagnosis 307
 S. Senthil Kumar, H. Hannah Inbarani, Ahmad Taher Azar, Hala S. Own, Valentina Emilia Balas and Teodora Olariu

Boosted Decision Trees for Vertebral Column Disease Diagnosis 319
 Ahmad Taher Azar, Hanaa S. Ali, Valentina E. Balas, Teodora Olariu and Rujita Ciurea

Hybrid Invasive Weed Optimization Method for Generating Healthy Meals 335
 Viorica R. Chifu, Ioan Salomie, Emil Șt. Chifu, Cristina Bianca Pop, Dan Valea, Madalina Lupu and Marcel Antal

Therapeutic Conduct and Management of Rehabilitate Treatment Measured with Zebris Device and Applied Using WinSpine Software 353
 Andrei Diana, Poenaru V. Dan, Nemes Dan, Surducan Dan and Gal-Nadasan Norbert

A Novel Approach on the Newborns’ Cry Analysis Using Professional Recording and Feature Extraction from the “First Cry” with LabVIEW 363
 F. Feier and I. Silea

Development of a Preliminary Mathematical Model to Predict the Indoor Radon Concentration in Normal and High Background Radiation Areas of Ramsar	373
S.M.J. Mortazavi, A. Zamani, A. Tavakkoli-Golpayegani and S. Taeb	
ASD: ML Perspective for Individual Performance Evaluation	379
D. López De Luise, M. Fernandez Vuelta, R. Azor, M. Agüero, C. Párraga, N. López, P. Bustamante, M. Marquez, R. Bielli, D. Hisgen, R. Fairbain and S. Planes	
Part V Neural Network and Applications	
Fermat Number Applications and Fermat Neuron	403
V.K. Madan, M.M. Balas and S. Radhakrishnan	
Data Clustering Using a Modified Fuzzy Min-Max Neural Network	413
Manjeevan Seera, Chee Peng Lim, Chu Kiong Loo and Lakhmi C. Jain	
Adaptive Neuro-Fuzzy System for Current Prediction in Electric Arc Furnaces	423
Manuela Panoiu, Loredana Ghiormez and Caius Panoiu	
Exact Hessian Matrix Calculation for Complex-Valued Neural Networks	439
Călin-Adrian Popa	
Functioning State Estimator of Pump-Motor Group of MOP-Type Drive Mechanisms Using Neural Networks	457
V. Nicolau and M. Andrei	
Part VI Knowledge-Based Technologies for Web Applications, Cloud Computing, Security, Algorithms and Computer Networks	
Self-organizing System for the Autonomic Management of Collaborative Cloud Applications	469
Bogdan Solomon, Dan Ionescu and Cristian Gadea	
An Architecture and Methods for Big Data Analysis	491
Bogdan Ionescu, Dan Ionescu, Cristian Gadea, Bogdan Solomon and Mircea Trifan	
Process Mining Functional and Structural Validation	515
Maria Laura Sebu and Horia Ciocârlie	

Evaluating the Performance of Discourse Parser Systems 525
 Elena Mitocariu

**Considerations Regarding an Algebraic Model for Inference
 and Decision on Heterogeneous Sensory Input 539**
 Violeta Tulceanu

Integrated Design Pattern for Intelligent Web Applications. 549
 Zsolt Nagy

Energy Performance Optimization of Wireless Sensor Networks 563
 Cosmina Illes, Cristian Vasar and Ioan Filip

**Jigsaw Inspired Metaheuristic for Selecting the Optimal Solution
 in Web Service Composition 573**
 Viorica Rozina Chifu, Ioan Salomie, Emil Șt. Chifu,
 Cristina Bianca Pop, Petru Poruțiu and Marcel Antal

Multimedia as a Tool for Learning Engineering. 585
 D. López de Luise, J. Gelvez, N. Borromeo, L. Maguet and L. Dima

Educational Assessment Engineering: A Pattern Approach 605
 Paul Hubert Vossen

**Feasibility of Extracting Unique Signature for Each User Based
 on Analysing Internet Usage Behaviours 621**
 Rozita Jamili Oskouei

Privacy Preserving Data Mining Survey of Classifications. 637
 Mahdi Aghasi and Rozita Jamili Oskouei

A Formal Analysis for RSA Attacks by Term Rewriting Systems 651
 Mohammad Kadhoda, Anis Vosoogh and Reza Nourmandi-Pour

Part VII Knowledge-Based Technologies

**Heuristic Optimization of Wireless Sensor Networks
 Using Social Network Analysis. 663**
 Alexandru Iovanovici, Alexandru Topirceanu, Cristian Cosariu,
 Mihai Udrescu, Lucian Prodan and Mircea Vladutiu

**Interactive Applications for Studying Mathematics
 with the Use of an Autostereoscopic Display. 673**
 Monica Ciobanu, Antoanela Naaji, Ioan Virag and Ioan Dascal

**Determining the Similarity of Two Web Applications
 Using the Edit Distance 681**
 Doru Anastasiu Popescu and Dragoș Nicolae

Generative Learning Object Assessment Items for a Set of Computer Science Disciplines 691
Ciprian-Bogdan Chirila

Performance Metrics for Persistent Routing 701
S.N. Orzen

Parity-based Concurrent Error-detection Architecture Applied to the IDEA NXT Crypto-algorithm 713
Andreea Bozesan, Flavius Opritoiu and Mircea Vladutiu

Invited Keynote Papers

Decision Support Systems in Practice



Prof. Lakhmi C. Jain
Faculty of Science and Technology
Data Science Institute, Bournemouth University
Poole
UK
e-mail: Lakhmi.jain@unisa.edu.au

Abstract This talk will summarize the research projects on safety undertaken by me and my research team in recent years. The progress made in developing the intelligent flight data monitoring system for improving the safety of aviation operations will be presented.

Short Biography

Lakhmi C. Jain, serves as Visiting Professor in Bournemouth University, UK, Adjunct Professor in the Division of Information Technology, Engineering and the Environment at the University of South Australia, Australia and University of Canberra, Australia.

Dr. Jain founded the KES International for providing to a professional community the opportunities for publications, knowledge exchange, cooperation, and teaming. Involving around 5000 researchers drawn from universities and companies worldwide, KES facilitates international cooperation and generates synergy in teaching and research. KES regularly provides networking opportunities for the professional community through one of the largest conferences of its kind in the area of KES. www.kesinternational.org

His interests focus on artificial intelligence paradigms and their applications in complex systems, security, e-education, e-healthcare, unmanned air vehicles, and intelligent agents.

Advances in Evolutionary Multi-objective Optimization and Applications



Kay Chen Tan

National University of Singapore, Singapore

e-mail: eletankc@nus.edu.sg

Abstract Multi-objective optimization is widely found in many fields, such as logistics, economics, engineering, or whenever optimal decisions need to be made in the presence of trade-offs. The problem is challenging because it involves the simultaneous optimization of several conflicting objectives in the Pareto optimal sense and requires researchers to address many issues that are unique to MO problems.

This talk will first provide an overview of evolutionary computation for multi-objective optimization (EMO). It will then discuss challenges faced in EMO research and present various EMO algorithms for good optimization performance. The talk will also discuss the application of evolutionary computing techniques for solving engineering problems, such as logistics, design optimization, and prognostic applications.

Short Biography

Dr. Kay Chen TAN received the B.E. degree with First Class Honors in Electronics and Electrical Engineering, and the Ph.D. degree from the University of Glasgow, Scotland, in 1994 and 1997, respectively. He is currently associate professor in the Department of Electrical and Computer Engineering, National University of Singapore.

Dr. Tan actively pursues research in the area of computational intelligence, with applications to multi-objective optimization, scheduling, automation, data mining, and games. He has published over 100 journal papers, over 100 papers in conference proceedings, co-authored five books including *Multiobjective Evolutionary Algorithms and Applications* (Springer-Verlag, 2005), *Modern Industrial Automation Software Design* (John Wiley, 2006; Chinese Edition, 2008), *Evolutionary Robotics: From Algorithms to Implementations* (World Scientific, 2006), *Neural Networks: Computational Models and Applications* (Springer-Verlag, 2007), and *Evolutionary Multi-objective Optimization in Uncertain Environments: Issues and Algorithms* (Springer-Verlag, 2009), co-edited four books including *Recent Advances in Simulated Evolution and Learning* (World Scientific, 2004), *Evolutionary Scheduling* (Springer-Verlag, 2007), *Multiobjective Memetic Algorithms* (Springer-Verlag, 2009), and *Design and Control of Intelligent Robotic Systems* (Springer-Verlag, 2009).

Dr. Tan has been an invited keynote/plenary speaker for over 40 international conferences in the area of computational intelligence. He is an elected member of AdCom for IEEE Computational Intelligence Society from 2014 to 2016. He serves

as the General Co-Chair for 2016 IEEE World Congress on Computational Intelligence to be held in Vancouver, Canada. He has also served in the international program committee for over 100 conferences and was involved in the organizing committee of over 50 international conferences, such as the General Co-Chair for 2007 IEEE Congress on Evolutionary Computation in Singapore, etc. He has actively served in various committees of the IEEE Computational Intelligence Society, such as conference committee, publication committee, nomination committee, awards committee, etc. He was also a Distinguished Lecturer of the IEEE Computational Intelligence Society from 2011 to 2013 and served as the Chair of Evolutionary Computation Technical Committee from 2008 to 2009.

Dr. Tan was the Editor-in-Chief of *IEEE Computational Intelligence Magazine* from 2010 to 2013. He currently serves as an Associate Editor/Editorial Board member of over 20 international journals, such as *IEEE Transactions on Evolutionary Computation*, *IEEE Transactions on Cybernetics*, *IEEE Transactions on Computational Intelligence and AI in Games*, *Evolutionary Computation* (MIT Press), *European Journal of Operational Research*, *Journal of Scheduling* etc.

Dr. Tan is a Fellow of IEEE. He was awarded “Outstanding Early Career Award” from the IEEE Computational Intelligence Society in 2012 for his contributions to evolutionary computation in multi-objective optimization. He also received the “Recognition Award” from the International Network for Engineering Education & Research (iNEER) in 2008 for his outstanding contributions to engineering education and research. He was a winner of the NUS Outstanding Educator Awards in 2004, the Engineering Educator Awards (2002, 2003, 2005), the Annual Teaching Excellence Awards (2002–2006), the Honour Roll Awards in 2007, and a Fellow of the NUS Teaching Academic from 2009 to 2012.

Hybrid Intelligent Techniques in Autonomous Complex Systems



Ioan Dumitrache
Romanian Academy
e-mail: ioandumitrache@yahoo.com

Abstract The complexity of physical infrastructures, the progress of knowledge in computational intelligence, and the increasing integration of computers, communications, and control strategies with physical processes have imposed a new vision on intelligent complex systems.

The paper presents some architectures of autonomous complex systems where the synergy of the intelligent methodology is thoroughly exploited.

There are presented some hybrid architectures as: neuro-fuzzy, geno-fuzzy, geno-neuro-fuzzy, and their real impact on the control performances for different types of applications. There are also presented some results in the fields of robotics and intelligent manufacturing.

Special attention is paid to the connections between computational intelligence and the new paradigm of Intelligent Complex Cyber-Physical Systems.

There are underlined some new research directions on these advanced integrative technologies: computer, communication, control and cognition, deeply enabled in physical systems.

Short Biography

Prof. Dr. Ing. Ioan Dumitrache graduated the Faculty of Energetics of the Polytechnical Institute of Bucharest in 1962 and received in 1970 a Ph.D. from the same institute in the field of Automatic Control. He is, from 1987, Ph.D. advisor in the field of Control and Systems Engineering.

He is a Fullbright Fellow (1970) with Oklahoma State University and invited professor of this university (1991, 1995) and of the Technical University of Vienna (1994–1999). Prof. Dumitrache is a corresponding member of the Romanian Academy (since 2003), member of the Technical Sciences Academy (since 1999) and Doctor Honoris Causa of Polytechnical University of Timisoara, University of Pitesti, University of Craiova, University of Arad and Technical University of Cluj. His research has addressed several areas, from automatic control to Cyber Physical Systems, including adaptive control, mobile and autonomous robotics, intelligent control systems, smart manufacturing, knowledge management, bioprocess control and so on.

He is an author of more than 250 scientific papers, published in international journals and conference proceedings, author of more than 20 books and monographs edited by national and international publishing houses, editor of more than 25 volumes and coordinator of research teams for more than 75 projects, nationally and internationally funded.

He was in the IPC of more than 100 international conferences, chaired or co-chaired more than 25, is the President of SRAIT–NMO of IFAC, member in the editorial board of several international scientific journals and Editor in Chief of CEAI Journal.

He was the President of CNCSIS between 1998 and 2011, Romanian representative in IFAC since 1979 and member in the Governors Board of JRC (2005–2013) and NSF (2003–2011).

Contemporary Software Challenges: Big Data and Cloud Computing



Prof. Dan Ionescu
School of Electrical Engineering and Computer Science
University of Ottawa
e-mail: ionescu@site.uottawa.ca

Abstract Cloud computing and data storage options lowering down the cost of hosting server farms, the rush for interpreting large amounts of data for predicting the advent of events of interest for business, politicians, social behaviors, or endemics changed the way the data were regarded and produced in the last decade.

The success stories of the results obtained by the Narval, the big data analytics used by the winner of the 2012 Presidential Elections in the US, demonstrated that it is not enough to have or host a huge amount of data, rather there is a need to know how to use it, too.

Recently, industries become interested in the high potential of big data, and many government agencies announced major plans to accelerate big data research and applications.

However, the data deluge in the big data era brings about huge challenges to data acquisition, storage, management, and especially in data analysis.

Many solutions for big data storage and processing have been experimented with. As such permanent storage and management of large-scale disordered datasets, distributed file systems, and NoSQL databases are mentioned as good choices for approaching big data projects.

Cloud computing's main goal is to provide hosting to huge computing and storing resources under concentrated management, thus providing big data applications with fine-grained computing and storage capacity.

In this talk, Dr. Ionescu will review the background and state of the art of big data research related to software technologies. After focusing on data generation, data acquisition, data storage, and data analysis discussing the technical challenges to the latest advances in the associated software technologies, the talk will make an attempt to associate big data analysis algorithms with Digital Signal Processing (DSP) techniques. Several representative applications of big data, including enterprise management, Internet of Things, online social networks, e-health applications, collective intelligence, and smart grid will be presented at the end.

Short Biography

Dr. Dan Ionescu is a Professor at the University of Ottawa (the Capital City University). He is the Director of the Network Computing and Control Technologies (NCCT) research laboratory since 1999. Former director of Computer Engineering at the above university from 1996 to 2000, Dr. Dan Ionescu is a senior member of various IEEE, IFIP, and IFAC groups.

His research at the University of Ottawa spans domains such as Artificial Intelligence, Machine Vision, Distributed Computing, Network Computing and Control, Internetworking Technologies, Web Collaboration platforms, and others. His contributions to Expert Systems, Image Processing, Temporal Logic, Discrete Event and Real-Time Systems materialized in a series of more than 250 papers, and a book. A series of industrial and governmental research grants were obtained by Dr. Ionescu which were used for equipping the NCCT with state-of-the-art high-end routing and switching devices, and large server farms, connected directly to Ca*net 4, Abelen, GEANT, and other main research-public networks. His research works were at the foundations of a few start-ups such as Diatem Networks, ARTIS, and Mgestyk.

His recent research efforts are directed at collaborative multimedia platforms, autonomic computing, big data, IoT, and new man–machine interface paradigm. Results of his research materialized into a Big Data Platform called M3Data in use at the Government of Canada.

DataFlow SuperComputing for ExaScale Applications



Jakob Salom
School of Electrical Engineering
University of Belgrade, Serbia
e-mail: jasadalom@yahoo.com

Abstract The strength of DataFlow computers, compared to ControlFlow ones, is in the fact that they accelerate the data flows and application loops by one or more orders of magnitude; how many orders of magnitude—that depends on the amount of data reusability within the loops. This feature is enabled by compiling down to levels much below the machine code, which brings important effects: much lower execution time, equipment size, and power dissipation.

The presentation’s goal is to describe and explain DataFlow programming paradigm:

Rather than writing one program to control the flow of data through the computer, one has to write a program to configure the hardware of the computer, so that input data, when it arrives, can flow through the computer hardware in only one way (the way the computer hardware has been configured). This is best achieved if the serial part of the application continues to run on the ControlFlow host and the parallel part of the application (BigData crunching and loops) is migrated into a DataFlow accelerator.

The presentation contains a few examples of successful implementations of DataFlow applications.

Short Biography

Dr. Jakob Salom graduated from University of Belgrade, School of Electrical Engineering in 1975, and started working in an IT company that was later acknowledged as the fastest growing IT company in the region.

During his tenure in the industry, his teams developed complete solutions for state payment systems agency, for banks and insurance companies, developed and managed large banking networks, and developed and established (in 1988) the first electronic banking network. He is now a consultant to Mathematical Institute of Serbian Academy of Sciences and Arts and to University of Belgrade, School of Electrical Engineering. His domains of expertise in recent years are:

- Use of Maxeler FPGA accelerators for HPC computing,
- Data warehousing, data archiving and data mining, and
- Cloud computing.

Advances in Urban Video-Based Surveillance Systems



Prof. Dr. Margarita N. Favorskaya
Russian Federation
e-mail: favor.edu@gmail.com

Abstract In recent years, a number of systems based on automatic video analysis for human security, traffic surveillance, home automation, and other applications are developed. Techniques of object and event recognition, behavior understanding, and action representation form a basis for such systems. The activity recognition in urban environment is the main problem of current investigations, which is built on data and knowledge representations of objects and reasoning scenarios. Such techniques are strongly dependent on low-level and middle-level vision tasks such as the filtering and motion segmentation following tracking.

The focus of this presentation is to discuss the applications of intelligent technologies and systems in vision-based urban surveillance. The application of intelligent paradigms improves efficiency and safety on the road networks (e.g., traffic alerts, estimated time to reach a destination and alternative routes, unmanned cars). The analysis of eyes and hands activity for automatic driving risk detection is one of the crucial problems in urban environment. Also car manufacturers, public transportation services, and social institutions are interested in detecting pedestrians in the surroundings of a vehicle to avoid dangerous traffic situations. The research on 3D computer graphic for the model representation of actual urban environment is also presented.

Short Biography

Margarita Favorskaya received her engineering diploma from Rybinsk State Aviation Technological University, Russia, in 1980 and was awarded a Ph.D. from St. Petersburg State University of Aerospace Instrumentation, St. Petersburg, in 1985. Since 1986 she is working in the Siberian State Aerospace University, Krasnoyarsk, where she is responsible for the Digital Image and Videos Processing Laboratory. Presently, she is a Full Professor and the Head of Department of Informatics and Computer Techniques, Siberian State Aerospace University. Her main research interests are in the areas of digital image and video processing, pattern recognition, fractal image processing, artificial intelligence, information technologies, and remote sensing. She has authored/co-authored more than 130 publications.

Margarita Favorskaya is a member of KES International organization and the IPC member of a number of national and international conferences.

She is on the editorial board of International Journal of Computer and Information Science and International Journal of Intelligent Decision Technology. She has won a number of awards from the Ministry of Education and Science of the Russian Federation for significant contribution in educating and training a number of highly qualified specialists over a number of years.

Robust Ensemble Learning for Data Mining



Sheryl Brahnam

Professor and Daisy Portenier Loukes Research Fellow in the School of COB, Computer Information Systems Department at Missouri State University
e-mail: sbrahnam@facescience.org

Abstract The field of machine learning is expanding at a rapid pace, especially in medicine. This pace is being driven by an information avalanche that is unprecedented. To handle these data, specialized research databases and metadatabases have been established in many domains. Machine learning technology applied to many of these databases has the potential of revolutionizing scientific knowledge. In the area of bioinformatics, for example, many large-scale sequencing projects have produced a tremendous amount of data on protein sequences. This has created a huge gap between the number of identified sequences and the number of identified protein structures. Machine learning methods capable of fast and accurate prediction of protein structures hold out the promise of not only reducing this gap but also of increasing our understanding of protein heterogeneity, protein-protein interactions, and protein-peptide interactions, which in turn would lead to better diagnostic tools and methods for predicting protein/drug interactions.

What are needed to handle the problems of today are not yesteryear's solutions, which were typically based on training a single classifier on a set of descriptors extracted from a single source of data. It is generally acknowledged that ensembles are superior to single classifiers, and much recent work in machine learning has focused on methods for building ensembles. In protein prediction some powerful ensembles have recently been proposed that utilize the combined information available in multiple descriptors extracted from protein representations. Particularly interesting, however, are ensemble systems combining multiple descriptors extracted from many protein representations that are trained across many databases. In this address, I shall describe the ensemble research that I am involved in with Drs. Loris Nanni and Alessandra Lumini. My focus will be on describing the methods our research group uses for building ensemble systems that work extremely well across multiple databases. Powerful general purpose ensembles are of value to both the general practitioner and expert alike. Such classifier systems can serve as a base for building systems optimized for a given problem. Moreover, general purpose ensembles can further our general understanding of the classification problems to which they are applied.

Short Biography

Sheryl Brahnham is a Professor and Daisy Portenier Loukes Research Fellow in the school of COB Computer Information Systems Department at Missouri State University. She is the Director/Founder of Missouri State University's infant Classification Of Pain Expressions (COPE) project. Her interests focus on medical decision support systems, machine learning, bioinformatics, biometrics, embodied conversational agents, and computer abuse. She has served as guest editor of several books and special issues on virtual reality and rehabilitation, technologies for inclusive well-being, agent abuse, and computational systems for medicine. She has published extensively in journals such as Bioinformatics, Pattern Recognition, Artificial Intelligence in Medicine, Amino Acids, Journal of Theoretical Biology, Expert Systems with Applications, Decision Support Systems, NeuroComputing, PLoS One, and Interacting with Computers, as well as in many conferences devoted to human-computer interaction, machine learning, and artificial intelligence. More about Dr. Brahnham can be found here: <http://www.brahnham.info>.

Part I
Image, Text and Signal Processing

A Comparative Study of Text-to-Speech Systems in LabVIEW

Manuela Panoiu, Cezara-Liliana Rat and Caius Panoiu

Abstract In this paper we propose to study the possibilities of transforming the written language into speech (text-to-speech) using the LabVIEW programming environment. To this aim we studied the text-to-speech interfaces provided by the Microsoft Speech SDK for TTS applications. The number and diversity of languages that can be used through these interfaces are also taken into consideration. Emphasis is on the advantages and the limitations of each class while analyzing the possibility of rendering languages that use special characters. It is well known that LabVIEW offers little support for special characters, special language characters being no exception, hence finding a functional method of correctly rendering speech for special character languages is an arduous task we proceeded to undertake. We have also researched the use of a speech synthesizer called MBROLA that provides support for a wide range of international languages. Together with open-source software, namely eSpeak, MBROLA becomes a complete text-to-speech (TTS) system. We have also analyzed the possibility of interfacing eSpeak with LabVIEW.

Keywords TTS · LabVIEW · SAPI · eSpeak · MBROLA · Lernout & Hauspie

M. Panoiu (✉) · C. Panoiu
Electrical Engineering and Industrial Informatics Department,
University Polytechnic Timisoara, Timisoara, Romania
e-mail: manuela.panoiu@upt.ro

C. Panoiu
e-mail: caius.panoiu@upt.ro

C.-L. Rat
University Polytechnic Timisoara, Timisoara, Romania
e-mail: cezara.liliana@gmail.com

1 Introduction

The utility of text-to-speech (TTS) systems consists of an easier means of communication and improved accessibility for the visually impaired [1–3]. High quality TTS systems, such as natural-sounding synthesizers [4], are complex systems that require the cooperation of various specialists resulting in a multidisciplinary project. Research on TTS synthesizers continues with the purpose of creating a wider range of languages and improving voice quality [1, 5]. Microsoft Speech SDK 5.1 is a software development kit designed primarily for developing speech applications in Microsoft Windows.

Microsoft Speech SDK allows programmers to write applications incorporating speech into them. The SDK contains the speech application programming interface (SAPI), the Microsoft continuous speech recognition engine and Microsoft concatenated speech synthesis (or text-to-speech) engine, and a collection of speech-oriented development tools for compiling source code and executing commands. The SDK components and the redistributable SAPI can serve to build applications that incorporate both speech recognition and speech synthesis capabilities. The Microsoft Speech SDK can be used with programming languages that support OLE automation, such as C, C++, Visual Basic, or C#.

SAPI has strong reliance on COM. SAPI 5.1 particularly supports OLE automation, hence programming languages that support OLE automation can use SAPI for application development. The SAPI application programming interface (API) reduces the code required for an application to use speech recognition or text-to-speech, making speech technology more accessible and robust. The Speech API provides a high-level interface between an application and speech engines while implementing all the low-level details needed to control and manage the real-time operations of various speech engines.

The Speech API architecture includes a collection of speech components that can directly manage the audio, training wizard, events, grammar compiler, resources, speech recognition manager, and a TTS manager. This provides low-level control and greater flexibility. The Speech API can also manage shared recognition events for running multiple speech-enabled applications. The two basic types of SAPI engines are TTS systems and speech recognizers. TTS systems synthesize text strings and files into spoken audio using synthetic voices. Speech recognizers convert human spoken audio into readable text strings and files [6].

The voices normally used by a Microsoft TTS engine would be Lernout & Hauspie voices. Lernout & Hauspie Speech Products, or L&H, was a company based in Belgium that was, in its day, the technology leader in speech recognition. L&H worked with Microsoft in making TTS voices for many international languages such as English (Mary—L&H TruVoice; Michelle—L&H TruVoice; Anna—L&H TruVoice; Sam—L&H TruVoice; Michael—L&H TruVoice; Mike—L&H TruVoice; Carol—TTS3000; Peter—TTS3000), Dutch (Linda—L&H TTS3000; Alexander—L&H TTS3000), French (Veronique—L&H TTS3000; Pierre—L&H TTS3000), German (Anna—L&H TTS3000; Stefan—L&H TTS3000), Italian

(Barbara—L&H TTS3000; Stefano—L&H TTS3000), Japanese (Naoko—L&H TTS3000; Kenji—L&H TTS3000), Korean (Shin-Ah—L&H TTS3000; Jun-Ho—L&H TTS3000), Portuguese (Juliana—L&H TTS3000; Alexandre—L&H TTS3000), Russian (Svetlana—L&H TTS3000; Boris—L&H TTS3000), Spanish (Carmen—L&H TTS3000; Julio—L&H TTS3000) [7].

Another approach to speech synthesis would be to use software provided by the MBROLA project. MBROLA is a non-commercial project that provides speech synthesizers for international languages. MBROLA 2.00 is a speech synthesizer based on the concatenation of diphones using a technique under the name of Multi Band Resynthesis OverLap Add, similar to the PSOLA methods [8], particularly the PSOLA methods that process the signal in time domain (TD-PSOLA) [9], which provides better solutions for the real time implementation of a TTS system [10]. This synthesizer is provided for free, for noncommercial, nonmilitary applications only. Executable files of this synthesizer have been made available for many computers/operating systems. MBROLA takes a list of phonemes as input, together with prosodic information (duration of phonemes and a piecewise linear description of pitch), and produces speech samples on 16 bits (linear), at the sampling frequency of the diphone database used. Diphone databases tailored to the MBROLA format are needed to run the synthesizer. It does not accept raw text as input therefore it is not a TTS synthesizer [5]. In order to obtain a complete TTS synthesizer we used eSpeak.

eSpeak is a compact open source speech synthesizer for Linux or Windows. eSpeak converts text into phonemes with pitch and length information. Therefore it can be used as a front-end to MBROLA diphone voices.

eSpeak is available as follows:

- A command line program to speak text from a file or from standard input.
- A shared library version for use by other programs.
- A SAPI5 version for Windows.
- eSpeak has been ported to other platforms.

It is written in C and includes several different voices whose characteristics can be altered. eSpeak executes text to speech synthesis for the following languages: Afrikaans, Albanian, Aragonese, Armenian, Bulgarian, Cantonese, Catalan, Croatian, Czech, Danish, Dutch, English, Esperanto, Estonian, Farsi, Finnish, French, Georgian, German, Greek, Hindi, Hungarian, Icelandic, Indonesian, Irish, Italian, Kannada, Kurdish, Latvian, Lithuanian, Lojban, Macedonian, Malaysian, Malayalam, Mandarin, Nepalese, Norwegian, Polish, Portuguese, Punjabi, Romanian, Russian, Serbian, Slovak, Spanish, Swahili, Swedish, Tamil, Turkish, Vietnamese, Welsh. Other languages may also be added. However, some of these may only be experimental attempts at the language and need to be improved. A major factor is the rhythm or cadence. A voice can be significantly improved by changing the relative length of stressed syllables. Identifying unstressed function words is also important to make the speech flow well [11].

2 Analysis of the TTS Interfaces Available in LabVIEW

The classic LabVIEW TTS example [12] uses the ISpeechVoice interface from the SpeechLib library. SpeechLib.ISpeechVoice can be used as an Activex Control. Once an application has created an ISpeechVoice object, the application only needs to call the Speak method to generate speech output from some text data. In addition, the ISpeechVoice interface also provides several methods for changing voice and synthesis properties such as speaking rate, output volume, and changing the current speaking voice.

This interface can access the Microsoft text-to-speech voices. The Microsoft text-to-speech voices are speech synthesizers that can be used in applications that are developed using the SAPI. These voices are Microsoft Sam, Microsoft Mary, and Microsoft Mike, all three being English voices. Microsoft Sam is the default text-to-speech male voice in Microsoft Windows 2000 and Windows XP. Microsoft Mike and Microsoft Mary are optional male and female voices [13]. Unfortunately, Lernout & Hauspie voices, such as Michael and Michelle, are not directly accessible through this interface; this representing is a serious limitation to a TTS program for foreign languages. Instead, the voices installed with MBROLA and eSpeak are available.

The classic LabVIEW example of TTS using the class ISpeechVoice adapted for calling MBROLA languages can be seen in Fig. 1a. The changes that were made to the program to enable this can be seen in Fig. 1b.

Another option in TTS programming would be to use the Microsoft TextToSpeech control, which is an ActiveX control installed with SAPI4 that wraps up the high-level Voice Text API. Accessing this control adds the generated type library import unit (HTTSLib_TLB.pas) to a package. The import unit contains the Object Pascal component wrapper for the ActiveX, which is called ItextToSpeech. This component will be installed by default on the ActiveX page of the Component Palette. The ActiveX is described as the High-Level Text To Speech Module.

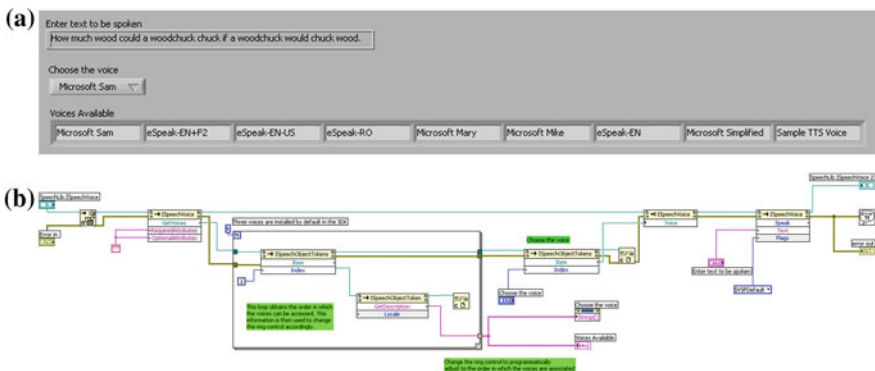


Fig. 1 A TTS that uses ISpeechVoice. **a** Front panel. **b** Block diagram

The primary interface it implements is `ITextToSpeech`. This ActiveX control can be used programmatically through the ClassID `CLASS_TextToSpeech` from the `HTTSLib_TLB` unit. The Windows registry describes this class as the `TextToSpeech Class`. The ActiveX component shows up as a colorful mouth. When the ActiveX is asked to speak, the mouth animates in sync with the spoken phonemes. It can also generate the `OnVisual` event which is used by the ActiveX mouth animation, but offers plenty of information that can be used for another animation [14].

The `HTTSLib.ITextToSpeech` interface can be used through an ActiveX control in LabVIEW. It can access the Microsoft default voices and the Lernout & Hauspie voices. The only drawback, which can be a significant one, is that it cannot access the MBROLA voices.

The second application, shown in Fig. 2, is TTS designed and implemented by the authors in LabVIEW using the `ITextToSpeech` interface and a number of Lernout & Hauspie languages. The application allows the user to select the speech voice and shows the voice information (name, gender, style, speaker, language ID). The animation associated to `ITextToSpeech` can also be seen in the figure.

3 The Use of Special Language Characters in LabVIEW

Accents, diacriticals, and special language characters, the use of which also constitutes a topic of interest, is a problem in LabVIEW. LabVIEW uses multibyte character strings (MBCS) in character representation and therefore it does not recognize special UNICODE characters. There are still ways to represent diacritics in LabVIEW [15], but they do not work for text from UNICODE documents and direct conversion methods can prove to be extremely complicated when the text does not originate from the LabVIEW program. Considering that an efficient TTS must be able to work with character strings regardless of their origin (programs that read books are an excellent example of this), a method of adapting LabVIEW to operate with these characters is required. The solution found by the authors is by employing an ActiveX object called `RichTextBox`.

This functions in UNICODE encoding, being able not only to correctly represent special language characters, but also to copy the format of the original text. `RichTextBox` permits text editing similar to WordPad. A `RichTextBox` object is also able to access the contents of stack memory so that it can programmatically paste copied text. But transmitting the text from this component through strings to an object of the `ISpeechVoice` interface or the `ITextToSpeech` interface would add up to the same result. Due to this, a text file-based communication was used. `RichTextBox` can write text files itself and correctly encode them. Because both `ISpeechVoice` and `ITextToSpeech` would require the programming environment to read the files with correct encoding or re-encode the text keeping the special characters represented correctly, we bypass the programming environment and send the text files through a programmatic command directly to `espeak.exe`. `eSpeak` is

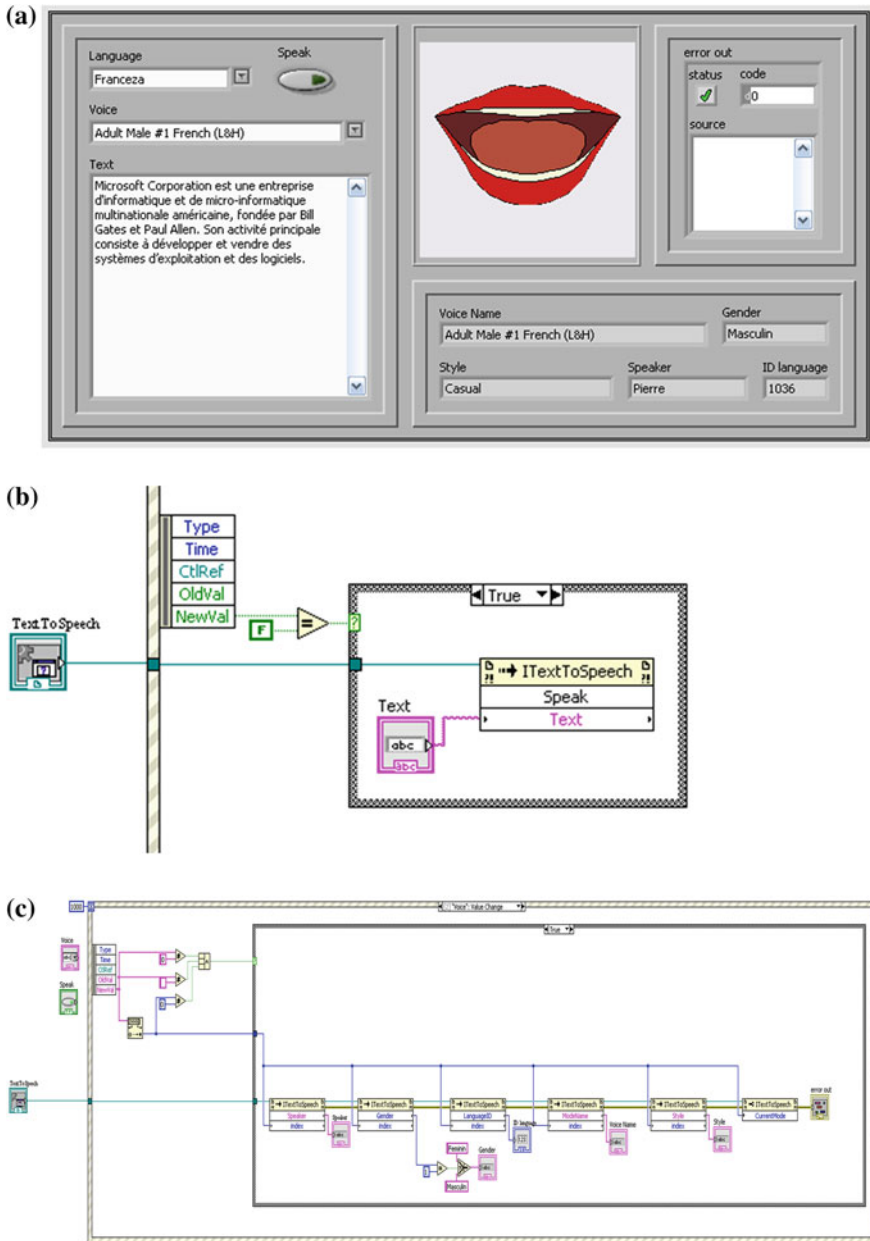


Fig. 2 An example TTS made using the ITextToSpeech class. **a** Front panel. **b** The use of the speak method of the ITextToSpeech class. **c** The use of some methods of the ITextToSpeech class in order to set the desired voice and obtain information about it

(for Polish this is Latin2, for Russian it is KOI8-R). This choice can be overridden by a line in the voices file to specify an ISO 8859 character set, example: charset 5. This means that ISO 8859-5 is used as the 8-bit character set rather than KOI8-R [11].

Because each of these actions, required in order to use special language characters, could be done manually, but are, in this case, executed programmatically, we can consider this program as an automation of a manual process.

The last application (Fig. 3) is a TTS implemented by technologies (eSpeak, MBROLA) other than the above-mentioned interfaces. This application has a built-in web browser (Fig. 3a). The presence of the RichTextBox component and how it is employed is evident. Figure 3b represents the speech algorithm that uses a command prompt component to access eSpeak.

4 Conclusions

There are various ways to create a TTS in LabVIEW. Complications arise when we want to build a TTS for a specific language or a particular voice quality. Question arises as to the character encoding in that language and whether there is software commercially available for that language. The answers all depend on what exactly one wants to achieve through the application.

Designing a TTS that can accurately render special language characters in LabVIEW was a very complicated task to undertake, given the limitations of the programming environment. This is particularly concerning when there are few synthesizers available for the language to be spoken. When choices are limited, the repercussions might be felt in the quality of the end-product. However, the authors have demonstrated that the task of building a TTS in LabVIEW with special character recognition is not impossible and that, in the process, LabVIEW is a highly versatile programming environment. If LabVIEW libraries are too restrictive for the needs of the application one can use methods other than classical ones for solving the challenges.

References

1. Azis NA, Hikmah RM, Tjahja TV, Nugroho AS (2011) Evaluation of text-to-speech synthesizer for Indonesian language using semantically unpredictable sentences test: IndoTTS, eSpeak, and Google Translate TTS. In: Proceedings of international conference on advanced computer science & information systems
2. Rafiee MS, Jafari S, Ahmadi HS, Jafari M (2011) Considerations to spoken language recognition for text-to-speech applications. In: 2011 UKSim 13th international conference on computer modelling and simulation (UKSim), pp 304–309
3. Falk TH, Mölle S (2008) Towards signal-based instrumental quality diagnosis for text-to-speech systems. *IEEE Signal Process Lett* 15:781–784

4. Hunt AJ, Black AW (1996) Unit selection in a concatenative speech synthesis system using a large speech database. In: Proceedings of the IEEE international conference on acoustics, speech, and signal processing, ICASSP-96, vol 1, pp 373–376
5. Dutoit T, Pagel V, Pierret N, Bataille F, van der Vrecken O (1996) The Mbrola project: towards a set of high quality speech synthesizers free of use for non commercial purposes. In: Proceedings of the fourth international conference on spoken language, ICSLP 96, vol 3, pp 1393–1396
6. Microsoft Speech SDK 5.1 Help
7. http://en.wikipedia.org/wiki/Lernout_%26_Hauspie
8. Bigorgne D, Boeffard O, Cherbonnel B, Emerard F, Larreur D, Le Saint-Milon JL, Metayer I, Sorin C, White S (1993) Multilingual PSOLA text-to-speech system. In: Proceedings of IEEE international conference on acoustics, speech, and signal processing, ICASSP-93, vol 2, pp 187–190
9. Dutoit T, Leich H (1993) MBR-PSOLA: text-to-speech synthesis based on an MBE re-synthesis of the segments database. *Speech Commun* 435–440
10. Moulines E, Charpentier F (1989) Pitch synchronous waveform processing techniques for text-to-speech synthesis using diphones. *Speech Commun* 9:5–6
11. <http://espeak.sourceforge.net/>
12. <https://decibel.ni.com/content/docs/DOC-2263>
13. http://en.wikipedia.org/wiki/Microsoft_text-to-speech_voices
14. <http://www.blong.com/Conferences/DCon2002/Speech/SAPI4HighLevel/SAPI4.htm>
15. <https://decibel.ni.com/content/docs/DOC-10153>

Parallel Neural Fuzzy-Based Joint Classifier Model for Grading Autistic Disorder

Anju Pratap, C.S. Kanimozhiselvi, R. Vijayakumar and K.V. Pramod

Abstract This article proposes a Parallel Neural Fuzzy (PNF) possibilistic classifier model and it is the application in autism assessment systems. An independent neural network and a fuzzy system work in parallel on a set of input and produces individual support (belief) regarding the output classes. The beliefs of heterogeneous classifiers are then fused using a possibilistic classifier to take a joint decision. A neural network is trained with samples to simulate expertise while the fuzzy system is embedded with theoretical knowledge, specific to a problem. This model has been implemented and applied as an assessment support system for grading childhood autism. Application specific observations demonstrate two advantages over an individual neural network classifier: first, an improved accuracy rate or decreased misdiagnosis rate and second, a certain or unique grading than an uncertain or vague grading. The proposed approach can serve as a guide in determining the correct grade of autistic disorder.

Keywords Childhood autism • Parallel neural fuzzy classification • PNF possibilistic classifier • Linear vector quantization • Local fuzzy model

A. Pratap (✉)

Anna University, Chennai, Tamilnadu, India
e-mail: anjuprathap@gmail.com

C.S. Kanimozhiselvi

Department of Computer Science and Engineering, Kongu Engineering College,
Erode, Tamilnadu, India
e-mail: kanimozhi@kongu.ac.in

R. Vijayakumar

School of Computer Sciences, Mahatma Gandhi University, Idukki, Kerala, India
e-mail: vijayakumar@mgu.ac.in

K.V. Pramod

Department of Computer Applications, Cochin University of Science and Technology,
Cochin, Kerala, India
e-mail: pramodkv4@gmail.com

1 Introduction

The main challenges in the domain of clinical decision-making processes are imprecision, uncertainty, and vagueness. The medical practitioners rely on their gained expertise from which they have to reason logically and infer correctly before making a decision regarding a disease. There are problem-specific clinical decision support systems developed with the aid of artificial intelligence, to support and improve this medical decision-making process. Artificial intelligence-based predictions in clinical diagnosis especially in the field of psychology has gained much research interest [1, 2]. Psychological disorders are usually assessed by observing the symptoms or features present in a human, where quantitative tests are having less involvement during a diagnosis. Hence, the differential diagnosis and grading of a disorder is comparatively difficult than that of a disease. Due to this qualitative assessment-based diagnosis, this chapter refers a decision support system as an assessment support system.

AI uses any classification or clustering technique which is a process of grouping individuals having the same characteristics into a set. A classifier can assign a class label to an object based on its object descriptions. Likewise, classifiers are applied to assign grade to a disorder based on the symptoms present on it. These have prompted research to progress into hybrid models, where the combinations enhance classification results. The objectives of this research article are:

- To illustrate the usage of some complementary soft computing techniques in streamlining the autism diagnostic process with higher accuracy or with lower misdiagnosis rate.
- To propose a parallel neural fuzzy possibilistic classifier model which gives better accuracy without any uncertainty in grading over an individual neural network that gives vague grading.

1.1 *Artificial Neural Networks (ANN) in Decision Making*

Various branches of science and technology use neural networks for different applications. The processing capability of ANN allows integrating diverse amount of clinical data to classify the output. Problem-specific diverse data can be processed by an ANN in the context of previous training history to produce clinically relevant output that supports a clinician to take accurate decision [3].

ANN belongs to the family of AI techniques due to its learning and generalization capabilities. ANN can model a highly nonlinear complex system in which the relationship between the variables are unknown. An ANN is formed as a series of nodes organized in layers and are connected through a weighted connection. The input layer receives input data and transfers to the hidden layer through the

weighted links for mathematical processing. The intermediate results are then transferred to the next layer, and finally the last layer provides the output. Thus, network can be represented as black box with 'x' inputs and 'y' outputs.

1.2 Fuzzy Systems in Decision Making

Fuzzy classification is the process of grouping individuals having same characteristics into a fuzzy set. The truth value of a fuzzy proposition function defines the membership function of the above said fuzzy set. Thus, a fuzzy classification corresponds to a membership function (μ) that indicates whether an individual is a member of a class; given its classification predicate (PI),

$(\mu): PF \times U \rightarrow T$, where

PF = Propositional function

U = Universe of Discourse

T = Set of truth values

A Fuzzy Rule-Based System contains fuzzy if-then rules of the form:

R_i :

If x is normal then the class is 1

If x is low then the class is 2

If x is medium then the class is 3

If x is high then the class is 4.

An individual vote of each rule is aggregated to find the output of a fuzzy classifier. The purpose of fuzzy classifiers in medical decision making is to mimic the behavior of a human expert physician who is able to diagnose the disease satisfactorily. To automate entire diagnosis process for supporting a human physician with a fuzzy classifier has to be made as computer software.

1.3 Classifier Combination Techniques in Decision Making

Multiple classifier fusion may generate more accurate classification than the constituent classifiers [4]. The outputs of homogeneous classifiers are then combined to form an ensemble for classifying novel patterns. The performance of the ensemble is strongly dependent on the accuracy of individual classifiers.

One of the most widely used ensemble structures is Ensemble Network. They are neural networks having same structure, but with different initializations that are applied to the same classification problem [5]. Such an ensemble network is a homogeneous classification system and the decisions of individual networks are fused using any decision fusion scheme. This ensemble homogeneous NN classifiers can be applied for developing a decision support system.

2 Problem Description and Related Works in Autistic Disorder

Childhood autism is a psychological disorder that disables the verbal and nonverbal communicative skills in a child especially social interaction. The differential grading of this disorder is highly challenging as it depends fully on the knowledge and expertise of a clinician. Autism expresses itself in diverse ways and hence it is prone to misdiagnosis. Early intervention and grading of disorder is necessary, because therapies like speech therapy, psychotherapy, etc., are the only methods to alleviate the problems happened due to the disorder. Conventionally, autism diagnosis and grading are based on assessment tools which are normally provided by a medical expert like: developmental pediatrician, psychologist, speech pathologist, etc. An experienced medical practitioner can easily spot an autistic child, and hence they rarely depends diagnostic tools for an initial screening about the presence of the disorder. Others will usually go for another opinion on any uncertainty in their diagnosis. But, the process of grading the severity of autistic disorder in an early childhood is not straight forward and even expert clinicians too feel difficulty and uncertainty [6]. The clear and vague grades are represented in a set ‘S,’ where G_i is as represented in Table 1.

$S = \{Normal (G1), Probably autistic (G23), Autistic (4)\}$ or

$S = \{Normal (G1), Mild to Moderate (G23), Moderate to Severe (G34), Severe (G4)\}$

The steps that lead to a diagnosis are as follows:

- Step 1: Child’s caretaker feels an abnormality in the language or behavior of the child, which led them bring it to the notice of a medical practitioner
- Step 2: Based on the expertise, the clinician makes an initial diagnosis of an autistic disorder
- Step 3: The child is then referred for an autism assessment that rely on standard diagnostic tools
- Step 4: Based on the observations made by the clinician using any of the tools, he sums up the score obtained for each qualitative symptom to calculate a

Table 1 Grade representation

Grade	Class name
G1	<i>Normal</i>
G2	<i>Mild</i>
G3	<i>Moderate</i>
G23	<i>Mild–moderate</i>
G34	<i>Moderate–severe</i>
G4	<i>Severe</i>

total score. This total score is then compared with the threshold of each grade and classify it accordingly

Step 5: This diagnosis ends up with a prediction that the child is either: *Normal*, *probably autistic*, or *severely autistic*

The main problem here is to confidently grade autism as *Normal* (G1), *Mild* (G2), *Moderate* (G3), and *Severe* (G3), where a correct assessment is needed to schedule the frequency of therapy or in other treatments.

This challenging uncertainty in the conventional grading and the improved predictive ability of hybrid soft computing techniques are the motivations behind this study. Better performance of an automated diagnostic system is depending on two factors. First is the identification of relevant symptoms that involves in a disease or disorder. The next factor is the formulation of appropriate function that relates these symptoms to a correct disease or disorder.

Soft computing techniques like fuzzy logic and neural networks have proven its application in clinical decision support systems [3, 7, 8]. Various studies on artificial intelligence techniques and its application in expert systems were conducted by many researchers [9]. The usage of NN for the diagnosis of autism has started in early 1990's, and on an average a back propagation neural network performed with an accuracy of 95 % [2]. Likewise, Multilayer Perceptron provided a classification of 92 % which was higher than the accuracy of a logistic regression model in autism diagnosis [6]. The combination of fuzzy techniques with neural network has succeeded in improving the classification function in diagnosis application [1, 10].

3 Parallel Neural Fuzzy Classifier Model: An Overview

Parallel neural fuzzy is based on an architecture that integrates an appropriate parallel structure of a neural network and a fuzzy logic. This joint classification mechanism involves two parallel classifiers: a nonknowledge-based neural network classifier and knowledge-based fuzzy logic classifier. The model consists of three layers: an input layer, a parallel neural fuzzy layer, and a joint classification layer (The probabilistic fuser). The neural network has already been trained with a set of training data and can able to classify it to a vague grade. Similarly, the fuzzy system is also built with problem-specific theoretical knowledge for a unique grading. To diagnose a new patient, the input layer sends the input data to the trained neural network and fuzzy system in parallel. The independent neural network and fuzzy system work in parallel and outputs their support or belief toward the grades. The supports of corresponding classes are then fused using a possibilistic classifier for a combined diagnosis.

Figure 1 represents a Parallel Neural Fuzzy (PNF) decision support system model for autism diagnosis, in which an LVQ neural network and a Local Fuzzy system are used in parallel to classify the grade of childhood autism. The algorithm PNF for this problem-specific PNF classifier is as shown in the Table 2. The output

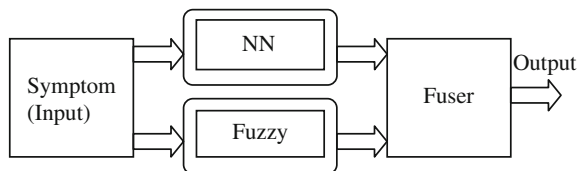


Fig. 1 PNF model

Table 2 Algorithm PNF

Algorithm: parallel neural fuzzy
Input: Symptom Vector ‘S’
Output: Autism Grade ‘Gi’
<ol style="list-style-type: none"> 1. Train the neural network (LVQ_NN) using history of samples to simulate practice 2. Create a Fuzzy Rule Base (FRB) using theoretical knowledge 3. Design a Rule-Based Possibilistic Classifier as a fuser 4. Read the symptom vector ‘S’ 5. Open a parallel processing environment 6. For $I = 6.1$ to 6.2 do in parallel <ol style="list-style-type: none"> 6.1. Run the LVQ_NN using ‘S’ for getting a vague grading (V) 6.2. Apply the FRB to ‘S’ for a unique grading (U) 7. End For 8. Apply ‘U’ and ‘V’ to the fuser to obtain a Joint Classification result, G_i

units of neural network are $G1$, $G23$, $G34$, $G4$ and that of fuzzy system are $G1$, $G2$, $G3$, and $G4$ where a G_i is represented in Table 2. The output grades of the fuser are also $G1$, $G2$, $G3$, and $G4$ with an improved accuracy.

4 Implementation Details

4.1 Knowledge Acquisition, Feature Selection, and Dataset Building

Accurate diagnosis of a disorder using any soft computing technique is based on the selection of input features. Knowledge acquisition was done through a group elicitation phase that includes: a developmental pediatrician, a psychologist, and a speech therapist. Major autistic features are addressed in Childhood Autistic Rating Scale (CARS) and a careful selection of suitable features have been carried out using CARS tool. Here, the features are represented through strength of the symptoms which is relevant in helping the grade of the disorder. These provide the information needed to discriminate different grades of childhood autism. Thus, a clinical dataset which contains CARS score of 100 autistic children whose

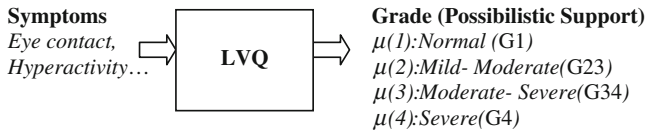


Fig. 2 LVQ model

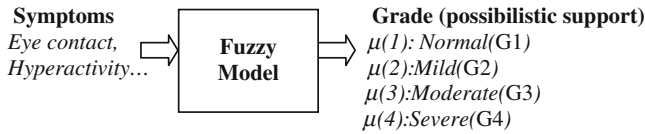


Fig. 3 Fuzzy model

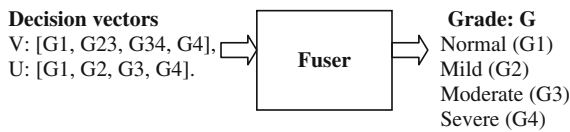


Fig. 4 The possibilistic fuser

diagnosis is already been made by clinicians were collected and evaluated to form training and testing samples (Figs. 2, 3 and 4).

The dataset properties include: 100 instances, 16 attributes, and 4 grades (G1, G23, G34, and G4). The prediction and generalization abilities of neural networks are strongly depending on the quality of input data and training method. Thus training sample is structured as a matrix (100 × 17), where each row refers to one autistic patient. The first 16 elements in a row represent input features and the last element represents the grade .This dataset have been used for network learning and verification.

4.2 LVQ Neural Network

In a LVQ, the input vectors are quantized to codebook values and are then used for pattern classification. It assumes that a set of codebook values, $W \{w_i | i = 1, 2 \dots q\}$ and a set of labeled training samples $X = \{x_i | i = 1, 2, 3 \dots n\}$ are available. Decision regions and boundaries are defined using a similarity measure, i.e., the Euclidean distance [11].

For each iteration ‘ k ’ until the stop criterion is not satisfied do steps 1–4:

1. For each x_i , find w_i that is closest to x_i . Denote it as w_c .
2. If the label on x_i belongs to w_c , i.e., correctly classified, then update $w_c(k + 1) = w_c(k) + \alpha(x_i - w_c(k))$. This moves w_c closer to x_i .
3. Otherwise, if x_i is incorrectly classified then update $w_c(k + 1) = w_c(k) - \alpha(x_i - w_c(k))$.
4. Consider the next element in X .

The Euclidean distances of all output units show the similarity between the input and the output units. This trained LVQ is able to classify an input to one output where the similarity distance is minimum. But the joint decision model takes one more stage to modify the output of LVQ, where the intention is not to find a single output unit. The similarity distances between the input and outputs are normalized to form a degree of support $\mu(i)$ or belief to all output units.

The normalization for a possibilistic support is as follows:

For each instance

1. For all output unit ‘ j ’
2. Calculate $d_j \forall j = 1, 0, 4$, where $d_j =$ Euclidean similarity measure
3. Create vector $D = [d_1, \dots, d_j]$
4. Find $E_j = \text{abs}(d_j - \max(D))$
5. Calculate Sum = $\sum_{i=1}^4 E_j$
6. $\text{Bel}(j) = \mu(j) = \frac{E_j}{\text{sum}}$

$\mu(j)$ represents the possibilistic value or the degree of support of LVQ to the j th class, where its value ranges in between [0, 1], and form a possibilistic decision vector ‘ V ’ as given in algorithm.

The conventional CARS-based assessment calculates a total score obtained through symptoms without considering the relationship between 15 input symptoms and its contribution to the overall disorder. In other words, grading is based on a single variable which is the total score. Hence, an LVQ is trained with the 15 symptoms along with the total score (16th feature) for a better accuracy. The outputs are vague grades: *Normal* (G1), *Mild–Moderate* (G23), *Moderate–Severe* (G34), *Severe* (G4). Result shows that rather than giving an accurate unique grading, LVQ performs better for vague grading similar to a clinician’s diagnosis. The class overlapping like *Mild–Moderate* and *Moderate–Severe* are unable to separate for giving a unique grading like *Normal*, *Mild*, *Moderate*, *Severe*.

LVQ uses clustering, which is a process of grouping similar data points into same group rather than across the groups. Thus, LVQ is implemented with 16 input units and 4 output units. Each input ‘ x_i ’ represents the strength of a symptom and the output ‘ y_i ’ represents a grade.

4.3 Fuzzy Rule-Base Design

To support and improve the accuracy of LVQ along with the refinement of overlapped grades, a fuzzy rule-based system is also run in parallel using the input data. This subsection describes about the design of a knowledge-based autism diagnosis system that uses a fuzzy logic concept. The knowledge obtained from the domain experts during the group elicitation phase are embedded as rules mostly in the form of If-then-Else statements. For example, if there is any history of seizures and its frequency is given, then generate warning as the proneness to autism.

A problem-specific local fuzzy model that uses a Takagi-Sugeno-Kang-type rules has been developed. Local fuzzy rules find the relationship between input (x_i) and the output (y_i), and hence the consequent parts are represented as functions. Thus, fuzzy model tries to find out the contribution of individual symptoms to the overall grade of the disorder and, so the rules are of single input and single output structure. The outputs are clear grades: *Normal* (G1), *Mild* (G2), *Moderate* (G3), *Severe* (G4). The model uses a triangular fuzzifier that fuzzifies the input symptoms individually, and the inference mechanism uses a first order function to map the input feature to a confidence value for a grade. The confidence value of each symptom to the respective grades is mapped correctly and calculates the cumulative confidence obtained for each grade. Then, the confidence values of 4 output grades are normalized to a possibilistic values to form a possibilistic decision vector ' U ', as follows:

For an instance

1. For all output grade, $j = 1$ to 4
2. Let c_j represents the cumulative confidence
3. Create vector $C = [c_1, \dots, c_j]$
4. Find $E_j = \text{abs}(c_j - \max(C))$
5. Calculate Sum = $\sum_{i=1}^4 E_j$
6. Degree of support (j) = $\mu(j) = \frac{E_j}{\text{Sum}}$

Since this system can give a clear grading, it is used to support and separate the overlapped grades decided by the LVQ, which is similar to the second opinion of a doctor. Thus for a given case, if LVQ classifies as *Mild-Moderate* (G23), then the Fuzzy system supports to refine it to an exact grade with an improved accuracy through a possibilistic classifier, i.e., either *Mild* (G2) or *Moderate* (G3).

4.4 Possibilistic Classifier—The Fuser

The decision vector of neural and fuzzy system contains (G1, G23, G34, G4) and (G1, G2, G3, G4), respectively and passes it to the last layer that contains a fuser.

The fuser considers a value in a decision vector as the belief or support to a grade by that individual classifier. In possibility theory, the belief potential of nested sets

Fig. 5 Nested sets

are called consonant evidences. Here, the overlapped grades G23 and G2 are consonant evidences supported by a neural network and fuzzy system, respectively. The fuser checks the supports of a grade by the neural network and fuzzy system, and possibilistic rules are applied to corresponding classes' accordingly. Consider the nested sets in Fig. 5, where $G2 \subset G23$. The belief of G2 based on the consonant evidence is as in Eq. 1.

$$\text{Bel}(G2) = \text{Bel}(G2 \cap G23) \quad (1)$$

Thus, evidences for grade “*Mild*” are obtained from G23 and G2, and the combined evidence is calculated using the min operator. Similarly, the evidence for “*Moderate*” is given through G23 and G34 by ANN, and G3 by Fuzzy system. Its combined evidence is calculated as:

$$\text{Bel}(G3) = \text{Bel}(G23 \cap G3) \cup (G34 \cap G3) \quad (2)$$

Thus, Possibilistic rules (Pr_i) for consonant evidences are as follows:

$$\text{Pr}_1: \text{Bel}(\textit{Mild}) = \min[\text{Bel}(\textit{Mild}), \text{Bel}(\textit{Mild-Moderate})]$$

$$\text{Pr}_2: \text{Bel}(\textit{Moderate}) = \max(\min[\text{Bel}(\textit{Moderate}), \text{Bel}(\textit{Mild-Moderate})], \min[\text{Bel}(\textit{Moderate}), \text{Bel}(\textit{Moderate-Severe})])$$

$$\text{Pr}_3: \text{Bel}(\textit{Severe}) = \max(\min[\text{Bel}(\textit{Severe}), \text{Bel}(\textit{Severe})], \min[\text{Bel}(\textit{Severe}), \text{Bel}(\textit{Moderate-Severe})])$$

$$\text{Pr}_4: \text{Bel}(\textit{Normal}) = \min[\text{Bel}(\textit{Normal}), \text{Bel}(\textit{Normal})]$$

The above rules are applied for all V_i and U_i , and the G_i having the maximum value is considered as the grade of the disorder.

5 Experimental Results and Discussions

This section contains two subsections: LVQ ANN-based autistic grading and its improvement through PNF-based autistic grading through a chart-based comparison.

Table 3 Confusion matrix of LVQ ANN

	<i>Normal</i>	<i>Mild–moderate</i>	<i>Moderate–severe</i>	<i>Severe</i>
<i>Normal</i>	10	0	0	0
<i>Mild–moderate</i>	0	46	2	0
<i>Moderate–severe</i>	0	0	23	0
<i>Severe</i>	0	0	4	15

Table 4 LVQ ANN performance

Sample size	100
Average reliability	94.8 %
Average accuracy	93.6 %
Overall accuracy	94 %
Training time	0.79 s
Error rate	0.060
MAE	0.060
RMSE	0.245
TP	0.94

5.1 LVQ ANN-Based Autistic Grading

The proposed model is implemented and tested using a matlab parallel processing pool. Table 6 shows a sample matlab code of the implemented PNF classifier model. To select a neural network for this application, both SOM and LVQ were designed and trained. The performance of LVQ is better than a SOM due to its supervised form of clustering; results show that LVQ can give a vague classification/grading of almost 94 % similar to a clinician during resubstitution testing using 100 samples. The confusion matrix of LVQ is calculated based on the experimental results which is given in Table 3.

Other performance parameters are also calculated using this confusion matrix and is shown in Table 4. To improve the accuracy of the ANN diagnosis and to separate the vague or overlapped grades, the diagnosis of LVQ is supported with a parallel fuzzy system.

Although the results of LVQ ANN were acceptable, it was unable to separate uncertain grades like G23 (*Mild–Moderate*) and G34 (*Moderate–Severe*). This is not only achieved by using a parallel neural fuzzy possibilistic classifier, but also a reduction in error rate or misdiagnosis was also seen.

5.2 Parallel Neural Fuzzy Based Autistic Grading

The similarity measures given by the LVQ are converted to certain possibilistic grades and a possibilistic decision vector ‘U’ is constructed, where some grades are overlapped. Similarly, the local fuzzy model also generates a possibilistic decision

Table 5 Possibilistic vectors

	$\mu(1)$	$\mu(2)$	$\mu(3)$	$\mu(4)$
NN	32.46425	35.79353	31.74222	0
FS	0	82.85714	17.14286	0
PNF	0	35.79353	17.14286	0

vector ‘V’, where the grades are certain. The result of joint decision is illustrated with an example.

In common, $\mu(1)$ and $\mu(4)$ represents Grades “Normal” and “Severe”, respectively. But $\mu(2)$ and $\mu(3)$ are represented by NN as “Mild–Moderate” and “Moderate–Severe”, where by FS and PNF are “Mild” and “Moderate”, respectively. Table 5 contains the possibilistic support for a grade by LVQ ANN (NN), Fuzzy system (FS), and the possibilistic fuser (PNF) for Case No:58 of the dataset, in which $\mu(I)$ represents the possibilistic support to Grade ‘i’. It is clear that LVQ gives maximum support to G23 and local fuzzy to G2. The possibilistic classifier, i.e., PNF takes the decision of NN and FS and joins the consonant evidences using max-min operators.

LVQ diagnoses Case No: 58 as “Mild–Moderate” due to the maximum possibilistic support for $\mu(2)$, and Fuzzy system calculates the maximum possibilistic support for “Mild” which is $\mu(2)$. The fuser calculates the percentage of support to “Mild” in “Mild–Moderate” which again is the maximum, i.e., $\mu(2)$.

5.3 Chart-Based Comparison

Figure 6 is chart representing around 100 cases and its grades diagnosed by an LVQ ANN. This shows that it is able to clearly grade G1: “Normal” and G4:

Fig. 6 Bar chart representing the vague grading of 100 cases by LVQ ANN

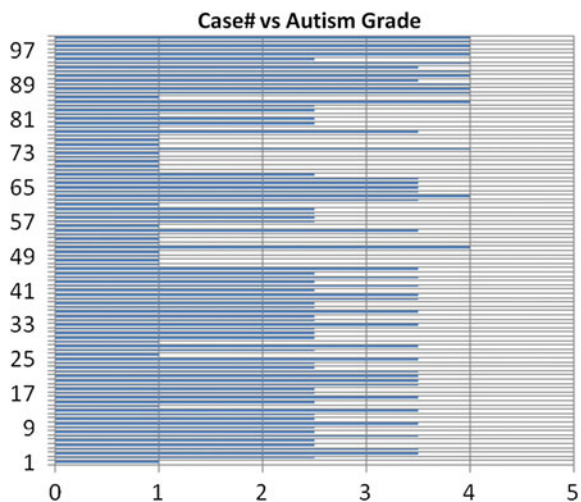
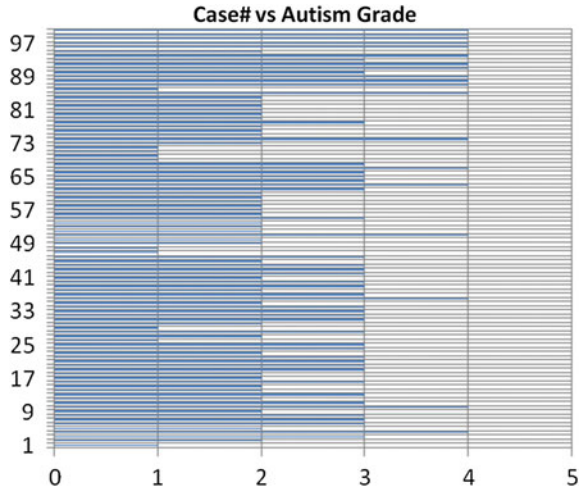


Fig. 7 Bar chart representing the clear grading of 100 cases by PNF classifier



“Severe” only and the majority of cases are G23: “Mild–Moderate” and G34: “Moderate–Severe”. Figure 7 represents the chart of PNF classifier in which all the cases have been graded clearly and separately.

References

1. Arthi K, Tamilarasi A (2008) Prediction of autistic disorder using neuro fuzzy system by applying ANN technique. *Int J Dev Neurosci* 26:699–704
2. Cohen IL, Sudhalter V, Landon-Jimenez D, Keogh M (1993) A neural network approach to the classification of autism. *J Autism Dev Disord* 23:443–466
3. Amato F, López A, Peña-Méndez EM, Vañhara P, Hampf A, Havel J (2013) Artificial neural networks in medical diagnosis. *J Appl Biomed* 11:47–58
4. Kuncheva LI, Bezdek JC, Duin RP (2001) Decision templates for multiple classifier fusion: an experimental comparison. *Pattern Recogn* 34:299–314
5. Karray FO, De Silva CW (2004) *Soft computing and intelligent systems design: theory, tools, and applications*. Pearson Education
6. Florio T, Einfeld S, Tonge B, Brereton A (2009) Providing an independent second opinion for the diagnosis of autism using artificial intelligence over the internet. *Couns, Psycho Health Use Technol Mental Health* 5:232–248
7. Sikchi SS, Sikchi S, Ali MS (2013) Fuzzy expert systems (FES) for medical diagnosis. *Int J Comput Appl* 63:7–16
8. Prasath V, Lakshmi N, Nathiya M, Bharathan N, Neetha P (2013) A survey on the applications of fuzzy logic in medical diagnosis. *Int J Sci Eng Res* 4:1199–1203
9. Veeraraghavan S, Srinivasan K (2007) Exploration of autism expert systems. In: *Proceedings of the international conference on information technology*, pp 261–264. IEEE Computer Society (2007)

10. Papageorgiou EI, Kannappan A (2012) Fuzzy cognitive map ensemble learning paradigm to solve classification problems: application to autism identification. *Appl Soft Comput* 12:3798–3809 (2012)
11. Jang JSR, Sun CT (1996) *Neuro-fuzzy and soft computing: a computational approach to learning and machine intelligence*. Prentice-Hall, Inc. (1996)

Image Processing with Android Steganography

Dominic Bucerzan and Crina Rațiu

Abstract Digital Steganography is a technique that provides confidential communications between two parties via Internet and Mobile Networks. This paper proposes a new solution of digital steganography based on Android operating system. The proposed method uses an improved LSB technique by a random selection function and has as cover BMP files. Image processing and image analysis using steganalytic techniques confirm the good quality of the proposed steganographic algorithm.

Keywords Steganography · SmartSteg · LSB · Cryptography · Android · Image processing

1 Introduction

Current trends in both hardware and software technology led industry toward the development of smaller, faster, and high-performance mobile devices, which can support a wide range of features and open-source operating systems [1].

Although digital technology has reached a high level of development, digital information security problems remain present. In today's modern society, digital information security is an interdisciplinary issue, having to be constantly optimized, developed, and innovated.

Figure 1 shows briefly a classification of the security techniques used today to ensure integrity, confidentiality, availability, authenticity, and non-repudiation of digital data.

D. Bucerzan (✉)

“Aurel Vlaicu” University of Arad, Arad, Romania

e-mail: dominic@bbcomputer.ro

C. Rațiu

“Vasile Goldis” Western University of Arad, Arad, Romania

e-mail: ratiu_anina@yahoo.com

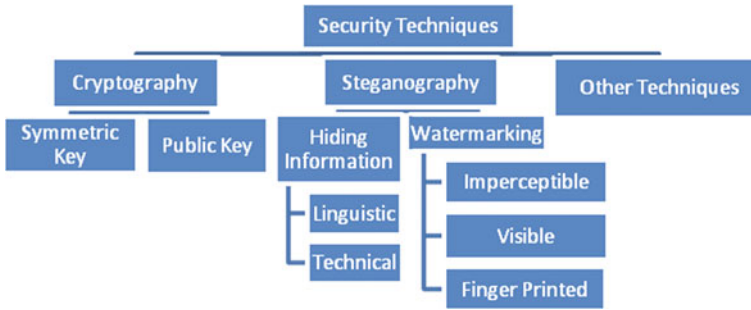


Fig. 1 Security techniques [9]

Cryptography and steganography are two important techniques used today to ensure the security of the information shared and transferred through open channels, vulnerable to interception. Often these techniques are combined and used together to optimize the security of digital information.

Cryptography is a technique that transforms information in such a way that it becomes *difficult to understand*. Steganography is a technique that hides information in different files (usually media files) hence its presence becomes *difficult to notice* [2].

One of the facts that made digital steganography popular was that some countries restricted the use of cryptography. Steganography was seen as a solution to this situation because a steganographic message could not be detected so its use could not be controlled [3].

Figure 2 shows briefly digital steganography techniques classification.

The majority of steganographic algorithms use as a cover different media files like images, audio, and video due to the ubiquity and the size of these data types so they do not raise suspiciousness [3].

This paper proposes a new solution to ensure secure and confidential communication between two parties via Internet and mobile networks. The proposed method uses secret key cryptography combined with an improved random LSB steganography method applied on BMP files. It works both on Windows and Android devices.

Image processing and image analysis by steganalytic techniques confirm the good quality of proposed algorithm.

In the proposed solution, the cryptographic method applied is not a complex one, its security relies on the secrecy of the key exchanged between the two parties by other means.

The solution proposed by the authors uses digital steganography in spatial domain, namely an optimized LSB algorithm. This method consists in hiding secret data inside a BMP file, applying changes to different pixels of the image.

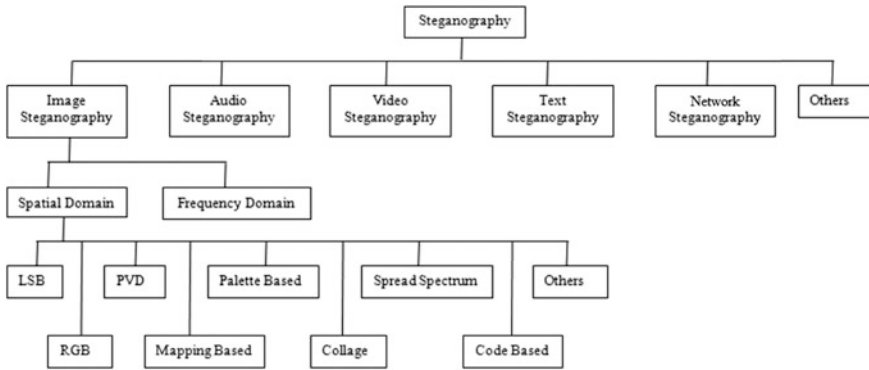


Fig. 2 Classification of spatial domain image steganography techniques [4]

The performance of steganographic methods is emphasized by the following characteristics [4]:

- *Capacity*—refers to the quantity of hidden information;
- *Security*—refers to the capability of hidden information to survive to different attacks like: cropping, scaling, filtering, addition of noise and others;
- *Imperceptibility*—refers to perceptual transparency;
- *Tamper resistance*—survival of the embedded data when an attacker attempts to modify it;
- *Computational complexity*—refers to the computational cost of embedding and extraction.

2 Proposed Solution

In the literature [5], steganography methods are divided into three main categories: pure steganography, secret key steganography, and public key steganography.

Based on Kerckhoff’s principle, we choose to work with a public algorithm based on secret key steganography. The security of the stego-system relies on the “stego-key” and on a random algorithm to choose the modified bits.

There is a similarity between a secret key steganography system and a symmetric cryptographic system [3]: the sender chooses an image as a transfer cover and embeds a secret message into it using a secret key. Once arrived at destination, the intended receiver uses the same secret key, to reverse the process and extract the secret message. It is assumed that all communication parties are able to trade secret keys through a secure channel as in cryptography.

At this stage of the project, SmartSteg provides confidential communication between computers that run Windows Operating System and devices that run Android. This means that a secret file that is encrypted and encoded with SmartSteg

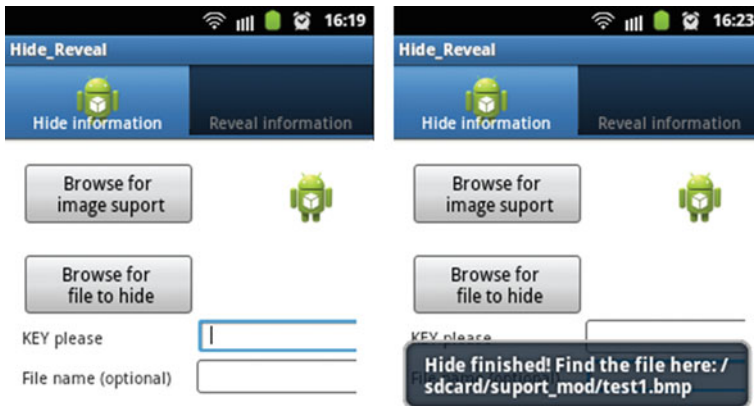


Fig. 3 Design for the SmartSteg application running on Android

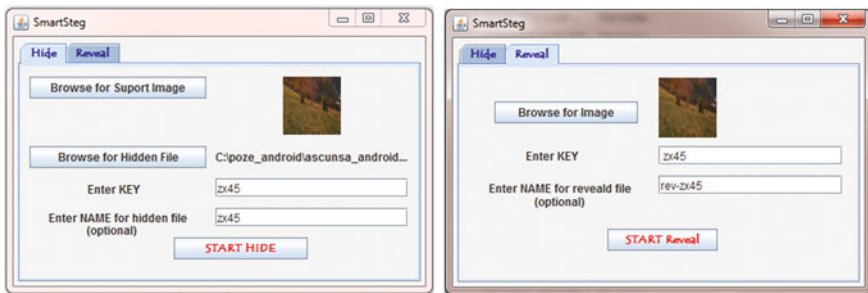


Fig. 4 Design for the application that runs under windows

using a computer can be revealed and decrypted with SmartSteg from a device that runs Android. Figures 3 and 4 show the design of the application chosen for the two version of SmartSteg.

We have considered that among the major issues that occur in this dynamic environment is the fact that almost all platforms have dedicated application. This fact is in contradiction with one of the principal characteristic of digital information, namely availability.

In other words, if a sender uses an iPhone to encode and hide some information, the receiver must also use an iPhone to unhide and decode the secret information. And this issue also applies when using a computer.

In the case when the sender is restricted to using a computer whereas the receiver has access only to a smartphone, the secret information is no longer available in this scenario. This is because an application designed for computers cannot work on smartphones.



Fig. 5 Histogram for Lily image

3 Implementation

In this environment, with an uncertain security for digital information and studded with threats, we considered opportune to continue the development and improvement of SmartSteg project.

SmartSteg is a solution for the security of digital data that is transferred through Internet and Mobile Networks. It is a project that started from the idea of creating a set of applications that will decode and unhide digital information, independent of the operating system used to code and hide them. Regardless of the device used (computer, smartphone, tablet) to encode and hide information, the intended receiver of the secret information may unhide and decode it without the need to use the same type of device as the sender did.

From the beginning, one of the targets that we want to achieve is to design an algorithm that allows to hide a larger quantity of digital data in a digital image, consuming minimal time resources and to minimize the steganalysis detection.

The design programming language used for implementing SmartSteg is JAVA using ECLIPSE environment.

Application interface is minimal (Figs. 3 and 4), we focused on achieving high performance for processing time and processing speed regarding encryption algorithm, random selection of bits and concealment of information.

Compared to other application that exists on Android market, SmartSteg is able to process cover image files of MB dimension instantaneously. Also it is able to conceal a large variety of files.

SmartSteg works on Windows and different Android versions and it does not depend on a specific type of device.

The security of the proposed model lies in the use of secret key.

4 Image Analysis with Steganalysis Method

The field of Steganalysis focuses on detection of steganography, estimation of message length, and its extraction [6].

Most popular steganalytic attacks include [6]:

- *Visual attacks*—look for suspicious artifacts using simple visual inspection. These attacks are simple, but difficult to generalize and their reliability is questionable;
- *Statistical analysis of pairs of values (histogram analysis)*—is fitted to any steganographic technique in which a fixed set of Pairs of Values are flipped into each other to embed message bits;
- *Dual statistics methods*—also known as RS Steganalysis;
- *Deriving the quantization matrix*—it is suitable for cover images that were initially saved in JPG format;
- *Universal blind steganalysis*—is a meta-detection method, meaning that it can be adjusted, after training on original and stego-images, to detect any steganographic method regardless of the embedding domain. This method is very flexible.

In Table 1, there are some samples of original images and images processed with SmartSteg under Android and Windows, images that contain embedded information.







The main parameters that are popular for measuring the changes made by embedded process to original image are as follows [4]:

- mean square error
$$\text{MSE} = \frac{1}{M \times N} \sum_{i=1}^M \sum_{j=1}^N (p_{ij} - q_{ij})^2 \quad (1)$$

where: $M \times N$ —pixel distribution, p —original image, q —image with hidden data;

- peak signal to noise ratio
$$\text{PSNR} = 10x \log_{10} \frac{C_{\max}^2}{\text{MSE}} \quad (2)$$

Table 1 Characteristics of the resulted image

Cover image original	Cover image with hidden information on Android	Cover image with hidden information on Windows
 <p>Lily image</p> <ul style="list-style-type: none"> • File type: image • BMP • Dimension: 4.44 MB • Pixel distribution: 1440 × 1080 	 <p>Lily image with embedded data</p> <ul style="list-style-type: none"> • File type: image BMP • Dimension: 4.44 MB • Pixel distribution: 1440 × 1080 	 <p>Lily image with embedded data</p> <ul style="list-style-type: none"> • File type: image BMP • Dimension: 4.44 MB • Pixel distribution: 1440 × 1080
 <p>Autumn image</p> <ul style="list-style-type: none"> • File type: image BMP • Dimension: 2.54 MB • Pixel distribution: 1155 × 679 	 <p>Autumn image with embedded data</p> <ul style="list-style-type: none"> • File type: image BMP • Dimension: 2.54 MB • Pixel distribution: 1155 × 679 	 <p>Autumn image with embedded data</p> <ul style="list-style-type: none"> • File type: image BMP • Dimension: 2.54 MB • Pixel distribution: 1155 × 679

where: C_{\max}^2 —maximum pixel value in the image;

- $$\text{correlation } r = \frac{\sum_{i=1}^M \sum_{j=1}^N (p_{ij} - \bar{p})(q_{ij} - \bar{q})}{\sqrt{\left(\sum_{i=1}^M \sum_{j=1}^N (p_{ij} - \bar{p})^2\right) \times \left(\sum_{i=1}^M \sum_{j=1}^N (q_{ij} - \bar{q})^2\right)}} \quad (3)$$

where: \bar{p} and \bar{q} are the average pixel value in the original image and image with embedded data.

Next, we present the results obtained when applying steganalysis techniques on the images with embedded information. In this process, we used a tool called Steganography Studio. It implements several algorithms highly configurable with a variety of filters. Also it implements image analysis algorithms for the detection of hidden information [7].

The histograms obtained after image analyses are shown in Figs. 5 and 6. Even though the random function that we developed changes between 0 and 2 bits per byte, the histogram of the original image and the histogram of the image processed with hidden information show very little differences.

This fact is sustained also by parameters obtained by running RS Analysis and Benchmark test on the images that we worked on.

Regarding RS Analysis, we mention that SmartSteg covers the entire surface of the original image with modified bits in order to remove the detection of the length of hidden information. Table 2 shows the result of RS Analyses that we obtained for the Lily and Autumn images.

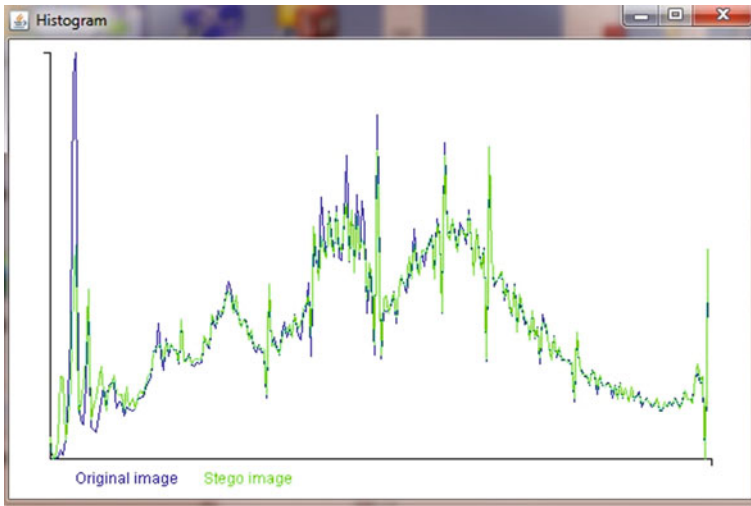


Fig. 6 Histogram for Autumn image

Table 2 Results of steganalysis—RS analysis

RS analysis (nonoverlapping groups)	Lily image	Autumn image
Percentage in red	89.48389	65.5219
Approximate length (in bytes) from red	521870.01894	218235.84368
Percentage in green	92.78612	64.28888
Approximate length (in bytes) from green	541128.6484	214128.99797
Percentage in blue	87.58843	66.88909
Approximate length (in bytes) from blue	510815.72677	222789.59366
<i>RS Analysis (overlapping groups)</i>	<i>Lily image</i>	<i>Autumn image</i>
Percentage in red	88.34037	66.06865
Approximate length (in bytes) from red	515201.04964	220056.92492
Percentage in green	88.71541	65.23375
Approximate length (in bytes) from green	517388.25351	217276.08351
Percentage in blue	87.61354	67.18678
Approximate length (in bytes) from blue	510962.15148	223781.1181
Average across all groups/colors	89.08796	65.86484

Table 3 Results of steganalysis—Benchmark tests

	Benchmark test	
	Lily image	Autumn
Mean squared error	3.8562950102880658	3.0002218364197533
Signal to noise ratio	43.5926257046439 dB	44.6827945326950 dB
Peak signal to noise ratio	51.5229318901347 dB	52.6131007181858 dB
Correlation quality	123.88306790889202	123.89825709285965

Table 3 shows the Benchmark test results. The main parameters of this test were discussed in the second section of this paper. The values obtained on PSNR parameter are over 50 dB. This is a performance to be noticed taking into consideration that the typical values for PSNR are between 20 and 40 dB [8].

5 Conclusions and Future Works

The solution proposed in this paper is a robust one, fact proved by the image analysis with steganalytic methods.

The project has major advantages like:

- Large volume of hidden data with low degradation of cover image;
- Large variety of hidden files;
- High level of security based on secret key cryptographic algorithm and on the random selection of the bits with secret information;

- High processing speed;
- Portability on Windows and Android Operating System.

In the near future, one of our goals will be to successfully implement this project on other mobile platforms, like IOS.

References

1. Wang Z, Murmura R, Stavrou A Implementing and optimizing an encryption filesystem on android. Department of Computer Science, George Mason University, Fairfax
2. Lubacz J, Mazurczyk W, Szczypiorski K (2014) Principles and overview of network steganography. *IEEE Commun Mag* 52(5)
3. Wolfel U (2011) Efficient and provably secure steganography. Dissertation, Universitat zu Lubeck, Institut fur Theoretische Informatik
4. Gandharba S, Saroj KL (2014) Classification of image steganography techniques in spatial domain: a study, Gandharba Swain et al. *Int J Comput Sci Eng Technol (IJCSET)* 5(03). ISSN:2229-3345
5. Katzenbeisser S, Petitcolas FAP (2000) Information hiding techniques for steganography and digital watermarking. Library of Congress Cataloging-in-Publication, Artech House Computing Library
6. Fridrich J, Goljan M (2002) Practical steganalysis of digital images—state of the art. *Proc. SPIE* 4675:1–13. Security and Watermarking of Multimedia Contents IV
7. <http://stegstudio.sourceforge.net/>. Accessed 20 May 2014
8. Cole E (2003) Hiding in plain sight: steganography and the art of covert communication. Wiley. ISBN:0-471-44449-9
9. Bucerzan D, Rațiu C (2013) SmartSteg: a new android based steganography application. *Int J Comput Commun Control* 8(5). Available at: <http://univagora.ro/jour/index.php/ijccc/article/view/642>

Part II
Intelligent Transportation

Social Cities: Redistribution of Traffic Flow in Cities Using a Social Network Approach

Alexandru Topirceanu, Alexandru Iovanovici, Cristian Cosariu, Mihai Udrescu, Lucian Prodan and Mircea Vladutiu

Abstract Motivated by the constantly growing interest and real-world applicability shown in complex networks, we model and optimize the network formed by road networks in cities from an innovative perspective. We detect traffic hotspots which lead to congestion using the betweenness centrality of the road graph. This is shown to have a power-law distribution which we set out to redistribute and equalize. Optimization at a macro-level is not feasible because of the graph size, and thus we recursively narrow down the methodology to a sub-optimization of city neighborhoods. To that end, the paper introduces a genetic algorithm which redistributes betweenness optimization at a neighborhood level, district level, and city level to reduce and/or eliminate congestion hotspots, by changing street directions, without adding any new roads. Experimental results yield an improvement with a factor of 4 times in terms of reducing load off from hotspots and transferring it to neighboring streets.

Keywords Road networks · Complex networks · Genetic optimization · Betweenness centrality · Community detection

A. Topirceanu (✉) · A. Iovanovici · C. Cosariu · M. Udrescu · L. Prodan · M. Vladutiu
Department of Computers and Information Technology, Politehnica University Timisoara,
Bd. Vasile Parvan 2, 300223 Timisoara, Romania
e-mail: alexandru.topirceanu@cs.upt.ro

A. Iovanovici
e-mail: iovanalex@cs.upt.ro

C. Cosariu
e-mail: cristian.cosariu@cs.upt.ro

M. Udrescu
e-mail: mudrescu@cs.upt.ro

L. Prodan
e-mail: lprodan@cs.upt.ro

M. Vladutiu
e-mail: mvlad@cs.upt.ro

1 Introduction

One increasingly demanding and unresolved problem of the century is coping with the traffic conditions in large or crowded cities around the world. It is a general known fact that traffic and the time spent by drivers in their cars can have a big impact on personal life, career, and safety. It causes stress, annoyance, and frustration to most inhabitants of crowded cities. Regardless of the causes, effects, and impromptu solutions, in this paper we take a step back from the current optimization techniques of traffic congestion, and reassess the underlying road topology. Thus, using concepts from complex and social networks analysis, we propose a low-level optimization at the topological level of street in any city.

Applying social network analysis principles in order to analyze and optimize road networks is nothing but natural as the social perspective provides an innovative means of analyzing the structure of entities with a social-like structure [1, 2]. Thus, we can detect influential nodes (i.e., intersections), patterns of communication, and also study dynamics inside the network. This strongly relates to road networks in large cities [3, 4], as it is important to disseminate which areas are critical for the traffic throughput, which nodes are more influential so that congestion can be controlled at those positions, and also because it we can model growth as the network coverage spreads in time.

Many scientifically important problems can be represented and empirically studied using networks. For example, biological and social patterns, the World Wide Web, metabolic networks, food webs, neural networks, and pathological networks are a few examples of real-world problems that can be mathematically represented and topologically studied to reveal some unexpected structural features [4, 5]. Most of these networks possess a certain community structure that has substantial importance in building an understanding regarding the dynamics of the network [3, 6–8]. Our approach revolves around finding congestion hotspots in a given road network, hotspots whose graph betweenness centrality we propose to reduce so that other adjacent intersections can help redistribute the throughput of cars. We do this by decentralizing the problem and solving it at the micro-level of neighborhoods, which is then replicated at the macro-level of the whole city.

The paper has the following structure: In Sect. 2, we describe the related work and the theoretical concepts behind complex networks analysis. Section 3 explains the methodology of heuristic reorganization of the road graph until the centrality distribution is evened out, and Sect. 4 discusses the results obtained from the local reorientation of streets.

2 State of the Art Traffic Assessment

2.1 *Traffic Optimization Techniques*

Significant research has been carried toward finding alternative approaches in analyzing the structure of cities and especially good patterns of roads, which maximize the car traffic throughput. Using graph theory was a clear choice based on the clear historic affiliation of the domain and the suitability of representing the relationships between intersections (nodes) and streets (edges). Much work was put into this segment and there are even some far fetched investigations into creating for example most real artificial driver, which acts as close to a real driver as possible [9].

Understanding how drivers interact and how road networks are created around specific points of interest (schools, shopping centers, concert halls, sports arenas) could lead to identifying the patterns—motifs—that can apply at different scales over several road networks to achieve increased traffic flow and consequently, less congestion.

Jiang and his team identify in [10, 11] a classical 80/20 behavior because roughly 20 % of the streets account for more than 80 % of the urban traffic. There is a clear distinction between some important streets (few) and some which are less important (many) which leads us to what could be easily presented as a hierarchical view of the urban structure [12].

Porta et al. present in [13] a methodology and a framework for analysis of urban environments emphasizing on the layout of the urban roads, in terms of both classical graph theory but also using complex network-specific metrics and algorithms.

There is a trend in measuring the optimality of a specific street layout and even finding algorithms and methodologies of dynamically reassigning the traffic light signaling policies in order to indirectly “reconfigure” the network as to maximize various throughput metrics and an approach based on complex networks analysis is used for this.

2.2 *Complex Network Approach*

We novelty introduced in this paper is the usage of complex network analysis principles to enhance the properties of a road infrastructure network topology. Through measurements performed over raw street networks, formed out of intersections (nodes) and streets (directed edges), our goal is to propose an optimal

redirection of streets—without actually adding new ones—over any given network so that we maximize the throughput and reliability of traffic, by evening out the betweenness distribution in the graph.

We have measured the basic network metrics: network size (nodes and edges), average path length, clustering coefficient, average degree, network diameter, density and modularity, and also the distributions of the degrees, betweenness, closeness, and (eigenvector) centrality [3]. After performing network analysis, we have concluded that an optimal way to leverage the street reorganization is through community detection and centrality algorithms.

We define the basic set of network analysis principles further used in this paper. The average path length of a network is the mean distance between two nodes, averaged over all pairs of nodes [3]. The degree of a node is defined as the total number of its (outgoing) edges. Thus, the average value of the degrees, measured over all nodes, is called the average degree of the network. Modularity is a measure that shows the strength of the division of a network into communities [7]. A high modularity means a strong presence of well-delimited communities. Betweenness centrality is the measure of a node's influence in a graph. It is measured as a ratio between the numbers of shortest paths which go through a node divided by the total number of shortest paths in the graph [3].

In the presented context, a node with high betweenness is an intersection with high influence. Moreover, influence is translated into an intersection through which more shortcuts pass. Based on this definition and on the driving habits of people, we deduce that the nodes with high betweenness in the city network are the intersections which are, or may become, hotspots for congestion.

3 Methodology

We obtain the road information data from the online repository OpenStreetMap. This data is parsed using a custom implemented python plugin. From there, we have all intersections as a node list, and all streets inside the city as edges between nodes. Further, we assemble this data into gexf file format which can be imported in Gephi [14], the leading tool in large graph data visualization. Any layout of intersections in a geographic space can be processed by our algorithm by importing it in Gephi, where our developed plugin can be used from. Further, our enhancement algorithm, called SocialCity, processes the topological data. The result is the same input road graph G but with a more even distributed betweenness of nodes. This is done solely by reorienting some of the existing streets, without adding new streets or new lanes.

The first step (A) is to apply a recursive breakdown of the road graph into smaller units. This helps solve a much simpler problem, and then reassemble the solutions. The division of the initial graph G is done using a community detection algorithm [15]. Most of these networks possess a certain community structure that has substantial importance in building an understanding regarding the dynamics of the network [3, 6–8]. We repeat the division for two times, and call the three different perspectives: city level ($\lambda = 0$), district level ($\lambda = 1$), and neighborhood level ($\lambda = 2$). The next step (B) is to measure a starting fitness for each neighborhood. This is achieved by measuring the betweenness distribution of the subgraph, and then the slope of the linear interpolation trend line.

Once the original road network G is divided into neighborhoods, each with its own fitness, the last step (C) consists of a heuristic optimization. For each independent community, the same principle applies, thus the problem can be parallelized. In a community, we start with pop solutions, which define the initial population. We have run experiments with pop = 100 and pop = 1000, with little difference in results. A solution S_j consists of the initial neighborhood graph in which one random street's orientation is reversed (source swapped with target). The new fitness is calculated for each solution S_j by measuring their betweenness distributions and computing the slope of the best linear approximation. This will result in a negative number which we want to decrease so that it evens out the betweenness distribution. Thus, the best fitness is the slope that is nearest to 0 as possible. The population of solutions is used in a genetic algorithm manner [16]. Consequently, we iterate over generations of solutions by following lines 12–17 in the given pseudo-code in Algorithm 1. The new generation consists of the best 10 % solution from the current population, 75 % new solutions obtained from crossing over two random solutions, and 15 % new solutions obtained from mutation. The percentages are not fixed, and can be changed based on empirical observations.

The crossover implementation is a simplified approach which produces one new solution from two random existing solutions. The two graphs are joint through union so that the changes in both graphs are taken into consideration. If the same street (edge) is found to have opposite directions, then the street is modeled as bidirectional. Mutation is implemented by picking a random street in a given road graph and changing its direction.

We call the initial division factor λ (lambda) and the use a default value of 2. The stop condition of the algorithm is when the best individual in the population has a better fitness than a required fitness. In other words, the algorithm repeats until the slope of the betweenness distribution drops to a smaller absolute value.

The motivation of the algorithm, as well as for choosing betweenness centrality, is depicted in Figs. 1, 2, and 3. Our experimentation comprises multiple cities, and we chose to discuss based on the analytic results obtained over the road network of Budapest. It is worth mentioning that the city lies in a part-flat, part-hilly region, and is divided into two by the river Danube.

Algorithm 1 SocialCity pseudo-code for a throughput-optimization network

Input: city road digraph $G = \{N, R\}$ with positional data (n_i, n_j) , and a fractal level \perp .

A: Split into communities
 // = 2: city!district!neighborhood
 1 : $Com0 \leftarrow G$
 2 : **for** $i = 0, i <$ **do**:
 3 : $Com_{i+1} \leftarrow \{\}$
 4 : **for each** com_j in Com_i :
 5 : $Com_{i+1} \leftarrow Com_{i+1}$ [detect communities $\{com_j\}$]

B: Measure centrality in each neighborhood
 6 : **for each** com_i in Com :
 7 : B_i betweenness distribution $\{com_i\}$
 8 : BS_i slope of distribution B_i

C: Reduce slopes for each BS_i :
 9 : **for** $j <$ pop:
 10 : S_j swap one random edge in com_i
 11 : fit_j slope(betweenness(S_j))
 12 : **sort** descending S_j by fit_j
 13 : S_{new} top 10% of solutions S_j (elite)
 14 : S_{new} 75% **crossover** between two solutions
 15 : S_{new} 15% **mutation** of a random solution S_j
 16 : $S_j \leftarrow S_{new}$
 17 : go to [line 12], while best fitness $<$ ' **Crossover two solutions from S :**
 18 : S_i random $\{S\}$
 19 : S_j random $\{S\}$, $S_i \neq S_j$
 20 : $S_k \leftarrow S_i \cup S_j$
 21 : **return** S_k

Mutation of one solution S_j
 22 : $edge$ random edge in S_j
 23 : $edge$ swap($edge$)
 24 : **return** S_j

Output: road network G with normalized betweenness distribution at fractal level \perp .

In each of the figures, one can see the community overview, which corresponds to the geographical proximity of streets and intersections. The nodes with high betweenness, the so-called congestion hotspots, are depicted in sub-figures (b), while the allocation of hotspots per community is depicted in sub-figures (c).

We also chose three other diverse cities for numerical analysis: Augsburg (in southern Germany, 272 K inhabitants, flat plateau region), Sibiu (in central Romania, 147 K inhabitants, hilly region, compact with narrow streets), and Constanta (in eastern Romania, 283 K inhabitants, along the seaside). The geographical information was retrieved from Wikipedia. We thus chose 3 normalized

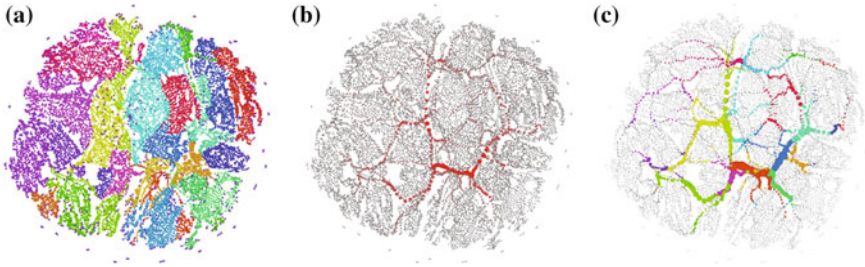


Fig. 1 Road network of Budapest, with each node representing an intersection. **a** Nodes colored by community (districts) detected using a community detection algorithm. **b** Nodes colored (*gray to red*) and sized (*small to large*) by their betweenness. Nodes with high betweenness highlight traffic-intensive hotspots. **c** Nodes colored by community and sized by betweenness. Highlights the hotspots per city district

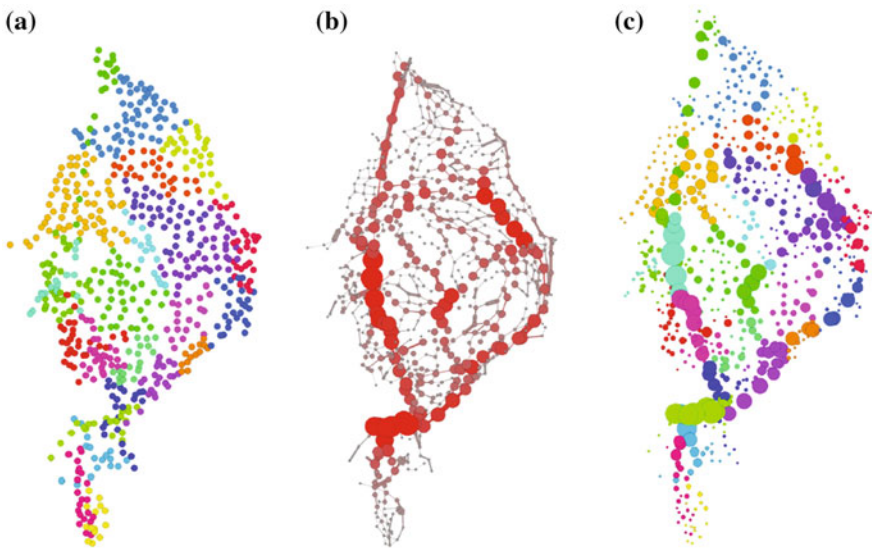


Fig. 2 Road network of a central district in Budapest. Nodes are colored by community **(a)** and sized by their betweenness **(b)**, **(c)**

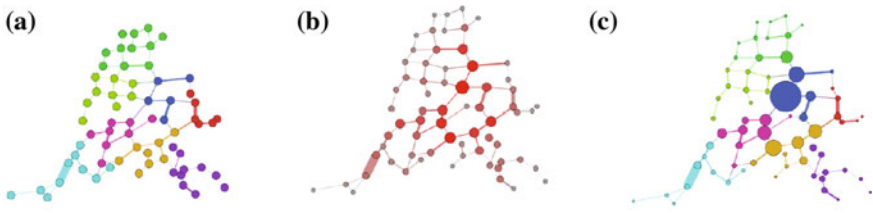


Fig. 3 Road network of local neighborhood in a district of Budapest. Nodes are colored by community **(a)** and sized by their betweenness **(b)**, **(c)**

cities, and one metropolis. Two cities are in a hilly region, two in a flat one; one is divided by a large river, which creates congestion along the few existing bridges, one is divided by a small river, connected by many bridges, one is compact and circular, and one is a seaside city.

4 Simulations and Results

Focusing on the experimentation over Budapest in this paper, we start out with an initial graph of 12,038 nodes and 17,309 edges. This graph is divided down into districts (500–1000 nodes), and then to neighborhoods (50–150 nodes). The preferential paths for high traffic throughput, but also congestion, are visible in Figs. 1b, 2b, 3b, and replicate down to the smaller levels of the city. Figure 4 shows the power-law betweenness distribution of the intersections in Budapest. The distribution is typical for social networks [1, 3, 17] and other complex networks [4, 8], but it does not represent a desideratum for the infrastructure in cities.

By applying the SocialCity algorithm over Budapest’s streets, we obtain encouraging results, as this is the first such approach, to the best of our knowledge. Figure 5a shows the initial (real) betweenness distribution over a representative neighborhood in Budapest (the same depicted in Fig. 3). The slope (s) of the betweenness at this stage is -0.0035 . Figure 5b represents the resulting (ideal) betweenness distribution on the same neighborhood after the genetic optimization. The new slope s of the linear trend line is -0.0008 . Thus, we are able to reduce the slope 4.375 times.

To consolidate our proposal, we apply the algorithm on the other three mentioned cities for a better validation due to the diversity of topological networks. Table 1 gives the initial and final (optimized) results for the betweenness slope s on

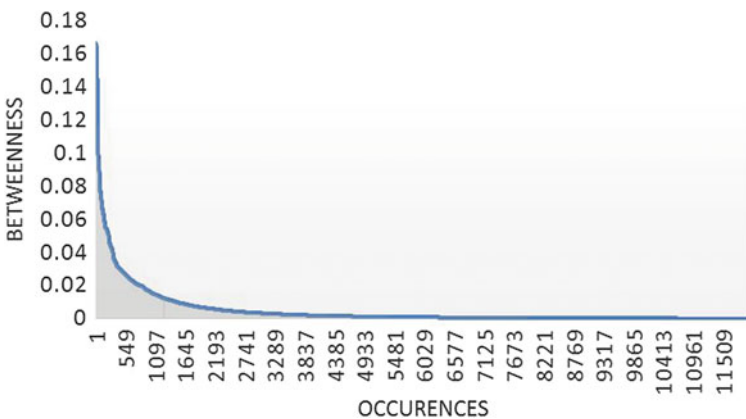


Fig. 4 Betweenness distribution—at city level—of Budapest. The few intersections with very high betweenness (*left side*) tend to form congestion hotspots at around traffic rush hours

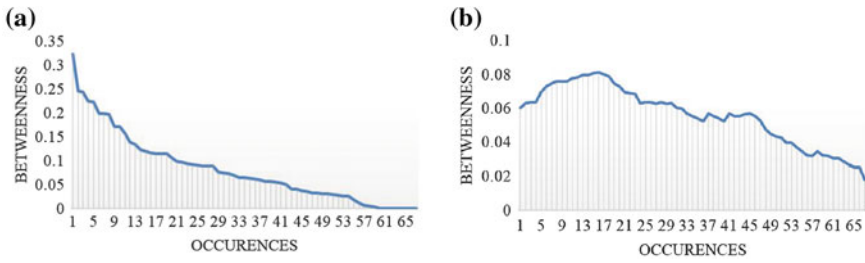


Fig. 5 Betweenness distributions—at block level—in a central neighborhood of Budapest. **a** Real distribution. **b** Obtained distribution after heuristic optimization. The resulting distribution has no more power-law behavior, but rather a normal-uniform distribution which eases traffic congestion

Table 1 Results of the block-level street optimization algorithm SocialCity applied on four different cities

City	Initial (s)	Optimized (s)	Improvement
Augsburg	-0.0028	-0.0006	4.6700
Budapest	-0.0035	-0.0008	4.3750
Constanta	-0.0040	-0.0011	3.6300
Sibiu	-0.0021	-0.0008	2.6200

The improvement ratio is the quantified improvement of the resulting betweenness optimization on each of the four cities. Higher ratios mean better improvement

the four tested cities: Augsburg, Budapest, Constanta, and Sibiu. The graph sizes of the introduced cities are 6097 nodes and 7929 edges for Augsburg, 2794 nodes and 3994 edges for Constanta, and 2260 nodes and 3056 edges for Sibiu. What is worth mentioning is that the algorithm behaves better on cities with regular structure in flat regions, with many existing road alternatives for the congested intersections. We obtain the worst results in Sibiu, where the city is already optimized as much as the hilly terrain allows for; on the other hand, Augsburg allows the best improvement ($\times 4.67$) as it consists of many perpendicular roads that can take the heavy flow of traffic from the large boulevards. Overall, SocialCity seems to be able to add consistent improvement to any type of city.

As there is no such similar approach to road infrastructure optimization, the discussion of the results remains theoretical, and the results are encouraging, as such a solution can be implemented in real life without any need for new streets or shortcuts to be constructed.

5 Conclusions and Future Work

To the best of our knowledge, our work represents a novel approach in redesigning the road infrastructure of a city. Using concepts from the area of network analysis and mapping to road networks, we succeed to add improvements to the theoretical

traffic throughput. Our research is focused around the algorithm we have devised, called SocialCity.

We envision this research as a framework for a much in depth analysis involving detailed physical and economical characteristics of the network. The simple solution given through heuristics by SocialCity is of particular importance for the demand of modern cities, with larger and larger street networks. Tackling the problem from a complex network point of view, we manage to point out the congestion paths using the betweenness centrality and are able to redistribute the load on the most congested hotspots. Intuitively, through a 4.375 times more even betweenness distribution obtained over the city of Budapest, we can conclude that the load can be lowered by 4 times, which is a consistent improvement.

Our future work is focused towards implementing the heuristic algorithm to automatically process any city road topology and adds an additional overlapping layer of optimally placed streets which increase the traffic throughput even further, both at a micro- and macro-level on the analyzed city. Consequently, we look forward to real-world testing of the SocialCity algorithm and a more insightful analysis of the functional requirements of the network with proven simulation tools.

Acknowledgments This work was partially supported by the strategic grant POSDRU/159/1.5/S/137070 (2014) of the Ministry of National Education, Romania, co-financed by the European Social Fund—Investing in People, within the Sectoral Operational Programme Human Resources Development 2007–2013.

References

1. Strogatz SH (2001) Exploring complex networks. *Nature* 410(6825):268–276
2. Wasserman S (1994) *Social network analysis: methods and applications*, vol 8. Cambridge University Press, Cambridge
3. Wang XF, Chen G (2003) Complex networks: small-world, scale-free and beyond. *IEEE Circuits Syst Mag* 3(1):6–20
4. Easley D, Kleinberg J (2010) *Networks, crowds, and markets*, vol 8. Cambridge University Press, Cambridge
5. Barabási A-L, Gulbahce N, Loscalzo J (2011) Network medicine: a network-based approach to human disease. *Nat Rev Genet* 12(1):56–68
6. Newman M (2003) The structure and function of complex networks. *SIAM Rev* 45(2):167–256
7. Newman ME (2006) Modularity and community structure in networks. *Proc Natl Acad Sci* 103(23):8577–8582
8. Barabási A-L (2013) Network science. *Philos Trans R Soc Math Phys Eng Sci* 371(1987):20120375
9. Juhlin O (1999) Traffic behaviour as social interaction-implications for the design of artificial drivers. In: *Proceedings of 6th world congress on intelligent transport systems (its)*, Held Toronto, Canada, 8–12 Nov 1999
10. Jiang B, Duan Y, Lu F, Yang T, Zhao J (2013) Topological structure of urban street networks from the perspective of degree correlations, vol. 1533. arXiv preprint arXiv:1308
11. Jiang B (2009) Street hierarchies: a minority of streets account for a majority of traffic flow. *Int J Geogr Inf Sci* 23(8):1033–1048

12. Tomko M, Winter S, Claramunt C (2008) Experiential hierarchies of streets. *Comput Environ Urban Syst* 32(1):41–52
13. Porta S, Crucitti P, Latora V (2006) The network analysis of urban streets: a dual approach. *Phys A* 369(2):853–866
14. Bastian M, Heymann S, Jacomy M (2009) Gephi: an open source software for exploring and manipulating networks. In: ICWSM
15. Blondel VD, Guillaume J-L, Lambiotte R, Lefebvre E (2008) Fast unfolding of communities in large networks. *J Stat Mech: Theory Exp* 2008(10):P10008
16. Mitchell M (1998) *An introduction to genetic algorithms*. MIT Press, Massachusetts
17. Barabási AL, Albert R (1999) Emergence of scaling in random networks. *Science* 286 (5439):509–512

The Computer Assisted Parking of a Bluetooth Controlled Car Using Fuzzy Logic

Caius Panoiu, Manuela Panoiu, Cezara-Liliana Rat and Raluca Rob

Abstract The aim of this paper is to present a computer assisted parking system modeled in NI LabVIEW using the fuzzy logic toolkit. This system itself is capable of autonomously parking a car from any position and angle within the parking ground. The experiments on this system were conducted on a remote controlled (RC) car, specifically a Bluetooth controlled car. This particular type of RC car is compatible with Bluetooth devices existing on laptops, making it possible to control the car directly from a laptop without any additional equipment. The position and orientation of the car are computed through image processing from a USB camera set directly above the parking lot and positioned in such a way as to capture the entire range of the parking ground (Li et al., Proceedings of the 2003 IEEE International Conference on Robotics and Automation, 2003). These parameters form the inputs of the fuzzy logic controller which selects the steering angle and direction that are converted to a command sent to the Bluetooth car. According to the command it receives, the Bluetooth car changes its position, executing the parking maneuvers. The system we choose to develop is generalized enough to be adapted to any mobile robot positioning system, being particularly useful in controlling vehicles with non-adjustable or set steering angle.

Keywords Parking · LabVIEW · Fuzzy · Image recognition · Bluetooth

C. Panoiu · M. Panoiu · C.-L. Rat · R. Rob (✉)
University Polytechnic Timisoara, Electrical Engineering and Industrial Informatics
Department, Timisoara, Romania
e-mail: raluca.rob@fih.upt.ro

C. Panoiu
e-mail: caius.panoiu@upt.ro

M. Panoiu
e-mail: manuela.panoiu@upt.ro

C.-L. Rat
e-mail: cezara.liliana@gmail.com

1 Introduction

This paper is structured according to the technologies used in implementing our project: Bluetooth communications, image identifications, fuzzy logic. We have also presented the experimental results in a separate chapter.

Our goal was to obtain a completely autonomous car parking system capable of autonomously parking a car from any position and angle within the parking ground. This would represent a significant improvement on modern-day assisted parking systems since even the most scientifically advanced of these is not completely autonomous [1]. We have successfully designed such a system. We have tested it using a Bluetooth remote controlled car, but the system itself can be adapted for use on a real car. This would include using a wireless camera and a car that has an onboard computer, but these requirements do not represent a major investment. Many parking lots are equipped with surveillance cameras and if these were wireless cameras available to the drivers that use the parking lot the system could use them. Using a camera instead of parking sensors does have the advantage of having a per-whole view of the car's surroundings, making it easier to find a vacant parking space and to maneuver toward it. A high-speed camera, if used, would be able to adapt to its surroundings in real-time and detect other cars that are maneuvering at the same time. This could prove to be an invaluable piece of information in accident prevention.

2 Bluetooth Technology

The BBZ203-A1 RC Car, which can be seen in Fig. 1, is Bluetooth 2.1 compliant, therefore being compatible with all Bluetooth compliant devices that use serial port profile (SPP), such as mobile phones or computers, a specific application being required in this case. This makes it possible to control the RC car directly from the laptop: laptops being Bluetooth through SPP devices can associate with the RC car to form a piconet. By associating these devices a virtual serial port (COM6) is created and it is through this port that the connection between the two devices is formed. The data transmission to this port is a serial transmission with the following specification: 9600 bps, 8 data bits, no parity, 1 stop bit, and no flow control.

The Bluetooth RC car works as a regular RC car with forward/backward direction and left/right steering [2]. The steering angle is a non-adjustable 45° angle, needing more complicated parking maneuvers than would be necessary for a real car, hence assuring that the system that was developed, is generalized enough to be fitted for many more machine positioning systems. Due to the high speed of the RC car and its variable acceleration according to the battery level, an open loop system based solely on a mathematical model of the car would make a very imprecise, if even a functional, parking program. Hence there was a need to receive the current position and orientation of the car in real-time. This is achieved with the help of a USB webcam that captures, frame by frame, the movements of the car within the parking ground.

Fig. 1 The FIAT 500 bluetooth RC car



3 Image Identification

The image obtained from the camera is processed using the NI Vision and Motion toolkit in order to locate the RC car. The process of identifying a moving object through image processing is called object tracking. There are many different approaches to object tracking in LabVIEW through the NI Vision and Motion toolkit. We have analyzed several of these to find which one better suits our system, namely shape detection, edge detection, and pattern matching. We obtained the following results. Shape detection was fast but unreliable since the shape of the car projected on the 2D view of the camera produced highly irregular shapes at certain angles. Due to the advantages this method would provide, such as simplicity and speed, painting a regular shape on the hood of the RC car was taken into consideration. But this was swiftly abandoned; no matter what shape we would have chosen, the angle between the car and the camera would have made it impossible to identify the shape in every position. Edge detection, although fast, has proven to be of little use when the car was in motion because of difficult and limited use in blurred images [3]. Pattern matching, although having limited real-time capabilities, was proven to be the best choice in our application. High speed was not a necessity in our case, but adaptation to slightly variable speed and bursts of acceleration was a necessity.

Therefore the technique we used for determining the position and orientation of the RC car is pattern matching. Pattern matching locates regions of a grayscale image that match a predetermined template. The major advantage of pattern matching is that it provides matches to the template regardless of the angle at which the object represented by the template is rotated. The template is a region of interest selected from an image representing the searched object, in this case the top of the Bluetooth car (Fig. 2).

The region of interest is graphically selected from a window displaying the image. This area will be used for further processing. The template is then saved as a.png file. Since the positioning of the car is made according to the center of the

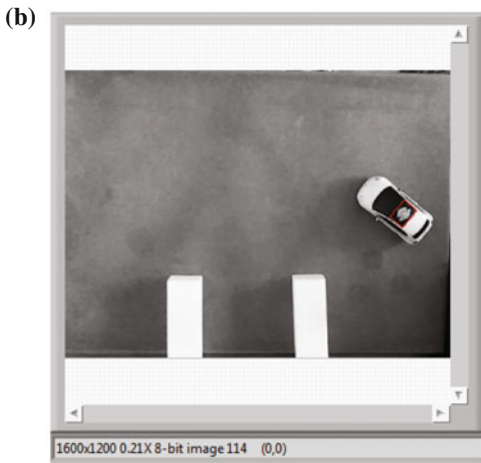
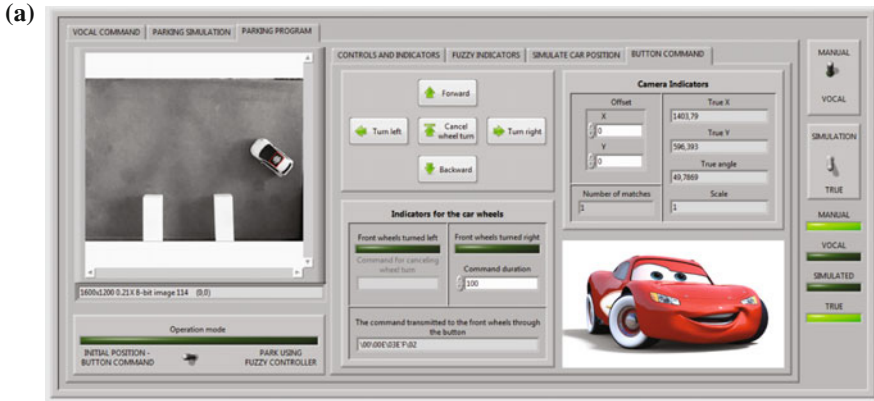


Fig. 2 The recognition of the RC car. **a** The results of the recognition are visible in the Camera indicators container. **b** The template is recognized and presented inside a red border. **c** The pattern template

match and not of its edges, a template that is representative of the car's movements but not likely to be influenced by shade or light is the best choice. This template has proven to be the top of the car.

The settings used in the pattern matching algorithm were as follows. The "Number of Matches to Find" is set at 1 and the "Minimum Match Score" is set at 600. This means that a minimum of 60 % of the found image is required to be identical to the template. This ensures that the program looks for the part of the image which is most similar to the template, but not identical to it. However, better results are obtained for a higher match score, a match score of 800 (80 % accuracy), but the program becomes sensitive to any sudden movement of the car, being

unable during motion to determine its position, not to mention its angle. Since the program is expected to process the position and angle of the car in real-time, such a setting will render the computer unable to control the car. In this case, a less accurate search provides more accurate results. Hence setting a minimum match score at 600 is mandatory in order to identify the car regardless of its rotation angle. Our experiments show that the results obtained by using this setting in combination with the “Subpixel Accuracy” setting are accurate enough for the software to control the car and park it.

The “Subpixel Accuracy” setting was used in order to compensate for the inexactitudes the low match score could cause. The subpixel accuracy option applies a bi-linear interpolation to the image. Bi-linear interpolation is used for interpolating functions of two variables on a regular grid. Interpolation is performed bidirectionally [4].

The “Search for Rotated Patterns” option along with the “Angle Range” of $\pm 180^\circ$ and the “rotation-invariant matching” option are selected in order find the car under any angle.

The image taken by the camera represents the search area. NI Vision will scan a rectangular portion of the acquisition window, forming a region of interest, in an attempt to find if there are any matches. Using pattern matching, NI Vision will return the number of matches and their coordinates within the region of interest. The results of this search will help determine the car’s position and orientation. This process will be executed a number of times in order to follow the car’s movement [5]. The block diagram of the subprogram responsible for this can be seen in Fig. 3. The image from the camera is acquired through the Vision Acquisition VI and processed through the Vision Assistant VI. The results are visible on the front panel of the application and on the acquired image, the identified area being bordered with red rectangle.

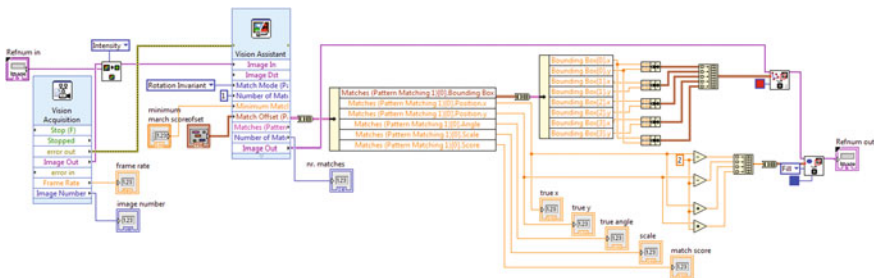


Fig. 3 The block diagram of the camera recognition program

4 Fuzzy Logic Control

The aim of the parking algorithm is to park a vehicle from an arbitrary starting position [6]. In everyday life, a driver can control a vehicle by constantly evaluating the current status of the vehicle, such as the distance from the target position and the orientation of the vehicle, to derive the correct steering angle. In this case, the place of the driver is taken by the computer. The method chosen for the control of this car is a fuzzy logic controller [7].

The first step in programming the fuzzy logic controller is defining the linguistic variables. The following input linguistic variables have been defined: x represents the vehicle position on the Ox axis in relation to the destination, orientation represents the orientation of the vehicle, and y represents the vehicle position on the Oy axis. The output linguistic variables are as follows: the steering angle, to represent the steering angle of the vehicle and the direction, to represent the direction of the vehicle movement (backward/forward) [8, 9].

The linguistic terms of Left, Center, and Right can be defined for the linguistic variable x (Fig. 4) to describe the possible positions of the vehicle in relation to the destination [8].

The linguistic terms of Left Down, Left, Left Center, Left Up, Up, Right Up, Right Center, Right, and Right Down can be defined for the linguistic variable orientation (Fig. 5) to describe the possible orientations of the vehicle [8].

The input linguistic variable y (Fig. 6) is not absolutely necessary in the parking algorithm, but due to the fact that, in practice, a parking spot is usually surrounded by other parking spots that may or may not be occupied and that have to be avoided during parking maneuvers. Also the space in which these maneuvers are made may also be limited. Hence, the linguistic terms corresponding to the linguistic variable y are Parking Lot, Parking Ground, and Edge [10].

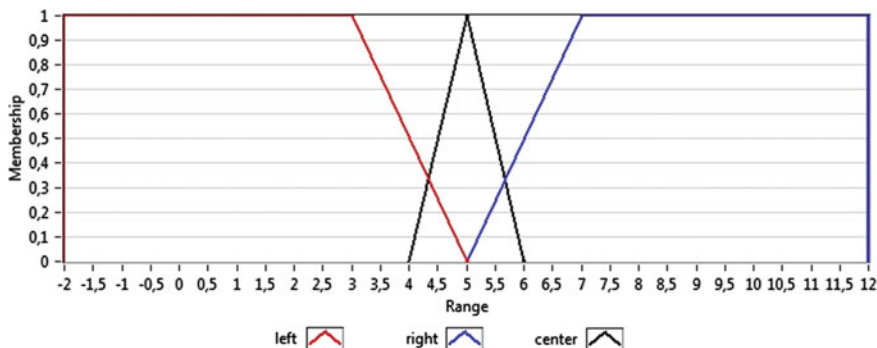


Fig. 4 Membership functions for input variable x

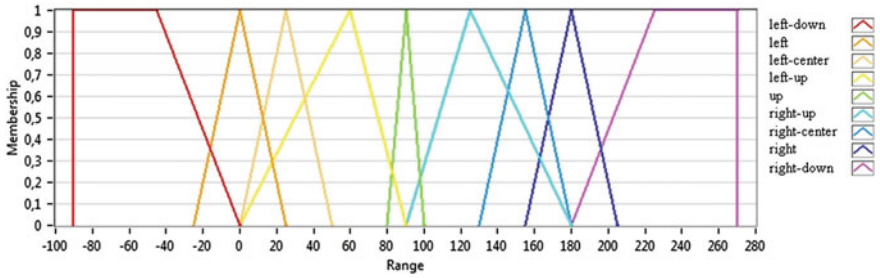


Fig. 5 Membership functions for input variable orientation

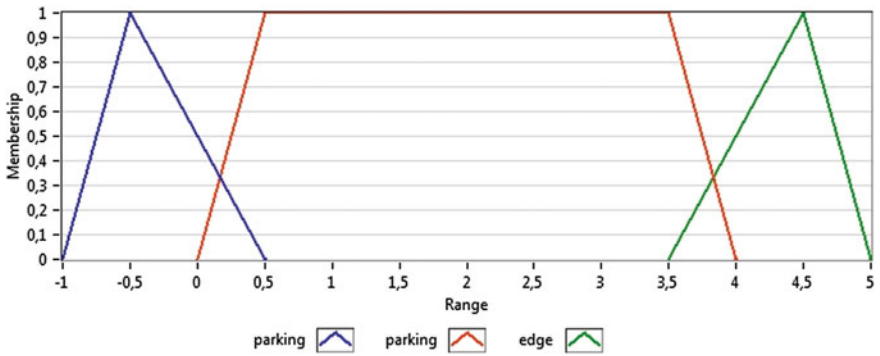


Fig. 6 Membership functions for input variable y

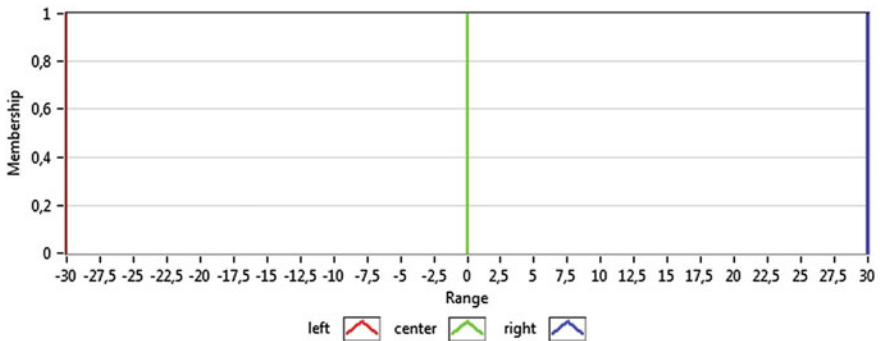


Fig. 7 Membership functions for output variable steering-angle

The linguistic terms of the steering-angle output linguistic variable (Fig. 7) are Left, Center, and Right. These variables are Singleton-type due to the fact that the car has a fixed steering angle of $\pm 45^\circ$.

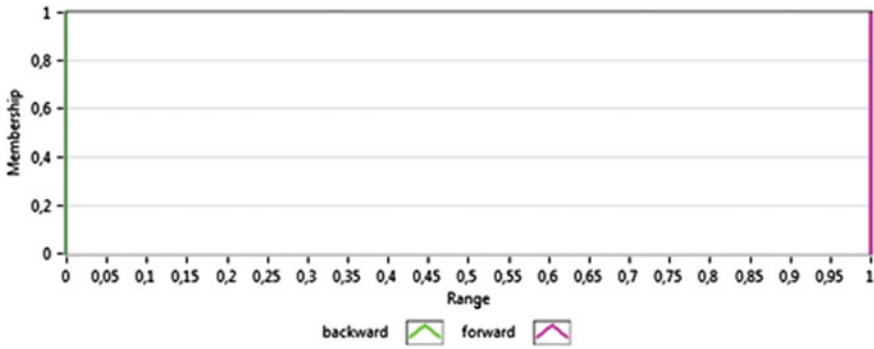
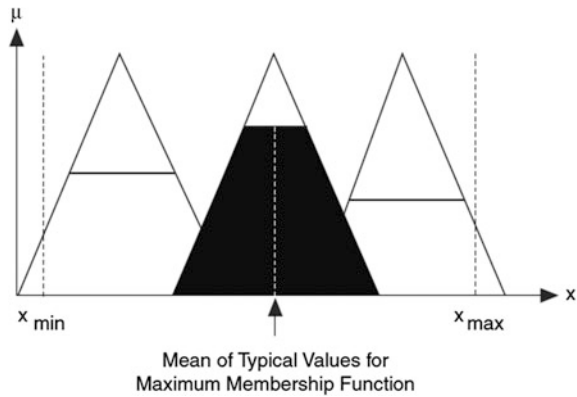


Fig. 8 Membership functions for output variable direction

Fig. 9 Mean of maximum (MoM) defuzzification method



The linguistic terms of the direction output linguistic variable (Fig. 8) are Backward and Forward. These variables are also Singleton-type.

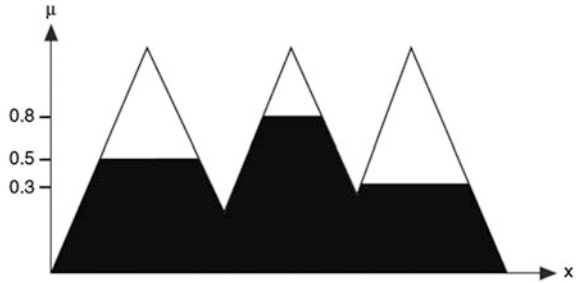
The defuzzification method used is Mean of Maximum (Fig. 9). Studies show that it offers the best results in pattern recognition and the least computational effort. It outputs the most typical value of the most probable answer. Mean of Maximum has proven experimentally to be the best method to use in our system [8].

The antecedent connective AND (Product) specifies to use the product of the degrees of membership of the antecedents.

The Minimum implication method (Fig. 10) is used to truncate the output membership functions to the value of the corresponding rule weights.

The degree of support, between 0 and 1, represents the relative significance of each rule and allows for fine-tuning of the rule base. In this case, the degree of support is set at 1 for all the rules. The final weight of a rule is equal to the degree of support multiplied by the truth value of the aggregated rule antecedent [8].

Fig. 10 Minimum implication method



The rules of the fuzzy system were determined based on experimental analysis. The aim of the rules was to get the car at a 90° in line with the parking lot. The rules used were the following:

An example of rules used in this system:

1. IF 'x' IS 'left' AND 'orientation' IS 'left-down' AND 'y' IS 'parking ground' THEN 'steering-angle' IS 'left' ALSO 'direction' IS 'backward'
connective: AND (Product); implication: Minimum; degree of support: 1.00
2. IF 'x' IS 'left' AND 'orientation' IS 'left-down' AND 'y' IS 'parking lot' THEN 'steering-angle' IS 'center' ALSO 'direction' IS 'backward'
connective: AND (Product); implication: Minimum; degree of support: 1.00
3. IF 'x' IS 'left' AND 'orientation' IS 'left' AND 'y' IS 'parking ground' THEN 'steering-angle' IS 'left' ALSO 'direction' IS 'backward'
connective: AND (Product); implication: Minimum; degree of support: 1.00.

Here is an example of the fuzzy logic controller in operation mode. If $x = 8$, orientation = 10°, and $y = 1$, the resulting output variables are steering angle = 16.9565 and direction = 1. The output surface of the fuzzy controller in this situation can be seen in Fig. 11.

Fuzzy systems can be implemented in LabVIEW using the LabVIEW PID and Fuzzy Logic toolkit. The system described before was made with the fuzzy system designer and saved in a file named car-control-1.fs. The file is then loaded in LabVIEW using the FL Fuzzy Controller VI. The output of the Fuzzy Control system can be seen in Fig. 12.

The initial position and orientation of the car are chosen by the user in order to facilitate experimental analysis. Upon receiving the parking command the program starts sending serial commands to the car in order to park it. Hence the car starts parking itself. This can be observed in Fig. 13a, b. When the car has officially parked the parking command is reset Tables 1, 2, 3, 4, 5, 6, and 7.

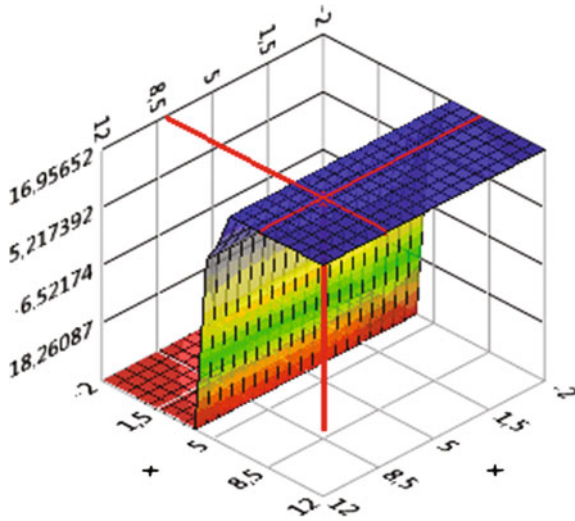


Fig. 11 The output surface of the fuzzy controller

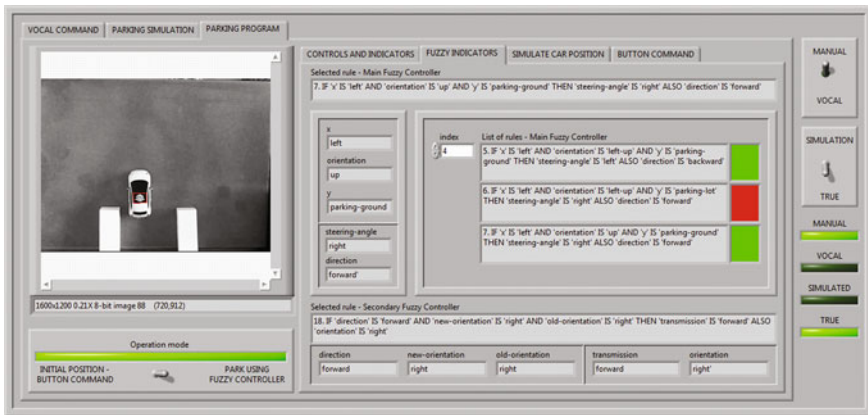


Fig. 12 The indicators of the fuzzy logic controller

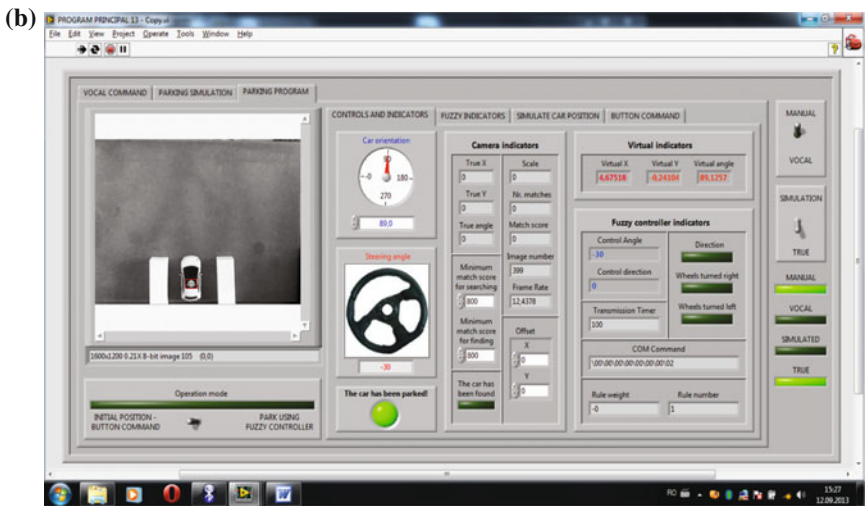
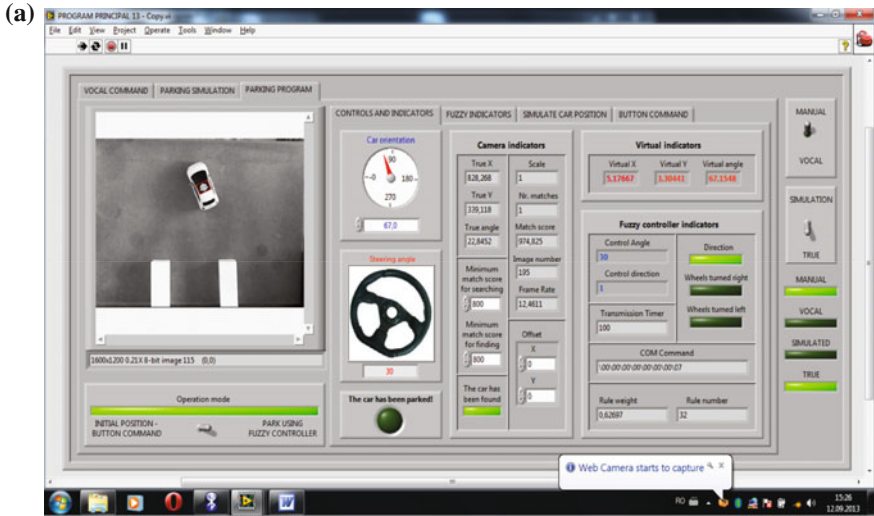


Fig. 13 The program commands the parking of the car. a The program is parking the car. b The program has parked the car

Table 1 Membership functions for input linguistic variable x

Membership function	Shape	Points
Left	Trapezoid	-2; -2; 3; 5
Right	Trapezoid	5; 7; 12; 12
Center	Triangle	4; 5; 6

Table 2 Membership functions for input linguistic variable orientation

Membership function	Shape	Points
Left-down	Trapezoid	-90; -90; -45; 0
Left	Triangle	-25; 0; 25
Left-center	Triangle	0; 25; 50
Left-up	Triangle	0; 60; 90
Up	Triangle	80; 90; 100
Right-up	Triangle	90; 125; 180
Right-center	Triangle	130; 155; 180
Right	Triangle	155; 180; 205
Right-down	Trapezoid	180; 225; 270; 270

Table 3 Membership functions for input linguistic variable y

Membership function	Shape	Points
Parking lot	Triangle	-1; -0.5; 0.5
Parking ground	Trapezoid	0; 0.5; 3.5; 4
Edge	Triangle	3.5; 4.5; 5

Table 4 Membership functions for output linguistic variable steering-angle

Membership function	Shape	Points
Left	Singleton	-30
Center	Singleton	0
Right	Singleton	30

Table 5 Membership functions for output linguistic variable direction

Membership function	Shape	Points
Backward	Singleton	0
Forward	Singleton	1

5 Experimental Results

Due to the high speed of the car and the errors that can appear in recognizing its position (image recognition is not a fast process) an impulse-based control was chosen. In this case the program sends four serial impulses to the Bluetooth port; the first three commanding the movement of the vehicle given by the fuzzy controller and one stop command. The time lapse between transmissions is dictated by a timer, being of 100 ms. During this time, the car maintains the movement dictated

Table 6 Rule table for output linguistic variable steering-angle

Steering-angle		Center		Right		
Orientation		Center		Right		
x		Center		Right		
Left		Center		Right		
y		Center		Right		
	Parking-lot	Parking-ground	Edge	Parking-lot	Parking-ground	Edge
Left-down	Center	Left	Center	Center	Center	Center
Left	Right	Left	Left	Center	Left	Center
Left-center	Right	Left	Center	Right	Center	Left
Left-up	Right	Left	Center	Right	Center	Center
Up	Center	Right	Center	Center	Center	Center
Right-up	Left	Right	Center	Left	Left	Center
Right-center	Left	Right	Center	Left	Center	Center
Right	Left	Left	Right	Center	Right	Right
Right-down	Center	Left	Center	Left	Left	Center

Table 7 Rule table for output linguistic variable direction

Direction	x			y		
	Parking-lot	Parking-ground	Edge	Parking-lot	Parking-ground	Edge
Orientation	Center			Right		
	Left					
Left-down	Backward	Backward	Forward	Backward	Backward	Forward
Left	Forward	Backward	Backward	Backward	Backward	Backward
Left-center	Forward	Backward	Backward	Forward	Forward	Backward
Left-up	Forward	Backward	Backward	Forward	Forward	Backward
Up	Forward	Forward	Backward	Backward	Backward	Backward
Right-up	Forward	Forward	Backward	Forward	Forward	Backward
Right-center	Forward	Forward	Backward	Forward	Forward	Backward
Right	Forward	Forward	Backward	Backward	Backward	Backward
Right-down	Backward	Forward	Forward	Forward	Forward	Forward

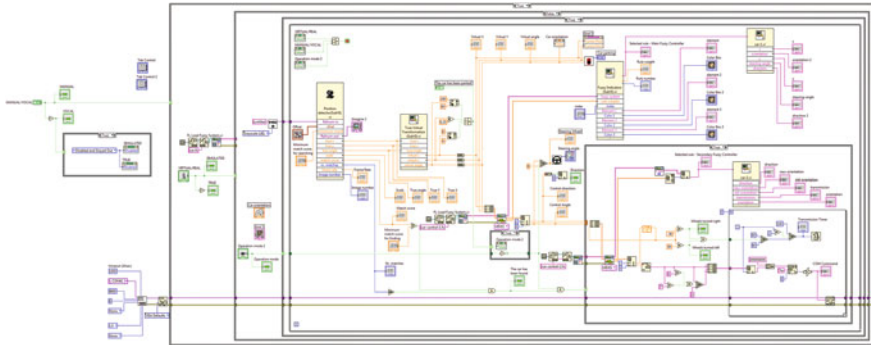


Fig. 14 The block diagram of the program

by the command not having enough time to stop completely, just to slow down. Therefore the car is controlled with a 75 % filling factor, this modifying the average speed of the car so that the program can control it more easily. The position of the car can be taken more accurately since the car is stationary when the camera grabs the next picture. The block diagram of the program can be seen in Fig. 14.

We recommend that the edges of the parking ground consist of separate limiters for the parking algorithm with a higher priority than the results of the fuzzy controller. This will ensure that the car will never maneuver out of the parking ground during parking. Out of the results obtained from tests we have concluded that the car will not go past the margins of the parking ground but it will go dangerously close to it. Therefore, we recommend using separate mechanisms that won't allow it to do this.

6 Conclusions

This system can be applied to real car in a real life parking situation by means of a wireless camera and the car's onboard computer. It does require an infrastructure (the camera has to be in a fixed position situated directly above the parking ground, but this camera could serve a double purpose: parking lot surveillance and parking sensor). This could also be helpful in accident prevention during parking maneuvers which are an issue for inexperienced drivers. It could also allow multiple cars to execute parking maneuvers at the same time. Since modern-day assisted parking systems are not completely autonomous [11] and the system we provide has this benefit, drivers could actually step out of their cars to let them park. It could also be retrofitted into any car with an onboard computer.

Our system could also be adapted as a robot positioning system, especially non-adjustable steering angle robots. Therefore it would be useful in an industrial environment. Possible improvements and extensions of the presented system

include Bluetooth interlocking and communication facilities, obstacle detection and avoidance, etc. Also the speed at which the parking process is performed could be increased with fast image processing techniques and high-speed cameras.

References

1. <http://auto.howstuffworks.com/car-driving-safety/safety-regulatory-devices/self-parking-car.htm>
2. http://www.bee-wi.com/site/user_guides/BBZ201_Multilingual_User_Manual.pdf
3. Ravi Kumar AV, Nataraj KR, Rekha KR (2012) Morphological real time video edge detection in labview, (IJCSIT). *Int J Comput Sci Inf Technol* 3(2):3808–3811
4. <http://digital.ni.com/public.nsf/allkb/4B426438875D67CA8625730100713972>
5. NI Vision Assistant Tutorial, August 2004, Nr. 372228A-01
6. Flores CDP, Ángel M, Gutiérrez H, Palomares RA (2005) Fuzzy logic approach to autonomous car parking using MATLAB. In: Proceedings of the 15th international conference on electronics, communications and computers (CONIELECOMP 2005)
7. Li THS, Chang SJ, Chen YX (2003) Implementation of autonomous fuzzy garage-parking control by an FPGA-based car-like mobile robot using infrared sensors. In: Proceedings of the 2003 IEEE international conference on robotics and automation, Taipei, Taiwan, 14–19 Sept 2003
8. PID and Fuzzy Logic Toolkit User Manual (June 2009) Nr. 372192D-01
9. Miah MS, Gueaieb W, Miah MS, Gueaieb W (2007) Intelligent parallel parking of a car-like mobile robot using RFID technology. In: ROSE 2007—IEEE international workshop on robotic and sensors environments, Ottawa, Canada, 12–13 Oct 2007
10. Cabrera-Cósetl R, Mora-Álvarez MZ, Alejos-Palomares R (2009) Self-parking system based in a fuzzy logic approach. In: 2009 international conference on electrical, communications, and computers
11. Li THS, Chang SJ (2003) Autonomous fuzzy parking control of a car-like mobile robot. *IEEE Trans Syst Man Cybern Part A Syst Humans* 33(4):451–465

A Location-Aware Solution for Predicting Driver's Destination in Intelligent Traffic Systems

Emilian Necula

Abstract This paper presents a methodology focused on learning driving tendencies using GPS data and time stamps to forecast future movement locations. People move throughout regions of time in established, but variable patterns and a person's normal movement can be learned by machines. Location extraction from raw GPS data in combination with a probabilistic neural network is proposed for learning human movement patterns. Using time as an input over a distribution of data, normal tendencies of movement can be forecasted by analyzing the probabilities of a target being at a specific point within a set of frequented locations. This model can be used to predict future traffic conditions and estimate the effects of using the same routes each day. Considering traffic density on its own is insufficient for a deep understanding of the underlying traffic dynamics and hence we propose a novel method for automatically predicting the capacity of each road segment. We evaluate our method on a database of GPS routes and demonstrate their performance. Ultimately, the results produced can contribute to the prediction of traffic congestion in urban areas.

Keywords Neural networks · Data mining · ITS · Congestion · Prediction · GPS data

1 Introduction

Predicting a driver's near-term future path could be useful for giving the driver warnings about upcoming road situations, delivering anticipatory information, and allowing the vehicle to automatically adapt to expected operating conditions. The problem of learning patterns of human behavior from sensor data arises in many applications, including intelligent environments [1], surveillance [2, 3],

E. Necula (✉)

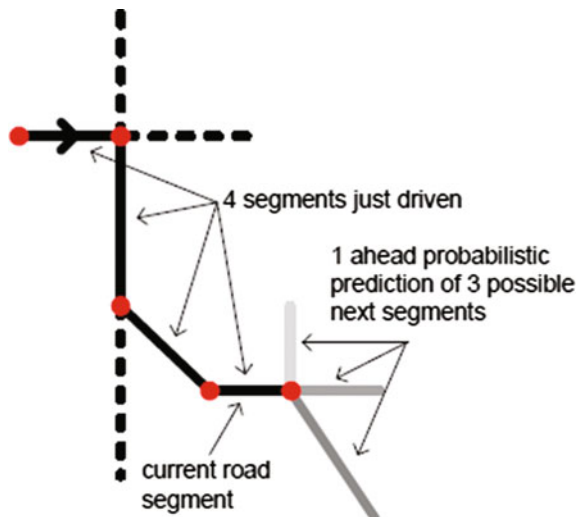
Faculty of Computer Science, University of Alexandru Ioan Cuza, Iasi, Romania
e-mail: emilian.necula@infoiasi.ro

human–robot interaction [4], and assistive technology for the disabled [5]. A focus of recent interest is the use of data from global positioning system (GPS) location data, to learn to recognize the routes which a driver is following over a period of many weeks and to further determine the relationship between his routes and the others that are important to the user [6–10]. The goal of this research is to mine smart driving directions from the historical GPS routes of a considerable number of drivers and provide a user with the practically fastest route to a given destination at a given departure time. Finding efficient driving directions has become a daily activity and been implemented as a key feature in many map services like Google and Bing Maps. A fast driving route saves not only the time of a driver but also energy consumption (as most gas is wasted in traffic jams). In practice, big cities with serious traffic problems usually have a large number of taxis traversing on road surfaces. For the sake of management and security, these taxis have already been embedded with a GPS sensor, which enables a taxi to report on its present location to a data center in a certain frequency. Thus, a large number of time-stamped GPS trajectories of taxis can be utilized to make assumptions.

Intuitively, experienced drivers can usually find out the fastest route to a destination based on their knowledge. When selecting driving directions, besides the distance of a route, they also consider other factors, such as the time-variant traffic flows on road surfaces, traffic signals, and direction changes contained in a route, as well as the probability of accidents. These factors can be learned but are too subtle and difficult to incorporate into existing routing engines. Therefore, historical trajectories, which imply the intelligence of experienced drivers, provide us with a valuable resource to learn practically fast driving directions.

This paper presents a prediction algorithm trained from a driver’s past history. Specifically, we train a neural network to probabilistically predict future road segments based on a short sequence of just-driven road segments, usually 1–10. A sketch of this basic approach appears in Fig. 1. The methodology for learning

Fig. 1 The prediction algorithm looks at a recent sequence of road segments to probabilistically predict future segments



route patterns proposed utilizes a probabilistic neural network (PNN), which is a form of artificial neural network that acts as a maximum a posteriori probability (MAP) estimator. A PNN learns from a distribution of data and then forms a MAP estimation based on the most likely probability of a certain class of output, given the current pattern of input data. PNNs are well suited for pattern recognition and have been used for forecasting in research by Guan et al. [11] for forecasting incidence of Hepatitis A, as well as in research by Saad et al. [12] for forecasting stock market activity. The PNN methodology used in this paper takes time and visited locations as input and outputs probabilities a target will be at one of their established locations within a given window of time. We show that the resulting accuracy is much better than random guessing; for instance, looking at the 10 most recent road segments, we can predict the next road segment with about 90 % accuracy. The algorithm is simple enough to be trained and executed on an in-vehicle navigation computer, and it needs no off-board network connection. We tested the accuracy of our predictions on GPS data from 20 drivers.

2 Related Work

Previous approaches to route detection and place labeling suffer from design decisions that limit their accuracy and flexibility. Ashbrook et al. [6] only reason about moving between significant places, without considering different types of places or different routes between places. In the context of indoor mobile robotics, Bennewitz et al. [4] showed how to learn different motion paths between places. However, their approach does not model different types of places and does not estimate the user's activities when moving between places. In other works [7, 13] they have developed a hierarchical dynamic Bayesian network model that can reason about different transportation routines between significant places. Gogate et al. [9] showed how to use deterministic constraints to more efficiently reason in such models.

Closely related to estimating traffic conditions are obtaining accurate estimates of the travel time between two points in a city. Blandin et al. [14] use kernel methods [15] to obtain a non-linear estimate of travel times on "arterial" roads; the performance of this estimate is then improved through kernel regression. Yuan and Zheng [16] propose constructing a graph whose nodes are landmarks. Landmarks are defined as road segments frequently traversed by taxis. They propose a method to adaptively split a day into different time segments, based on the variance and entropy of the travel time between landmarks. This results in an estimate of the distributions of the travel times between landmarks.

The research most relevant to this paper is those which attempt to model and/or predict traffic conditions. Guhnmann et al. [17] use GPS data to construct travel time and speed estimates for each road segment, which are in turn used to estimate emission levels in different parts of the city. Their estimates are obtained by simply averaging over the most recent GPS entries; this is closely related to the historical means baseline we compare our algorithm against. Singliar and Hauskrecht [18]

studied two models for traffic density estimation: conditional autoregressive models and mixture of Gaussian trees. This work was designed to work with a set of traffic sensors placed around the city, and not with GPS-equipped vehicles. The authors assume the Markov property for traffic flows: the state of a road segment in the immediate future is dependent only on the state of its immediate neighbors. We adopt a similar assumption in our construction of a model. Lippi et al. [19] use Markov logic networks to perform relational learning for traffic forecasting on multiple simultaneous locations, and at different steps in the future. This work is also designed for dealing with a set of traffic sensors around the city. Su and Yu [20] used a genetic algorithm to select the parameters of a support vector machine (SVM), trained to predict short-term traffic conditions. Their method is meant to work with either traffic sensors or GPS-equipped vehicles. However, their empirical evaluation is quite limited and falls short of fully convincing the reader of their method's practicality. Herring et al. [21] use Coupled Hidden Markov Models [22] for estimating traffic conditions on arterial roads. They propose a sophisticated model based on traffic theory which yields good results. Nevertheless, we argue that this type of sophistication is, in a sense, "overkill". Taking into account the coarse regularity of traffic flow during the week to construct a model yields very good results, without having to resort to more sophisticated and computationally expensive, methods. One of the main motivations driving this research is the application of these results in a real-time setting, where computationally expensive proposals are unsuitable.

Yuan et al. [23] used both historical patterns and real-time traffic to estimate traffic conditions. However, the predictions they provide are between a set of "landmarks" which is smaller than the size of the road network. Although suitable for many applications (such as optimal route planning), the coarseness of their predictions makes them less suited for a detailed understanding of a city's traffic dynamics.

3 Data Acquisition

In order to show the effectiveness of the proposed methodology, it was necessary to run tests over real data. For the experiment, 4 weeks of real GPS data was gathered on a series of test subjects. This approach is based on GPS-enabled smart phones, leveraging the fact that increasing numbers of smart phones or PDAs come with GPS as a standard feature. This technique can provide more accurate location information and thus more accurate traffic data such as speeds and/or travel times. Additional quantities can potentially be obtained from these devices, such as instantaneous velocity, acceleration, and direction of travel. Fontaine and Smith [24] used cell phone for traffic monitoring purposes, and mentioned the need of having GPS-level accuracy for position to compute reasonable estimates of travel time and speed. Yim and Cayford [25] and Yim [26] concluded that if GPS-equipped cell phones are widely used, they will become a more attractive and

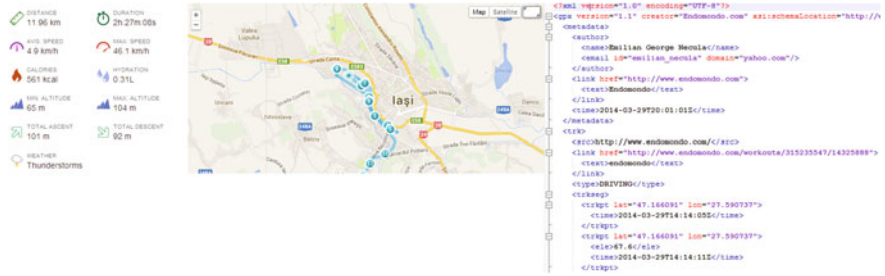


Fig. 2 Endomondo web interface that displays driver’s route and (*left*) and the equivalent GPX file (*right*)

realistic alternative for traffic monitoring. GPS-enabled mobile phones can potentially provide an exhaustive spatial and temporal coverage of the transportation network when there is traffic, with a high positioning accuracy achieved by a GPS receiver. Some concerns regarding this technology include the need of a specifically designed handset, and the fact that the method requires each phone to send information to a center [27, 28], which could potentially increase the communication load on the system. Another issue is the knowledge of vehicle position and velocity provided by this technology, which needs to be used in a way which does not infringe on privacy. The subject driver carried a smart phone with an application installed on it that tracks his daily routes while driving. The application is freely available for any Android or MacOs device. Any driver that has an account on Endomondo [29] can save his routes easily. As we are using it for academic purpose there is no copyright infringement involved. We are planning to develop soon our own mobile tracking application. These routes can be exported to our external application in GPX format—Fig. 2 in order to be processed. The GPS receiver used by the mobile devices was accurate to less than 15 m under optimal conditions, however, due to lack of satellite verification, satellite acquisition time, terrain topology, etc., the data obtained was noisier than what an optimal system would have provided. Ashbrook et al. [6] discuss lapses in data acquisition and there are numerous papers, of which Schmid et al. [30] present a particularly eloquent methodology for dealing with location extraction (location extraction acts as a filtering mechanism that extracts meaningful locations from noisy data).

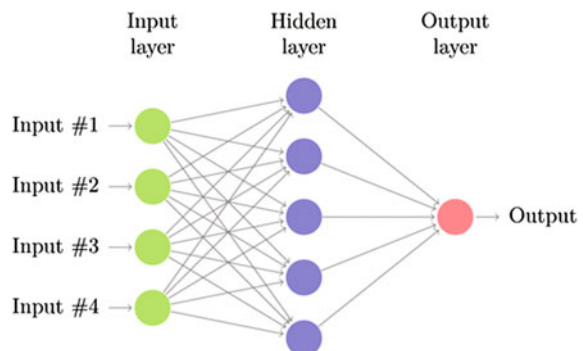
4 The Methodology

4.1 Prediction Model

The inputs to the PNN for the first set of experiments dealt with the modeling of normal tendencies of movement and the only inputs for this experiment were four membership functions representing time. These membership functions are time

inputs representing the degree to which the current time is close to 0:00, 6:00, 12:00, and 18:00 h. For the first set of experiments the data was separated into seven different sets, one for each day of the week. This was done based on the assumption that a person's pattern of movement depends heavily on the day of the week. Each of the different datasets needed a separate PNN, so a total of 7 PNNs would be needed to learn normal tendencies of movement for a target over each day of the week. The second set of experiments dealt with forecasting a person's next location. There are additional inputs for these experiments which represent the set of locations a person has visited on the specific day in question. After analyzing the routes that a driver followed on each day the inputs for the PNN can be grouped according to different representative regions: Input #1, Input #2, Input #3, Input #4. It was only necessary to use one PNN for these experiments because the pattern of visited locations for a given day of the week distinguished that day from others in the distribution and the PNN was able to group the patterns of visited locations together in relation to the time inputs. These additional inputs give the network more insight into the day being classified, and they change the problem. When the network is given this information, it is no longer just trying to model a normal day but instead a normal day given a certain set of locations the person has visited. As the day goes on, the network gets more information about the movement of the subject and can therefore more accurately forecast where the subject will potentially be. To represent the locations a person has visited, the number of inputs used is equal to the number of locations the person visited over the distribution of data. If a location is visited on a given day, its input variable is set to 1 for the rest of the day; else it is set to 0. The number of outputs for a network is equal to the number of locations the person has visited over the distribution of data. Each output represents a certain location. The output for the forecasted location is set to 1 and the rest of the outputs are 0. The architecture used, as mentioned earlier, is a PNN, and therefore contains four layers. The first layer is the input layer. The second is the pattern layer implementing a Gaussian activation function. This layer consists of one node for each of the patterns in the distribution of data. The third layer is a summation layer where probabilities are summed and the probability for each individual class is surmised. In this layer there is one node for each individual class which is surmised. In this layer there is one node for each potential class in the data distribution. These last two layers are grouped into the "Hidden Layer" and the

Fig. 3 Probabilistic neural network that takes as input four membership functions accordingly to 00:00, 6:00, 12:00, 18:00 h and outputs the most likely destination



graphical representation of the PNN can be seen in Fig. 3. Finally the fourth layer is a “winner takes all” layer where the class with the highest probability wins. The second layer contains the only parameter in the PNN that is variable and this parameter is the smoothing factor, or standard deviation. It can be varied to alter the sensitivity of nodes to particular patterns. For the experiment the best smoothing factor was found using the standard iterative approach which is discussed by Saad et al. [12]. The iterative approach increments the parameter in a discrete fashion until it finds the optimum results over the training data.

The implementation of this model is divided into six steps and considers an isolation of the observations using a time-series pattern matching approach.

- Step 1 *Time Series*: A time-series dataset $T = t_1, \dots, t_m$, an ordered set of m real-valued variables, is considered
- Step 2 *Subsequence*: Given a time series of T length, a subsequence C_p of T is a sample of length $w < m$ of contiguous positions from T , that is, $C_p = t_p, \dots, t_{p+w-1}$ for $1 \leq p \leq m - w + 1$. The process of extracting subsequences from a time series is achieved through the implementation of a sliding window
- Step 3 *Sliding Window*: Given a time series T of length m , and a user-defined subsequence length of w , all possible subsequences can be extracted by sliding a window of size w across T and extracting each subsequence C_p . Using this process, the subsequence following C_p is $C_{p+1} = t_{p+1}, \dots, t_{p+w}$
- Step 4 *Pattern Definition*: The pattern of each subsequence C_p is characterized by the slope of the best-fit line generated for each subsequence C_p . The change of slope between consecutive subsequences is then measured to identify the similarity of the subsequences
- Step 5 *Pattern Similarity*: The inclusion of a point in a time-series subsequence which falls outside the linear regime introduces non-linearity which results in a large change of slope in the linear behavior of the subsequence and provides a low R^2 value for the best-fit line, indicating non-linear behavior. Using this assumption, the points introducing non-linearity in the traffic time-series data are identified
- Step 6 *Time-Series Classification*: A subsequence C_p which is characterized by a R^2 value of a beyond a defined lower limit and the difference of slope, θ , between C_p and C_{p-1} is beyond a threshold T classifies the sequence as non-linear. The threshold T can be the lower limit of the 95 % confidence interval of a change of slope distribution calculated using historical time-series datasets. The lower limit of the R^2 value, L , can be the average value calculated using historical time-series datasets.

The abovementioned steps are followed to identify the traffic route regions a driver has followed. These observations are preprocessed to introduce a calibration into our predictive model. It can be seen, that each set of information on driver's route, average speed, and time of observation, t , is a vector that can be represented as $X(q, u, t)$. The observations can be adjusted using the following conditions:

$$\begin{aligned} &\text{for } \theta < T \text{ and } R^2 < L \\ &X(q, u, t_i) = E(X(q, u, t_i)), i = 1, \dots, M \end{aligned} \quad (1)$$

where $X(q, u, t_i)$ defines the driver's routes in region q , average speed u , and time t of the day; M is the number of days on which traffic data is collected; E denotes the expectation. We will describe the neuron j as

$$u_q = \sum_{p=1}^m w_{pq} x_p \quad a_q = \varphi(u_q + b_q) \quad (2)$$

where x_1, x_2, \dots, x_p are driver's routes, w_{pq} is the connection weight from neuron p in the layer l to neuron q in layer $l + 1$, u_q is the linear combiner output due to the driver's routes, b_q is the bias, $\varphi(\dots)$ is the activation function, and a_q is the output signal of the neuron.

The *feed forward back propagation neural network* (FFBPNN) consists of both a forward and a backward phase. The input vector contains N elements which is equal to the number of traffic instants at which the route data is collected within a day. Output values are calculated using Eq. (2) and a log-sigmoid function is used as the activation function in this case. The back propagation (BP) phase compares the neural network outputs a_{pq} , calculated with the target values, t_{pq} , and is an iterative optimization of the error function that represents the performance of the network. This function of error, E , is defined as:

$$E = \frac{1}{2} \sum_{p=1}^M \sum_{q=1}^N (t_{pq} - a_{pq})^2 \quad (3)$$

where N and M are defined as before. E is minimized using the gradient descent optimization technique. The partial derivative of the error function in relation to each weight provides a direction of steepest descent. The corrections to the connection weights within the network are adjusted for each iteration using this partial derivative. The weight updating equation is:

$$w_{pq}(k+1) - w_{pq}(k) = \Delta w_{ipq}(k) = -\mu \frac{\delta E(k)}{\delta w_{ipq}(k)} \quad (4)$$

where μ is the learning rate, a small positive constant. If the difference between neural network output and desired output becomes negligible or acceptable then the learning process terminates.

4.2 The Algorithm

The algorithm used is a derived from the Viterbi algorithm (VA) that can be simply described as an algorithm which finds the most likely path through a trellis given a set of observations. The trellis in this case represents a graph of a finite set of states from a finite state machine (FSM). Each node in this graph represents a state and each edge a possible transition between two states at consecutive discrete time intervals. An example of a trellis is shown below in Fig. 4a and the FSM that produced this trellis is shown in Fig. 4b. The FSM referred to here is often referred to in the literature as a Markov model (MM). For each of the possible transitions within a given FSM there is a corresponding output symbol produced by the FSM. This data symbol does not have to be a binary digit, it could instead represent like in our situation a location. The outputs of the FSM are viewed by the VA as a set of observed locations with some of the original data corrupted by some form of noise. This noise is usually inherent to the low GPS signal that reflects on the exact position of a driver from the GPX file.

To format the data for input into the neural network, the raw GPS data must first be preprocessed because of inherent noise. Once the data is preprocessed, meaningful locations are extracted. For the experiments in this paper, locations were defined as a person being within a 200 m for at least 7 min. After the locations are extracted, each of the individual logged coordinates over 15 min time regions is averaged. The assumed longitude and latitude for the each time region is the calculated averaged of its logged coordinates. Once the 15 min intervals are obtained they are classified. If the location for a time region overlaps with an extracted location, or the person was within 15 min of an extracted location, the interval is classified as being at the visited location. If a person was not at a location and not within 15 min of arriving at a location, the interval is classified as unknown.

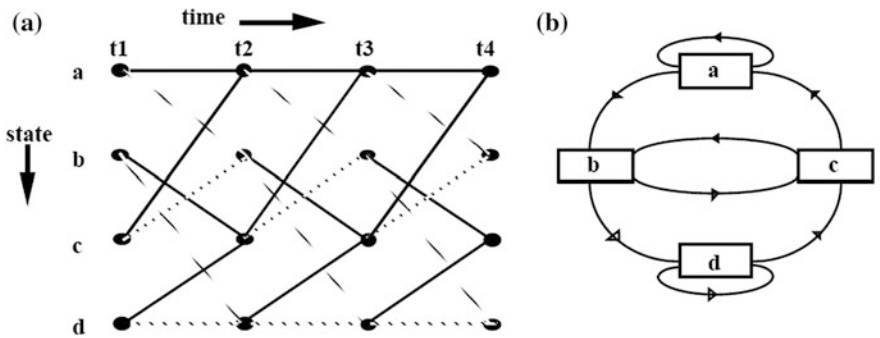
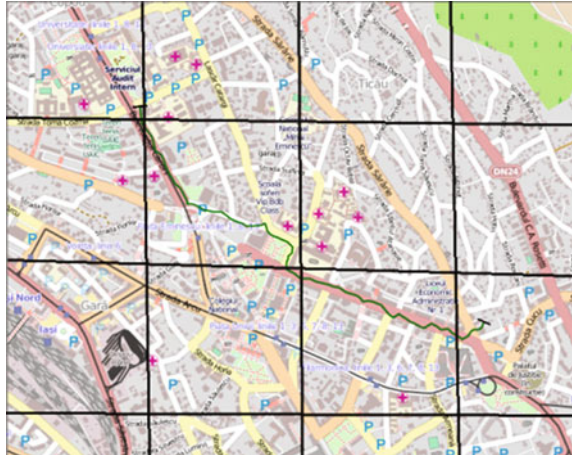


Fig. 4 Showing a trellis diagram spread over time and b the corresponding state diagram of the FSM

Fig. 5 Map showing the area with the grid. The cells are squares, one square kilometer in size



Finally, for the second set of experiments it was necessary to formulate inputs that represented the locations a person had visited on a given day. To obtain this, each 15 min time region was processed and if a region was classified as being at a location the corresponding input for that location was set to 1 for the rest of the day.

We represent a region as a 40×40 , two-dimensional grid of square cells, each cell 1 km on a side, as shown in Fig. 5. Each cell represents one discrete location. Our destination prediction is aimed at picking the cell in which a driver will conclude his or her trip based on which cells the driver has already traversed and on the characteristics of each cell. This particular discretization of space is a heuristic choice, and we could have chosen a different tiling, size, and number of discrete cells. Each of the $N = 1600$ cells is given an index $i = 1, 2, 3, \dots, N$.

Because our methods are probabilistic, we ultimately compute the probability of each cell being the destination, i.e. $P(D = i | \mathbf{X} = \mathbf{x})$, where D is a random variable representing the destination and \mathbf{X} is a random variable representing the vector of observed features from the trip so far. While we shall focus on trajectory-centric observations, other factors can be included in \mathbf{X} , such as time of day and day of week.

We decompose the inference about location into the prior probability and the likelihood of seeing data given that each cell is the destination. Applying Bayes rule [31] gives:

$$P(D = i | \mathbf{X} = \mathbf{x}) = \frac{P(\mathbf{X} = \mathbf{x} | D = i)P(D = i)}{\sum_{j=1}^N P(\mathbf{X} = \mathbf{x} | D = j)P(D = j)}$$

Here $P(D = i)$ is the prior probability of the destination being cell i . We compute the prior probability with two sources of map information. $P(\mathbf{X} = \mathbf{x} | D = i)$ is the likelihood of cell i being the destination based on the observed measurements \mathbf{X} .

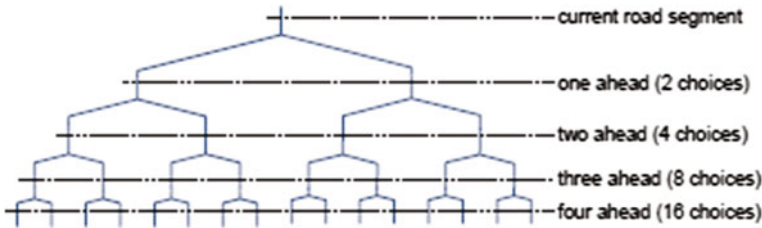


Fig. 6 The tree that models the choice for the future road segments

The model gives a probabilistic prediction over future road segments based on past road segments. The model is sensitive to the two most recent road segments $((1)|X(-1), X(0))$. In particular, looking at the two most recent road segments gives a sense of the direction of travel along a road, which helps significantly. This model can be used to predict beyond just the next road segment. We can clearly build $((2)|X(0))$, which is the distribution over the road segments after the next one, given the current one. We can also use higher order models to make these farther out predictions, e.g. $((2)|X(-1), X(0))$. In general, we can build an n th order Markov model ($n \geq 1$) to predict the m th next encountered segment ($m \geq 1$). We denote our general n th order model as

$$P(X(m)) = P(X(m)|X(-n + 1), X(-n + 2), \dots, X(0))$$

In the Results section we will look at how prediction accuracy changes as we increase n , the number of segments we look at into the past (better). We also look at how prediction accuracy changes as we increase m , the number of segments we predict into the future. Predicting two segments into the future would involve making two of these random choices. In fact, the road segment choices are conveniently represented as a tree, as shown in Fig. 6. The branching factor for this tree is two, given that each node splits into two as the tree gets deeper.

4.3 Determination of the Future Locations and Road Capacities

We propose a novel method for determining the capacity of the different road segments, based on the previous routes and speed readings. For each edge-orientation pair (e, o) and minute m we compute $vel((e, o), m)$, defined as the average velocity of all drivers passing by (e, o) in minute m . In the computation of this average velocity we apply some simple filtering schemes, such as ignoring the velocity of cars that are parked: parked cars are not navigating the network so are not a proper indication of the average speed through (e, o) and will bring down the computed average velocity.

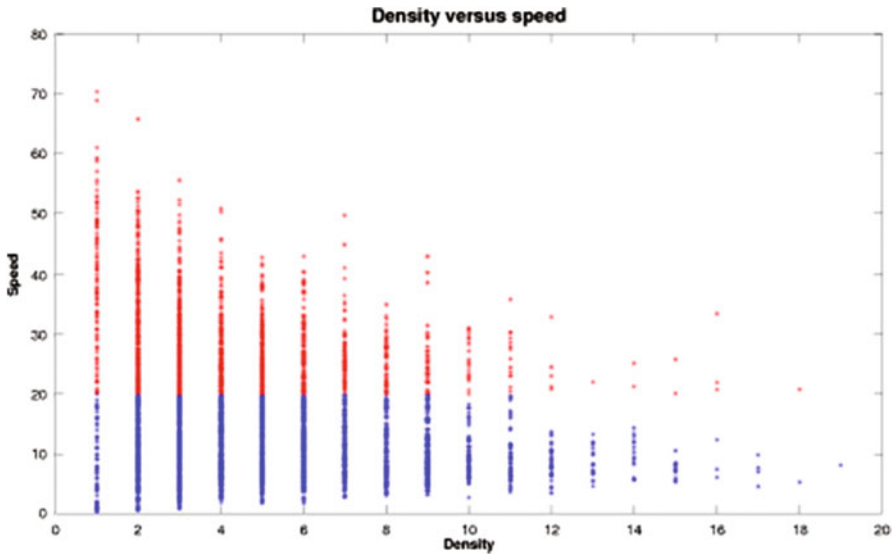


Fig. 7 Density versus speed for one edge-orientation pair

We can use average velocity as an indication of when a road is congested. Schafer et al. [32] define a congested road as one where the average velocity is below 10 km/h. In this paper we say a road segment is congested if the velocity of the majority of cars is below 20 km/h, in a manner that will be made more precise below. We choose 20 km/h as our cutoff as this is already quite low, even for residential areas. In Fig. 7 we plot density versus average speed for a particular edge-orientation pair; that is, every point in the figure corresponds to one of the 7200 min in a week. We color the points above our 20 km/h limit in red, and those below in blue. We will refer to the red points as the high points, and the blue points as the low points. As one would expect, the velocity tends to go down as the density goes up. It is inevitable that even with low densities we will have low speed readings, and simply using averages may underestimate the road’s true capacity. So we will compute for each density level d , the ratio of high points, high_d to low points, low_d :

$$\text{ratio}(d) = \frac{|\text{high}_d|}{|\text{low}_d|}$$

We define the capacity of an edge-orientation pair (e, o) , as the density level d , with sufficient data points, whose ratio unambiguously drops below 0.4 (there are at least 250 % more low points than high points). A density level d has sufficient data points if $|\text{high}_d| + |\text{low}_d| > 500$. The unambiguous drop criterion is meant to exclude outlier “spikes” that will affect the real road capacity values.

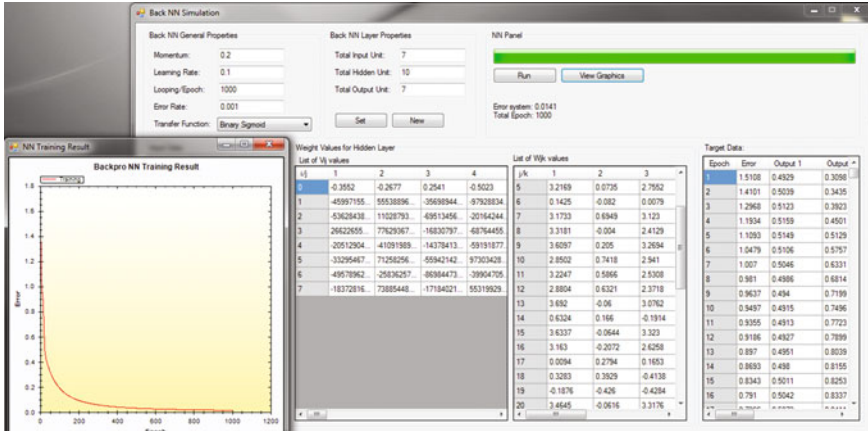


Fig. 8 Screenshot from the C# application that learn driver’s route and displays in the end the prediction accuracy for future segments

The data presented to the probabilistic neural network for the experiments was partitioned into three sets of data, training data (2 weeks), testing data (used to prevent overfitting—1 week), and a production set (1 week) used to evaluate the performance of the network on unseen data. As mentioned already there were two different sets of experiments performed for this paper. For one set of experiments a single PNN was used to classify the entire distribution of data while in the other experiment seven PNNs were used and each PNN dealt only with a specific day of the week. We developed for these experiments a C# application—Fig. 8 that can display in the end the prediction accuracy for the further route segments.

To allow the PNN to learn, it is desirable to have multiple weeks of data in the training set because a person’s movement varies from day to day but exhibits patterns over time. When more data is presented to a PNN the network can obtain a better understanding of the subject’s movement patterns. The real data used was limited to 4 weeks of data so we were only able to use 2 weeks in the training dataset. The testing set that was used to prevent overfitting was a contiguous set of data encompassing 1 week of logged GPS coordinates (latitude, longitude) from the GPX routes obtained as we mentioned in Sect. 2. It was necessary to partition this set so that each different day of the week had a representative example in the testing set, since the different days all present different patterns of movement. The time-series nature of the data makes using a continuous block of data as the testing set desirable. Finally, the production set was partitioned in the same fashion as the testing set.

5 Experimental Results

We tested our prediction algorithm on data from 10 drivers in our primary studies. On average, we observed each of the 10 drivers for a total of 30 days. The traffic data logs and their dimensions (expressed in GPS trace points) that were used in this research are detailed in Table 1.

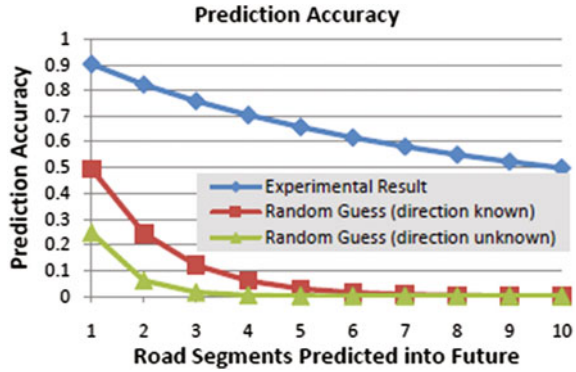
In testing a given set of parameters, e.g. m and n , we used leave-one-out testing, where we trained the model with all first 2 week trips and tested it on the remaining trips. Doing this gives an average accuracy figure over all the trips. An example result is shown in Fig. 9. This shows the accuracy of predicting one road segment ahead, two segments ahead, and up to ten segments ahead based on the last ten observed road segments. The predicted road segment for our experiments is the one with the highest probability from the model. In this case, the model predicts the next road segment with slightly over 90 % accuracy. As expected, the prediction accuracy drops the farther it looks into the future. At 10 segments ahead (almost 2 km), our prediction accuracy lowers to 50 %. This can be looked as the worst scenario in our experiments (3000 tests conducted; 1000 for each method and 100 for each added segment that represents far-away predictions).

Figure 9 also shows the accuracy of prediction using random guessing as a way to see the benefits of our model. Random guessing would involve randomly predicting the next road segment at each choice point. For instance, on a road segment that connects two four-way intersections, the random algorithm would assign a probability of 1/6 to each of the six possible next road segments and randomly pick one for the next segment (we are not taking into account the possibility of a U-turn in our analysis of random guessing). Predicting two segments into the future would involve making two of these random choices (branching factor of two). If the

Table 1 Experiment subject data summary

Driver ID	GPS trace points	Number of trips	Number of different destinations	Period of data collection
1	45.345	21	5	4
2	21.853	7	4	3
3	29.382	11	5	3
4	38.854	19	8	4
5	24.560	7	9	2
6	52.897	25	14	2
7	16.734	7	5	1
8	63.459	21	6	3
9	26.622	14	5	2
10	22.334	11	7	2

Fig. 9 Graph that shows how the prediction accuracy of our model drops as prediction go farther into the future



branching factor is b , and if we are predicting m segments into the future, the number of possible choices at that future point is b^m .

For a given prediction depth m and branching factor b , the probability of randomly guessing the right segment is $1/b^m$. If we know the direction of travel, then the branching factor is halved, because we know which end of the current segment is next. In this case, the probability of making the correct prediction by random guessing is $1/(0.5b)^m$. These two curves are shown in Fig. 9, showing that the predictions based on our model are significantly better than random guessing.

Finding driver’s location at a moment of time was also analyzed in the experiments. Because of the limited period of observations (1 month) our model classified correctly 65 %, incorrectly classified 7 %, and was unable to classify 28 %. The results of the experiments show that there is more information supplied by the model than just a single forecast as to where someone will be. While the percent classified correct is an important feature to analyze, another important piece of information provided by the neural network is the probability of a person being at different locations they have been known to frequent. This provides useful information even when the model misclassifies where the person actually is because it gives insight into where else the person could be. Table 2 shows example output from the probabilistic neural network for the real data over a certain range of time from Friday. The probabilities that the test subject will be at all the different locations that were extracted for the distribution of data are shown in the columns titled *Loc n*, the actual location of the test subject (from the production data) is shown in the column titled *Actual*, the time column represents what time region the forecast is pertaining to, and there is also a classification for unknown (this is when the subject is at least 15 min away from any location).

6 Conclusions and Future Work

The article contribution was to find a simple and accurate prediction algorithm. Based on GPS data collected from 10 drivers, on a period of 1 month we have shown that a probabilistic neural network based model is a simple, effective way to predict near-term, future road segments. Taking into account the most recent 10 segments into the past, we can predict the next segment with about 90 % accuracy. We look forward to validate our methodology considering a more large traffic routes database. We envision that predictions of this type could be used to warn drivers of upcoming traffic hazards, provide anticipatory information and may be triggering automatic vehicle behaviors.

The mechanism presented in this paper for automatically determining the capacity of road segments is one of the few, and provides a powerful tool for obtaining a deep understanding of the traffic dynamics. In future this kind of information might be useful to predict congestion in a city road network. Besides its use for automatically determining the capacity of a road segment, the density versus speed plots can provide additional useful information about road segments.

Future work along the direction outlined in this paper could include experiments that show how prediction accuracy changes with the number of days that a driver is observed. We expect prediction accuracy to generally rise with observation time, eventually reaching an optimum. The experiments described in this paper have shown how a neural network in conjunction with a Markov Model based algorithm can learn normal patterns of movement for a person given at least 1 month of logged GPS coordinates of that person. Obtaining more data would test how robust the methodology is, as well as its ability to adapt to different types of movement in a real scenario. To this point the scarcity of data is one of the biggest limitations. Another area of research for destination prediction is to implement methodology mentioned by Luper et al. [33] to isolate abnormal days in a distribution of data. This would allow for the removal of abnormal days from training data which would be beneficial because it would ensure the network was only trained on days that were classified as normal, in essence only learning normal patterns of movement and eliminating days that would be “noise”.

Acknowledgments This paper is supported by the sectoral operational programme human resources development (SOP HRD), financed from the European Social Fund and by the Romanian Government under Contract Number POSDRU/150/1.5/S/133675.

References

1. Brumitt B, Meyers B, Krumm J, Kern A, Shafer S (2000) Easyliving: technologies for intelligent environments. *Handheld and Ubiquitous Computing*
2. Bui HH, Venkatesh S, West G (2001) Tracking and surveillance in wide-area spatial environments using the abstract hidden markov model. *Int J Pattern Recogn Artif Intell* 15(1)

3. Dee H, Hogg D (2005) On the feasibility of using a cognitive model to filter surveillance data. In: Proceedings of the IEEE international conference on advanced video and signal based surveillance
4. Bennewitz M, Burgard W, Cielniak G, Thrun S (2005) Learning motion patterns of people for compliant robot motion. *Int J Robot Res (IJRR)* 24(1)
5. Patterson D, Etzioni O, Fox D, Kautz H (2002) Intelligent ubiquitous computing to support Alzheimer's patients: enabling the cognitively disabled. In: *UbiCog '02: first international workshop on ubiquitous computing for cognitive aids*
6. Ashbrook D, Starner T (2003) Using GPS to learn significant locations and predict movement across multiple users. *Pers Ubiquitous Comput* 7(5)
7. Liao L, Fox D, Kautz H (2004) Learning and inferring transportation routines. In: Proceedings of the national conference on artificial intelligence (AAAI)
8. Liao L, Fox D, Kautz H (2005) Location-based activity recognition using relational Markov networks. In: Proceedings of the international joint conference on artificial intelligence (IJCAI)
9. Gogate V, Dechter R, Rindt C, Marca J (2005) Modeling transportation routines using hybrid dynamic mixed networks. In: Proceedings of the conference on uncertainty in artificial intelligence (UAI)
10. Liao L, Fox D, Kautz H (2005) Hierarchical conditional random fields for GPS-based activity recognition. In: Proceedings of the international symposium of robotics research (ISRR)
11. Guan P, Huang D-S, Zhou B-S (2004) Forecasting model for the incidence of hepatitis a based on artificial neural network. *World J Gastroenterol*. ISSN:1007-9327 CN 14-1219/R
12. Saad EW, Prokhorov DV, Wunsch DC, II (1998) Comparative study of stock trend prediction using time delay, recurrent and probabilistic neural networks. *IEEE Trans Neural Networks* 9(6)
13. Patterson D, Liao L, Gajos K, Collier M, Livic N, Olson K, Wang S, Fox D, Kautz H (2004) Opportunity knocks: a system to provide cognitive assistance with transportation services. In: *International conference on ubiquitous computing (UbiComp)*
14. Blandin S, Ghaoui LE, Bayen A (2009) Kernel regression for travel time estimation via convex optimization. In: Proceedings of the 48th IEEE conference on decision and control
15. Scholkopf B, Smola A (2002) *Learning with kernels*. MIT Press
16. Yuan J, Zheng Y (2010) T-Drive: driving directions based on taxi trajectories. In: *ACM Sigspatial GIS*
17. Guhnmann A, Schafer R, Thiessenhusen K (2004) Monitoring traffic and emissions by floating car data. In: *Institute of transport studies Australia*
18. Singliar T, Hauskrecht M (2007) Modeling highway traffic volumes. In: Proceedings of the 18th European conference on machine learning, ECML'07
19. Lippi M, Bertini M, Frasconi P (2010) Collective traffic forecasting. In: Proceedings of the 2010 European conference on machine learning and knowledge discovery in databases: Part II
20. Su H, Yu S (2007) Hybrid GA based online support vector machine model for short-term traffic flow forecasting. In: Proceedings of the 7th international conference on advanced parallel processing technologies
21. Herring R, Hofleitner A, Abbeel P, Bayen A (2010) Estimating arterial traffic conditions using sparse probe data. In: Proceedings of the 13th international IEEE conference on intelligent transportation systems
22. Brand M (1997) Coupled hidden markov models for modeling interacting processes. In: *Technical report, the media lab, Massachusetts institute of technology*
23. Yuan J, Zheng Y, Xie X, Sun G (2011) Driving with knowledge from the physical world. In: Proceedings of the 17th ACM SIGKDD international conference on knowledge discovery and data mining
24. Fontaine M, Smith B (2007) Investigation of the performance of wireless location technology-based traffic monitoring systems. *J Transp Eng* 133(3):157-165
25. Yim Y, Cayford R (2001) Investigation of vehicles as probes using global positioning system and cellular phone tracking: field operational test. In: *California PATH working paper UCB-ITS-PWP-2001-9, institute of transportation studies, University of California, Berkeley, CA*

26. Yim Y (2003) The state of cellular probes. In: California PATH working paper UCB-ITS-PRR-2003-25, institute of transportation studies, University of California, Berkeley, CA
27. Rose G (2006) Mobile phones as traffic probes: practices, prospects, and issues. *Transp Rev* 26(3):275–291
28. Qiu Z, Chen P, Jing J, Ran B (2007) Cellular probe technology applied in advanced traveler information. *Int J Technol Manag* (Accepted for Publication)
29. Endomondo—web page. <http://www.endomondo.com/>
30. Schmid F, Richter KF (2006) Extracting places from location data streams. In: Zipf A (ed) Workshop proceedings (UbiGIS). MÜNster, Germany
31. Olshausen B (2004) Bayesian probability theory
32. Schafer R-P, Thiessenhusen K-U, Wagner P (2002) A traffic information system by means of real-time floating-car data. In: 9th world congress on intelligent transport systems
33. Luper D, Cameron D, Miller JA, Arabnia HR (2007) Spatial and temporal target association through semantic analysis and GPS data mining. In: IKE'08—the 2008 international conference on information and knowledge engineering

Advances in Urban Video-Based Surveillance Systems: A Survey

M. Favorskaya

Abstract The focus of this paper is on providing the perspective intelligent technologies and systems for video-based urban surveillance. The development of intelligent transportation systems improves the safety on the road networks. Car manufacturers, public transportation services, and social institutions are interested in detecting pedestrians in the surroundings of a vehicle to avoid the dangerous traffic situations. Also the study of driver's behavior has become a topic of interest in intelligent transportation systems. Another challenge deals with the intelligent vision technologies for pedestrians' detection and tracking, which are fundamentally different from the crowd surveillance in public places during social events, sport competitions, etc. The detection of abnormal behavior is also connected with the human safety tasks. Some perspective methods of natural disaster surveillance such as earthquakes, fire, explosions, and terrorist attacks are briefly discussed.

Keywords Surveillance system · Vehicle tracking · Driver's behavior · Pedestrians' tracking · Crowd surveillance · Abnormal behavior · Unmanned aerial vehicles · Unmanned ground vehicles · Micro aerial vehicles

1 Introduction

In recent years, the systems for human safety, traffic surveillance, home automation, among others, based on automatic video analysis are developed. Methods of object and active actions' recognition as well as a behavioral understanding lay in the basis of such systems. The activity recognition in urban environment is the main problem of current investigations, which are built on data and knowledge representations of objects and reasoning scenarios. These techniques strongly depend on the low-level

M. Favorskaya (✉)

Institute of Informatics and Telecommunication, Siberian State Aerospace University,
31, Krasnoyarsky Rabochoy Av., 660014 Krasnoyarsk, Russia
e-mail: favorskaya@sibsau.ru

(filtering) and the middle-level (spatio-temporal segmentation with following object tracking) vision tasks. A great variety of vision projections in the real environment make useless the model-based methods. The stochastic approaches based on Bayesian networks, boosting and bagging algorithms are the most popular for object and event recognition in real scenes with all possible artifacts (luminance changing, night lighting, unsuccessful shooting, and meteorological effects). In the high-level vision task, the clustering and classification techniques, an evolution modeling, and the prediction methods can be successfully applied for events monitoring in urban environment.

The urban surveillance includes many complicated and unsolved tasks. Each of them may be considered as a separate sub-task in the following investigations. The reality is such that the researchers make contribution to their fields of investigation but do not take care about the neighboring issues. This approach does not lead to the redundancy in data analysis, computational resources, and possible inconsistency. The goal of the paper is the attempt to analyze the intelligent techniques in order to optimize the structure of urban surveillance framework.

The rest of this paper is structured as follows. A framework for urban surveillance is presented in Sect. 2. Two issues of vehicle tracking and driver's behavior are in the focus of Sect. 3. Section 4 provides the people surveillance techniques in order to understand the behavior of a single pedestrian and a crowd. Some modern techniques for natural disaster recovery are briefly discussed in Sect. 5, and the conclusion is mentioned in Sect. 6.

2 Framework for Urban Surveillance

At present, an urban environment is equipped with hundreds or thousands of cameras, optical and infrared, for traffic light regulators, vehicle tracking systems, and surveillance in public accommodations. Such systems provide a dissemination of comprehensive information including real-time data and video. Smart urban surveillance system involves the sub-domains, which can be considered as the intelligent systems with data and knowledge processing according to their assignments:

- Intelligent Traffic Surveillance System including a network tracking cars, buses, trains, and underground trains in cities.
- Intelligent People Surveillance System (airports, sports competition, exhibitions, and smart house). Due to high activities of people, these systems can be sub-divided into pedestrians tracking domain, crowd surveillance domain, and domain of abnormal human activity.
- Intelligent Natural Disaster Surveillance System in order to monitor earthquakes, fire, explosions, terrorist attacks, etc.

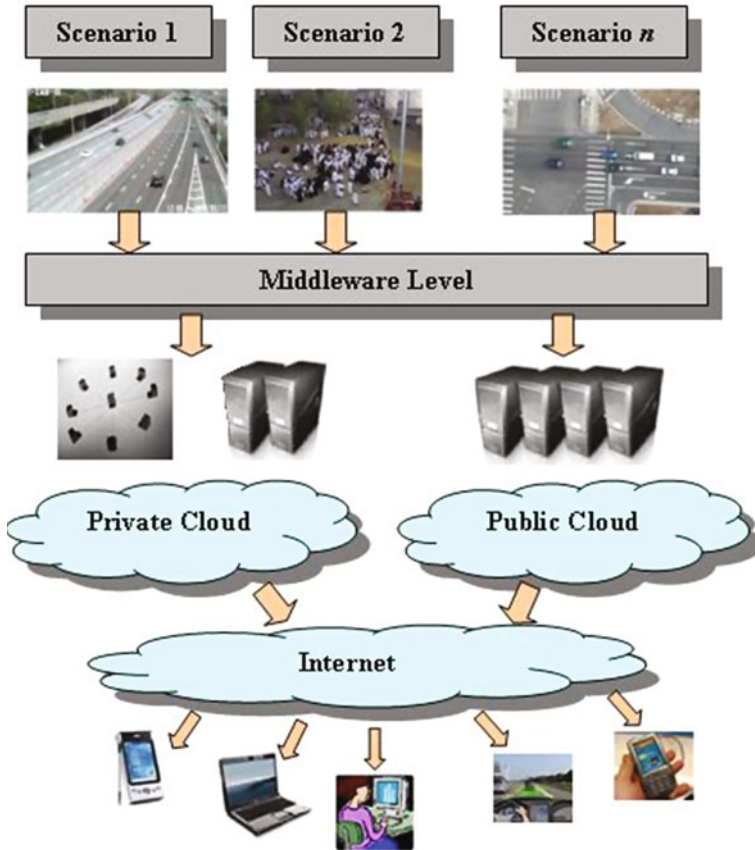


Fig. 1 Architecture for urban vision-based surveillance

The proposed architecture for urban surveillance represented in Fig. 1 can be extended by multiple new tasks of surveillance due to rapid development of cloud and fog technologies, advances in telecommunication networks, and innovations in vision-based technologies. Static surveillance in city urban areas called as conventional infrastructure involves data provided by static sensors. Recently, a new mobile infrastructure had been proposed, named Vehicular Sensor Networks (VSN) [1], when taxis and busses are equipped with mobile sensors, and the information is gathered by the GPS path.

The proposed data model of Conventional Infrastructure (CI) DM_{CI} includes operators of shooting from a single camera O_{sh-sc} and multiple cameras O_{sh-mc} , a transmission operator to predetermined local nodes O_{tr-dn} , a processing by algorithms operator O_{pr-al} , and a transmission operator of detected events to private or public clouds O_{tr-en} . This model is provided by Eq. (1), where S_c is a set of single

cameras, S_v is a set of view areas, S_{fr} and S_{pi} are sets of frames and panoramic images, respectively, S_{ev} is a set of events, and t is a time instant.

$$DM_{CI} = \left\{ \left(O_{sh-sc}(S_c, S_v fr) \mid_t, O_{sh-mc}(S_c, S_v pi) \mid_t \right), O_{tr-dn}(S_{fr}, S_{pi}), \right. \\ \left. O_{pr-al}(S_{fr}, S_{pi}), O_{tr-en}(S_{ev}) \right\} \quad (1)$$

The data model of Mobile Infrastructure (MI) involves the close operators excluding a transmission operator to predetermined local nodes O_{tr-dn} , which is replaced by a transmission operator to nearest local nodes O_{tr-nn} during a movement of vehicle or a transmission operator to clouds O_{tr-cl} (Eq. 2).

$$DM_{MI} = \left\{ \left(O_{sh-sc}(S_c, S_v \rightarrow S_{fr}) \mid_t, O_{sh-mc}(S_c, S_v \rightarrow S_{pi}) \mid_t \right), \right. \\ \left. \left(O_{tr-dn}(S_{fr}, S_{pi}), O_{tr-cl}(S_{fr}, S_{pi}) \right), O_{pr-al}(S_{fr}, S_{pi}), O_{tr-en}(S_{ev}) \right\} \quad (2)$$

The CI and MI data models represent a typical task of big data processing, however, very complicated. Optimization is possible in every step of Eqs. (1) and (2). Volume optimization requires the hardware algorithms' implementation close to single or multiple cameras in order to reduce traffic significantly. Such smart cameras are needed in future. Nowadays, the heuristic algorithms prevail, and only a framework of digital image and video processing is determined by the scientific community in computer vision. A Data-Centric Storage (DCS) and a DIstributed Storage (DIS) are two main appropriate decisions. The DCS means data storage on the predefined locations that causes unnecessary communication cost by migrating data from cameras to local node. The DIS provides a distributed storage and a data transmission, when it is necessary.

Let us briefly discuss the interesting reasonable approaches in common issues of any surveillance, which are well known but at present not solved in complicated scenes, such as a background modeling, illumination change models, and a multi-camera surveillance.

One of the challenges in video-based surveillance is a truth creation of background model. Many algorithms were proposed and successfully used in practical applications beginning from the simplest (background subtraction) and ending the complex based on various statistical estimations. For scenes with shadows and slow changeable brightness, a background subtraction model jointly with statistic color estimations was used in the research [2]. The truth and fast computing background model of a scene is very important because it provides the fundamentals for following object detection and tracking. One can find many approaches for static scene analysis in the literature. At present, this type of surveillance is used in many commercial protective systems. However, from a scientific point of view the dynamic scene is a weak-studied subject. Two problems, such as illumination

changes and so-called “dynamic textures” (trees, water waving in a wind, etc.), may be mentioned. One of the constructive approaches combining global and local background estimations was proposed by Zhao et al. in [3], where the authors presented the spatio-temporal patch-based background modeling. The background spatio-temporal patches, called bricks, lie in a low dimensional background subspace under all possible lighting conditions. At the same time, the moving foreground bricks are widely distributed outside. The authors show that their online subspace learning method based on the candid covariance-free incremental principal component analysis simulates the illumination changes in a scene more robustly than the traditional pixel-wise, block-wise, or motion-based methods.

The illumination change model using a chromaticity difference model and a brightness ratio model was proposed by Choi et al. [4]. The authors built their model under the assumption that the fixed background pixels become the “false” foreground pixels by the influence of illumination change. Then such “false” foreground pixels should be separated to detect the moving objects accurately. Usually in the illumination models, it is assumed that all objects in a scene are perfectly opaque and have Lambertian surfaces [5, 6]. The Enhanced Multi-Scale Retinex algorithm based on the adaptive logarithmic equalization of spectral ranges for dark and bright areas of grayscale and color images was developed by Favorskaya and Pakhirka [7].

The multi-camera surveillance has been applied in objects tracking, sport scenes, urban 3D reconstruction, among others. The synchronized multi-cameras may accurately measure the depth of a scene. They provide a wide viewing angle and, therefore, more information about the scene. Input video sequences can be synchronized manually, by time-stamp-based synchronization, or by use of built-in expensive hardware. The special algorithms provide more productive way without a preliminary tuning. In early works, a video synchronization was achieved by use of the epipolar geometry for the measurements of temporal correspondence between two video sequences [8]. Another approach uses a feature-based sequence-to-sequence alignment method [9], when a spatial alignment is obtained by a homography or a fundamental matrix. The following step is a sequence alignment in both spatial and time domains. In all cases, the cameras are required to remain fixed to each other. Liu et al. proposed the trajectory-to-trajectory temporal alignment in video sequences based on the correspondences of events [10]. The authors referred to an event as a significant change of a scene such as the change of illumination or kinetic changes of moving objects. Excellent review of intelligent multi-camera video surveillance provided by Wang [11] includes five main issues mentioned below:

- Multi-camera calibration, when the intrinsic parameters (focal length, principal point, skew, and distortion coefficients) and extrinsic parameters (the position of the camera center and the camera’s orientation in 3D world coordinates) are estimated. Manual calibration, when salient points are predetermined in the scene, is unsuccessful in comparison to the automatic calibration algorithms by use of known planar templates, vanishing points from static structures with

parallel and orthogonal lines (buildings, landmarks), solar shadows of objects, various keypoint detectors, local descriptors, among others.

- The topology of a camera network has to be arranged in order to overlap camera views for continuous object tracking. Sometimes “blind areas” between two adjacent but disjoint camera views appear that makes multi-camera tracking difficult. The prediction algorithms may be successfully used for tracking an object that leaves one view and appears in some adjacent areas.
- Multi-camera tracking includes intra-camera tracking within a single camera view and inter-camera tracking, which provides the tracks of objects in different camera views. A comprehensive survey for intra-camera tracking can be found in [12]. An inter-camera tracking is usually based on multi-camera calibration (the use of a priori known topology camera views, recursive Bayesian estimation, particle filter) or integrated cues of objects’ motion (a Bayesian approach to integrate the colors and the sizes of objects with velocities, the Expectation–Maximization algorithms, clustering technologies).
- Object re-identification in order to match image regions received from different camera views in spatio-temporal domain and recognize the same object or not is observed. The same object is observed in different camera viewpoints that cause significant variations of poses, resolutions, and lightings. Color histograms [13], Histogram of Oriented Gradients (HOG) [14], various methods based on local texture features’ extraction [15, 16], spatio-temporal features, exemplar-based representations [17], or the photometric transformation between camera views can be recommended to solve this challenge.
- Multi-camera activity analysis for automatic recognition of activities and/or detection abnormal activities in a large area provided by multiple camera views. The supervised approaches require manual labeling of training samples that becomes impossible in different camera views. Nowadays, the unsupervised approaches are prevailed without a necessity for labeling of training samples. The activities of objects can be determined by moving patterns, the complete trajectories, trajectory network [18], among others.

Recent development of multi-camera surveillance and different solutions is compared in [11].

3 Traffic Surveillance

The traffic surveillance includes various sub-tasks, among which two issues are crucial for urban traffic monitoring systems, i.e. vehicle tracking and driver’s behavior. In general, a single-target tracking technology is classified into four major categories: a region-based tracking, a model-based tracking, a contour-based tracking (active contour or kernel), and a feature-based tracking [19]. Sometimes, the Kalman and particle filters are used to predict a magnitude and a direction of motion. Most of the algorithms are developed for stationary surveillance systems

with a shooting from the Earth. The principal unsolved problem for wide implementation in the practice of such intelligent algorithms is their high computational cost and impossibility of real-time implementation. At present, the efforts of researchers are directed towards the development of a mobile surveillance system, for example, based on airborne platforms. This shooting is different from the Earth surface shooting, causes the development of algorithms considering the air shooting conditions (particularly, the non-stabilized video sequences), and provides more suitable area of view and visibility of moving vehicles.

Cao et al. proposed the effective approach for surveillance groups in airborne videos [20]. This approach involves a multi-vehicle tracking in a dynamic scene with the higher level tracking, when the target vehicles are divided into different groups based on the magnitude and direction of velocity, and the lower level tracking, when the position of single target is predicted by Kalman filter and histogram matching algorithm. In spite of all strengths, such surveillance seems vulnerable due to possible fast changing of groups updating, a high computational cost, and the meteorological effects.

The warning system for driver and pedestrian safety was designed by Chien et al. [21]. In this work, the idea is developed to utilize the multiple types of cameras for tracking vehicle movements and driver's intents suggested in [22]. The front-facing stereo cameras determine the vehicle's movements to extract the following types of information:

- The lane boundaries and deviation of the vehicle from the lane center.
- The distance to the vehicle ahead, and the type of lane markings.
- The presence of a pedestrian crossing in front of the vehicle.

A fuzzy system determines, whether the direction of car is legal and safe during a regular driving. The driver line-of-sight camera is directed on a driver, and the algorithm estimates a direction of a driver view and his/her normal or abnormal state. The study of driver's behavior has become a topic of interest in intelligent transportation systems. It has been estimated that 25–50 % of all vehicle crashes are caused by the human factors [23]. According to Kircher [24], three main categories of driver distraction exist:

- A cognitive distraction, when a driver does not concentrate on the driving task. It can appear despite a correct driver's position (eyes in the road and hands on the wheel).
- A visual distraction, when a driver makes secondary tasks such as reading or looking for information in a mobile phone or configuring a GPS, while driving.
- A manual distraction, when a driver has bad hand positions over the steering wheel executing a secondary task (mobile phone calls) or is resting his/her arms out of the steering wheel area.

Cheng et al. modeled the driver activities by a hidden Markov model-based classifier [25]. A driver's intention was detected by tracking of hands and head in the predetermined situations (e.g. turn left, turn right). The risks of a hurried driving are presented in [26]. The risk model was built on the distribution of collision risk

for the preceding vehicle and the continuous time gazing at the rear vehicle. The risk analysis of vehicle and the road parameters in simulated traffic accidents was proposed in [27]. The emotion and the hand gesture recognition of a driver is a future stage of investigation for a traffic safety.

The advanced assistance systems promote a safe urban environment. Thus, traffic sign recognition systems inform drivers about current state of the road for better navigation. In spite of a restricted set of traffic signs as planar rigid objects with different shapes and colors, an automatic recognition of traffic signs in an uncontrolled environment is still a complicated and open challenge. In real-life scenarios, one can mention a set of shooting artifacts such as poor image quality due to low resolution, motion blur, varied lighting conditions, weather conditions, cluttered background, affine and projection transformations, and occlusions. Among well-known classification methods such as Support Vector Machine (SVM), Zernike moments, AdaBoost classification, Haar wavelets, Bayesian classifiers, some original methods are developed. The Error Correcting Output Codes (ECOC) by means of a forest of optimal tree structures embedded in the ECOC matrix is one of such interesting approaches [28]. The ECOC is based on an ensemble of binary classifiers that are trained on a bi-partition of classes. The codebook model represents the continuous visual features with discrete prototypes predefined in a vocabulary due to the Bag-of-Words (BoW) representation model [29]. The matter is in that the off-line training on a set of idealized template sign images cannot provide the significant recognizing results. Large life-like dataset—the German Traffic Sign Recognition Benchmark (GTSRB) including more than 50,000 traffic sign images, which are divided in 43 classes, is often used in experiments [30].

4 People Surveillance

The detection of people plays an essential role in many applications. This task may be divided into two large sub-tasks: the pedestrians tracking and the crowd surveillance. Various algorithms are used for these sub-tasks because of their differences in scale and a visible human shape. However, the common difficulties and requirements can be mentioned, among them are the following:

- A human diversity in appearance by changing pose, sizes, clothes, the objects being carried, and a viewpoint of camera.
- The environment diversity with a cluttered background, illumination changing, and weather effects.
- The partial occlusions of visual projects in dynamic and uncontrolled backgrounds at any time of day and night.
- Camera position fixed or changeable. The shooting by fixed camera (static scenes) requires more simple and reliable algorithms in surveillance systems. The analysis of dynamic scene (more often real-life cases) is a subject for following development.

- The real-time or pseudo real-time processing. The pedestrian detection is an essential, but not a single part in the surveillance systems. To make these algorithms as fast as possible requires the attraction of advanced software and hardware (servers, personal computers, and telecommunication networks).

The algorithms for pedestrian detection and tracking are discussed in Sect. 4.1, while Sect. 4.2 provides the approaches for the crowd surveillance.

4.1 Pedestrian Detection and Tracking

The detection of pedestrian is a subject for research in two past decades due to its essential role in intelligent video-based surveillance and vehicle vision-based systems. In general, a procedure of pedestrian detection is divided into the Region Of Interest (ROI) detection and the following classification. Two basic approaches for ROI detection, image-based and feature-based, prevail. In the image-based approach, often the artificial neural networks are used. Gavrilu [31] proposed the two-step procedure, when, first, contour features are extracted, and a hierarchical template matching is built in order to receive the candidates for ROIs. Second, the intensity features and radial basis function neural network are used to validate these candidates. Sometimes, the convolution neural network [32], SVM [33], or even adapted Principal Component Analysis (PCA) based reconstruction to detect pedestrians [34] is applied for pedestrian detection in video sequences.

The feature-based approach is more popular than the image-based methods. Similar to the first approach, it also uses some learning algorithms such as SVM, AdaBoost [35], and neural networks for classification. However, instead of intensity values, it utilizes the gradients, Haar-like features [36], Histogram of Oriented Gradient (HOG) descriptors [37], or shape features [38]. The technique for efficient pedestrian detection using bidirectional PCA was proposed in [39].

A human tracking is a high computational procedure with linear or non-linear model of prediction. Usually the motion estimation methods without prediction or based on the equation of optical flow with following 3D structural tensor calculations are used. In the last case, two tensor components describe the displacements of objects in the XOY plane and the third component estimates the inter-frame differences in a temporal domain [40]. Also the famous Lucas–Kanade tracking algorithm [41] or its modifications are implemented widely.

The following task is the recognition of human active actions in a scene. Various approaches were developed such as a boosted space–time classifier [42], a frequency-based cross-correlation [43], the histograms of spatio-temporal gradients [44], and the body parts trackers [45]. However, these tools often fail in real video data. The combined approach based on the spatial scale invariant features, the motion estimators, the region descriptions, and the multiple vocabulary trees of object-action categories is represented in [46].

4.2 *Crowd Surveillance*

The crowd monitoring became possible due to the appearance of closed-circuit television networks in public places, the increase of the computer power, and the advantages in computer vision. The security of people and monitoring of public events are gradually entrusted to automatic control systems. As it follows from the surveys on crowd analysis [47, 48] and human visual analysis [49], the crowd detection is generalized into three main ways:

- The detection of separate pedestrians from a background or a group of pedestrians. It requires a close camera position to obtain a human shape. This method cannot be applied, if a crowd is too dense and a number of occlusions is large.
- The adapted background subtraction method classifies the detected objects as pedestrian or non-pedestrian. Such technique cannot process video streams from the mobile cameras. However, it is very efficient to monitor the public places such as pedestrian zones, stadiums, or fairs, where only pedestrians are expected [50]. The use of head detector to find the best position for 3D human models with silhouette obtained via background subtraction is proposed in [51].
- The motion estimation algorithms are developed under the assumption that a crowd is never static, and an environment is non-dynamic. Two approaches, among others, are the most productive. The first one is based on a set of particles combined with an optical flow algorithm to detect the “direction” of crowd motion [52]. The second approach performs a crowd image as a texture, and the model is built as a density estimation of such “crowd texture” [53].

Ali and Dailey proposed the automatic algorithm to detect and track multiple humans in high-density crowds, in which they combined a head detector as the most reliably visible part of the human body and a particle filter for estimation of the expected human height [54]. For tracking, the AdaBoost detection cascade and a particle filter were used. For modeling, the color histograms were applied. To reduce false detections due to a non-ideal shooting, a 3D head plane method was developed that reduced false errors. This algorithm provides the unsupervised learning without any a priori extrinsic camera calibration.

4.3 *Detection of Abnormal Activities*

Detection of abnormal activities is necessary for public security and safety. The learning of an automatic system to detect the suspicious events, which would carry a potential threat, is a very hard task because of short or long duration of event, static or dynamic, involving a single human or a group of intruders. All mentioned facts are very important for security management. Some researches are devoted to detection abnormalities in crowd flows, among which are the works of Sharif and Djeraba [55], Ihaddadene and Djeraba [56], Ivanov et al. [57], Xiang and Gong [58],

and Mehran et al. [59]. A system based on unsupervised learning of motion patterns for anomaly detection and behavior prediction in a scene with multiple objects was presented in [60]. Very difficult task is to detect the rarely unusual events, i.e. to determine automatically, the current event may be interpreted as unusual with a potential threat or not [61]. We can summarize that a multi-level surveillance for detecting the threats in a crowd is a reasoning way, when, first, a video stream of crowd is analyzed for any abnormal activities and, second, a zooming visualization provides in detail a local scenario including personalization and identification of participants.

Visual detection and recognition of targets has a critical role in security systems especially at night time or in conditions with a lower illumination. The fusion technologies combining conventional television (TV) and Infrared (IR) images are well known and effective. Many systems of improved vision are built in such paradigms, when the strengths of both types of shooting provide a satisfactory image for the end-user. In research [62], Smeelen et al. consider the Gated Viewer (GV) images fused with TV or IR images. The GV systems include a time controlled camera with a pulsed laser illumination source. However, such technology works into small depths of a scene, 15–45 m.

An intelligent image fusion scheme typically uses the fusion rules. In recent years, many excellent image fusion schemes have been proposed [see, e.g. 63, 64]. Two basic approaches called the pixel-based and the region-based fusion schemes dominate. The pixel-based fusion algorithms generate a fused image defining each pixel from a set of pixels in various source images (a transform domain). The region-based fusion algorithms initially segment the input image and then select the required regions in the fused image. This approach is less sensitive to noise, produces the higher contrast images, and allows the use of semantic fusion rules. Smeelen et al. [62] proposed the weighted average and the multi-resolution fusion schemes with the corresponding fusion rules.

5 Natural Disaster Recovery

Natural disasters such as fires, earthquakes, floods, hurricanes, and tornados are the unforeseeable events and cannot be prevented. However, their effect can be minimized through warnings of population and post-disaster recovery surveillance. In such situations, Unmanned Aerial Vehicles (UAVs) are very useful for monitoring urban territories [65]. The interesting idea for collaborative urban surveillance, a crowd control, and the individuals in a crowd by using the UAVs and the Unmanned Ground Vehicles (UGVs) was proposed by Grocholsky et al. [66]. The UAVs have a global target view. However, the accuracy suffers from the speed and altitude limits and on-board sensor resolution. The UGVs demonstrate the accurate sensing capability with smaller observation range and possible object occlusions. Both the UAVs and UGVs can be considered as mutual complemented devices with fusion information technologies.

Autonomous Micro Aerial Vehicles (MAVs) are playing an increasingly important role for both civil and military purposes. The MAVs can be used in various hazardous tasks such as environment exploration, surveillance, search, disaster monitoring and relief operation, inspection of hazardous or hostile areas, without taking the risk of human lives. One of the most challenging scenarios for the MAVs is the exploration of 3D enclosed industrial and civil environments such as auditoriums, underground mines, nuclear power plants, subway stations, etc., after disasters (such as earthquakes, fire, explosions, terrorist attacks).

Li et al. [67] developed a system including the following main modules:

- The Red Green Blue-Depth (RGB-D) odometry for tracking and matching features from image and depth data of the surrounding environments captured by the Kinect sensor.
- The data fusion of a relative motion from the RGB-D with the on-board inertial measurement units for accurate estimation of the MAV velocity and position for MAV control, as well as for 3D map building.
- The 3D environment modeling uses the consecutive 3D point clouds and data fusion estimations for the path planning and the obstacle avoidance.
- The path planning generates the feasible trajectories for a good tradeoff between a human and a MAV.

However, the surveillance systems with different capabilities require the regulatory mechanisms to minimize their impacts on civil liberties. The personal information through the privacy enhancing technologies should be protected by encryption, as well as the current non-public information ought to be available to the restricted number of administrators and managers.

6 Conclusion

In this paper, it is shown that various urban scenarios can be analyzed by three-level processing with universal methods and algorithms of computer vision. However, the concrete differences also exist. They provide a “thin tuning” on traffic, people, or disaster surveillance that is very important for safety and well-being of citizens. At present, the separate surveillance systems are developed successfully. The following task is to join them in the uniform distributed information space with a reliable protection of private information and a timely notice of public information. One of the perspective approaches for visualization of video-based data is a performance of urban scenes as a virtual environment using the real data from the conventional/infrared cameras in a multi-camera mode and data from a laser locator.

References

1. Lee U, Magistretti E, Gerla M, Bellavista P, Corradi A (2009) Dissemination and harvesting of urban data using vehicular sensor platforms. *IEEE Trans Vehiclar Technol* 58(2):882–901
2. Favorskaya M, Pyankov D, Popov A (2013) Motion estimations based on invariant moments for frames interpolation in stereovision. *Procedia Comput Sci* 22:1102–1111
3. Zhao Y, Gong H, Jia Y, Zhu SC (2012) Background modeling by subspace learning on spatio-temporal patches. *Pattern Recogn Lett* 33(9):1134–1147
4. Choi JM, Chang HJ, Yoo YJ, Choi JY (2012) Robust moving object detection against fast illumination change. *Comput Vis Image Underst* 116(2):179–193
5. Lai AN, Yoon H, Lee G (2008) Robust background extraction scheme using histogram-wise for real-time tracking in urban traffic video. In: *Proceedings of 8th IEEE international conference on computer and information technology (CIT 2008)*, Sydney, Australia, pp 845–850
6. Pilet J, Strecha C, Fua P (2008) Making background subtraction robust to sudden illumination changes. In: *Proceedings of 10th European conference on computer vision (ECCV 2008)*, Marseille, France, pp 567–580
7. Favorskaya M, Pakhirka A (2012) A way for color image enhancement under complex luminance conditions. In: *Smart innovation, systems and technologies*, vol 14. pp 63–72
8. Pádua FLC, Carceroni R, Santos G, Kutulakos K (2010) Linear sequence-to-sequence alignment. *IEEE Trans Pattern Anal Mach Intell* 32(2):304–320
9. Caspi Y, Simakov D, Irani M (2006) Feature-based sequence-to-sequence matching. *Int J Comput Vision* 68(1):53–64
10. Liu Y, Yang M, You Z (2012) Video synchronization based on events alignment. *Pattern Recogn Lett* 33(10):1338–1348
11. Wang X (2013) Intelligent multi-camera video surveillance: a review. *Pattern Recogn Lett* 34(1):3–19
12. Yilmaz A, Javed O, Shah M (2006) Object tracking: a survey. *ACM Comput Surv* 38(4): article no. 13
13. Cheng ED, Piccardi M (2006) Matching of objects moving across disjoint cameras. In: *Proceedings of IEEE international conference on image processing (IPC 2006)*, Atlanta, GA, USA, pp 1769–1772
14. Schwartz W, Davis L (2009) Learning discriminative appearance-based models using partial least squares. In: *Proceedings of XXII Brazilian symposium on computer graphics and image processing (SIBGRAPI)*, Rio de Janeiro, Brazil, pp 322–329
15. Bay H, Tuytelaars T, Gool LV (2006) Surf: speed up robust features. *Comput Vis Image Underst* 110(3):346–359
16. Forssen PE (2007) Maximally stable colour regions for recognition and matching. In: *Proceedings of IEEE international conference on computer vision and pattern recognition (CVPR 2007)*, Minneapolis MN, USA, pp 1–8
17. Guo Y, Shan Y, Sawhney H, Kumar R (2007) Peet: prototype embedding and embedding transition for matching vehicles over disparate viewpoints. In: *Proceedings of IEEE international conference on computer vision and pattern recognition (CVPR 2007)*, Minneapolis, MN, USA, pp 1–8
18. Wang X, Tieu K, Grimson E (2010) Correspondence-free activity analysis and scene modeling in multiple camera views. *IEEE Trans Pattern Anal Mach Intell* 32(1):56–71
19. Liu M, Wu C, Zhang Y (2008) A review of traffic visual tracking technology. In: *Proceedings of international conference on audio, language and image processing (ICALIP 2008)*, Shanghai, pp 1016–1020
20. Cao X, Shi Z, Yan P, Li X (2013) Tracking vehicles as groups in airborne videos. *Neurocomputing* 99(1):38–45
21. Chien JC, Lee JD, Chen CM, Fan MW, Chen YH, Liu LC (2013) An integrated driver warning system for driver and pedestrian safety. *Appl Soft Comput* 13(11):4413–4427

22. Trivedi MM, Gandhi T, McCall J (2007) Looking-in and looking-out of a vehicle: computer-vision-based enhanced vehicle safety. *IEEE Trans Intell Transp Syst* 8(1):108–120
23. Klauer SG, Dingus TA, Neale VL, Sudweeks JD, Ramsey DJ (2006) The impact of driver inattention on near-crash/crash risk: an analysis using the 100-car naturalistic driving study data. In: Technical report DOT HS 810 594 of the Virginia tech transportation institute, NHTSA
24. Kircher K (2007) Driver distraction: a review of the literature. In: Technical report 594A of the Swedish national road and transport research institute
25. Cheng SY, Park S, Trivedi MM (2007) Multi-spectral and multi-perspective video arrays for driver body tracking and activity analysis. *Comput Vis Image Underst* 106(2–3):245–257
26. Wada T, Yoshida M, Doi S, Tsutsumi S (2010) Characterization of hurried driving based on collision risk and attentional allocation. In: Proceedings of 13th international IEEE conference on intelligent transportation systems (ITSC'10), Funchal, Portugal, pp 623–628
27. Wang J, Zhu S, Gong Y (2010) Driving safety monitoring using semi-supervised learning on time series data. *IEEE Trans Intell Transp Syst* 11(3):728–737
28. Baro X, Escalera S, Vitria J, Pujol O, Radeva P (2009) Traffic sign recognition using evolutionary adaboost detection and forest-ecoc classification. *IEEE Trans Intell Transp Syst* 10(1):113–126
29. Stallkamp J, Schlipsing M, Salmen J, Igel C (2012) Man vs. computer: benchmarking machine learning algorithms for traffic sign recognition. *Neural Netw* 32:323–332
30. Chang CC, Hsieh YP (2012) A fast VQ codebook search with initialization and search order. *Inform Sci* 183(1):132–139
31. Gavrila D (2000) Pedestrian detection from a moving vehicle. In: Proceedings of 6th European conference on computer vision (ECCV 2000), Dublin, Ireland, Part II, pp 2241–2248
32. Szarvas M, Yoshizawa A, Yamamoto M, Ogata J (2005) Pedestrian detection with convolutional neural networks. In: Proceedings of IEEE intelligent vehicles symposium, Nevada, USA, pp 224–229
33. Zhang G, Gao F, Liu C, Liu W, Yuan H (2010) A pedestrian detection method based on SVM classifier and optimized histograms of oriented gradients feature. In: Proceedings of 6th international conference on natural computation (ICNC 2010), Yantai, Shandong, vol 6. pp 3257–3260
34. Malagon-Borja L, Fuentes O (2007) Object detection using image reconstruction with PCA. *Image Vis Comput* 27(1–2):2–9
35. Geronimo D, Sappa AD, Lopez A, Ponsa D (2006) Pedestrian detection using adaboost learning of features and vehicle pitch estimation. In: Proceedings of 6th IASTED international conference on visualization (VIIP 2006), Palma De Mallorca, Spain, pp 400–405
36. Jones M, Viola P (2003) Detecting pedestrians using patterns of motion and appearance. In: Proceedings of IEEE international conference on computer vision (ICCV 2003), Nice, France, vol 2. pp 734–741
37. Dalal N, Triggs B (2005) Histograms of oriented gradients for human detection. In: IEEE computer society conference on computer vision and pattern recognition (CVPR 2005), San Diego, CA, USA, vol 1. pp 886–893
38. Hota VVRN, Rajagopal A (2007) Shape based object classification for automated video surveillance with feature selection. In: Proceedings of 10th international conference on information technology (ICIT 2007), Orissa, India, pp 97–99
39. Nguyen THB, Kim H (2013) Novel and efficient pedestrian detection using bidirectional PCA. *Pattern Recogn* 46(8):2220–2227
40. Favorskaya M (2012) Motion estimation for object analysis and detection in videos. In: Kountchev R, Nakamatsu K (eds) *Advances in reasoning-based image processing, analysis and intelligent systems*, vol 29. Springer, Berlin, Heidelberg, pp 211–253
41. Lucas B, Kanade T (1981) An iterative image registration technique with an application to stereo vision. In: Proceedings of 7th international joint conference on artificial intelligence (IJCAI'81), San Francisco, USA, vol 2. pp 674–679

42. Laptev I, Marszalek M, Schmid C, Rozenfeld B (2008) Learning realistic human actions from movies. In: Proceedings of IEEE conference on computer vision and pattern recognition (CVPR 2008), Anchorage, AK, USA, pp 1–8
43. Efros A, Berg A, Mori G, Malik J (2003) Recognizing action at a distance. In: Proceedings of 9th IEEE international conference on computer vision (ICCV 2003), Washington, DC, USA, vol 2. pp 726–733
44. Zelnik-Manor L, Irani M (2001) Event-based analysis of video. In: Proceeding of the 2001 IEEE computer society conference on computer vision and pattern recognition (CVPR 2001), Kauai, HI, USA, vol 2. pp 123–130
45. Park S, Aggarwal JK (2006) Simultaneous tracking of multiple body parts of interacting persons. *Comput Vis Image Underst* 102(1):1–21
46. Mikolajczyk K, Uemura H (2011) Action recognition with appearance–motion features and fast search trees. *Comput Vis Image Underst* 115(3):426–438
47. Silveira Jacques JCS, Musse RS, Jung RC (2010) Crowd analysis using computer vision techniques. *IEEE Signal Proc Mag* 27(5):66–77
48. Zhan B, Monekosso D, Remagnino P, Velastin S, Xu LQ (2008) Crowd analysis: a survey. *Mach Vis Appl* 19(5–6):345–357
49. Gerónimo D, López A, Sappa AD (2007) Computer vision approaches to pedestrian detection: visible spectrum survey. *Pattern Recogn Image Anal* 4477:547–554
50. Dong L, Parameswaran V, Ramesh V, Zoghلامي I (2007) Fast crowd segmentation using shape indexing. In: Proceedings of 11th international conference on computer vision (ICCV’2007), Rio de Janeiro, Brazil, pp 1–8
51. Wang L, Yung NHC (2009) Crowd counting and segmentation in visual surveillance. In: Proceedings of 16th IEEE international conference on image processing (ICIP’2009), Cairo, Egypt, pp 2573–2576
52. Ali S, Shah MA (2007) A lagrangian particle dynamics approach for crowd flow segmentation and stability analysis. In: Proceedings of IEEE international conference on computer vision and pattern recognition (CVPR 2007), Minneapolis, MN, pp 1–6
53. Fagette A, Courty N, Racoceanu D, Dufour JY (2014) Unsupervised dense crowd detection by multiscale texture analysis. *Pattern Recogn Lett* (2014) (in print)
54. Ali I, Dailey MN (2012) Multiple human tracking in high-density crowds. *Image Vis Comput* 30(12):966–977
55. Sharif MdH, Djeraba C (2012) An entropy approach for abnormal activities detection in video streams. *Pattern Recogn* 45(7):2543–2561
56. Ihaddadene N, Djeraba C (2008) Real-time crowd motion analysis. In: Proceedings of 19th international conference on pattern recognition (ICPR 2008), Tampa, FL, USA, pp 1–4
57. Ivanov I, Dufaux F, Ha TM, Ebrahimi T (2009) Towards generic detection of unusual events in video surveillance. In: Proceedings of international conference on advanced video and signal based surveillance (AVSS’09), Genova, Italy, pp 61–66
58. Xiang T, Gong S (2008) Video behavior profiling for anomaly detection. *IEEE Trans Pattern Anal Mach Intell* 30(5):893–908
59. Mehran R, Oyama A, Shah M (2009) Abnormal crowd behavior detection using social force model. In: Proceedings of international conference computer vision and pattern recognition (CVPR 2009), Miami, FL, USA, pp 935–942
60. Hu W, Xiao X, Fu Z, Xie D, Tan T, Maybank SJ (2006) A system for learning statistical motion patterns. *IEEE Trans Pattern Anal Mach Intell* 28(9):1450–1464
61. Stauffer C, Grimson WL (2000) Learning patterns of activity using real-time tracking. *IEEE Trans Pattern Anal Mach Intell* 22(8):747–757
62. Smeelen MA, Schwering PBW, Toet A, Loog M (2014) Semi-hidden target recognition in gated viewer images fused with thermal IR images. *Inform Fusion* 18:131–147
63. Zaveri T, Zaveri MA (2011) A novel region based multimodality image fusion method. *J Pattern Recogn Res* 6(2):140–153
64. Krishnamoorthy S, Soman KP (2010) Implementation and comparative study of image fusion algorithms. *Int J Comput Appl* 9(2):25–35

65. De Filippis L, Guglieri G (2012) Path Planning strategies for UAVs in 3D environments. *J Intell Rob Syst* 65(1):247–264
66. Grocholsky B, Keller J, Kumar RV, Pappas GJ (2006) Cooperative air and ground surveillance. *IEEE Robot Autom Mag* 13(3):16–25
67. Li Q, Li DC, Wua QF, Tang LW, Huo Y, Zhang YX, Cheng NL (2013) Autonomous navigation and environment modeling for MAVs in 3-D enclosed industrial environments. *Comput Ind* 64(9):1161–1177

Traffic and Pedestrian Risk Inference Using Harmonic Systems

I. Acuña Barrios, E. García, Daniela López De Luise, C. Paredes,
A. Celayeta, M. Sandillú and W. Bel

Abstract Vehicle and pedestrian risks can be modeled in order to advise drivers and persons. A good model requires the ability to adapt itself to several environmental variations and to preserve essential information about the area under scope. This paper aims to present a proposal based on a Machine Learning extension for timing named Harmonic Systems. A global description of the problem, its relevance, and status of the field is also included.

Keywords Risk prediction · Harmonic systems · Time mining

I. Acuña Barrios · E. García · D.L.D. Luise (✉) · C. Paredes · A. Celayeta · M. Sandillú ·
W. Bel

Researcher at CI2S Lab, Pringles 10 2nd FL, C1183ADB Buenos Aires, Argentina
e-mail: mdl1@ci2s.com.ar

I. Acuña Barrios
e-mail: acunai@ci2s.com.ar

E. García
e-mail: egarcia@ci2s.com.ar

C. Paredes
e-mail: cparedes@ci2s.com.ar

A. Celayeta
e-mail: ecelayeta@ci2s.com.ar

M. Sandillú
e-mail: msandillu@ci2s.com.ar

W. Bel
e-mail: wbel@ci2s.com.ar

1 Introduction

Traffic bottlenecks and environmental hazards are a big concern [1–4]. This problem, that affects many cities in the world, is very complex and carries many consequences. Among others, collisions involving pedestrians. They are a leading cause of death and injury in many countries [1, 2]. Risk in roads is high for vehicles and for pedestrians, who are considered vulnerable due to their lack of protection and limited biomechanical tolerance to violent forces if hit by a vehicle [5].

The risk of pedestrian injuries is increased by a number of factors that relate to the road environment, including:

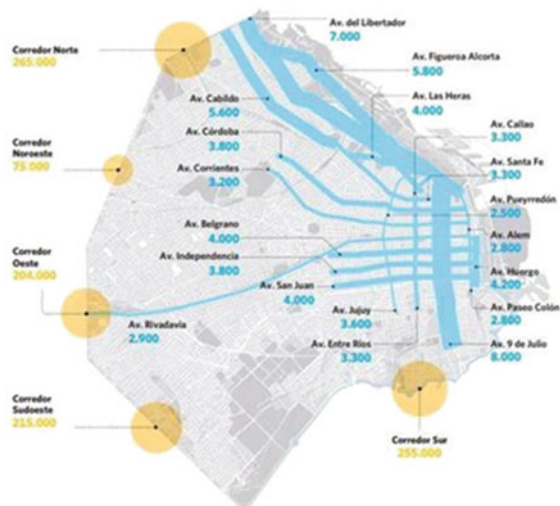
- High speed of traffic (increases severity)
- Poorly maintained, obstructed footpaths
- Inadequate crossing facilities
- Lack of pedestrian crossing opportunities (traffic volume)
- Number of lanes to cross
- Complexity and unpredictability of traffic movements at intersection
- Inadequate separation from traffic
- Poor crossing sight distance.

The city has certain key locations for vehicle inputs and movement. In Fig. 1 there is a map showing those places that are relevant.

Orange dots represent the input locations, with the amount of transportation in numbers. The thickness of the blue lines indicates the number of vehicles moving in every main street. The precise numbers are detailed in blue, next to every road.

There are many studies that precede this project and serve as a basis for it. Among others, Cathy evaluated the incidence age of pedestrians [6], but organizations like

Fig. 1 Buenos Aires traffic flow



Transport for London Surface (TFL) [7] consider more subtle tips such as crowd management, pedestrian attitudes, and footway width. The same happens in [8]. The approach explained in this paper uses criteria like these.

It also deserves to mention the proposal in [9] that aims to pay more attention to other traffic-related actors and suggests modifying the physical environment. In [10] there is an interesting set of tips listed, many of them related to the same idea of [9]. In [11] indirect risk ranking is mentioned, in order to find the most reliable measures for safety improvement of pedestrian crossings. The Swinburne University of Technology [12] developed a Traffic Management Hazard Identification and Risk Assessment Control Form, that checks relevant causes and events related.

Although certain authors [13, 14] consider education and prevention initiatives as the best way to decrease mortality, there are many prototypes. It can be mentioned of the G20/OECD methodological framework on disaster risk assessment and risk financing [1]. In [15] there is a proposal to develop a novel approach to assessing the risk of collision with a pedestrian based on the scenario and the behavior of the pedestrian. The risk assessment is based on extensive off-line Monte Carlo simulations relying on a simple, yet representative, stochastic model of the pedestrian. A Pedestrian Data System for Safety Analyses [16] uses national/local censuses, surveys of travel and activity, pedestrian monitoring systems, public transport tracking systems, counts, and surveys and generates the estimation of pedestrian exposure for Melbourne.

In [17] there is a case-control approach and GIS Methods to inform pedestrian safety policies regarding the environmental characteristic of locations associated with higher collision risk, and to guide road design safety standards for environments where walking is a common mode of travel.

The micro-simulation model with surrogate safety assessment model (SSAM, developed by FHWA, USA) [18] assesses the risk of intersection traffic accident using a prediction model developed for USA. The micro-simulation model is based on a safety analysis using vehicle trajectories produced during the simulation. The trajectory data provide vehicle's position, speed, and acceleration for user-defined time resolution.

In reference [19] a methodological tool is presented: a tailor-made statistical tool to identify whether there is a relationship between a set of potential risk factors and accident involvement or accidental injury.

Journey risk management (JRM) [20] is a system that tracks images and information toward understanding interactions between causes and devising a pre-journey advice module for road users undertaking highway journeys. The complete list of prototypes and proposals is very long and is not under the scope of this work.

As a consequence of the multiple analyses and the evolution of several systems, there are many useful findings to design a ubiquitous model for traffic and pedestrian risks. For instance, in [21], authors perform statistics and define exposure as the product of the numbers of pedestrians and vehicles observed in the same section in the same 5-min. interval. Other approaches are traditional averages or simple sex-specific weighted averages [22].

This paper describes a proposal based on Harmonics Systems [3], an approach that takes events as data vectors that can resonate certain patterns and consequently fire-specific modeling features. This is a kind of plastic, flexible, and self-trained learning from data. A resonance in this context can be thought of as a pattern matching with weighted features and changing patterns. This modeling approach is being applied as the KRONOS prototype, an Intelligent System for pedestrian and car risk evaluation. Additionally, the model allows rendering advices for intersection of streets, and any other place in a map under the system's control.

As the prototype is still under construction, it is not possible to perform real tests. Therefore, statistical evaluation is not under the scope of this paper.

The following sections describe the status and relevance of traffic and pedestrian security (Sect. 2), the overall architecture of KRONOS prototype (Sect. 3), a general presentation of the model knowledge inferred (Sect. 4), and conclusions and future work (Sect. 5).

2 Traffic and Pedestrian

Intelligent systems (IS), like Kronos, have been used in the past after several years as a complement of traditional methods. They reached also the transport field, playing a key role in these last years and will become the most promissory industry in the next years and will be an important part of transportation and infrastructure sectors [23, 24].

Kronos is a smart system that can assess the risk for accidents in certain locations, advise alternate paths and learning dynamically from contextual information. Due to the high number of human beings lost it is intended to avoid or reduce crashes and any other accidents and thereby the number of victims [25]. For that reason we consider it is relevant to be able to have a system that is able to detect anomalies and risks on the fly. According to Dr. Pablo Martínez Carignano, chair of the public guard of Buenos Aires city, users most vulnerable are pedestrians: about 30 % of deaths in traffic accidents. Furthermore, he explained that bikers' deaths increased by 300 % between years 2004 and 2010 due to the increase of bottlenecks in main cities of the country [26].

Almost 3500 persons die every day in streets, and about 100,000 persons are injured. This way traffic is one of the most important causes of death in the world, with 1.3 million deaths every year, as claimed by the World Health Organization. For that reason, traffic accidents may be considered as epidemic. Ninety percent of deaths for this reason take place in locations with medium to low income.

In India, the number scales to 160,000 persons per year (400 every day); in Brazil it is 38,000 (100 every day); and in Mexico 28,000 (75 every day). As a consequence it may be concluded that traffic and risks in the streets are one of the most important problems [27].

The problem requires a system to evaluate risks using local and specific information and most probably, a business model that works on a customer-requirement

basis. It could be available not only for public institutions but also for individuals. The prototype is intended to give the user different alternatives for preventing the traffic bottlenecks and accidents in crucial streets of a city.

The service will require information that can be provided regularly by other institutions, such as:

- Location information of every vehicle accident
- Programmed events that may alter the throughput of the transit
- Information about semaphores
- Information about public transportation.

Besides, it will be mandatory to compile and keep updated the map of the streets.

Those information requirements may be covered by hiring personnel or by paying a third party company.

3 Architecture Description

The design corresponds to a smart system to avoid transit accidents. It is very important, because it provides possibilities to prevent dangerous streets intersections, that increased day by day varying during the day; and this way avoids a chaos in the traffic. Furthermore, every day there are more vehicles in the streets of many cities in the world, which generates a reduction of the control of possibilities at the vehicle traffic.

Because of this, it is very important to fulfill the needs of society, in terms of road safety, because at present this situation affects, directly or indirectly, too many people; and thus protects their life considerably, avoiding unnecessary danger.

The architecture is based on a few modules that are presented in the diagram of Fig. 2.

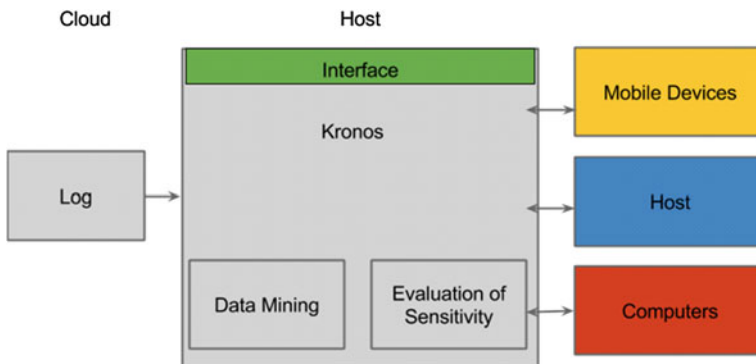


Fig. 2 Kronos architecture

The key features of every component are described in the following sections with more details.

A. Cloud

It is the main source of information. In the graphic it is represented by a log, extracted from any device in the cloud (a web server, web services, a local server, or other host); it is converted into an array vector, that is processed using an Advanced Data Mining Approach, based on the Kronos project [23].

The implementation is an Apache Tomcat (c) as Servlet container for accessing web servers or web services. PostgreSQL (c) in the case where the logs are in the local host.

B. Host

The core of Kronos is a Harmonic System based on real-time data prediction [3], applied to a particular field: dangerous intersections generated from traffic problems.

- **Evaluation of Sensitivity:** The proposal is based on the “Harmonics Systems for Time Mining” Theory [23], which first analyzes and evaluates the time patterns. Later on, it applies pattern matching (resonance), to dynamically build a model.
- **Interface:** It is the place for data customization. Through this channel, the devices communicate with Kronos. It constitutes a friendly environment, making it simple for the user to interact with the system. The technology uses Java Development Kit, for programming the modules.
- **Data mining:** Several traditional algorithms are implemented to produce intermediate results with Java Development Kit, for programming the modules.
- **Kronos:** Implements the core of the Harmonic Systems using Java Development Kit, for programming the modules.

C. Devices

There are two mobile devices:

- One designed to use “Android Flow Monitoring—Flowoid”, that supports mobile users.
- The other called “Location—LOCS”, that is used for finding the user’s location. It can receive information and notifications about dangerous locations, depending on the current position.

D. Special remarks

The WEB may be used as another market target of the information by using personal email accounts and providing customized information.

In all the cases it may be possible to insert Adds along with the information.

4 Model Support

The model has to learn using the techniques described in [23]. To show the complexity of the model, the following is a list of some rules automatically learnt from data.

System Traffic information balance [22], patterns of injury considering age and gender, typified risk factors [28], main risk factors [3, 21], driver conditions [11], sidewalks, intersections, curbs, ramps, and landings for people with disabilities, bicycles [16], opportunities for crashes and conflicts [10], are some of the sources of general information and validation criteria.

In Tables 1, 2, 3, and 4 there are some of the rules that handle the system: they relate to car conditions, weather, driver conditions, corners/intersections [29], and risk.

It is important to note that although many considerations have to be taken into account, the model successfully learned a global risk assessment using the main risk factors as grouped into the following types [28]:

- Factors influencing exposure to risk
- Factors influencing crash involvement

Table 1 Relationship between car conditions and risk

If	Then
(car.speed > 120) and (car.zone = 1) and (num.car > 10) and (car.time => wheater.sunset)	car.risk.level = HIGH car.risk.description="You exposed a risk accident" car.risk.type = 1
(car.lightning = false) and (car.breaking = false) and (car.documents = false)	car.risk.level = HIGH car.risk.description = "You exposed an risk accident" car.risk.type = 1
(car.dimensions >= (4365,2113,1639)) and (car.velocity >= 30 km/hs)	car.risk.level = MEDIUM car.risk.description = ("You're exposed to the risk of a severe accident") car.risk.type = 3

Table 2 Relationship between weather conditions and risk

If	Then
(wheater.visibility < 15 km) and (weather.wind > 30 km/hs) and (car.time > weather.sunset)	car.risk.level = HIGH car.risk.description = "The weather and time, you exposed an risk accident" car.risk.type = 2
(accident.state = true) and (acciden.crossing = false) and (traffic.num => 10)	car.risk.level = LOW accident.description = "An accident took place close to a crossing, but not exactly at a crossing" car.risk.type = 4

Table 3 Relationship between driver conditions and risk

If	Then
(individual.alcohol < 0.15) and (car.time > weather.sunset)	car.risk.level = LOW individual.alcohol.level = LOW individual.risk.description = "You're perfects conditions" individual.risk.type = 0
(individual.alcohol > 0.15) and (car.time > weather.sunset)	car.risk.level = LOW individual.alcohol.level = LOW individual.risk.description = "You experimented decreased reflexes" individual.risk.type=1
(individual.alcohol > 0.20) and (car.time > weather.sunset)	car.alcohol.level = LOW individual.alcohol.level = LOW individual.alcohol.description = "Decreased reflexes, dysmetria, and velocity underestimation" car.alcohol.type = 1

Table 4 Relationship between intersection conditions and risk

If	Then
(intersectionstreets.walk-signals = false) and (intersectionstreets.sidewalks-sections = false) and (intersectionstreets.lightnings-cross = false)	car.risk.level = MEDIUM car.risk.description = "Have a problem in intersection streets.zone" car.risk.type = 2
(driver.alcohol > 0.15) and (car.time > weather.sunset)	car.risk.level = LOW car.risk.description = "You experimented a decreased reflexes" car.risk.type = 1
(driver.alcohol > 0.20) and (car.time > weather.sunset)	car.alcohol.level = LOW car.alcohol.description = "Decreased reflexes, dysmetria, and velocity underestimation" car.alcohol.type = 1

- Factors influencing crash severity
- Factors influencing post-crash injury outcomes

Exposure was defined as the product of the numbers of pedestrians and vehicles observed in the same section in the same 5-min interval [21].

5 Conclusion and Future Work

There are a number of approaches to evaluate pedestrian and car risks, and many proposals to reduce them. Many authors agree that it is convenient to provide risk information and to give advice about alternate paths in advance. The proposal mentioned in the KRONOS prototype is to perform an automatic learning modeling

from several well-known rules of practice, mining statistics from the environment, and external devices. As the prototype is still under construction, it is not possible to perform on-site tests and statistical evaluation of the performance.

References

1. OECD. Organization for economic co-operation and development (OECD) (2014). <http://www.oecd.org>
2. Alex Quistberg D, Jaime Miranda J, Ebel B (2010) Reducing pedestrian deaths and injuries due to road traffic injuries in Peru: interventions that can work. *Revista Peruana de Medicina Experimental y Salud Pública. Rev Peru Med Exp Salud Publica* vol 27, n. 2 Lima Apr/Jun 2010. ISSN 1726-4634. <http://dx.doi.org/10.1590/S1726-46342010000200014>
3. López De Luise D (2013) Harmonics systems for time mining. *Int J Mod Eng Res (IJMER)* 3 (6):2719–2727. ISSN: 2249-6645
4. Wash O (1998) Assessing pedestrian risk locations : a case study of WSDOT efforts. Department of Transportation. Washington State Library. Electronic State Publications
5. Oxley J (2004) Improving pedestrian safety. Curtin—Monash Accident Research Centre. Fact Sheet No. 6
6. Cathy T, Packman D (1995) Risk and safety on the roads: the older pedestrian. Foundation for Safety Research. New Castle University
7. TFL (2012) Transport for London surface. Transport roads directorate guidance on the assessment of pedestrian guardrail. SQA-00234
8. TSO (2009) Generic risk assessment 4.1. TSO Publisher. www.tsoshop.com.uk
9. Rodríguez-Hernández M, Campuzano-Rincón J (2010) Primary prevention measures for controlling pedestrian injuries and deaths and improving road safety. *Revista Salud Pública. Rev. salud pública* vol 12, no. 3
10. Thomas L, Hamlett C, Hunter W, Gelinne D (2009) Final report to North Carolina department of transportation. North Carolina Department of Transportation, Traffic Engineering and Safety Systems Branch
11. Antov D, Rõivas T, Antso I, Sürje P (2011) A method for pedestrian crossing risk assessment. *Trans Wessex Inst.* doi:[10.2495/UT110501](https://doi.org/10.2495/UT110501)
12. Traffic Management Hazard Identification & Risk Assessment Control Form (2009) Swinburne University of Technology. <http://www.docstoc.com/docs/24507714/Traffic-Management-Health-Safety-Checklist>
13. Hart J (2004) Measuring pedestrian risk and identifying methods to prevent pedestrian accidents in langley park. National Fire Academy
14. Health and Safety Comission (2001) Reducing at-work road traffic incidents. Report to Government and the Health and Safety Commission, DTLR
15. Alavi H, Charlton J, Newstead S, Archer J (2014) A pedestrian data system for safety analyses. Monash University Accident Research Center (MUARC), Melbourne, Victoria, Australia
16. De Nicolao G, Ferrara A, Giacomini L (2007) On-board sensor-based collision risk assessment to improve pedestrians' safety. *IEEE Trans Veh Technol* 56(5):2405–2413. doi:[10.1109/TVT.2007.899209](https://doi.org/10.1109/TVT.2007.899209)
17. Jiao J, Moudon A Using a Case-control approach and GIS methods to assess the risk of pedestrian collision in Seattle, USA
18. Kim K, Sul J (2001) Development of intersection traffic accident risk assessment model transportation & environment research institute Ltd. kijoonkim@hotmail.com, 82-(0) 2-10-8752-1851

19. Hautzinger H (2007) Analysis methods for accident and injury risk studies. Project No. 027763 TRACE. Deliverable 7.3.2007
20. Journey risk management® (JRM®). <http://www.irte.com/journey-risk-management.html>
21. Cameron MH (1982) A method of measuring exposure to pedestrian accident risk. *Accid Anal Prev Elsevier* 14(5):397–405
22. Chisholm D, Naci H (2008) HSF discussion paper road traffic injury prevention: an assessment of risk exposure and intervention cost-effectiveness in different world regions. World Health Organization. Department of Health Systems Financing
23. López De Luise D (2012) La tecnología al servicio del transporte inteligente. ITS Argentina, n. 86
24. María J (2012) Improvements on the enforcement process based on intelligent transportation techniques. Model and mechanisms for electronic reporting, offense notification and evidence generation. Universidad Carlos III de Madrid
25. Quinti D (2013) Más autos y atascos en la calle, y crecen los tiempos de viaje. *Clarín Ciudades*. http://www.clarin.com/ciudades/atascos-calle-crecen-tiempos-viaje_0_955704555.html
26. Leonetti J (2013) La voz del tránsito. *Control de Transito*. <http://www.controldetransito.com.ar>
27. Bazán B (2013) El Metrobus porteño entre los peores del mundo. *PropAMBA*. <http://propamba.wordpress.com/2013/10/16>
28. Indian Institute of Technology and WHO (2006) Risk factors for road traffic injuries. Transport Research and Injury Prevention Programme (TRIPP). Training Manual
29. <https://www.cesvi.com.ar/revistas/r87/alcohol.pdf>

Part III
Modeling and Applications

The Electronic Verification of the Weight and the Amount of Food Consumed by Animals in a Farm

Doru Anastasiu Popescu and Nicolae Bold

Abstract In this paper we will present a modality of controlling the quantity of food that animals eat in a farm. This would be a very efficient way of determining if an animal part of the effective has problems concerning the food and to establish the type of problem that is faced by it. The application would be an important aid for those who run currently a business of this type, apart from the visual control that can be made easier, in case of the situation where animals are fewer and bigger, or harder, when the number of animals is larger. The amount of food consumed by an animal and the weight of the animal are the main parameters that are measured by sensors in order to collect information for each of them and to determine when a problem appears. In both cases of an infectious disease or a not infectious, but dangerous one, contracted by the animal, the possibility of spreading the disease would be little, and respectively the problem would be signaled faster and prompter.

Keywords Weight · Food · Sensor · Livestock · Bovines · Farm management

1 Introduction

The control of the food that animals consume is very important because this is the variable that shows the state of the health of an animal, apart from the weight of the animal. Generally, an animal consumes food regularly and it is not eaten if the

D.A. Popescu (✉)

Faculty of Mathematics and Computer Sciences, University of Pitesti,

Pitesti, Romania

e-mail: dopopan@yahoo.com

N. Bold

University of Agronomic Science and Veterinary Medicine of Bucharest,

Slatina Branch, Bucharest, Romania

e-mail: bold_nicolae@yahoo.com

animal has a problem. In this matter, this application uses two variables (the weight of the animal and the quantity of food left after consumption) to determine if a disease or any other type of problem exists. The application is usable for larger animals. In this article the example of bovines was taken.

These types of systems are also used in health domains, for elders living alone, the problem being studied for many years and in many articles such as [1–3].

Section 1 presents a short introduction of the article.

In Sect. 2 general notions that characterize animals and their behaviour, including the types of food and growth, will be presented. These are very important because they are implicated in the process of the livestock.

The components of the system of monitoring will be shown in Sect. 3. The room, sensors and the software will be detailed in this section to create an impression of the whole system.

The model of the process will be discussed in Sect. 4. A description and several schemes will be given here. The mathematical model of this problem is presented in Sect. 5. A study case will be presented in Sect. 6.

In the end, conclusions and future work for this system will be presented in Sect. 7.

2 Notions Regarding Animals and Their Behaviour

Because of the fact that we are studying in particular the large animals, bovines more exactly, we should remind one of several facts regarding their growth, the types of food consumed or characteristics related to the shelters.

In the beginning, we can say that two major types of growth systems exist: semi-opened systems, where animals can move inside the shelter, and closed systems, separate boxes for each animal. We should not also forget about the ecological growth of the animals, which has different principles [4].

The medium weight of bovines is included in the interval 600–650 kg. In the closed system, the minimum space per bovine is approximately 1.5 m. The principal types of food consumed by the animals are grits (formed, for example, from corn, fodder wheat, wheat bran, sunflower meal and concentrates), fodder, hay, corn, barley, oat, alfalfa or pasturage (directly from the grassland).

We should also differentiate the purpose of the growth of bovines. In this matter, the bovines are raised for milk or for their meat. This classification leads to different needs for animals, different ratios for food, even a distinct schedule and different rates of growth.

The most known breeds of bovines are presented in the next list:

- bovines grown for milk: e.g. Holstein, Romanian Spotted
- bovines grown for meat: e.g. Angus

We should also consider that animals have a schedule established by their own needs and the type of livestock (the purpose for which the animals are grown).

These are few characteristics of livestock, particularly the growth of bovines which would help in the process of the system.

3 General Components of the System

The system consists of three major components, presented schematically in Fig. 1, each of them having its own features. Generally, the system is formed of the room where the animals live, the place where the equipment is placed. Composed of several sensors, the hardware part is the one that helps in the process of collecting data. The software interprets the information received from the sensors and draws the principal lines for acting in case of problems. They will be presented separately in each subchapter and detailed in order to emphasize their importance. According to Bamis et al. [1], a system must respond to tasks such as: queries (in our case, what is the weight of the animal and the quantity of food left), alarms and notifications, detection of the anomalies, recognition of specific events and actuation. In a simpler classification of tasks, the system:

- (a) Observes the animals
- (b) Uses data (interpret)
- (c) Gives answers to the tasks listed above

It is also extremely important that the equipment must not agitate the animals, because it can alter the measurement or there may exist damages or deterioration that make sensors unusable, conducting to false results, a consequence that brings further costs, extra stress and false alarms for the owner, the products being contaminated with stress products from the animal. Also, the room should not be packed with sensors [1], for the reasons presented above, and, at the same time, not

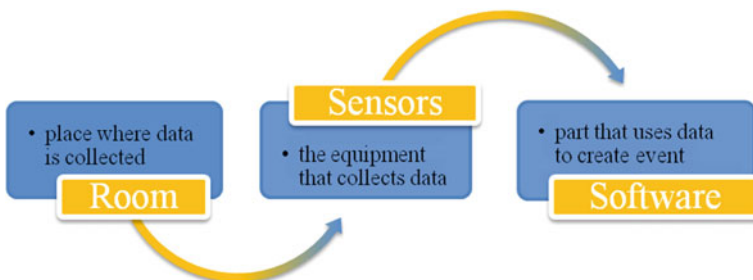


Fig. 1 Components of the system

to aggravate the activity of the farm, breaking the laws related to this area at the same time.

3.1 *The Room*

Considered very important in the process of livestock, the room (stable) is characterized by specific parameters, like temperature, percentage of oxygen or light. In ecological livestock, because of the nature of agriculture, the farmers renounce the room in the daytime—the animals are usually held outdoors—and, as a result, the parameters can be measured with more difficulty.

It is the place where animals eat, sleep and make the actions that they need to do in order to make a living. Generally, the room consists of a stable with separate boxes for each animal, depending on the type of livestock, in case of bovines and horses, or in halls and boxes for birds (especially hens and chickens for meat). These places give data (in our case, the weight of the animal and the quantity of food consumed by it), values that are very important because they give an image of the condition of the health of the animal.

3.2 *Sensors*

The equipment or, simpler, the sensors, are those which measure specific parameters. The sensors that are commonly used in domains like nursery are PIR (passive-infrared) and image sensors [1]. Using these types of sensors leads to the fabrication of new sensors, called macroscopic sensors [5], which are derived from patterns obtained from gross information. The macroscopic sensors are a matter of routine and they are used to observe abnormal behaviour, a fact that could mean that the animal would have contracted a disease; these types of sensors are strongly related to the respecting of the schedule. In this case, weight sensors will be used and, in this matter, a special attention must be given to weight sensors, because they are extremely important for obvious reasons (they must measure this parameter).

Sensors would be placed where the animals are milked in the case of animals grown for milk or in a place where animals go together for the calculation of the weight of the animal and under the spaces where food is stored and eaten for the determination of the weight of the food left by every animal. They could even be placed in the floor of the establishment—therefore they are recommended to be wireless sensors, because the equipment would be more effective.

3.3 Software Components

This component is a very important one, given the fact that here are displayed the results and the notifications and alarms are being shown. It consists of a program that uses the data collected from the equipment and interprets it in order to actuate and recognize events. The input data is taken from specified files, obtained from sensor measurements, processed and a message is displayed.

The software component will be presented in the next rows.

The main window contains a menu and three tabs, one for the short description of the application, the second for the verification of the weight of the animal and the third one allows the user to find the amount of food consumed by each animal.

As it can be seen, the application shows a rough scheme of the stable and the boxes and where problems are found they are represented in a red colour. If problems do not appear, the box is represented in blue. Also, for each red box the weight of the animal is shown and the difference from the normal weight is calculated, as it can be seen in Fig. 2.

The same method is applied for the calculation of the food consumed by the animal and the output is shown in Fig. 3.

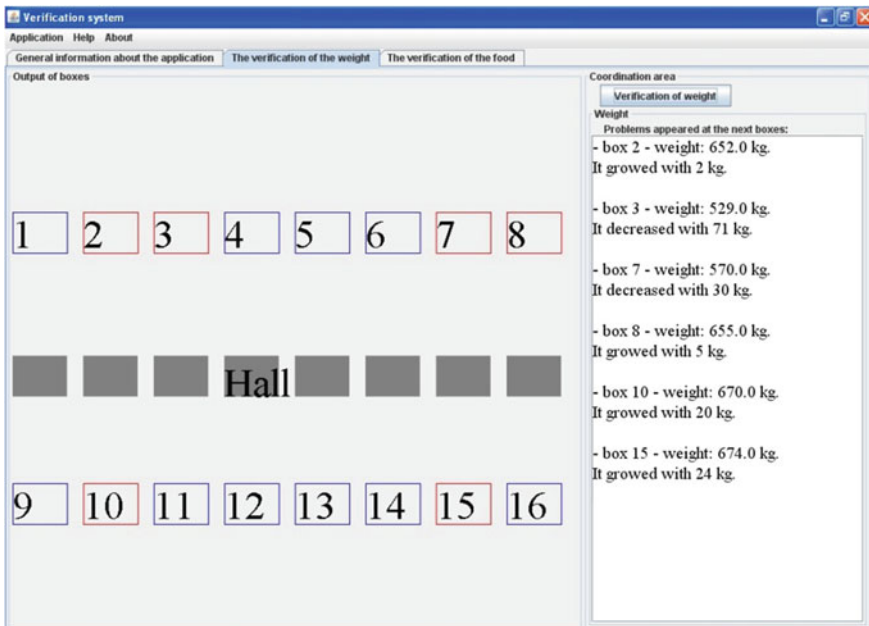


Fig. 2 Software output for weight measurement

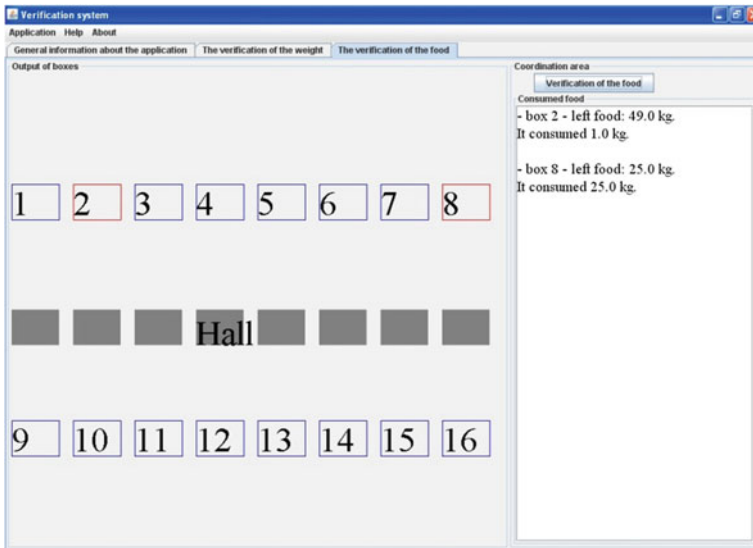


Fig. 3 Software output for food measurement

4 The Animal Monitoring Model

We will present the model in the next rows. It uses the amount of food consumed by the animal and its weight as input data and the results obtained will consist of a warning in case of a problem or a message if there is not a problem.

- Step 1. Sensors take the data that is needed and the files that contain it are filled out with the quantity of food and, respectively, the weight of the animal
- Step 2. The input data are taken from files and compared with determined values (e.g. in case of a particular animal, the amount of food consumed is known previously by the farmer)
- Step 3. If problems appear, a message with a warning containing the location and other information will appear
- Step 4. If there are no problems, a message of confirmation will appear

The utility can be run periodically, helping the manager to take decisions and solving problems that can strike.

The data contains details about the location (number of the box, the number of the hall), weight of the animal and the quantity of food left to eat.

It could be used as an alternative using motion histogram, as in [2, 5, 6]. This is used in medicine, nursing or other domains studied in articles such as [3, 7–9]. This

histogram detects the presence of the motion and its size. This type of measurement can bring the opportunity to create relative motion patterns or routines, [1, 10], used to detect anomalies in a schedule of an animal and, in this way, is a very precise modality of the identification of the problems (for example, an animal which does not come to eat may have a possible physical problem). This alternative would consist in a future work and will be used for measuring other types of parameters.

5 The Mathematical Method

We will formalize below the model used in the monitoring application. To do so, we number the animal rooms $1, 2, \dots, n$, and the animals $1, 2, \dots, n$ (the animal i is in the room i , $i = 1, 2, \dots, n$). The areas where the animals eat will be numbered $1, 2, \dots, m$. An animal can only eat from a single area ($n \leq m$).

At each time point t , because of the sensors we know the weight of each animal and the amount of food in each area. Thus, we can define five functions:

$F_t : \{1, 2, \dots, n\} \rightarrow R$, $F_t =$ weight of the animal i at the time t .

$C_t : \{1, 2, \dots, n\} \rightarrow R$, $C_t =$ the amount of food remaining in the area $Z(i)$ at time t .

$Z : \{1, 2, \dots, n\} \rightarrow \{1, 2, \dots, m\}$ is an injective function, $Z(i) =$ the number of the zone where the animal numbered i eats, $i = 1, 2, \dots, n$.

$X_t : \{1, 2, \dots, n\} \rightarrow R$, $X_t(i) =$ the normal weight the animal i should have at the time t , $i = 1, 2, \dots, n$.

$Y_t : \{1, 2, \dots, m\} \rightarrow \{1, 2, \dots, m\}$, $Y_t(i) =$ the minimum amount that may remain in the area i at time t .

For rigorous control of animal development, it is preferable to use, from experience, t values in the set $\{0, 1, 2, \dots, 24\}$, i.e., checking every hour of the day.

For a given t , $F_t(i)$ and $C_t(i)$ are calculated using the sensors, $i = 1, 2, \dots, n$.

The algorithm underlying the application from Sect. 3 checks for different values of t if there is at least one of the following situations:

- There is i in $\{1, 2, \dots, n\}$ with the property that $|F_t(i) - X_t(i)| > V_i$, where V_i is the maximum tolerance approved by studies conducted so far.
- There is i in $\{1, 2, \dots, n\}$ with the property that $C_t(i) > Y_t(Z(i))$.

Statements previously presented are displayed with corresponding details using the data structures which contain the values used in the previously defined functions.

6 Case Study

We are studying in this section data regarding a specific disease that is dangerous and infectious, tuberculosis having the potentiality to infect people too (it is a zoonosis). We can count among the symptoms of tuberculosis the loss in weight, a parameter that the application monitors. In this way, the infected bovines can be found quickly. We present in the next rows some statistical data about tuberculosis infections in the United Kingdom [11], the situation being presented in Fig. 4.

The total number of bovines in the UK is presented in the next graph (in the period between 2008 and 2012 years, Fig. 5) [12].

In a short account, we observe that the disease infected between 0.3 and 0.4 % from the total population of bovines. Based on this case study and taking into account that an average weight of a bovine is included in the interval 600–650 kg, we created artificially generated data for a farm of 20 bovines. The results are shown in Fig. 6.

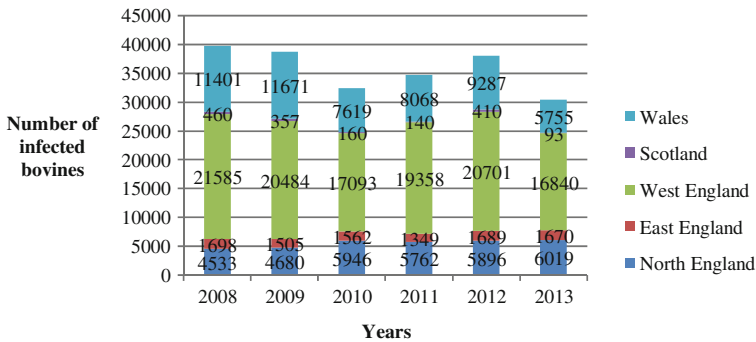


Fig. 4 Number of bovines infected with tuberculosis (TB) in the United Kingdom (2008–2013)

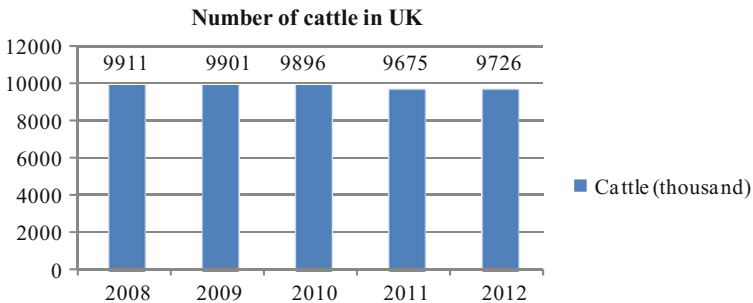


Fig. 5 Number of bovines in the United Kingdom (2008–2012)

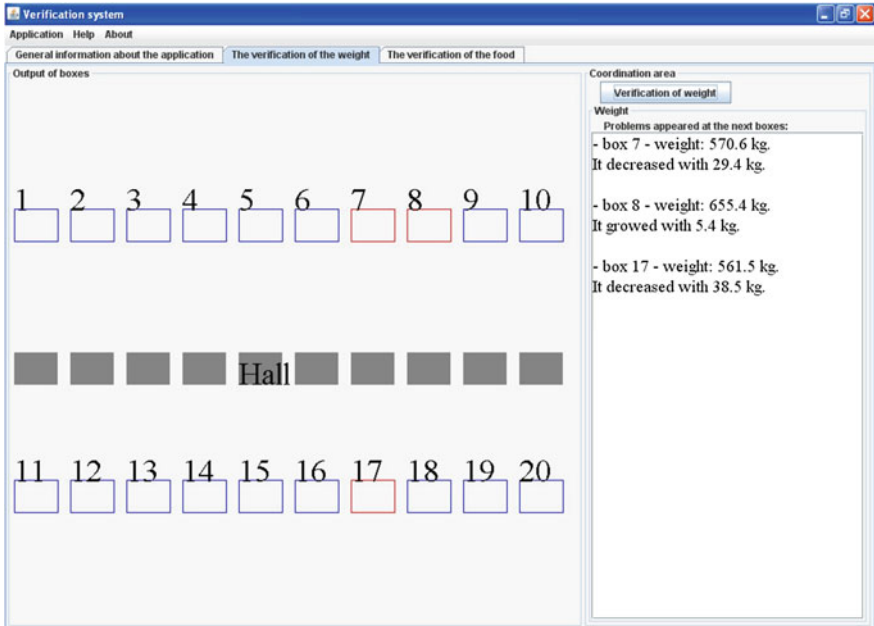


Fig. 6 The software output for the example mentioned above

7 Conclusions

As we reminded in the Introduction, the control of the condition of the animals is very important because it keeps a clear view of the general state of the animals in a farm. The diseases can be signalled in a reasonable time and the infection would not be spread. At the same time, a faster signalization leads to a wide range of treatments, a prompter reaction for the competent authorities, less important negative consequences for the animal and the avoidance of financial loss for the business. For these reasons, this application tries to help the manager or the farmer to signal a problem faster than usual. The types of systems as those presented in the literature can increase autonomy and independence while minimizing risks [1] (Fig. 7).

A future task that could be accomplished would be the extension of the application for smaller animals, the ones stocked in a semi-opened system or in the case of the animals which are grown in common (such as the chickens for meat). The software component could also be developed, leading to a more precise measurement or a better design.

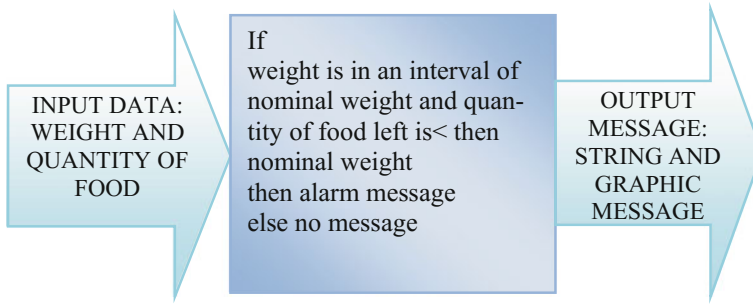


Fig. 7 A scheme for the mathematical model

The measurement can raise some questions regarding the stress created by the modality of weighting for the animals. In this matter, this process is designed not to stress the animals or, in the worst case, to keep the stress in the lowest rates.

References

1. Bamis A, Lymberopoulos D, Teixeira T, Savvides A (2010) The BehaviorScope framework for enabling ambient assisted living. *Int J Pers Ubiquitous Comput* 2–3
2. Bamis A, Lymberopoulos D, Teixeira T, Savvides A (2008) Towards precision monitoring of elders for providing assistive services. In: *International conference on pervasive technologies related to assistive environments (PETRA'08)*, p 4
3. Lymberopoulos D, Bamis A, Savvides A (2008) Extracting spatiotemporal human activity patterns in assisted living using a home sensor network. In *PETRA'08: Proceedings of the 1st international conference on pervasive technologies related to assistive environments*. New York, NY, USA pp 2, 6
4. <http://www.recolta.eu/arihiva/cresterea-si-exploatarea-bovinelor-in-conditii-ecologice-9424.html>
5. Bamis A, Fang J, Savvides A (2010) Poster abstract: discovering routine events in sensor streams for macroscopic sensing composition. In: *Proceedings of the 9th ACM/IEEE international conference on information processing in sensor networks*, p 408 (IPSN 2010)
6. Teixeira T, Savvides A (2007) Lightweight people counting and localizing in indoor spaces using camera sensor nodes. In: *First ACM/IEEE international conference on distributed smart cameras, ICDSC'07*, pp 36–43, Sept 2007
7. Ivanov YA, Bobick AF (2000) Recognition of visual activities and interactions by stochastic parsing. *IEEE Trans Pattern Anal Mach Intell* 22(8):852–872
8. Moore D, Essa I (2002) In *Recognizing multitasked activities from video using stochastic context-free grammar*. Menlo Park, CA, USA, AAI, pp 770–776
9. Ogale AS, Karapurkar A, Aloimonos Y (2005) View-invariant modeling and recognition of human actions using grammars. *ICCV'05*, Oct 2005
10. Heierman E, Youngblood M, Cook DJ (2004) Mining temporal sequences to discover interesting patterns. In: *KDD workshop on mining temporal and sequential data*
11. <http://www.parliament.uk/briefing-papers/sn06081.pdf>
12. https://www.gov.uk/government/uploads/system/uploads/attachment_data/file/183227/defra-stats-foodfarm-landuslivestock-farmstats-dec2012-130314.pdf

FEM Modeling of Some Raising Effects of the Magnetic Liquids Around Vertical Conductors with a Current Flow

D. Vesa, M. Greconici and I. Tatai

Abstract This paper analyzes the mechanism of the magnetic liquid raising around two parallel, vertical, straight conductors with a current flow compared with the mechanism of the magnetic liquid raising around a vertical conductor with a current flow. A FEM modeling was made in order to establish the magnetic field inside the magnetic fluid and, using these values in Matlab, the forces that act in a magnetic liquid were computed. The magnetic liquid will be considered as a linear and non-conducting medium placed in a stationary field.

Keywords Conical meniscus · Forces in magnetic liquids · FEM modeling

1 Introduction

The effect called “conical meniscus” [1, 2] consists in the response of a pool of magnetic liquid to the magnetic field of a steady electrical current flowing through a vertical, straight conductor. This effect can be used in car suspensions or some biomedical applications, so it is important to know the effects of magnetic field forces in a magnetic liquid.

Trying to explain the effects of field forces in magnetic fluids, the literature systematically refers to discrete models, inspired by microscopic technique. It refers to various approximations in the micro–macro transition [3], which, implicitly, ignore the magnetostriction contribution. In this way, some global equivalent quantitative formulations have been made [4–6], but improper from the point of

D. Vesa (✉) · M. Greconici · I. Tatai
“Politehnica” University of Timisoara, Timisoara, Romania
e-mail: daniela.vesa@upt.ro

M. Greconici
e-mail: marian.greconici@upt.ro

I. Tatai
e-mail: ildiko.tatai@upt.ro

view of the force localizations and of the actual physical mechanism produced as a field effect.

Thus, using the expression of the force exerted by field on an elementary magnetic dipole [1, 2] (similar to ferromagnetic particle from the suspension), the force density exerted by field on a ferrofluid was deduced as:

$$f_v = -\frac{1}{2}H^2 \text{grad } \mu \quad (1)$$

The relation (1) is valid only for a uniform field H and if the forces interactions between the elementary dipoles are neglected. Also, considering the liquid as homogeneous medium (when $\text{grad } \mu = 0$), the expression (1) leads to a superficial location of forces, the surface being treated as a continuous layer of rapid variation of the permeability μ . Thus, knowing that the liquid–air boundary is a field surface and in the absence of magnetostriction, the surface force expression is [1]:

$$f_s = \frac{\mu - \mu_0}{2} H^2 n_{12} \quad (2)$$

where n_{12} is the normal unit vector being oriented toward the second medium (air).

The force oriented outward of the liquid, having the n_{12} direction, leads to the conclusion that the rise of the liquid is due to the traction exerted by this force on the fluid–air surface. It is known that the liquids do not support tractions so the interpretation above is inadequate. The fact will be proved by taking into account the magnetostrictive term in the forces expressions, a term that cannot be neglected.

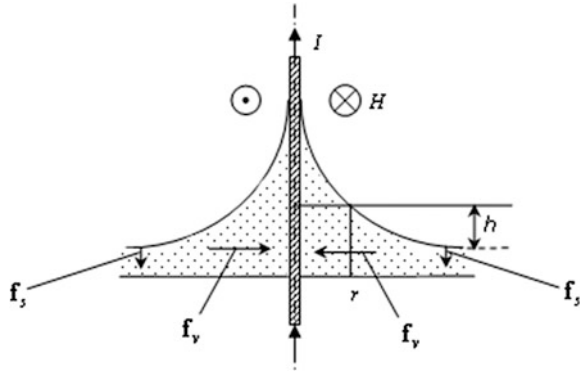
The original experimental arrangement with two vertical straight conductors [7] was used to make a comparison between the “conical meniscus” effect for this case, and the “conical meniscus” effect in the case of one conductor. The rise in height will be higher than in the case of single conductor with a current flow [1, 2].

2 The Raising Effect of the Magnetic Liquid Along the Conductors with a Current Flow

Taking into account the magnetostrictive term in the volume and surface forces expressions [8, 9], it is observed that the forces f_v act also in the fluid volume, having the direction toward the more intensive field area. This fact is valid even for homogeneous media (when $\partial\mu/\partial\tau = \text{const.}$), but placed in a non-uniform field:

$$f_v = \frac{1}{2} \tau \cdot \text{grad} \left(H^2 \frac{\partial\mu}{\partial\tau} \right) \quad (3)$$

Fig. 1 The spatial localization of the forces



where τ is the mass density of the fluid. For the “conical meniscus” experiment, the force f_v is oriented in the radial direction (Fig. 1), and it exerts a pressure against the magnetic liquid. This pressure acts in the opposite direction to the force of gravity and it raises the liquid along the straight conductors [3, 8, 10].

Moreover, on the liquid surface (which initially is a field surface), the forces f_s act as a compression and not as traction (Fig. 1), explaining how it resulted in the absence of the magnetostrictive term [11]:

$$f_s = -\frac{\chi(\mu - \mu_0)}{2} H^2 n_{12} \tag{4}$$

χ being the magnetic susceptibility.

Thus, the force f_s induces in the magnetic liquid an additional pressure and, the resulting magnetic pressure due to the simultaneous action of volume and surface forces generates the rise h of the liquid [11]:

$$h = \frac{\mu - \mu_0}{2\tau g} H^2 \tag{5}$$

where g is the acceleration due to gravity.

Because the maximum value of the field H , in the case of the “conical meniscus” effect for a single conductor with a current flow, is obtained at the conductor surface [7], the height h of rise is maximum here (Fig. 2).

Comparatively, the “conical meniscus” effect in the case of two conductors with a current flow obtains the maximum height of rise between conductors when the two are very close (Fig. 3). In this particular case, the magnetic field intensity produced by the two conductors is almost two times higher than the magnetic field intensity produced by a single conductor [7].

Fig. 2 Conical meniscus in the case of one vertical conductor with external radius $r = 3$ mm

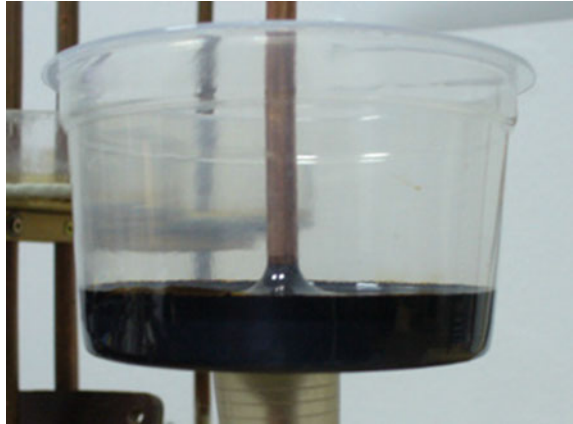
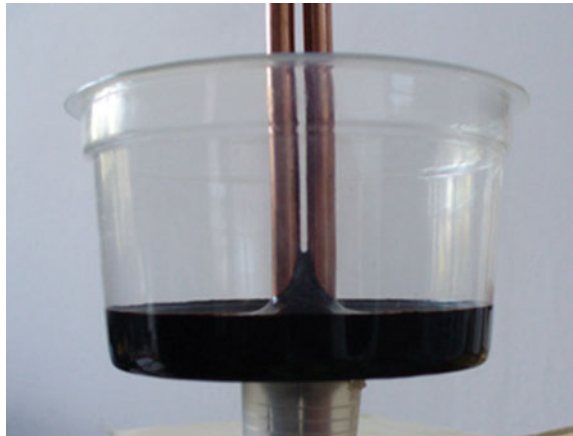


Fig. 3 Conical meniscus in the case of two vertical conductors with external radius $r = 3$ mm

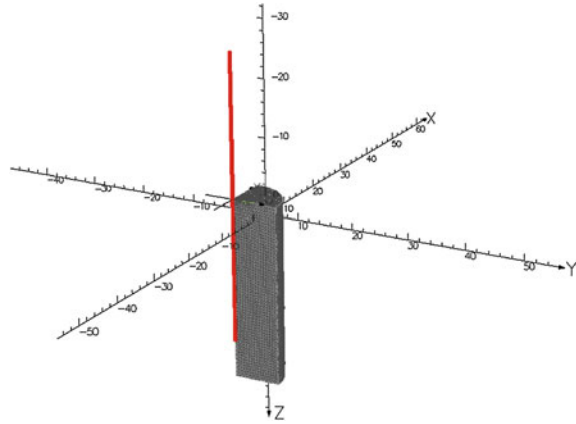


3 The Finite Element Formulation

The aim of the numerical method is to establish the magnetic field intensity generated by the conductors in any point of the magnetic liquid in the case of two treated effects, and to calculate the volume and surface forces which act on it. This computation is necessary because the volume and the surface forces cannot be determined experimentally, and it is important to understand their effects on the magnetic liquid.

The 3D-FEM program Opera 13 of Vector Fields has been used in order to solve the field problem numerically, [12]. The analysis program used to solve this problem was TOSCA. Among other things, TOSCA algorithm can analyze magnetostatic fields from defined current sources. This algorithm is based on vector potential formulation. In magnetostatic problems two potentials are used. The total

Fig. 4 FEM formulation for conical meniscus



magnetic vector potential is used in magnetic materials and the reduced magnetic vector potential is used in regions which contain source currents. The normal flux and the tangential field intensity interface conditions exactly determine the relationship between the two types of vector potential.

The two models are composed by the magnetic liquid sample which has a cylindrical form before applying the magnetic field, the vertical straight conductors, and the surrounding air. Due to the symmetry of the models and in order to use at maximum the mesh capabilities of Opera 13, one-eighth of the entire model was kept (Fig. 4).

In the magnetic liquid and the surrounding air domains of the model, the magnetic potential vector A fulfills a Laplace equation $\Delta A = 0$, as $\text{div } \mathbf{B} = 0$, $\text{curl } \mathbf{H} = 0$, $\mathbf{B} = \mu \mathbf{H}$ in the magnetic liquid and $\mathbf{B} = \mu_0 \mathbf{H}$ in the surrounding air. In all analyses, the following boundary conditions were used: the two rectangular boundaries, parallel to the z axis, are normal magnetic boundaries ($\text{curl } \mathbf{A} \times \mathbf{n} = 0$), and all the rest are tangential magnetic boundaries ($\mathbf{A} \times \mathbf{n} = 0$).

As many as 40,000 nodes have been used in all the analyzed cases. Both linear and quadratic elements were used. A part of the finite elements used in models are presented in Fig. 4.

4 The Simulation Numerical Results

The values of the geometrical quantities used in simulation are: the conductor radius $r = 3$ mm, the conductor length $l = 50$ cm, the magnetic liquid radius $r_l = 38.5$ mm, and the initial height of the magnetic liquid $h_i = 9$ mm. The magnetic liquid was considered as a linear medium having the relative magnetic permeability $\mu_r = 2.4$.

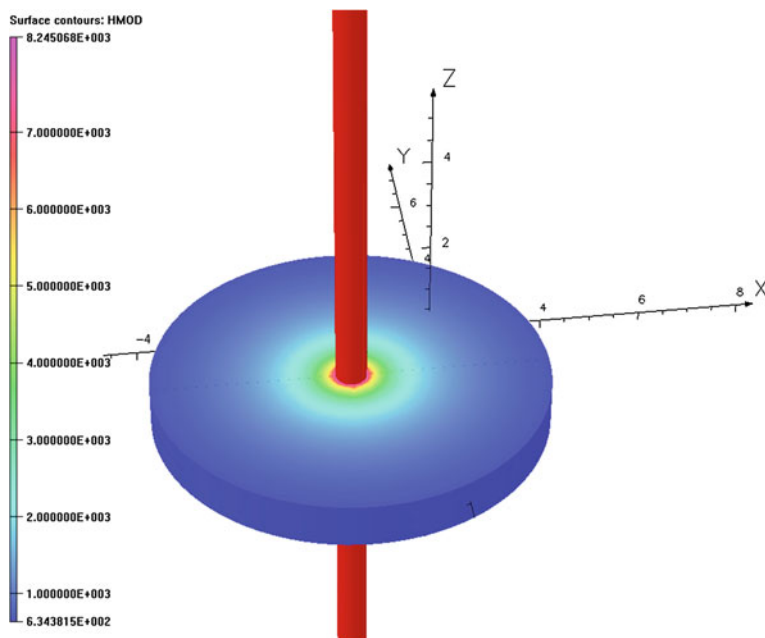


Fig. 5 Magnetic field intensity distribution in the case of one vertical conductor

The values of the forces in “conical meniscus” effect for a single conductor case have been calculated numerically using the magnetic field intensity values from Opera 13 (Fig. 5) and using a program developed in Matlab.

This program uses expressions (3) and (4) in the forces calculus. Considering the magnetic liquid as homogeneous media and knowing that it is weak magnetic media, $\tau \cdot (\partial\mu/\partial\tau) = \mu\chi$ in (3). The volume force density was calculated in several points of a vertical plane having the coordinate $y = 0$ cm and being parallel to the x axis which passes through the conductor. Also, the surface force density was calculated in several points of the liquid surface. The results are presented in graphical form (Figs. 6 and 7).

As it can be seen in the figures above, the forces obtain both positive and negative values. The sign gives information about the forces orientation. Thus, considering the magnetic liquid as homogeneous media, the volume forces are function of $\text{grad } H^2$, their values being positive in the left half and negative in the right half of the considered plane. So, these forces have the orientation toward the conductor (due to symmetry, for all vertical planes), exerting a pressure in the magnetic liquid, with larger values near the conductor. The surface force is negative in all surface points, being oriented toward the liquid and exerting compression on it. This pressure is larger in the points placed near the conductor and decreases in the rest. It can be seen that the volume forces have larger values than the surface

Fig. 6 The volume force density distribution in the case of one vertical conductor

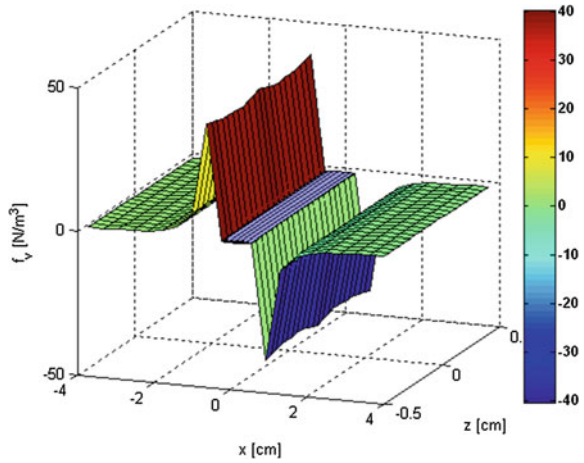
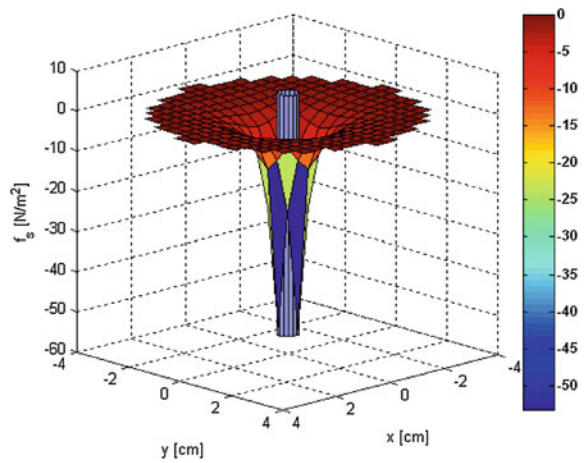


Fig. 7 The surface force density distribution in the case of one vertical conductor



forces, as a consequence their higher pressure compensates the pressure due of surface forces, causing the rise of the liquid around the conductor (Fig. 2).

Using the magnetic field intensity values calculated with Opera 13 in the case of two very close conductors (Fig. 8), and expression (3), the volume forces have been calculated in several points of two vertical planes. The first plane has the coordinate $y = 0$ cm, being parallel to the x axis and passing through both conductors. The second plane has the coordinate $x = 0$ cm, being parallel to the y axis and placed between the conductors.

The volume forces values in both planes are presented in graphical form (Figs. 9 and 10).

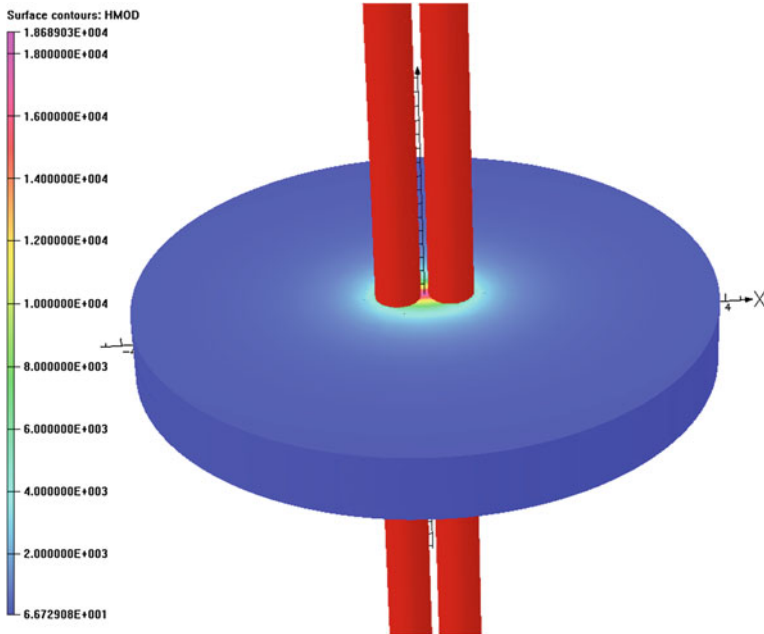
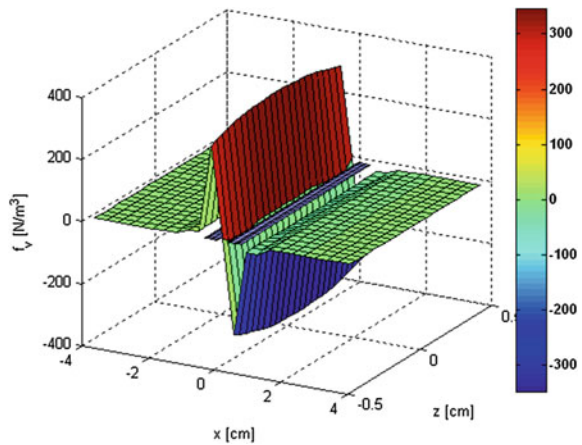


Fig. 8 Magnetic field intensity distribution in the case of two vertical conductors

Fig. 9 The volume force density distribution in the case of two vertical conductors for $y = 0$ cm



As it can be seen in the figures above, the volume forces obtain both positive and negative values in both planes, so these forces have the orientation toward the middle of the magnetic liquid, having larger values in this area. So, these forces exert a pressure in the magnetic liquid having the radial direction toward the conductors.

Fig. 10 The volume force density distribution in the case of two vertical conductors for $x = 0$ cm

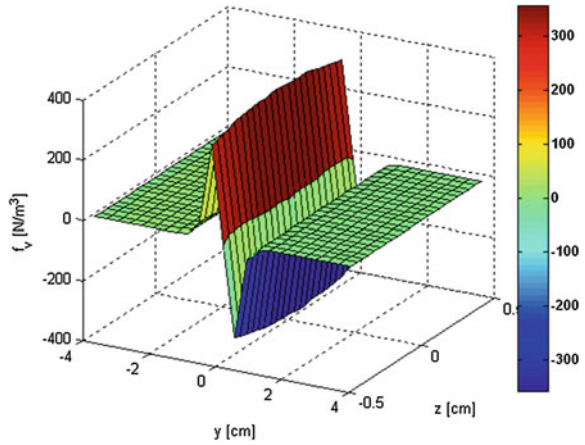
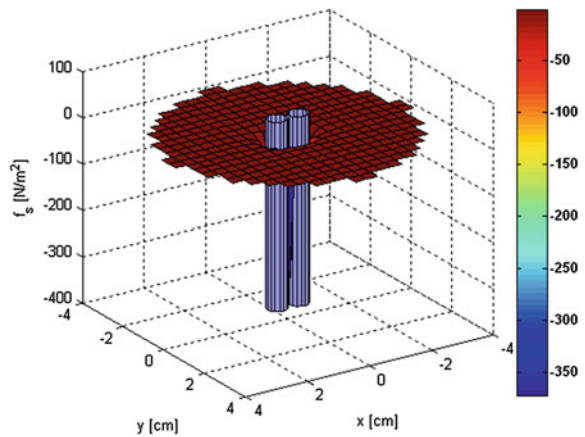


Fig. 11 The surface force density distribution in the case of two vertical conductors



Using the magnetic field intensity values calculated with Opera 13 (Fig. 8) and expression (4), the surface forces have been calculated in several points of the liquid surface. The results are presented in graphical form (Fig. 11).

Similar to the “conical meniscus” effect in the case of a single conductor, the surface force is negative in all surface points, being oriented toward the liquid and exerting compression on it. This pressure is larger in the points placed between the conductors and decreases in the rest. Since the pressure due to surface forces has smaller values than the pressure due to volume forces, their compound effect causes the rise of the magnetic liquid. Since the distance between conductors is very small (1 mm), and the pressure due to volume forces in this area is very high, the magnetic liquid rises along the conductors, the rise h being maximum here (Fig. 3).

5 Conclusions

This paper analyzes from the point of view of magnetic forces, the mechanism of the magnetic liquid raising around two parallel, vertical, very close straight conductors with a current flow compared with the mechanism of the magnetic liquid raising around a vertical conductor with a current flow. Thus, in the presence of the magnetostrictive term in the expressions of volume and surface forces, both act in a magnetic liquid. Also, in the first case it can be seen that, due to the proximity of two conductors, these forces produce a rise h of magnetic liquid four times higher (Fig. 3) than in the case of a single conductor (Fig. 2).

Moreover, the volume and surface forces which act in a magnetic liquid in the case of the experiment with one conductor and in the case of the experiment with two very close conductors were calculated numerically in this paper. Comparing the modeling results for the case of one conductor with those obtained in the case of two very close conductors, it results that the magnetic field effects are more pronounced in the second case due to much higher values of the specific volume forces. However, the modeling results do not provide information about the rise h of magnetic liquid around the conductors. These information can be obtained by experimental measurements.

References

1. Rosensweig RE (1985) *Ferrohydrodynamics*. Edited by Cambridge University Press, New York
2. Luca E, Calugaru G et al (1978) *Ferrofluids and theirs industry applications*. Edited by Ed. Tehn. Bucuresti, Roumania (in Roumanian)
3. Tamm IE (1952) *The electricity fundaments*. Edited by Ed. Tehnica Bucuresti (in Roumanian)
4. Neuringer JL, Rosensweig RE (1964) *Ferrohydrodynamics*. *Phys Fluids* 7(12):1927–1937
5. May K, John T, Stannarius R (2011) Experimental study on the meniscus of a ferrofluid around a vertical cylindrical wire carrying electric current. In: Annual general meeting of the chemical and polymer physics division
6. Mayer D (2008) Future of electrotechnics: ferrofluids. *Adv Electr Electron Eng J* 7(1,2):9–14
7. Vesa D., Greconici M (2010) About some raising effects of the magnetic liquids placed in a stationary field. In: National symposium on theoretical electrical engineering Bucuresti
8. Abraham M., Becker R (1932) *Theorie der elektrizität, Bd.1*. Edited by Teubner-Verlag, Leipzig (in German)
9. Straton JA (2007) *Electromagnetic theory*. Edited by McGraw-Hill Book Company, New York and London. Reprinted by IEEE Press Series on Electromagnetic Wave Theory
10. Durand E (1953) *Electrostatics and magnetostatics*. Edited by Masson et Cie Paris (in French)
11. Vesa D, Greconici M (2010) Physical mechanism of the magnetic liquid raising around a vertical conductor with a current flow. In: Proceedings of international PhD seminar on computational electromagnetics and optimization in electrical engineering, Sofia, pp. 124–127
12. Opera 13: 3D-Reference manual (2009) Edited by Vector Fields

Hard as a Rock or Deformation Controlled?

Gheorghe Sima, Glavan Dan, Popa Alexandru and E. Muncut

Abstract In our days we are considering that it is not anymore a problem if structures that are applied to static or dynamic loads are reacting in multiple ways if we can measure the displacement of the theoretical point of contact between the cutting tool and the object manufactured in order to take measures to compensate the errors, fact that allowed us to obtain almost maximum precision.

Keywords Structures · Static load · Dynamic load · Precision · Manufacturing

1 Introduction

The first solution to reach higher precision in manufacturing is to increase the rigidity of the structure in this case obtaining a minimum for deformations.

Getting stronger structure means more material, more weight and higher costs but anyway this point of view is not 100 % acceptable due to the law of small plastic deformation that are present in every elastic deformation, their cumulated effects will affect the precision of the whole structure of the machine, so on long term the precision of the machine will be affected.

This type of judgement in designing tool machinery structures was easy to realize so for many years it was considered to be the only one capable to offer an

G. Sima (✉) · G. Dan · P. Alexandru · E. Muncut
Faculty of Engineering, University “Aurel Vlaicu” of Arad, B-Dul Revoluției Nr. 77,
P. O. BOX 2/158, 310130 Arad, România
e-mail: gheorghe.sima@klastorf.ro

G. Dan
e-mail: glavan@fortuna.com.ro

P. Alexandru
e-mail: alexpopaarad@yahoo.com

E. Muncut
e-mail: muncutstela@yahoo.com

answer to the high precision problem by almost all the engineers involved in design of structures.

Our alternative is taking in consideration that it is not inconvenient the fact that the structure is changing itself as dimensions and basic shape if we can determine the exact value of deformation in the cross section where the tool is working.

2 Formulating the Problem

In order to reach maximum precision, that means almost zero errors we have to know the value of the displacement in the mentioned cross section of the structure.

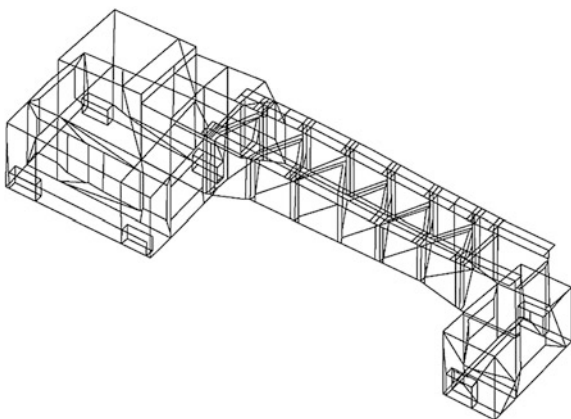
As a procedure the things seems to be very clear and easy, but when we transfer the theory in tool machinery engineering due to the complex shapes and irregular section calculating the deformations becomes a very serious and complicated thing.

How can be calculated the value of deformation is the cross section of the tool is our main problem that we are trying to offer an answer for. This requires not classic material resistance methods but methods that can deal with multiple non-determined in the system of equations that can be attached to the model.

An example of applying of the classic methods (Fig. 1) for a turning machine follows.

For this particular example we can use the classic equilibrium equations, along the axes of the reference triple orthogonal system for the forces and around the axes for torques. Those six equations resulting are completely nonsufficient, the number of unknown parameters being in total at least eight so the double undetermined system must be solved. We can add equations that are coming from the real process but this will conduct us to additional parametrical equations.

Fig. 1 Classic methods of calculating forces



3 Classic Solutions

The value of the cutting forces are resulting from the technological process, the reaction forces and the friction forces we will calculate them taking in consideration the coordinates of the applying points of each one and finally we can write the equations.

It is obvious that with six equation system available we cannot determine eight unknown parameters the conclusion being that we need two supplementary equations.

With classic resistance material methods it is almost impossible to find those two equations, so we will try to get them out from the particular shape of the structure and from the manufacturing process characteristics fact that leads us to the final results.

The value of the cutting forces F are resulting from the technological process, the reaction forces R and the friction forces we will calculate them taking in consideration the coordinates of the applying points of each one and finally we can write the equations.

It is obvious that with six equation system available we cannot determine eight unknown parameters the conclusion being that we need two supplementary equations.

With classic resistance material methods it is almost impossible to find those two equations, so we will try to get them out from the particular shape of the structure and from the manufacturing process characteristics fact that leads us to the final results that will look like:

$$f = \frac{\sqrt{M_{2v}^2 + M_{2H}^2}}{E \left(\frac{BH^3}{12} + a_2^2 BH + \frac{bh^3}{12} - a_3^2 bh \left(\frac{\pi}{8} - \frac{8}{9\pi} \right) \frac{B^4}{16} + a_1^2 \frac{\pi B^2}{8} \right)} \tag{1}$$

$$= \frac{\frac{1-x_2}{1} \sqrt{F_1^2 x_1^2 + F_2^2 x_2^2 + 2F_1 F_2 x_1 x_2 \cos \alpha}}{E \left(\frac{BH^3}{12} + a_2^2 BH + \frac{bh^3}{12} - a_3^2 bh \left(\frac{\pi}{8} - \frac{8}{9\pi} \right) \frac{B^4}{16} + a_1^2 \frac{\pi B^2}{8} \right)}$$

$$\varphi = \frac{T_f}{EI_z} \tag{2}$$

$$\varphi = \frac{\frac{F_1 x_1 + F_2 x_2 \cos \alpha}{1}}{E \left(\frac{BH^3}{12} + a_2^2 BH + \frac{bh^3}{12} - a_3^2 bh \left(\frac{\pi}{8} - \frac{8}{9\pi} \right) \frac{B^4}{16} + a_1^2 \frac{\pi B^2}{8} \right)}$$

where

f represents the value of displacement of the structure in the cutting cross section area

φ represents the angle of rotation of the structure in the same cross section

$F_{x,y,z}$ represents the component of the cutting force projected on the axes ox , oy and oz

$M_{x,y,z}$ represents the torques around the axes ox , oy and oz
 x,y,z , etc. are linear values (distances) between particular points of the structure.

4 Improving Classic Solutions

In this point it is clear that we cannot write supplementary equations that are 100 % sure (only in the situation of a particular cross section-regular one, symmetric, etc.) but we can add only some equations that are coming from the practice experience that means they have just a probability to be sure. In fact if we are adding two of those types of equations we need a third one that will confirm or not our suppositions (equations coming from practice experience).

The whole process can be described now like an algorithm; in conclusion we can determine a logic process that is happening as follows:

1. To describe the structure as requested to be use by the finite element method;
2. Based on the parameters of process (speed, feed, materials, etc.) we can calculate the range of stress that the structure will be exposed at;
3. Choosing a convenient increment we can use the method step by step covering the whole interval;
4. The results (deformations) will be organized in a data base;
5. During the manufacturing process we will use the variation of only one parameter, in order to accelerate the algorithm, that parameter being in the case of a turning machine the principal cutting force, controlled by the adaptive force control device of the machine;
6. In order to speed the process it will be used not the function of force that is coming out from the device like information but the first or even the second derivate of this function that offers us a predictability of the evolution for the force, with evident gain in time to control the parameters of the process;
7. The information that we own in this point permit us to go now to the data base of deformation and make an interpolation of the values of forces we can approximate acceptably the deformation;
8. The deformation being calculated, we can command a very fast reaction on the machine in order to compensate it using non-conventional sources of movement (engines) like the magnetostrictive engine having the principal advantage the very short time of reaction.

Using this procedure we can also improve the structure itself.

The value of the cutting forces are resulting from the technological process, the reaction forces and the friction forces we will calculate them taking in consideration the coordinates of the applying points of each one and finally we can write the equations.

5 New Methods

Using this logic we can obtain or not the results in real time, everything depending on the inspiration of choosing the supplementary equations.

We know that the finite element method is the right solution but to use it is another discussion, the method being applied to calculate structures that are let say “static”, or our case suppose almost instantaneous calculation and then instantaneous corrective action from the machine, things that are not possible basic because of two problems:

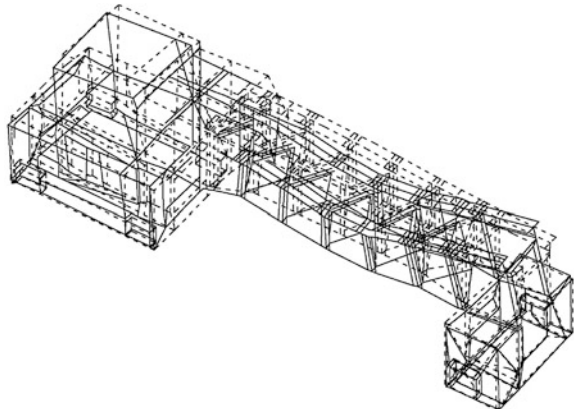
1. The method requires a strong enough software and the very strong computer to be able to apply the method in real time (time enough for the machine to take the result and make the correction);
2. The mechanical systems on the machine are not fast enough to do the correction in real time, most of them, classic used, being too slow.

For example for the structure mentioned above the finite element method will show in Fig. 2.

It is impossible to use the finite element method in real time, and in order to obtain some advantages from the excellent precision that the finite element method is offering, we apply the method, the results for deformation being saved in data bases for each particular situation, in this way we could generate fields of data from where the computer could choose the right value for the deformation, making linear interpolation between the closest pre calculated values the following of the cutting force function proving to be (especially when the derivate was use to show the trend).

In fact we cannot use the method in real time, and in order to obtain some advantages from the excellent precision that the finite element method is offering us we can anticipate the evolution of the structure.

Fig. 2 Finite element method



6 Conclusions

Depending on the particular situation both classic or modern methods can be applied, the results are very much influenced by the way the engineer manages to extract mathematic information's from the manufacturing process.

Bibliography

1. Jacobson MO (1966) Tehnologia stankostroenia. "Maşinostroenie", Moscova
2. Pronicov AC (1957) Iznov i dolgovecinosti stankov. Maşghiz, Moscova
3. Dreucean A (1984) Maşini unelte şi control dimensional. Litografia UPT, Timişoara
4. <http://www.schrauben-jaeger.de/tradepro/shop/artikel/docs/DIN981.pdf>, 19.06.2013, 18.27
5. http://www.stamel.ro/files/produse/fise-tehnice/1277816133_din39.pdf, 19.06.2013, 21.25
6. Drăghici I (1981) Îndrumar de proiectare în construcţia de maşini vol.1. Editura tehnică Bucureşti
7. Paizi G, Stere N, Lazăr D (1977) Organe de maşini şi mecanisme. Editura didactică şi pedagogică Bucureşti
8. Ioan R (2001) Mecanica—vol II Cinematica Editura Mirton Timişoara
9. Ioan R, Dan G (2001) Elemente de vibraţii mecanice. Editura Universităţii "Aurel Vlaicu" Arad
10. Gheorghe S (2004) Sisteme senzoriale utilizate la sudare. Editura, Viata Arădeana Arad
11. Doina M, Lavinia S, Theoharis B, Lucian G (2006) Autocad 2006, partea I— modelarea 2d, Îndrumător pentru uzul studenţilor. Editura Universităţii "Aurel Vlaicu", Arad

Cast-Resin Dry-Type Transformer Thermal Modeling Based on Particle Swarm Optimization

Davood Azizian and Mehdi Bigdeli

Abstract In this research paper, a novel approach for dynamic thermal modeling of cast-resin dry-type transformer is introduced. In order to analyze the dynamic behavior of the temperatures in this type of transformer, a new thermal model has been introduced which is based on the particle swarm optimization (PSO) algorithm. Selecting a typical 400 kVA dry-type transformer, the models parameters have been estimated (by employing the PSO) and validated using the experimental data. The PSO is used to estimate the models parameters with a good performance. The estimated second-order model describes the thermal behavior of the cast-resin transformer completely. Using this model, dynamic thermal behavior of the transformer has been analyzed and the effects of load variation on thermal behavior of transformer have been discussed in this paper. It has been shown that the newly introduced thermal model that is estimated using the PSO is an accurate and efficient model for analyzing the dynamic thermal behavior of the cast-resin dry-type transformer.

Keywords Cast-resin transformer · Dynamic behavior · Thermal modeling · Particle swarm optimization (PSO)

D. Azizian (✉)

Department of Electrical Engineering, College of Engineering, Abhar Branch,
Islamic Azad University, Abhar, Iran
e-mail: d.azizian@abhariau.ac.ir

M. Bigdeli

Department of Electrical Engineering, Zanzan Branch, Islamic Azad University,
Zanzan, Iran
e-mail: bigdeli_aznu@yahoo.com

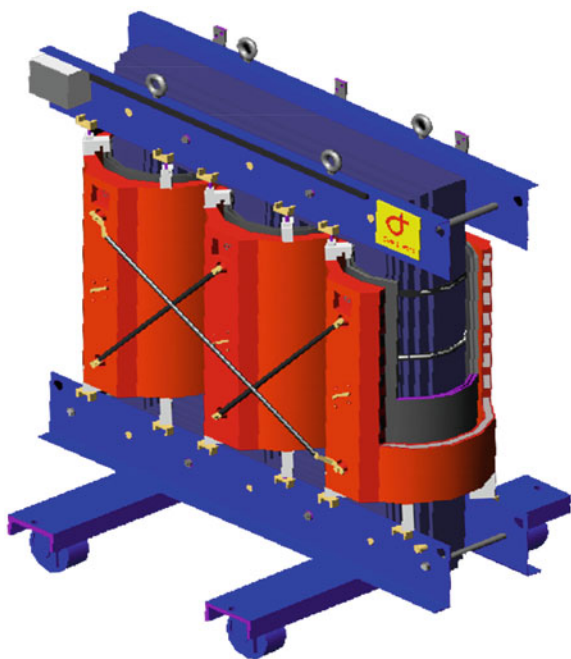
1 Introduction

In some applications such as traction systems, ships, military areas, and residential regions, transformers have to be protected from explosion. Oil-immersed transformers are risky to be used in such regions; thus, the industry tends to use special types of transformers. Therefore, non-flammable materials, such as Askarel, silicon fluid, high temperature hydrocarbons, tetrachloroethylene, and epoxy resins, have been presented for using as transformer insulations. In the past 40 years, the usage of Askarel is gradually being discontinued because of its harmful nature to the environment. Among the mentioned insulations, epoxy resin is the best one that can be used in a transformer.

Consequently, cast-resin dry-type transformer (Fig. 1) has been developed for better protection against flame and moisture absorption.

Cooling in a cast-resin transformer (CRT) is carried down by the air and the CRT does not have any cooling fluid; so the temperature range is higher than oil-immersed transformers. Temperature variations affect the life-time of insulations in a transformer. Therefore, studying the thermal behavior of CRT is vital. The steady-state temperature calculation of dry-type transformers was studied previously [1–6]. However, it is essential to analyze the dynamic thermal behavior of CRT. Thus it is helpful to introduce an applicable model for dynamic thermal analysis and life-time estimation in the CRT. Different life-time [7] and transient thermal models [8–10] have been introduced for oil-immersed transformers and

Fig. 1 A cut of windings in cast-resin transformer (CRT)



several techniques have been presented for parameter estimations in the existing thermal models [11–14].

But there is only one research on the dynamic thermal behavior of the dry-type transformer [14]. Reference [14] introduces genetic algorithm (GA) based thermal models for transient temperature estimation in a typical dry-type transformer. The mentioned paper introduces two simple (first and second order) models for studying the average temperature of windings (average temperature of the low and the high voltage windings). Thus, in this paper a new third-order model has been introduced for detailed thermal modeling of both low and high voltage windings. As difficulties are faced when applying GA in dynamic thermal model determination, here a method that is based on particle swarm optimization (PSO) has been used for parameter estimation of the introduced dynamic thermal model. It has been shown that the introduced model can estimate the dynamic thermal behavior of CRT with a good performance. The estimated model has been verified using experimental data extracted from a typical 400 kVA CRT. Afterwards, the introduced dynamic thermal model has been used to study the effect of loading procedure on the thermal behavior of a typical CRT.

It has been shown that the PSO estimates the models parameters rapidly and the estimated third-order model can estimate the windings temperatures accurately. Thus the introduced dynamic thermal model is an appropriate model for on-line and off-line temperature monitoring of the CRT and can be used by both CRT designers and power system experts.

2 Dynamic Thermal Models for CRT

2.1 Discredited Heat Transfer Equations

The CRT has a symmetrical geometry and its windings can be assumed as concentric cylinders. Applying the cylindrical symmetry, the transient behavior of the winding temperatures in the CRT can be described as

$$\frac{1}{r} \frac{\partial}{\partial r} \left(r \frac{\partial \theta}{\partial r} \right) + \frac{\partial^2 \theta}{\partial z^2} + \frac{q''}{k} = \frac{1}{\alpha} \frac{\partial \theta}{\partial t} \quad (1)$$

where q'' is the generated heat flux, θ is the temperature, k is the thermal conductivity, and α is the coefficient of thermal diffusion.

According to heat transfer mechanisms, the CRT can be divided into two main parts: windings and peripheral surfaces. Solving Eq. (1) in these parts and especially for natural convection in peripheral surfaces is complicated and impossible; thus some numerical methods are needed. A numerical technique that is called as resistive elements [3, 15] is employed to solve the heat transfer equations. In this technique, the windings are divided into separate units and each unit is connected to other units via thermal resistances. This is shown in Fig. 2.

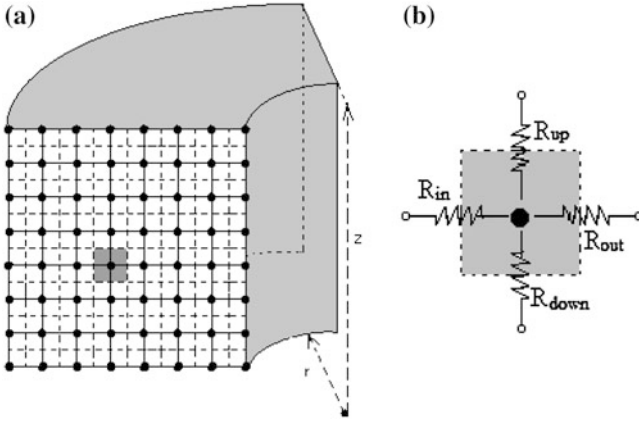


Fig. 2 **a** Winding divisions in the resistive elements method, and **b** thermal resistances

Resistive elements technique employs the energy conversion law (unit losses – heat transferred to neighbor units = thermal energy stored in the unit) to discretize Eq. (1). In spite of the steady state, the stored energy in a unit is not zero in transient condition. In transient condition, each unit behaves as a thermal capacitor and the energy conversion law for this unit (i, j) can be rewritten as follows [15]:

$$\begin{aligned}
 Q_{i,j} - \frac{(\theta_{i,j} - \theta_{i-1,j})}{R_{in}} - \frac{(\theta_{i,j} - \theta_{i+1,j})}{R_{out}} - \frac{(\theta_{i,j} - \theta_{i,j-1})}{R_{down}} - \frac{(\theta_{i,j} - \theta_{i,j+1})}{R_{up}} \\
 = C_{i,j} \frac{\partial \theta_{i,j}}{\partial t}
 \end{aligned} \quad (2)$$

where R_{in} , R_{out} , R_{down} , and R_{up} are the radial and axial thermal resistances related to the neighboring nodes, $C_{i,j}$ is the thermal capacitance of the unit, $Q_{i,j}$ is the unit losses, and $\theta_{i,j}$ is the unit temperature.

2.2 Thermal Equivalent Circuit Based on the Concept of Duality

Here, each winding is represented by a single unit. Heat transferred from bottom and top surfaces of the windings is negligible and it can be ignored [3]. Thus, heat transfer of the windings is understood to occur only in the radial direction and thermal resistances in axial directions can be removed. Therefore, ignoring the axial thermal resistances, Eq. (2) can be simplified as below for a single node selected in each winding.

$$Q_{LV} - \frac{\theta_{LV} - \theta_a}{R_{LV}} = C_{LV} \frac{\partial \theta_{LV}}{\partial t} \tag{3}$$

$$Q_{HV} - \frac{\theta_{HV} - \theta_a}{R_{HV}} = C_{HV} \frac{\partial \theta_{HV}}{\partial t} \tag{4}$$

where θ_{LV} and θ_{HV} are the windings temperatures, θ_a is the temperature of cooling air on the top of windings, Q_{LV} and Q_{HV} are the windings losses, R_{LV} and R_{HV} are the thermal resistances between the windings and the air, and C_{LV} and C_{HV} are the windings thermal capacitances.

It can be seen that Eqs. (3) and (4) express two first-order models. The models that are extracted based on the concept of duality are shown in Fig. 3.

For simplification, one can assume θ_a as the ambient temperature [3]. But usually, it is convenient to model the air temperature in addition of the windings temperatures.

Similarly, the cooling air can be considered as a single unit (or node). Thermal conduction between the duct’s walls is negligible and it can be ignored [3]. Thus, heat transfer in the air ducts and the outer surface is solely convection. Consequently, Eq. (2) can be expressed as Eq. (5) for a single node selected in the cooling air.

$$Q_a - \frac{\theta_a - \theta_{amb}}{R_a} = C_a \frac{\partial \theta_a}{\partial t} \tag{5}$$

where Q_a is the total heat flow to the cooling air, R_a is the cooling air’s thermal resistance, and C_a is the cooling air’s thermal capacitance.

Similarly, it is clear that Eq. (5) expresses a first-order model for the cooling air temperature (Fig. 4).

Combining the first-order models in Figs. 3 and 4, a new third-order equivalent circuit can be extracted as shown in Fig. 5.

One may assume that the temperatures of the low and the high voltage windings are independent of each other. This can truly occur if the distance (duct) between these windings is big enough. In this case, the third-order model can be simplified into two split second-order models [14].

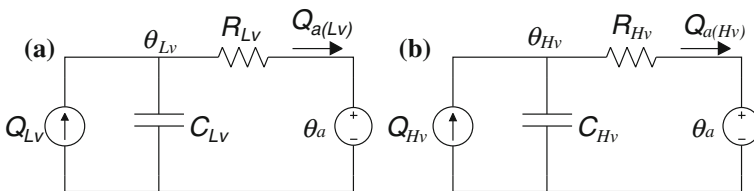


Fig. 3 First-order equivalent circuits describing **a** LV and **b** HV winding temperatures

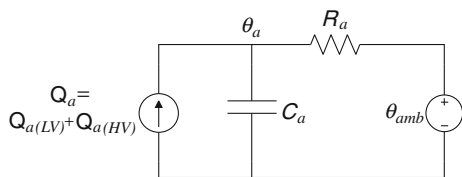


Fig. 4 First-order equivalent circuit describing the cooling air’s temperatures

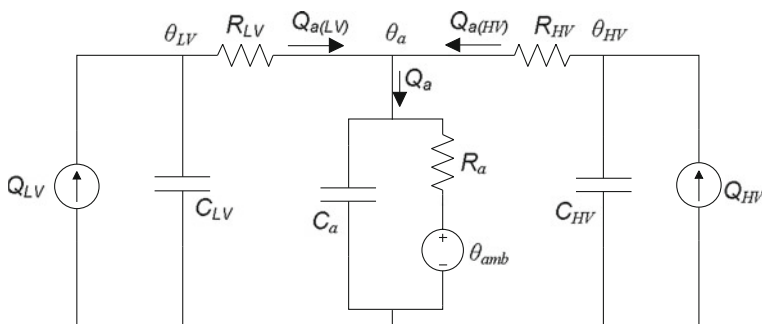


Fig. 5 Detailed thermal equivalent circuit for dynamic thermal analysis of the windings and the cooling air in the CRT

The winding’s losses in Fig. 5 depend on the winding’s current and it can be expressed as

$$Q_w(I) = Q_w(I_0)K^{2n_w} \tag{6}$$

where K is the ratio of the load current to the nominal current and n_w is an experimental adjustment coefficient that differs from one winding to another [16].

2.3 Temperature Dependent Parameters of the Thermal Model

Additionally, it is known that the thermal resistors and capacitors depend on temperature. Temperature dependency can be taken into account to have a better accuracy for dynamic thermal modeling of CRT. This dependency is negligible in windings parameters. On the other hand, the effect of temperature on the cooling air parameters is considerable. It can be shown that the correlation between these parameters and the temperature obeys the equations mentioned below:

$$R_a \approx (0.0046\theta_a + 0.4816)R_{a(b)} \quad (7)$$

$$C_a \approx (-0.0036\theta_a + 1.3592)C_{a(b)} \quad (8)$$

where $R_{a(b)}$ and $C_{a(b)}$ are the thermal resistor and capacitor of the air in the reference temperature.

Consequently, winding's losses vary due to the winding's temperature [3].

3 Thermal Model Estimation Based on PSO

3.1 Particle Swarm Optimization (PSO)

PSO is an efficient algorithm and has developed in recent years. PSO is one of the new algorithms invented by Kennedy and Eberhart in 1995 [17, 18]. This algorithm was inspired from social behavior of animals such as bird flocking or fish schooling. In comparison with other optimization algorithms, PSO has considerable search for complex optimization problems with faster convergence rate. As an advantage in programming, PSO requires fewer parameters for regulation than other optimization algorithms. Implementation steps of this algorithm are as follows:

1. Random generation of primary population,
2. Particles' fitness calculation with respect to their current positions,
3. Comparison of the current fitness of particles with their best experience:

$$\text{If } F(P_i) \geq pbest_i \rightarrow \begin{cases} pbest_i = F(P_i) \\ \overrightarrow{xpbest}_1 = \overrightarrow{x_1(t)} \end{cases} \quad (9)$$

4. Comparison of the current fitness of particles with the best experience of all particles

$$\text{If } F(P_i) \geq gbest_i \rightarrow \begin{cases} gbest_i = F(P_i) \\ \overrightarrow{xgbest}_1 = \overrightarrow{x_1(t)} \end{cases} \quad (10)$$

5. Change in velocity of each particle according to Eq. (11).

$$\overrightarrow{v_1}(t) = \overrightarrow{v_1}(t-1) + \rho_1 (\overrightarrow{xpbest}_1 - \overrightarrow{x_1}(t)) + \rho_2 (\overrightarrow{xgbest}_1 - \overrightarrow{x_1}(t)) \quad (11)$$

6. The particle position change to new position according to Eq. (12).

$$\vec{x}_1(t) = \vec{x}_1(t - 1) + \vec{v}_1(t) \quad (12)$$

7. Algorithm is iterated from step 2 until the convergence is obtained.

In the above algorithm, $\vec{x}_1(t)$, $F(P_i)$, $Pbest_i$, and \vec{xpbest}_1 are position, fitness, best fitness, and best fitness position of i th particle. Also $gbest_i$ and \vec{xgbest}_1 are best fitness of the population and its position.

3.2 General Notes on Implementation of PSO

Number of Particles The number of particles in search space is chosen by the trial-and-error method to get better convergence. Since PSO application is relatively based on swarm intelligence, more particles lead to a better response. On the other hand, more particles require more calculations and therefore the method will be time consuming.

Velocity Limitation One higher limit for velocity prevents particles from jumping with high speed in the searching region. Consequently, space is searched to reach better region accurately. Additionally, this limitation prevents algorithm divergence due to high velocities of particles. After updating velocity vector, the following conditions are checked:

$$\text{If } V_i(t) \geq V_{\max} \rightarrow V_i(t) = V_{\max} \quad (13)$$

$$\text{If } V_i(t) \leq -V_{\max} \rightarrow V_i(t) = -V_{\max} \quad (14)$$

The maximum value of velocity is selected with respect to change of position vector parameters. However, researches [19, 20] have shown that if Eq. (11) is applied for updating velocity vector (as follows); it does not require to check previous conditions.

$$\vec{v}_1(t) = k(\vec{v}_1(t - 1) + \rho_1(\vec{xpbest}_1 - \vec{x}_1(t)) + \rho_2(\vec{xgbest}_1 - \vec{x}_1(t))) \quad (15)$$

where

$$k = \frac{2}{|2 - \rho - \sqrt{\rho^2 - 4\rho}|}, \quad \rho = (\rho_1 + \rho_2) > 4 \quad (16)$$

Inertia Weight This parameter controls the effect of previous velocity on current velocity. Its large certainly causes wide search space and vice versa. Implementation of inertia weight can be done by using Eq. (17):

$$\vec{v}_1(t) = \varphi \vec{v}_1(t-1) + \rho_1 (\overrightarrow{xpbest}_1 - \vec{x}_1(t)) + \rho_2 (\overrightarrow{xgbest}_1 - \vec{x}_1(t)) \quad (17)$$

Preliminarily inertia weights are initialized by value 1 and reduce along algorithm. Also, Eq. (15) must be true. If not, PSO's behavior becomes oscillatory and maybe divergence [19, 20]:

$$\varphi > \frac{1}{2}(C_1 + C_2) - 1 \quad (18)$$

3.3 Implement of PSO Algorithm

As was mentioned earlier, the models parameters can be determined using artificial optimization methods such as PSO. This algorithm overcomes inaccuracies that arise mostly due to the errors in analytical formulae. PSO, for each model with specified number of model units, is used to determine the model parameters optimally, starting with the initial values. Beside initial values, a suitable fitness function is required for any optimization algorithm, to find the model parameters that most improve the accuracy of the original model. For our purpose a proper fitness function yielding satisfactory optimizations is formulated as follows:

$$\text{Fitt} = \sum_t (\alpha_{LV}^t |\theta_{LV}^c(t) - \theta_{LV}^e(t)| + \alpha_{HV}^t |\theta_{HV}^c(t) - \theta_{HV}^e(t)| + \alpha_a^t |\theta_a^c(t) - \theta_a^e(t)|) \quad (19)$$

where θ_{LV}^c , θ_{HV}^c , and θ_a^c are the estimated temperatures, θ_{LV}^e , θ_{HV}^e , and θ_a^e are the measured temperatures, and α_{LV}^t , α_{HV}^t , and α_a^t are the weights of the windings and air temperatures in the fitness function.

3.4 Parameter Estimation

In this paper, a load sequence (50 % of the nominal load for 5 h and 100 % for 4 h) was applied to a typical transformer [21] and temperatures of the windings and cooling air were measured. The gathered experimental data have been employed to estimate the parameters of the thermal model using the PSO algorithm. Figure 6 shows the process of fitness function optimization in the PSO algorithm.

Consequently, parameters of the introduced thermal model have been estimated using the PSO algorithm (Figs. 7 and 8). The PSO has good performance in

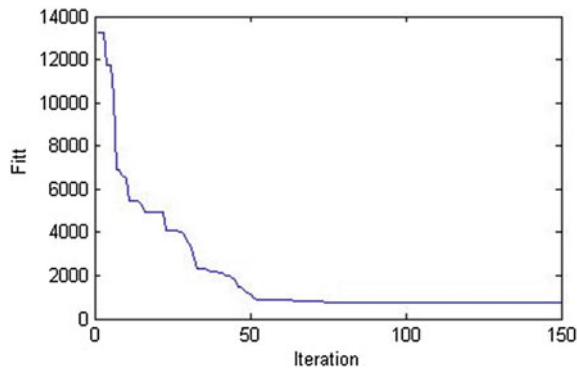


Fig. 6 Variation of the fitness function due to the iteration of PSO

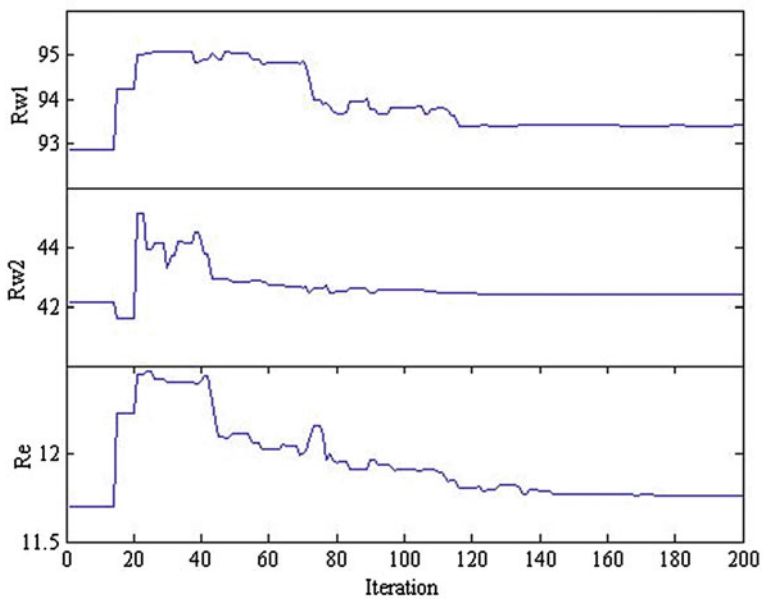


Fig. 7 Thermal resistance estimations due to the iteration of PSO

parameter estimation of the thermal model. In addition to its good accuracy, it is very fast in comparison with the GA [3].

Figure 9 shows the correlation between models parameters and the temperature. Actually, it had been seen that considering the temperature dependency, it causes no significant increase in accuracy of the introduced model.

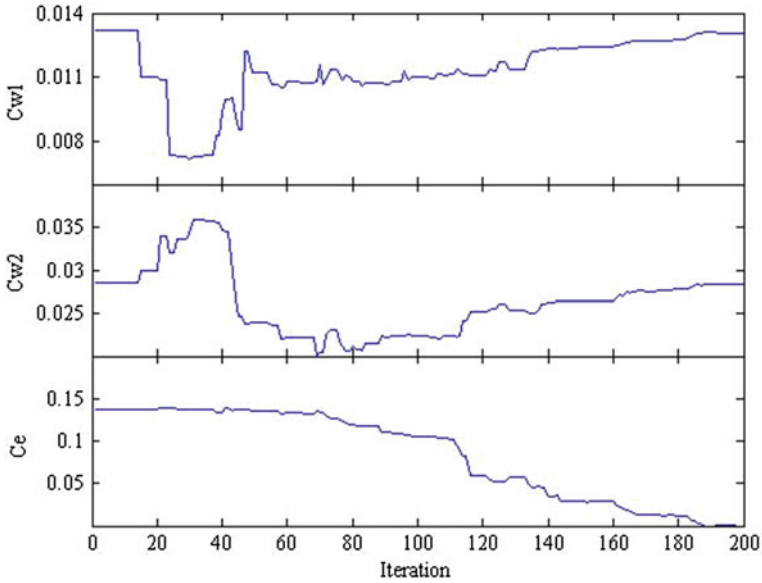
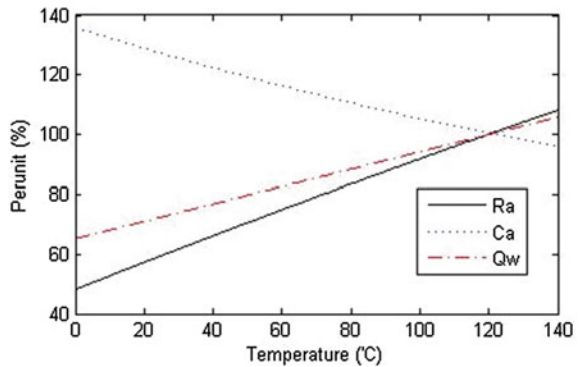


Fig. 8 Thermal capacitor estimations due to the iteration of PSO

Fig. 9 Temperature dependency of the thermal model parameters



4 Model Validation and Dynamic Thermal Analysis of CRT

In order to validate the thermal model, a typical loading sequence (Fig. 10) had been applied to the estimated thermal model and the results have been verified using the experimental data (Fig. 10).

As it is shown in these figures, the introduced thermal model has a good accuracy and it can be used for dynamic thermal modeling and on-line monitoring

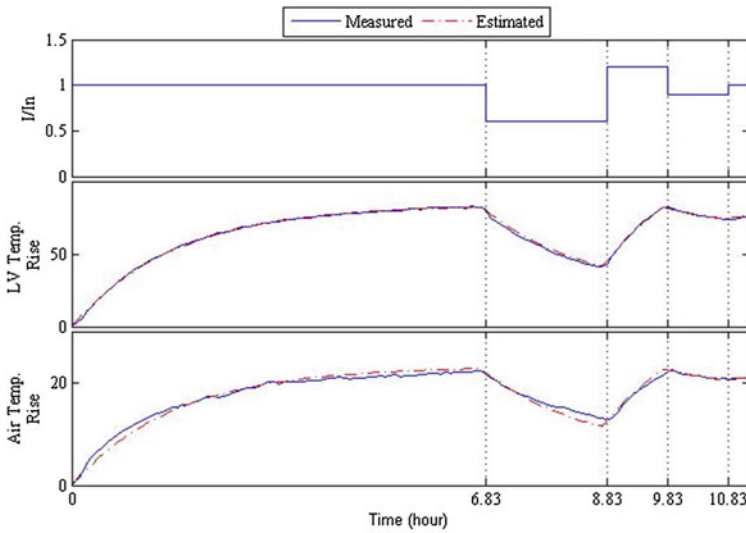


Fig. 10 Arbitrary load cycle, the LV winding temperature rise, and the cooling air temperature rise

of the CRT. Considering the effect of temperature on thermal model's parameters increases the accuracy of results; but actually in many cases, this effect can be neglected for simplification.

5 Conclusions

The paper is presenting a new detailed dynamic thermal equivalent circuit model based on PSO for the CRT. With the help of the experimental data, the model has been estimated and validated. The PSO has good performance in parameter estimation of the thermal model. In addition to its good accuracy, it is very fast in comparison with the GA.

It was shown that the introduced thermal equivalent circuit is an accurate model for dynamic thermal analysis of the CRT. Using the introduced thermal model, the effects of different factors on the windings temperatures and thus the life-time of CRT can be studied.

By considering the temperature-dependent parameters in the thermal equivalent circuit, the accuracy of the introduced model has been improved. But it can be shown that the temperature dependency of the parameters does not have a considerable effect on windings temperatures.

References

1. Pierce LW (1992) An investigation of the temperature distribution in cast-resin transformer windings. *IEEE Trans Power Delivery* 7:920–926
2. Lee M, Abdullah HA, Jofriet JC, Patel D, Fahrioglu M (2011) Air temperature effect on thermal models for ventilated dry-type transformers. *J Electr Power Syst Res* 81:783–789
3. Rahimpour E, Azizian D (2007) Analysis of temperature distribution in cast-resin dry-type transformers. *Electr Eng* 89(4):301–309
4. Eslamian M, Vahidi B, Eslamian A (2011) Thermal analysis of cast-resin dry-type transformers. *J Energy Convers Manag* 52:2479–2488
5. Dianchun Z, Jiexiang Y, Zhenghua W (2000) Thermal field and hottest spot of the ventilated dry-type transformer. In: *IEEE Proceedings of the 6th international conference on properties and applications of dielectric materials*, Xi'an, China, June 2000
6. Cho HG, Lee UY, Kim SS, Park YD (2002) The temperature distribution and thermal stress analysis of pole cast resin transformer for power distribution. In: *IEEE conference international symposium on electrical insulation*, Boston, USA, April 2002
7. Jian H, Lin C, Zhang SY (2007) Transformer real-time reliability model based on operating conditions. *J Zhejiang Univ* 8(3):378–383
8. Randakovic Z, Feser KA (2003) New method for the calculation of hot-spot temperature in power transformers with ONAN cooling. *IEEE Trans Power Deliv* 18(4)
9. Susa D, Palola J, Lehtonen M, Hyvärinen M (2005) Temperature rises in an OFAF transformer at OFAN cooling mode in service. *IEEE Trans Power Deliv* 20(4)
10. Susa D, Lehtonen M, Nordman H (2005) Dynamic thermal modeling of distribution transformers. *IEEE Trans Power Deliv* 20(3)
11. Wang S, Xu X (2006) Parameter estimation of internal thermal mass of building dynamic models using genetic algorithm. *Energy Convers Manag* 47:1927–1941
12. Taghikhani MA (2012) Power transformer top oil temperature estimation with GA and PSO methods. *Energy Power Eng* 4(1):41–46
13. Ghareh M, Sepahi L (2008) Thermal modeling of dry-transformers and estimating temperature rise. *Int J Electr Electron Sci Eng* 2(9)
14. Azizian D, Bigdeli M, Firuzabad MF (2010) A dynamic thermal based reliability model of cast-resin dry-type transformers. In: *International conference on power system technology*, Hangzhou, China, Oct 2010
15. Incropera FP, DeWitt DP (2002) *Fundamentals of heat and mass transfer*. John Wiley and Sons Inc
16. IEC Std. 60076-12. (2008) *Loading Guide for Dry-Type Power Transformers*. IEC Nov 2008
17. Kennedy J, Eberhart R (1995) Particle swarm optimization. In: *IEEE International conference on neural networks*, Perth, Australia, vol 4, pp. 1942–1948
18. Shi Y, Eberhart R (1999) Empirical study of particle swarm optimization. In: *Proceeding of the 1999 congress on evolutionary computation*, CEC 99, vol 3, pp. 1945–1950
19. Zheng Y, Ma L, Zhang L, Qian I (2003) On the convergence analysis and parameter selection in particle swarm optimization. In: *Proceedings of international conference machine learning cybern*, pp 1802–1807
20. Clerc M, Kennedy J (2002) The particle swarm-explosion, stability, and convergence in a multidimensional complex space. *IEEE Trans Evol Comput* 6:58–73
21. Design Sheets for 400kVA Transformer. ITRD025, Dry-Type Transformers Technical Office. IRAN TRANSFO Company

Geometric Model of a Railway Wheel with Irregular Contour

T. Mazilu

Abstract Modeling the irregularities of the rolling surfaces in a wheel/rail system is of utmost importance from the accuracy perspective in predicting the wheel/rail interaction. This paper proposes a new geometric model of the wheel with irregular contour, which takes into account the wheel curvature. Upon using this model, the interaction between a wheel flat and a smooth rigid rail is simulated.

Keywords Wheel/rail geometry · Irregular contour · Contact · Wheel flat

1 Introduction

The irregularities of the wheel/rail rolling surfaces have many agents, such as manufacturing tolerances [1], wear [2], material fatigue, malfunction of the braking system [3], etc. Moreover, the wheel/rail interaction in the presence of the irregularities of the rolling surfaces has different effects of practical interest: wear of rolling surfaces [4, 5], rolling noise [6, 7], degradation of the ballast [8], ground vibration [9, 10], and even increasing irregularities or track fatigue, due to dynamic loads [11, 12].

Studying the wheel/rail interaction implies an adequate modeling of the rolling surfaces irregularities. The most difficult task consists in modeling the irregular contour of the wheel, due to the wheel curvature and the possibility of the double contact point. Classical models are based on the so-called equivalent indentation on the railhead [13]. Hence, the problem of the contact between a wheel with irregular contour and a smooth rail is replaced by the one of the contact between a smooth wheel and a rail with an equivalent indentation on its head.

T. Mazilu (✉)

Railway Vehicles Department, University Politehnica of Bucharest,
Bucharest, Romania

e-mail: trmazilu@yahoo.com

This paper focuses on a new geometric model of the contact between a wheel with irregular contour and a smooth rail. This model is more realistic since it takes the wheel curvature into account. The interaction between a flat wheel and a rigid smooth rail is being studied, by using the new geometric model.

2 Wheel/Rail Geometry

This chapter deals with a wheel with irregular contour that is rolling without slipping along a perfectly smooth rigid rail, as seen in Fig. 1. The irregular contour of the wheel is described by the function

$$\rho = \rho(\theta), \tag{1}$$

where ρ and θ are the polar coordinates in respect to the wheel center O_w .

Point M on the wheel contour has the coordinates x and y in respect to the orthogonal reference Oxy , where the origin point O belongs to the wheel contour

$$x = \rho \sin \theta \tag{2}$$

$$y = \rho_o - \rho \cos \theta, \tag{3}$$

where ρ_o is the distance from the wheel center O_w to the point O .

The orthogonal reference Oxy is attached by the head of the rigid rail.

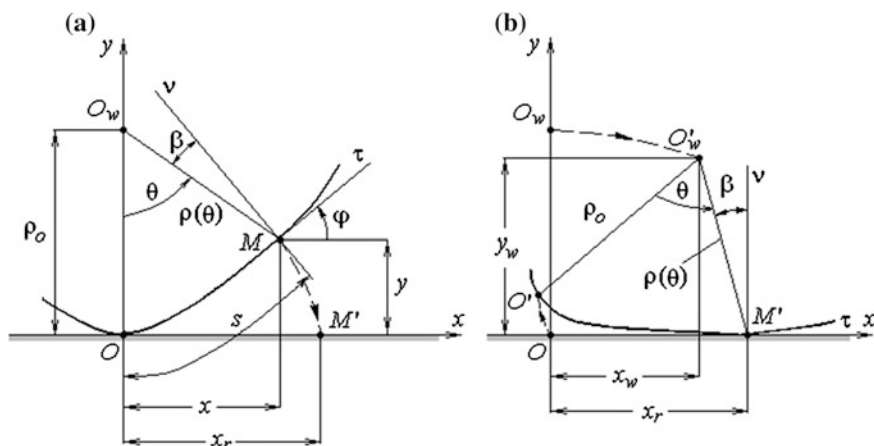


Fig. 1 Wheel/rail geometry: **a** reference position; **b** particular position

The slope of the tangent $M\tau$ is given as

$$\tan \varphi = \frac{dy}{dx}. \quad (4)$$

By differentiating relations (2) and (3), it is obtained

$$dx = (\rho \cos \theta + \rho' \sin \theta)d\theta \quad (5)$$

$$dy = (\rho \sin \theta - \rho' \cos \theta)d\theta, \quad (6)$$

where

$$\rho' = \frac{d\rho}{d\theta}. \quad (7)$$

Inserting the above differentials in (4), it reads

$$\frac{dy}{dx} = \tan \varphi = \frac{\rho \sin \theta - \rho' \cos \theta}{\rho \cos \theta + \rho' \sin \theta}. \quad (8)$$

The geometrical considerations drive to the angle between the O_wM and the normal $M\nu$

$$\beta = \theta - \varphi. \quad (9)$$

When the wheel rolls without slipping on the rail, the initial contact point O between the wheel and the rail arrives in O' , the point M comes in the point M' on the rail head; when the wheel center O_w arrives in the point O_w' (Fig. 1b), the abscissa of the M' point is x_r .

We are interested in calculating the coordinate (x_w, y_w) of the wheel center when the wheel turns around the center point at the angle θ . To this end, the length of the arch OM has to be known.

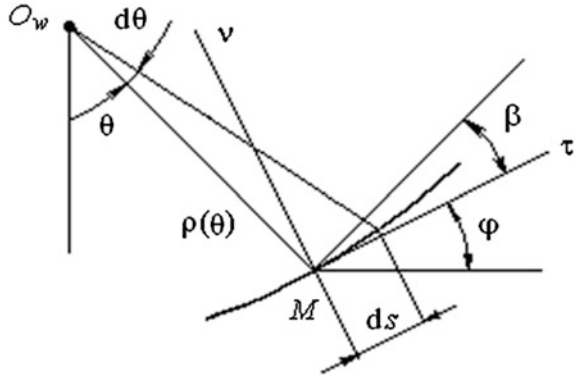
According to the geometrical correlation in Fig. 2, the length of an infinitesimal element of the wheel contour is

$$ds = \frac{\rho}{\cos \beta} d\theta \quad (10)$$

and the length of the wheel contour between O and M points is

$$s = \int ds = \int_0^\theta \frac{\rho}{\cos \beta} d\theta \quad (11)$$

Fig. 2 Explanation for the calculus of infinitesimal element of the wheel contour



When the wheel rolls on a rigid rail and the wheel rotation angle is θ , the distance between the initial contact point O and the current wheel–rail contact point M' and the arch length are equal

$$x_r = s. \tag{12}$$

According to Fig. 1b, the coordinates of the wheel center are as follows

$$x_w = x_r - \rho \sin \beta \tag{13}$$

$$y_w = \rho \cos \beta. \tag{14}$$

In the preceding geometrical considerations, we tacitly suppose that the wheel and the rail have a single contact point. However, this hypothesis has to be verified. To this purpose, the curvature of the wheel contour must be calculated

$$C = \frac{\frac{d^2y}{dx^2}}{\left[1 + \left(\frac{dy}{dx}\right)^2\right]^{3/2}}. \tag{15}$$

The derivation dy/dx is given by Eq. (8), while the derivation of second order can be computed according to the equation

$$\frac{d^2y}{dx^2} = \frac{d}{d\theta} \left(\frac{dy}{dx}\right) \frac{1}{\frac{dx}{d\theta}} = \frac{\rho^2 - \rho\rho' + 2\rho'^2}{(\rho \cos \theta + \rho' \sin \theta)^3}. \tag{16}$$

Upon inserting Eqs. (8) and (16) in (15), it is obtained

$$C = \frac{\rho^2 - \rho'' + 2\rho'^2}{(\rho^2 + \rho'^2)^{3/2}} \text{sign}(\rho \cos \theta + \rho' \sin \theta). \quad (17)$$

When the wheel and the rail have a single contact point, the curvature takes a positive value for $-\pi/2 < \theta < \pi/2$ and a negative value for all the others.

3 Kinematics of Wheel/Rail

In this section, the velocity and acceleration of the wheel center will be calculated. The velocity components of the wheel center can be formulated as follows

$$\frac{dx_w}{dt} = \frac{dx_w}{d\theta} \frac{d\theta}{dt}, \quad \frac{dy_w}{dt} = \frac{dy_w}{d\theta} \frac{d\theta}{dt}. \quad (18)$$

When using Eqs. (13) and (14), it is obtained

$$\frac{dx_w}{dt} = \dot{\theta} \left(\frac{\rho}{\cos \beta} - \rho' \sin \beta - \rho \beta' \cos \beta \right), \quad (19)$$

$$\frac{dy_w}{dt} = \dot{\theta} (\rho' \cos \beta - \rho \beta' \sin \beta), \quad (20)$$

where $\dot{\theta} = \frac{d\theta}{dt}$.

The acceleration components of the wheel center can be calculated via the following equations

$$\begin{aligned} \frac{d^2x_w}{dt^2} = & \ddot{\theta} \left(\frac{\rho}{\cos \beta} - \rho' \sin \beta - \rho \beta' \cos \beta \right) \\ & + \dot{\theta}^2 \left(\frac{\rho' \cos \beta + \rho \beta' \sin \beta}{\cos^2 \beta} - \rho'' \sin \beta - 2\rho' \beta' \cos \beta - \rho \beta'' \cos \beta + \rho \beta'^2 \sin \beta \right) \end{aligned} \quad (21)$$

$$\begin{aligned} \frac{d^2y_w}{dt^2} = & \ddot{\theta} (\rho' \cos \beta - \rho \beta' \sin \beta) \\ & + \dot{\theta}^2 (\rho'' \cos \beta - 2\rho' \beta' \sin \beta - \rho \beta'' \sin \beta - \rho \beta'^2 \cos \beta), \end{aligned} \quad (22)$$

For practical purposes, it is interesting to notice the case when the x component of the wheel center velocity is constant, which means that

$$\frac{dx_w}{dt} = V, \quad \frac{d^2x_w}{dt^2} = 0, \quad (23)$$

where V is the forwardness speed of the wheel, and the correspondent component of the acceleration is zero.

The y component of the wheel center velocity can be computed using the following formula

$$\frac{dy_w}{dt} = \frac{dy_w}{dx_w} \frac{dx_w}{dt}. \quad (24)$$

From Eqs. (13), (12), and (10), it follows

$$dx_w = dx_r - (\rho' \sin \beta + \rho \beta' \cos \beta) d\theta = \left(\frac{\rho}{\cos \beta} - \rho' \sin \beta - \rho \beta' \cos \beta \right) d\theta. \quad (25)$$

Also, from Eq. (14) we have

$$dy_w = (\rho' \cos \beta - \rho \beta' \sin \beta) d\theta. \quad (26)$$

Finally, the y component of the wheel center velocity is given as

$$\frac{dy_w}{dt} = V \frac{\rho' \cos \beta - \rho \sin \beta}{\frac{\rho}{\cos \beta} - \rho' \sin \beta - \rho \beta' \cos \beta}. \quad (27)$$

The y component of the wheel center acceleration can be obtained from Eq. (24)

$$\frac{d^2y_w}{dt^2} = \frac{d}{dt} \left(\frac{dy_w}{dx_w} \right) \frac{dx_w}{dt} + \frac{dy_w}{dx_w} \frac{d^2x_w}{dt^2} = \left(\frac{dx_w}{dt} \right)^2 \frac{d^2y_w}{dx_w^2} + \frac{dy_w}{dx_w} \frac{d^2x_w}{dt^2}. \quad (28)$$

Taking into account Eq. (23), the y component of the wheel center acceleration becomes

$$\frac{d^2y_w}{dt^2} = V^2 \frac{d^2y_w}{dx_w^2}, \quad (29)$$

where the derivation of second order is

$$\frac{d^2y_w}{dx_w^2} = \frac{d}{d\theta} \left(\frac{dy_w}{d\theta} \frac{1}{\frac{dx_w}{d\theta}} \right) \frac{1}{\frac{dx_w}{d\theta}} = \frac{\frac{dx_w}{d\theta} \frac{d^2y_w}{d\theta^2} - \frac{d^2x_w}{d\theta^2} \frac{dy_w}{d\theta}}{\left(\frac{dx_w}{d\theta} \right)^3} \quad (30)$$

with

$$\frac{dx_w}{d\theta} = \frac{\rho}{\cos \beta} - \rho' \sin \beta - \rho \beta' \cos \beta \quad (31)$$

$$\frac{d^2x_w}{d\theta^2} = \frac{\rho' \cos \beta + \rho \beta' \sin \beta}{\cos^2 \beta} - \rho'' \sin \beta - 2\rho' \beta' \cos \beta + \rho \beta'^2 \sin \beta - \rho \beta'' \cos \beta \quad (32)$$

$$\frac{dy_w}{d\theta} = \rho' \cos \beta - \rho \beta' \sin \beta \quad (33)$$

$$\frac{d^2y_w}{d\theta^2} = \rho'' \cos \beta - 2\rho' \beta' \sin \beta - \rho \beta'' \sin \beta - \rho \beta'^2 \cos \beta. \quad (34)$$

In the next section, Eq. (29) is used to solve the equations of motion.

4 Equations of Motion

A loaded wheel with the irregular contour is being considered, which rolls without slipping along a smooth rigid rail (Fig. 3). The forwardness speed of the wheel is constant, V . The wheel load is Q and the wheel mass is m .

According to Newton's Laws of Motion, the governing equations of motion are

$$m \frac{d^2y_w}{dt^2} = N - Q \quad (35)$$

$$J \frac{d^2\theta}{dt^2} = -N \rho \sin \beta, \quad (36)$$

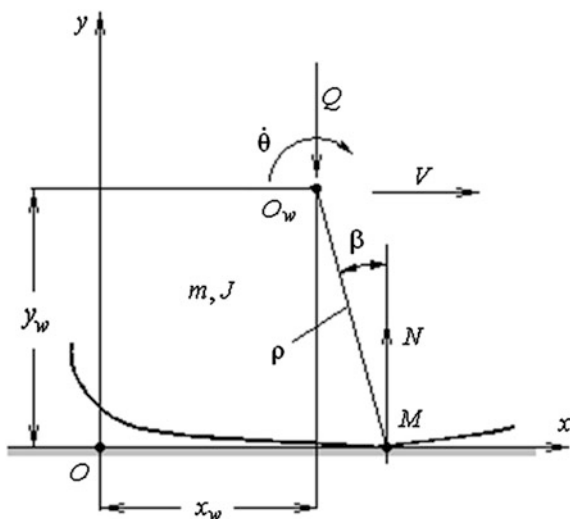
where J is the mass moment of the wheel and N is the reaction of the rail.

The unknown quantities in the equations of motion are the angle θ and the reaction N . The vertical displacement of the wheel center y_w depends on the angle θ via Eqs. (29–34).

From Eqs. (29) and (35), the reaction of the rail results as

$$N = Q + mV^2 \frac{d^2y_w}{dx_w^2} \quad (37)$$

Fig. 3 The model of a wheel with irregular contour rolling along a smooth rail



or

$$N = Q + mV^2 \frac{\frac{dx_w}{d\theta} \frac{d^2 y_w}{d\theta^2} - \frac{d^2 x_w}{d\theta^2} \frac{dy_w}{d\theta}}{\left(\frac{dx_w}{d\theta}\right)^3}, \tag{38}$$

if considering Eq. (30). It can be noticed that the rail reaction has two components —one equals the wheel load and the other is proportional to the wheel mass and increases with V^2 .

Finally, by substituting N from Eq. (36), we have the equation

$$J \frac{d^2 \theta}{dt^2} = - \left[Q + mV^2 \frac{\frac{dx_w}{d\theta} \frac{d^2 y_w}{d\theta^2} - \frac{d^2 x_w}{d\theta^2} \frac{dy_w}{d\theta}}{\left(\frac{dx_w}{d\theta}\right)^3} \right] \rho \sin \beta, \tag{39}$$

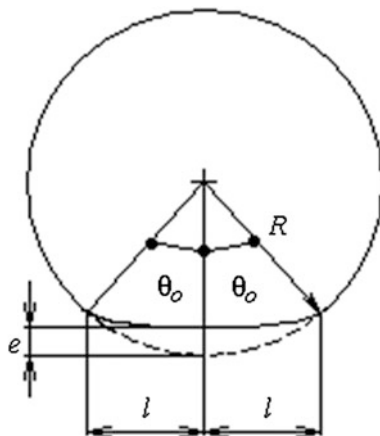
which needs a solution.

5 Application

Here, the previously presented theory applies in the case of a wheel flat of radius R , which has the length of the flat defect $2l$ and the depth e (Fig. 4).

The mathematical shape of the flat defect can be given as

Fig. 4 Wheel flat



$$\rho = R - \frac{e}{2} \left(1 - \cos \pi \frac{\theta - \theta_o}{\theta_o} \right), \tag{40}$$

where $\theta_o = \arcsin(l/R)$.

Next, the following values of the wheel parameters are to be taken into account: $V = 10 \text{ m/s}$, $R = 460 \text{ mm}$, $l = 30 \text{ mm}$, $e = 0.35 \text{ mm}$, $m = 750 \text{ kg}$, $J = 120 \text{ kg m}^2$ and the wheel load $Q = 100 \text{ kN}$. Figure 5 shows the flat defect contour and the wheel ideal contour.

When using Eqs. (13) and (14), the trajectory of the wheel center can be computed, (Fig. 6), and it has a characteristic shape [14].

The angular velocity of the wheel is displayed in Fig. 7 for the case when the forwardness velocity is constant. When the wheel passes over the first part of the flat defect, the angular velocity increases since the distance between the wheel center and the wheel/rail contact point becomes smaller. Certainly, this tendency reverses in the second part of the passing over the flat defect.

Fig. 5 Wheel flat: dashed line, ideal contour; line, flat contour

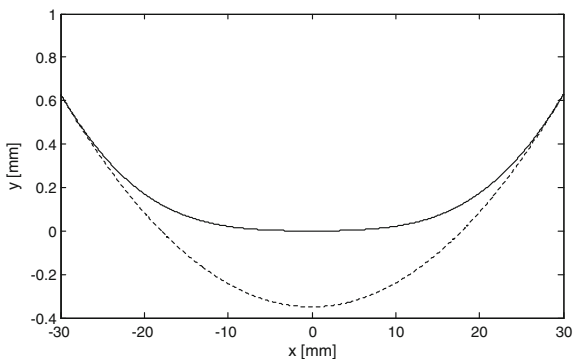


Fig. 6 The trajectory of the wheel center

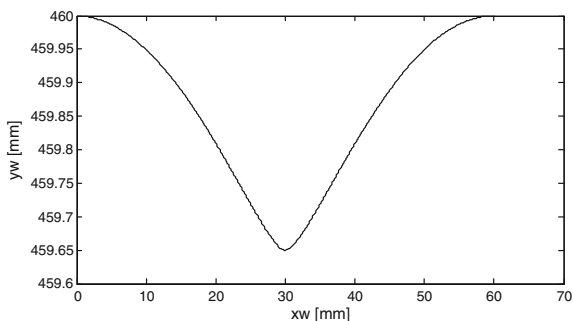
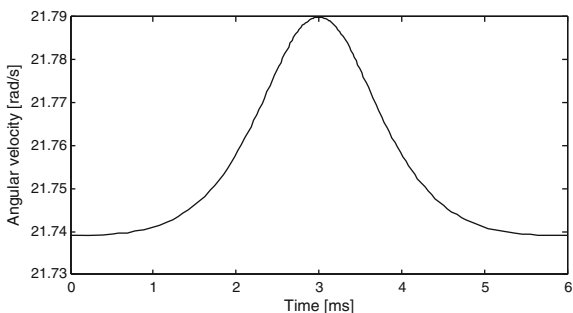


Fig. 7 The angular velocity of the wheel



6 Conclusions

The railway wheel contour is irregular due to many causes, such as local defects, roughness, short waves, etc.

This paper deals with a new geometric model of the irregular contour of a wheel. This model takes into account the real irregular contour of the wheel and therefore, it is more realistic than the classical ones which imply the equivalent rail indentations. The model has been used to simulate the interaction between a wheel flat and a perfectly smooth rigid rail.

The presented model can be developed to study the wheel/rail interaction deriving from any shape of the irregularities in the rolling surfaces.

References

1. Mazilu T, Dumitriu M (2013) Technology manufacturing and repair of railway rolling stock (Tehnologia fabricării și reparării materialului rulant de cale ferată), Matrix Rom, Bucharest
2. Nielsen JCO, Lunden R, Johansson A, Vernersson T (2003) Train-track interaction and mechanisms of irregular wear on wheel and rail surfaces. *Vehicle Syst Dyn* 40(1-3):3-54
3. Cruceanu C (2009) Brakes for railway vehicles (Frâne pentru vehicule feroviare) Matrix Rom, Bucharest, 3rd edn

4. Oostermeijer KH (2008) Review on short pitch rail corrugation studies. *Wear* 265:1231–1237
5. Ignesti M, Malvezzi M, Marini L, Meli E, Rindi A (2012) Development of a wear model for the prediction of wheel and rail profile evolution in railway systems. In: *Wear* 284–285, pp 1–17
6. Remington JP (1988) Wheel/rail rolling noise: what do we know? what don't we know? where do we go from here? *J Sound Vib* 120:203–226
7. Thompson DJ, Jones CJC (2000) A review of the modelling of wheel/rail noise generation. *J Sound Vib* 231:519–536
8. Popp K, Kruse H, Kaiser I (1999) Vehicle-track dynamics in the mid-frequency range. *Vehicle Syst Dyn* 38(1–3):345–488
9. Sheng X, Jones CJC, Thompson DJ (2004) A theoretical model for ground vibration from trains generated by vertical track irregularities. *J Sound Vib* 272:937–965
10. Lombaert G, Degrande G (2009) Ground-borne vibration due to static and dynamic axle loads of InterCity and high-speed trains. *J Sound Vibration* 319(3–5):1036–1066
11. Dumitriu M (2012) On the dynamic vertical wheel-rail forces at low frequencies. In: *Fiability and Durability/Fiabilitate si Durabilitate, Supplement no 1*, pp 11–17
12. Dumitriu M (2013) Influence of the primary suspension damping on the vertical dynamic forces at the passenger railway vehicles. In: *U.P.B. Scientific Bulletin Series D*, vol 75, iss 1, pp 25–40
13. Wu TX, Thompson DJ (2002) A hybrid model for the noise generation due to railway wheel flats. *J Sound Vib* 251:115–139
14. Mazilu T (2008) Wheel/rail vibrations (Vibrații roată-șină). Matrix Rom, Bucharest

Grafting, Locations, and Ordinal Dispersion

Tiberiu Spircu

Abstract Locations, fulfilling the conditions that measures of location should satisfy, and dispersions whose behavior mimics that of entropy, are introduced in the framework of weighted rooted trees. Ordinal dispersion, introduced by Leti in 1983 as a measure of dispersion for ordinal variables, is generalized in this framework, and a relation with dispersions of classical type is established. A concordance measure coherent with ordinal dispersion is introduced.

AMS Classification 62H20 · 05C05

Keywords Measure of dispersion · Ordinal dispersion · Rooted tree

1 Introduction

Several attempts have been made in the last decades to define measures of dispersion for ordinal variables [11, 20] with satisfactory properties, taking into account the systematic work of Bickel and Lehmann [2, 3] in the 1970s, summarized by Oja [14], about location and dispersion measures.

On the other hand, recent advances have been made in the theory of operads [4, 12, 18, 21, 22] since its applications in the quantum theory.

Some basic ideas on operads lead to a reasonable approach to define location, (classical) dispersion, and ordinal dispersion from a natural point of view, namely by using a grafting framework, well known from combinatorics.

This approach is very helpful in an attempt to coherently define “covariances” and “correlations” in the ordinal context.

T. Spircu (✉)

Institute of Mathematics of the Romanian Academy, 21 Calea Griviței,
010736 Bucharest, Romania
e-mail: spircut@yahoo.com

Sections 2 and 3 are introductory; the main classical notions that will be used in the sequel, namely those of weighted rooted tree and grafting, are remembered here.

Sections 4 and 5 are devoted to the study of location measures in the context of weighted rooted trees.

Sections 6 and 7 show how dispersions appear in this context, and how their properties are similar to those of Shannon's entropy.

An ordinal dispersion has been introduced in [11] (pp. 290–297) and intensively used in several studies on university courses' evaluation (see [7, 8]). Section 8 is devoted to the natural introduction of the ordinal dispersion and, eventually, Section 9 presents the way of coherently introducing ordinal covariance and correlation.

2 Rooted Trees and Grafting

The notion of **tree** is well known and we remind it only for the sake of completeness; it is a pair $T = (V_T, E_T)$, where V_T is the (finite) set of **vertices** and E_T is the set of edges, such that either of the following conditions is fulfilled (see [1], Chap. XVI, Theorem 1):

- (i) As a graph, T is connected and $|E_T| = |V_T| - 1$;
- (ii) Any pair of vertices is linked by a unique chain.

The number of vertices $|V_T|$ is called the **order** of T .

A **rooted tree** is a tree $T = (V_T, E_T)$ together with a selected vertex r_T . This vertex induces a natural ordering on V_T , such that V_T becomes a partially ordered set (poset—see [22]) having r_T as the (unique) smallest element.

The maximal elements in this poset are called **leaves** of the rooted tree. In rooted trees, the condition (ii) above becomes:

- (ii') Any pair of vertices is linked by a unique chain and in particular

(ii'') Any vertex $v \in V_T$ is linked to the root r_T by a unique path.

The length of this path is called the **depth** of v and is denoted in the sequel by $d_T(v)$.

The maximum length of paths linking the root r_T with leaves is called the **height** of tree T and is denoted in the sequel by $h(T)$. In what follows the height of trees and the depth of vertices will be by far more important than the order of trees.

Of course, $d_T(r_T) = 0$. If $d_T(v) = 1$ for all other vertices $v \in V_T$, then we say that T is an **n -corolla** (here $n + 1$ is the order of T). Of course, $h(C) = 1$ for any corolla C .

The **trivial** rooted tree τ will be an exceptional tree, with only one vertex, its root. This single vertex will be considered, simultaneously, as root and as leaf.

In a non-trivial rooted tree we denote by $y \rightarrow x$ an existing arrow, instead of the ordinary notation $(y, x) \in E_T$. The vertex x will be called **child** of the vertex y , and

y will be called **parent** of x . By convention, all the arrows will be oriented toward leaves.

The **reduction** of a (non-trivial) rooted tree $T = (V_T, E_T)$ consists of repeatedly:

- (a) Replacing the root by its unique neighbor, in case only one arrow is adjacent to the initial root r_T ; of course, in this case the old root and its adjacent arrow will be removed;
- (b) Removing any vertex that has only one parent and one child, and replacing its two adjacent arrows by a single arrow directly linking the parent to its child.

In the sequel all rooted trees will be either trivial, or **reduced**. Hence, in non-trivial rooted trees, all vertices—except the leaves—will have at least two children.

The notion of subtree usually means the following: any subgraph of a tree which is itself a tree (see [19]). However, we will use it with a slight different meaning. Namely, a **subtree** of a rooted tree, **rooted at vertex** v , is the tree of all descendants (toward the leaves) of v . Obviously it is a rooted tree, having v as root.

The height of rooted trees and the depth of vertices introduced above allow inductive proofs of some results for all rooted trees, provided they have been established for corollas.

Definition 1 Consider two rooted trees S and T , with roots r_S res. r_T , and suppose a leaf l of S is selected. In this context, the **graft** of T over S along l , denoted $S \circ_l T$, is the rooted tree such that:

- Its set of vertices is $V_S \cup V_T - \{l\}$;
- Its set of edges (arrows) is $E_S \cup E_T$;
- Its root is r_S .

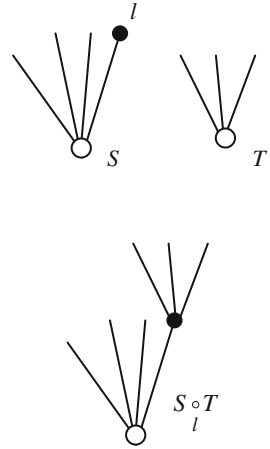
Obviously, the leaf l selected to perform the grafting is destroyed in the process, the leaves of this new rooted tree $U = S \circ_l T$ are all the other leaves of S and all the leaves of T .

The depth $d_U(u)$ of a vertex u of $S \circ_l T$ is equal to $d_S(u)$ if u is a vertex of S , and is equal to $d_T(u) + d_S(l)$ if u is a vertex of T . As for the height $h(U)$, only the obvious inequalities $\max\{h(S), h(T)\} \leq h(U) \leq h(S) + h(T)$ can be established (Fig. 1).

Although the graft of T over S along l can be constructed for arbitrary rooted trees S and T , we suppose these trees are reduced. Of course, $S \circ_l T$ will be reduced as well.

Keeping fixed the rooted tree S , the grafting operation can be repeated as long as not all the leaves of S have been destroyed, provided for each leaf l_k a rooted tree T_k is considered. In this way, if l_1, \dots, l_p are all the leaves of S (labeled in a particular order), and T_1, \dots, T_p are arbitrary rooted trees (labeled accordingly, and composing a “forest”), by repeated grafting we obtain the “full graft” rooted tree

Fig. 1 Grafting



$$S \circ \{T_1, T_2, \dots, T_p\} = (\dots((S \circ_{l_1} T_1) \circ_{l_2} T_2) \dots \circ_{l_p} T_p). \tag{1}$$

For this rooted tree we have $h(S \circ \{T_1, T_2, \dots, T_p\}) = \max_{1 \leq k \leq p} \{h(T_k + d_S(l_k))\}$ and, in case S is a corolla, $h(S \circ \{T_1, T_2, \dots, T_p\}) = \max_{1 \leq k \leq p} \{h(T_k)\} + 1$.

If T' is the subtree of T rooted at vertex v , then by removing the subtree from T and by transforming v into a leaf we obtain another tree T'' whose root is that of T . It is obvious that T coincides with the graft $T' \circ_v T''$.

The following result has an obvious proof.

Proposition 1 (See [21], Prop. 0.2.6). *Let T be a rooted tree, with root r . Suppose r_1, \dots, r_m are all the vertices of T of depth 1 (i.e. directly above r , ordered in a particular order). Let T_k be the subtree that contains the vertex r_k as root and everything above it in T . Then*

$$T = C \circ \{T_1, \dots, T_m\}$$

where C is the m -corolla consisting of r as root and $\{r_1, \dots, r_m\}$ as the set of leaves.

Corollary *Any reduced rooted tree T , of height h , can be expressed in a unique way as a full graft*

$$C \circ \{T_1, \dots, T_m\}$$

where C is a m -corolla with the same root as T , and T_1, \dots, T_m are reduced rooted trees of heights $\leq h - 1$.

Indeed, $h(T_k) \geq h$ means the existence of a path of length $\geq h$ linking a leaf l of T_k to r_k , hence the existence of a path of length $\geq h + 1$ from l to r , and this contradicts the hypothesis $h(T) = h$.

In fact, the “full grafting” operation \circ is exactly the Butcher product of the tree T_1 with the “forest” $\{T_2, \dots, T_m\}$ (see [4, 12]). The graft $S \circ_l T$ of T over S along l is in fact the “full graft” $S \circ \{\tau, \dots, T, \dots, \tau\}$, where T is in position l .

Obviously the leaves of $S \circ \{T_1, \dots, T_m\}$ are the elements of the set $\bigcup_{k=1}^m L_k$, where L_k is the set of leaves of T_k . If l_{k1}, \dots, l_{kj_k} are all the leaves from L_k , and if $\{U_{k1}, \dots, U_{kj_k}\}$ is a forest (of rooted trees), then obviously the forest can be grafted over T_k , giving the rooted tree $T_k \circ \{U_{k1}, \dots, U_{kj_k}\}$. On the other hand, $\bigcup_{k=1}^m \bigcup_{j=1}^{j_k} U_{kj}$ is an adequate forest for grafting over $S \circ \{T_1, \dots, T_m\}$. The “pseudo-associativity” relation

$$\left(S \circ \bigcup_{k=1}^m \{T_k\} \right) \circ \bigcup_{k=1}^m \bigcup_{j=1}^{j_k} U_{kj} = S \circ \bigcup_{k=1}^m \left\{ T_k \circ \bigcup_{j=1}^{j_k} \{U_{kj}\} \right\}$$

is in fact an operad-type associativity (see [18]).

3 Weights and Weighted Rooted Trees

Our notion of weighted rooted tree is somewhat different from other similar notions (see [10, 15]). It resembles most that of weighted graph [6], in which each edge has a positive weight attached. However, we will define weights on vertices, not on edges (arrows).

If τ is the trivial rooted tree, with root r , and if $\omega \in R_+$, a weight w will be defined by $w(r) = \omega$.

Consider $T = (V, E)$ a non-trivial rooted tree with root r . A **weight** (on T) is a function $t : V \rightarrow R_+$ such that

$$t(y) = \sum_{\substack{x \in V \\ y \rightarrow x}} t(x) \text{ for each vertex } y \in V. \tag{2}$$

It is obvious that such a weight is completely determined by its values on leaves, and that the weight of the root is $t(r) = \sum_{l \in \text{leaf of } T} t(l)$.

Definition 2 A **weighted rooted tree** is either trivial, or a rooted tree $T = (V, E)$ endowed with a function $t : V \rightarrow R_+$ such that (2) is fulfilled.

We pointed out above that any subtree T' of T is rooted at a particular vertex v of T and contains all the descendants of v . When t is a weight on T , by restriction it

obviously induces a weight t' on T' . Thus $t'(x) = t(x)$ for each vertex x of T' . The subtree T' , together with the induced weight t' , is obviously a weighted tree, which is said to be **induced** by (T, t) .

Definition 3 Let (T, t) and (T', t') be (non-trivial) weighted rooted trees. We will say that (T, t) **extends** (T', t') if T' is a subtree of T and $t'(x) = t(x)$ for each vertex x of T' , i.e. if (T', t') is induced by (T, t) .

Given (T, t) and (S, s) two weighted rooted trees, once a leaf l of S is selected, we are able to construct the rooted tree $U = S \underset{l}{\circ} T$, whose root r_U coincides with the root r_S of S . This rooted tree can be naturally endowed with a weight u , defined as follows:

$$u(x) = \begin{cases} s(x) & \text{if } x \text{ is a vertex of } S, \text{ except for } x = l \text{ (which, in fact, is destroyed)} \\ t(x) \cdot s(l)/t(r_T) & \text{if } x \text{ is a vertex of } T, \text{ where } r_T \text{ is the root of } T, \end{cases}$$

and, as a consequence, the following equality is straightforward:

$$u(r_u) = \sum_{\substack{l' \text{ leaf of } S \\ l' \neq l}} u(l') + \sum_{l' \text{ leaf of } T} u(l')$$

This weight u can be denoted as $s \underset{l}{\circ} t$, i.e. it can be considered as the graft of t over s along l . It is natural to denote (U, u) as $(S, s) \underset{l}{\circ} (T, t)$.

The propagation formula (1) allows us to deal with particular weights in an inductive manner. If l_1, \dots, l_p are all the leaves of (S, s) , and if for each leaf l_k a weighted rooted tree (T_k, t_k) is considered, then the full grafted rooted tree $S \circ \{T_1, T_2, \dots, T_p\}$ is naturally endowed with a weight. This weight obviously coincides with the repeated graft $(\dots((s \underset{l_1}{\circ} t_1) \underset{l_2}{\circ} t_2) \dots \underset{l_p}{\circ} t_p)$, will be denoted by $s \circ \{t_1, t_2, \dots, t_p\}$, and will be called the **full graft** of s and $\{t_1, t_2, \dots, t_p\}$. The weighted rooted tree which appears in this way will be denoted $(S, s) \circ \{(T_1, t_1), \dots, (T_p, t_p)\}$.

Since the root r of the full grafted rooted tree $S \circ \{T_1, T_2, \dots, T_p\}$ is exactly the root of S , the following two equalities are obvious:

$$(s \circ \{t_k\}_{1 \leq k \leq p})(r) = \sum_{1 \leq k \leq m} s(l_k) \text{ and } s(l_k) = \sum_{l \text{ leaf of } T_k} t_k(l).$$

The following result is an immediate extension of the Corollary of Proposition 1 above.

Proposition 2 Any (reduced) weighted rooted tree (T, t) , of height $h > 1$, can be expressed in a unique way as a full graft

$$(C, c) \circ \{(T_1, t_1), \dots, (T_m, t_m)\}$$

where (C, c) is a weighted m -corolla having the same root as (T, t) , and $(T_1, t_1), \dots, (T_m, t_m)$ are weighted rooted trees, of heights $\leq h - 1$, either trivial or reduced.

In fact, c and t_k are all restrictions of the weight t , $T = C \circ \{T_1, \dots, T_m\}$ as rooted tree and the weight t is exactly the full graft $c \circ \{t_1, \dots, t_m\}$.

4 Locations Over Weighted Rooted Trees

Consider $V \approx R^n$ a (finite dimensional) real vector space. The notion of pre-location (over a reduced weighted rooted tree, in short rwr-tree) with values in V will be defined by induction on the height of the tree.

The rwr-trees of height 0 are the trivial rooted tree τ plus a weight ω attached to the root r . A pre-location γ over a trivial rwr-tree (τ, ω) is simply a vector $\gamma(r) \in V$.

The rwr-trees of height 1 are the weighted m -corollas. A pre-location γ over a m -corolla (C, c) —with vertex set V and root r —is a function $\gamma : V \rightarrow V$ which satisfies the condition

$$\gamma(r) = \frac{1}{c(r)} \sum_{r \rightarrow x} c(x)\gamma(x), \quad \text{i.e.} \quad \gamma(r) = \frac{1}{c(r)} \sum_{l \text{ leaf of } C} c(l)\gamma(l).$$

Suppose pre-locations—with values in V —have been defined for all rwr-trees (T, t) of given height $h \geq 1$, as functions $\gamma : V \rightarrow V$, where V is the vertex set of T , satisfying the condition

$$\gamma(y) = \frac{1}{t(y)} \sum_{y \rightarrow x} t(x)\gamma(x) \text{ for each vertex } y \text{ of } T, \tag{3}$$

and consequently the condition

$$\gamma(r_T) = \frac{1}{t(r_T)} \sum_{l \text{ leaf of } T} t(l)\gamma(l) \tag{4}$$

where r_T is the root of T . Clearly any pre-location γ is perfectly determined by its restriction $\bar{\gamma} : L \rightarrow V$ defined on the set L of leaves of T , i.e. by the family $\{\gamma(l)\}_{l \in L}$ of vectors from V .

Let (U, u) be a rwr-tree of height $h + 1$ and let V res. L be its set of vertices res. leaves. Identify the basic corolla C of U , composed of the root r_U as root and all the vertices r_1, \dots, r_m of depth 1 as leaves. Denote by T_k the subtree of U having r_k as root and V_k res. L_k as set of vertices res. leaves. The restriction t_k of the weight u to

T_k makes (T_k, t_k) a rwr-tree of height at most h , and it is obvious that L is the union of sets L_1, \dots, L_m .

Now, if $\bar{\gamma} : L \rightarrow V$ is a function, its restrictions $\bar{\gamma}_k : L_k \rightarrow V$ can be extended to pre-locations $\gamma_k : V_k \rightarrow V$ over (T_k, t_k) , thus satisfying (3). In addition, $\gamma_k(r_k) = \frac{1}{t_k(r_k)} \sum_{l \in L_k} t_k(l) \gamma_k(l) = \frac{1}{u(r_k)} \sum_{l \in L_k} u(l) \gamma(l)$.

The vectors $\gamma_k(r_k) \in V$ identify in fact a function $\bar{\gamma}_*$ from the set of leaves $\{r_1, \dots, r_m\}$ of the corolla C , given by $\bar{\gamma}_*(r_k) = \gamma_k(r_k)$. This is obviously extended to a function γ_* such that

$$\gamma_*(r_U) = \frac{1}{u(r_U)} \sum_{1 \leq k \leq m} u(r_k) \gamma_*(r_k) = \frac{1}{u(r_U)} \sum_{1 \leq k \leq m} \sum_{l \in L_k} u(l) \gamma(l).$$

The function $\gamma : V \rightarrow V$ defined by $\gamma(x) = \gamma_k(x)$ for $x \in V_k$ and $\gamma(r_U) = \gamma_*(r_U)$ is clearly a pre-location over the rwr-tree (U, u) . The relation $\gamma(r_U) = \frac{1}{u(r_U)} \sum_{l \text{ leaf of } U} u(l) \gamma(l)$ is immediate.

Hence, condition (3) can be used to define pre-locations over arbitrary (non-trivial) rwr-trees, and condition (4) is a consequence.

Let now (S, s) and (T, t) be two (reduced) weighted rooted trees, and l a leaf of S . By grafting along l , the new rwr-tree $(U = S \circ_l T, u = s \circ_l t)$ appears.

Suppose $\gamma_S : V_S \rightarrow V$ and $\gamma_T : V_T \rightarrow V$ are two pre-locations, respectively, over the “initial” rwr-trees. We will say that γ_T is **concordant with γ_S on the leaf l** of S if $\gamma_T(r_T) = \gamma_S(l)$, where r_T is the root of T . In short, **concordant** if no confusion about the leaf is possible. In case of concordant pre-locations, it is easy to construct from them a pre-location over (U, u) , obviously defined as follows:

$$\gamma_U(x) = \begin{cases} \gamma_S(x) & \text{if } x \text{ is a vertex of } S, \\ \gamma_T(x) & \text{if } x \text{ is a vertex of } T, \end{cases}$$

for which condition (4) looks as follows:

$$\gamma_U(r_U) = \frac{1}{u(r_U)} \sum_{\substack{x \text{ leaf of } S \\ x \neq l}} u(x) \gamma_S(x) + \frac{1}{u(r_U)} \sum_{y \text{ leaf of } T} u(y) \gamma_T(y)$$

It is natural to denote by $\gamma_S \circ_l \gamma_T$ this pre-location over $(S \circ_l T, s \circ_l t)$.

By extension, if (S, s) is a non-trivial rwr-tree with $\{l_1, \dots, l_p\}$ as set of leaves, and if for each leaf l_k a rwr-tree (T_k, t_k) —possibly trivial—is considered, then we may construct the full graft rooted tree $U = S \circ \{T_1, \dots, T_p\}$ and a corresponding weight $u = s \circ \{t_1, \dots, t_p\}$ on it. If $\gamma_{T_1}, \dots, \gamma_{T_p}$ are given pre-locations (with values in V), concordant with γ_S , then the full graft $\gamma_U = \gamma_S \circ \{\gamma_{T_1}, \dots, \gamma_{T_p}\}$ appears in a natural way. It is defined as follows:

$$\gamma_U(x) = \begin{cases} \gamma_S(x) & \text{if } x \text{ is a vertex of } S, \text{ except the leaves } l_1, \dots, l_p \text{ (which are destroyed by grafting)} \\ \gamma_{T_k}(x) & \text{if } x \text{ is a vertex of } T_k. \end{cases}$$

Conversely, suppose the reduced rooted tree U is expressed as a full graft $S \circ \{T_1, \dots, T_p\}$ and is endowed with a weight u . Consider a pre-location γ over (U, u) , with values in $V \approx R^n$. In fact, γ is fully determined by a set function $\bar{\gamma} : L \rightarrow V$, where L is the set of leaves of U , i.e. γ is in fact the family $\{\gamma_l\}_{l \in L}$ of vectors from V .

On one hand, each T_k is endowed with the restriction of weight u (denoted by t_k), and γ induces in a natural way, by restriction, a pre-location γ_k over (T_k, t_k) . This pre-location is fully determined by the sub-family $\{\gamma_l\}_{l \in L_k}$, where L_k is the set of leaves of T_k .

On the other hand, the rwr-tree S is endowed with the restriction of u (denoted by s), and γ induces by restriction a pre-location γ_S over (S, s) . It is obvious that each γ_{T_k} is concordant with γ_S . The relation $\gamma = \gamma_S \circ \{\gamma_{T_1}, \dots, \gamma_{T_p}\}$ is immediate. In fact, we proved the following proposition.

Proposition 3 *If the rwr-tree (U, u) is decomposed as a full graft $(S, s) \circ \{(T_k, t_k)\}_{1 \leq k \leq p}$, and if γ is a pre-location over (U, u) with values in the vector space $V \approx R^n$, then γ decomposes as a full graft $\gamma_S \circ \{\gamma_k\}_{1 \leq k \leq p}$ where γ_S is a pre-location over (S, s) and each γ_k is a pre-location over (T_k, t_k) with values in V .*

Conversely, if $\{\gamma_{T_k}\}_{1 \leq k \leq p}$ are concordant with γ_S pre-locations over rwr-trees (T_k, t_k) res. (S, s) , all with values in $V \approx R^n$, then the full graft $\gamma_S \circ \{\gamma_{T_k}\}_{1 \leq k \leq p}$ is a pre-location over the full graft rwr-tree $(S, s) \circ \{(T_k, t_k)\}_{1 \leq k \leq p}$.

*Consider $V \approx R^n$ a (finite dimensional) real vector space. A **location** over the rwr-tree (T, t) , with values in V , is a vector $\gamma(r) \in V$, where $\gamma : V \rightarrow V$ is a pre-location over (T, t) , r is the root of T , and V is the set of its vertices.*

Since the pre-location γ is fully determined by the family $\{\gamma(l)\}_{l \in L}$ of vectors from V , where L is the set of leaves of T , we will denote the location $\gamma(r)$ by $\Gamma[(T, t), \{\gamma(l)\}_{l \in L}]$ or simply $\Gamma[T, \{\gamma(l)\}_{l \in L}]$ when no confusion on weights is possible.

5 Main Properties of Locations

In what follows, (T, t) will be a rwr-tree, with root r , vertex set V , and L set of leaves. Given the vector space $V \approx R^n$, denote by L the set of locations over (T, t) with values in V . Recall an element $\gamma \in L$ is fully determined by a family $\{\gamma(l)\}_{l \in L}$ of vectors of V , where γ is a pre-location over (T, t) .

Denote by G the group: (a) whose elements are the pairs $g = (\alpha, v)$ where α is an automorphism of V and v is a vector of V ; (b) whose neutral element is the pair $(1_V, 0)$, and (c) whose composition law \cdot is given by the formula $(\alpha, v) \cdot (\alpha', v') = (\alpha \circ \alpha', \alpha(v') + v)$. It is in fact the “affine” group of dimension n over the field R .

The group G operates on V , as follows:

$$(\alpha, v) * w = \alpha(w) + v$$

and in consequence it operates coordinatewise on the Cartesian product V^L .

On the other hand, the group G operates on L , as follows:

$$(\alpha, v) * \Gamma[T, \{\gamma(l)\}_{l \in L}] = \Gamma[T, \{\alpha(\gamma(l)) + v\}_{l \in L}].$$

The proof of the following proposition is a simple check.

Proposition 4 *Under the notations above, if $g = (\alpha, v) \in G$ and $\Gamma[T, \{\gamma(l)\}_{l \in L}] \in L$, then*

$$g * \Gamma[T, \{\gamma(l)\}_{l \in L}] = \Gamma[T, g * \{\gamma(l)\}_{l \in L}]. \quad (5)$$

In other words, the location “commutes” with the actions of G .

Suppose a basis e_1, e_2, \dots, e_n has been selected in the vector space V . Since the vector space V is naturally ordered, at least in two ways:

(1) The product order $v \leq w$, meaning $v_i \leq w_i$ in each coordinate $1 \leq i \leq n$;

(2) The lexicographic order $v \prec w$, meaning $v_1 < w_1$ or $v_1 = w_1, v_2 < w_2$, or $v_1 = w_1, v_2 = w_2, v_3 < w_3 \dots$

The two orderings extend to pre-locations γ, γ' over a rwr-tree (T, t) , as follows:

(1') $\gamma \leq \gamma'$ if $\gamma(l) \leq \gamma'(l)$ for all leaves l of T ;

(2') $\gamma \prec \gamma'$ if $\gamma(l) \prec \gamma'(l)$ for all leaves l of T .

Since the weights $t(l)$ are positive real numbers, it is easily deduced that:

(1'') from $\gamma \leq \gamma'$ it follows that $\gamma(x) \leq \gamma'(x)$ for all vertices x of T , in particular $\gamma(r_T) \leq \gamma'(r_T)$;

(2'') from $\gamma \prec \gamma'$ it follows that $\gamma(x) \prec \gamma'(x)$ for all vertices x of T , in particular $\gamma(r_T) \prec \gamma'(r_T)$.

Since every location over (T, t) is fully determined by a family of vectors $\{\gamma(l)\}_{l \in L}$, it is easy to deduce from (1'') and (2'') above the following:

$$\text{If } \gamma \leq \gamma' \text{ then } \Gamma[T, \{\gamma(l)\}_{l \in L}] \leq \Gamma[T, \{\gamma'(l)\}_{l \in L}] \quad (6)$$

$$\text{If } \gamma \prec \gamma' \text{ then } \Gamma[T, \{\gamma(l)\}_{l \in L}] \prec \Gamma[T, \{\gamma'(l)\}_{l \in L}]. \quad (7)$$

Conditions (6)/(7) and (5) are similar to the conditions that a location in the probabilistic framework should satisfy according to [2] (see also [13]). Surprisingly enough, condition (8) that follows appears to be new. More precisely, in connection

with grafting, the locations exhibit a nice property, expressed in the following proposition.

Proposition 5 *If $\Gamma[(U, u), \{\gamma(l)\}_{l \in L}]$ is a location over the rwr-tree (U, u) with values in $V \approx \mathbb{R}^n$, and if (U, u) is decomposed as a full graft $(S, s) \circ \{(T_k, t_k)\}_{1 \leq k \leq p}$, then this location can be expressed in an iterated manner as $\Gamma[(S, s), \{\Gamma[(T_k, t_k), \{\gamma(l)\}_{l \in L_k}]\}_{1 \leq k \leq p}]$.*

The **proof** is immediate, taking into account Proposition 3 above, since by definition $\Gamma[(U, u), \{\gamma(l)\}_{l \in L}] = \gamma(r_U)$ where r_U is the root of U , and r_U coincides with r_S , the root of S . Moreover, the leaves of S are exactly the roots r_k of T_k and it is clear that $\gamma_{T_k}(r_k) = \Gamma[(T_k, t_k), \{\gamma(l)\}_{l \in L_k}]$.

Consequently, the following formula can be written as

$$\Gamma[S \circ \{T_k\}_{1 \leq k \leq p}, \{\gamma(l)\}_{l \in L}] = \Gamma[S, \{\Gamma[T_k, \{\gamma(l)\}_{l \in L_k}]\}_{1 \leq k \leq p}] \tag{8}$$

when no confusion on weights is possible.

6 Entropy of Reduced Weighted Rooted Trees

In order to give a general definition of the entropy in the framework of rwr-trees, set $H(\tau) = 0$ for each trivial reduced weighted rooted tree τ .

For a weighted m -corolla (C, c) , with leaves r_1, \dots, r_m and root r , let

$$H(C, c) = -\frac{1}{c(r)} \sum_{1 \leq k \leq m} c(r_k) \log c(r_k) + \log c(r).$$

Hence the entropy H is defined in a classical way (see [16]) on each rwr-tree of height 1. By induction, H will be defined on every rwr-tree.

Let now (T, t) be a rwr-tree of height $h > 1$. According to Proposition 2 above, (T, t) can be expressed in a unique way as a full graft

$$(C, c) \circ \{(T_1, t_1), \dots, (T_m, t_m)\}$$

where (C, c) is a weighted m -corolla, and (T_k, t_k) are rwr-trees of height $\leq h - 1$. By definition,

$$H(T, t) = H(C, c) + \frac{1}{t(r)} \sum_{1 \leq k \leq m} t(r_k) H(T_k, t_k)$$

where r is the root of T and r_k is simultaneously a leaf of C and the root of T_k .

In this way, by induction on the height h , the **entropy** H appears as a real function defined on the family of rwr-trees. Its main property is expressed in the following proposition.

Proposition 6 *Suppose the rwr-tree (U, u) decomposes as the graft of (T, t) over (S, s) along the leaf l of S . Then*

$$H(U, u) = H(S, s) + \frac{u(l)}{u(r)}H(T, t)$$

where r is the root of U .

Proof Let r_1, \dots, r_m be all the depth 1 vertices of U , determining the basic corolla (C, c) from the decomposition $(C, c) \circ \{(T_1, t_1), \dots, (T_m, t_m)\}$. By definition,

$$H(U, u) = H(C, c) + \frac{1}{u(r)} \sum_{1 \leq k \leq m} u(r_k)H(T_k, t_k). \tag{9}$$

Two cases may appear.

Case 1: The depth of leaf l is 1, thus l coincides with, let us say, r_1 . In this case (T_1, t_1) coincides with (T, t) , and (C, c) is the basic corolla of (S, s) . By replacing the tree (T, t) with a trivial one τ , we have $(S, s) = (C, c) \circ \{\tau, (T_2, t_2), \dots, (T_m, t_m)\}$. Taking into account that all weights s, t_k, c are induced by u , we have $H(S, s) = H(C, c) + \frac{1}{u(r)} \sum_{2 \leq k \leq m} u(r_k)H(T_k, t_k)$. It

follows that $H(U, u) = H(S, s) + \frac{u(l)}{u(r)}H(T, t)$ in this case.

Case 2: The depth of leaf l is > 1 , thus l is a descendant of, let us say, r_1 . Now (T_1, t_1) decomposes as $(S', s') \circ_l (T, t)$ and (S, s) decomposes as $(C, c) \circ_{r_1} (S', s')$. An induction argument allows the use of relations $H(T_1, t_1) = H(S', s') + \frac{u(l)}{u(r)}H(T, t)$ and $H(S, s) = H(C, c) + \frac{u(r_1)}{u(r)}H(S', s')$ together with the definition relation (9) in order to obtain $H(U, u) = H(S, s) + \frac{u(l)}{u(r)}H(T, t)$.

7 Dispersions Over Reduced Weighted Rooted Trees

Consider the norm $\|\cdot\|_A$ over the vector space $V \approx R^n$ determined by the symmetric positive definite (in short, s.p.d.) matrix A , i.e. such that $\|v\|_A = v^T A v$.

If τ is a trivial rwr-tree, any pre-location γ over τ is in fact a vector $\gamma(\cdot) = v \in V$. Define $D_A(\tau, \gamma) = 0$ for each given norm $\|\cdot\|_A$.

If (C, c) is a weighted m -corolla with leaves r_1, \dots, r_m and root r , and if γ is a pre-location over (C, c) with values in the vector space V , define the dispersion induced by γ as

$$D_A((C, c), \gamma) = \frac{1}{c(r)} \sum_{1 \leq k \leq m} c(r_k) \|\gamma(r_k) - \gamma(r)\|_A^2 \text{ for each given norm } \|\cdot\|_A.$$

Suppose now dispersions induced by pre-locations γ —with values in V —have been defined for all rwr-trees (T, t) of given height $h \geq 1$, for all norms $\|\cdot\|_A$, as real numbers $D_A((T, t), \gamma)$.

Let now (U, u) be a rwr-tree of height $h + 1$ and let γ be a pre-location over (U, u) —with values in V . Identify the basic corolla (C, c) of (U, u) having the vertices r_1, \dots, r_m as leaves. Denote (T_k, t_k) the subtree of (U, u) having r_k as root.

Consider the restrictions of γ to the corolla (C, c) and to the subtrees (T_k, t_k) , denoted by γ_C res. γ_k . By induction, the real numbers $D_A((C, c), \gamma_C)$ and $D_A((T_k, t_k), \gamma_k)$ have been defined. For the initial rwr-tree, the dispersion induced by γ —and associated to the norm $\|\cdot\|_A$ —will be defined as follows

$$D_A((U, u), \gamma) = D_A((C, c), \gamma_C) + \frac{1}{u(r)} \sum_{1 \leq k \leq m} u(r_k) D_A((T_k, t_k), \gamma_k) \tag{10}$$

Condition (10) is similar to that describing entropy (9). In fact, it is known since Ronald A. Fisher (see [5]) that variance of a set of numbers behaves similarly to the entropy.

This similarity allows us to prove an analog of Proposition 6, namely the following.

Proposition 7 *If the rwr-tree (U, u) decomposes as the graft of (T, t) over (S, s) along the leaf l of S , and if γ is a pre-location with values in V defined on (U, u) , then γ induces pre-locations γ_S res. γ_T on (S, s) res. (T, t) . Among the corresponding induced dispersions the following relation is valid*

$$D_A((U, u), \gamma) = D_A((S, s), \gamma_S) + \frac{u(l)}{u(r)} D_A((T, t), \gamma_T) \text{ for each given norm } \|\cdot\|_A,$$

where r is the root of U .

Recall the “affine” group G of dimension n (over R) operates on the vector space V and coordinatewise on the Cartesian product V^L once a basis has been fixed.

If L is the set of leaves of the rwr-tree (T, t) , the pre-locations γ over (T, t) are fully determined by families $\{\gamma(l)\}_{l \in L}$ of vectors from V . Of course, G operates on the set P of these pre-locations, as follows:

$(\alpha, v) * \gamma$ is the pre – location determined by the family $\{(\alpha, v) * \gamma(l)\}_{l \in L}$,

where α is an automorphism of V and v is a vector of V .

The group G operates in an induced manner on the set D of dispersions induced by pre-locations and by norms, as follows:

$$(\alpha, v) * D_A((T, t), \gamma) = D_A((T, t), (\alpha, v) * \gamma).$$

If a basis of V as vector space has been fixed, the automorphism α is perfectly determined by an invertible matrix M of order n . The following is immediate.

Proposition 8 Under the notations above,

$$D_A((T, t), (\alpha, v) * \gamma) = D_{M^{-1}AM}((T, t), \gamma). \quad (11)$$

Relation (11) is the analog of conditions (1.4)–(1.5) from [3] that a measure of dispersion in the probabilistic framework should satisfy (see also [13]).

8 Ordinal Dispersions

In sociological investigations based on questionnaires where respondents' answers to questions are given according to Likert scales, the respondents are naturally grouped in clusters and the clusters in larger clusters, and so on. Usually what is of interest is the possible relation between answers in clusters or in larger clusters.

Recall a general Likert scale question admits n possible answers, ordered as follows $A_1 \prec A_2 \prec \dots \prec A_{n-1} \prec A_n$, where \prec signifies “is worse than”. Any respondent has the right to choose only one of these answers, but in a group of N respondents some diversity may exist. If N_i is the number of respondents that have chosen A_i as answer, the relative frequency $f_i = N_i/N$ is easily computed, and it is obvious that $\sum_{1 \leq i \leq n} f_i = 1$. Probably most people agree that the median answer A_μ defined by $\sum_{1 \leq i \leq \mu} f_i \leq \frac{1}{2}$, $\sum_{1 \leq i \leq \mu+1} f_i > \frac{1}{2}$ is the “best” measure of location, but this agreement is not attained when selecting a “good” measure of dispersion is the objective. Leti proposes in [11] the “ordinal dispersion” based on cumulative frequencies. Recall the cumulative frequencies F_i are computed as $\sum_{1 \leq j \leq i} f_j$, and it is obvious that $0 \leq F_1 \leq F_2 \leq \dots \leq F_\mu \leq \frac{1}{2} < F_{\mu+1} \leq F_{n-1} \leq F_n = 1$.

In the vector space $V \approx \mathbb{R}^n$, in which a basis e_1, e_2, \dots, e_n has been selected, consider the fundamental simplex S composed of all vectors $v = (v_i)_{1 \leq i \leq n}$ such that $0 \leq v_1 \leq \dots \leq v_{n-1} \leq v_n = 1$. In particular, let 1 be the vector with all coordinates equal to 1.

According to Leti [11], the **ordinal dispersion** associated to the vector $v \in S$ is the real number $\Delta(v) = \sum_{1 \leq i \leq n} v_i(1 - v_i)$, which can be rewritten as $\Delta(v) = \frac{n}{4} - \sum_{1 \leq i \leq n} [v_i - \frac{1}{2}]^2$.

Our definition below will be a little more general, allowing, for example, the treatment of different coordinates of v according to their specific “importance”.

Definition 4 The *A*-**ordinal dispersion** $\Delta_A(v)$ associated to $v \in S$ is defined as

$$\Delta_A(v) = v^T A(1 - v) = \frac{1^T A 1}{4} - \left[v - \frac{1}{2} 1 \right]^T A \left[v - \frac{1}{2} 1 \right] \tag{12}$$

where A is a symmetric positive definite real matrix of order n .

Consider now a rwr-tree (T, t) with root r , and a pre-location γ over it, with values in S .

If the rwr-tree is trivial, then the pre-location is determined by a single vector $\gamma(r) \in S$. Its *A*-ordinal dispersion $\Delta_A(\gamma(r))$ is the ***A*-ordinal dispersion associated to the rwr-tree**.

If (T, t) is a m -corolla, with leaves r_1, r_2, \dots, r_m , then given a pre-location γ over it, with values in S , on one hand $m + 1$ *A*-ordinal dispersions $\Delta_A(\gamma(r))$ and $\Delta_A(\gamma(r_1)), \dots, \Delta_A(\gamma(r_m))$ exist, and on the other hand there is a dispersion induced by γ and determined by $\|\cdot\|_A$. A simple check shows that:

$$\Delta_A(\gamma(r)) = \frac{1}{t(r)} \sum_{l \text{ leaf of } T} t(l) \Delta_A(\gamma(l)) + D_A((T, t), \gamma) \tag{13}$$

Suppose formula (13) is valid for all rwr-trees of height $\leq h$, and let (T, t) be a rwr-tree of height $h + 1$, having r as root and r_1, r_2, \dots, r_m vertices of depth 1. Let us decompose (T, t) as $(C, c) \circ \{(T_k, t_k)\}_{1 \leq k \leq m}$, where (C, c) is the basic corolla.

If γ is a pre-location over (T, t) , with values in S , then it induces pre-locations γ_C res. γ_k over (C, c) res. (T_k, t_k) . We know, by the induction hypothesis, that

$$\Delta_A(\gamma(r_k)) = \frac{1}{t(r_k)} \sum_{l \text{ leaf of } T_k} t(l) \Delta_A(\gamma(l)) + D_A((T_k, t_k), \gamma) \quad (1 \leq k \leq m)$$

and for the basic corolla we know

$$\Delta_A(\gamma(r)) = \frac{1}{t(r)} \sum_{1 \leq k \leq m} t(r_k) \Delta_A(\gamma(r_k)) + D_A((C, c), \gamma).$$

Exploiting formula (10) above, since the leaves of T are exactly the leaves of all subtrees T_k , it follows that (13) is valid for the rwr-tree (T, t) of height $h + 1$ too, thus is valid for all rwr-trees.

In other words, the following proposition is proved.

Proposition 9 For each *rwr-tree* (T, t) , having r as root and L as set of leaves, for each *s.p.d.* matrix A of order n and for each pre-location γ over (T, t) with values in S , the dispersion induced by γ and associated to the norm $\|\cdot\|_A$ can be expressed in terms of *A-ordinal dispersions*, as follows:

$$\Delta_A(\gamma(r)) - \frac{1}{t(r)} \sum_{l \in L} t(l) \Delta_A(\gamma(l)).$$

9 Ordinal Covariances and Correlations

In classical statistics, concordance between sets of data extracted from a sample when taking into account two different numeric variables is evaluated by using the so-called Pearson correlation coefficient, whose formula involves variances and covariance all defined in a coherent manner. By contrast, in sociological investigations based on questionnaires, the concordance between sets of answers given—according to Likert scales—on two different questions is currently evaluated according to indices—such as Somers’ delta [17], Kendall’s tau [9], gamma, and so on—defined on principles which are completely different from those used in defining dispersion.

In this section we try to produce a coherent approach, starting from formula (12) proposed as definition of the *A-ordinal dispersion* associated to a vector $v \in S$:

$$\Delta_A(v) = \frac{1^T A 1}{4} - \left[v - \frac{1}{2} 1 \right]^T A \left[v - \frac{1}{2} 1 \right],$$

that gives a real number in $\left[0, \frac{1^T A 1}{4} \right]$.

This formula allows an immediate extension. Namely,

Definition 5 Given two vectors $v, w \in S$, the *A-ordinal covariance* $K_A(v, w)$ between them is defined as:

$$K_A(v, w) = \frac{1^T A 1}{4} - \left[v - \frac{1}{2} 1 \right]^T A \left[w - \frac{1}{2} 1 \right] = \frac{1}{2} [v^T A w + w^T A v].$$

This gives a real number in $\left[0, \frac{1^T A 1}{2} \right]$.

Based on the above evaluations, it is easy to establish the following inequality:

$$\left[K_A(v, w) - \frac{1^T A 1}{4} \right]^2 \leq \Delta_A(v) \Delta_A(w) + \left[\frac{1^T A 1}{4} \right]^2$$

and consequently an ordinal correlation coefficient can be defined as follows:

$$R_A(v, w) = \left[K_A(v, w) - \frac{1^T A 1}{4} \right] / \sqrt{\Delta_A(v) \Delta_A(w) + \left[\frac{1^T A 1}{4} \right]^2} \tag{14}$$

Of course, the possible values of $R_A(v, w)$ range from -1 to $+1$. Unfortunately, such a “correlation coefficient” is far from having the usual properties of the classical Pearson correlation coefficient. For example, $R_A(\frac{1}{2} 1, v) = 0$ for each $v \in S$, and $R_A(v, w) = 0$ only if there exists an index k such that $v_i = \frac{1}{2}$ for $i < k$ and $w_i = \frac{1}{2}$ for $i \geq k$.

The classical approach, based on the fact that $\frac{1}{2}$ can be considered an “average” of the coordinates $(v_i)_{1 \leq i \leq n}$ of any vector $v \in S$, naturally leads to defining the dispersion as $[v - \frac{1}{2} 1]^T A [v - \frac{1}{2} 1]$, the covariance as $[v - \frac{1}{2} 1]^T A [w - \frac{1}{2} 1]$, and the Pearson correlation coefficient as

$$\rho_A(v, w) = \left[v - \frac{1}{2} 1 \right]^T A \left[w - \frac{1}{2} 1 \right] / \sqrt{\left[v - \frac{1}{2} 1 \right]^T A \left[v - \frac{1}{2} 1 \right] \left[w - \frac{1}{2} 1 \right]^T A \left[w - \frac{1}{2} 1 \right]}.$$

However, this “coefficient” is not always defined, it cannot be defined for $v = \frac{1}{2} 1$ or $w = \frac{1}{2} 1$. Another drawback is its much skewed distribution, under the hypothesis of uniformly distributed v, w . For example, in Fig. 2 above it can be seen that in

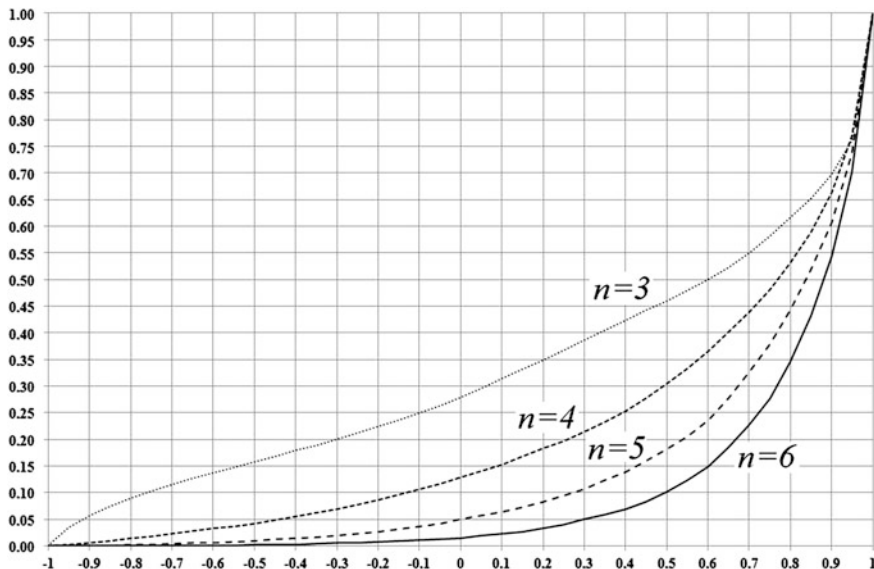


Fig. 2 Distribution functions of $\rho_I(v, w)$ in dimensions 3, 4, 5, and 6 ($I =$ unit matrix)

case of a 5-step Likert scale only about 5 % of the values of $\rho_I(v, w)$ are negative, and more than 80 % are over 0.8. Thus $\rho_I(v, w)$ is unsatisfactory from this point of view; the number $R_A(v, w)$ given by the formula (14) seems to be a valid candidate.

The use in sociological investigations of this $R_A(v, w)$ as “correlation coefficient” is bounded by a thorough knowledge of its distribution (as a random variable, when v and w are considered as uniformly distributed in S). This knowledge is not yet available.

References

1. Berge C (1967) *Théorie des Graphes et ses Applications*. Dunod, Paris
2. Bickel PJ, Lehmann EL (1975) Descriptive statistics for nonparametric models. II. Location. *Ann Statist* 3:1045–1069
3. Bickel PJ, Lehmann EL (1976) Descriptive statistics for nonparametric models. III. Dispersion. *Ann Statist* 4:1139–1158
4. Butcher JC (1972) An algebraic theory of integration methods. *Math Comp* 26(117):79–106
5. Fisher RA (1925) Theory of statistical estimation. *Proc Cambridge Phil Soc* 22:700–725
6. Fletcher P, Hoyle H, Patty CW (1991) *Foundations of discrete mathematics*. PWS-KENT Publ. Co., Boston
7. Grilli L, Rampichini C (2002) Scomposizione della dispersione per variabili statistiche ordinali. *Statistica* 12(1):111–116
8. Grilli L, Rampichini C, Petrucci A (2004) Analysis of university course evaluations: from descriptive measures to multilevel models. *Stat Methods Appl* 13:357–373
9. Kendall M (1938) A new measure of rank correlation. *Biometrika* 30(1–2):81–89
10. Kundu S, Misra L (1977) A linear tree partitioning algorithm. *SIAM J Comput* 6(1):151–154
11. Leti G (1983) *Statistica Descrittiva*, Il Mulino. Bologna
12. Lundervold A (2011) Lie-Butcher series and geometric numerical integration on manifolds, PhD thesis, University of Bergen (2011)
13. Oja H (1983) Descriptive statistics for multivalued distributions. *Statis Probab Lett* 1:327–332
14. Oja H (2012) Descriptive statistics for nonparametric models. The impact of some Erich Lehmann’s papers. In: Rojo O (ed), *Selected Works of E. L. Lehmann, Selected Works in Probability and Statistics*, ©Springer Science + Business Media, 2012, pp. 451–457
15. Rojo O, Robbiano M (2007) On the spectra of some weighted rooted trees and applications. *Linear Algebra Appl* 420:310–328
16. Shannon CE (1948) A mathematical theory of communication. *Bell Syst Tech J* 27(3):379–423
17. Somers RH (1962) A new asymmetric measure of association for ordinal variables. *Am Sociol Rev* 27:799–811
18. Stasheff J (2004) What is an operad? *Notices of the Amer Mat Soc* (2004), 630–631
19. Subtree. *MathWorld—A Wolfram Web Res.* <http://mathworld.wolfram.com/Subtree.html>
20. Tastle WJ, Wierman MJ (2007) Consensus and dissention: a measure of ordinal dispersion. *Intern J Approx Reasoning* 45:531–545
21. Weiss I (2007) *Dendroidal sets*, PhD Thesis, University of Utrecht (2007)
22. Weiss I (2011) From operads to dendroidal sets. In: Sati H, Schreiber U (eds), *Mathematical foundations of quantum field theory and perturbative string theory*. In: *Proceedings Symposia in Pure Mathematics*, vol 83, pp 31–70. American Mathematical Society Publication

Software Solution for Reliability Analysis Based on Interpolative Boolean Algebra

Nemanja Lilić, Bratislav Petrović and Pavle Milošević

Abstract In this paper, our objective is to present a software solution for evaluating and analyzing reliability of a system. Applying the principles of Interpolative Boolean algebra (IBA) our software can model both classical systems, with a discrete $\{0, 1\}$ -valued structural function and systems whose operability can be represented by a continuous fuzzy measure. The proposed software solution uses Generalized Boolean polynomial (GBP) to determine an algebraic representation of the system structural function and thus evaluate its reliability. As the complexity of analysis exponentially grows with the number of the system's components, automated calculation of a system that is quite complex is often the only choice.

Keywords Reliability · Software solution · Structural function · Interpolative Boolean algebra · Generalized Boolean polynomial

1 Introduction

One of the most common concepts in reliability theory is the system's structural function [1], a mapping from the state of the system's components to the state of the whole system. Both are usually represented by discrete states $\{0, 1\}$ —working or not working, but in general the state of the whole system can be represented by a continuous $[0, 1]$ space state that pertains to the case when despite the failure of some its components, the system continues to work with a diminished capacity. In the case fuzzy measure [2] can be used to model these states of the system.

N. Lilić (✉) · B. Petrović · P. Milošević
Faculty of Organizational Science, University of Belgrade, Belgrade, Serbia
e-mail: nemanja.lilic@gmail.com

B. Petrović
e-mail: bratislav.petrovic@fon.bg.ac.rs

P. Milošević
e-mail: pavle.milosevic@fon.bg.ac.rs

Several different approaches to determine the algebraic representation of structural function were proposed. Since structural function is Boolean function, Shannon decomposition [3] may be seen as one of the initial methods. Minimal path and cut sets from graph theory were also applied [1, 4]. Radojević [5, 6] introduced the multiplicative discrete Choquet integral for determining reliability of a system when arithmetical product is applied as a fuzzy t -norm.

Interpolative Boolean algebra (IBA) [7, 8] is a consistent real-valued realization of Boolean algebra (BA) in the manner that it preserves all the laws Boolean algebra relies on. Unlike conventional fuzzy logic, which is based on the principle of truth functionality, IBA separates the structure of the logical expressions from the values of logical variables. So far, IBA has been successfully applied to numerous fields, including uncertainty analysis [9], consensus decision making [10], expansion of Analytical Hierarchy Process [11], etc. However, there have not been many software platforms that support IBA [9].

In this paper, we propose a software solution for evaluating and analyzing the reliability of a system. Our software solution expands the inherent capability of propositional logic to model the reliability of a system to a non-Boolean framework, so that we can model both non parallel-series systems and systems with continuous space states of components. We use a consistent aggregation [7] to analyze and determine the structural function of a system in an algebraic form, and thus its reliability. As the calculation complexity of this polynomial is exponential by nature, we propose a software solution for this analysis. Our software supports IBA reliability analysis with nine logical connectives, and may calculate the reliability of a system with up to 64 components.

This paper is structured in the following manner. In Sect. 2 we present some basic concepts of reliability theory. Section 3 reviews some of the main principles of IBA. In Sect. 4 we show the application of IBA concepts to reliability theory, along with examples of using GBP to determine the structural function and the reliability of a system. Section 5 deals with our software solution for reliability analysis based on IBA. Final section concludes this paper.

2 Basic Concepts of Reliability Modelling

To every system made out of n components, we could associate a state vector

$x = (x_1, x_2, \dots, x_n)$, $x_i \in [0, 1]$, $i = 1, \dots, n$. When $x_i = 1$ it means that i th component of the system is working, and when $x_i = 0$ it is not working. We need to determine whether the whole system is working for a certain state vector of components.

Definition 1 [1] Consider the space $\{0, 1\}^n$ of all possible state vectors for an n -component system. The structural function $\varphi = \{0, 1\}^n \rightarrow \{0, 1\}$ is a mapping that associates those state vectors x for which the system works with the value 1 and those state vectors x for which the system fails with the value 0.

In other words, for every subset of the component's power set, the system's structural function will determine whether the system is working or not.

2.1 Parallel-Series Systems

Every parallel-series system or system that can be decomposed to parallel-series can be represented by propositional logic. A logical formula that distinctly corresponds to a specific system can be devised. This logical formula can be evaluated for every subset of the component's power set so that we can determine the structural function of the system.

For instance, the system shown in Fig. 1 can be represented by the following logical formula φ :

$$\varphi = (r_1 \vee r_2) \wedge ((r_3 \wedge r_4) \vee r_5) \wedge r_6 \tag{1}$$

where $r_i, i = 1, \dots, 6$ are reliabilities of the components, respectively.

2.2 Non Parallel-Series Systems

More complex systems that we encounter in real use, e.g. computer networks, cannot always be modelled using a set of parallel-series connections. We will represent these kind of systems by a vector of the values of their structural function σ_φ ordered by the subsets of the component's power set. This vector we will call a structural vector [5].

The system in Fig. 2 can be represented by a structural vector. All possible state vectors (2^n) are power set of the set of system's components. If an element is a member of the current subset of the power set, it is assumed to be working, otherwise it is not. When following combinations of components are working, the whole system is working: $\{a_1, a_2\}$, $\{a_1, a_2, a_4\}$, $\{a_1, a_3, a_4\}$, $\{a_2, a_3, a_4\}$, $\{a_1, a_2, a_3, a_4\}$. For these state vectors, the value of the structural vector is 1. For any other state vector the system is out of order, and the element of the structural vector is 0.

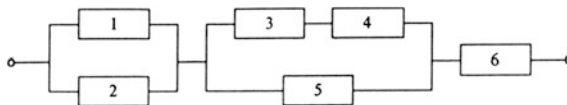


Fig. 1 Combined parallel-series system

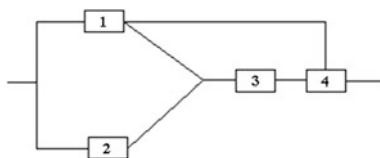


Fig. 2 Non parallel-series system

We could enhance this concept of structural vector for the systems that continue to work despite the failure of some of their key components, but with a diminished capacity. Like an airplane which had one of its engines gone off, but can still be flown with other engines working. These systems can be modelled using a fuzzy measure, $\mu : \{0, 1\}^n \rightarrow [0, 1]$.

Both in discrete and continuous cases, structural vector/fuzzy measure is assumed to be monotonous, since repairing a component cannot make the system worse. If the system contains no irrelevant components, such that their state cannot in any way influence the state of the whole system, we will say that such system is coherent. In Fig. 2, if component 2 were to be connected to component 4, the system would not be coherent as component 3 would be irrelevant.

3 Interpolative Realization of Boolean Algebra

Interpolative Boolean algebra is a consistent real-valued realization of Boolean algebra (BA) in the sense that it preserves all the laws Boolean algebra relies on [7, 12]. Unlike conventional fuzzy logic that is based on the principle of truth functionality, logic based on IBA separates the structure of the logical expressions (symbolic level of IBA) from the values of logical variables (value level). On the symbolic level IBA is identical to Boolean algebra with a finite number of elements.

3.1 Algebraic Representation of IBA

A set of primary (basic) Boolean variables $\Omega = \{a_1, \dots, a_n\}$ generates the finite Boolean algebraic domain $\text{BA}(\Omega)$. The algebraic structure of BA is:

$$\langle \text{BA}, \wedge, \vee, \neg \rangle \quad (2)$$

where BA is set with a finite number of elements, \wedge and \vee are binary operators of conjunction and disjunction, respectively, and \neg is the unary operator of negation.

Table 1 Atomic elements of Boolean algebra for two variables

S	$\alpha(S)$
\emptyset	$\neg a \wedge \neg b$
$\{a\}$	$a \wedge \neg b$
$\{b\}$	$\neg a \wedge b$
$\{a, b\}$	$a \wedge b$

The set BA can be defined by the following expression:

$$BA = P(P(\Omega)) \tag{3}$$

Definition 2 [7] Atomic attributes $\alpha(S)$, ($S \in P(\Omega)$) are the simplest elements of the Boolean algebraic domain of attributes $BA(\Omega)$ in the sense that they do not include in themselves anything except a trivial Boolean constant 0.

The atomic attributes of $BA(\Omega)$ are described by the following expressions [8]:

$$\alpha(S) = \bigwedge_{a_i \in S} a_i \bigwedge_{a_j \in \Omega \setminus S} \neg a_j, S \in P(\Omega) \tag{4}$$

Atomic attributes of Boolean algebra for $\Omega = \{a, b\}$ are given in Table 1.

The atoms are the simplest elements in the sense that they are not included in any other element except in themselves and in a Boolean zero constant. The conjunction (standard intersection) of any two atomic elements is equal to a Boolean 0 (empty set). The disjunction (standard union) of all atomic attributes is 1 (universe). The structure of any element $\varphi \in BA$ is determined by atomic elements included in φ . It is in fact a characteristic function of the subset of atoms that comprise that element from the set of all atoms.

The structural function of primary Boolean variables is defined by the following expression:

$$\sigma_\varphi(S) = \begin{cases} 1, & \alpha(S) \subseteq \varphi \\ 0, & \alpha(S) \not\subseteq \varphi \end{cases} \tag{5}$$

where $\varphi \in BA, S \in P(\Omega)$.

In structural functionality [12] concept that IBA advocates, logical operations are performed not on the value level, but on the structure level. For every logical variable we can determine its structural vector and on them we will perform logical operations as they are defined in classical Boolean algebra. The principle of structural functionality states that these operations are to be performed under the following rules:

$$\begin{aligned}
\sigma_{\varphi \wedge \psi}(S) &= \sigma_{\varphi}(S) \wedge \sigma_{\psi}(S) \\
\sigma_{\varphi \vee \psi}(S) &= \sigma_{\varphi}(S) \vee \sigma_{\psi}(S) \\
\sigma_{\neg \varphi}(S) &= 1 - \sigma_{\varphi}(S)
\end{aligned} \tag{6}$$

where $\varphi, \psi \in \text{BA}, S \in \mathcal{P}(\Omega)$.

3.2 Value Level and Generalized Product

All Boolean attributes have their realizations on value level. In case of Boolean logic, they are discrete $\{0, 1\}$ -valued, in fuzzy case, these attributes take their value form $[0, 1]$ interval. The conventional fuzzy logic applies algebraic operators in the shape of t -norms (and adequate t -conorms) directly to the values of these attributes. In IBA, algebraic operations are completed on symbolic, structural level. All t -norms can be used in IBA in the form of generalized product, but it is only an arithmetic operation on value level, not algebraic/logical operator as it is perceived in conventional fuzzy logic. A generalized product as a subclass of t -norms [13] can be any function $\otimes : [0, 1] \times [0, 1] \rightarrow [0, 1]$ that satisfies four axioms of t -norms (commutativity, associativity, monotonicity, and boundedness), along with the additional non-negativity condition:

$$\sum_{K \in \mathcal{P}(\Omega/S)} (-1)^{|K|} \otimes a_i(x) \geq 0, \tag{7}$$

where $S \in \mathcal{P}(\Omega), a_i^v(x) \in [0, 1], a_i \in \Omega, i = 1, \dots, n$.

Generalized product defined in this manner is an operator that is between the Lukasiewicz t -norm and minimum:

$$\max(0, a + b - 1) \leq a \otimes b \leq \min(a, b) \tag{8}$$

Corresponding to the atomic attributes on symbolical level, IBA introduces atomic polynomials on value level. Atomic generalized Boolean polynomials are defined by the following expression:

$$\alpha^{\otimes}(S)(a_1^v, \dots, a_n^v) = \sum_{K \in \mathcal{P}(\Omega/S)} (-1)^{|K|} \otimes_{a_i \in K \cup S} a_i^v \tag{9}$$

where $S \in \mathcal{P}(\Omega), a_i \in \Omega, a_i^v \in [0, 1], i = 1, \dots, n$.

4 GBP and Application in Reliability Analysis

Definition 3 [7] Generalized Boolean polynomial, which corresponds to φ analyzed element of Boolean algebra $\text{BA}(\Omega)$, is equal to the sum of relevant atomic GBPs:

$$\begin{aligned}\varphi^{\otimes}(a_1^v, \dots, a_n^v) &= \sum_{S \in \mathcal{P}(\Omega) | \sigma_\varphi=1} \alpha^{\otimes}(S)(a_1^v, \dots, a_n^v) \\ &= \sum_{S \in \mathcal{P}(\Omega)} \sigma_\varphi(S) \alpha^{\otimes}(S)(a_1^v, \dots, a_n^v).\end{aligned}\quad (10)$$

For any element φ of the Boolean algebra, GBP calculates their value, based on the values of the primary Boolean variables a_1, \dots, a_n that φ is comprised of. Based on the definition of atomic generalized Boolean polynomial, GBP can be represented in the following form:

$$\varphi^{\otimes}(a_1^v, \dots, a_n^v) = \sum_{S \in \mathcal{P}(\Omega)} \sigma_\varphi(S) \sum_{K \in \mathcal{P}(\Omega, S)} (-1)^{|K|} \bigotimes_{a_i \in K \cup S} a_i^v \quad (11)$$

$$(\varphi \in \text{BA}(\Omega), a_i^v(x) \in [0, 1], a_i \in \Omega).$$

If the structural vector of a function σ_φ is defined as follows:

$$\vec{\sigma}_\varphi = [\sigma_\varphi(S) | S \in \mathcal{P}(\Omega)] \quad (12)$$

and the vector of atomic Boolean polynomials:

$$\vec{\alpha}^{\otimes}(S)(a_1^v, \dots, a_n^v) = [\alpha^{\otimes}(S)(a_1^v, \dots, a_n^v) | S \in \mathcal{P}(\Omega)]^T \quad (13)$$

the generalized Boolean polynomial can be represented as a scalar product of these two vectors:

$$\varphi^{\otimes}(a_1^v, \dots, a_n^v) = \vec{\sigma}_\varphi \vec{\alpha}^{\otimes}(S)(a_1^v, \dots, a_n^v). \quad (14)$$

With structural vectors defined in this manner, all Boolean axioms (associativity, commutativity, absorption, distributivity, excluded middle, and contradiction), as well as all Boolean theorems (idempotency, boundedness, identity, De Morgan's laws, and involution) are valid.

The law of excluded middle and the law of contradiction are followed in IBA. In case of contradiction: $\varphi \Leftrightarrow a \wedge \neg a$, conventional fuzzy logic treats this Boolean theorem as a 2^2 dimensional problem by applying the binary operator of conjunction to both a and its negation. The IBA shows that this is a 2^1 dimensional

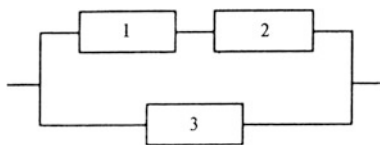


Fig. 3 A parallel-series system

problem— $P(\Omega) = \{\emptyset, \{a\}\}$, with only one logical variable. The resulting GBP for this logical formula is identically equal to zero, irrespective of the value of logical variables, and the law of contradiction is preserved. Similarly, it can be shown that the law of excluded middle is a tautology in IBA.

Since reliabilities of individual components are probabilistic, $[0, 1]$ -values and no normalization are needed, the consistent realization of fuzzy logic, Interpolative Boolean algebra, is a natural framework for modelling systems which we analyze in terms of reliability.

4.1 Parallel-Series and Non Parallel-Series Systems

We will use the parallel-series system from Fig. 3 to show how Generalized Boolean polynomial can be used for determining the algebraic representation of structural function and evaluating system reliability.

Case 1 Logical formula equivalent to the system shown in Fig. 3 is $\varphi \Leftrightarrow a_1 \wedge a_2 \vee a_3$. By evaluating this formula for every state vector x we can determine the structural vector of this system. Atomic polynomials for 3-variable formula can be determined from Eq. 9. In Table 2, we present structural functions and atomic polynomials:

Table 2 Atomic elements of Boolean algebra for three variables

$P(\Omega)$	$\sigma_{a_1}(S)$	$\sigma_{a_2}(S)$	$\sigma_{a_3}(S)$	$\sigma_\varphi(S)$	$\alpha^\otimes(S)(a_1^v, a_2^v, a_3^v)$
\emptyset	0	0	0	0	$(1 - a_1^v) \otimes (1 - a_2^v) \otimes (1 - a_3^v)$
$\{a_1\}$	1	0	0	0	$a_1^v \otimes (1 - a_2^v) \otimes (1 - a_3^v)$
$\{a_2\}$	0	1	0	0	$(1 - a_1^v) \otimes a_2^v \otimes (1 - a_3^v)$
$\{a_3\}$	0	0	1	1	$(1 - a_1^v) \otimes (1 - a_2^v) \otimes a_3^v$
$\{a_1, a_2\}$	1	1	0	1	$a_1^v \otimes a_2^v \otimes (1 - a_3^v)$
$\{a_1, a_3\}$	1	0	1	1	$a_1^v \otimes (1 - a_2^v) \otimes a_3^v$
$\{a_2, a_3\}$	0	1	1	1	$(1 - a_1^v) \otimes a_2^v \otimes a_3^v$
$\{a_1, a_2, a_3\}$	1	1	1	1	$a_1^v \otimes a_2^v \otimes a_3^v$

where $S \in P\{\Omega\}$, $\Omega = \{a_1, a_2, a_3\}$, $\sigma_{a_1}(S)$, $\sigma_{a_2}(S)$ and $\sigma_{a_3}(S)$ are structural vectors of Boolean variables, and a_1, a_2, a_3 are components' reliabilities. The structural function of this system in GBP form is:

$$\begin{aligned} \varphi^{\otimes}(a_1^v, a_2^v, a_3^v) &= 1 \cdot (1 - a_1^v) \otimes (1 - a_2^v) \otimes a_3^v + 1 \cdot a_1^v \otimes a_2^v \otimes (1 - a_3^v) \\ &\quad + 1 \cdot a_1^v \otimes (1 - a_2^v) \otimes a_3^v + 1 \cdot (1 - a_1^v) \otimes a_2^v \otimes a_3^v \\ &\quad + 1 \cdot a_1^v \otimes a_2^v \otimes a_3^v \\ &= a_1^v \otimes a_2^v + a_3^v - a_1^v \otimes a_2^v \otimes a_3^v \end{aligned} \quad (15)$$

The resulting algebraic representation of GBP is accurate and consistent with other procedures for determining the system's structural function already used in the theory of reliability, like Shannon decomposition of binary functions [3], or the multiplicative discrete Choquet integral [6].

Case 2 For non parallel-series system shown in Fig. 2, the system structural function determined using GBP is:

$$\begin{aligned} \varphi^{\otimes}(a_1^v, a_2^v, a_3^v, a_4^v) &= a_1^v \otimes a_4^v + a_2^v \otimes a_3^v \otimes a_4^v \\ &\quad - a_1^v \otimes a_2^v \otimes a_3^v \otimes a_4^v \end{aligned} \quad (16)$$

4.2 Generalized Pseudo-Boolean Polynomial in Reliability Analysis

Systems that continue to work with diminished capacity in case of failure of some components can be modelled by a fuzzy measure. We can use Pseudo-Boolean polynomial to determine their reliability. Their continuous structural function can be represented as a linear convex combination of discrete algebraic elements. We can define a generalized measure μ [7] of Pseudo-Boolean polynomial φ_{π} as a set function that maps:

$$\mu : P(\Omega) \rightarrow [0, 1], \quad \Omega = \{a_1, \dots, a_n\} \quad (17)$$

and can be expressed as a weighted sum of discrete elements of BA:

$$\mu(S) = \sum_{i=1}^m w_i \sigma_{\varphi_i}(S), \quad (18)$$

where $S \in P(\Omega)$, $\varphi_i \in \text{BA}(\Omega)$, $\sum_{i=1}^m w_i = 1$, $w_i \geq 0, i = 1, \dots, m$.

If we define the vector of a generalized measure, as a linear combination:

$$\vec{\mu}(S) = \sum_{i=1}^m w_i \vec{\sigma}_{\phi_i}(S) \quad (19)$$

generalized Pseudo-Boolean polynomial in this case is the scalar product of the vector of generalized measure and the vector of atomic Boolean polynomials.

5 A Software Solution for IBA-Based Reliability Analysis

As the complexity of calculation of GBP depends exponentially on the number of the system's components— $O(n2^n)$, we developed a software solution for reliability analysis based on IBA: Reliability analysis software, developed in MATLAB environment. Both classical parallel-series systems (defined by logical expressions) and more complex non parallel-series systems (defined by their structural function, discrete or continuous) can be represented. Figure 4 shows an interface for defining

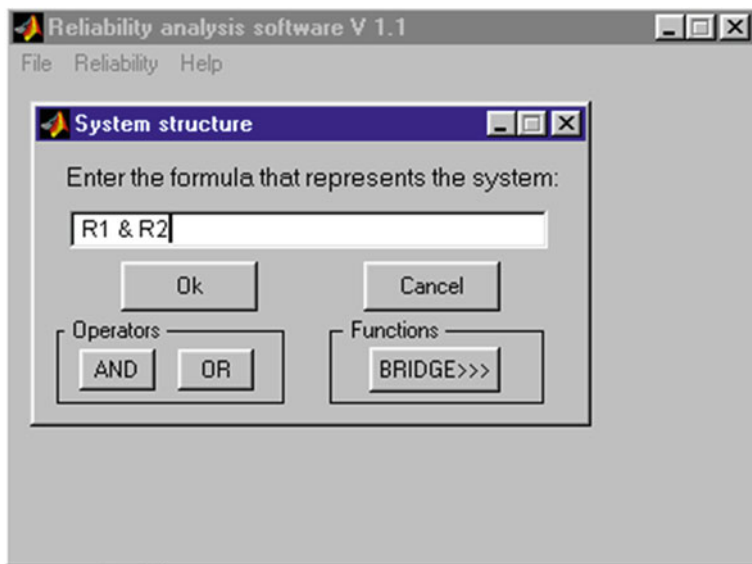


Fig. 4 Defining the system structure through logical expression

the structure of the parallel-series system. The software also supports some commonly met structures in reliability, like the bridge substructure (see Case 3).

In our implementation of GBP, we chose the arithmetic product as a generalized product since it is a common operator for dealing with probabilities. The inherent structure of GBP allows us to have only one state vector x in the memory at a time and in this way we resolved potential dimension problem with the length of structural vector (2^n). Due to this fact, our software can analyze systems comprised of up to 64 components (number determined by the length of unsigned 64-bit long integer). In every iteration the product of the current element of the structural vector and the corresponding atomic polynomial is computed and cumulatively added to the sum of previous iterations. For less complex systems (up to 20 components) our software can determine their structural function in symbolic, algebraic form that is expanded and simplified by MATLAB's Symbolic Math Toolbox.

As the problems of reliability and the evaluating propositional fuzzy logical expressions are closely related, our Reliability analysis software can also be used for the latter. Table 3 shows logical operators and their MATLAB equivalents that can be used in our software:

Non parallel-series systems can be represented through structural functions, both discrete or continuous (fuzzy measure). Figure 5 shows the input form where we can enter previously ascertained measures that for any state vector determine whether the system is working or not (or in which capacity).

Our software also supports some commonly met structures in reliability analysis, like the bridge structure presented in Fig. 6.

Table 3 Logical operators supported by reliability analysis software

Logical operator	Name	MATLAB equivalent
\wedge	Conjunction (AND)	&
\vee	Disjunction (OR)	
\Leftrightarrow	Equivalence	==
\Rightarrow	Right implication	<=
\Leftarrow	Left implication	>=
$\underline{\vee}$	Exclusive disjunction (XOR)	Xor (a, b)
\neg	Negation (NOT)	~
$ \Rightarrow$	Inhibition (A and not B)	<
$\Leftarrow $	Inhibition (B and not A)	>

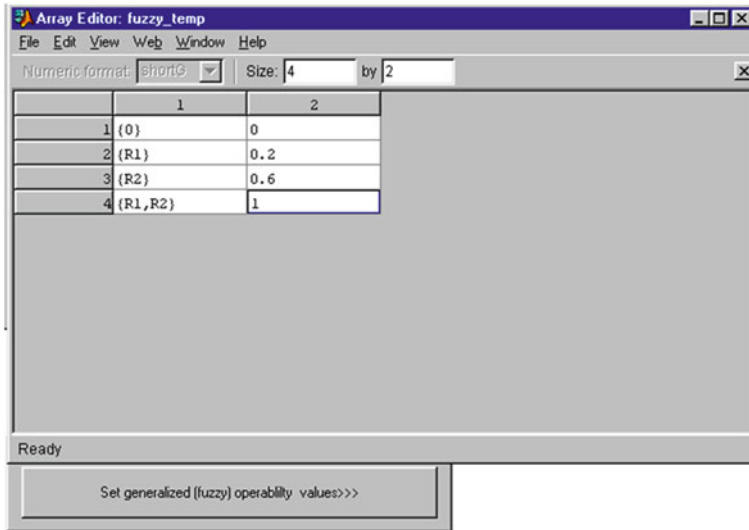


Fig. 5 Two-component system represented by fuzzy measure

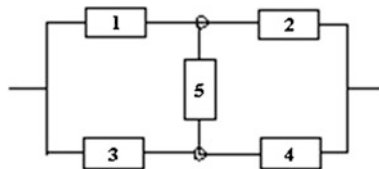


Fig. 6 Bridge system with five components

Case 3 Using our software we will determine the reliability of the bridge system. The bridge substructure can be entered as part of a logical formula using the reserved word *bridge*: *Bridge*("(r1 & r2) | (r3 & r4)", "r5"), or just as *Bridge*("r1 r2 r3 r4 r5"). The rightmost element is considered to be the one bridging the parallel connection. When we enter the reliabilities of individual components, we can choose *Classical reliability analysis* option from the menu (see Fig. 7).

The system structural function is represented in algebraic form for the 5-component bridge system, and the reliability of this system is computed (Rsys).

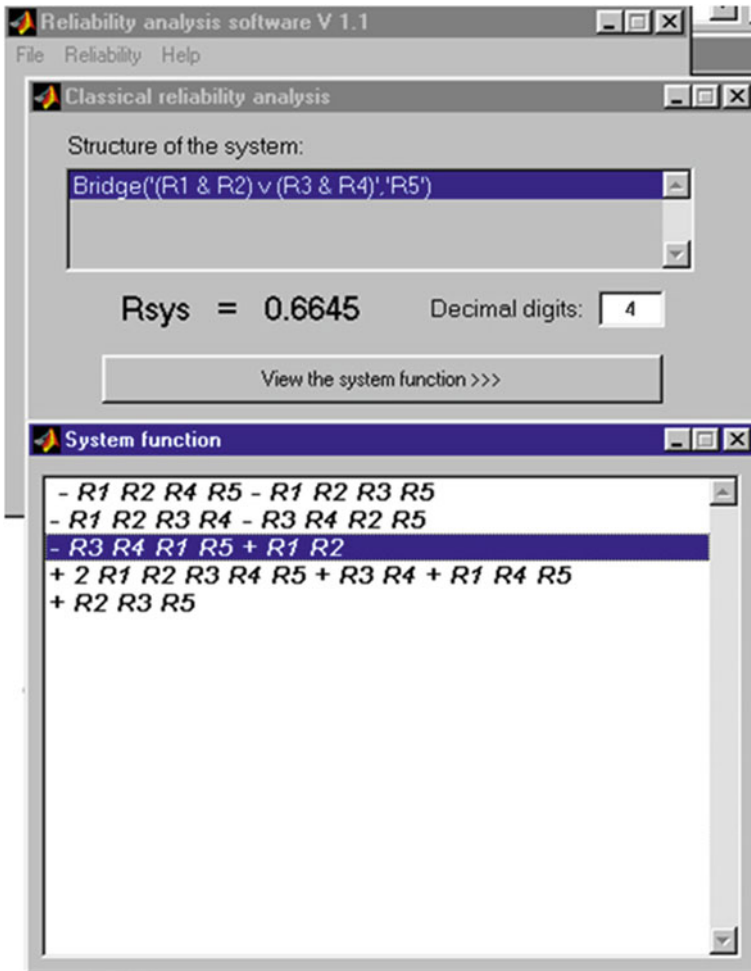


Fig. 7 Reliability and structural function of Bridge system

6 Conclusion

In this paper, we propose IBA, consistent realization of fuzzy logic, as the adequate tool for reliability analysis. Parallel-series systems can be modelled by propositional fuzzy logic and non parallel-series systems by the structural function which also plays a pivotal role when computing GBP as a logical aggregation. We showed that GBP can be used also in the analysis of systems for which failure of some components does not necessarily lead to the failure of the whole system, but the system continues to work in a decreased capacity. In this case, the structural function of the system is a fuzzy measure and can also be logically aggregated through GBP.

We developed a software solution within MATLAB environment for these types of reliability analysis based on IBA. Our results were consistent with classical reliability theory. In fact, Interpolative Boolean algebra can be viewed as a consistent metamathematical framework for reliability analysis. We operate with a set of logical operators and relations in MATLAB so that our software can also be used for evaluating fuzzy propositional expressions, since operators other than AND and OR (e.g. XOR, implication, equivalence) are seldom used in reliability analysis. Due to the inherent structure of GBP that allows us to have only one state vector in memory at any given time, our solution can be used to analyze very complex systems comprised of up to 64 components.

References

1. Samaniego FJ (2007) *System signatures and their applications in engineering reliability*. Springer, New York
2. Yager RR (2014) A fuzzy measure approach on system's reliability modeling. *IEEE Trans Fuzzy Syst* 5(22):1139–1150
3. Shannon CE (1949) The synthesis of two-terminal switching circuits. *Bell Syst Tech J* 28 (1):59–98
4. Singhal M, Chauhan RK, Sharma G (2010) Network reliability computation by using different binary decision diagrams. *Int J Distrib Parallel Syst* 1(1):82–91
5. Radojević D (2000) [0, 1]-Valued logic: a natural generalization of boolean logic. *Yugoslav J Oper Res* 10(2):185–216
6. Letic D, Radojević D (1999) System reliability analysis and multiplicative Choquet integral. In: Zimmermann HJ (ed) *Proceedings of 7th European congress on intelligent techniques and soft computing (EUFIT '99)*. Verlag Mainz, Aachen (1999)
7. Radojević D (2008) Logical aggregation based on interpolative boolean algebra. *Mathw. Soft Comput.* 15:125–141
8. Radojević D (2008) Interpolative realization of Boolean algebra as a consistent frame for gradation and/or fuzziness. In: Nikraves M, Kacprzyk J, Zadeh LA (eds) *Forging new frontiers: fuzzy pioneers II. Studies in Fuzziness and Soft Computing* 218, pp 295–317. Springer (2008)
9. Milošević P, Petrović B, Radojević D, Kovačević D (2014) A software tool for uncertainty modeling using interpolative Boolean algebra. *Knowl-Based Syst* 62:1–10
10. Poledica A, Milošević P, Dragović I, Petrović B, Radojević D Modeling consensus using logic-based similarity measures. *Soft Comput* doi:[10.1007/s00500-014-1476-5](https://doi.org/10.1007/s00500-014-1476-5)
11. Dragović I, Turajlić N, Petrović B, Radojević D (2014) Combining Boolean consistent fuzzy logic and AHP illustrated on web service selection problem. *Int J Comput Intell Syst* 7(Supp 1):84–94
12. Radojević D (2008) Fuzzy set theory in Boolean frame. *Int J Comput Commun Control* 3:121–131
13. Klement EP, Mesiar R, Pap E (2002) *Triangular norms*. Kluwer Academic Publishers, Dordrecht

Local Search Algorithms for Solving the Combinatorial Optimization and Constraint Satisfaction Problems

Y. Kilani, A. Alsarhan, M. Bsoul and A.F. Otoom

Abstract Local search is a metaheuristic for solving computationally hard optimization problems. In the past three decades, local search has grown from a simple heuristic idea into a mature field of research in combinatorial optimization that is attracting ever-increasing attention. It is still the method of choice for NP-hard problems as it provides a robust approach for obtaining high-quality solutions to problems of a realistic size in reasonable time. Optimization problems such as the shortest path, the traveling salesman, pin packing, and the Knapsack problems. Local search techniques have been successful in solving large and tight constraint satisfaction problems. Local search algorithms turn out to be effective in solving many constraint satisfaction problems. This chapter gives an introduction to the local search algorithms, the optimization and the constraint satisfaction problems, and the local search methods used to solve them.

Keywords Local search · Introduction · Combinatorial optimization problems · Constraint satisfaction problems

Y. Kilani (✉) · A. Alsarhan

Department of Computer Information Systems, Faculty of Prince Al-Hussein Bin Abdullah II for Information Technology, Hashemite University, Zarqa, Jordan

e-mail: ymkilani@hu.edu.jo

A. Alsarhan

e-mail: ayoubm@hu.edu.jo

M. Bsoul

Department of Computer Science and Applications, Faculty of Prince Al-Hussein Bin Abdullah II for Information Technology, Hashemite University, Zarqa, Jordan

e-mail: mbsou@hu.edu.jo

A.F. Otoom

Department of Software Engineering, Faculty of Prince Al-Hussein Bin Abdullah II for Information Technology, Hashemite University, Zarqa, Jordan

e-mail: aotoom@hu.edu.jo

1 Introduction

Combinatorial optimization arise in situations where discrete choices must be made, and solving them amounts to finding an optimal solution among a finite or countably infinite number of alternative [1]. Optimality relates to some cost criterion, which provides a quantitative measure of the quality of each solution [1]. The optimization problems include the shortest path, the traveling salesman, pin packing, and the Knapsack problems.

The constraint paradigm is a useful and well-studied framework expressing many problems of interest in artificial intelligence and other areas of computer science [2]. A constraint satisfaction problem requires a value, selected from a given finite domain, to be assigned to each variable in the problem, so that all constraints relating the variables are satisfied [3].

Constraint-based local search has been quite successful in solving problems that prove difficult for constraint solvers based on constructive search [4]. In computer science, local search is a metaheuristic method for solving computationally hard optimization problems [5, 6]. In the past three decades, local search has grown from a simple heuristic idea into a mature field of research in combinatorial optimization that is attracting ever-increasing attention [7]. A basic local search problem-solving strategy for either *constraint satisfaction problem* (CSP) or *combinatorial optimization problem* (COP) consists of starting from an initial randomly chosen *valuation* and trying to improve it through repeated small changes. At each of this repetition the current valuation is slightly modified, the function to be optimized is tested, the change is kept if the new valuation is better, otherwise another change is tried.

It is a common knowledge that the CSPs and COPs are NP-hard problems. It is generally believed that NP-hard problems cannot be solved to optimality within polynomial bounded computation times [7].

2 The Combinatorial Optimization Problems

Optimization problems can be divided into two categories depending on whether the variables are continuous or discrete [8]. An optimization problem with discrete variables is known as a COP [8]. Solving combinatorial problems is increasingly crucial in business applications, in order to cope with hard problems of practical relevance [9]. Our interest in this chapter is in the COP.

A COP is a tuple (Z, D, C, O, Ω) , where Z is a finite set of variables, D defines a finite set D_x , called the *domain* of x , for each $x \in Z$, C is a finite set of *hard constraints* restricting the combination of values that the variables can take, O is a finite set of *soft constraints*, and Ω is the objective function, which would be either

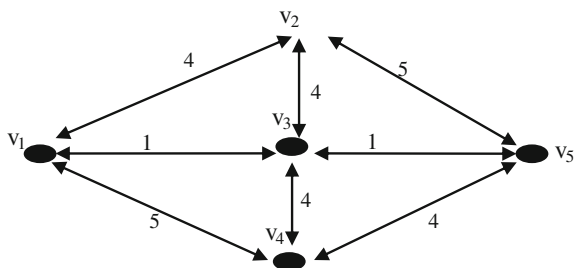
maximized or minimized. A *valuation (state)* is a complete assignment for each variable y , $y \in Z$, a value from its domain D_y . A *feasible solution* is a valuation that satisfies all the hard constraints. A COP which has feasible solution is called *satisfiable*. Otherwise, it is *unsatisfiable*. There can be many feasible solutions to any one problem [10]. Note that the feasible solution may violate some or all of the soft constraints (O) and this depends on the difficulty of the COP being solved. The *optimal feasible solution* is a feasible solution with the highest or smallest objective value in the maximization or minimization problems, respectively that Ω can take. The objective in solving the COP is to find an optimal feasible solution. Obtaining an optimal feasible solution is not always an easy task. Therefore, usually, the goal is to find a feasible solution with the highest or smallest possible objective value of Ω in the maximization or minimization problems, respectively within a limited time. The *search space* for a COP is the set of all valuations. It is a fact of life that most interesting optimization problems are NP-hard [1].

The COP is rooted in the theory of linear programming, and has strong links with discrete mathematics, probability theory, algorithmic computer science, and complexity theory [11]. Some problems in the area are relatively well understood and admit solution to optimality in polynomial time [11].

COP such as the shortest path, the traveling salesman, pin packing, scheduling different jobs on a set of available machines, the Knapsack problems, integrated circuit design, factory floor layout, job-shop scheduling, automatic programming, telecommunications network optimization, internet data packet routing, protein structure prediction, combinatorial auctions winner determination, finding model of propositional formulae, and vehicle routing and portfolio management. The following is an example of the COP.

Example 2.1 Consider the *directed weighted graph* in Fig. 1. It consists of 5 vertices and 16 edges. The figure also shows the weight for each edge. The vertices are: $v_1, v_2, v_3, v_4,$ and v_5 and the edges are: $(v_1, v_2), (v_2, v_1), (v_1, v_3), (v_3, v_1), (v_1, v_4), (v_4, v_1), (v_2, v_5), (v_5, v_2), (v_3, v_5), (v_5, v_3), (v_3, v_4), (v_4, v_3), (v_5, v_4), (v_4, v_5), (v_2, v_3),$ and (v_3, v_2) . The problem is to find the shortest path from v_1 to v_5 with minimum weight. Figure 2 gives the answer. The shortest path is: $v_1 \Rightarrow v_3 \Rightarrow v_5$ of weight 2. There are many paths from v_1 to v_5 such as: $v_1 \Rightarrow v_2 \Rightarrow v_5$ of weight 9 and $v_1 \Rightarrow v_4 \Rightarrow v_5$ of weight 9, $v_1 \Rightarrow v_4 \Rightarrow v_3 \Rightarrow v_5$ of weight 10, etc.

Fig. 1 A directed weighted graph



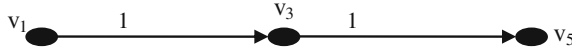


Fig. 2 The shortest path from v_1 to v_5

3 The Constraint Satisfaction Problems

A CSP [12] is a tuple (Z, D, C) , where Z is a finite set of variables, D defines a finite set D_x , called the *domain* of x , for each $x \in Z$, and C is a finite set of constraints restricting the combination of values that the variables can take [13]. A *valuation (state)* is a complete assignment for each variable $f, f \in Z$, a value from its domain D_f . A *solution* is an assignment to each variable of a value in its domain so that all constraints are satisfied simultaneously [13]. A CSP which has a solution is called *satisfiable*. Otherwise, it is *unsatisfiable*. The *search space* for the CSP is the set of all valuations. CSPs are well-known to be NP-complete in general [13].

Many real-life problems can be expressed as a CSP. Some examples are scheduling, configuration, hardware verification, graph coloring, molecular biology, model checking, model finding, planning bioinformatics, security, and network routing.

The state-of-the-art local search solvers for solving constraint satisfaction problems include: localizer [14], CometTM [15], kangaroo [4], and Oskar [16].

A satisfiability (SAT) problem is a special type of CSP. In SAT, the variables are *propositional/Boolean* variables that each can take the value of either true or false. A *literal* l_i is a variable x_i or its negation $\neg x$. For every variable x , there are two literals: x (*positive*) and $\neg x$ (*negative*). A *clause* in SAT represents a constraint in CSP. A clause is a disjunction of literals $c_i = l_1 \vee l_2 \dots \vee l_n$. A clause is satisfied when at least one of its literals is true. Otherwise, it is unsatisfied (false). A solution for a SAT is an assignment of true or false for each variable that satisfies all the clauses.

Nowadays, local search techniques for solving SAT are very hot topic. Local search algorithms for SAT testing are still the best methods for a large number of problems, despite tremendous progresses observed on *complete search algorithms* over the past few years [17]. The state-of-the-art local search solvers for solving SAT problems include: UBCSAT [18], gNovelty⁺ [19], the exponentiated sub-gradient algorithm (ESG) [20], TNM [21], adaptG²wsat2009++ [22], QingTing [23], SAPS [24], and PAWS [25].

Note that the difference between the COP and CSP is that COP contains soft constraints, while CSP does not contain soft constraints. The following gives an example of CSP, the *n-queens problem* which is a well-known problem among CSP community.

Example 3.1 The *n-queens problem* is to place n -queens on a square board of size $n \times n$ in such a way that the queens do not attack each other. Queen x attacks queen y or vice versa if x and y on the same row, column, or diagonal. This problem can be modeled in a CSP as follows. The n variables: x_1, x_2, \dots, x_n represent the n -queens,

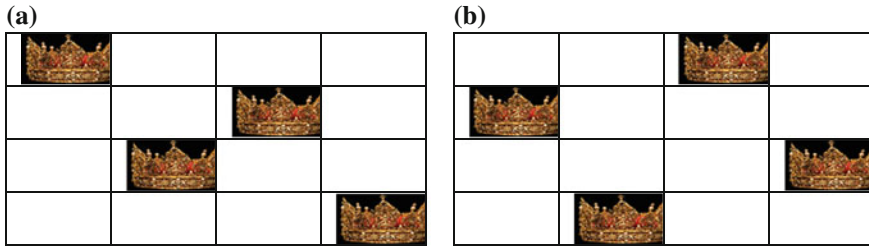


Fig. 3 The 4-queens problem. **a** Not a solution, **b** a solution

where x_i corresponds to a queen in a row i on the board. $Dx_i = \{1, 2, \dots, n\}$, $i = 1, 2, \dots, n$. There must be one queen per row. The assignment of value j to the variable x_i , $x_i = j$, where $j \in Dx_i$ means, a queen is placed on row i column j . Figure 3 shows an example of the 4-queens problem. Part *a* shows a valuation: $x_1 = 1, x_2 = 3, x_3 = 2, x_4 = 4$ which is not a solution since each of the queens on the first and last rows, $x_1 = 1$ and $x_4 = 4$, and the second and third rows, $x_2 = 3$ and $x_3 = 2$ on the same diagonal. But, part *b* shows a valuation: $x_1 = 3, x_2 = 1, x_3 = 4, x_4 = 2$ which is a solution.

4 State-of-the-Art Techniques for Solving the COPs and CSPs

There are two classes of high-performance algorithms for solving instances of the optimization and CSPs: the *complete (systematic)* and *incomplete (not systematic)* algorithms. The systematic approach explores the search space in a systematic manner by enumerating the search space and checking whether each valuation is a solution or a feasible solution in CSP or COP, respectively or not. The incomplete search algorithms include stochastic local search, genetic [26, 27], and neural network algorithms. Our interest in this chapter is in local search algorithms.

Local search techniques have been successful in solving large and tight CSPs [13]. Local search algorithms turn out to be effective in solving many CSPs [28].

Although local search algorithms are not systematic, they have two key advantages: (1) they use very little memory—usually a constant amount; and (2) they can often find reasonable solutions in large or infinite (continuous) state spaces for which systematic algorithms are unsuitable [28].

Local search algorithms traverse the search surface of a usually enormous search space to look for solutions using some heuristic function [13]. It starts the search from an initial randomly selected valuation by giving each variable a random value from its domain. This valuation represents the *current valuation*. There is a set of *neighbor valuations* called *neighborhood* for each valuation. The neighborhood differs from local search to another. Many of the local search algorithms consider the

neighborhood of valuation Z to be a set of valuations that each differs in a single variable assignment from Z . Local search then moves from the current valuation to a *better* neighbor valuation. The notion of better differs from local search to another. One criteria we may consider that valuation x is better valuation than y when x satisfies more constraint than y . Local search continues such move from the current valuation to a better neighbor valuation until it reaches a solution in CSP, a good feasible solution in COP, or the resources is exhausted; time or number of moves.

Some local search algorithms give every constraint a *weight* which is initially initialized to one. The weight w of constraint c reflects the degree of violations c is involved in. Local search often faces a situation in which there is no better neighbor valuation than the current valuation. In this case, it makes learning in order to avoid such situation again. In learning, it increases the weights of the currently unsatisfied constraints.

Local search uses many heuristic techniques which have great influence on its performance like: *restart*, *tabu list*, the choice of the variable x in the current valuation to change its value in order to move to a better neighbor valuation, the choice of the value for x from D_x . The restart and tabu list techniques proven are experimentally to be very effective. Local search makes restart when the search progress becomes very slow, and usually the number of moves before restart is set up in advance as a parameter. A *trial* is the local search moves from the initialization/restart to restart. Usually, local search makes number of trials before terminating the search. It uses tabu list to avoid choosing the same variable in the coming moves. When the variable d is chosen to change its value to move from the current valuation to a better neighbor valuation, d is added to the tabu list, and therefore d is not allowed to be chosen again in the next n moves, where n is a parameter. The following example illustrates how local search works.

Example 4.1 referring to Example 3.1 and Fig. 3. In this CSP, 4-queens(Z, D, C), $Z = \{x_1, x_2, x_3, x_4\}$, $D = \{D_{x1}, D_{x2}, D_{x3}, D_{x4}\}$, where $D_{x1} = D_{x2} = D_{x3} = D_{x4} = \{1, 2, 3, 4\}$, and $C = \{c_1, c_2, \dots, c_{13}\}$. C is shown in Table 1. In addition, Table 1 shows the meaning of each constraint. The constraint $\text{Alldiff}(x_1, x_2, x_3, x_4)$ means no any two variables of the set $\{x_1, x_2, x_3, x_4\}$ have the same values; all must be different. Two variables having the same values means that there are 2-queens on the same column.

We demonstrate the steps of local search as follows. Suppose we have chosen the random valuation: $s_0 = \{x_1 = 2, x_2 = 1, x_3 = 2, x_4 = 4\}$. s_0 violates c_2 and c_9 . Suppose the neighborhood consists of the set of the states that differ in a single variable assignment from the current state which most of the current local search algorithms do. Table 2 shows that there are 12 neighbors for s_0 : n_1, \dots, n_{12} . n_2 and n_6 are the best neighbors since each of these constraints violates one constraint only, n_2 violates c_9 , and n_6 violates c_1 , while n_3 , for instance, violates three constraints: c_1, c_5 , and c_9 . We want to move to one of the best neighbors randomly. Suppose we moved to n_2 . Name the current state n_2 as s_1 . Similarly, we found the set of neighbors for s_1 . Table 3 shows the set of neighbors $\{n_1, \dots, n_{12}\}$ for s_1 . n_9 is the best neighbor. Let us move to n_9 and name it s_2 . Similarly, we want to move to the

Table 1 The constraints of the 4-queens problem and the meaning of each constraint

Constraint number	The constraint	The meaning
c_1	Alldiff(x_1, x_2, x_3, x_4)	To prevent 4-queens be on the same column
c_2	$x_1 \neq x_2 + 1$	To prevent the queens on the first and second rows be on the same diagonal
c_3	$x_1 \neq x_2 - 1$	
c_4	$x_1 \neq x_3 + 2$	To prevent the queens on the first and third rows be on the same diagonal
c_5	$x_1 \neq x_3 - 2$	
c_6	$x_1 \neq x_4 + 3$	To prevent the queens on the first and fourth rows be on the same diagonal
c_7	$x_1 \neq x_4 - 3$	
c_8	$x_2 \neq x_3 + 1$	To prevent the queens on the second and third rows be on the same diagonal
c_9	$x_2 \neq x_3 - 1$	
c_{10}	$x_2 \neq x_4 + 2$	To prevent the queens on the second and fourth rows be on the same diagonal
c_{11}	$x_2 \neq x_4 - 2$	
c_{12}	$x_3 \neq x_4 + 1$	To prevent the queens on the third and fourth rows be on the same diagonal
c_{13}	$x_3 \neq x_4 - 1$	

Table 2 The current state s_0 and the neighborhood to $s_0 = \{x_1 = 2, x_2 = 1, x_3 = 2, x_4 = 4\}$ is the set of the neighbor states: $\{n_1, n_2, \dots, n_{12}\}$

The neighbors	The variables				Constraint violations
	x_1	x_2	x_3	x_4	
	2	1	2	4	c_3, c_9
n_1	1	1	2	4	c_1, c_9
n_2	3	1	2	4	c_9
n_3	4	1	2	4	c_1, c_5, c_9
n_4	2	2	2	4	c_1, c_{11}
n_5	2	3	2	4	c_1, c_3, c_8
n_6	2	4	2	4	c_1
n_7	2	1	1	4	c_1, c_2
n_8	2	1	3	4	c_2, c_{13}
n_9	2	1	4	4	c_1, c_2, c_5
n_{10}	2	1	2	1	c_1, c_2, c_{12}
n_{11}	2	1	2	2	c_1, c_2, c_9
n_{12}	2	1	2	3	c_1, c_3, c_{11}

best neighbor of s_2 . Table 4 shows the neighbors of s_2 . In this table, we found that n_{11} is a solution while evaluating the neighbors. We stop the search since we found the solution. Therefore, we found a solution in three steps: $s_0 \Rightarrow s_1 \Rightarrow s_2 \Rightarrow$ solution.

Table 3 The current state s_1 and the neighborhood to s_1 is the set of the neighbor states: $\{n_1, n_2, \dots, n_{12}\}$

	The variables				Constraint violations
	x_1	x_2	x_3	x_4	
The s_1 neighbors					The current state s_1
	3	1	2	4	c_9
n_1	1	1	2	4	c_1, c_7, c_9
n_2	2	1	2	4	c_1, c_2, c_9
n_3	4	1	2	4	c_1, c_4, c_9
n_4	3	2	2	4	c_1, c_2, c_{11}
n_5	3	3	2	4	c_1, c_8
n_6	3	4	2	4	c_1, c_3
n_7	3	1	1	4	c_1, c_4
n_8	3	1	3	4	c_1, c_{13}
n_9	3	1	4	4	c_1
n_{10}	3	1	2	1	c_1, c_{13}
n_{11}	3	1	2	2	c_1, c_9
n_{12}	3	1	2	3	c_1, c_{13}

Table 4 The current state s_2 and the neighborhood to s_2 is the set of the neighbor states: $\{n_1, n_2, \dots, n_{12}\}$ and n_{12} is the solution

	The variables				Constraint violations
	x_1	x_2	x_3	x_4	
The s_2 neighbors					The current state
	3	1	4	4	c_1
n_1	1	1	4	4	c_1, c_7
n_2	2	1	4	4	c_1, c_2, c_5
n_3	4	1	4	4	c_1
n_4	3	2	4	4	c_1, c_2, c_{11}
n_5	3	3	4	4	c_1, c_9
n_6	3	4	4	4	c_1, c_3
n_7	3	1	4	4	c_1
n_8	3	1	1	4	c_1, c_9
n_9	3	1	2	4	c_9, c_{11}
n_{10}	3	1	3	4	c_1
n_{11}	3	1	4	2	The solution
n_{12}	3	1	4	1	

4.1 *The State-of-the-Art Local Search Techniques for Solving CSPs and COPs*

Constraint-based local search is based on a view of constraint satisfaction as an optimization problem [4]. Therefore, the same solvers which are used for solving CSPs are used for solving the COPs and vice versa. The state-of-the-art local search solvers for solving the CSPs and the COPs include: Oscar CBLS engine [16, 29], Localizer [14, 37], Comet [15], Kangaroo [4]. In the following, we detail each of these solvers.

4.1.1 Oscar CBLS Engine

Oscar Constraint-Based Local Search (Oscar CBLS) engine is based on the reference book titled “Constraint-based Local Search” [30]. The Oscar CBLS engine offers a powerful [29]:

- framework for *invariant* declaration, with an engine that is able to perform incremental update of these invariants. Invariants are meant to incrementally maintain the value of some output variable based on some input variables [31].
- library of standard invariants, which can be extended.
- framework for declaring constraints.
- library of standard constraints.

Oscar CBLS engine is used for solving COP and CSP. First, we *model* the CSP or COP and find the variables and constraints that represent the problem being solved. Second, we then implement this model by using the Oscar CBLS engine. In Oscar CBLS engine, there is a way to define the variables, the domain for each variable, and the constraints. A CBLS framework includes support for declaring constraints and a library of standard constraints (alldiff, equalities, etc.).

The page [29] gives an example of how to solve the n -queens problem using the Oscar CBLS engine.

The main features of the Oscar CBLS engine includes:

- **Complex data types** to maintain the structure of the problem in the problem definition and to enable the writing of complex neighborhood rules.
- **The Oscar CBLS engine is open**, so that one can fully tailor the search heuristics to its precise problem [29]. For instance, one can implement the standard metaheuristics such as taboo, random restart, etc.
- **Libraries of standard invariants and constraints** include logic, numeric, min/max, and set invariants. Constraint library includes few global constraints: Alldiff, AtLeast, AtMost, and equalities over integers.
- **The violation degree propagates upward through the static propagation graph**. Each constraint has a weight which is usually initialized to one. Each variable x has a violation degree associated with each constraint system. This

degree is equal to the sum of the weights of the violated constraints (i.e., *currently unsatisfied constraints by the current state*) in which x occurs. This violation degree propagates upward through invariants. The propagation rule enables us to find the most problematic variable assignment that contributes the most to the overall constraints' violation.

- **Propagation graph can be cyclic.** Some of the propagation graphs can include cycles and this enable the implementation of some problems from *standard invariants*. *Propagation rules* are the rules that describe how a change of the mark of a component in the dependency graph will affect status of other components in the dependency graph this component interacts with [32].
- **No differentiation in invariants.** The engine relies on propagation to explore the neighborhood and it uses *partial propagation* to keep neighborhood exploration relatively fast. The partial propagation is able to quickly compute a difference even if this involves complex structure involving invariants [29].
- **Lightweight.** The Oscar CBLS engine has been kept small and well structured to ensure that it can be easily understood and extended [29].

4.1.2 Localizer

Localizer is a modeling language for implementing local search algorithms [33]. This model shortens the development time of these algorithms. Localizer makes it possible to express local search algorithms in a notation close to their informal descriptions in scientific papers [33]. It offers support for defining traditional concepts like neighborhoods, acceptance criteria, and restarting states [33]. Using localizer, we declare the maximum number of local search moves, and after each move, localizer tests if the state is a solution (in CSPs) or an acceptable feasible solution (in COPs), then the search has finished. Otherwise, it selects a candidate move in the neighborhood and moves to this new state if this is acceptable. If no solution is found after maximum trials or when the local condition is false, localizer restarts the search. The algorithm returns the best valuation found at the end of the computation.

4.1.3 Comet

Comet is the world's most comprehensive software platform for solving complex COPs [34]. Comet combines the methodologies used for constraint, linear, and integer programming, constraint-based local search, and dynamic stochastic combinatorial optimization a language for modeling and searching. One of the key innovations of the Comet system is constraint-based local search, the idea of specifying local search algorithms as two components [35]:

- (1) a high-level model describing the applications in terms of constraints, constraint combinators, and objective functions.

- (2) a clearly separated search procedure that implicitly takes advantage of the model in a general fashion.

Comet represents the life's work of Pascal Van Hentenryck—the Dynadec's founder (see <http://dynadec.com/technology/the-comet-story/>). Dynadec's hybrid platform incorporates constraint-based local search, which merges ideas from constraint programming and local search, and dynamic stochastic optimization.

Constraint-Based Local Search Capabilities in Comet [35]:

- Local search on high-level optimization models.
- Invariants and differential invariants for incremental computations.
- Rich constraint and objective language, including arithmetic, logical, and global/combinatorial constraints.
- Ability to model *soft constraints* (i.e., *the constraints which may be violated. For instance, the constraint of voiding a student to have two or three exams in a day in exam timetable scheduling in universities may be considered as soft constraint*) and preferences.
- Support for metaheuristics, including tabu-search, simulated annealing, variable-depth neighborhood search, guided local search, and hybrid evolutionary algorithms.

4.1.4 Kangaroo

Kangaroo [4] is a constrain-based local search system framework which has not been implemented yet. Newton et al. [4] presented the key details of Kangaroo implementation and aimed to improve Comet in both time and memory usage. Kangaroo differs from Comet in several aspects [4]:

- it currently provides a C++ library, not a separate language; it employs a lazy strategy for updating invariants,
- it uses well-supported simulation to explore neighborhoods, rather than directly using invariants as Comet seems to, and
- it uses data structures that are encapsulated at the system level instead of at the object level as Comet does. Nevertheless, Kangaroo provides many of the capabilities of Comet and is also very efficient.

5 Conclusions

This chapter gives an introduction to the local search algorithms, the optimization and the constraint satisfaction problems, and the local search methods used to solve them. In addition, it presents the state-of-the-art local search solvers for solving the CSPs or the COPs like Oscar CBL engine, Localizer, Comet, and Kangaroo [4].

References

1. <http://www.cs.cmu.edu/~venkatg/RD-approx.html>. Accessed 15 Aug 2012
2. Veřmřovský K (2003) Algorithms for constraint satisfaction problems. Master thesis, Faculty of Informatics, Masaryk University Brno, Czech Republic
3. Brailsford SC, Pott CN, Smith BM (1999) Constraint satisfaction problems: algorithms and applications. *Eur J Oper Res* 119:557–581
4. Newton MAH, Pham D, Sattar A, Maher M (2011) Kangaroo: an efficient constraint-based local search system using lazy propagation. In: *Proceedings of 17th international conference on principles and practice of constraint programming*
5. Letombe F, Joao Marques-Silva J (2008) Improvements to hybrid incremental SAT algorithms. In: *Proceeding of the international conference on theory and applications of satisfiability testing*
6. [http://en.wikipedia.org/wiki/Local_search_\(optimization\)](http://en.wikipedia.org/wiki/Local_search_(optimization)). Accessed 14 Nov 2014
7. Aarts EHL, Lenstra EJK (2003) *Local search in combinatorial optimization*. Princeton University Press, Princeton
8. http://en.wikipedia.org/wiki/Optimization_problem. Accessed 08 Aug 2014
9. Mancini T, Flener P, Pearson JK (2012) Combinatorial problem solving over relational databases: view synthesis through constraint-based local search. In: *Proceedings of the 27th annual ACM symposium on applied computing*, pp 80–87
10. <http://hsc.csu.edu.au/sdd/core/cycle/feasibility/feasibility.html>. Accessed 08 Aug 2014
11. Aardal KI, van Hoesel S, Lenstra JK, Stougie L (1997) A decade of combinatorial optimization. Technical report, Utrecht University, Information and Computing Sciences, Issue 1997–12
12. Mackworth A (1977) Consistency in networks of relations. *J Artif Intell* 8(1):99–118
13. Fang H, Kilani Y, Lee JHM, Stuckey PJ (2007) The Island confinement method for reducing search space in local search methods. *J Heuristics* 13:557–585
14. Michel L, Van Hentenryck P (1999) A modeling language for local search. *INFORMS J Comput* 11:1–14
15. Van Hentenryck P, Michel L (2009) *Constraint-based local search*. MIT Press, Honolulu
16. <http://www.hakank.org/oscar/>. Accessed 2 Aug 2014
17. Audemard G, Simon L (2007) GUNSAT: a greedy local search algorithm for unsatisfiability. In: *Proceeding of the international joint conference on artificial intelligence*
18. Tompkins DA, Hoos HH (2004) UBCSAT: an implementation and experimentation environment for SLS algorithms for SAT and MAX-SAT. In: *Proceeding of the 7th international conference on theory and applications of satisfiability testing*, pp 37–46
19. Pham D-N, Thornton J, Gretton C, Sattar A (2007) Advances in local search for satisfiability. In: *Proceedings of the 20th Australian joint conference on artificial intelligence*
20. Schuurmans D, Southey F, Holte R (2001) The exponentiated subgradient algorithm for Heuristic Boolean Programming. In: *Proceeding of the international joint conference on artificial intelligence*, pp 334–341
21. Wei W, Li CM (2009) Switching between two adaptive noise mechanisms in local search for SAT
22. Li CM, Wei W (2009) Combining adaptive noise and promising decreasing variables in local search for SAT, (2009). SAT2009. <http://www.cril.univ-artois.fr/SAT09/>
23. Li XY, Stallmann MF, Brglez F (2003) QingTing: a fast SAT solver using local search and efficient unit propagation. In: *Proceedings of international conference on theory and applications of satisfiability testing*
24. Hutter F, Tompkins DAD, Hoos HH (2002) Scaling and probabilistic smoothing: efficient dynamic local search for SAT. In: *Proceedings of the eighth international conference on principle and practice of constraint programming (CP-02)*. *Lecture Notes in Computer Science (LNCS)*, vol 2470, pp 233–248

25. Thornton J (2005) Clause weighting local search for SAT. *J Autom Reasoning* 35(1–3):97–142. ISSN 0168-7433
26. Ho SY, Shu LS, Chen JH (2004) Intelligent evolutionary algorithms for large parameter optimization problems. *IEEE Trans Evol Comput* 8(6):522–541. <http://ieeexplore.ieee.org/stamp/stamp.jsp?arnumber=01369245>
27. Yang P (2007) A hybrid evolutionary algorithm by combination of PSO and GA for unconstrained and constrained optimization problems. In: *IEEE international conference on control and automation*
28. Russell S, Norvig P (2009) *Artificial intelligence: a modern approach*, 3rd edn. Prentice Hall, Englewood Cliffs
29. <https://bitbucket.org/oscarlib/oscar/wiki/CBLS>. Accessed 29 July 2014
30. Van Hentenryck P (2009) *Constraint-based local search*. MIT Press, Cambridge
31. <https://bitbucket.org/oscarlib/oscar/wiki/ExtendCBLS>. Access 4 Aug 2014
32. <http://ripples.sourceforge.net/ripples/manual/concepts/propagationrules.html>. Accessed 4 Aug 2014
33. Micheal L, Van Hentenryck P (2000) Localizer. *J Constraints* 5(1–2):43–84
34. <http://dynadec.com/technology/>. Accessed 13 Dec 2013
35. <http://dynadec.com/technology/constraint-based-local-search/>. Accessed 12 Aug 2014

Remote Tuning of Magnetron Frequency in an RF Linac

Vijay Sharma, V.K. Madan, S.N. Acharya and K.C. Mittal

Abstract A 6 MeV electron beam, RF Linac system was developed to operate at a frequency of 2856 MHz. The RF power source to the Linac is a magnetron. During operation of the Linac, loss of RF power changes frequency of both the Linac as well as magnetron. The magnetron RF output power frequency needs to be changed remotely to feed maximum power into the Linac. This paper presents theory and the developed system.

Keywords RF—Radio frequency · OFHC—Oxygen-free high-conductivity copper · OACCL—On axis coupled cavity linac · PLC—Programmable logic controller

1 Introduction

A 6 MeV oxygen-free high-conductivity, OFHC, copper cavity based RF linear particle accelerator, Linac, was developed for X-ray generation. Microwave power source was used to provide RF power in the Linac cavity. The RF power develops electromagnetic fields in the cavity to accelerate the electron beam. For X-rays of beam energy of 6 MeV and maximum average beam power of 1.0 kW, the RF source required should have peak power capability in the range of 2.0–3.0 MW and average power of 3.0 kW. The RF source used in the Linac is a magnetron of 5.5 MW (peak power) and 3.2 kW (average power). The magnetron is operating at a frequency of 2856 MHz with 4 μ s pulse width and 0.12% duty cycle. The magnetron output RF power is fed to the center fed on axis coupled cavity Linac, OACCL. The whole structure has been cooled by low-conductivity chilled water

V. Sharma (✉) · S.N. Acharya · K.C. Mittal
Bhabha Atomic Research Centre (BARC), Mumbai, India
e-mail: vijay9819420563@gmail.com

V.K. Madan
(Ex-BARC) Kalasalingam University, Krishnankoil, India

with conductivity less than 3.2 mS/cm, and with temperature not exceeding 30 °C at 45 psi. For utilization of RF power in the cavity, the RF frequency should match with the resonance frequency of the Linac. In order to match the frequency of the magnetron, RF output is tuned remotely such that the reflected RF power from Linac is minimum.

2 System Description

The block diagram of the RF section of the Linac is shown in Fig. 1. A TTL trigger pulse of 4 μs and PRF 250 Hz is given to the magnetron modulator. The magnetron modulator drives the magnetron and feeds the RF power into the cavity to establish the accelerating field in the cells of the cavity. The magnetron generates the RF power at a tuned frequency. Any change needed in the RF output of the magnetron is done using the tuning knob of the magnetron.

3 Operation of the System

During the operation of Linac, the magnetron and Linac temperature changes due to loss of RF power in the system. The magnetron RF power output frequency can be achieved from 2856–2859 MHz. However, tuner setting can change frequency by 630 kHz per kW power in the mean input power. The frequency shift at different power level operation can be adjusted up to 50 kHz around the center frequency using a mechanical tuning knob provided with the magnetron. The tuner of the

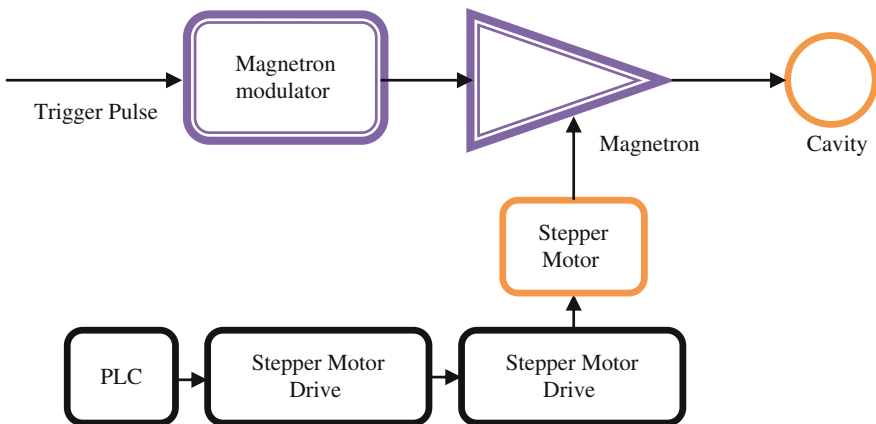


Fig. 1 Block diagram of the Linac RF system

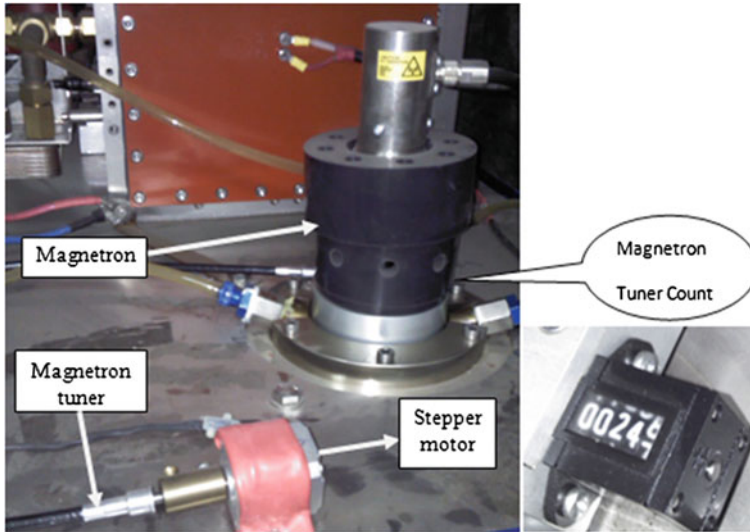


Fig. 2 Motor interfacing to magnetron tuner

magnetron is coupled with an accelerator cable. The accelerator cable is linked to the stepper motor as shown in Fig. 2. For remote operation of the tuning knob a PLC-based pulse generator system was developed to drive the stepper motor. The PLC is programmed to generate set number of pulses at its output. The PLC pulse output is fed to the stepper motor drive unit, and that drives the stepper motor driving the magnetron tuner. The PLC output of 200 pulses corresponds to rotations of tuning knob by 360° , hence giving a resolution of $1.8^\circ/\text{pulse}$ with an accuracy of 3–5 % with noncumulative error. The current position of the knob is tracked by counting the number of rotations taken by the tuning knob in terms of pulses given to the motor. The current position of the knob is saved in battery backed memory of the PLC and any rotation command given to the motor is updated in PLC memory to indicate the current position of the magnetron frequency tuning knob. The control system allows the motor to be rotated clockwise or anticlockwise to make a shift in the RF power frequency both increase or decrease from the current value. The user interface for the motor control is built using a touch panel human machine interaction, HMI. The user can set position of tuning knob by entering the number of knob rotations needed such as 1.5 turns, and direction of rotation as either clockwise/anticlockwise. Pressing the RUN button sets the magnetron tuning knob to the set position given by the user, and hence adjusts the RF signal frequency to the desired value. The operator sees the current frequency output of the magnetron on spectrum analyzer and whenever there is any shift in the frequency, he rotates the stepper motor to bring the magnetron frequency back to the original frequency.

4 Summary

The Linac is located in a concrete shielded cell area and all the related RF systems are kept close to it. During operation of the Linac X-ray radiations it covers the cell area and that makes adjustment of the frequency tuning difficult. But with the use of this PLC-based manual tuner for magnetron RF frequency the Linac operation has become convenient for a human operator. A system is being developed to automatically adjust tuning of the frequency to keep the reflected power from cavity at a minimum. We are designing a system to adjust the tuner position automatically in close loop control by monitoring the reflected RF power from cavity as feedback signal to rotate the motor in either of the two direction and right number of steps so that a minima is achieved on the reflected RF power. The control algorithm will be implemented using a PLC.

Part IV
Biomedical Applications

Using Modern Technologies to Facilitate Translating Logical Observation Identifiers Names and Codes

Daniel-Alexandru Jurcau, Vasile Stoicu-Tivadar
and Alexandru Serban

Abstract This paper presents the result of a research study aimed at reducing the amount of time and effort required to translate the Logical Observation Identifiers Names and Codes (LOINC[®]). The first section introduces LOINC and its role in interconnecting medical units. The structure of the LOINC terms is analyzed and various ways of decomposing the terms are presented. These involve finding and applying various patterns and storing the results in a database. The database is used by a website aimed at allowing medical staff to easily and efficiently translate the terms into any language. The LOINC codes are then recomposed from the translated fragments. The paper shows the key points of creating this website. The emphasis is placed on usability and a rich client interface. The advantage of the suggested method is decrease of the translation effort. A social network is used for authentication, relieving the users of the need to remember a new password. In the end, the paper presents the result of piloting the website by medical staff and students.

1 Introduction

In today's world, a lot of medical information needs to be transferred from one unit to another. One way of achieving this connection electronically is with the help of HL7 Clinical Document Architecture (CDA) messages [1].

D.-A. Jurcau (✉) · V. Stoicu-Tivadar · A. Serban
Faculty of Automatics and Computer Science, Politehnica University Timisoara,
2, Piata Victoriei Street, 300006 Timisoara, Romania
e-mail: djurcau@gmail.com

V. Stoicu-Tivadar
e-mail: vasile.stoicu-tivadar@aut.upt.ro

A. Serban
e-mail: alex.serban81@yahoo.com

The CDA describes XML documents as being composed of two parts (a header and a body) [2]. The body contains a lot of coded information. However, if each producer of such messages (e.g., laboratories) was to use his own internal codes, then understanding of the message by receiver would become problematic without adopting the sender's codes. The situation can become even more complicated if there are multiple sources [3].

This is where Logical Observation Identifiers Names and Codes (LOINC[®]) comes in. According to the official manual, LOINC “provides a set of universal names and ID codes for identifying laboratory and clinical test results” [3]. By implementing the LOINC codes on both ends of the communication's channel, the problem described above would disappear.

LOINC, developed by Regenstrief Institute, is an open standard and is freely available for download from the LOINC website [4]. Outside the US, LOINC is used in Brazil, Canada, Germany, The Netherlands, Mexico, Rwanda, Spain, Singapore, and Korea [5]. To help mapping the local test names to LOINC, a software tool called RELMA is also provided [6].

A first step in adopting LOINC in a country is translating it to the country's native language, should such a translation not already be available. Daniel J. Vreeman describes the challenges of translating LOINC into Italian [5]. The focus is placed on converting terms into separate pieces for independent translation.

Based on this, the current article seeks to find better, more detailed ways of reducing the effort required for translating LOINC into other languages. The article also presents the process of building a modern web application for medical staff to use while translating LOINC codes. The emphasis is on ease of use and increased productivity.

2 Analyzing the Available Data

The English language version of LOINC table is available for download from the official website (<https://loinc.org/downloads>) in a variety of formats, including a simple comma-separated value (CSV) file. At the moment of this writing, the latest version is 2.46, released on December 26th 2013 [4].

The following sections will detail the process of analyzing the content of the LOINC data table with the goal of creating an efficient translation strategy.

2.1 Observations at a Glance

Each row in the table is identified by a unique value stored in the first column, also called LOINC_NUM. This unique value is composed of two integers, joined together by a minus sign, e.g., 10,092 - 5.

Table 1 Summary of the data found in the LOINC table

Measurement	Value
Number of rows	73,115
Number of columns	48
Number of null (empty) values	1,904,784
Number of non-string values	497,721
Number of string values	1,107,015
Number of unique string values	261,115
Total length of unique string values	23,785,626
Average length of unique string values	91.09

The remaining columns store various pieces of information in the form of numeric values, date values and more or less complicated strings. Table 1 summarizes the content of the LOINC data.

The main reason for splitting up string values from non-string values is that the latter do not require translations in any language. Thus, after counting out the duplicates, only 261,115 string values would require translation. This number is still pretty high, keeping in mind that the average length of such an entry is 91.09 characters.

However, as with any data, various patterns have been observed, which are detailed next.

2.2 Observed Data Patterns

The next step after filtering out the immediate duplicates is analyzing the remaining values in the hope of finding various patterns. These patterns would then help in converting large cells into smaller, atomic¹ elements.

The main reason why the average length of each value is so high is that a lot of them contain enumerations of multiple atomic elements, e.g.:

- Person name; Point in time; Random; Cardiac rehabilitation Tx plan; Nominal
- Dx.primary; Dx; Interpretation; Interp; Impression; Impressions; Point in time; Random; Alcohol-substance abuse rehabilitation Tx; Alcohol-substance abuse rehabilitation Tx; Narrative; Report
- Immune globulin G; Immunoglobulin G; Arbitrary concentration; Point in time; Random; Serum; SR; Quantitative; QNT; Quant; Quan; ABS; Antibodies;

¹Throughout this article, the term `atomic` will be used in the sense of a word or series of words that can be individually translated into any language and then reassembled back into the (larger) cell value, without relying on any particularities of the English language, like word order. Thus, a series of sentences could be separated into individual ones, that would be separately translated, however a sentence would not be split into individual words, because, for example, the word order would be different when translating into another language.

Autoantibody; Antibody; Autoantibodies; Antby; Aby; Anti; species; spp; Microbiology

- Coxiella burnetii phase II; C burnet Ph2; Q fev; C burnetii; Qfever; Coxiella burnetii; Q fever; Dilution factor; Titer; Titre; Ttr; Ttered; Point in time; Random; Serum; SR; Quantitative; QNT; Quant; Quan; ACIF; FA; Fluorescent antibody; Immune fluorescence; Fluoresent; Immunoflour; Immunofluor; Immunofluorescence; IFA; Time Resolved Fluorescence; Anticomplement Immunofluorescence; TRF; ABS; Antibodies; Autoantibody; Antibody; Autoantibodies; Antby; Aby; Anti; Microbiology

From a translation point of view, these terms are not related to each other, so splitting up each value into its individual atoms would result in translating much smaller terms that also have a big chance of being repeated. Similarly, other cells contain narrative text, even five or more sentences in the same table cell. These could also benefit from being individually translated.

Another simple pattern involves short values that do not require any translation because they represent various identifiers or value/measurement unit pairs, e.g.:

- 25 mg/dL
- 30 mg/dL
- mU/mL;mcU/mL
- umol/L
- mm[Hg]

Various columns have led the way to the discovery of more complex patterns. One of these consists of specifying what has been detected/observed, and where, the unit of measurement and, optionally, the number of the specimen:

- Lutropin [Units/volume] in Serum or Plasma—1st specimen
- Thyrotropin [Units/volume] in Serum or Plasma—4th specimen
- Adenosine deaminase [Enzymatic activity/mass] in Chorionic villus sample
- Beta-cortolone/Cortisol [Mass Ratio] in Urine

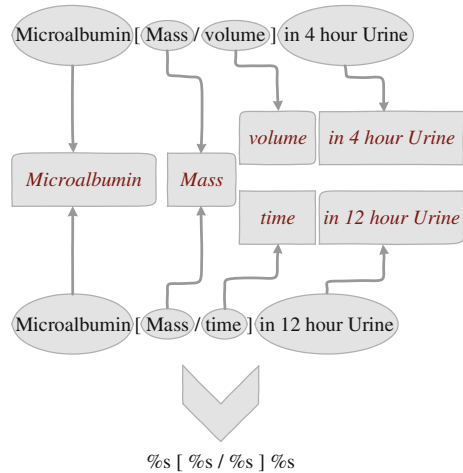
After having discovered these patterns, it was time to make use of them in order to break the data apart in as many atomic parts as possible.

2.3 *Applying Patterns*

In order to break the data apart into atomic parts, a C# application has been developed. The role of this application is to apply various patterns in a recursive manner.

The easiest breaking-up to be applied involves splitting up the values into array of strings based on common delimiters such as;,—or :\t. A total of 18 such delimiters were implemented. A simple dot for delimiting various sentences could not be easily used because it would generate unacceptable false-positives, like in

Fig. 1 Splitting a LOINC value into patterns



E. coli. To overcome this, a rule was implemented that only splits multiple sentences based on dots if the word before the dot contains at least four characters (and thus is not an abbreviation) and a white-space comes after the dot.

The rest of the patterns are much more complicated and require the use of regular expressions. Specially created expressions would split the text up into groups as detailed in Fig. 1. Each expression is accompanied by a string format used to recompose the values into the original text. This pattern is very similar to the one used by the C standard library `printf()` function. One such pattern could be `%s [%s/%s] %s`. The regular expression would extract four groups of string values corresponding to the four placeholders in the format. These values are then individually translated and the key benefit is that they appear multiple times in various cells (the matching is case-sensitive). Non-letter values such as brackets are skipped as much as possible and only appear in the format.

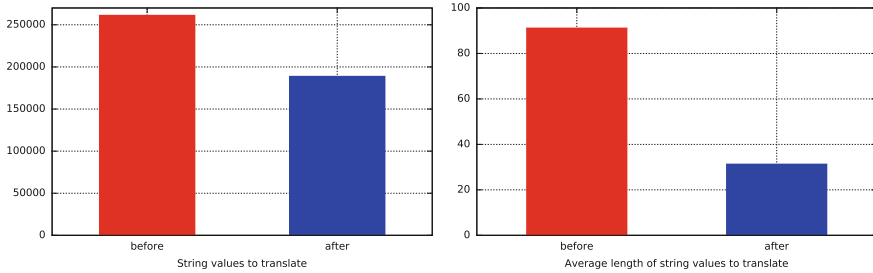
A total of 25 regular expressions have been used, e.g.:

- `(.*) \((.*)\) (I\g[A-Z][0-9]*) ([A-Z][a-zA-Z]+) $`
- `^(.*) ([0-9.]+) ([^ -:]*) / ([^ -:]*) ([^a-zA-Z0-9]*) $`
- `^(.*) ([\t]+) (PhenX) $`

In order to benefit the most from using these regular expressions, they are applied in a recursive manner. So, a group matched by one expression could then be further split up into multiple other groups and formats by other expressions. Technically, this is achieved by using a programming technique called Metaprogramming [7]. A text template has been written which contains all the patterns and regular expressions. This text template also contains C# code that is then executed by the `TextTemplatingFileGenerator` to produce a C# class [8] that is used in the actual project, and which does the job of recursively applying the patterns.

Table 2 Result of applying patterns to the LOINC data

Measurement	Value
Number of values that do not require translation	7,661
Number of values to translate	188,646
Total length of values to translate	5,894,023
Average length of values to translate	31.24

**Fig. 2** Comparison of the number of values (*left*) to be translated and their average length (*right*) before and after applying patterns

In the last step, some of the values are, for example, numeric and do not require any translation. A rule has been introduced so that any value that does not contain more the one consecutive letter is considered as not requiring translation (e.g., 10.5%, A10).

The result of applying the patterns is presented in Table 2. Figure 2 compares the number of values to be translated and their average length before and after applying the patterns.

All these results have been stored in a database which is presented in the next section.

3 Creating the Database

In order to create a web application to support the translation of LOINC terms, a relational database was first created to store the results of applying the patterns. Figure 3 describes the database schema.

The main table is called `TableValues` and it stores the content of each non-empty cell in the LOINC data table. The cell is identified by the `LOINC_NUM`, stored as a two-part integer and by the column, stored also as an integer. If cell contains an integer, decimal, date, or boolean value, the value is stored in the same table in the corresponding column. If cell contains a simple string value, it stores a reference to the actual value from the `StringValues` table. Should the cell however contain a string value that was matched by patterns, the values table will

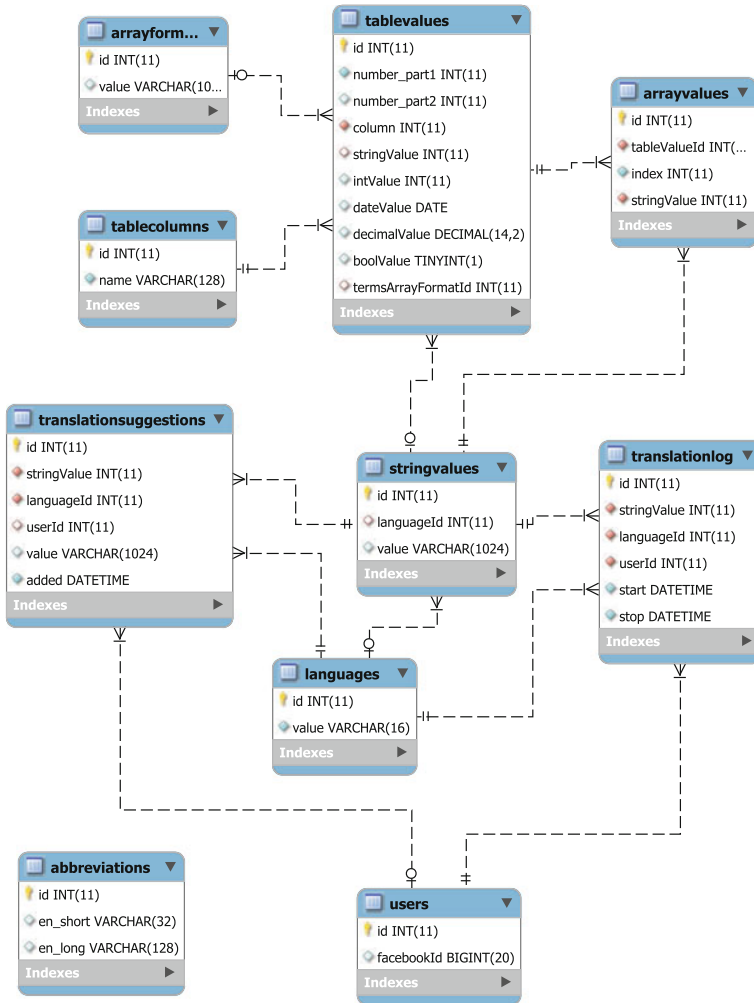


Fig. 3 The database schema used for the translation of LOINC terms

store a reference to the format used to reassemble the original value and will make use of an N-N relationship with the StringValues table, via the intermediate ArrayValues table, to store the actual atomic values found by the patterns.

The StringValues table stores all the atomic string values and differentiates between those that require translation and those that do not. A lot of these values repeat multiple times so translating them once brings the advantage of multiple use.

In order to validate the correctness of the database, an application was created that analyzes each value stored in the database and compares it to the value from the original spreadsheet. The validation was successful.

Information relating to the users that will perform the translations is stored in a table called `Users`. When someone submits a translation in a specific language, it is stored in `TranslationSuggestions` and a log table, `TranslationLog` stores metrics regarding when the translations were made and how long the translation process took.

The database also contains a table used for expanding abbreviations. The data inside was manually collected from the LOINC documentation [3].

4 Building the Website

In order to allow medical staff to translate the English LOINC terms, a website has been built using PHP as the server-side language together with their PDO classes for accessing the MySQL database in an object-oriented manner [9].

The development of the website was focused more on the client-side programming. By using asynchronous JavaScript with the help of jQuery, the website provides a rich and smooth client interface [10, 11]. The client-side scripts have been split into modules and loaded with the help of RequireJS [12].

The first feature provided by the web application is allowing the users to browse through all the LOINC records. An interactive table displays 50 rows/page and allows the user to select the columns of interest. As presented in Fig. 4, abbreviations are highlighted and expanded on mouse over. The caching of string values allows the web client to minimize the number of server requests during the browsing of the data table.

The most important feature of the web application is allowing the users to submit translations.² As presented in Fig. 5, the user is shown a LOINC term to translate and an input textbox. The user is also presented with three buttons:

- *Save*—Saves the current translation
- *Does not require translation*—The current term does not require any translation
- *Change term*—The user is presented with another term.

If the term to be translated has already been translated by someone else, the user is presented with the other translations as suggestions, ranked by the number of users who provided them.

In order to know who provides translations, all the users of the web application are required to authenticate themselves. As this has become so popular, the Facebook API is used for this purpose, relieving the users of the need to remember another password [13].

Multiple medical graduates and students have been granted access to the website and have been invited to participate in evaluating it by translating various terms. The process has been benchmarked and the results are presented in the next section.

²The web application has been localized to provide translations into Romanian.

LOINC NUM	COMPONENT	RELATEDNAMES2	SHORTNAME	ORDER OBS
10093-3	ST initial amplitude 6 ms lead V6	ST I-Amp 6ms L-V6; PB; Electrical potential; Voltage; Point in time; Random; Hrt; Cardiac; Quantitative; QNT; Quant; Quan; Electrocardiogram; Electrocardiograph; ECG; EKG.MEASUREMENTS; EKG.MEASUREMENTS	ST I-Amp 6ms L-V6	Observation
10094-1	ST slope.lead AVF	ST Slope L-AVF; PB; Voltage rate; Amperage; Point in time; Random; Hrt; Cardiac; Quantitative; QNT; Quant; Quan; Electrocardiogram; Electrocardiograph; ECG; EKG.MEASUREMENTS; EKG.MEASUREMENTS	ST Slope L-AVF	Observation

Fig. 4 The LOINC table displayed on the web page with *highlighted* abbreviations

CACNA1A gene allele 1.CAG repeats

traducere în română

🔄 Salvează

↔ Nu necesită traducere

🔄 Schimbă termenul

Fig. 5 Input area for the users translation—localized to Romania

5 Translation Results

A number of 12 medical staff and students have accepted the invitation to pilot the website and translate LOINC terms into Romanian. They have translated a total of 179 terms, Table 3 summarizing their results. Time has been measured from the moment the user was displayed the term to translate, until the translation was submitted. The measurement is approximate.

By extrapolating, a team of 20 translators would require about 1154 h to translate the entire LOINC table, estimating that each term would be translated by an average of two people.

Table 3 Summary of translating LOINC terms into Romanian

Measurement	Value
Number of translators	12
Number of terms translated	179
Total time spent translating	02:31:52
Average time spent translating/user	00:12:39
Average length of translated English terms	29.15
Average length of resulting Romanian terms	35.46
Average time spent translating /English character	1.74 s

6 Conclusions

In conclusion, the research on finding ways to reduce the amount of time required to translate the LOINC codes has proved successful.

By analyzing the format and structure of the LOINC terms in depth, various patterns of data have been observed, allowing the cell values to be split up into more atomic parts that can easily be individually translated and reassembled, without being affected by the particularities of the English language.

The total number of unique values to be translated has been reduced by about 27 %. Although, at first glance, this value does not seem so important, one has to remember that, by splitting a large value into many small ones, the total number of values actually increases. The fact that after eliminating duplicates the number of values to be translated has decreased and by over 25 % hints at a good output. This is further confirmed by comparing the average length of the values before and after applying the patterns. Here a decrease of over 65 % can be observed.

Creating a website for allowing medical staff to translate the LOINC codes has also proved a success. The focus on usability has led to a product that was easy to use and led to increased productivity, as presented by Table 3. The modern social network Facebook has also played its role by allowing the users to use the same credentials when authenticating to the translation website.

Although localized to Romania, the database and website have been designed with internationalization in mind, allowing the product to be adapted to any language. Further translations will be performed to gather more data and increase the accuracy of the estimates.

References

1. Vida M (2012) Contributions on medical information systems interoperability demonstrated at electronic healthcare records systems. Editura Politehnica, Timisoara
2. Vida M, Gomoi V, Stoicu-Tivadar L, Stoicu-Tivadar V (2010) Generating medical computer-based protocols using standardized data transmission. In: 4th international workshop on soft computing applications, pp 155–158
3. McDonald C, Huff S, Deckard J, Holck K, Vreeman DJ (2013) Logical observation identifiers names and codes (LOINC) users' guide. Regenstrief Institute, Inc., Indianapolis
4. LOINC from Regenstrief (2013) <https://loinc.org/>
5. Vreeman DJ, Chiaravalloti MT, Hook J, McDonald CJ (2012) Enabling international adoption of LOINC through translation. *J Biomed Inform* 45:667–673
6. Kim H, El-Kareh R, Goel A, Vineet F, Chapman WW (2012) An approach to improve LOINC mapping through augmentation of local test names. *J Biomed Inform* 45:651–657
7. Hazzard K, Bock J (2013) Metaprogramming in .NET. Manning, Shelter Island
8. Design-Time Code Generation by using T4 Text Templates (2013) <http://msdn.microsoft.com/en-us/library/dd820620.aspx>
9. PHP Data Objects (2014) <http://www.php.net/manual/en/book.pdo.php>

10. Freeman A (2013) Pro jQuery 2.0. Apress, New York
11. jQuery (2014) <http://jquery.com/>
12. RequireJS—A Javascript Module Loader (2014) <http://requirejs.org/>
13. Facebook SDK for PHP. <https://developers.facebook.com/docs/reference/php> (2014)

Data Analysis for Patients with Sleep Apnea Syndrome: A Complex Network Approach

Alexandru Topirceanu, Mihai Udrescu, Razvan Avram
and Stefan Mihaicuta

Abstract Network science is an emerging paradigm branching over more and more aspects of physical, biological, and social phenomena. One such branch, which has brought cutting edge contributions to medical science, is the field of network medicine. Along this direction, our proposed study sets out to identify specific patterns of developing obstructive sleep apnea (OSA), by taking into consideration the multiple connections between risk factors in a relevant population of patients. For this purpose, we create a social network of patients based on their common medical conditions and obtain a community based society which pinpoints to specific—and previously uncharted—patterns of developing OSA. Eventually, this insight should create incentives for predicting the apnea stage for any new patient by evaluating its network topological position.

Keywords Network medicine · Complex networks · Disease development pattern · Emergent medical diagnosis · Obstructive sleep apnea

A. Topirceanu (✉) · M. Udrescu · R. Avram
Department of Computers and Information Technology, Politehnica University of Timisoara,
Bd. Vasile Parvan 2, 300223 Timisoara, Romania
e-mail: alext@cs.upt.ro

M. Udrescu
e-mail: mudrescu@cs.upt.ro

S. Mihaicuta
Department of Pneumology, Victor Babes University of Medicine and Pharmacy,
Piata E. Murgu 2, 300041 Timisoara, Romania
e-mail: stefan.mihaicuta@umft.ro

1 Introduction

Many scientifically important problems can be represented and empirically studied using networks. For example, biological and social patterns, the World Wide Web, metabolic networks, food webs, neural networks, and pathological networks are few examples of real world problems that can be mathematically represented and topologically studied to reveal some unexpected structural features [1, 2]. Most of these networks possess a certain community structure that has substantial importance in building an understanding regarding the dynamics of the network [3–6].

Sleep apnea is a disorder that consists of abnormal breathing pauses, irregular or superficial breathing that occurs during sleep [7]. It has often been indicated as a serious, frequent but mostly underrated clinical problem [8]. The reported incidence of apnea varies, due to different backgrounds of patient groups that were taken into account. Nonetheless, in [9] it was reported that there are 70 million people in USA with obstructive sleep apnea (OSA), so that 1 in 4 men and 1 in 10 women have developed this disorder. Other studies have reported estimates of 3–7 % prevalence of OSA [10]. Obviously, these are high figures which indicate the magnitude of the situation; hence it comes as no surprise that the occurrence of sleep apnea is referred by many as epidemic [9–11]. The morbidity risks entailed by the fact that many sleep apnea cases are not discovered and treated in time are well documented by many comprehensive studies. Maybe the best known link is between sleep apnea and cardiovascular problems [12–15], leading to hypertension, stroke, and even death [16]. This is one of the reasons which indicate the paramount importance of early diagnosis of these severe cases [17].

The economic implications of all these risks are significant and must be dealt with, by adopting appropriate procedures for patient management [18, 19] which, in turn, are underpinned by methods for early detection of moderate and severe apnea cases. Taking a step forward, reference [11] argues that the available traditional methods for identifying patients at risk (based on randomized trials) are not efficient enough, and that new, innovative, and ultimately better ways are required.

This paper proposes such an innovative approach, based on identifying specific patterns of developing apnea by taking into consideration the multiple connections between risk factors in a relevant population of patients. The main idea is based on the assumption that there is a connection between the way of acquiring apnea and the severity of this disease. Thus, by using tools that were put forward by the new network science [4–6] which spurred cutting edge research in the field of network medicine [2, 20], this work proposes a methodology of associating apnea risk groups to each such apnea pattern. Eventually, this insight creates incentives for predicting the apnea severity for any new patient, by evaluating its network topological position, based only on simple clinical aspects such as sex, neck circumference, obesity, etc. This allows for introducing an easy-to-use scorecard that will accurately indicate the risk group that the potential patient pertains to.

This paper has the following structure: in Sect. 2 we describe the medical dataset of patients and how the study was conducted. Section 3 explains the

methodology of creating and clustering the patient database into a complex network, and Sect. 4 discusses the results obtained from the clustering of patients in the obtained communities.

2 Data Acquisition

We acquired data for our apnea database at Timisoara Pneumology Clinic, in Timisoara, Romania, from March 1, 2001 to 31, 2011. The cardiorespiratory polysomnography was performed using Poly-Mesam 4 1998, Alice 5 Respirationics 2005, and Stardust Respirationics 2005 devices. The population group is represented by all consecutive persons referred to be evaluated in the sleep laboratory with suspicion of sleep breathing disorders.

The study was conducted in accordance with the New England Journal of Medicine protocol (available at NEJM.org). The protocol was approved by the local ethics committee. We used standard and noninvasive, effortless procedures only, which therefore did not require any kind of compensation or supplementary costs. Their identities and personal data were not used, thus assuring the complete confidentiality of our study. The authors vouch for the completeness and veracity of the reported work as well as the fidelity of the reported work to the protocol.

3 Network Approach

A final database of 1367 consecutive patients from the sleep lab of Timisoara “Victor Babes” Hospital, with over 100 measured criteria, is used as input for a methodology inspired by the Network Medicine approach [2, 20]. Each patient is considered a node in a network, where the link between two nodes is inserted if there is a risk compatibility relationship between the two corresponding patients. The risk compatibility exists if the two nodes have at least 5 out of 7 identical parameters: *sex* (male or female), *age* (group 0: ≤ 20 years; group 1: 20–40 years; group 2: 40–60 years; group 3: > 60 years), *blood pressure* (with/without hypertension), obesity (not obese: $BMI \leq 30$; obese: $BMI > 30$), *neck circumference* (normal circumference: < 40 cm for women, < 43 cm for men), *mean- and desaturation index*. The graphical representation is generated with Gephi 0.8.1 [21], in order to extract the most important network attributes, as well as revealing the compatibility clusters. A compatibility cluster uniquely defines the specific pattern for acquiring apnea. We chose Gephi as it is the leading tool in large dataset visualization, and because it is open source, allowing us to create custom tools on top of the graph processing framework. In Fig. 2 we use the AHI (apnea–hypopnea index) parameter to classify the four stages of apnea: group 0: $0 \leq AHI \leq 4$, group 1: $5 \leq AHI \leq 14$, group 2: $15 \leq AHI \leq 29$, group 3: $30 \leq AHI$.

The algorithm for mapping the patient database onto the apnea risk clusters is detailed below. The construction of the graph has a time complexity of $O(n^2)$. The relevant health parameters of each two (distinct) patients are compared, and the compatibility degree is increased on each match. Line 4 compares the mappings of each of the 7 described risks. The condition on line 5 acts as an edge weight filter, i.e., only edges with weight ≥ 5 out of 7 is actually added to the graph. The resulting graph is discarded of weights.

```

Patient database to complex network G:
1 :for each pair of patients  $(p_i, p_j)$ :
2 :  compat = 0
3 :  for each risk  $r_k$ :
4 :    if risk  $r_k(p_i) = r_k(p_j)$  then compat $\leftarrow$ compat+1
5 :  if compat $\geq$ 5 then G.addEdge( $p_i, p_j$ )

```

Once the patient graph is obtained, the nodes have to be classified into compatibility clusters. As such, we extract the modularity, a graph measure which is designed to measure the strength of division of a network into communities [3]. This is achieved using the modularity algorithm [22], with a corresponding default resolution of 1.0 [23], detailed in the pseudocode below. Further, for each obtained community independently, we inventory the number of occurrences of each risk of each patient (line 3). Finally, the risks with a high occurrence per community are marked as significant for the risk cluster. A risk is considered significant if it is present in $\geq 75\%$ of patients from that community (line 5).

```

Extract significant features of risk clusters from G:
1 :communities  $c_{[1..n]}$  = modularity(G)
2 :for each patient  $p_i$  in each  $c_j$ :
3 :  mapRisks( $p_i$ )  $\rightarrow$ risks( $c_j$ )
4 :for each risk  $r_k$  in risks( $c_j$ ):
5 :  if  $75\% \leq r_k \leq 100\%$  then markSignificant( $r_k, c_j$ )
6 :  else if  $50\% \leq r_k < 75\%$  then markCharacteristic( $r_k, c_j$ )

```

The reason for choosing the limit of 5 out of 7 as the threshold t for adding edges to the graph was made empirically. The goal of the study was to clusterize the patient database based on ad hoc properties, in such a way that the visualization is relevant for human understanding and clinical processing: not too many, or too few clusters were required. Thus, Fig. 1a, b depict the visualizations of the resulting graphs for a threshold $t = 4$, and $t = 6$ out of 7, while the ideal clustering for $t = 5$ is depicted in Fig. 1c. A lighter condition ($t < 5$) results in too many edges being added and the community structure disappears. A stronger condition ($t > 5$) results in too few edges added, thus too many small communities. The threshold $t = 5$

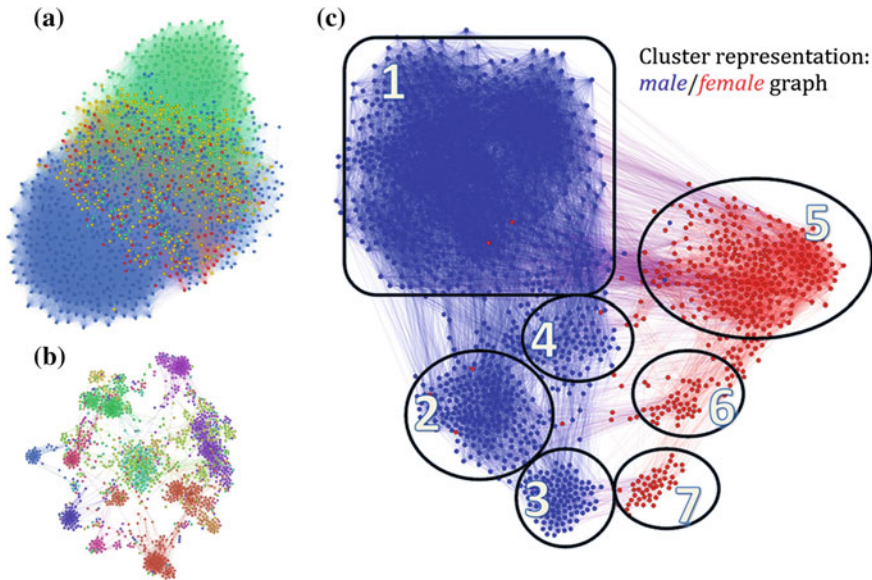


Fig. 1 The visualization of the patient graph with a threshold of: **a** 4 out of 7 (4 communities, too dense), **b** 6 out of 7 (162 communities, too sparse). The node color is according to the assigned communities, **c** the 7 resulting clusters, colored by gender, using the threshold 5

offers the best results, but it is no rule of thumb for other datasets. This aspect has to be tested empirically and adjusted accordingly for other studies (Fig. 2).

4 Results

Using the complex network cluster analysis [9, 10] that we provide, 7 distinct compatibility clusters were found. Each of these clusters corresponds to a specific patient profile which leads to a certain probability of developing the disease, as shown in Fig. 1c. There are 3 clusters of patients with severe apnea (1, 2, and 5) and 3 clusters which generally do not have severe apnea (3, 6, and 7). Cluster 4 is special in that it seems to reflect a transitory stage between the clusters indicating severe illness and the others; moreover, it shows that it cannot be characterized by a stable AHI group: ~47 % are group 3, 26 % are group 2, ~17 % are group 1, and 7 % pertain to group 0.

Each obtained community holds a particular distribution of the 7 risks, however, only some are statistically relevant to a cluster. In order to extract the most relevant features for each cluster we have developed a data mining tool in Gephi which extracts these relevant features. We consider these results to pave way for defining the characteristic patterns of each cluster of patients to develop sleep apnea. Also,

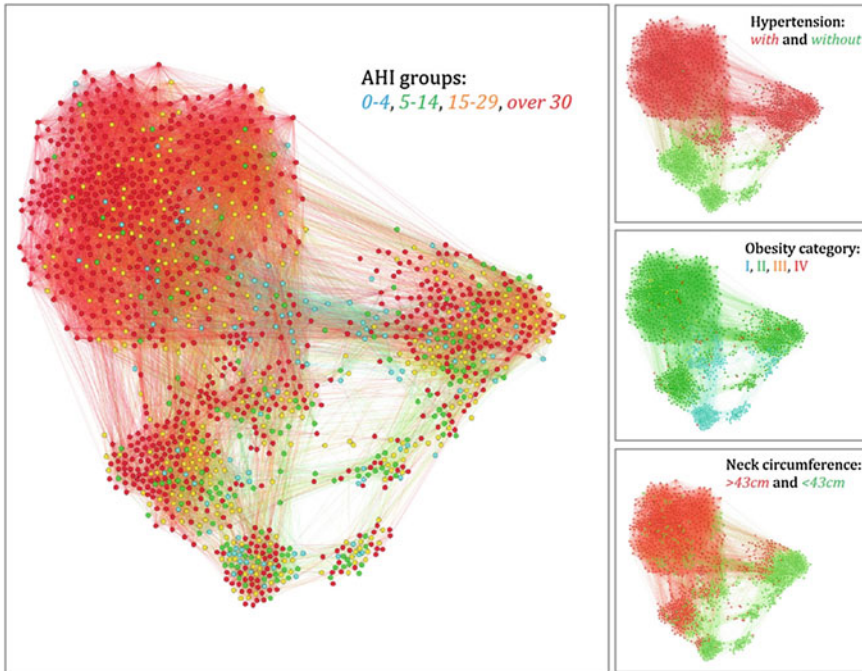


Fig. 2 Graphical representation of the patient population with clinical apnea signs: node colors are assigned in order to depict, as indicated: AHI groups, hypertension, obesity, and neck circumference

each cluster can be correlated with a type of prevention and treatment scheme. The characteristic features for each obtained cluster are:

- cluster 1: male, obese, with hypertension, neck circumference > 43 cm, desaturation < 90 (73 % have AHI > 30);
- cluster 2: male, obese, no hypertension, neck circumference > 43 cm, desaturation 90–95 (55 % have AHI > 30);
- cluster 3: male, no hypertension, neck circumference < 43 cm, desaturation > 95 (39 % have AHI > 30);
- cluster 4: male, not obese, all other risk factors are variable (56 % have AHI > 30);
- cluster 5: female, obese, with hypertension, neck circumference < 43 cm, desaturation 93–97, (52 % have AHI > 30);
- cluster 6: female, obese, without hypertension, neck circumference < 43 cm, normal desaturation 93–97, (33 % have AHI > 30);
- cluster 7: female, not obese, no hypertension, neck circumference < 43 cm, desaturation > 95, (39 % have AHI > 30).

Table 1 The apnea risk matrix is a table which facilitates a statistical diagnosis of apnea patients

Gender	M	M	M	M	F	F	F
Hypertension	1	0	0	X	1	0	0
Obesity	1	1	0	0	1	X	0
Neck	1	1	0	X	X	X	0
Desaturation	<90	90–95	>95	X	93–97	93–97	>95
<i>Cluster</i>	<i>1</i>	<i>2</i>	<i>3</i>	<i>4</i>	<i>5</i>	<i>6</i>	<i>7</i>
Normal (0–4)	5 %	6 %	15 %	7 %	10 %	10 %	9 %
Moderate (5–14)	6 %	14 %	22 %	14 %	13 %	28 %	22 %
High (15–29)	16 %	25 %	24 %	23 %	25 %	29 %	30 %
Very high (≥30)	73 %	55 %	39 %	56 %	52 %	33 %	39 %

It is based on the following simple measurable criteria: gender (M/F), hypertension (0/1), obesity (0/1), neck (0/1), mean desaturation (0–100 %). Each of the seven resulting clusters can be described by the set of characteristic features represented in the table. We mark with ‘x’ the fact that a criteria can take both values (i.e. is irrelevant). In the lower part of the table, we represent the apnea risk probability that a patient included in either one of the clusters will have. These values result from the analysis of the network with over 1300 patients

In light of the goal of this study, namely to facilitate the efficiency of diagnosing OSA, we have developed the apnea risk matrix based on the cluster analysis. Using the apnea risk matrix, a doctor may identify patients with a possible risk of apnea through a survey, without the need for an initial specialized control. Once the measurements are done on a patient, the doctor will use the matrix in Table 1 to fit the results into one of the seven clusters (columns). When the cluster corresponding to the patient is found, the doctor will use the apnea risk percentages to formulate the diagnosis. If the patient’s risk toward apnea results as statistically high, then specialized control is recommended.

5 Conclusions and Future Work

Obstructive sleep apnea is an underrated respiratory problem with very high incidence among the world’s population. Correlated with obesity, studies indicate it has become a pandemic killer, as 1 in 4 men and 1 in 10 women are diagnosed with OSA in the USA. However, it is still a widely unknown and underrated clinical problem. The diagnosis and treatment involves a time- and money-consuming methodology. In light of the emerging field of network medicine, we pave the way for a much improved methodology of diagnosing OSA before patients actually reach specialized help.

We set out to process clinical data collected over the period of 2001–2011 which we model as a social network of patients. Using a proposed compatibility clustering we obtain a new perspective on patterns that lead to acquire OSA. The fact that there is a clear node clustering within the graph suggests that there are some

(we identified seven) specific patterns for apnea, which are defined by the way the risk factors relate to each other. This may pave way for automatically predicting, with a high degree of accuracy, if a patient is prone to developing this disease.

Measuring simple (anthropometric) parameters may pave a way for automatically predicting the probability that a new patient has, or is prone to developing apnea. This model may be useful to categorize OSA severity and triage patients for diagnostic evaluation.

References

1. Easley D, Kleinberg J (2010) Networks, crowds, and markets. Cambridge Univ Press 6(1):1–6
2. Barabási A-L, Gulbahce N, Loscalzo J (2011) Network medicine: a network-based approach to human disease. *Nat Rev Genet* 12(1):56–68
3. Newman ME (2006) Modularity and community structure in networks. *Proc Natl Acad Sci* 103(23):8577–8582
4. Wang XF, Chen G (2003) Complex networks: small-world, scale-free and beyond. *IEEE Circuits Syst Mag* 3(1):6–20
5. Newman ME (2003) The structure and function of complex networks. *SIAM Rev* 45(2):167–256
6. Barabási A-L (2013) Network science. *Philos Trans R Soc A Math Phys Eng Sci* 371 (1987):20120375
7. Simon S, Collop N (2012) Latest advances in sleep medicine latest advances in obstructive sleep apnea obstructive sleep apnea. *CHEST J* 142(6):1645–1651
8. Sharma SK, Agrawal S, Damodaran D, Sreenivas V, Kadiravan T, Lakshmy R, Jagia P, Kumar A (2011) Cpap for the metabolic syndrome in patients with obstructive sleep apnea. *N Engl J Med* 365(24):2277–2286
9. Young T, Peppard PE, Gottlieb DJ (2002) Epidemiology of obstructive sleep apnea: a population health perspective. *Am J Respir Crit Care Med* 165(9):1217–1239
10. Punjabi NM (2008) The epidemiology of adult obstructive sleep apnea. *Proc Am Thorac Soc* 5 (2):136
11. Memtsoudis SG, Besculides MC, Mazumdar M (2013) A rude awakening—the perioperative sleep apnea epidemic. *N Engl J Med* 368(25):2352–2353
12. McNicholas W, Bonsignore M et al (2007) Sleep apnoea as an independent risk factor for cardiovascular disease: current evidence, basic mechanisms and research priorities. *Eur Respir J* 29(1):156–178
13. Rossi VA, Stradling JR, Kohler M (2013) Effects of obstructive sleep apnoea on heart rhythm. *Eur Respir J* 41(6):1439–1451
14. Utriainen KT, Airaksinen JK, Polo O, Raitakari OT, Pietilä MJ, Scheinin H, Helenius HY, Leino KA, Kentala ES, Jalonen JR et al (2013) Unrecognised obstructive sleep apnoea is common in severe peripheral arterial disease. *Eur Respir J* 41(3):616–620
15. Sánchez-de-la Torre M, Campos-Rodriguez F, Barbé F (2013) Obstructive sleep apnoea and cardiovascular disease. *Lancet Respir Med* 1(1):61–72
16. Yaggi HK, Concato J, Kernan WN, Lichtman JH, Brass LM, Mohsenin V (2005) Obstructive sleep apnea as a risk factor for stroke and death. *N Engl J Med* 353(19):2034–2041
17. Pelletier-Fleury N, Meslier N, Gagnadoux F, Person C, Rakotonanahary D, Ouksel H, Fleury B, Racineux J (2004) Economic arguments for the immediate management of moderate-to-severe obstructive sleep apnoea syndrome. *Eur Respir J* 23(1):53–60

18. Jurcevic D, Shaman Z, Krishnan V (2012) A new category: very severe obstructive sleep apnea has worse outcomes on morbidity and mortality. *Chest* 142(4):1075A–1075A. Meeting Abstracts
19. Parati G, Lombardi C, Hedner J, Bonsignore MR, Grote L, Tkacova R, Levy P, Riha R, Bassetti C, Narkiewicz K et al (2012) Position paper on the management of patients with obstructive sleep apnea and hypertension: Joint recommendations by the european society of hypertension, by the european respiratory society and by the members of european cost (cooperation in scientific and technological research) action b26 on obstructive sleep apnea. *J Hypertens* 30(4):633–646
20. Loscalzo J, Barabasi A-L (2011) Systems biology and the future of medicine. *Wiley Interdisc Rev Syst Biol Med* 3(6):619–627
21. Bastian M, Heymann S, Jacomy M (2009) Gephi: an open source software for exploring and manipulating networks. In: ICWSM, pp 361–362
22. Blondel VD, Guillaume J-L, Lambiotte R, Lefebvre E (2008) Fast unfolding of communities in large networks. *J Stat Mech Theory Exp* 2008(10):P10008
23. Lambiotte R, Delvenne JC, Barahona M (2008) Laplacian dynamics and multiscale modular structure in networks. arXiv preprint [arXiv:0812.1770](https://arxiv.org/abs/0812.1770)

Mobile Applications Supporting Healthy Lifestyle

Oana-Sorina Lupșe, Adrian Căprioru
and Lăcrămioara Stoicu-Tivadar

Abstract The quality of life is continually improved by various activities and applications supporting the style of living by sports, healthy food, or other activities. In this paper, we propose a mobile application that supports healthy lifestyle. The FitAndWin application is launching fitness challenges and keeps food and calories logs. The application integrates Facebook features and uses Windows Azure as a cloud solution for ubiquitous access. The new approach launching challenges on Facebook contributes to adding motivation for people in having an active style of life with best results. The paper describes the design and implementation of the application and presents the advantages of the solution.

1 Introduction

The aim of the paper is to present a mobile application for a healthy life, that includes a social and fitness application. In our days, the people work a lot and for this reason they do not have generally a healthy lifestyle. The food is eaten in hurry and in many cases is fast food, generally an unhealthy food. Most of the people ignore the physical activity and in this way they become fat or obese. No physical activity, unhealthy food, and an unhealthy lifestyle have as consequence a lot of diseases that lower the life quality and raise costs in society.

The lifestyle behavior has an important role in prevention and treatment of a lot of diseases, or in controlling certain chronic diseases. The software applications

O.-S. Lupșe (✉) · A. Căprioru · L. Stoicu-Tivadar
Faculty of Automation and Computer Science,
University Politehnica Timișoara, Timișoara, Romania
e-mail: oana.lupse@aut.upt.ro

A. Căprioru
e-mail: adrian.caprioru@yahoo.com

L. Stoicu-Tivadar
e-mail: lacramioara.stoicu-tivadar@upt.ro

have the potential to change the behavior of the people. Computers progress very fast and have the possibility to help people in their work and also in their life. Familiar devices that may change the personal lifestyle are the mobile devices. They may be a support at hand suggesting or reminding certain activities. The new mobile devices, the smartphones are also connected to social applications and other types of apps helping people [1].

In 2013, more than 4.3 billion people in the world were using mobile devices, and in the next 4 years specialists estimate that 5.1 billion people will use mobile phones around the world [2]. In this way, the mobile phones are becoming more popular than personal computers and will be able to see, read, hear, and understand human language [3]. Given these things, the mobile applications are gaining more popularity than other types of applications.

To help people who use these mobile devices, the nutrition specialists try to develop a lot of dietary applications that suggest healthy food and correct doses of calories to be consumed (Fig. 1).

The majority of existing mobile nutrition and health applications are focused on specific health problems like stress, diet, or physical activity. These applications monitor and support people in their behavior [4].

Our application allows creating fitness challenges and keeping a food and calories journal. To be more attracting for people, it integrates also Facebook features and maintains all the data in Windows Azure cloud platform.

In the next section, we present existing lifestyle mobile applications, and in Sect. 3 the impact of social applications in our life. Section 4 presents the

Fig. 1 Workflow in mobile nutrition apps



architecture of a mobile application and the description of the developed mobile application FitAndWin, and in Sect. 5 we conclude the paper and present future work.

2 Existing Lifestyle Mobile Applications

The presented applications are selected from the most complex applications for nutrition and physical activities.

The first chosen application is the Weight Watchers Mobile that was designed to count the calories consumed daily. It uses a database that contains over than 31,000 dishes. This application is well known for interactive graphics that displays real weight loss. The mobile application has the following characteristics: counts calories and daily activities, interactive graphics with personal characteristics, search for recipes, and looking for information about health and weight maintenance [5].

Another mobile application is MyFitnessPal [6]. This app counts calories and helps to decrease or maintain the desired weight. The application has a database of over 2,000,000 kinds of food and types of exercises that help to eliminate excess fat. The application has been selected by PC Magazine Editor's Choice Selection and Wired Magazine's Editor's Pick as the best application type for lifestyle.

The MyNetDiary [7] is described as the most comprehensive diet app for Android operating system. With over 485,000 dishes, the database includes free access to the personal computer via the web interface and data backup. The application is focused on determining the amounts of calories consumed. This application has a potential audience of over 2.5 million of people.

My Diet Coach-Pro [8] is a virtual application that helps to motivate people lose weight quickly and easily. It informs about the daily calories consumed using Body Mass Index and Basal Metabolic Rate. Calculation is based on weight, age, sex, and activity level to obtain the real need for calories.

Diet Assistant Pro-Weight Loss [9] is an application that helps people to lose weight. To configure the application, the first thing to do is to establish the desired weight, then follow weight loss programs offered by the application. Weight loss application contains plans for vegetarian diets and also for people that eat more protein to increase muscle mass. The application helps lose weight but also to build a healthy lifestyle.

After studying these applications, the most complex application is MyFitnessPal, containing a large variety of food and the possibility to add and scan others menus. Also good applications, but not so complex, are MyNetDiary or My Diet Coach-Pro.

Our application FitAndWin is a mobile application supporting people creating fitness challenges and keeping a food and calories journal. It is based more on sport activities and has the possibility to give rewards to motivate people to continue their sport activities. Also, FitAndWin is connected to social media applications and shares sport performances or rewards with friends.

3 The Impact of Social Applications in Our Life

Currently, the social apps are commonly used. Social media platforms like Facebook, Twitter, and Google+ are used by people everyday to communicate with their friends. They have become a media in which we also shop and get our information. Their influence has spread beyond the confines of the online world and has affected every aspect of our lives. News are made and distributed through social media even before traditional media is informed of the events and sometimes help in solving crises [10].

One of the terms coined by the social media is the “viral” concept, which has brought a plethora of marketing campaigns and huge profits to the companies that employed such marketing techniques. This has ushered in a new golden age of software development by allowing software companies to take advantage in creating applications that offer novel ways to connect with friends, while pushing great amounts of commercials.

Facebook and Twitter are two of the greatest inventions of our generation, a way we communicate with each other, shop, and get our information. One of their biggest impacts is on communication between citizens. Anybody can post something on social media that may be seen by anyone else. It offers the possibility to get in touch with old friends and family that are spread in the whole world. Websites like Facebook and Twitter have revolutionized the way we organize our social lives, the way people relate to one another, the visibility people have into one another’s lives. They allow social friendships, but you can also follow people and conversations that are relevant to you.

As we can see, these social applications are very important for people today. For these reasons in our application, we integrate also Facebook features.

4 FitAndWin Mobile Application

The FitAndWin solution consists in a mobile application that allows creating fitness challenges and keeping food and calories journal. The application integrates Facebook features while using Windows Azure for storing information. The architecture is presented in Fig. 2.

The application is an Android app that is used for keeping track of physical activities.

The login in the application is done through Facebook, so that social information is available. Communication between the applications is made through a web service provided by Windows Azure, to store the data.

The structure of the application is presented in Fig. 3.

The application uses personal information, so it is paramount to provide a secure method of authentication. To this purpose, the application uses a Facebook

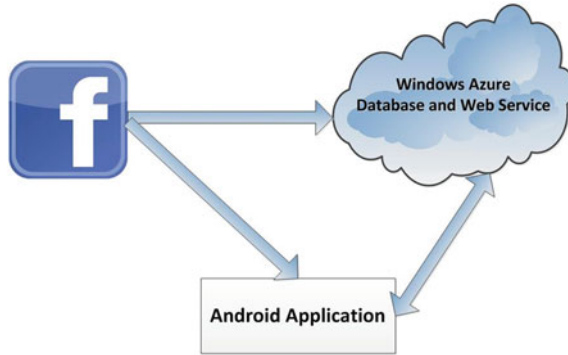


Fig. 2 Solution architecture

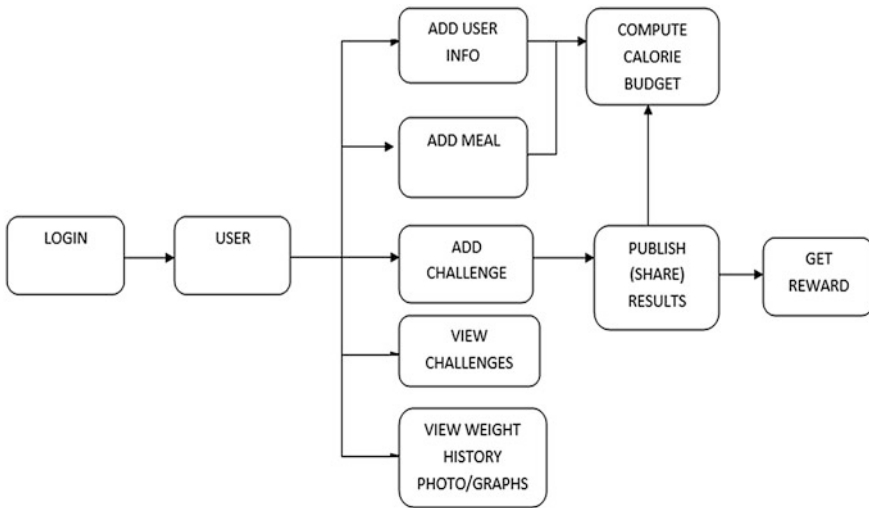
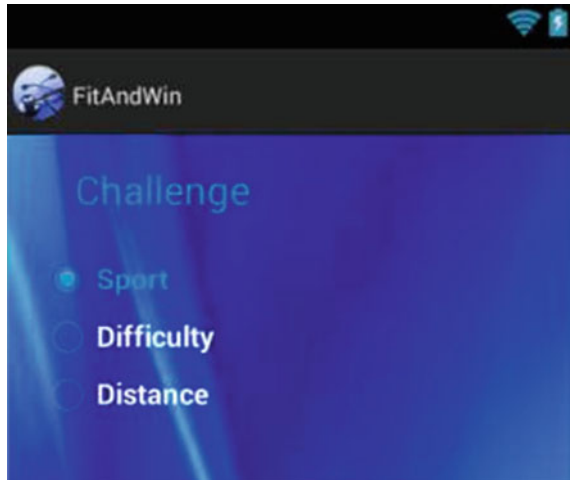


Fig. 3 Application architecture

authentication login to access its features. The login screen allows the user to input the username to start the login process. If the username is found in the database, the Facebook login credentials are retrieved and the Facebook authentication can continue.

The User Info screen displays general information like the age, height, and weight and allows the user to input its weight. These are used to compute the maximum calories intake for the day.

The meal screen suggests dishes that allow the users to comply with the maximum calories intake limitation (computed using personal info) and helps them

Fig. 4 Challenges menu

keep track of the meal they have had during the day. The dishes are split into categories.

The social component of the app comes not only from its Facebook use for authentication, but from its use of Facebook to create fitness challenges. The Challenges screen allows the user to create and view challenges (Fig. 4). A challenge implies choosing a physical activity and time or distance goal and sharing it with your friends through Facebook. Whoever manages to finish it first will win the reward set by the creator of the challenge.

The reward screen allows the user to create and view rewards that are used in the challenges self or others have created. These may be used in newly created challenges.

Figure 5 presents the steps followed in the application.

The mobile user, after starting the application, can choose add meal. If he/she wants to add, he/she can add more types of food in the application. He/she also can choose the calculation of calories, let the application choose her/his state (obesity, malnutrition or normal), and according to this state, the application searches some food. After filtering the food, if the person who wants eat has some allergies, the application filters the food again considering these allergies.

Our application can also monitor the user data, and according to this data it decides if he/she needs sports. The application suggests a physic activity according the plan. When the user of the application has done successfully some activity, he/she can receive some rewards. Also, all the activities, rewards, and meals can be shared with Facebook friends.

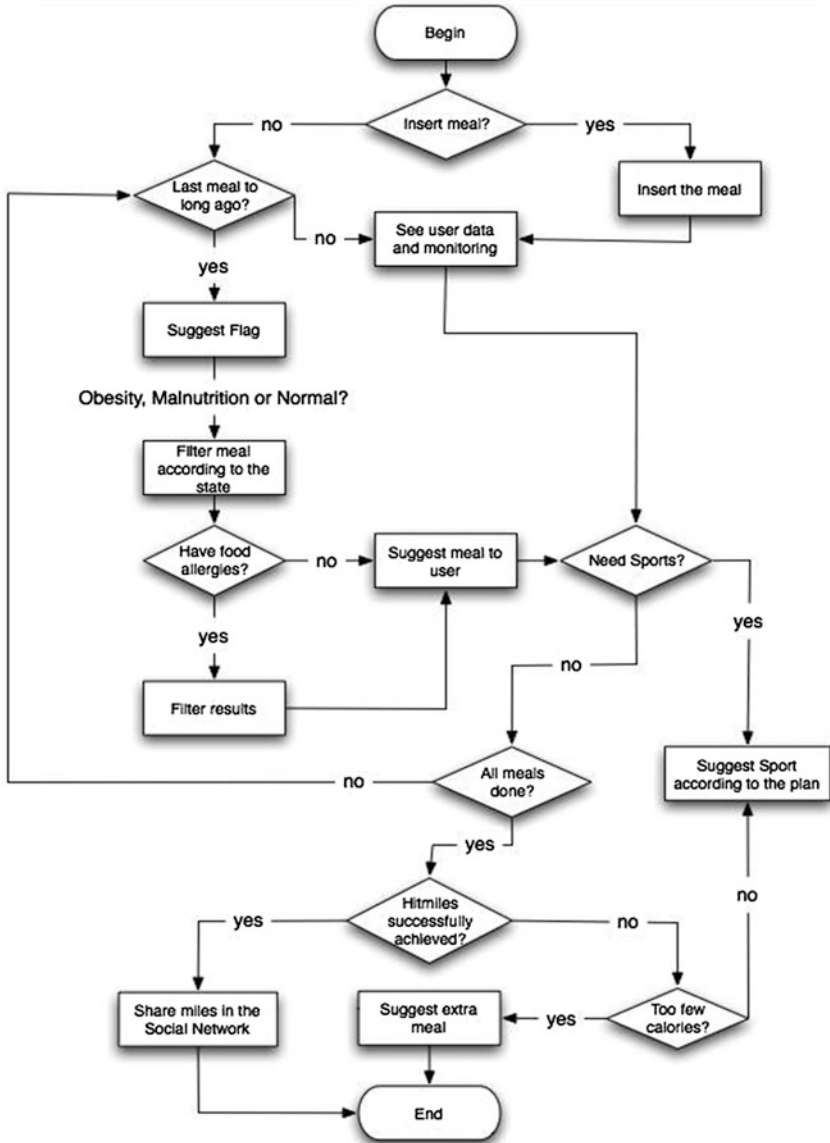


Fig. 5 Workflow of the application

5 Conclusions and Future Works

The FitAndWin solution is a very useful application for mobile users. It can be downloaded from Android Market and used everyday. To motivate the person how to use the application, it has an option to give him/her a reward.

Also the application contains a Facebook feature that helps people to communicate results with the friends.

In future works, the application will be improved using the new concept of cognitive apps with personalized advice contributing to a better and healthier life.

References

1. Gasser R, Brodbeck D, Degen M, Luthiger J, Wyss R, Reichlin S (2006) Persuasiveness of a mobile lifestyle coaching application using social facilitation. In: Lecture notes in computer science, vol 3962. Springer, Berlin, pp 27–38. ISBN 978-3-540-34291-5
2. Mashable (2014). <http://mashable.com/2013/10/03/mobile-phones-2017/>. Accessed 20 May 2014
3. Alagöz F, Valdez AC, Wilkowska W, Ziefle M, Dörner S, Holzinger A (2010) From cloud computing to mobile Internet, from user focus to culture and hedonism: the crucible of mobile health care and Wellness applications. In: 2010 5th international conference on pervasive computing and applications (ICPCA), pp 38–45, 1–3 Dec 2010. doi:[10.1109/ICPCA.2010.5704072](https://doi.org/10.1109/ICPCA.2010.5704072)
4. Lane ND, Mohammad M, Lin M, Yang X, Lu H, Ali S, Doryab A, Berke E, Choudhury T, Campbell AT (2011) Bewell: a smartphone application to monitor, model and promote wellbeing. In: International ICST conference on pervasive computing technologies for healthcare
5. Weight Watchers Mobile (2014). <https://play.google.com/store/apps/details?id=com.weightwatchers.mobile&hl=en>. Accessed 03 May 2014
6. Calorie Counter—MyFitnessPal (2014). <https://play.google.com/store/apps/details?id=com.myfitnesspal.android>. Accessed 03 May 2014
7. Calorie Counter PRO MyNetDiary (2014). <https://play.google.com/store/apps/details?id=com.fourtechnologies.mynetdiary.ad>. Accessed 03 May 2014
8. My Diet Coach—Pro (2014). <https://play.google.com/store/apps/details?id=com.inspiredapps.mydietcoachpro>. Accessed 03 May 2014
9. Diet Assistant Pro-Weight Loss (2014). <https://play.google.com/store/apps/details?id=com.aportela.diets.pro.view>. Accessed 03 May 2014
10. Social Media and the Search for the Boston Bombing Suspects (2014). <http://www.cbsnews.com/news/social-media-and-the-search-for-the-boston-bombing-suspects/>. Accessed 03 May 2014

Fuzzy Expert System Prediction of Lumbar Spine Subchondral Sclerosis and Lumbar Disk Hernia

Norbert Gal, Diana Andrei, Vasile Stoicu-Tivadar, Dan Ion Nemeş and Emanuela Nădăşan

Abstract One of the first degenerative diseases of the lumbar spine is the subchondral sclerosis from which other degenerative complications can occur. The first symptom of the subchondral sclerosis and herniated disk is the low back pain. The subchondral sclerosis and herniated disk is often associated with obesity, high body fat index, and high stress on the vertebral spine. This paper proposes a fuzzy expert system which predicts that a patient will suffer from subchondral sclerosis. The expert system correlates the body mass index (BMI) with the body fat (BF) percentage and the daily activity expressed by the consumed calories. In total 60 inference rules were created and the first results present a correlation of 0.91 with the results from the control group. Using this system, a compliant patient can avoid serious spinal cord problems.

Keywords Expert system · Prediction · Quality of life · Subchondral sclerosis

1 Introduction

Intervertebral disk degeneration is characterized by dehydration of the pulpous nucleus and annulus fibrosis wear as a result of multiple mechanical and biochemical factors. A number of degenerative changes can be described as processes of destabilization followed by restabilizing processes.

N. Gal (✉) · V. Stoicu-Tivadar
Politehnica University of Timisoara, Timisoara, Romania
e-mail: norbert.gal@aut.upt.ro

D. Andrei · D.I. Nemeş
Victor Babes University of Medicine and Pharmacy, Timisoara, Romania
e-mail: andreidiana81@gmail.com

E. Nădăşan
City Emergency Hospital—Medical Rehabilitation and Rheumatology Department,
Victor Babes University of Medicine and Pharmacy, Timisoara, Romania

Initially, the lesions of annulus fibrosis result in the loss of the pulposus nucleus contentment ability. The internal concomitant changes of the pulposus nucleus lead to obstructing the joint space and to a reduced loading capacity of that vertebral segment. The nuclear material is not firmly fixed within the intervertebral disk and will migrate in the direction of least resistance, which is usually toward posterior or posterolateral.

This migration leads to a “prominent” or “encapsulated hernia” of the annulus fibrosis toward the vertebral hole or root canal. If the means of the ring contention lose their stability, the nuclear material can herniate. This is the so-called “real hernia” or “non encapsulated hernia” [1, 2].

It is important to note that both types of hernia are the result of a degenerative process. In a disk that has not suffered from degenerative processes, the rupture after a trauma occurs typically at the cartilaginous vertebral plaque level; a normal intervertebral disk, which is traumatized, will rarely herniate [3]. After internal disjunction of the intervertebral disk, the loss of the disk height and the reduction of the annulus fibrosis stabilization capacity represent the main mechanisms through which the stability of the mobility segment is affected (segmental instability) [4]. As a result of this situation, on the margins of the vertebral body and the vertebral arch there is a process of reactivate bone formation that leads to the classic radiologic appearance of osteophytes [5]. The degenerative process is defined by structural changes but the way the changes produce symptoms is less clear. Theories may be issued of how clinical pain occurs and shows, depending on each degenerative stage.

One of the degenerative changes on the margins of the vertebral body and the vertebral arch is the classic radiologic appearance of the osteophytes and subchondral sclerosis [6]. These degenerative changes can lead to intervertebral herniated disk. The general symptom of the subchondral sclerosis is an acute low back pain (LBP).

It has been shown that annulus fibrosis present at its exterior free nerve endings and vascular channels, thus affecting these tissues, with or without migration of nuclear material was proposed as a major cause for LBP. The concept of the disk prominence which results from the internal disjunction of the intervertebral disk was investigated as a primary major cause for LBP [7]. The disk space obstruction associated with degenerative intervertebral disk changes, influences the mechanical joint movement and was postulated as a major cause of segmental instability, can also be associated with LBP.

LBP is not a specific to this disease, but rather a complaint that may be caused by a large number of underlying problems of varying levels of seriousness [8]. The majority of LBP does not have a clear cause, but is believed to be the result of nonserious muscle or skeletal issues such as sprains or strains [9].

The laboratory examinations for the subchondral sclerosis are:

- Radiography excludes other causes of back pain: fractures, primitive or secondary spinal tumors, structural abnormalities. Nuclear Magnetic Resonance (NMR)—allows bone and soft tissue visualization using a magnetic field and radio waves. It allows highlighting herniated disks and spinal stenosis

- Computed tomography—allows recording on a radiographic film of cross sections in bone and soft tissues. It is used rarely, because in the case of the spine NMR is more efficient
- Discograma—allows visualization of the intervertebral disk by injecting a contrast agent
- Myelogram—allows visualization of the spinal canal by injecting a contrast agent into the dural sac
- Nerve conduction velocity/EMG—allows highlighting conditions in the nerve root or peripheral nerve caused by a herniated disk.

In the assessment of the LBP done by doctor [10], he/she will insist in the medical history of the injury mechanism, progression of symptoms, previous treatments and their results, medical history, sleep disorders, including sleep surface of the patient and used pillow, postures in which he performs NMR and the evolution of symptoms during these postures and activities.

As you can observe that this pathology is rather complex and a correct diagnosis is hard to formulate.

In this paper, we propose a novel method to indicate the predisposition of the patient to the subchondral sclerosis and other types of LBP. This is done by creating an expert system that correlates the body mass index (BMI) of the patient with the body fat (BF) and the daily activity expressed in the daily consumed calories. These three parameters are directly linked to the physical and mechanical characteristics of the body and influence the mechanical stress on the spinal cord. This mechanical stress is the main cause for the LBP.

Our method is used as a prevention tool for the subchondral sclerosis and its complications.

This tool was created for two reasons: first the medical staff needed a prediction tool that can correlate the mentioned parameters with the presence of the LBP and second according to the literature review, this is the first system that predicts the possibility of LBP.

Essentially an early indication of the subchondral sclerosis, a compliant patient and a competent physician can substantially influence the result of the disease, the complications, and its quality of life [11, 12].

2 Used Predictive Attributes

The proposed prediction system takes in consideration of three numerical clinical data and one Boolean attribute: the BMI, the Body Fat the daily activity expressed in calories, and the sex of the patient.

(a) Body Mass Index (BMI)

Body Mass Index is a simple indicator of weight that is used to classify underweight, overweight, and obesity in adults [13]. It is calculated using the following formula:

$$\text{BMI} = m/h^2 \quad (1)$$

where m is the mass of the patient in kg and h is the height of the patient in meters (Table 1).

BMI values are age-independent and the same for both sexes. However, BMI may not correspond to the same degree of fatness in different populations due, in part, to different body proportions. The health risks associated with increasing BMI are continuous and the interpretation of BMI grading in relation to risk may differ for different populations.

(b) Body Fat (BF)

The BF% of a human or other living being is the total mass of fat divided by total body mass; body fat includes essential body fat and storage body fat. Essential body fat is necessary to maintain life and reproductive functions. The percentage of essential fat is 3–5 % in men, and 8–12 % in women (referenced through NASM). Storage body fat consists of fat accumulation in adipose tissue, part of which protects internal organs in the chest and abdomen. The BF % is a measure of fitness level, since it is the only body measurement which directly calculates a person's relative body composition without regard to height or weight. The BF % is in relation with the BMI [14].

The formula that is used to calculate the BF% is the following [15]:

$$\text{BF}\% = (1.29 \times \text{BMI}) + (0.20 \times \text{Age}) - (11.4 \times \text{gender}) - 8.0 \quad (2)$$

where BMI is the calculated BMI, the Age is the age of the patient and gender is for male = 1 and female = 0.

A BF% of 25 % for men and 30 % of BF for women can be considered as the lowest point for obesity.

(c) Consumed daily calories

The daily activity parameter refers to the calories needed by the patient to perform his daily living activities. It is computed using formulas derived from WHO estimation of metabolic rate [16] and it depends upon the gender and daily activity of the patient.

Table 1 BMI categories

Classification	BMI value
Underweight	<18.50
Normal range	18.50–24.99
Overweight	≥25.00
Obese	≥30.00

Table 2 Recommended loss of daily calories

Age	Male (calories/day)	Female (calories/day)
10–18	$16.6P + 77T + 572$ (3)	$7.4P + 482T + 217$ (7)
18–30	$15.4P - 27T + 717$ (4)	$13.3P + 334T + 35$ (8)
30–60	$11.3P + 16T + 901$ (5)	$8.7P - 25T + 865$ (9)
After 60	$8.8P + 128T - 1071$ (6)	$9.2P + 637T - 321$ (10)

P is the weight of the patient and T is the height of the patient

Parameter P represents the weight of the patient and parameter T represents the height of the patient (Table 2).

For a more precise activity calculation, the daily activities categories were used [10]: reduced physical activity: $M = 1.56, W = 1.56$; average physical activity: $M = 1.78, W = 1.64$; increased physical activity: $M = 2.10, W = 1.82$, where M is man and W is woman.

3 The Expert System

Fuzzy logic extends the Boolean logic by introducing a degree of uncertainty. The fuzzy inference system is constructed from four major parts: the fuzzification system which converts the numerical data in linguistic data, the linguistic variables, the inference rules which infer a result, and the defuzzification process. Our system bypasses the defuzzification process and gives the result in linguistic form. This is achieved by using a modified Sugeno-type inference system [17]. The system returns 2 fuzzy possibilities: healthy patient or predisposed patient. Our fuzzy inference system is presented in Fig. 1.

Due to the fact that a numerical result is not important the defuzzification processes is eliminated from the fuzzy inference system.

(a) Linguistic variables

In our case, we have used 4 linguistic variables. One of the variables describes the sex of the patient and three of the variables describe the physical constitution of the patient using the BMI, BF, and the consumed calories. The linguistic variables were created according to the Marsh rule [18]:

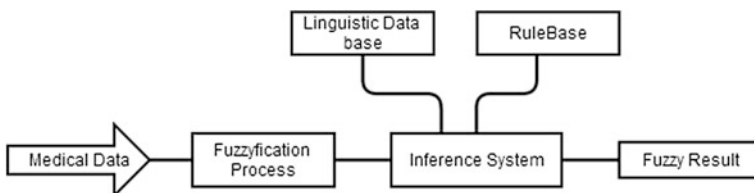


Fig. 1 The fuzzy inference system

$$\text{Overlap Ratio} = \frac{X4 - X3}{x6 - x1} \quad (11)$$

$$\text{Overlap Robustness} = \frac{\int_{x3}^{x4} (u1 + u2) dx}{2 * (x4 - x3)} \quad (12)$$

where x_i , $i = 1 \rightarrow 6$ are the maximum and minimum points of truth of two trapezoidal membership functions. $u1$ and $u2$ are the intersections of the 2 membership functions.

The linguistic variables are constructed according to the following list:

- SEX: Male–Female represented by singletons;
- BMI: 0–18 Underweight, 18–25 Normal, 25–29 Overweight, and 30–50 Obese;
- BF: 0–10 Low, 10–20 Normal, 20–30 Medium, 30–60 High;
- Calories: 1500–1800 Low, 1700–2500 Normal, 2400–4000 High;

The fuzzy inference system is created using XML files and the computational form of the linguistic variables are the following:

```
<Input>
  <Name>Calories</Name>
  <Range MIN="1500" MAX="4000" />
  <Type>Trapezoidal</Type>
  <Labels>
    <Low v0="1500" v1="1600" v2="1700" v3="1800" />
    <Normal v0="1700" v1="1800" v2="2400" v3="2500" />
    <High v0="2400" v1="2500" v2="3800" v3="4000" />
  </Labels>
</Input>
```

Except for the sex each linguistic variable is constructed using trapezoidal membership functions.

(b) The rules for the expert system

These rules are similar to the rules that are used in common language communication. In their general form these rules consists of several antecedents and a result separated by the “THEN” statement. The antecedent is a conjunction of several fuzzy terms and several logical operators (AND, OR, NOT) between the active membership functions.

The antecedents of the rules are the collected clinical data and the result of the rules is a prediction if the patient has or has not predisposition for subchondral sclerosis.

In our case, 60 rules were computed by the medical staff based on their knowledge by taking into consideration the relation between the BMI and the BF [17]. This relation presents that a person with high BMI cannot have a low BF.

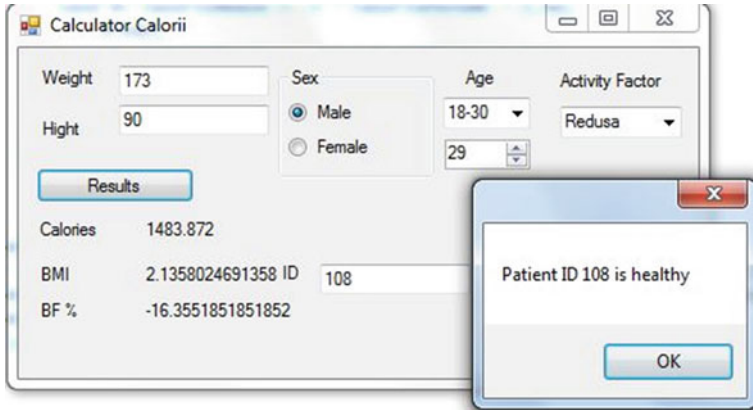


Fig. 2 The expert system prototype

Several of the inference rules are presented below:

IF SEX IS MALE AND BMI IS UNDERWEIGHT AND BF IS LOW AND CALORIES IS HIGH THEN PREDISPOSITION IS HIGH

IF SEX IS MALE AND BMI IS OBESE AND BF IS MEDIUM AND CLORIES IS HIGH THEN PREDISPOSITION IS HIGH

IF SEX IS MALE AND BMI IS NORMAL AND BF IS NORMAL AND CALORIES IS NORMAL THEN PREDISPOSITION IS LOW

A total of 44 of the rules indicate the need to start an early prevention if the there is no LBP and 16 of the rules indicates a healthy patient. The clinical trial of the system is a work in progress and is developed in Visual Studio.NET 2013 using C# language and the AForge.NET open source software platform (Fig. 2).

4 Discussion and Conclusions

The first test of the system was realized using a group of 201 control patient’s use in a double blind test.

Form the test group, 147 patients were diagnosed by the M.D. with subchondral sclerosis and the rest were healthy patient. A comparison between the results of the control group assessed by the MD and the assessment of the same group made by the fuzzy system is presented in Fig. 1.

In 5 situations, there was a difference between the results of the control group and the fuzzy system. In 2 situations, the fuzzy system indicated that a diagnosed patient is healthy and in 3 cases it is indicated that a healthy patient will develop subchondral sclerosis (Fig. 3).

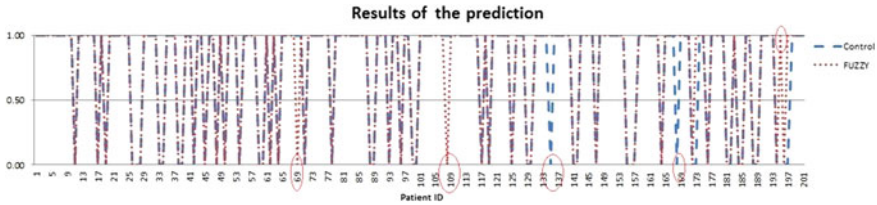


Fig. 3 Initial results of the fuzzy prediction system. Results: 1-predisposition, 0-healthy patient

Table 3 The confusion table of the system

	Back pain positive	Back pain negative
Fuzzy positive	146	4
Fuzzy negative	2	49

These differences appeared in patients who were at the limit of overweight and high BF %. The correlation index between the results of the control group and fuzzy system is 0.91, a good correlation (Table 3).

The clinical testing of the systems is in progress, but the initial results are encouraging.

The study shows that a percentage with high BF % at the limit of overweight will develop more likely subchondral sclerosis and other complications that normal weighted patients.

References

- Halbert I et al (1996) Proc Natl Acad Sci USA 93: 9748
- Herbert CM, Lindberg KA, Jaysonivi I, Bailey AJ (1975) Proceedings: Intervertebral disc collagen in degenerative disc disease. Ann Rheum Dis 34(5):467–468
- Klippel JH, Dieppe PA (1994) Rheumatology. Mosby, London
- Boszczyk BM, Boszczyk AA, Korge A, Grillhosl A, Boos WD, Putz R, Iviilz S, Benjamin M (2003) Immunohistochemical analysis of the extracellular matrix in the posterior capsule of the zygapophysial joints in patients with degenerative L4-5 motion segment instability. J Neurosurg 99(1 Suppl):27–33
- Berlemann U, Gries NC, Moore RJ, Fraser RD, Vernon-Roberts B (1998) Calciumpyrophosphate dihydrate deposition in degenerate lumbar discs. Eur Spine J 7 (1):45–49
- Berlemann U, Gries NC, Moore RJ, Fraser RD, Vernon-Roberts B (1998) Calcium pyrophosphate dehydrate deposition in degenerate lumbar discs. Eur Spine J 1:45–49
- Borenstein DG (1997) Epidemiology, etiology, diagnostic evaluation, and treatment of low back pain. Curr Opin Rheumatol 9:144–150
- Pierre B (2013) An Evidence-based approach to the evaluation and treatment of low back pain in the emergency department. Emerg Med Pract 15:1–23
- Low Back Pain Fact Sheet, National Institute of Neurological Disorders and Stroke. National Institute of Health. Accessed 28 Jan 2014
- Klippel JH, Dieppe PA (1994) Rheumatology. Mosby, London

11. Fitzpatrick F, Badley EM (1996) An overview of disability. *B J Rheumatol* 35:184–187
12. Guccione AA, Jette AM (1988) Accessing limitations in physical function in patients with arthritis. *Arthritis Care Res* 1:170–176
13. http://apps.who.int/bmi/index.jsp?introPage=intro_3.html. Accessed 14 Jan 2014)
14. Frankenfield DC, Rowe WA, Cooney RN, Smith JS, Becker D (2001) Limits of body mass index to detect obesity and predict body composition. *Nutrition* 17:26–30
15. Deurenberg P, Yap M, van Staveren WA (1998) Body mass index and percent body fat. A meta analysis among different ethnic groups. *Int J Obes Relat Metab Disord* 22:1164–1171
16. Human Energy Requirements: Energy Requirement of Adults (2014) Report of a Joint FAO/WHO/UNU Expert Consultation. Food and Agriculture Organization of the United Nations. Accessed 16 Oct 2013
17. Araujo E (2008) Improved Takagi-Sugeno fuzzy approach. In: *IEEE International Conference on Fuzzy Systems, 2008. FUZZ-IEEE 2008. (IEEE World Congress on Computational Intelligence)*, pp 1154–1158, 1–6 June 2008
18. Marsh S, Wei Huang Y, Sibigtroth J (1994) Center for emerging computer technologies, Motorola, Inc.: Fuzzy Logic Program 2.0

Server-Side Image Segmentation and Patient-Related Data Storage

Ioan Virag, Lăcrămioara Stoicu-Tivadar, Mihaela Crișan-Vida and Elena Amăricăi

Abstract Image segmentation is one of the most important operations used in computer vision to detect regions inside the analyzed image where some properties of the component pixels can vary within a specific range of values. This paper describes a server-side automatic segmentation method in the context of a browser-based application. The system uses the slices of patient's DICOM (Digital Imaging and Communications in Medicine) files in order to build a 3D model that can be superimposed using augmented reality on the body area of interest. The proposed method will isolate the relevant anatomical data inside each slice from the surrounding background using thresholding, still preserving the details needed for interpretation, detecting the edges of the studied area. The images will be processed, and stored in a cloud-based server in order to retrieve them whenever needed by the physicians in the future.

Keywords Image segmentation · Thresholding · Edge detection · Cloud storage

1 Introduction

The system under development uses NanoDICOM toolkit in order to extract the images from the patient's DICOM files on the server side, which after segmentation, will be sent to the browser and recombined in a 3D model using Three.js API

I. Virag (✉) · L. Stoicu-Tivadar · M. Crișan-Vida
Politehnica University of Timișoara, Automation and Computer Science Faculty,
Timișoara, Romania
e-mail: ioan.virag@aut.upt.ro

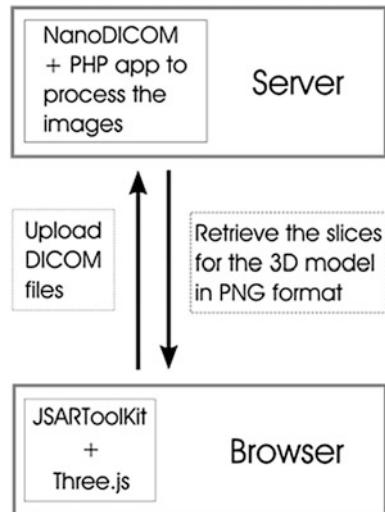
E. Amăricăi
Victor Babeș, University of Medicine and Pharmacy Timișoara,
Rehabilitation Department, Timișoara, Romania

on the client side. Following that, the 3D model will be virtually attached to the specific body area using JSARToolKit (JavaScript Augmented Reality Toolkit) allowing it to rotate and move in the same time as the patient. Figure 1 presents the relation between the building blocks of the system involved in the image processing and rendering.

Due to the fact that most servers have a maximum execution time limit our solution is to develop a simple and fast method that can extract the relevant image area from each uploaded slice. Even that image segmentation is not a trivial task by itself, the main problem we were facing was that the resulting images had to contain all the initial anatomical details needed for the final 3D model. For this reason we could not apply local [1, 2] or multilevel thresholding [3] techniques. The first option was to try first-scan label-equivalence-based connected-component labeling [4] but that would not solve the specific problems we were facing, since that method still has to process three neighboring pixels. The current method we propose, even if it uses two raster scans, checks only one neighboring pixel in order to decide if it belongs to the foreground. The second pass is used to detect the edges and to assign the color to the pixels.

Associating cloud computing, an already frequently used solution in healthcare applications, with our system results in benefits in ubiquitous information access and in economic efficiency. Cloud computing solution ensures accessing the information in real time, sharing the information, scalability of data, and provides more detailed analyses without additional computational infrastructure [5].

Fig. 1 The relation between the software technologies involved in the image processing



2 Software Libraries

The application is based on open-source software libraries, in order to make it possible for others to modify and adapt it to different fields of study where visualizing and manipulating 3D models can have a key role. Another important aspect we focused on during the development process was to make the system work on any operating system or mobile device that has a suitable browser. The toolkits and technologies we chose to use supported this approach.

2.1 *NanoDICOM*

NanoDICOM is a server-side, open-source DICOM file parser that allows the accessing of attached patient-related data and visualization of the medical images inside a browser window.

2.2 *Three.js*

Three.js is a JavaScript API used for the rendering of 3D models inside a web browser. We use it to combine the modified slices of patients MRI or CT images into a 3D model that can be added on top of the camera feed of patient's real-time images using JSARToolKit.

2.3 *JSARToolKit*

JSARToolKit is an open-source augmented reality library written in JavaScript and it is used to compute the distance from the camera to a physical marker in real time, making it possible to virtually attach a 3D model to the detected marker inside the camera feed.

3 The Proposed Method

In order to build the 3D model we had to isolate the relevant anatomical area inside each slice of the patient's DICOM files. For this purpose, we used NanoDICOM to extract the image data from the slices and transform them into transparent PNG files. After the image processing this files are sent back to the browser and used for reconstruction using Three.js.

Our first approach was to transform the surrounding black pixels into transparent pixels and retain only the image area of interest. As Fig. 2 shows, emphasizing the noise, it is not a good approach since the pixels can have different lightness values and they do not always form a unique blob that could be easy to eliminate. In the presented example we had to eliminate the irrelevant data from both sides, but this is not always the case depending on the subject of the studied body area.

The second approach was to detect pixels that are over a certain threshold and transform only the pixels with a darker tone. As we can see it in Fig. 3 this leads to better results since we managed to have most of the relevant image data separated in each new slice.

The problem with this method is that the anatomical image may also contain darker regions that are needed in order to interpret the slices by physicians and we need to preserve them after the transformation. In many cases this darker regions may indicate the exact region that needs to be further investigated during the diagnosis.

Fig. 2 Using transparent pixels to replace black pixels

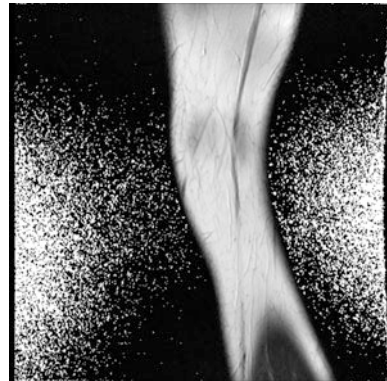


Fig. 3 Using transparent pixels to replace black pixels within a certain tone range



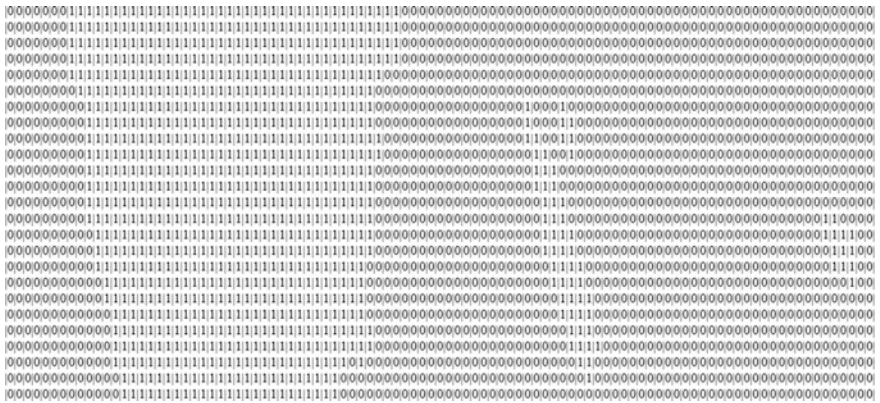


Fig. 4 A binary representation of the *bottom-center* part of the image based on the threshold value

The implementation solution uses a two-dimensional array to separate the background pixels from the ones that compose the actual image marking the pixels under the threshold value with 0 and the other ones with 1 as shown in Fig. 4.

The problem with this method was that it transformed the pixels marked with 0 to transparent pixels and copied the original color of the pixel for the ones marked with 1 eliminating relevant parts of the resulting image. The solution to this issue was to determine the first and the last occurrence of the pixels that belong to the relevant part of the image in each row. For this purpose, we added another processing part that read each row into an array, determined the index of the first and the last occurrence of the pixels marked with 1, and replaced the pixels marked with 0 between them with ones. The resulting image as presented in Fig. 5 solved the problem.

The proposed method preserves the medically relevant image area even if it is below the threshold limit. This is also important because we intend to add a col- orization module in order to allow physicians to highlight different areas in the slices.

Fig. 5 The resulting image using the new method



4 Cloud Storage of Medical Images

The resulting images related to each patient will be stored in cloud servers in order to ensure ubiquitous and at any time access to them. The system will use only the images from the patients DICOM files. This is very important in order to hide personal data associated with the images. The sets will have a unique identifier that will be associated with patient-related information only by the doctors when they will study a specific set.

Our solution uses Windows Azure platform which is a cloud computing platform and infrastructure developed by Microsoft, for building and managing applications and services through a global network of Microsoft datacenters. We use the blob storage which contains the images, a collection of binary data stored as a single entity in a database management system. Figure 6 presents an interface of the application in the cloud storing images.

Figure 7 presents a capture of the container making available the images for user access.

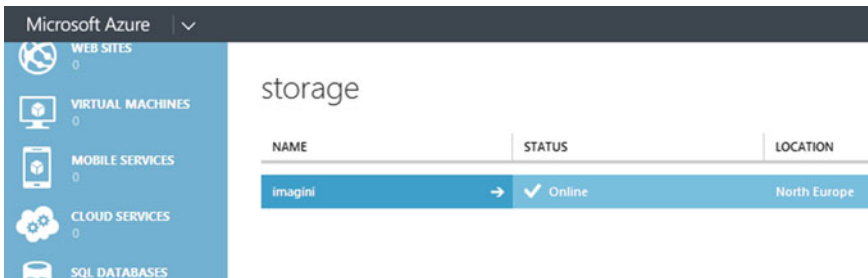


Fig. 6 Windows Azure cloud

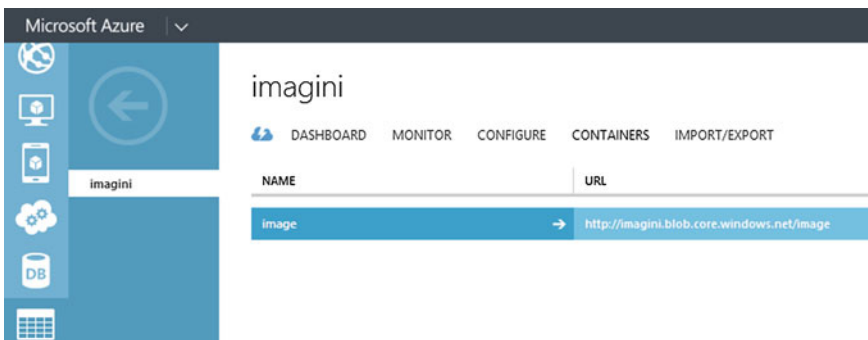


Fig. 7 Windows Azure container

5 Medical Benefits

Cloud computing offers many opportunities to improve healthcare services from the viewpoint of management, technology, security, and legality [6]. Moving the infrastructure to the cloud, valuable data extracted from different databases of treatment, patients, diseases, and so on will be accessible to doctors to perform analytical studies and see statistical results. Hiding personal patient details, data may be shared between doctors and even hospitals, and may be available as cross-referenced information from different diseases and treatments [7].

Using telematic applications, the time dedicated to personalized clinical attention to patients increases, and clinicians may more effectively schedule and manage that time. Also it avoids unnecessary travel by patients, while allowing them to feel closely monitored by the clinician [8].

With data interoperability, a clinical consultation, research, and educational platform may be established where regional and international clinicians, researchers, and students can upload or download clinical data including image files, and medical reports to review and discuss pathological signs and diagnostic results [7].

The proposed system helps the physicians to make a more accurate and a faster interpretation of the patient's segmental imaging. Physicians of different specialties (orthopedic, rehabilitation specialist, or radiologist) who are treating a patient suffering of a musculoskeletal disorder can analyze and interpret simultaneously the scanning images. Afterwards, the physician establishes a treatment plan. According to the concerned musculoskeletal lesion the physician requires further imaging investigations. The patient is examined after 3 months, 6 months, or 1 year. The physicians will compare the staged imaging scans. They will then conclude upon the patient's evolution and will take decisions regarding the next treatments.

The system is also cost-effective. It will eliminate the costs of transportation for patients that are living in remote locations. The costs implied by consulting physicians who are working in different countries and who are asked for a second opinion are reduced. Work productivity can be increased taking into account that most of the targeted patients are young or adult with an active professional status.

The proposed system contributes to the e-Health field by providing a model to support medical software, saving resources, and improving the management of patients who are dealing with musculoskeletal lesions. It also supports tendencies that may be used to improve the current treatments to be generated and analyzed.

6 Conclusions

The proposed system will use a new approach in image processing. Preserving the data associated with the pixels in the original image will allow the automatic segmentation and colorization of the images based on the intensity values. Cloud computing and high level image processing has the potential to be effective, efficient, and raise the quality of recovery after injury.

Acknowledgments This paper is supported by the Sectoral Operational Programme Human Resources Development POSDRU/159/1.5/S/137516 financed from the European Social Fund and by the Romanian Government.

References

1. Wei QR, Feng DZ, Yuan MD (2013) Automatic local thresholding algorithm for SAR image edge detection. In: IET international radar conference, Xi'an, pp 1–5
2. Batenburg KJ, Sijbers J (2009) Optimal threshold selection for tomogram segmentation by projection distance minimization. *IEEE Trans Med Imaging* 28(5):676–686
3. Adollah R, Francis EU, Mashor MY, Harun NH (2012) Bone marrow image segmentation based on multilevel Thresholding. In: International conference on biomedical engineering (ICoBE), Penang, pp 457–461
4. He L, Chao Y, Suzuki K (2010) An efficient first-scan method for label-equivalence-based labeling algorithms. *Pattern Recogn Lett* 31(1):28–35
5. Pardamean B, Rumanda RR (2011) Integrated model of cloud-based E-medical record for health care organizations. In: Gaol FL, Strouhal J (eds) Proceedings of the 10th WSEAS international conference on E-Activities (E-ACTIVITIES'11), World Scientific and Engineering Academy and Society (WSEAS), Stevens Point, Wisconsin, USA, pp 157–162
6. Kuo AMH (2011) Opportunities and challenges of cloud computing to improve health care services. *J Med Internet Res* 13(3):e67
7. Jui-Chien H, Ai-Hsien L, Chung-Chi Y (2013) Mobile, cloud, and big data computing: contributions, challenges, and new directions in telecardiology. *Int J Environ Res Public Health* 10:6131–6153. doi:[10.3390/ijerph10116131](https://doi.org/10.3390/ijerph10116131)
8. Vilaplana J, Solsona F, Abella F, Filgueira R, Rius J (2013) The cloud paradigm applied to e-Health. *BMC Med Inform Decis Mak* 14(13):35. doi:[10.1186/1472-6947-13-35](https://doi.org/10.1186/1472-6947-13-35)

Dedicated BSN for Personal Indoor Monitoring

Ștefan Mocanu

Abstract In 1995, the concept of “ubiquitous computing” was introduced by Weiser. A particular case is represented by ambient intelligence (AmI) which denotes an environment dedicated to supporting people’s everyday activities at home. Even more, another concept, ambient assisted living (AAL) was introduced for designating an AmI system oriented to support elderly or disabled people in their daily lives, allowing them to grow old in their homes or their familiar community as long as possible with a minimum intervention of a medical or social assistant. For this to be possible, latest hardware, software, and communication technologies need to work together. The core of any assistive system is represented by WSN (wireless sensor network). In this paper, a particular case of WSN is presented as a personal monitoring system. The main features of this system include: vital signs monitoring (heart rate, temperature—others may be added), fall detection, and pedometer. In addition, the system can send alerts to an emergency center in case anomalies are detected in subject’s normal behavior.

Keywords Personal monitoring · AAL · PAL · BSN · WSN · Healthcare services · Home care

1 Introduction

During the past few years, many statistics regarding social, medical, and qualitative aspects of elderly and disabled peoples’ life were presented. Some of the most trustful ones were made by EUROSTAT [1].

A simple analysis of the data reveals that life expectancy of elderly people in today’s societies is growing [1–3] while as the birth rate is constantly decreasing. Although the first may be considered a positive fact proving that modern medical

Ș. Mocanu (✉)
University Politehnica of Bucharest, Bucharest, Romania
e-mail: smocanu@rdslink.ro

technology and medication along with the increase of living conditions (especially in cities) are at peak level, it also hides some negative aspects. The unbalance between unemployed vs. employed population will cause severe problems to social and health funds and medical systems, which are all expected to collapse. Actual figures already reveal alarming trends of reducing the medical personnel and medical facilities (hospitals, clinics) as presented in [2, 3].

Another category that must be taken into consideration is represented by the disabled or partially disabled people. Most relevant data were collected by the World Health Organization (WHO) [4].

In a recent report of WHO, it is stated: “*An estimated 10 % of the world’s population—approximately 650 million people, of which 200 million are children—experience some form of disability. The most common disabilities are associated with chronic conditions such as cardiovascular and chronic respiratory diseases, cancer and diabetes; injuries, such as those due to road traffic crashes, falls, landmines and violence; mental illness; malnutrition; HIV/AIDS and other infectious diseases. The number of people with disabilities is growing as a result of factors such as population growth, ageing and medical advances that preserve and prolong life. These factors are creating considerable demands for health and rehabilitation services.*”

Available data and statistics lead to alarming conclusions from which one already severely affects millions of people: incapacity of public social and medical systems to offer elderly or disabled people the care and attentions they need.

A very important aspect of today’s and future health strategies of EU and worldwide concerns the quality of life. For example, back in 2005, healthy life years (HLY) was included as a Lisbon Structural Indicator, to point out that population’s life expectancy must also consider the quality of life not only the length of life. This factor was considered to be one of the key factors of economic growth. On March 15, 2010, the Declaration of European Cooperation on e-Health was signed in Barcelona by the Ministers of Health from the EU States, as a joint decision for improving health services at the EU level.

Other measures were taken or proposed in order to reduce or eliminate the predicted problems previously exposed. Those measures may be classified as follows:

(a) *Economic—financial*

- consolidation and decentralization of social and medical funds;
- elimination of useless expenses, better selection of suppliers;
- restrictions for certain categories of people;

(b) *Politic—administrative*

- increase of retirement age;
- employment restrictions;

(c) *Research and development*

- development of new data acquiring, storage and, distribution systems;
- development of medical assistive systems;
- development of autonomous monitoring and assistance systems for elderly or disabled;
- interdisciplinary approaches: medical, engineering, networking, and sensor development.

One solution may be represented by the use of ICT technologies for supporting everyday home life of old, partly disabled, or convalescent people. These represent the groups of people that traditionally would be treated or receive care in specialized institutions such as hospitals or asylums. Personal assisted living (PAL) can offer cheaper solutions than the traditional treatment or care methods when it comes to persons that do not need permanent assistance from a specialized human assistant. Of course, severe cases that require permanent medical attention will have to be treated accordingly in proper institutions, by well-trained personnel. When it comes to personal assistance, some guidelines must be taken into consideration. For instance, studies conducted by WHO revealed that many accidents that occur indoor are not reported in time and may have dramatic consequences. In the early 2000, statistics showed that, worldwide, every 15 min a death occurs indoor and every 5s a severe accident should be reported.

2 Related Work

Homecare or PAL represents a particular type of ambient assisted living (ALL). The concept denotes an intelligent, autonomous system [5] customized for monitoring and assisting elderly, disabled people, or patients at home. The main goal of these systems is to allow users to have a virtually normal life in a friendly environment. Although many studies indicate that elderly people are reserved when they have to deal with new technologies, in case of ALL systems the general opinion is a positive one and a high degree of acceptance is expected. The explanation is simple: people do not need to learn anything new and, furthermore, reducing costs are welcomed, not to mention the benefits of living in their own homes instead of hospitals or asylums.

During the past few years, many assistive systems have been proposed, especially for indoor environments. Most of them perform a single task (fall detection, localization, and monitoring of vital signs) and do not aim integration with other assistive modules such as environment control and customization. The simplest form of assistive system is represented by a radio transmitter which sends a distress signal when the user pushes a button. This kind of systems suffers from a limited usage given the fact that severe conditions (heart attack, stroke, and falls followed by head injuries) can prevent the user to push the alert button. Assistive systems

based on telephony can offer a remote interaction between the subscriber and an operator from a call center. Although the operator can call the subscriber in order to get information about current health state, subjective description of health condition by the patient may be a serious inconvenient. Moreover, a critical event (stroke, heart attack, and fall) can appear as soon as the call is over and the next call may be too late to help the subscriber. More complex systems architectures were presented in [2, 3, 6, 7] but, unfortunately, none of them have been deployed on a large scale.

Discussions with medical specialists revealed most important aspects regarding short-term health parameters which should be considered when implementing an ALL-PAL system. The SEPSIS condition represents a dangerous body status caused by a severe inflammation that can soon lead to a fatal result. There are some symptoms that can be immediately detected by body sensors and remotely reported to a medical specialist or an emergency center. The symptoms include: high fever, high skin humidity (perspiration), increased heart rate and low blood pressure. Abnormal heart rate and temperature are the first symptoms that may indicate SEPSIS condition.

Another big problem regarding the well being and health of elderly people is represented by falls. Statistics show that more than 30 % of the people older than 65 years suffer various forms of fractures from indoor falls. Even worse, over 20 % of those suffer a severe form of hip fracture that lead to death within a year from the event. As if it is not enough, over 70 % of accidental deaths of elderly people older than 70 years are provoked by late detected falls.

An efficient assistive system should be able to immediately detect abnormal situations and report them to the medical teams from the emergency center according to a well-defined protocol. The core of almost all proposed assistive systems is represented by wireless sensor networks (WSN) or body sensor network (BSN) [8].

In our previous work, the architecture of a complex AAL system named AmiHomeCare and parts of its software implementation was presented [2, 3]. In this paper, additional features for the MHSDMCS module (Medical Home Surveillance Devices Monitoring and Coordination System) [2] and the way it can interact with other AAL modules will be presented.

3 System Description and Functionality

The purpose of this personal monitoring system is to observe and record the short-term evolution of human vital signs in order to detect and report abnormal behaviors that can put the user in danger. Also, the system will report such situations to an emergency call center so that a medical team will immediately go to the user's residence.

As stated before, the system is based on WSN/BSN concept. For each monitored parameter, a dedicated wireless sensor is used, all the data being collected and processed at the central node level. Due to spatial, energy and radiation constraints,

a centralized STAR-based architecture was chosen. The functional architecture of the system is depicted in Fig. 1. As one can notice, there are two different ways the monitoring system can work. In one scenario, the system can work independently and send alert messages via Internet and GSM network to a call center in case a critical situation was identified. In another scenario, the personal monitoring system can be integrated in a more complex AAL-PAL system where it can collaborate with an environment monitoring module. This is the most likely situation since such integrated solutions can offer an increased reliability. This aspect will be discussed later in this paper.

Once data are processed by the central node, the results can be transmitted as alert messages or stored in a database located at the environment monitoring module level if an extended AAL-PAL architecture is chosen. From the personal monitoring system perspective, in this case, the environment monitoring module also acts like a transmission relay since wireless routers or access points are part of the latter [2, 3]. The importance of logging parameters locally is also presented in [2].

Data exchange between the modules is made using two different types of messages. On one hand, there are logging messages which contain only the instant values received from the wireless sensor nodes and on the other hand, there are alert messages which contain not only the monitored parameters but also indication of which one of them is abnormal. The decision is exclusively made by the central node of the personal monitoring system. All the messages contain a time stamp, very useful in case medical reports or statistics are required.

Since costs of implementation were aimed to be as low as possible, cheap development platforms from Texas Instruments were used. The first development platform used for temperature monitoring, data transmission, and energy consumption optimization was TI eZ430—RF 2500 [9]. Giving the similarities of the sensors in that concerns the output, virtually any kind of sensor can be integrated into the system. The coverage range indicated by the supplier was about 25–50 m but, in reality, less than 2 m were initially achieved. Several improvements were operated within the application, and a reasonable 5–6 m range in the presence of

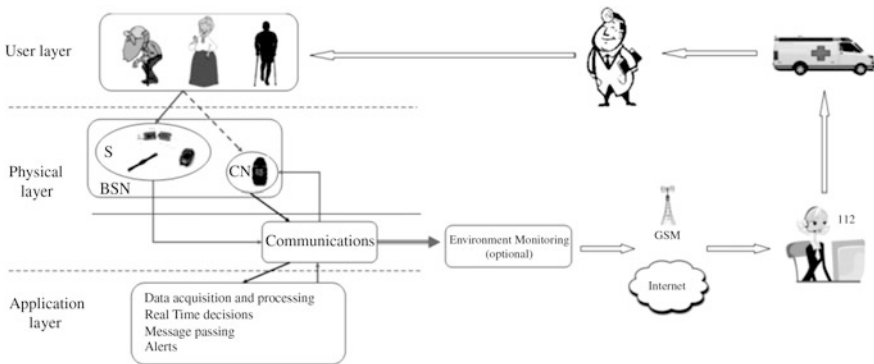


Fig. 1 The architecture of personal monitoring system

solid obstacles (walls, furniture, and electronic devices) was achieved while the life of the power supply increased by 10 %. In a real-life scenario, improvements must be made at the environment monitoring system module, most likely by placing several access points in order to overcome the specific problems generated by reinforced concrete walls, electrical engine home appliances or microwave ovens with regards to wireless communications.

The second development platform used for implementing the personal monitoring system was TI—Chronos (Texas Instruments 2013). This is a more user friendly platform presented as a hand watch with several embedded sensors (temperature, 3 axis accelerometer, and pressure sensor). TI-Chronos allows communications with external wireless sensors via proprietary protocol named BlueRobin. In our case, this facility was used to connect with a thoracic belt as presented in Fig. 2. TI-Chronos can also connect with a computer through a dedicated access point based on a proprietary protocol named SimpliciTI.

Low power consumption required by any WSN application is guaranteed by the use of CC430 platform [9] which is, as vendor says, “*the industry’s lowest power consumption, single-chip radio-frequency family for microcontroller-based applications.*”

Based on the conclusions taken after the discussions with the medical specialists, a decision was made to monitor the first symptoms of SEPSIS (heart rate and fever) and, also, to detect falls. Since the system is modular and scalable, extended functionalities can be easily added. It was our goal to implement a “proof of concept” model not only from the sensors point of view, but also from the integration and communication point of view.

Previous results were partially published in [2, 3, 10] but some clarifications are needed. For instance, in Fig. 3, results from the temperature monitoring procedure are presented. As one observe, the real temperature values (measured independently with a high-precision medical thermometer) are not even close to the values indicated by TI-Chronos. This suggests a high imprecision of Chronos’s temperature sensor which can not be compensated due to its variability in time and high

Fig. 2 TI Chronos development kit and BMI thoracic belt



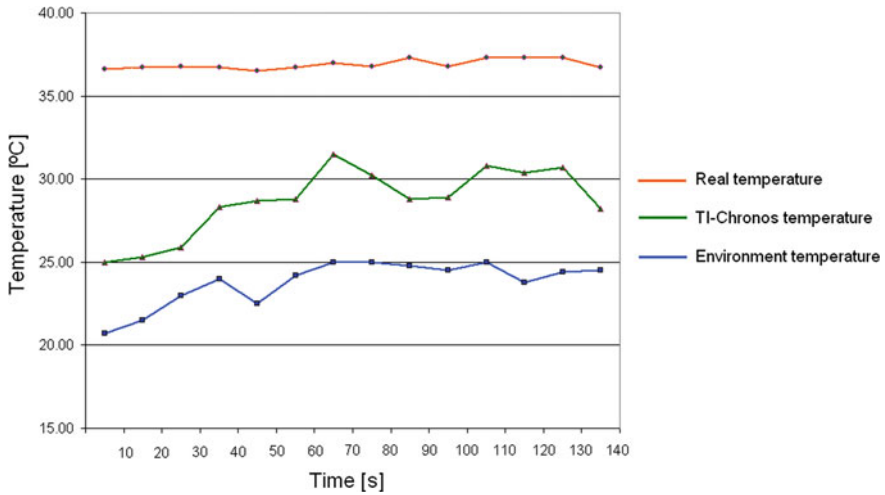
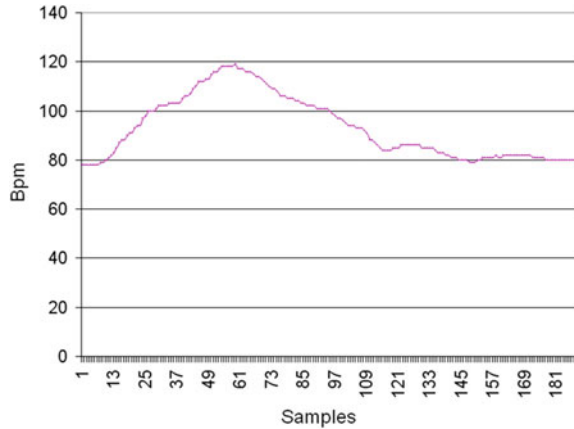


Fig. 3 Temperature monitoring

dependence of environmental temperature. However, a more precise, specialized sensor can be used with greater chances of success. In addition, this is a good opportunity to highlight the importance of complex AAL-PAL systems in which different modules can cooperate. For instance, if the ambient temperature is high, an increased body temperature is justified and does not necessarily indicate an abnormal situation. Take, for example, the case when a monitored person is taking a shower [11]. Even if an alert message is issued, the human operator from the call center can choose not to send an emergency team this way reducing the operating costs.

As opposed to temperature monitoring, the heart rate monitoring offered more realistic values as presented in Fig. 4. The thoracic belt from BMI was used for this experiment. The monitored human subject (male, 36 years) was observed during an interval of about 5 min in which he made a low to moderate effort followed by a period of total relaxation. As one can observe in Fig. 4, heart rate does not have a linear increase nor decrease. Also, a certain inertia and oscillation have been noticed during the experiments. Since TI-Chronos does not offer simultaneous wireless communications the readings from the BMI thoracic belt data processing was performed offline based on real values that were recorded in TI-Chronos internal memory while it worked as a data logger.

The third analyzed sensor was the accelerometer. The purpose of this investigation is based on facts and statistics (previously mentioned) which point that fall detection should be included in all personal monitoring applications. There are many commercial products that offer only this functionality but none of them is integrated into a complex AAL-PAL system. For the fall detection, an algorithm was designed and implemented. The first challenge was to design a calibration procedure for the accelerometer since no technical details were available from the

Fig. 4 Heart rate monitoring

manufacturer. Figure 5a presents the data acquired with a demonstrative application from Texas Instruments. It is easy to observe that, as it is, data cannot be used for numerical processing.

Figure 5b presents the raw data from the accelerometer, while Fig. 5c presents the calibrated data. Calibration process can be performed “on-line” by the central node.

In order to apply the fall detection algorithm, several filters were applied. First, a median filter was chosen, with a window size of 15 elements. The output became input for an extended FIR filter with a window of 36 elements. This is double the size of the windows considered relevant in literature related to fall detection. At the end, a fall detection algorithm was applied; the results are presented in Fig. 6. The threshold was determined empirically after real tests (falls).

As one can see, the reported events depend on the threshold value: if the threshold is too low, a big number of false falls will be reported; if the threshold is too high, there is a possibility of not detecting a real fall. Another thing one can observe in Fig. 6 is that only the second reported event was, indeed, a fall. The first event, falsely reported, was due to a severe shake of the accelerometer but it is easy to observe that vertical acceleration did not drop and stay around 0, as expected.

Based on the fall detection algorithm, an additional feature, a pedometer, was implemented for the personal monitoring system. Since a sedentary life leads to obesity and other-related problems, especially when it comes to elderly or disabled people [12], reporting the amount of moving per day may represent a good motivation for preventing and avoiding those bad habits.

In Fig. 7 movement monitoring is presented. The slightly different values for each identified step (in the range of 5 %) are justified by the different accelerations values. Similar to fall detection algorithm, a threshold was conveniently selected but, in this case, fine tuning is recommended for each user since people have different ways of walking/running. Another difference consists in giving different weights for the accelerations of different axes. In particular, due to the specific requirements, the vertical acceleration received the highest weight.

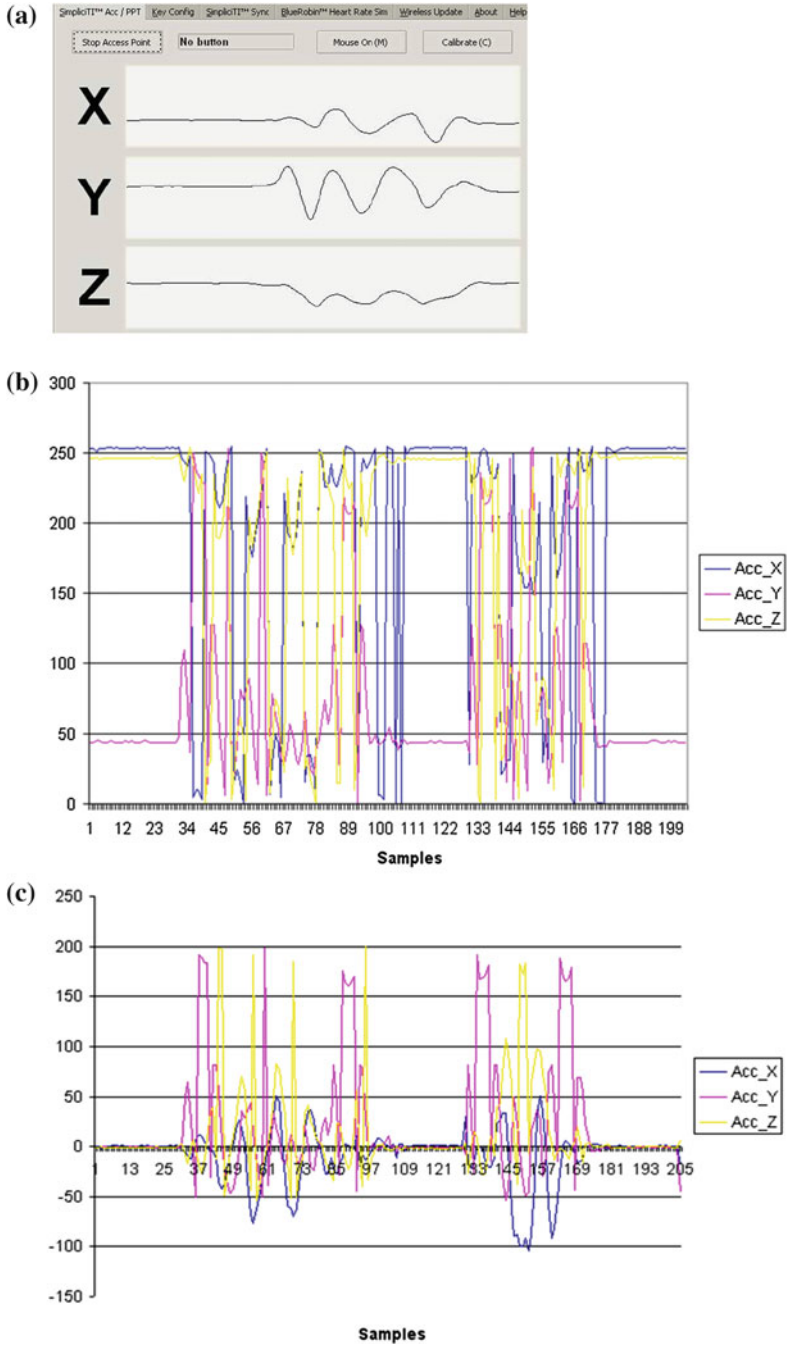


Fig. 5 a Data acquired from accelerometer with a demonstrative TI application. b Raw data from accelerometer. c Calibrated data

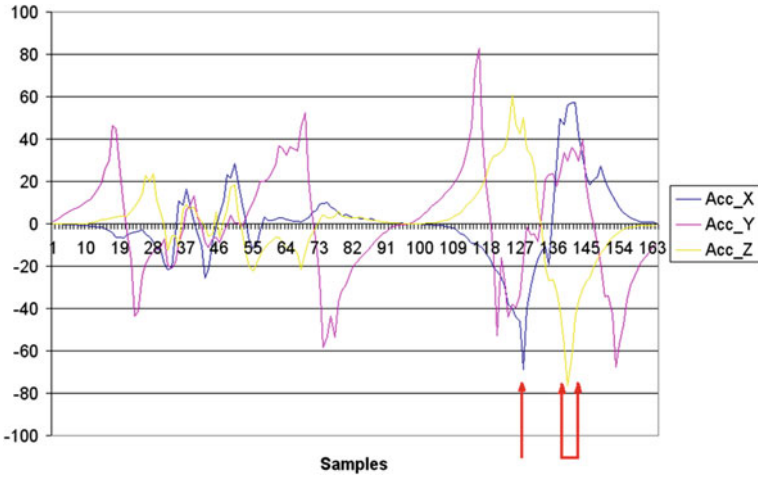


Fig. 6 Filtered data and detected events (possible falls)

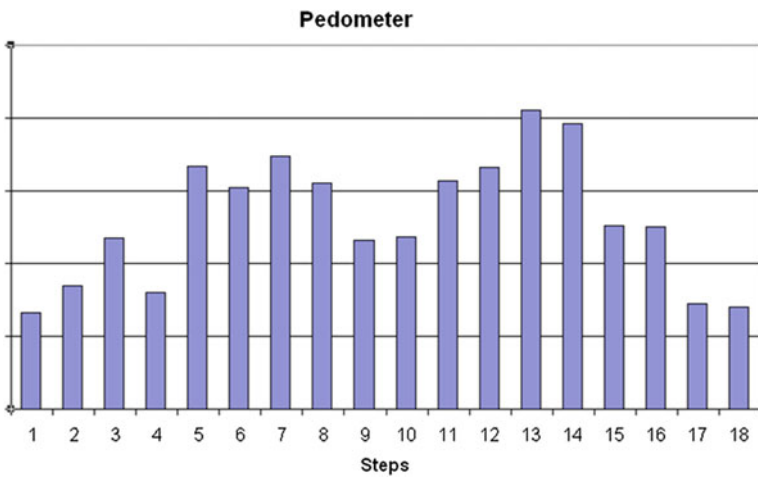


Fig. 7 Pedometer function of personal monitoring system

The final objective for the personal monitoring system was the communication with an environment monitoring system so it can send log or alert messages. All inter-module communications are wireless and are based on WLAN (wireless LAN) concepts. Figure 8 presents a sample communication session, in particular one in which a high rate is reported to be too high. Consequently, an alert message was issued.

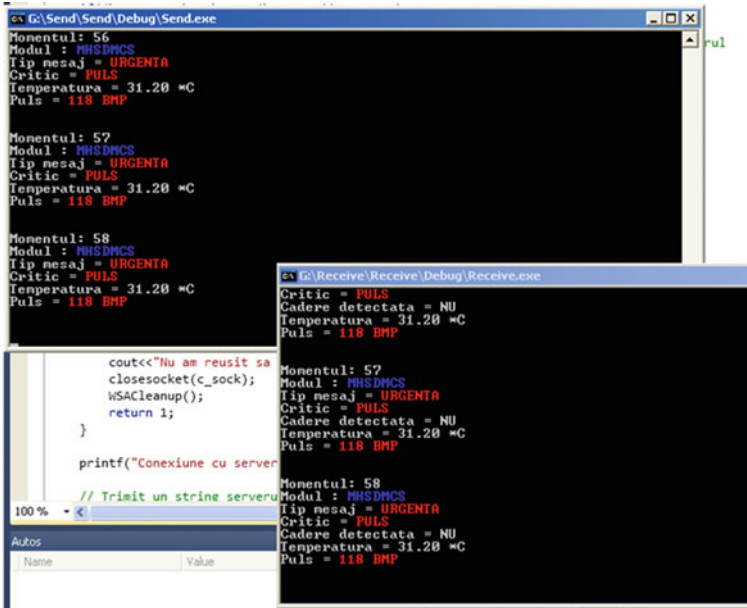


Fig. 8 Sample inter-module communication

4 Conclusions and Discussions

In this paper, a fully functional personal monitoring system was presented. The system not only can work as an independent module, but also can be integrated into an advanced AAL system with personal monitoring facilities. The second option is preferred because, as presented in the paper, there are many situations when cooperation between different modules and sensor data fusion offers a more reliable behavior for the system.

For a “proof of concept” model cheap hardware devices were used. As presented, this option was good enough for demonstrating the viability of the concept but cannot be the basis of a functional, real-life, system. For this, state of the art sensors and communication modules must be used in order to guarantee the accuracy of the data and reliability of transmissions. Most important vital signs are monitored; others may be easily added due to the system scalability.

One of the key aspects regarding the design and implementation of the personal monitoring system was represented by the costs. Even if high-end components are used, the total costs for implementing and using such a system will be far smaller than the costs required by providing personal care in a dedicated facility.

In addition to the advantages given by lower costs, the users, either elderly or disabled persons, can benefit from warmer, familiar environment represented by their own homes. Unfortunately, the solution cannot be applied to persons with severe health problems which need more careful medical attention, but this is a step

forward. In conclusion, given the good results obtained so far, it is clear that AAL–PAL systems will continue to develop and become more and more popular in a near future.

References

1. EUROSTAT (2013) <http://epp.eurostat.ec.europa.eu/portal/page/portal/eurostat/home>
2. Mocanu S, Mocanu I, Anton S, Munteanu C (2011) AmIHomCare: a complex ambient intelligent system for home medical assistance. In: Proceedings of the 10th international conference on applied computer and applied computational science, pp 181–186
3. Munteanu C, Caramihai S, Mocanu I, Mocanu S, Vacher M, Portet F, Chahuara P (2014) Indoor personal monitoring, supervising and assistance sweet-home and AmiHomeCare case studies. *J Control Eng. Appl. Inform* 16(1):50–61
4. WHO—World Health Organization (2014). www.who.int
5. Ramos C, Augusto J, Shapiro D (2008) Ambient intelligence—the next step for artificial intelligence. *IEEE Intell Syst* 23:15–18
6. Abascal J, Bonail B, Marco A, Casas R, Sevillano JL (2008) AmbienNet: an intelligent environment to support people with disabilities and elderly people. In: ASSETS-2008, 10th ACM conference on computers and accessibility, Halifax, Canada, p 293
7. Dobrescu R, Popescu D, Nicolae M, Mocanu S (2009) Hybrid wireless sensor network for homecare monitoring of chronic patients. *Int J Biol Biomed Eng* 3(2):19–26
8. Chen M, Gonzalez S, Vasilakos A, Cao H, Leung VCM (2011) Body area networks: a survey. *Mobile Netw Appl Springer Media* 16(2):171–193
9. Texas Instruments (2014). www.ti.com
10. Munteanu C, Mocanu S (2013) Person and environment monitoring for home healthcare services. In: Davila C (ed) *Fostering innovation in healthcare services*, Chapter 2.4, pp 59–64
11. Steen EE, Frenken T, Eichelberg M, Frenken M, Hein A (2013) Modeling individual healthy behavior using home automation sensor data: Results from a field trial. *J Ambient Intell Smart Environ* 5:503–523 (IOS Press)
12. Kaluža B, Gams M (2012) Analysis of daily-living behaviour. *J Ambient Intell Smart Environ* 4:403–413 (IOS Press)

Romanian Sign Language Oral Health Corpus in Video and Animated Avatar Technology

Ionut Adrian Chiriac, Lăcrămioara Stoicu-Tivadar
and Elena Podoleanu

Abstract The goal of this article is to respond to a research question: what are the appropriate steps and challenges in building a parallel collection of data required for e-health systems design and implementation for deaf people both in avatar and video technology? The paper presents the steps taken in order to create a parallel collection of dentistry data for prevention education needed in development of medical education system for deaf people. The specific feature of this type of applications is that the medical information and concepts are converted in sign language for deaf users through an avatar. Two types of avatars are taken into consideration: the animated avatar will display an animated figure, and the video avatar will display recorded humans in order to make a comparative analysis between video technology and animated technology used in e-health applications for deaf people using avatars. The study starts with the project phase and continues with implementation followed by results analysis. The two collections of data are stored in different formats. In the case of the avatar video format, the collection is stored as files in video format. In the case of the animated avatar, the collection of files contains expressions and phrases in *SiGML* animated format. The content must be prepared in advance in both forms before assembling the applications. An important part of this paper covers detailed description of the process of editing signs for both forms of the avatars. The application software and the format of the files are presented in extenso. The final part consists of results of the comparative analysis and foreshadows the next steps to be made for future research.

I.A. Chiriac (✉) · E. Podoleanu
University of Medicine and Pharmacy “Carol Davila”,
Bucharest, Romania
e-mail: chiriaci@gmail.com

E. Podoleanu
e-mail: elena.podoleanu@gmail.com

L. Stoicu-Tivadar
Faculty of Automatics and Computers, University Politehnica,
Timișoara, Romania
e-mail: lacramioara.stoicu-tivadar@aut.upt.ro

Keywords Sign language · Avatar · Animated avatar · Medical education system · E-health application · E-health education

1 State of the Art

In the last years, many projects were developed involving animated avatar technology for deaf sign languages. In the following are shortly presented the most important in the field.

TESSA Project is an experimental system, with the goal to translate a clerk's speech from a Post Office in sign language for deaf clients [1–3].

ASL Synthesizer Project is a joint project involving institutions from USA with the aim of translating English into American Sign Language with the main priority to produce animations which are not only grammatically accurate and understandable, but also are natural and would be acceptable as examples of correct signing [4, 5].

American Sign Language Animation Generation Technologies—Researchers from USA developed a project with the goal to make avatar animations more understandable and natural-looking for ASL signers. The project explored the development of educational software including animations of the human figure, for the deaf users to practice their communication skills [6, 7].

The TEAM project is an English-to-ASL translation system with animated virtual humans as signing avatar and complex linguistic system focusing on morphological variations, facial expressions, and sentence mood [4, 8].

The South African SL Project has developed South African Sign Language (SASL) translation using SignWriting notation system [4, 9].

ASL—Animation Speaks Louder—is a research project developed by a group from USA whose aim was to develop a 3D animation-based software tool—ASL. This tool allows the deaf persons teachers to add sign language translation to digital media in the form of 3D character animations [10–12].

eSIGN Project is a European multinational project with the goal to provide flexible means by which any organization can provide for the deaf community information in sign language on screen-based media (data points, kiosks, displays, web sites, etc.) [13, 14].

SignTel Project—SignTel is a European multinational project whose aim is to add avatars to computer-based assessment tests that can 'sign' questions for deaf candidates [15].

Dicta-Sign Project is a European research project with the aim of making online communications more accessible to deaf sign language users with three laboratory prototypes: Search-by-Example tool, SL-to-SL translator, and sign-Wiki [16].

Sign Speak Project—main goal is to provide new e-services and to make possible continuous sign language recognition and translation in order to improve the

communication between the deaf community and the hearing community, and the other way around [17].

The research documentation upon previously presented projects containing design models involved in health education applications for deaf people returned modest results. In the paper “**Designing Health Care Applications for the Deaf**” written by Paolo Prinetto, Gabriele Tiotto, Andrea Del Principe [4, 18] is treated the subject of the architecture of design of an application with the aim of improving the accessibility and the service quality of health care for deaf people. The system allows the automatic translation from Italian to Italian Sign Language through a virtual avatar.

The state of the art research worldwide did not locate any concrete projects regarding **health education systems** for deaf people, neither with animated avatar nor with video technology avatar. No systematic comparative research between animated and video technology avatars was found. The international projects were focused main on automatic translation and better integration of the deaf people in social activities.

Prospective research on computerized projects in Romanian sign language returned very modest results. The most important projects refer to dictionaries for sign language using video technology. The research did not return any results regarding projects with animated avatars or e-health for deaf people in Romania.

2 General Overview

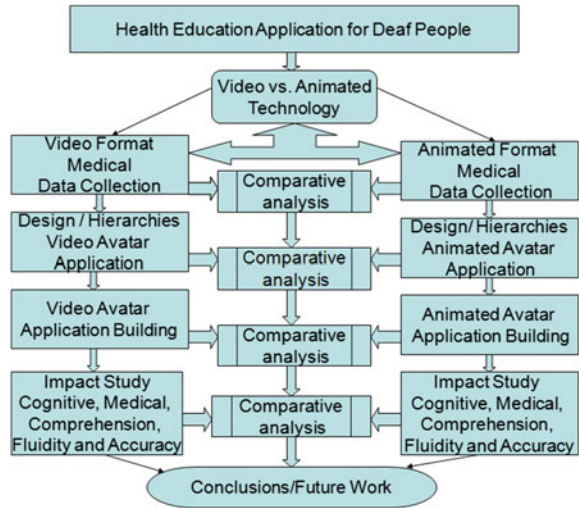
The paper presents the steps followed in order to create a parallel collection of dentistry data for prevention education needed in development of a medical education system for deaf people.

Two types of avatars are taken into consideration: the animated avatar will display an animated figure and the video avatar will display recorded humans in order to make a comparative analysis between video technology and animated technology used in e-health applications for deaf people using avatars. The study starts with the project phase and continues with the implementation followed by results analysis (Fig. 1).

The study of complex applications with avatar for medical education to the hearing impaired is a national and international premiere (Fig. 1).

- The study of avatar hierarchies involved in the design of the applications for medical education destined to hearing impaired is a national and international premiere.
- Building a collection of words and phrases in medical domain with both video and animated avatar technology is a national premier (for Romanian sign language).

Fig. 1 Block diagram of the general research project



- Domain: The creation of avatar applications in health education field for persons with hearing disabilities is a national and international premiere.
- Comparative study of the hierarchies involved in the design of the applications for medical education destined to hearing impaired is a national and international premiere.
- Comparative study of the cognitive and medical impact of the applications in video and animated avatar technology is a premier national and international.
- Comparative study of comprehension, fluidity, and accuracy of the individual signs, phrases, and message of the program is a national premiere.

This article deals with the first part of the research presented in the upper part of the diagram (Fig. 1).

Previous recent work in a collaboration of colleagues from Health Education, Behavioral Sciences and Oral Health disciplines, from the faculty of Medicine, University of Medicine and Pharmacy “Carol Davila,” Bucharest, Romania together with persons involved in the deaf education, resulted in building a corpus of words and key phrases from Oral Health domain.

3 Oral Health Corpus in Video Format Technology

The previously mentioned group of keywords and phrases was previously translated as signs and signs phrases performed by two different signers from different regions of Romania and recorded in video format.

The first recordings were done in Bucharest, using a specific language from this region, in collaboration with a team of professors from Deaf School no 1,

Fig. 2 Ana demonstrating “carbonated drinks” sign



Fig. 3 Andreea demonstrating “pain” sign



Bucharest. The work consisted in translating 68 words and key phrases according to the language used in this environment and were recorded with Ana as sign operator (Fig. 2).

The second recording session was done with Andreea as operator, student at faculty of Dentistry, University of Medicine and Pharmacy “Carol Davila,” Bucharest, Romania. The student graduated the deaf school and the deaf high school in Sibiu.

She is using a set of different signs than the one recorded with the first team, according to the specific sign language used in her region (Fig. 3). Consequently, there were recorded 162 words and key phrases with Andreea as sign operator.

The results of both recordings were filtered and selected in collaboration with Prof. Florea Barbu working that time at the faculty of Sociology, University of Pitesti, a well-known specialist of the domain. Following this operation, the

collection consisted in 101 useful words and key phrases, 37 from Ana and 64 from Andreea.

This collection, recorded in video format, performed by human operators, will be later integrated as video files in the experimental model, in the video avatar technology version of the application.

4 Oral Health Corpus in Animated Avatar Technology

To approach the topic of oral health corpus in animated avatar technology, the main goal was to edit the collection of keywords and phrases from medical domain previously recorded, as movements performed by an animated avatar and converting them as a file in SiGML [19] format that allows integration in web format.

“Signing Gesture Markup Language”—“Marking of gesture Sign Language” (SiGML), is a modified version of XML 2. SiGML was designed at University of East Anglia in order to “translate” HamNoSys symbol sequences in codes sequences that can be processed and executed by a computer. SiGML contains codes that processed in a synthesizer will put in motion the geometry of the animated agent [19] (Fig. 4).

In synthesis SiGML (Signing Gesture Markup Language) [19] is an XML application that enables transcription of sign language gestures. The SiGML variant used by eSIGN [20, 21] builds on HamNoSys [22] essentially and is encoding the HamNoSys manual features, accompanied by a representation of nonmanual aspects.

eSIGN Editor allows editing avatar movements using HamNosys symbols (Fig. 5). The editor allows setting the hand position and location, type, and range of motion, palm format, and the distance from the body where the sign is executed.

Working with eSIGN involves mandatory to learn the phonetic notation system HamNoSys (Hamburg Sign Language Notation System) and to combine these symbols in different ways in order to obtain a sign (Fig. 5).

In Fig. 5 is shown the HamNoSys sequence for the sign “pain” only with the manual features in the first editing step.

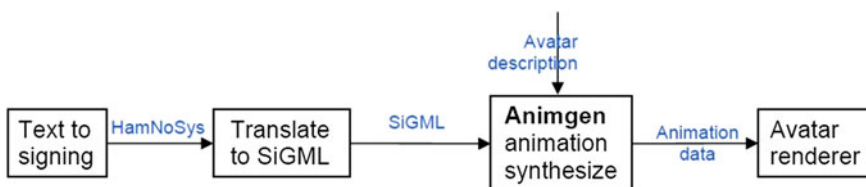


Fig. 4 Block diagram representing the process performed in order to produce an animation of a sign

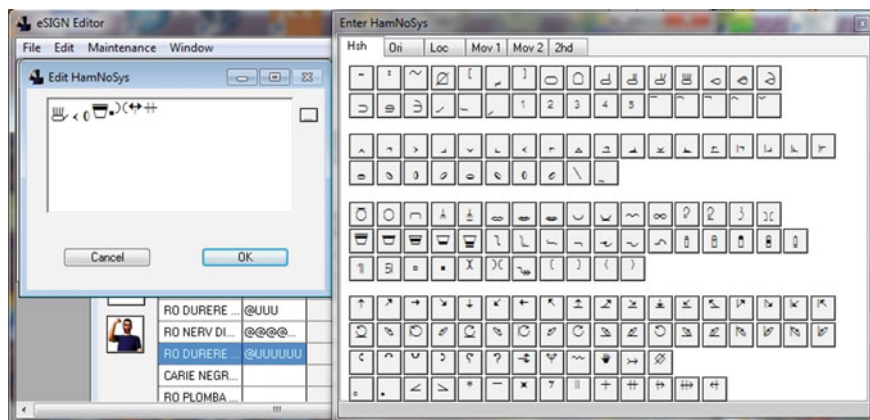
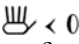
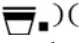
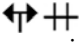


Fig. 5 eSIGN HamNoSys editor for individual signs

 converted in SiGML sequence is [`<hamfinger2345/> <hamthumboutmod/> <hamextfingerl/> <hampalml/>`] and give instructions about palm format and orientation (Figs. 6 and 7).

 converted in SiGML sequence is [`<hamshouldertop/> <hamlrat/> <hamclose/>`] and give instructions about the hand position relative to the body (Figs. 6 and 7).

 converted in SiGML sequence is [`<hamswinging/> <hamrepeatfromstartseveral/>`] and give instructions about the nature of the movement for the hand (Figs. 6 and 7).

In Fig. 7 is shown the SiGML sequence for the sign “pain” only with manual features in the first editing step. The sequence does not include the nonmanual features that will be added later.

For the palm, the sequence `<hamfinger2345/>` shows that the fingers 2, 3, 4, and 5 are opened. The line `<hamshouldertop/>` defines the level and the position where the movements with the palm are made. `<hamswinging/>` shows that the hand is swinging. `<hamrepeatfromstartseveral/>` shows that the movement is repeated several times.

eSign editor (Fig. 8—left) works with HamNoSys symbols and the player (Fig. 8—right) transform them in avatar’s movements.

eSIGN editor (Fig. 8—left) also allows visualizing signs phrases in SiGML format. The SiGML Player (Fig. 8—right) is a software written in java that displays one or several avatars (until 7 variants) which perform the signs or phrases edited in eSIGN. The SiGML URL Player App allows the avatars to perform signs from a URL location.

Sometimes the same sign may be obtained in different ways of editing in HamNoSys and may be edited in different versions as can be seen in Fig. 8—left. In Fig. 8—right is shown the avatar Luna performing the sign “pain” previously recorded with Andreea as operator and can be compared in Fig. 3.



Fig. 6 HamNoSys transcription of the manual components in the sign “pain”

```
<sigml>  
  <hns_sign gloss="RO DURERE BUN FB">  
    <hamnosys_nonmanual>  
    </hamnosys_nonmanual>  
    <hamnosys_manual>  
      <hamfinger2345/>  
      <hamthumboutmod/>  
      <hamextfinger/>  
      <hampalm/>  
      <hamshouldertop/>  
      <hamlrbeside/>  
      <hambetween/>  
      <hamchin/>  
      <hamlrbeside/>  
      <hamclose/>  
      <hamswinging/>  
      <hamrepeatfromstartseveral/>  
    </hamnosys_manual>  
  </hns_sign>  
</sigml>
```

Fig. 7 SiGML sequence for the sign “pain” only with manual features

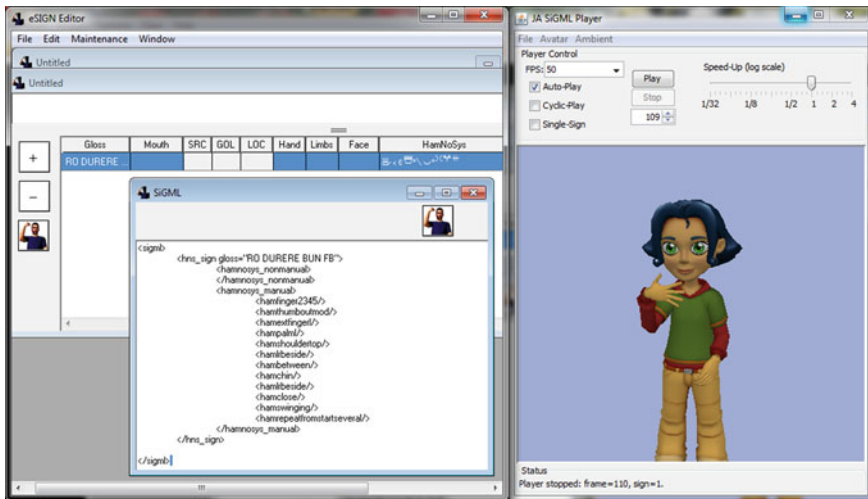


Fig. 8 eSIGN signs editor (right) and JA SiGML Player (left) for the sign “pain” only with manuals features

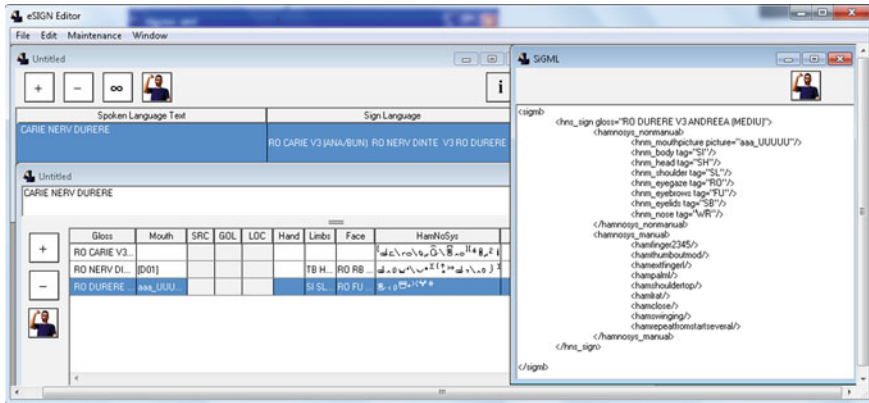


Fig. 11 Phrase/Words/Nonmanuals/HamNoSys/SiGML

shaking left right. For the face: RO—rolling eyes, FU—eyebrows furrowed, SB—lips narrowed, almost closed, and WR- nose wrinkled.

In Fig. 11 left is shown the phrases editor integrated into eSIGN with the words that compose the phrase succession “caries,” “nerve,” and “pain.” ALT key in combination with right click on the PLAY button makes appear in the right window the SiGML succession that compose the selected sign. In Fig. 11 right is shown the SiGML sequence for the sign “pain” with both manuals and nonmanual features.

In Fig. 12 is shown the SiGML sequence for the complex sign “pain” with both manuals and nonmanual features.

In the first part of the sequence, the nonmanual occurs. For the mouth, the movement <hnm_mouthpicture picture = “aaa_UUUUU”/> makes the avatar to simulate the aaa_UUUUU phonemes enunciation. For the Limbs <hnm_body tag = “SI”/>—SI—sigh, for the head <hnm_head tag = “SH”/>—SH—head is shaking left right. For the nose <hnm_nose tag = “WR”/>—WR—nose wrinkled.

The HamNoSys notation system has some natural limitations and sometimes a complicated sign may be realized as a succession of his composed parts as a phrase or part of a phrase. This event happened for the “Carbonated” sign part of “Carbonated Drinks” phrase. This sign presents a double symmetry that cannot be developed directly in HamNoSys. An inventive solution came to decompose first the sign in four components parts (Fig. 13).

With the eSIGN phrases editor, the complete sign “Carbonated” was recomposed inside the phrase “Carbonated Drinks,” repeating twice the four parts that compose the sign (Fig. 14—left). In Fig. 14—right is shown the avatar Luna performing the sign “Carbonated,” previously recorded with Ana as operator and can be compared in Fig. 2.

The phrases edited in eSIGN are saved by default in the special format eSIGN, and the resulted files have the extension *. esign. Those files can be edited with notepad or any other simple text editor (Fig. 15).

This collection of animated signs performed by avatars in SiGML Service Player realized with eSIGN editor and will be later integrated as SiGML files in the experimental model, in the animated avatar technology version of the application.

5 Conclusions

In what regards the two collections, those differ mainly in terms of data format and this determines the main features of the two variants.

In the case of the video avatar format, the recordings were made first in MOV format. The recorded files were further converted in MP4 format for better handling in the editing process. Sometimes the editing process implied changing proportions and crop editing. The final conversion will be made in FLV format for better integration in the application.

Video technology advantages: higher quality of the images, smoothness of movement, expressivity of the face, and more precision for details. In present times, normal and hd quality is less expensive and very accessible. The sign languages phrases can be recorded very easy using a device with video recording capabilities.

Video technology disadvantages: less flexibility in editing and some phrases may require postproduction.

In the case of the animated avatar, the collection of files contains words and phrases in SiGML animated format. The editing process is complex and involves time and dedicated work for every sign and phrase. Some of the signs may require several days of work as in the case of “carbonated drink.”

Avatar technology advantages: less space used on storage devices and flexibility in editing changes.

Avatar technology disadvantages: lower quality (mechanical movements), less expressivity of the face, and less precision for details. Sign language phrases require time and specialists to work with the editing tools.

The content must be prepared in advance in both formats before assembling the applications. The two alternatives presented in this paper will further influence the architecture of the two applications. The differences will be mainly in the conversion/translation module and in the Avatar Interface [23].

The set of records in video format, performed by human operators, will be edited and later integrated as video files in the experimental model, in the video avatar technology version of the application [23].

The series of animated signs performed by avatars in SiGML Service Player realized with eSIGN editor will be later integrated as SiGML files in the experimental model, in the animated version technology of the application [23].

The comparative research will continue with the implementation process and the study of the impact of the two categories of applications tested on the impaired users on different groups on different age categories [23].

In the next lines will be described the possible directions of research and development by improving the capabilities of editing of the eSIGN software and sign concepts.

Proposing the concept of MetaSigns that represents the signs that are more complex and long is a possible development in conceptualisation and edit of the signs. MetaSigns should be a unique complex sign obtained from the composition of several component parts which are edited separately.

The extension of the main menu used to edit the manual parts in order to be able to edit MetaSigns is a possible direction for development. Also a menu dedicated for editing MetaSigns is a possibility of improvement.

Regarding the improvements possible of the editor of eSIGN the proposal of a format converter between eSIGN format and SiGML for MetaSigns may represent an improvement. This converter could be another way to edit MetaSigns. The editor already allows the construction of sentences in eSIGN format and export them as SiGML files. As stated earlier in the article, the phrase “carbonated” was edited as a phrase consisting of four component parts. The existence of a converter could allow editing the MetaSigns by converting the sentence from eSIGN format to a specific SiGML sequence for individual signs. A menu that allows directly converting and saving the phrases in SiGML unique word format may also solve this problem although the essence of the issue is the same.

A menu that allows users to edit on the time axis the synchronization between the manual parts of the sign with the nonmanual parts would be a good direction for research and development. This menu should be developed further in the section menus for nonmanual components of signs.

Acknowledgments I would like to express my gratitude to Professor John Glauert providing guidance and all the necessary programs to work with animated avatars without which all this research on animated avatars would not have been possible in this form. Professor John Glauert is head of the Virtual Humans Group research team, School of Computing Sciences, University of East Anglia, Norwich. Thanks are also due to Prof. Florea Barbu for his dedicated guidance and assistance in the work for the preparation of the words and phrases in Romanian sign language.

References

1. Tessa. ViSiCAST. <http://www.visicast.co.uk/news/Tessa.html>
2. ViSiCAST. www.visicast.cmp.uea.ac.uk/Summary/summary1.htm
3. Visicast Home Page. www.visicast.co.uk
4. Morrissey S (2008) Data-driven machine translation for sign languages. Dublin City University, Dublin, Ireland. PhD Thesis
5. Wolfe R, Cook P, McDonald JC, Schnepf J (2011) Linguistics as structure in computer animation: toward a more effective synthesis of brow motion in American sign language. In: Herrmann A, Steinbach M (eds) Nonmanuals in sign language special issue of sign language & linguistics, pp 179–199. <http://asl.cs.depaul.edu/papers/WolfeCookMcDonaldSchnepf.pdf>
6. Linguistic and Assistive Technologies Laboratory (LATLab). <http://latlab.cs.qc.cuny.edu/index.html>

7. Linguistic and Assistive Technologies Laboratory (LATLab) -Research. <http://latlab.cs.cq.cuny.edu/research.html>
8. Huenerfauth, MP (2003) American sign language natural language generation and machine translation systems. Technical Report, computer and information sciences, University of Pennsylvania. MS-CIS-03-32. <http://eniac.cs.cq.edu/matt/pubs/huenerfauth-2003-ms-cis-03-32-asl-nlg-mt-survey.pdf>
9. van Zijl L, Olivrin G (2008) South African sign language assistive translation. In: Eighth international ACM SIGACCESS conference on computers and accessibility. ASSETS 2006, pp 233–234
10. ASL System User Guide. http://idealab.tech.purdue.edu/ASL/tutorial/asl_tutorial.htm
11. jason1.wmv. <http://www.youtube.com/watch?v=9mP2sySx3zM>
12. Nicoletta Adamo-Villani-Research Projects. http://www2.tech.purdue.edu/cgt/facstaff/nadamovillani/funded_projects.htm
13. ESIGN Project Website. (Essential sign language information on government networks), <http://www.sign-lang.uni-hamburg.de/esign/>
14. esign_summary02.ppt. www.sign-lang.uni-hamburg.de/esign/esign_summary02.ppt
15. SigntelProject. The University of East Anglia. (Citat: 04 04 2012). www.uea.ac.uk/cmp/research/graphicsvisionspeech/vh/signtel+project
16. Dicta-Sign—ProjectPresentation. www.dictasign.eu/ and http://www.dictasign.eu/attach/Main/HomePage/project_presentation.pdf
17. Sign Speak Project website. www.signspeak.eu/
18. Prinetto P, Tiotto G, Principe AD Designing health care applications for the deaf. <http://eudl.eu/pdf/10.4108/ICST.PERVASIVEHEALTH2009.6072>
19. Rubén San-Segundo Hernández Translated by Robert Smith—Extract from improvement and expansion of a system for translating text to sign language—Chapter 5. Representation of the signs downloaded from <http://vhg.cmp.uea.ac.uk/tech/hamnosys/An%20intro%20to%20eSignEditor%20and%20HNS.pdf>
20. http://vh.cmp.uea.ac.uk/index.php/SiGML_Tools
21. Hanke T, Popescu H EDC-22124 ESIGN / 27960 deliverable D2.3. Virtual humans research for sign language animation. (Interactiv) (Citat: 06 04 2012). <http://vhg.cmp.uea.ac.uk/tech/esigneditor/eSIGN-D23rev2.pdf>
22. HamNoSys, Description, Website University of Hamburg downloaded from <http://www.sign-lang.uni-hamburg.de/projects/hamnosys.html>
23. Chiriac IA, Stoicu-Tivadar L, Podoleanu E (2014) Health education applications for deaf people—design models, hierarchies and levels. In: Proceedings of the 10th international scientific conference “eLearning and software for education. Bucharest, vol 2, April 24–25. <http://proceedings.elseconference.com/index.php?r=site/index&year=2014&index=papers&vol=14#>

Hybrid Neuro-Fuzzy Approaches for Abnormality Detection in Retinal Images

D. Jude Hemanth, Valentina E. Balas and J. Anitha

Abstract Abnormality detection in human retinal images is a challenging task. Soft computing techniques such as neural approaches and fuzzy approaches are widely used for these applications. However, there are significant drawbacks associated with these approaches. Artificial Neural Networks (ANN) yield high accuracy only when the training data is sufficiently large and accurate. On the other hand, fuzzy approaches are quite accurate but require significant computational time. Hence, a combination of neural and fuzzy approach is tested in this work which yields high accuracy within a reasonable time. The neuro-fuzzy model used in this work is Adaptive Neuro-Fuzzy Inference Systems (ANFIS) which possess the benefits of neural approaches and fuzzy approaches. The applicability of these techniques is explored in the context of categorizing the normal and abnormal retinal images. The performance of the classifiers is analyzed in terms of sensitivity, specificity, and classification accuracy and convergence time. Representatives from neural approaches and fuzzy approaches are also implemented for comparative analysis. The neural and fuzzy approach used in this work is Kohonen Neural Network and Fuzzy C-Means (FCM), respectively. Experimental analysis suggests promising results for the hybrid approach.

Keywords ANFIS · Neural network · Fuzzy C-means · Retinal images and classification accuracy

D. Jude Hemanth (✉) · J. Anitha
Department of ECE, Karunya University, Coimbatore, India
e-mail: jude_hemanth@rediffmail.com

J. Anitha
e-mail: rajivee1@rediffmail.com

V.E. Balas
Department of Automation and Applied Informatics, Aurel Vlaicu University
of Arad, Arad, Romania
e-mail: balas@drbalas.ro

1 Introduction

Image classification is a method of pattern recognition in which the abnormal images are differentiated from normal images. This methodology is widely preferred for medical image analysis and specifically in the field of ophthalmology. Conventionally, the abnormality is identified by the human observer which is highly prone to error. Several automated systems have been developed to overcome this drawback of wrong identification of abnormalities. ANN and fuzzy systems hold significant positions among these automated systems.

Several works have been developed based on ANN and fuzzy systems. A detailed analysis of the various applications of ANN in the medical field is given in [1]. The merits and demerits of the ANN are highlighted in this work. Pixel-based retinal image classification is implemented in [2]. Back propagation neural networks are used for this application. Multilayer feed forward neural networks based retinal abnormality identification is available in [3]. Bilevel classification is performed in this work and various performance measures are analyzed. Retinal blood vessel analysis using ANN is developed by [4]. Filtering methodologies in conjunction with the ANN are used for enhancing the performance of the system. ANN-based retinal image abnormality identification is also performed by [5]. Single layer neural networks are used in this work and a detailed analysis of the proposed approach is also shown in this report. However, the accuracy of such ANN-based approaches is limited which shows the nonfeasibility of such systems for real-time applications.

Fuzzy based classification approaches have been also reported in the literature. X-ray image classification using fuzzy membership functions is available in [6]. A comparative analysis with other classifiers is also shown in this work. Classification between different types of ultrasound medical images is carried out by [7]. A combination of fuzzy logic theory and Support Vector Machine (SVM) is used for this implementation. Fuzzy approaches have been also used to classify the abnormal mammogram images [8]. SVM is used in conjunction with the fuzzy approaches to classify the images. Few other fuzzy based medical image classification techniques are available in [9, 10]. The interesting fact about these earlier works is that the approaches are efficient in terms of accuracy but requires huge time for convergence.

One of the methodologies to incorporate the advantages of ANN and fuzzy is to develop a hybrid methodology. In this work, the application of the hybrid systems such as ANFIS for medical image classification is analyzed. Real-time retinal images are collected from hospitals and used in this work to test the efficiency of the proposed system. The proposed system is analyzed in terms of various performance measures which include the efficiency measures and convergence rate measures. A comparative analysis with the neural classifier and the fuzzy classifier validates the superior nature of the hybrid systems over the other approaches.

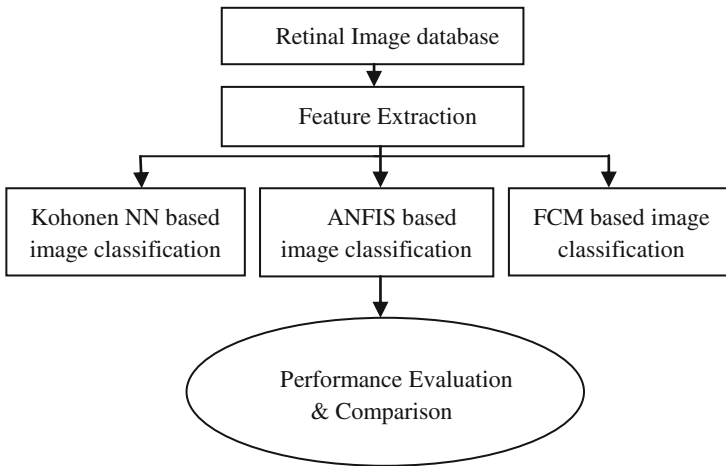


Fig. 1 Proposed framework of the automated system

2 Materials and Methods

The proposed flow diagram of the automated retinal image classification system is shown in Fig. 1.

The automated classification system consists of two parts: (a) Image database and feature extraction and (b) Classification using various approaches. The retinal images used in this work are collected from Lotus Eye Care Hospital, Coimbatore, India. Around 550 images are used in this work among which 260 images are from normal category and 290 images are from abnormal Diabetic Retinopathy (DR) category.

An extensive feature set is extracted from the input raw images. The features are then supplied as input to the classifiers. The classifiers are initially trained and then tested with unknown images. The performance measures are then analyzed from the experimental results.

3 Feature Extraction

Feature extraction is one of the important aspects of any image processing applications. The feature extraction concept is induced to represent the input categories in a specific manner. The features extracted from the normal category images must be significantly different from the features extracted from the abnormal category. The second objective of the feature extraction methodology is to reduce the complexity of the classifiers. Since only few extracted features represent the whole image, the computational complexity is significantly reduced.

In this work, 12 features are used to represent each image. Thus, an image of size 256×256 is reduced to 1×12 . Feature selection is very important, since the presence of irrelevant features may reduce the accuracy of the overall system. The features used in this work are Mean, Standard Deviation, Kurtosis, Skewness, Energy, Entropy, Correlation coefficient, Contrast, Variance, Cluster shade, Cluster prominence, and Inverse Difference Moment. These features are mostly textural features and they work well for any retinal image classification system. A detailed explanation on estimating these features are given in [11].

4 Classifiers

Three different types of classifiers are used in this work. One corresponds to the neural category, another corresponds to the fuzzy category, and the third classifier belongs to the hybrid neuro-fuzzy category.

4.1 Kohonen Neural Network

Kohonen neural network [12] belongs to the unsupervised neural network category. Since expert knowledge is not always available in prior, these unsupervised approaches are found to be more suitable for medical imaging applications. The significant advantage of Kohonen neural network is its simplicity which is essential for practical applications. The training algorithm is used to train the neural architecture, which stores the significant features in the neural network. The testing process is further used to categorize the unknown testing images.

4.1.1 Architecture

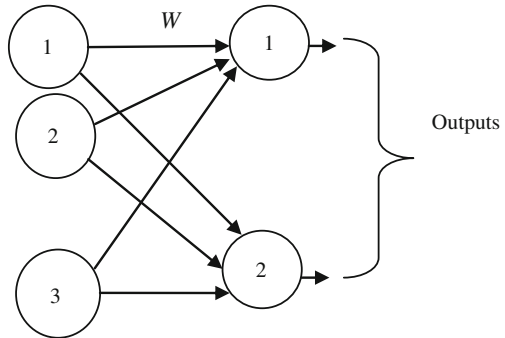
The framework of the Kohonen neural network is shown in Fig. 2.

The Kohonen neural network is a single layer network with an input layer and output layer. The number of neurons in the input layer is based on the number of input features and the number of neurons in the output layer is based on the number of output classes. A single weight matrix W is used to connect the two layers. It is essential to determine the values of the weight matrix which is done using the training algorithm.

4.1.2 Training Algorithm

The training algorithm of Kohonen neural network employs the “winner take-all” algorithm for the weight adjustment process. In this method, only the weights

Fig. 2 Architecture of Kohonen neural network



associated with the winner neuron will be adjusted while the other weight values remain the same. The detailed algorithm is given in the following steps.

- Step 1: Supply the inputs, randomly initialized weights, and the learning rate (α).
- Step 2: Determine the Euclidean distance between the inputs and the randomly initialized weights for each output layer neuron j .

$$D(j) = \sum (x_i - w_{ij})^2 \tag{1}$$

- Step 3: Find the output layer neuron j for which the distance value is minimum.
- Step 4: Adjust the weights of the links associated with the winner neuron using the following formula:

$$w(\text{new}) = w(\text{old}) + \alpha \cdot (y - w(\text{old})) \cdot x_i \tag{2}$$

- Step 5: Repeat the process for a specified number of iterations.
- Step 6: The stabilized set of weights is obtained when the maximum number of iterations is reached.

These stabilized set of weights are stored in the form of a matrix. The features are then extracted for an unknown input image and fed to the network. The distance measure is estimated with the stabilized weights. Each neuron in the output layer corresponds to the predefined class. The unknown input image is assigned to the class for which the distance value is minimum. The testing process is very quick, since it is free from iterations.

4.2 Fuzzy C-Means Approach

FCM algorithm [13] is an unsupervised algorithm which is mainly used for image segmentation. FCM involves the concept of fuzzy logic theory which mainly improves the accuracy of the overall system. Even though it is used for clustering

applications, few post-processing steps are included for the FCM to perform the operation of image classification.

4.2.1 FCM Algorithm

The detailed algorithm is given below through mathematical steps.

- Step 1: Initialize the number of clusters for the FCM algorithm. In this work, the number of clusters c is two which corresponds to the normal category and the abnormal category.
- Step 2: Initialize the membership values of each pixel for the different categories. These membership values, given by u_{ij} vary between 0 and 1. Thus, each pixel has two values for both the categories.
- Step 3: Calculate the centroid values using the following formula

$$c_i = \frac{\sum_j u_{ij}^m \cdot x_j}{\sum_j u_{ij}^m} \quad (3)$$

In this work, i varies from 1 to 2 and x_j corresponds to the j th data. Initially, the two-dimensional (2D) input image is rearranged to one-dimensional (1D) column for easier implementation.

- Step 4: Using the cluster center values, refine the initial membership values using the following formula

$$u_{ij} = \frac{1}{\sum_{k=1}^c \left(\frac{d_{ij}}{d_{kj}}\right)^{2/m-1}} \quad (4)$$

In the above equation, d_{ij} corresponds to the distance between the i th cluster center and j th input data. The constant m is called as fuzzy exponent and the value is greater than 2.

- Step 5: Using these membership values, the cluster center is again adjusted. This process continues till the following condition is reached.

$$u_{ij}(\text{new}) - u_{ij}(\text{old}) < \beta \quad (5)$$

In the above equation, β corresponds to the error tolerance value. If the difference between the current iteration's membership value and the previous iteration's membership value are very small, then it can be stated that the membership values are converged to the correct values.

- Step 6: After convergence, the membership value of each pixel is observed. The pixel is allotted to the category for which the membership value is maximum. The same procedure is used for all the pixels and the pixels are categorized to any one of the category.

Step 7: Check if at least one pixel belongs to the abnormal category. If yes, then that image is assigned to the abnormal category. If all the pixels belong to the normal category, then it is assigned to the normal category.

The same procedure is repeated for all the images and the entire input dataset is categorized either to the normal category or the abnormal category. The accuracy of such systems is usually good, but the time requirement for convergence is very high which limits the practical applications of such approaches.

4.3 Hybrid Neuro-Fuzzy Systems

ANN is comparatively quicker than fuzzy systems, but less accurate than fuzzy systems. However, practical applications demand both high accuracy and quick convergence. Thus, there is significant necessity for hybrid systems in order to incorporate both performance measures in the same system. In this work, a hybrid ANFIS system is proposed for the retinal image classification system.

4.3.1 Fuzzy IF-THEN Rules

Fuzzy IF-THEN rules are used to represent the input information in an accurate manner which is otherwise not accurate. The total number of input features used in this work is 12 and the number of output classes is 2. The total number of fuzzy rules used in this work is 4096. Some sample IF-THEN rules are shown below:

IF x_1 is a and x_2 is b ...and x_{12} is m , THEN output is class 1.

IF x_1 is r and x_2 is t ...and x_{12} is u , THEN output is class 2.

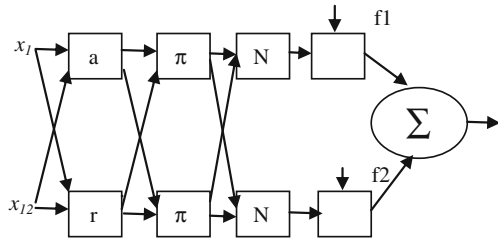
In the above rules, x_1, x_2, \dots, x_{12} corresponds to the input features. Even though many rules are framed, only one rule will be fired and used in the system for further processing.

4.3.2 Architecture

The architecture of Sugeno model ANFIS is shown in Fig. 3.

The architecture shown is the general ANFIS and it can be extended to any inputs and any number of fuzzy rules. These changes are usually reflected in Layer 1 of ANFIS which consists of premise parameters. The layer 2 performs the multiplication operation and Layer 3 performs the normalization operation. Layer 4 multiplies the inputs with the unknown function f_l which in turn consists of consequent parameters. Finally, the layer 5 performs the summation operation of all the

Fig. 3 Architecture of ANFIS



inputs to yield the overall output of the ANFIS system. The next step is the training process of ANFIS which sets the premise and consequent parameters.

4.3.3 ANFIS Training Ethodology

The proper selection of the number, the type, and the parameter of the fuzzy membership functions and rules is crucial for achieving the desired performance and in most situations, it is difficult. These parameters are often chosen based on trial and error method. This fact highlights the significance of tuning the fuzzy system. The ultimate aim of training the ANFIS system is to determine the optimal premise and consequent parameters.

The training algorithm is implemented in two paths: forward path and the reverse path. The entire algorithm is summarized below. The parameter set S is divided into two sets

$$S = S_1 \oplus S_2 \tag{6}$$

- S set of total parameters
- S_1 set of premise parameters
- S_2 set of consequent parameters
- \oplus direct sum.

For the forward path, least square method is applied to identify the consequent parameters. For a given set of values of S_1 , the following matrix equation can be obtained by plugging the training data.

$$A\Theta = y \tag{7}$$

where Θ contains the unknown parameters in S_2 . This is a linear square problem and the solution for Θ , which minimizes $\|A\Theta - y\|^2$, is the least square estimator.

$$\Theta^* = (A^T A)^{-1} A^T y \tag{8}$$

For the backward path, the error signals propagate backward. The premise parameters are updated by descent method, through minimizing the overall quadratic cost function

$$J(\Theta) = \frac{1}{2} \sum_{n=1}^N [y(k) - \hat{y}(k, \Theta)]^2 \tag{9}$$

in a recursive manner with respect to $\Theta_{(S_2)}$. The update of the parameters in the i th node can be written as

$$\hat{\Theta}_i(k) = \hat{\Theta}_i(k - 1) + \eta \frac{\partial^+ E(k)}{\partial \hat{\Theta}_i(k)} \tag{10}$$

where η is the learning rate and the gradient vector

$$\frac{\partial^+ E}{\partial \hat{\Theta}_i} = \varepsilon_i \frac{\partial \hat{z}_i}{\partial \hat{\Theta}_i} \tag{11}$$

where $\partial \hat{z}_i$ is the node output and ε_i is the back propagated error signal. The training algorithm identifies the optimal set of parameters which are further used for the testing process. If the output neuron value is greater than 0.5, then the input image is allotted to the second category. If it is less than 0.5, it is allotted to the first category. These categories are predefined and it is set based on the user application.

5 Experimental Results and Discussions

The experiments are carried out on the processor with 2 GB RAM and 1.66 clock frequencies. The software used for the implementation is MATLAB. The dataset used for the implementation is shown in Table 1.

The complete dataset is initially divided into the training data and the testing data. Initially, feature extraction is performed on these images. The features extracted from these images are sufficiently different between the categories but similar within the categories. The extracted features are supplied as input to the classifiers. The confusion matrix obtained for the classifiers for both the categories is shown in Table 2.

The level of correct classification and misclassification rate is illustrated in Table 2. In the above Table, class 1 corresponds to the normal category and class 2

Table 1 Experimental dataset

Input image category	Training dataset	Testing dataset
Normal	130	130
Abnormal	140	150

Table 2 Confusion matrix of the classifiers

Classifiers		Class 1	Class 2
Kohonen	Class 1	94	36
	Class 2	48	102
FCM	Class 1	111	19
	Class 2	25	125
ANFIS	Class 1	121	9
	Class 2	12	138

Table 3 Performance measures of the classifiers

Classifiers		TP	TN	FP	FN	Sensitivity	Specificity	CA (%)
Kohonen	Class 1	94	102	48	36	0.72	0.68	70
	Class 2	102	94	36	48	0.68	0.72	70
FCM	Class 1	111	125	25	19	0.85	0.83	84.2
	Class 2	125	111	19	25	0.83	0.85	84.2
ANFIS	Class 1	121	138	12	9	0.93	0.92	92.8
	Class 2	138	121	9	12	0.92	0.93	92.8

corresponds to the abnormal category. In Kohonen neural classifier, 94 images are correctly classified in the normal category and 102 images are correctly classified in the abnormal category. Thus, 196 images are correctly classified among 280 testing images. Similarly, 236 images are correctly classified for the FCM classifier and 259 images are correctly classified by the ANFIS classifier. The performance measures are further estimated from Table 2. The results are shown in Table 3.

In Table 3, TP corresponds to True Positive, TN corresponds to True Negative, FP corresponds to False Positive, and FN corresponds to False Negative. These values are estimated from the confusion matrix, and the performance measures are further estimated. The ideal values of sensitivity, specificity, and classification accuracy are infinity. A close observation of the results shown in Table 3 proves the efficiency of the ANFIS system in terms of accuracy. The sensitivity and specificity parameters are also better than the other classifiers.

FCM is better in comparison to the neural classifier in terms of accuracy but still inferior to the ANFIS system. The performance analysis in terms of convergence rate is shown in Table 4.

From Table 4, it is evident that the convergence rate is better for the hybrid neuro-fuzzy classifier than the other classifiers. Thus, this work has highlighted the necessity of hybrid systems for performance enhancement in practical applications.

Table 4 Convergence rate analysis of the classifiers

Classifiers	Convergence time (CPU seconds)
Kohonen neural network	6120
FCM	10,654
ANFIS	1251

6 Conclusion

In this work, the significance of hybrid neuro-fuzzy systems is emphasized in the context of retinal image classification. It has been also verified that ANN-based classifiers are quick, but less accurate than fuzzy systems. The experimental results of FCM show that the time required for convergence is very high but relatively accurate. The main objective of this work is proved with the experimental results which illustrates that hybrid systems possess the advantages of both ANN and fuzzy systems. Thus, an alternate for conventional neural and fuzzy systems is suggested in this work for medical image analysis applications.

Acknowledgments The authors thank Dr. A. Indumathy, Lotus Eye Care Hospital, Coimbatore, India for her help regarding database validation. The authors also wish to thank Council of Scientific and Industrial Research (CSIR), New Delhi, India for the financial assistance toward this research (Scheme No: 22(0592)/12/EMR-II).

References

1. Yasmin MS, Mohsin S (2013) Neural networks in medical imaging applications: a survey. *World Appl Sci J* 22:85–96
2. Marin D, Aquino A, Arias MEG, Bravo JM (2010) A new supervised method for blood vessel segmentation in retinal images by using gray level and moment invariant based features. *IEEE Trans Med Imaging*. doi:10.1109/TMI.2010.2064333
3. Shaeidi A (2010) An algorithm for identification of retinal microaneurysms. *J Serbian Soc Comput Mech* 4:43–51
4. Baroni M, Fortunato P, Pollazzi L, Torre LA (2012) Multiscale filtering and neural network classification for segmentation and analysis of retinal vessels. *J Webmed Cent Biomed Eng* 3:1–16
5. David J, Krishnan R, Kumar AS (2008) Neural network based retinal image analysis. *Proc IEEE Int. Congr Signal Image Process* 2:49–53
6. Ghofrani F et al (2012) Fuzzy based medical X-ray image classification. *J Med Signals Sens* 2:73–81
7. Md. Sohail AS, et al (2011) Classification of ultrasound medical images using distance based feature selection and fuzzy-SVM. In: *Pattern recognition and image analysis (LNCS)*, vol 6669, pp 176–183
8. Bai X, Qian X (2008) Medical image classification based on fuzzy support vector machines. *Proc Int Conf Intell Comput Technol Autom* 2:145–149
9. Jaganathan Y, Vennila I (2013) A hybrid approach based medical image retrieval system using feature optimized classification similarity framework. *Am J Appl Sci* 10:549–562
10. Tsai DY et al (2004) Medical image classification using genetic algorithm based fuzzy logic approach. *J Electron Imaging* 13:780–788
11. Haralick RM et al (1973) Textural features for image classification. *IEEE Trans Syst Man Cybern* 3:610–621
12. Fausett L (2008) *Fundamentals of neural networks-architectures algorithms and applications*. Pearson Education, New Delhi
13. Jang JSR et al (1997) Neurofuzzy and soft computing-a computational approach to learning and machine intelligence. *IEEE Trans Autom Control* 42:1482–1484

Optimistic Multi-granulation Rough Set-Based Classification for Neonatal Jaundice Diagnosis

S. Senthil Kumar, H. Hannah Inbarani, Ahmad Taher Azar,
Hala S. Own, Valentina Emilia Balas and Teodora Olariu

Abstract Neonatal jaundice diagnosis has been approached by various machine learning techniques. Pattern recognition algorithms are capable of improving the quality of prediction, early diagnosis of diseases, and disease classification. Pattern recognition algorithm results in Neonatal jaundice diagnosis or description of jaundice treatment by the medical specialist. This research focuses on applying rough set-based data mining techniques for Neonatal jaundice data to discover locally frequent identification of jaundice diseases. This work applies Optimistic Multi-granulation rough set model (OMGRS) for Neonatal jaundice data classification. Multi-granulation rough set provides efficient results than single granulation rough set model and soft rough set-based classifier model. The performance of the proposed Multi-granulation rough set-based classification is compared with other Naïve bayes, Back Propagation Neural Networks (BPN), and Kth Nearest Neighbor (KNN) approaches using various classification measures.

S. Senthil Kumar (✉) · H. Hannah Inbarani
Department of Computer Science, Periyar University, Salem 636011, India
e-mail: pkssenthilmca@gmail.com

H. Hannah Inbarani
e-mail: hhinba@gmail.com

A.T. Azar
Faculty of Computers and Information, Benha University, Banha, Egypt
e-mail: ahmad_t_azar@ieee.org

H.S. Own
National Research Institute of Astronomy and Geophysics, Helwan, Egypt
e-mail: halaown@gmail.com

V.E. Balas
Aurel Vlaicu University, Arad, Romania
e-mail: balas@drbalas.ro

T. Olariu
Vasile Goldis West University of Arad, Satu Mare, Romania
e-mail: olariu_teodora@yahoo.com

Keywords Rough set · Optimistic multi-granulation rough set · Neonatal jaundice data · Classification · and Comparative analysis of classification measures

1 Introduction

Neonatal jaundice is emerging as an increasingly common problem in newborns. Jaundice is the most common disease of the newborn, and although being benign in most cases it can lead to severe neurological consequences if poorly evaluated. In different areas of medicine, data mining has contributed to improve the results obtained with other methodologies. Neonatal jaundice is the most common clinical manifestation of newborns. Hyperbilirubinemia, the cause of jaundice, appears in approximately 60 % of the newborns at term and almost in all preterm neonates, with prevalence greater than 80 %. The correct identification of newborns at risk of developing severe hyperbilirubinemia and kernicterus is essential for early treatment. Therefore, preventing the newborn from toxic bilirubin levels, especially for their immature central nervous system, has become a main concern for pediatricians. Assessing the risk of neonatal jaundice is currently done with the support of specific monograms that take into account the age of the newborns, the serum or transcutaneous bilirubin levels, and associated risk factors [1–3].

Rough set introduced by Pawlak, is a mathematical tool for dealing with uncertainty or incomplete information and knowledge [4–6]. Rough Set theory has become a valuable tool in the resolution of various problems, such as representation of uncertain or imprecise knowledge; knowledge analysis; evaluation of quality and availability of information with respect to consistency; identification and evaluation of data dependency; reasoning based on uncertain and reduct of information data. The extent of rough set applications used today is much wider than in the past, principally in the ranges of medicine, analysis of database attributes and process control. In the past 15 years, several extensions of the rough set model have been proposed in terms of various requirements, such as the rough set model based on tolerance relation, the soft rough set model, the rough soft set model, the fuzzy rough set model, and the rough fuzzy set model [7]. In the view of granular computing, a general concept labeled by a set is always characterized via the so-called upper and lower approximations under a single granulation, i.e., the concept is showed by known knowledge induced from a single relation (such as equivalence relation, tolerance relation, and reflexive relation) on the universe. Multi-granulation rough set approximations are defined by using multi-equivalence on the universe. In Example 1, the approximation of a set is discussed by using two equivalence relations on the universe, i.e., the target concept is described by two granulation spaces. This paper discusses how optimistic multi-granulation rough set theory [5, 8–13] can be used for the analysis of Neonatal jaundice data [14–16], and for generating classification rules from a set of observed samples of the Neonatal jaundice data. Despite the use of different methodologies to assess the risk of

developing neonatal hyperbilirubinemia, this studies point out a growing resurgence of bilirubin encephalopathy and kernicterus, identifying the need to improve diagnosis. This paper is organized as follows. Section 2 describes theoretical concepts of rough set and multi-granulation rough set data analysis. Section 3 describes the overall structure of methodology. Section 4 describes proposed algorithm, which is relevant to the work and rule generation algorithm is presented. Section 5 describes dataset information. Experimental results are reported and Comparison with Naïve bayes, KNN, and BPN classifier algorithm is given in Sect. 6. Section 7 describes discussion about experimental results. Finally, conclusion is discussed in Sect. 8.

2 Preliminaries

2.1 Rough Sets

Rough set theory was initiated by Pawlak [4–6] for dealing with vagueness and granularity in information systems. This theory handles the approximation of an arbitrary subset of a universe by two definable or observable subsets called lower and upper approximations. It has been successfully applied to machine learning, intelligent systems, inductive reasoning, pattern recognition, image processing, signal analysis, knowledge discovery, decision analysis, expert systems, and many other fields.

Definition 1 Let R be an equivalence relation on U . The pair (U, R) is called a Pawlak approximation space. The equivalence relation R is often called an indiscernibility relation. Using the indiscernibility relation R , one can define the following two rough approximations:

$$R_*(x) = \{x \in U[x]_R \subseteq X\} \quad (1)$$

$$R^*(x) = \{x \in U : [x]_R \cap X \neq \emptyset\} \quad (2)$$

$R_*(x)$ and $R^*(x)$ are called the Pawlak lower approximation and the Pawlak upper approximation of X , respectively.

2.2 Optimistic Multi-Granulation Rough Sets

Rough set models are based on single granulation; they also called the single granulation rough sets. In the optimistic multi-granulation rough set (OMGRS), the target is approximated through the multiple granulations. In lower approximation, the word optimistic is used to express the idea that is in multiple independent granulations, we need only at least one of the granulations to satisfy with the

inclusion condition between knowledge granule and target concept [8, 10–13, 15, 17–19]. The upper approximation of OMGRS is defined by the complement of the lower approximation.

Definition 2 Let $S = (U, AT, f)$ is called a complete target information system if values of all attributes AT and D for all objects from U are regular (known), where AT is called the conditional attributes and D is called the decision attribute, \hat{P}, \hat{Q} be two partitions on the universe U , and $X \subseteq U$. The lower approximation and the upper approximation of X in U are defined by the following:

$$\underline{X}\hat{P} + \hat{Q} = \{x : \hat{P}(x) \subseteq X \text{ or } x: \hat{Q}(x) \subseteq X\} \tag{3}$$

$$\overline{X}\hat{P} + \hat{Q} = \sim(\sim X)\hat{P} + \hat{Q} \tag{4}$$

Example 1 Table 1 depicts a sample information system containing some information about a project. L and P are the conditional attributes of the system, whereas D is the decision attribute.

Let $X = \{e1, e2, e6, e8\}$. Three partitions are induced from Table 1 as follows:

$$\begin{aligned} \hat{L} &= \{\{e1, e7\}, \{e2, e3, e4, e5, e6\}, \{e8\}\} \\ \hat{P} &= \{\{e1, e2\}, \{e3, e4, e5\}, \{e6, e7, e8\}\} \\ \widehat{L\hat{P}} &= \{\{e1\}, \{e2\}, \{e3, e4, e5\}, \{e6\}, \{e7\}, \{e8\}\} \end{aligned}$$

Optimistic Multi-granulation Lower Approximation

The lower approximation of a target concept in complete information systems using multi-equivalence relation is defined as follows:

$$\underline{X}\hat{P} + \hat{Q} = \{x : \hat{P}(x) \subseteq X \text{ or } x : \hat{Q}(x) \subseteq X\} \tag{5}$$

Table 1 A sample information system

U	L	P	Decision
$e1$	1	1	1
$e2$	2	1	1
$e3$	2	2	0
$e4$	2	2	0
$e5$	2	2	0
$e6$	2	3	1
$e7$	1	3	0
$e8$	3	3	1

For example, for Table 1

$$\underline{X}\hat{P} + \hat{Q} = \{e8\} \cup \{e1, e2\} = \{e1, e2, e8\}$$

Optimistic Multi-granulation Upper Approximation

Multi-granulation upper approximation is a complement of multi-granulation lower approximation.

$$\bar{X}\hat{P} + \hat{Q} = \sim(\sim X)\hat{P} + \hat{Q} \tag{6}$$

For example for Table 1, $\underline{X}\hat{P} + \hat{Q} = \{e1, e2, e3, e4, e5, e6, e7, e8\} \cap \{e1, e2, e6, e7, e8\} = \{e1, e2, e6, e7, e8\}$

But, the lower approximation and the upper approximation of X based on Pawlak’s rough set theory are as follows:

$$\begin{aligned} \underline{X}\widehat{LUP} &= \{Y \in \widehat{LUP} : Y\} = \{e1, e2, e6, e8\} \\ \bar{X}\widehat{LUP} &= \{Y \in \widehat{LUP} : Y \cap X \neq \emptyset\} = \{e1, e2, e6, e8\} \end{aligned}$$

3 Methodology

Figure 1 show over all structure of classification. First stage of classification is data acquisition. Data acquisition is the process of taking data which should be acceptable to the computing device for further processing.

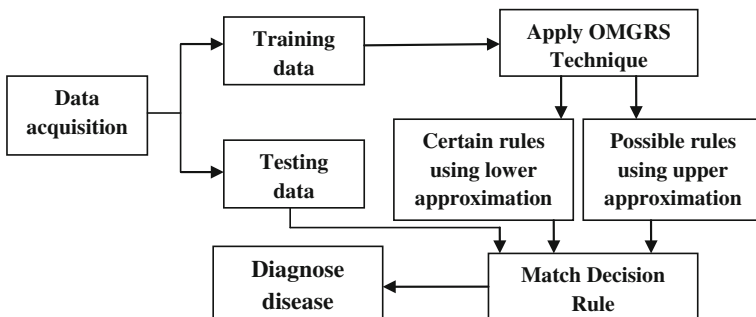


Fig. 1 Proposed classification structure

Table 2 Proposed algorithm

Proposed Algorithm: OMGRS-based classification

Input: Given Dataset with conditional attributes 1, 2, ..., n - 1 and the Decision attribute n.
Output: Generated Decision Rules

Step 1: Construct the OMGRS-based lower approximation for the given dataset.

$$\underline{X}\hat{P} + \hat{Q} = \{x : \hat{P}(x) \subseteq X \text{ or } x : \hat{Q}(x) \subseteq X\} \quad (7)$$

Step 2: Construct the OMGRS-based upper approximation for the given dataset

$$\bar{X}\hat{P} + \hat{Q} = \sim(\sim X)\hat{P} + \hat{Q} \quad (8)$$

Step 3: Generate certain rules using OMGRS-based lower approximation.
Step 4: Generate possible rules using OMGRS-based upper approximation.

Data acquisition is usually made by sensors, digitizing machine, and scanners. Second stage is data analysis. Later data acquisition, the task of analysis begins. During data analysis step, the learning about the data takes place and information is collected about the different events and pattern classes available in the data. This information or knowledge about the data is used for further processing. Dataset presented to a classification is divided into two sets: training set and testing set. The efficiency of classifier is checked by presenting testing set to it. Proposed algorithm is depicted in Table 2. During third stage, multi-granulation rough set classification is applied for training data. Its fortitude is to decide the group of new data on the basis of knowledge generated from certain rules and possible rules. In the next step, matching decision rules are applied for test data. Finally, classification measures are applied to evaluate the performance of various classification approaches for Neonatal jaundice disease diagnosis.

4 Proposed Algorithm

Optimistic Multi-granulation Rough set based classification approach is presented in Table 2. In this approach, OMGRS lower approximation of the given dataset based on Decision class C are constructed in step 1. In the second step, OMGRS upper approximation of the given dataset based on Decision class C are constructed. In the third step, certain rules are generated based on OMGRS lower approximation. In the fourth step, possible rules are generated based on OMGRS upper approximation.

The decision rules generated using proposed algorithm for the example presented in Table 1 is given in Table 3.

Table 3 Example for proposed work

A sample of the dataset is an example 1 in order to extract the rules.

Input: Conditional attributes L and P . Decision attribute X
Output: Generate decision rules

Step 1: Construct the OMGRS lower approximation for the given data in Table 1.

$$\underline{X}\hat{P} + \hat{Q} = \{e1, e2, e8\}$$

Step 2: Construct the OMGRS upper approximation for the given data in Table 1.

$$\overline{X}\hat{P} + \hat{Q} = \{e1, e2, e6, e7, e8\}$$

Step 3: Generate certain rules using OMGRS lower approximation

$$\begin{aligned} \text{If } L = 1 \text{ and } P = 1 & \Rightarrow D = 1 \\ \text{If } L = 2 \text{ and } P = 1 & \Rightarrow D = 1 \\ \text{If } L = 3 \text{ and } P = 3 & \Rightarrow D = 1 \end{aligned}$$

Step 4: Generate possible rules using OMGRS upper approximation

$$\begin{aligned} \text{If } L = 1 \text{ and } P = 1 & \Rightarrow D = 1 \\ \text{If } L = 2 \text{ and } P = 1 & \Rightarrow D = 1 \\ \text{If } L = 2 \text{ and } P = 3 & \Rightarrow D = 1 \\ \text{If } L = 1 \text{ and } P = 3 & \Rightarrow D = 0 \\ \text{If } L = 3 \text{ and } P = 3 & \Rightarrow D = 1 \end{aligned}$$

5 Data Description

A total of 808 medical records were collected from newborns during January–December 2007 in Neonatal Intensive Care Unit in Cairo, Egypt. Retrospective data of all neonatal jaundice cases were collected from patient’s files and descriptive analysis of these data was done. These data include the following: sex, gestational age, postnatal age, and weight at day of presentation, the day of onset of jaundice after delivery, and duration of stay in hospital. The ratio of 474 male to 334 female was 1.4:1. There were 643 full terms (79.58 %), 53 near terms (6.55 %), and 113 preterms (13.98 %). The mean postnatal age of patients on admission was 5.75 ± 4 days (ranging from 1 to 20 days except one case diagnosed as Crigler–Najjar syndrome, was admitted to NICU at 60-days old). The median age of onset of jaundice was three days with the interquartile range (IQR) of one day. The mean weight of patients was 2658.6 ± 710 g (ranging from 740 to 4900 g). The mean duration of stay is of 7.21 ± 8.72 days (ranging from 1 to 86 days). The total and direct bilirubin levels were measured several times for the studied patients with the detection of peak of total bilirubin and the day on which the peak occurred. The peak of total bilirubin ranged from 6.5 to 65.5 mg/dl with a mean value of 24.55 ± 9.16 at mean age 6.2 ± 3.58 days (ranging from 1 to 33 days). Among 808 studied cases, a peak of total bilirubin was reported in files of 781 cases. The total bilirubin level was measured at day of presentation, then after 24 hour later, then after two days, afterwards before discharge or death. The mean values were 23.1 ± 9.87 (ranging from 2.1 to 65.5 mg/dl), 19.85 ± 6.76 (ranging from 4.9 to 49.5 mg/dl), 16.09 ± 5.84 (ranging from 3.1 to 51.3 mg/dl), and 12.34 ± 6 (ranging from 0.74 to 51.7 mg/dl),

respectively. The direct bilirubin level was measured at the same time with total bilirubin. The mean values were 1.55 ± 3.4 (ranging from 0.02 to 38 mg/dl), 1.58 ± 3.21 (ranging from 0.03 to 25.36 mg/dl), 1.65 ± 3.35 (ranging from 0.01 to 24.8 mg/dl), and 1.22 ± 2.64 (ranging from 0.01 to 25.36 mg/dl), respectively. These data are presented for prediction of the risk of neonatal jaundice and extreme hyperbilirubinemia of newborns. The dataset of 808 records, 16 predictor variables, and 1 target variable was constructed. The target variable “pattern” has three possible values “1” (indirect hyperbilirubinemia), “2” (changed from indirect to direct hyperbilirubinemia), and “3” (direct hyperbilirubinemia) [1].

6 Experimental Analysis

Classification [10, 14, 15, 20] of complex measurements is essential in an analysis process. Accurate classification of measurements may in fact be the most critical part of the diagnostic process. Several classification measures are available in the pattern recognition techniques. The proposed algorithm is applied to training data and the generated classification rules are matched with test data to determine exact class. The attributes in these data sets are all numerical. 80 % of the data is chosen as the training set and 20 % as testing data. In this chapter, seven classification measures such as precision, recall, F-measure Folke–Mallows, Kulczynski, Rand and Russel–Rao indexes were applied for evaluating the accuracy of classification [21]. Precision, recall, and F-measure are external measures in classification analysis and other four measures are internal measures in classification analysis. Most of the researchers have applied only external measures. In this chapter, external measures along with four internal measures are applied to validate the proposed approaches. Various validation measures are applied to evaluate the accuracy of proposed classification approaches for diagnostic process. Table 5 and Fig. 2 presents different algorithms for the detection of Neonatal jaundice disease and effectiveness of those algorithms are computed using various validation measures. Table 4 depicts various validation measures used in this work.

Fig. 2 Comparative analysis of classification algorithms for neonatal jaundice dataset

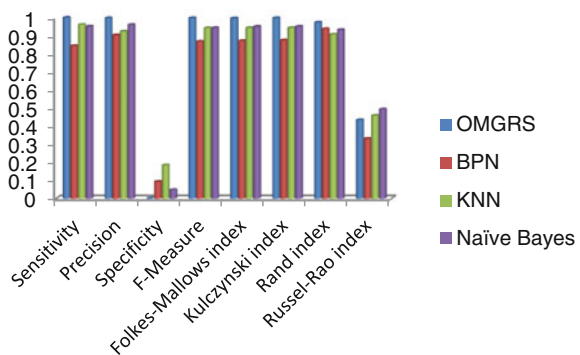


Table 4 Various classification measures

Precision = $\frac{\text{True positive}}{\text{True positive} + \text{False positive}}$
Recall (Sensitivity) = $\frac{\text{True positive}}{\text{True positive} + \text{False negative}}$
Specificity = $\frac{\text{True positive}}{\text{True positive} + \text{True negative}}$
F-Measure (Czekanowski–Dice index) = $2 * \frac{\text{Precision} * \text{Recall}}{\text{Precision} + \text{Recall}}$
Folkes–Mallows index = $\sqrt{\text{Precision} * \text{Recall}}$
Kulczynski index = $\frac{1}{2}(\text{Precision} + \text{Recall})$
Rand index = $\frac{(\text{True positive} + \text{False negative})}{(\text{True positive} + \text{True negative} + \text{False positive} + \text{False negative})}$
Russel–Rao index = $\frac{\text{True positive}}{(\text{True positive} + \text{True negative} + \text{False positive} + \text{False negative})}$

7 Discussion

When compared with the traditional methods, the prediction with the application of data mining techniques offered interesting results. Optimistic multi-granulation rough sets are widely and successfully used models for classification, forecasting, and problem solving. OMGRS is proposed for the diagnosis of Neonatal jaundice diseases. The main idea of this data set is to construct the proposed model, which will perform the presumptive diagnosis of Neonatal jaundice data. To evaluate the effectiveness of the Optimistic multi-granulation rough set technique, Neonatal jaundice data set is used. A number of useful performance metrics in medical applications which include Precision, Recall, Specificity, F-measure, Folke–Mallows, Kulczynski, Rand and Russel–Rao indexes are computed. The results are analyzed and compared with those from other methods available in the literature. The experimental outcomes positively demonstrated that the OMGRS classification method is effective in undertaking Neonatal jaundice data classification tasks. However, in practice, because it presents better accuracy results, the pediatricians base their assessment in the combination of clinical risk factors with the measures presented by the newborns. Table 5 and Fig. 2 illustrated the performance of proposed as well as compared classification approaches. As illustrated in the figure, OMGRS-based classification outperforms all the other classification approaches for Neonatal jaundice data set. Precision, Recall, Specificity, F-measure, Folke–Mallows, Kulczynski, and Rand indexes of OMGRS-based classification are higher than that of KNN, BPN, and Naïve bayes. Based on, Russell-Rao index Naïve bayes classification approaches, more importantly, the multi-granulation rough set only is able to produce good results than naïve bayes, BPN, and KNN. As a result, domain users (i.e., medical practitioners) are able to comprehend the prediction

Table 5 Performance analysis of classification algorithms for Neonatal jaundice dataset

	OMGRS	BPN	KNN	Naïve Bayes
Sensitivity	1.000	0.845	0.961	0.951
Precision	0.998	0.904	0.924	0.961
Specificity	0.002	0.093	0.185	0.049
<i>F</i> -Measure	0.998	0.868	0.942	0.943
Folkes–Mallows index	0.997	0.871	0.943	0.950
Kulczynski index	0.998	0.875	0.943	0.950
Rand index	0.974	0.938	0.908	0.932
Russel–Rao index	0.435	0.331	0.458	0.494

given by the multi-granulation rough set technique; hence its role is essential as a medical decision tool. Overall, the results indicate that multi-granulation rough set method performs better than all other methods. This multi-granulation rough set can be applied to a variety of Neonatal jaundice data. However, methods that are specialized to particular applications can often achieve better performance by taking into account former information. Selection of an applicable approach to a classification problem can therefore be a difficult dilemma. In consequence, still there is much room for over current medical data classification tasks. Therefore, there is a great potential for the use of data mining techniques for Neonatal jaundice data classification, which has been fully examined and would be one of the interesting directions for future research.

8 Conclusion

In this chapter, four classification techniques in data mining to predict Neonatal jaundice disease in patients are compared: rule-based OMGRS, BPN, Naïve bayes, and KNN. These techniques are compared on basis of classification measures of Precision, Recall, Specificity, *F*-Measure, Folke–Mallows, Kulczynski, Rand and Russel–Rao indexes. Our studies showed that OMGRS model turned out to be the best classifier for Neonatal jaundice disease prediction. In future, we intend to improve performance of these basic classification techniques by creating meta-model which will be used to predict medical disease in patients.

Acknowledgments The second author would like to thank UGC, New Delhi for the financial support received under UGC Major Research Project No. F-41-650/2012 (SR).

References

1. Ferreira D, Oliveira A, Freitas A (2012) Applying data mining techniques to improve diagnosis in neonatal jaundice. *BMC Med Inform Decis Mak* 12(7):143. doi:[10.1186/1472-6947-12-143](https://doi.org/10.1186/1472-6947-12-143)
2. Owna HS, Abraham A (2012) A new weighted rough set framework based classification for Egyptian Neonatal Jaundice. *Appl Soft Comput* 12(3):999–1005
3. Colletti JE, Kothari S, Jackson DM, Kilgore KP, Barringer K (2007) An emergency medicine approach to neonatal hyperbilirubinemia. *Emerg Med Clin North Am* 25(4):1117–1135
4. Pawlak Z (1982) Rough sets. *Int J Comput Inf Sci* 11(5):341–356
5. Pawlak Z, Skowron A (2007) Rough sets: some extensions. *information. Science* 177(1):28–40
6. Pawlak Z, Skowron A (2007) Rough sets and Boolean reasoning. *Inf Sci* 177:41–73
7. Dubois D, Prade H (1990) Rough fuzzy sets and fuzzy rough sets. *Int J Gen Syst* 17(2–3):191–209
8. Raghavan R (2013) Validation over basic set operations of internal structure of multi granular rough sets. *Int J Latest Res Eng Comput(IJLREC)* 1(2):34–42
9. Tripathy BK, Panda GK, Mitra A (2012) Incomplete multigranulation based on rough intuitionistic fuzzy sets. *UNIASCIT* 2(1):118–124
10. Chen W, Wei X, Xibei Y, Lijuan W (2014) A variable precision rough set model based on multi-granulation and tolerance. *Int J Eng Innov Technol* 3(7):1–6
11. Xu W, Zhang X, Wang Q (2012) A generalized multi-granulation rough set approach. *Bio-Inspired Comput Appl Lect Notes Comput Sci* 6840:681–689
12. Yang X, Song X, Dou H, Yang J (2011) Multi-granulation rough set: from crisp to fuzzy case. *Ann Fuzzy Math Info* 1(1):55–70
13. Qian Y, Liang J, Yao Y, Dang C (2010) MGRS: a multi-granulation rough set. *Inf Sci* 180(6):949–970
14. Seera M, Lim CH (2014) A hybrid intelligent system for medical data classification. *Expert Syst Appl* 41(5):2239–2249
15. Kumar SS, Inbarani HH, Udhayakumar S (2014) Modified soft rough set for multiclass classification. *Adv Intell Syst Comput* 246:379–384. doi:[10.1007/978-81-322-1680-3_41](https://doi.org/10.1007/978-81-322-1680-3_41)
16. Kumar SU, Inbarani HH, Kumar SS: Bijective soft set based classification of medical data. In: *International conference on pattern recognition, informatics and medical engineering (PRIME)*, Salem, pp 517–521, 21–22 Feb 2013
17. Zhang M, Xu W, Yang X, Tang Z (2014) Incomplete Variable Multigranulation Rough Sets Decision. *Int J Appl Math Inf Sci* 8(3):1159–1166
18. Raghavan R, Tripathy BK (2011) On some topological properties of multigranular rough sets. *Adv Appl Sci Res* 2(3):536–543
19. Raghavan R, Tripathy BK (2013) On some comparison properties of rough sets based on multigranulations and types of multigranular approximations of classifications. *Int J Intell Syst Appl* 06:70–77
20. Kumar SU, Inbarani HH, Kumar SS (2014) Improved bijective-soft-set-based classification for gene expression data. *Adv Intell Syst Comput* 246:127–132
21. Desgraupes B (2013) Clustering indices, University of Paris Ouest—Lab Modal’X, 1–34, 2013

Boosted Decision Trees for Vertebral Column Disease Diagnosis

Ahmad Taher Azar, Hanaa S. Ali, Valentina E. Balas, Teodora Olariu and Rujita Ciurea

Abstract Vertebral column diseases are of the main public health problems which cause a negative impact on patients. Disk hernia and spondylolisthesis are examples of pathologies of the vertebral column which cause intensive pain. Data mining tools play an important role in medical decision making and deal with human short-term memory limitations quite effectively. This paper presents a decision support tool that can help in detection of pathology on the vertebral column using three types of decision trees classifiers. They are Single Decision Tree (SDT), Boosted Decision Tree (BDT), and Decision Tree Forest (DTF). Decision Tree and Regression (DTREG) software package is used for simulation and the database is available from UCI Machine Learning Repository. The performance of the proposed structure is evaluated in terms of accuracy, sensitivity, specificity, ROC curves, and other metrics. The results showed that the accuracies of SDT and BDT in the training phase are 90.65 and 96.77 %, respectively. BDT performed better than SDT for all performance metrics. Value of ROC for BDT in the training phase is 0.9952. In the validation phase, BDT achieved 84.84 % accuracy, which is superior to SDT (81.94 %) and DTF (84.19 %). Results showed also that grade of spondylolisthesis is the most relevant feature for classification using BDT classifier.

A.T. Azar (✉)

Faculty of Computer and Information, Benha University, Benha, Egypt
e-mail: Ahmad_t_azar@ieee.org

H.S. Ali

Faculty of Engineering, Zagazig University, Zagazig, Sharkia, Egypt
e-mail: hanahshaker@yahoo.com

V.E. Balas

Aurel Vlaicu University of Arad, Arad, Romania
e-mail: balas@drbalas.ro

T. Olariu · R. Ciurea

Vasile Goldis West University of Arad, Arad, Romania
e-mail: olariu_teodora@yahoo.com

R. Ciurea

e-mail: dr.ciurea@yahoo.com

Keywords Vertebral column · Disk hernia · Spondylolisthesis · Machine learning · Single decision tree · Boosted trees · Tree forest · Accuracy · Sensitivity · Specificity · ROC

1 Introduction

The vertebral column is a system composed of a group of vertebrae, intervertebral disks, nerves, muscles, medulla, and joints. It plays an important role in the biomechanical system [6, 34]. The main function of the vertebral column is to provide support for the human body and to protect the spinal cord and nerve roots. The spinal cord is a major pathway for traveling motor and sensory signals between brain and the peripheral nervous system. When a spinal cord injury occurs, the spinal tracks carrying signals between the brain and organs are disrupted. The vertebral column is also responsible for body's movement axes making movement possible in three levels: frontal, sagittal, and transversal [1, 28, 29].

This complex system can suffer dysfunctions that cause backaches. The most common examples of pathologies of the vertebral column are disk hernia and spondylolisthesis. When the core of the intervertebral disk migrates from the center of the disk to the periphery, disk hernia appears. This may occur suddenly in an event such as a fall or an accident or may occur gradually with repetitive straining of the spine. Spondylolisthesis occurs when one of vertebrae slip in relation to the others. This slipping occurs generally toward the base of the spine in the lumbar region, causing a weakness in the rings of the lumbar vertebrae [22].

Several challenging problems in the biomedical domain and the set of powerful Machine Learning (ML) techniques have resulted in a new domain on its own, where the power and beauty of these techniques can be fully exploited to obtain proper solutions to these challenges. Machine learning techniques such as Support Vector Machines (SVM) and Artificial Neural Networks (ANN) are widely applied to several medical fields. The reason is that the capacity of human diagnostic is significantly worse than the neural system's diagnostic under adverse conditions such as stress, fatigue, and little technical knowledge [15, 22]. One of the most attractive features of ML is that it shares problems and tools with other fields such as statistics and signal processing. It takes advantage of the synergy of these fields thus providing robust solutions that use different fields of knowledge [23]. In general, ML methods use training data to induce general models that can detect the presence or absence of patterns in new (test) data. A learning algorithm is applied to the set of training vectors, generating a classifier model. Multi-class pattern recognition has a wide range of applications and is applied in many real-world problems which require the discrimination of different categories. The main aim of the classification problems is to construct robust, stable, successful, and fast classification models utilizing features of the problem dataset [5, 15, 18].

In this paper, decision trees classifiers are used for the detection of pathology on the vertebral column. Three types of classifiers are used; Single Decision Tree (SDT), Boosted Decision Tree (BDT), and Decision Tree Forest (DTF). These systems classify the cases in two categories: normal and abnormal. The normal ones are those characterizing a healthy patient. The abnormal ones include disk hernia and spondylolisthesis.

The rest of the paper is organized as follows. Section 2 depicts the related work. Subjects and methods are introduced in Sect. 3. Data analysis using the proposed systems is described in Sect. 4. Results and discussion are presented in Sect. 5. Finally, conclusion and future directions are given in Sect. 6.

2 Related Work

Neto and Barreto [21], reported a performance comparison among standalone machine learning algorithms and their combinations when applied in the field of orthopedics to a medical diagnosis problem. They used SVM, Multiple Layer Perceptron (MLP), and Generalized Regression Neural Network (GRNN) for classification. They also reported confusion matrices of all learning algorithms, and studied the effects of diversity in the design of the ensembles. Their results indicated that the ensembles of classifiers have better generalization performance than standalone classifiers. The accuracy obtained was 82 % using SVM, 83 % using MLP, and 75 % using GRNN. After ensembling these classifiers they become C-SVM, C-MLP, and C-GRNN, and reached 94, 88, and 81 %, respectively. Neto et al. [22], analyzed the incorporation of the reject option to hold a decision on the diagnostic of pathologies on the vertebral column. They applied their technique on the same UCI dataset and compared it with several machine learning techniques. Incorporation of the reject option provided better results than traditional learning techniques, even when rejecting few instances. They could reach average approximate accuracy of 85 %. A hybrid Case-Based Reasoning (CBR) and Artificial Neural Network (ANN) is used for the classification by Abdrabou [1]. The application was developed using eZ-CBR shell which showed a great potential in the hybridization between CBR and NN systems. Using UCI database, an average approximate accuracy of 85 % was obtained, which is almost the same obtained from other ML techniques. Babalik et al. [5] introduced an Artificial Bee Colony (ABC) algorithm as a preprocessor to improve the accuracy of the SVM classifier. RBF kernel was used as the kernel function in SVM. K-fold cross-validation algorithm was used to improve the reliability of the study. Optimum parameters of SVM are obtained using grid search algorithm. The weight vectors are obtained using associated optimum parameters with related SVM model. Mattos and Barreto [19], introduced two ensemble models that are built using Fuzzy ART (FA) and Self Organizing Map (SOM) Neural Networks as base classifiers. They described three different strategies to convert these unsupervised learning algorithms to supervised ones to be applied for the vertebral column classification task.

A metaheuristic solution based on a hybrid Particle Swarm Optimization (PSO) was used for parameter optimization. Ten datasets including vertebral column dataset was used for comprehensive performance evaluation. Results showed that FA and SOM-based ensemble classifiers outperform ensembles built from standard supervised neural networks. Average accuracy obtained during their experiments was approximately 83 %. A Computer-Aided Diagnosis (CAD) system which can help diagnosis of pathology on the vertebral column was introduced by Unal and Kocer [32]. Various artificial intelligence methods were used for the classification of the UCI database. The classification accuracy obtained was approximately 85.5 % using Multi-Layer Perceptron and 83.3 % using Naïve Bayes. Huang et al. [16], introduced a study that employed the ANN and rough set theory. The study used Back-Propagation Neural Network (BPNN), Rough Set Theory Genetic Algorithm (RS-GA), and Rough Set Theory Johnson Algorithm (RST_JA) to test the UCI database. Results showed that the BPNN is superior to RST-GA and RST-JA and has higher accuracy. The classification accuracy of BPNN was 90.32 %.

3 Subjects and Methods

3.1 Database

The database applied in this work is available from UCI Machine Learning Repository [31]. This database was collected during a medical residence in Spine Surgery. It contains about 310 patients obtained from sagittal panoramic radiographies of the spine. A total of 100 patients have normal anatomy. The rest of the data are from the patients operated due to disk hernia (60 patients) or spondylolisthesis (150 patients). The categories of disk hernia and spondylolisthesis could be merged into a single category named as abnormal (210 patients). Two different but related classification tasks can be implemented using UCI database. The first task is classifying patients as belonging to one of three categories (normal, disk hernia, spondylolisthesis). For the second task, disk hernia and spondylolisthesis can be merged into a single category and the classification is implemented using two classes (normal, abnormal). Each patient is represented in the dataset as a vector or pattern with six biomechanical attributes derived from the shape and orientation of the pelvis and lumbar spine. Standing lateral X-rays of a cohort of symptomatic young adult volunteers were obtained and on each radiograph, a simplified model of the spine and pelvis was created using dedicated software. The six attributes are: angle of Pelvic Incidence (PI), angle of Pelvic Tilt (PT), lordosis angle, Sacral Slope (SS), pelvic radius, and grade of slipping. Figure 1 describes graphically these attributes. The correlation between the vertebral column pathologies and these attributes was originally proposed in [7].

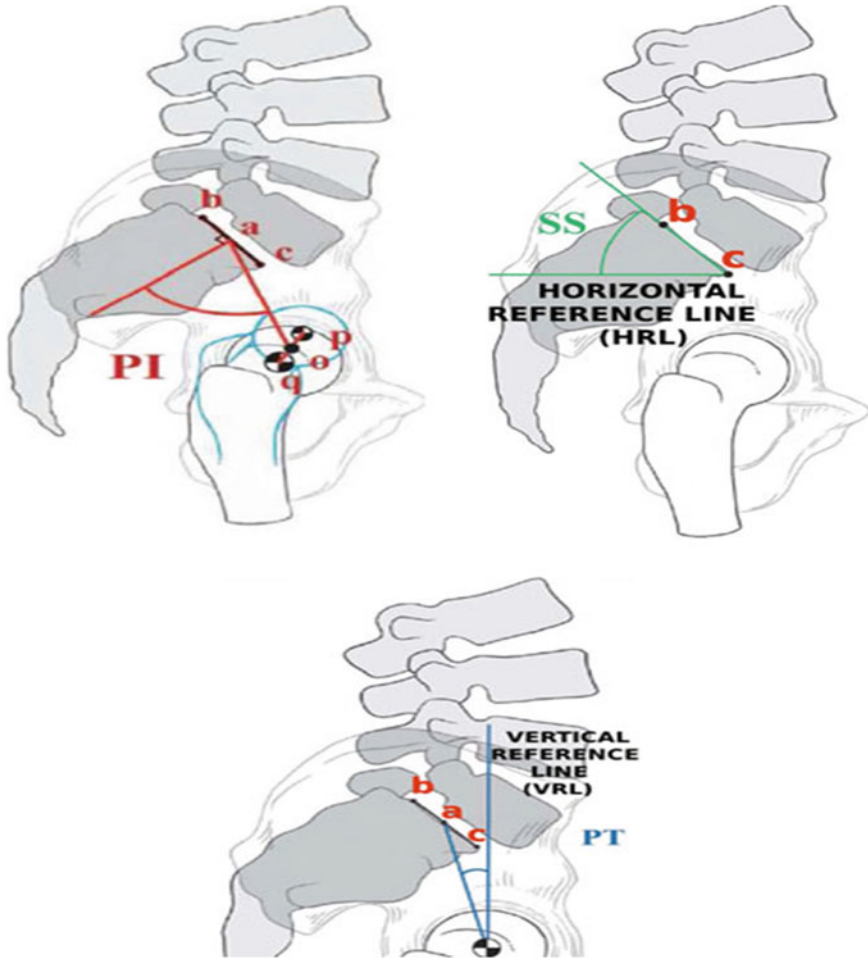


Fig. 1 Spino-pelvic system

3.2 Decision Trees

Decision trees are a form of multiple variable or multiple effect analyses. These types of analyses allow us to predict, explain, describe, or classify an outcome. Decision trees are one of the classification algorithms in current use in data mining and machine learning. The multiple variable analysis capability helps to go beyond simple one-cause, one-effect relationships, and describes things in the context of multiple influences. While it is easy to setup one-cause, one-effect relationships, this approach can lead to misleading outcomes [8, 10]. A definition of a decision tree was given by Russel and Norvig [26], as a construct which takes as input an object or situation described by a set of properties and outputs a yes/no decision.

When a set of input values is identified as having a strong relationship to a target value, then all of these values are grouped in a bin that becomes a branch on the decision tree. The tree is constructed by recursively partitioning a dataset into purer, more homogenous subsets based on a set of tests applied to one or more attribute values at each branch or node in the tree [4, 9, 10].

3.2.1 Single Decision Tree (SDT)

Every binary split of a node generates two descendant nodes. Tree splitting is based on a node impurity function. Let $I(t)$ denote the impurity at node t . The impurity function should be zero if all of the patterns that reach the node bear the same category, and should be large if the categories are equally represented. Entropy impurity as given by Eq. (1) is the most popular measure [30]

$$I(t) = - \sum_{i=1}^M P(\omega_i|t) \log_2 P(\omega_i|t) \quad (1)$$

where $P(\omega_i|t)$ denotes the probability that a vector X_t belongs to the class ω_i and M is the total number of classes. The impurity function will be minimized for a node that has elements of only one class (pure). The impurity gradient is given by:

$$\Delta I(t) = I(t) - a_R I(t) - a_L I(t) \quad (2)$$

where a_R and a_L are the proportions of the samples at node t , assigned to the right node and left node, respectively. The strategy is to choose the feature that maximizes $\Delta I(t)$.

To stop splitting, there are two basic strategies. The first criterion is to continue splitting until each leaf has zero impurity. Such a tree will not generally perform well on general datasets. This problem can be solved with pruning. In this process, any two leaves that are attached to a parent node are eliminated and their parent node is tuned into a leaf. Pruning can be done if it leads to a small increase in impurity. The second criterion is to stop splitting when a leaf has an acceptable impurity. The use of a threshold value for impurity decreases, and does not always lead to optimum tree size. It stops the tree growing either too early or too late. The most common approach is to grow a tree up to a large size and then prune its nodes [20, 30]. Once splitting is stopped, a node is declared to be a leaf, and a class label ω_j is given using the majority role:

$$j = \arg \max_i P(\omega_i|t) \quad (3)$$

A leaf of the tree is assigned to the class where the majority of the vectors X_t belong to.

3.2.2 Boosted Decision Tree (BDT)

Boosting is a general method for improving the accuracy of any learning algorithm. The AdaBoost algorithm is based on a learning algorithm repeatedly in a series of rounds $t = 1, 2, \dots, T$. The algorithm takes as input a training set (x_i, y_i) where x_i belongs to some domain X and y_i belongs to some label set Y . One of the main ideas of the algorithm is to maintain a set of weights over the training set and select the best weights and tree structure. The weights of this distribution on training example i on round t is $D_t(i)$. The first step of this boosting procedure is to build a SDT from the training data. This tree will usually contribute to errors for some cases in the training data. On each round, the weights of incorrectly classified examples are increased so that the weak learner is focused on the hard examples in the training data [2, 13, 24, 25]. The job of the learner is to find a hypothesis h_t appropriate for the distribution D_t . The goodness of the hypothesis is measured by its error given by Eq. (4) [14]

$$\varepsilon_t = \sum_{i:h_t(x_i) \neq y_i} D_t(i) \tag{4}$$

Once the hypothesis h_t has been received, the algorithm chooses a parameter α_t which measures the importance that is assigned to h_t . α_t gets larger as ε_t gets smaller.

$$\alpha_t = \frac{1}{2} \ln \left(\frac{1 - \varepsilon_t}{\varepsilon_t} \right) \tag{5}$$

The distribution D_t is updated to increase the weight of examples misclassified by h_t . The final hypothesis is given by:

$$H(x) = \text{sign} \left(\sum_{i=1}^T \alpha_i h_i(x) \right) \tag{6}$$

where H is a weighted majority vote in $= 1, 2, \dots, T$, α_i is the weight of h_i . It is clear that AdaBoost has the ability to reduce training error.

3.2.3 Decision Tree Forest (DTF)

A random forest is an ensemble of unpruned decision trees. Each tree is built from a random subset of the training dataset. In each decision tree model, a random subset of the available variables is used to choose how to partition the dataset at each node. The resulting tree models of the forest represent the final ensemble model [33]. Unlike boosting where the base models are trained and combined using a weighting scheme, the trees are trained independently and the predictions of the trees are

combined [11]. To classify a new object, put the object input vector down each of the trees in the forest, every classifier records a vote for the class to which it belongs and the object is labeled as a member of the class with the most votes. The randomness introduced by the random forest model in selecting the dataset and the variables gives robustness to noise and delivers substantial computational efficiencies. Also, very little, if any, preprocessing of the data needs to be performed. The need of the variable selection is avoided since the algorithm effectively does its own [3, 17, 33].

4 Data Analysis Using Decision Trees

The classification process starts by dividing the data into a training set and a validation set. The Decision Tree and Regression (DTREG) software package [27] is used for decision trees implementation. When building classification trees, the goal of splitting is to produce child nodes with minimum impurity. The basic aim is to favor homogeneity within each child node, and heterogeneity between child nodes. In a pure node, all rows have the same value of the target variable and the impurity value is zero. Gini and Entropy are the two methods provided by DTREG for evaluating the quality of splits when building classification trees. For deciding how large a tree should be, DTREG uses relaxed stopping criterion and builds an overly large tree. It then uses backward pruning to obtain the optimal tree size much more accurately. In decision trees modeling, tenfold cross-validation is used to prune back the trees to minimum cross-validated relative error [12]. The software is also used to compute the importance of features. Scores are given as relative values to the most important variable scaled to 100 %. Score “0” is the minimum score, while score “100” is the highest one indicating that the feature is the most important one. Various performance metrics are used to evaluate the performance of each classifier. The most important metrics are: accuracy, sensitivity, specificity, PPV, NPV, F-measure, and area under ROC curve.

5 Results and Discussion

5.1 *Single Decision Tree (SDT) Analysis*

SDT parameters are summarized in Table 1 and the SDT model is shown in Fig. 2. For single tree models, the model size is the number of terminal nodes in the tree. The full tree has 16 terminal (leaf) nodes. The primary goal of the pruning process is to generate the optimal size tree that can be generalized to the other data beyond the learning dataset. As shown in Fig. 3, the minimum validation relative error

Table 1 Training parameters of a SDT model

Parameter type	Value
Maximum splitting levels	10
Splitting algorithm	Gini
Minimum rows allowed in a node	5
Maximum categories for continuous predictors	1000
Tree pruning and validation method	Cross-validation
Number of cross-validation folds	10

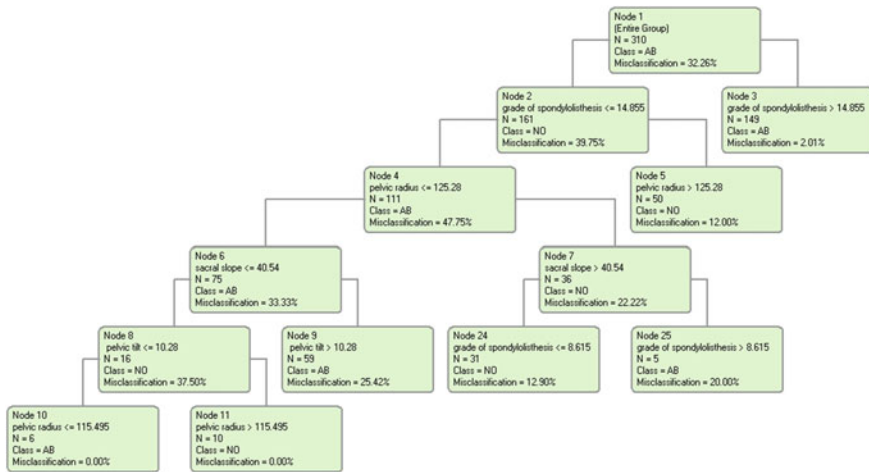


Fig. 2 SDT model for vertebral column diagnosis

occurs with 7 nodes. The relative error value is 0.5600 with a standard error of 0.0521. Therefore, the tree will be pruned from 7–16 nodes.

5.2 Boosted Decision Tree (BDT) Analysis

BDT parameters are summarized in Table 2. BDT can benefit from pruning to obtain the optimal size to minimize the error on a test dataset. Pruning in this case consists of truncating the series to the optimal number of trees.

As shown in Fig. 4, the full series has 600 trees. The minimum error with the training data occurs with 522 trees. The minimum error with the test data occurs with 270 trees. Therefore, the tree series will be pruned to 270 trees.

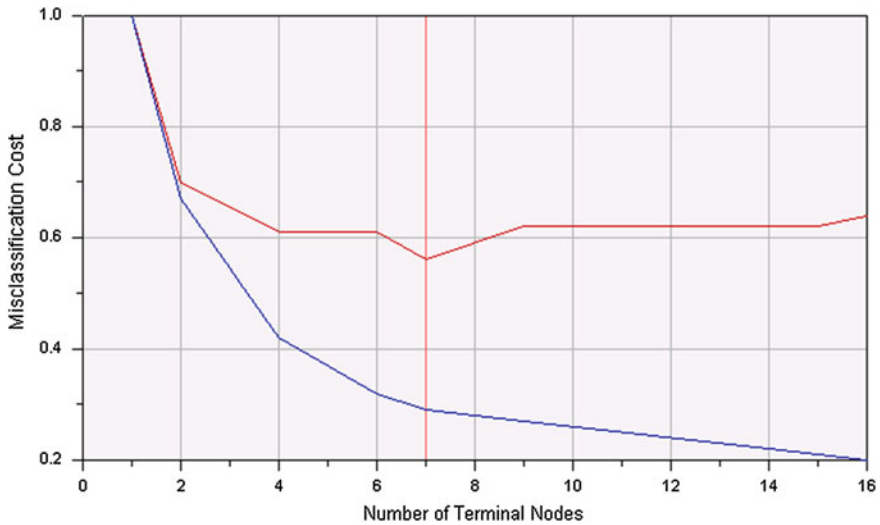


Fig. 3 SDT optimal model size during training (*blue line*) and validation phases (*red line*)

Table 2 Training parameters of a BDT model

Parameter type	Value
Maximum trees in tree boost series	600
Maximum splitting levels	5
Minimum size node to split	10
Maximum categories for continuous predictors	1000
Validation method	Cross-validation
Number of cross-validation folds	10
Tree pruning criterion	Minimum absolute error

5.3 Decision Tree Forest (DTF) Analysis

Using DTF, size can be controlled by changing the number of trees in the forest or by changing the size of each individual tree. Parameters of DTF are summarized in Table 3.

5.4 Performance Analysis

The performance analysis of the training phase by SDT and BDT classifiers is given in Table 4. The results show that the overall accuracies of SDT and BDT are 90.65 and 96.77 %, respectively. Random forests never report results on training data.

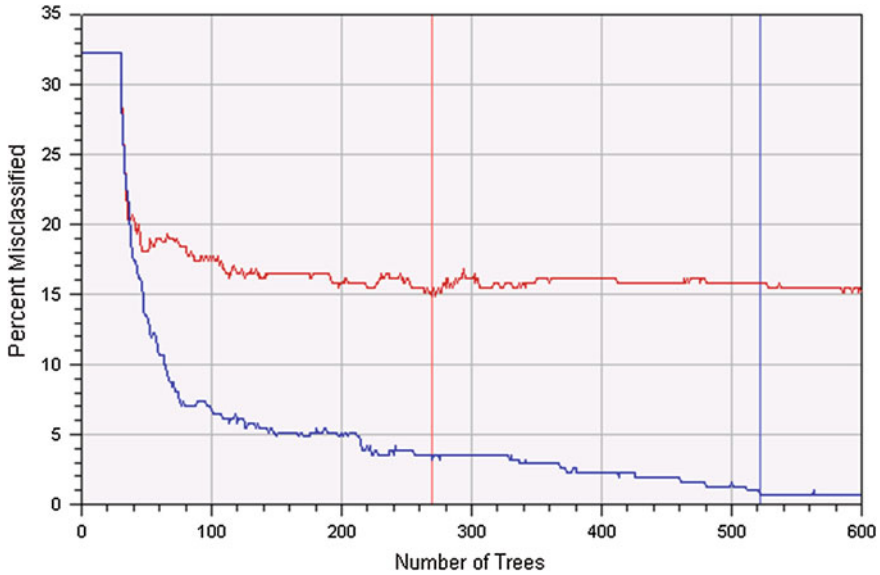


Fig. 4 BDT optimal model size during training (*blue line*) and validation phases (*red line*)

Table 3 DTF model parameters

Parameter type	Value
Maximum trees in decision tree forest	1400
Maximum splitting levels	50
Minimum size node to split	4
Maximum categories for continuous predictors	1000
Use surrogate splitters for missing values	Yes
Always compute surrogate splitters	No
Tree validation method	Out of Bag (OOB)

When trees are grown out to maximal size, near perfect classification on training data is expected, but this result is not useful for model assessment.

It is necessary to validate the quality of the resulting model after identifying the model structure and parameters. Performance metrics for validation phase of the three classifiers are shown in Table 5. It can be noted that, BDT achieved 84.84% accuracy, which is superior to SDT (81.94 %) and DTF (84.19 %). The results indicated that BDT performed better than the other two classifiers for approximately

Table 4 Performance indices for training phase of SDT and BDT classifiers

Performance index	SDT	BDT
Accuracy	90.65 %	96.77 %
Sensitivity	81.00 %	92.00 %
Specificity	95.24 %	99.05 %
Geometric mean of sensitivity and specificity	87.83 %	95.46 %
Positive Predictive Value (PPV)	89.01 %	97.87 %
Negative Predictive Value (NPV)	91.32 %	96.30 %
Geometric mean of PPV and NPV	90.16 %	97.08 %
Precision	89.01 %	97.87 %
Recall	81.00 %	92.00 %
F-measure	0.8482	0.9485
Area under ROC curve (AUC)	0.9392	0.9952

Table 5 Performance indices for validation phase of DT classifiers

Performance index	SDT	BDT	DTF
Accuracy	81.94 %	84.84 %	84.19 %
Sensitivity	74.00 %	75.00 %	74.00 %
Specificity	85.71 %	89.52 %	89.05 %
Geometric mean of sensitivity and specificity	79.64 %	81.94 %	81.18 %
Positive Predictive Value (PPV)	71.15 %	77.32 %	76.29 %
Negative Predictive Value (NPV)	87.38 %	88.26 %	87.79 %
Geometric mean of PPV and NPV	78.85 %	82.61 %	81.84 %
Precision	71.15 %	77.32 %	76.29 %
Recall	74.00 %	75.00 %	74.00 %
F-measure	0.7255	0.7614	0.7513
Area under ROC curve (AUC)	0.84655	0.91600	0.92167

all performance indices. BDT model showed the highest sensitivity which means that boosting is also useful to alleviate instability. ROC curves for the abnormal class in the testing phase for BDT is shown in Fig. 5.

The importance of features calculated by BDT classifier is given in Table 6. All scores are scaled to have values between 0 and 100. It can be noted that grade of spondylolisthesis is the most relevant attribute while pelvic incidence is the less important one. Results showed that the proposed BDT system provided satisfactory results for the vertebral column diseases diagnosis. It can be used by clinicians to further assist the selection of appropriate treatments for patients.

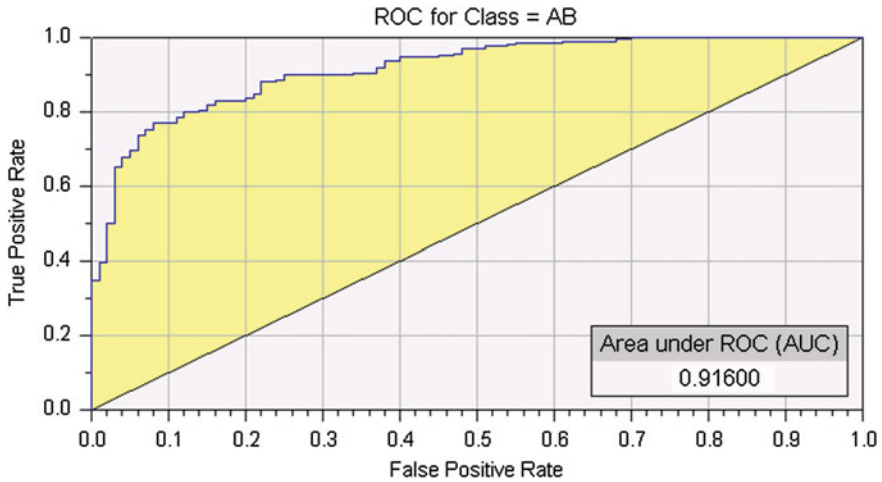


Fig. 5 ROC curve for the abnormal class in the testing phase using BDT model

Table 6 Importance of features by BDT classifier

Features	Attribute description	Importance (%)
F1	Grade of spondylolisthesis	100
F2	Pelvic radius	32.931
F3	Sacral slope	30.819
F4	Pelvic tilt	18.877
F5	Lumbar lordosis angle	15.075
F6	Pelvic incidence	12.329

6 Conclusion and Future Work

The prediction of vertebral column pathologies has been a challenging research problem. Decision trees are very useful data mining techniques used in classification problems. The aim to develop a robust, stable, and successful model for utilizing attributes of the problem dataset. Selection of the classifier influences the success of the classification accuracy. In this work, SDT, BDT, and DTF classifiers are used as decision support tools for detection of pathology on the vertebral column. The performance of the proposed classifiers is evaluated in terms of accuracy, sensitivity, specificity, ROC, and other metrics. The results showed that the accuracy of BDT in the training phase is 96.77 %, compared to 90.65 % using SDT. BDT performed better than SDT for all performance indices. ROC achieved a value of 0.9952 using BDT which is superior to SDT classifier. During the validation phase, BDT achieved 84.84 % which is superior to SDT (81.94 %) and DTF (84.19 %). The obtained value of ROC using BDT in the testing phase was 0.9160.

Future work can include integrating the tree structure into the Markov random field-based relabeling system to improve the accuracy. Another future direction is to combine more than one classifier using a suitable fusion technique.

References

1. Abdrabou E (2012) A hybrid intelligent classifier for the diagnosis of pathology on the vertebral column. In: Markov K (ed) Artificial intelligence methods and techniques for business and engineering applications. ITHEA, Rzeszow, pp 297–310
2. Arditi D, Pulket T (2005) Predicting the outcome of construction litigation using boosted decision trees. *J Comp Civil Eng* 19(4):387–393
3. Azar AT, El-Metwally SM (2013) Decision tree classifiers for automated medical diagnosis. *Neural Comput Appl* 23(7–8):2387–2403 (Springer). doi:[10.1007/s00521-012-1196-7](https://doi.org/10.1007/s00521-012-1196-7)
4. Azar AT, Elshazly HI, Hassanien AE, Elkorany AM (2014) A random forest classifier for lymph diseases. *Comput Methods Prog Biomed* 113(2):465–473 (Elsevier)
5. Babalik A, Babaoglu I, Ozkis A (2012) A pre-processing approach based on artificial bee colony for classification by support vector machine. *IJCEE* 2(1):68–70. doi:[10.7763/IJCEE.2013.V2.139](https://doi.org/10.7763/IJCEE.2013.V2.139)
6. Banik S, Rangayyan RM, Boag GS (2010) Automatic segmentation of the ribs, the vertebral column, and the spinal canal in pediatric computed tomographic images. *JDI* 23(3):301–322
7. Berthounaud E, Dimnet J, Roussouly P, Labelle H (2005) Analysis of the sagittal balance of the spine and pelvis using shape and orientation parameters. *J Spinal Disord Tech* 18(1):40–47
8. Breiman L, Friedman J, Olshen R, Stone C (1984) Classification and Regression Trees. Wadsworth & Brooks/Cole Advanced Books & Software, California
9. Clark LA, Pregibon D (1992) Tree-based models. In: Chambers JM, Hastie TJ (eds) Statistical models (Chap. 9). S. Chapman & Hall, New York, pp 377–420
10. de Ville B (2006) Decision trees for business intelligence and data mining. SAS Institute Inc., Cary
11. Denil M, Matheson D, de Freitas N (2014) Narrowing the gap: random forests in theory and in practice. In: Proceedings of the 31st international conference on machine learning, Beijing, China, vol 32. JMLR: W&CP
12. Diamantidis NA, Karlis D, Giakoumakis EA (2000) Unsupervised stratification of cross-validation for accuracy estimation. *ArtifIntell* 116(1–2):1–16
13. Freund Y, Schapire RE (1996) Experiments with a new boosting algorithm. In: Proceeding of the 13th international conference on artificial intelligence: machine learning, international machine learning society, pp 148–156
14. Freund Y, Schapire RE (1999) A short introduction to boosting. *J Jpn Soc Artif Intell* 14(5):148–156
15. Gonzalez FA, Romero E (2010) Biomedical image analysis and machine learning technologies: applications and techniques. IGI Global, ISBN13: 9781605669564, ISBN10: 1605669563, EISBN13: 9781605669571. doi:[10.4018/978-1-60566-956-4](https://doi.org/10.4018/978-1-60566-956-4)
16. Huang M, Hung Y, Liu D (2014) Diagnostic prediction of vertebral column using rough set theory and neural network technique. *Inf Technol J* 13(5):874–884. doi:[10.3923/itj.2014.874.884](https://doi.org/10.3923/itj.2014.874.884)
17. Kulkarni Y, Sinha P K (2013) Efficient learning of random forest classifier using disjoint partitioning approach. In: Proceedings of the World Congress on Engineering 2013, vol II. WCE 2013, London, U.K, 3–5 July 2013
18. Ma Y, Guo G (eds) (2014) Support vector machines applications. Springer, ISBN: 978-3-319-02299-4. doi:[10.1007/978-3-319-02300-7](https://doi.org/10.1007/978-3-319-02300-7)

19. Mattos CLC, Barreto GA (2013) ARTIE and MUSCLE models: building ensemble classifiers from fuzzy ART and SOM networks. *Neural Comput Appl* 22(1):49–61. doi:[10.1007/s00521-011-0747-7](https://doi.org/10.1007/s00521-011-0747-7)
20. Mingers J (1989) An empirical comparison of selection measures for decision tree induction. *Mach Learn* 3(4):319–342
21. Neto ARR, Barreto GA (2009) On the application of ensembles of classifiers to the diagnosis of pathologies of the vertebral column: a comparative analysis. *IEEE Latin Am Trans* 7(4). doi:[10.1109/TLA.2009.5349049](https://doi.org/10.1109/TLA.2009.5349049)
22. Neto ARR, Sousa R, Barreto GA, Cardoso JS (2011) Diagnostic of pathology on the vertebral column with embedded reject option. In: Vitria J, Sanches JM, Hernández V, Jordi S, Miguel J, Hernández M (eds) *Pattern recognition and image analysis. 5th Iberian conference, IbPRIA 2011. Lecture Notes in Computer Science*, vol 6669. Las Palmas de Gran Canaria, Spain, Springer, Heidelberg, 8–10 June 2011. doi:[10.1007/978-3-642-21257-4](https://doi.org/10.1007/978-3-642-21257-4)
23. Olivas ES, Guerrero JDM, Martínez-Sober M, Magdalena-Benedito JR, López AJ (2010) *Handbook of research on machine learning applications and trends: algorithms, methods, and techniques*. IGI Global, ISBN13: 9781605667669, ISBN10: 1605667668, EISBN13: 9781605667676. doi:[10.4018/978-1-60566-766-9](https://doi.org/10.4018/978-1-60566-766-9)
24. Quinlan JR (1993) *C4. 5: programs for machine learning*. Morgan Kaufmann, San Mateo
25. Quinlan JR (2003) *Data mining tools See5 and C5.0*. RuleQuest Research, Austria. <http://www.rulequest.com/see5-info.html>
26. Russell S, Norvig P (2002) *Artificial intelligence: a modern approach*. Prentice-Hall, New Jersey
27. Sherrod PH (2012) DTREG predictive modeling software. www.dtreg.com
28. Simon S (1998) *Bones: our Skelton system*. HarperCollin, New York
29. Tay B, Hyun JK, Oh S (2014) A machine learning approach for specification of spinal cord injuries using fractional anisotropy values obtained from diffusion tensor images. *Comput Math Methods Med*. doi:[10.1155/2014/276589](https://doi.org/10.1155/2014/276589)
30. Theodoridis S, Koutroumbas K (2006) *Pattern recognition*, 3rd edn. Elsevier, Amsterdam
31. UCI (2012) *Machine learning repository*. <http://archive.ics.uci.edu/ml/index.html>
32. Unal Y, Kocer HE (2013) Diagnosis of pathology on the vertebral column with backpropagation and Naïve Bayes classifier. In: *International Conference on Technological Advances in Electrical, Electronics and Computer Engineering (TAEECE)*, Konya, 9–11 May 2013. doi:[10.1109/TAEECE.2013.6557285](https://doi.org/10.1109/TAEECE.2013.6557285)
33. Williams G (2011) *Data mining with rattle and R: the art of excavating data for knowledge discovery*. Springer Science + Business Media, LLC, New York
34. Yao J, O' Connor SD, Summers RM (2006) Automated spinal column extraction and partitioning. In *Proceedings of the 3rd IEEE international symposium on biomedical imaging: nano to macro*, Arlington, VA, pp 390–393, 6–9 Apr 2006. doi:[10.1109/ISBI.2006.1624935](https://doi.org/10.1109/ISBI.2006.1624935)

Hybrid Invasive Weed Optimization Method for Generating Healthy Meals

Viorica R. Chifu, Ioan Salomie, Emil Șt. Chifu, Cristina Bianca Pop,
Dan Valea, Madalina Lupu and Marcel Antal

Abstract This paper presents a hybrid invasive weed optimization method for generating healthy meals starting from a given user profile, a diet recommendation, and a set of food offers. The method proposed is based on a hybrid model which consists of a core component and two hybridization components. The core component is based on the invasive weed optimization algorithm, and the hybridization components rely on PSO-based path relinking as well as on tabu search and reinforcement learning. The method proposed has been integrated into an experimental prototype and evaluated on various user profiles.

1 Introduction

In the last decades, governmental and non-governmental health institutions give more attention to increase the quality and duration of people's life. This is a measure to overcome the fact that death caused by chronic diseases, in the case of young and mature population, dramatically increases in the last years. For example, in Romania, cardiovascular diseases represent the main cause of death, leading to a mortality rate of 26.5 %, and are caused by high blood pressure (31.8 % of deaths), tobacco (16.3 % of deaths), high cholesterol (14.4 %), high BMI (13.9 %), alcohol (12.4 %), low fruit and vegetable intake (7.1 %), and physical inactivity (6.6 %) [1]. By adopting a healthy lifestyle, the quality of life can be improved even for people

V.R. Chifu (✉) · I. Salomie · E.Șt.Chifu · C.B. Pop · D. Valea · M. Lupu · M. Antal
Technical University of Cluj-Napoca, Barițiu 26-28, Cluj-Napoca, Romania
e-mail: Viorica.Chifu@cs.utcluj.ro

I. Salomie
e-mail: Ioan.Salomie@cs.utcluj.ro

E.Șt.Chifu
e-mail: Emil.Chifu@cs.utcluj.ro

C.B. Pop
e-mail: Cristina.Pop@cs.utcluj.ro

with chronic diseases (e.g., diabetes, hypertension, cardiovascular diseases). Many of these chronic diseases can be managed with proper eating, physical activity, and sound medical supervision [2]. Proper management of eating or physical activity is essential because unmanaged disease can be associated with high risk for other diseases. For example, unmanaged diabetes is associated with high risk for heart disease and other health problems [2].

Statistics demonstrate that, by adopting a healthy lifestyle (i.e., healthy nutritional diet, physical activity) more than 200,000 premature deaths can be prevented annually [2]. Some of the benefits of adopting a healthy nutritional diet are (i) reducing the risk of heart disease, stroke, or diabetes; (ii) better management of diseases (by reducing high blood pressure, by lowering the cholesterol); (iii) keeping muscles, bones, organs, and other parts of the body healthy; and (iv) ensuring the corresponding energy level in the body [3]. The prevention or management of diseases is a worldwide concern as the governmental institutions not only aim to decrease the mortality rate, but also to save a lot of money which would have been spent on treatment. For instance, reducing cholesterol concentrations or blood pressure levels by 5 % would lead to annual money savings of up to 100 million pounds, while reducing salt intake by 3 g/day would lead to annual money savings of up to 40 million pounds a year [4].

This paper presents a hybrid invasive weed optimization-based method for generating healthy meals starting from a given user profile, a diet recommendation, and a set of food offers. To improve the performance of the classical invasive weed optimization algorithm, the method proposed here is hybridized with a path re-linking component, as well as with a tabu search and reinforcement learning component [5, 6]. The method proposed has been integrated into an experimental prototype and evaluated on a set of scenarios describing various user profiles.

The paper is organized as follows. Section 2 presents related work. Section 3 presents the hybrid invasive weed optimization model, while Sect. 4 describes the hybrid algorithm. Section 5 presents the experimental prototype as well as the experimental results. We end our paper with conclusions.

2 Related Work

This section presents the state-of-the art in the field of generating healthy lifestyle recommendations.

In [7], the authors propose a counseling system for food or menu planning that can be successfully used in a clinical/hospital or at home. The system proposed consists of two main parts: a Food Ontology and an expert system. The Food Ontology contains information about ingredients, substances, nutrition facts, and recommended daily intakes for different regions, dishes, and menus. The expert system uses an inference engine that provides appropriate suggestions for meals and dishes. The suggestions are taken based on the information stored in the ontology as

well as the preferences introduced by the customer by means of a graphical user interface (e.g., their favorite ingredients, ingredients to avoid, favorite flavors).

In [8], the authors propose a personalized nutrition and food planning system for older people. The system proposed consists of four parts: a user interface, a personal health record, a knowledge base, and a food planning system. The user interface has the following purposes: (1) it allows patients and hospital staff to introduce information about the patient profile and the patient favorite food (i.e., favorite ingredients or disliked ingredients); and (2) it displays to the user the most appropriate food menu per meal, day, or week. The personal health record contains medical information such as name, gender, age, weight, height, blood pressure, pulse rate, or chronic diseases of a patient. The knowledge base stores information about food and nutrition collected from food and nutrition experts or from books. It consists of (i) a food and nutritional ontology, (ii) a set of rules and conditions for generating a menu of foods for the patient, and (iii) a database containing information about food and nutrition. The food planning system uses an inference engine for planning the food menu based on the personal health record, the information stored in the knowledge base, and patient's food favorites.

In [9], the authors present a decision support system for menu recommendation based on the rough set theory. The system generates menu recommendations based on the information provided by customers by means of questionnaires. In the questionnaires, the customer must specify what he/she likes or dislikes from ten randomly selected kinds of menu. Based on this information, a preference rule is extracted that will be used for generating the menu recommendation for the customer.

The authors of [10] present a personalized recommender system based on multi-agents and the rough set theory. The system proposed consists of five layers: viewer layer, control layer, agent service layer, lucene service layer, and data service layer. The viewer layer provides a user interface which ensures the interaction between the learners and the system. The control layer is responsible for transferring information from the user to the agent service layer. The agent service layer is the core of the system, and it contains two types of agents: learner agents and recommender agents. The learner agent is behind of each online learner. Using the rough set theory, the recommender agent recommends learning resources. The learning resources are recommended based on the online behaviors of the user. The lucene service layer is used to build a personalized retrieval function to support recommendation. The data service layer is responsible for data storage (i.e., information on learner's features, records of learner's activities, learning resources).

In [11], the authors propose an automated menu generator for people suffering from cardiovascular diseases. The menus are generated in such a way that a set of nutritional constraints is satisfied and the food items of the menu can be combined. In addition, the menu generator takes into account the user's preferences and other user-related information (e.g., gender). A commercial nutritional database for Hungarian lifestyle and cuisine is used to obtain information about recipes and their ingredients including a classification of the ingredients as well as their nutritional information. To generate a menu, genetic algorithms are used. An individual is

modeled either as a single meal or a daily menu. A daily menu consists of meals having dishes associated. The genetic crossover, mutation, and selection operators are used to evolve the individuals of the genetic algorithm. The crossover operator swaps the attributes of two individuals in a randomly chosen crossover point. The mutation operator randomly replaces a randomly chosen dish with another suitable one. A penalty-based fitness function is used to evaluate an individual. In addition, an individual is evaluated to check whether the food items contained can be combined, using a set of penalty-based rules. The initial population consists of individuals who have been generated previously for other similar problems.

3 Hybrid Invasive Weed Optimization Model

This section describes the invasive weed optimization-based component (as the core component) as well as the path relinking-based component and the tabu search-based component, the latter two being used to hybridize the invasive weed optimization meta-heuristic [12].

3.1 *The Invasive Weed Optimization-Based Component*

In nature, weeds profit of the unused resources from the soil and grow until they become mature weeds that produce seeds. The number of seeds of each weed depends on the quantity of resources consumed and on the ability to adapt to the environment (i.e., the fitness of the weed in the colony). The seeds produced are scattered over the ground and grow until they become mature weeds. The process is repeated until the unused resources from the soil are totally depleted.

The invasive weed optimization-based component represents the core component of our hybrid model and it is based on the phenomenon of colonization of invasive weeds in nature [12]. This component is defined by mapping the concepts of the invasive weed optimization meta-heuristic onto the concepts of generating healthy lifestyle recommendations, as follows: (i) a weed (i.e., a solution) is represented as a set of food offers from different providers representing the food items for breakfast, snacks, lunch, or dinner; (ii) the seed of a weed represents a new set of food offers obtained by performing a random mutation of the old set of food offers in a number of mutation points (i.e., replacing a food offer with another one according to the user's constraints and the recommended diet constraints); (iii) the colony represents the whole population of weeds (i.e., sets of food offers); and (iv) the fitness is a value representing how good a solution is, regarding the quantity of nutrients and vitamins contained, price, and delivery time.

In our approach, a weed is formally represented as

$$\text{sol} = \{\text{FI}_b, \text{FI}_{s1}, \text{FI}_l, \text{FI}_{s2}, \text{FI}_d\} \quad (1)$$

where FI_b represents the set of food items that can be eaten at breakfast, FI_{s1} and FI_{s2} are sets of food items that can be eaten at snacks, FI_l at lunch, and FI_d at dinner, during one day.

The set FI_b of food items that can be eaten at breakfast is defined as

$$\text{FI}_b = \{\text{foodItem}_{b1}, \text{foodItem}_{b2}, \dots, \text{foodItem}_{bn}\} \quad (2)$$

In Eq. (2), foodItem_{bi} is a food item that can be eaten at breakfast during one day, and n is the number of food items that can be consumed at breakfast during one day. The other components of a solution (a solution being a weed) are defined similarly to FI_b .

The fitness function used to evaluate the quality of a solution (i.e., weed) is defined as

$$\text{Fitness}(\text{sol}) = \alpha_1 * F_p(\text{sol}) + \alpha_2 * F_t(\text{sol}) + \alpha_3 F_n(\text{sol}) \quad (3)$$

where

- $\alpha_i \in [0, 1]$ are the weighting coefficients and $\sum_{i=1}^3 \alpha_i = 1$;
- $F_p(\text{sol}) = \sum_{\text{foodItem}_i \in \text{sol}} \text{Price}(\text{foodItem}_i)$ evaluates the price associated to a solution and is computed as the sum of the prices of the solution components (each solution component being a food item in our case¹);
- $F_t(\text{sol}) = \max_{\text{foodItem}_i \in \text{sol}} \text{Time}(\text{foodItem}_i)$ evaluates the delivery time associated to a solution and is computed as the maximum time among the delivery times of the solution components;
- $F_n(\text{sol}) = \sum_{i=1}^4 \omega_i f_i(\text{sol})$, $\omega_i \in [0, 1]$, and $\sum_{i=1}^4 \omega_i = 1$ is the fitness value which evaluates the nutritional features (i.e., calories, proteins, lipids, and carbohydrates) of a solution (i.e., a menu). In this formula, $f_i(\text{sol})$ is computed as

$$f_i(\text{sol}) = \frac{\tau_i - (\text{optVal}_i - \sum_{\text{foodItem} \in \text{sol}} \text{NF}_i(\text{foodItem}))}{\tau_i} \quad (4)$$

where (i) $\text{NF}_i(\text{foodItem})$ is a particular nutritional feature (i.e., one of the following four: calories, proteins, lipids, and carbohydrates) contained in a solution component; (ii) optVal_i is the optimal value for a particular nutritional feature; this value is taken from [13]; and (iii) τ_i is the threshold value that is accepted for this particular nutritional feature and is computed as 25 % of optVal_i .

¹Even if, according to formulae (1) and (2), a solution is a set of food offers (one for breakfast, another one for lunch, etc.), each of which being a set of food items, in what follows in the rest of the paper, we will consider a solution as a flat set of food items (for simplicity reasons).

Additionally, we have defined a set of constraints which we will consider in evaluating a solution (i.e., a menu):

$$C_j(y) = \sum_{y_i \in sol} \sum_{k=1}^{n(y_i)} q_{ik} * p_{kj} \quad (5)$$

where (i) $n(y_i)$ is the number of ingredients in food item y_i ; (ii) p_{kj} is the percent of nutrient j that is contained into ingredient k ; and (iii) q_{ik} is the quantity of ingredient k contained into a food item y_i .

These constraints are satisfied if they take values in an interval of values $[\min_j, \max_j]$, where \min_j is the minimum daily requirement for a particular nutrient j (e.g., sodium, iron, A, B1 or C vitamins), and \max_j is the maximum daily requirement for nutrient j .

We mention that the values of the components of the fitness function as well as the values of the constraints are normalized.

3.2 Hybridization Components

This section presents the components that will be used to hybridize the invasive weed optimization-based component.

1. Tabu Search and reinforcement learning component. The tabu search and reinforcement learning component improves the search capabilities of the core component by means of long-term and short-term memory structures borrowed from tabu search [5]. The long-term memory (see Eq. (6)) contains the history of food item replacements and the associated rewards and penalties and it is consulted each time a new solution is generated.

$$M_l = \{m_l | m_l = (\text{foodItem}_i, \text{foodItem}_j, \text{rlScore})\} \quad (6)$$

where foodItem_i is the food item that has been replaced by foodItem_j , and rlScore is the reinforcement learning score used for recording rewards and penalties for the tuple $(\text{foodItem}_i, \text{foodItem}_j)$. The concepts of rewards and penalties are borrowed from the reinforcement learning technique. The rlScore value of a food item replacement is updated each time the specified replacement takes place in order to modify a solution. If the replacement improves the quality of a solution, then the rlScore is increased (a reward is granted), otherwise the rlScore is decreased (a penalty is granted). The short-term memory structure is defined as

$$M_s = (\text{foodItem}_i, \text{foodItem}_j, \text{noIt}_{tab}) \quad (7)$$

where the solution component foodItem_i has been replaced with another component foodItem_j , and noIt_{tab} represents the number of iterations in which the component replacement cannot be performed. During the processing, this parameter number of iterations (noIt_{tab}) is reset dynamically according to the current need for exploration versus

exploitation. When rather exploration is currently needed, then $noIt_{tab}$ is increased, otherwise when rather exploitation is currently needed then $noIt_{tab}$ is decreased.

2. Path relinking component. Path relinking [6] is a search technique that exploits the search space by finding paths between two solutions (i.e., the initial solution and the guiding solution). The main idea of this technique is to obtain the guiding solution by applying a set of modification strategies on the initial solution. This way, each time a modification strategy is applied on the initial solution, the intermediate solution obtained will be more similar with the guiding solution and less similar with the initial one. By this searching technique, new paths between the initial and the guiding solution are generated, and the solutions on these paths could be a source for generating new paths.

In our approach, the path relinking-based component is used to generate new solutions by considering the **best solution from the set of seeds** as initial solution, and the currently optimal solution as the guiding solution. For generating new solutions, we have used two path relinking-based strategies: one which applies a crossover operator to modify the initial solution toward the guiding solution, and another one which applies a PSO modification strategy.

The **path relinking strategy** based on crossover operator is applied between the best solution in the set of child seeds and the currently optimal solution as follows: The initial solution (the best in the set of child seeds) is updated until arriving at the currently optimal solution by iteratively performing a one-point crossover (the crossover point being randomly chosen) between the two solutions (see example below).

- Initial solution: $sol_i = (\text{foodItem}_1, \text{foodItem}_2, \text{foodItem}_3, \text{foodItem}_4)$, Guiding solution: $sol_g = (\text{foodItem}'_1, \text{foodItem}'_2, \text{foodItem}'_3, \text{foodItem}'_4)$
- First Step—Applying Crossover: one-point crossover on sol_i and sol_g . The solutions obtained are $sol'_i = (\text{foodItem}'_1, \text{foodItem}_2, \text{foodItem}_3, \text{foodItem}_4)$, $sol'_g = (\text{foodItem}_1, \text{foodItem}'_2, \text{foodItem}'_3, \text{foodItem}'_4)$
- Second Step—Applying Crossover: one-point crossover on sol'_i and sol'_g . The solutions obtained are $sol''_i = (\text{foodItem}'_1, \text{foodItem}'_2, \text{foodItem}_3, \text{foodItem}_4)$, $sol''_g = (\text{foodItem}_1, \text{foodItem}_2, \text{foodItem}'_3, \text{foodItem}'_4)$
- Third Step—Applying Crossover: one-point crossover on sol''_i and sol''_g . The solutions obtained are $sol'''_i = (\text{foodItem}'_1, \text{foodItem}'_2, \text{foodItem}'_3, \text{foodItem}_4)$, $sol'''_g = (\text{foodItem}_1, \text{foodItem}_2, \text{foodItem}_3, \text{foodItem}'_4)$

The **PSO-based path relinking strategy** is applied between the best solution in the set of child seeds and the current globally optimal solution as follows:

- The initial solution (the best in the set of child seeds) is updated until arriving at a new solution having a fitness higher than the current globally optimal solution, by iteratively applying the PSO-based updating formula [14]:

$$sol_i = (1 - \beta) * sol_{\text{initial}} + \beta * sol_{\text{guiding}} + \text{Random} \tag{8}$$

where (i) β represents a value in the interval (0, 1) used to compute the percentage of solution components from $\text{sol}_{\text{initial}}$ that will be substituted with new components from $\text{sol}_{\text{guiding}}$, and (ii) Random is a randomly generated vector of 0's and 1's with a length equal to the length of the initiating and guiding solution.

To illustrate how formula (8) is applied, we consider the following example:

- Initial solution = (foodItem₁, foodItem₂, foodItem₃, foodItem₄), Guiding solution = (foodItem₁', foodItem₂', foodItem₃', foodItem₄'), $\beta = 0.7$
- We apply formula (8) as follows:
 - $0.3 * (\text{foodItem}_1, \text{foodItem}_2, \text{foodItem}_3, \text{foodItem}_4) + 0.7 * (\text{foodItem}_1', \text{foodItem}_2', \text{foodItem}_3', \text{foodItem}_4') = (\text{foodItem}_1, \text{foodItem}_2', \text{foodItem}_3', \text{foodItem}_4') \rightarrow$ one component of the initial solution is kept, while the others are taken from the guiding solution. This process is guided by the information from the short-term and long-term memories.
 - $(\text{foodItem}_1, \text{foodItem}_2', \text{foodItem}_3', \text{foodItem}_4') + (1, 0, 0, 1) = (\text{foodItem}_1, *, *, \text{foodItem}_4') \rightarrow$ 0 indicates that the element of the initial solution is randomly replaced with another compatible component (represented as a '*').

4 Hybrid Invasive Weed Optimization Algorithm

The hybrid invasive weed optimization-based algorithm takes as input the following parameters: *FoodOff*—the set of food offers, *PersonalProfile*—the personal profile of a user, *popSize*—the population size, *maxSeeds*—the maximum number of seeds, *minSeeds*—the minimum number of seeds, *noIt*—the number of iterations, and *noIt_{tab}*—the number of iterations for which a tuple of food items is tabu. The algorithm returns a set of optimal or near-optimal combinations of food items for a healthy menu. The algorithm consists of an initialization stage and an iterative stage. In the initialization stage, the initial population of individuals is generated based on the food offers, the user profile (i.e., personal profile), and the diet recommendation. Then the iterative stage identifies the optimal or near-optimal configuration of food items. The operations below are performed in the iterative stage, until a stopping condition (i.e., a predefined number of iteration) is satisfied:

- The locally optimal solution is identified among the set of individuals in the population.
- For each individual in the population, the steps below are performed:
 - The number of child seeds is computed based on the following formula:

$$nrSeeds(plant) = maxSeeds - \frac{(maxSeeds - minSeeds) * i}{MaxPopSize} \quad (9)$$

where (i) *maxSeeds*—represents the maximum number of seeds, (ii) *minSeeds* represents the minimum number of seeds, (iii) *MaxpopSize*

is the maximum population size, and (iv) i is the index of the plant the Population set (the plants in the Population set are stored in a descending order according to their fitness value—the best plant has index 1).

- The children are generated based on the number of child seeds computed as above.

ALGORITHM: Invasive Weed Optimization

Input: *FoodOff, PersonalProfile, MedicalDiet, popSize, maxPopSize, maxSeeds, minSeeds, noIt_{tab}, noMut, repProc*

Output: *Menu*

Begin

Population = **Randomly_Generate_Pop**(*popSize, FoodOff, PersonalProfile, MedicalDiet*)

ChildPop = {}

$M_s = \{\}, M_l = \{\}$

while (*stopping condition not satisfied*) **do**

Rank(Population)

$sol_{opt} = \mathbf{Get_Highest_Fitness_Solution}$ (Population)

foreach plant **in** Population **do**

$noSeeds = \mathbf{Compute_No_of_Seeds}$ (*maxSeeds, minSeeds,*

$\mathbf{Get_Index}$ (plant, Population), *maxPopSize*)

ChildSeeds = **Generate_Child_Seeds**(plant, *noSeeds*)

ChildSeeds* = **Mutate**(ChildSeeds, *FoodOff, PersonalProfile, MedicalDiet, M_s, M_l, noMut, noIt_{tab}*)

Update (M_l)

ChildPop = ChildPop \cup ChildSeeds*

bestSeed = **Get_Highest_Fitness_Solution**(ChildSeeds*)

if ($\mathbf{Fitness}$ (bestSeed) > $\mathbf{Fitness}$ (sol_{opt})) **then**

$sol_{opt} = \text{bestSeed}$

ChildSeeds* = ChildSeeds* - {bestSeed}

end if

end foreach

ChildPop = ChildPop \cup **Path_Relinking** ($\mathbf{Get_Highest_Fitness}$ (ChildSeeds*), sol_{opt})

Update(M_s)

Population = Population \cup ChildPop

Population = **Rank**(Population)

Population = **Elim_Lowest_Fitness**(Population, *maxPopSize*)

Population = **Replace_Lowest_Fitness**(Population, *repProc*)

end while

return $\mathbf{Get_Highest_Fitness}$ (Population)

End

- The child seeds are submitted to a mutation process by taking into account the user profile, the food offers, the diet recommendation, and the information stored in the long-term and short-term memory structures.
 - The long-term memory structure is updated.
 - The best child is identified from the population of children.
 - The locally optimal solution is updated if necessary.
- The population of children is updated by applying a path relinking-based strategy between the children population and the locally optimal solution.
 - The short-term memory structure is updated.
 - The updated population of children is added to the population of individuals, and a number *repProc* representing the worst individuals in the whole population is replaced with new individuals randomly generated.

5 Prototype Implementation and Case Studies

This section presents the experimental prototype as well as a case study to illustrate how the hybrid weed optimization method is used for generating healthy menus starting from a given user profile and a medical diet recommendation.

5.1 Experimental Prototype

To validate our hybrid invasive weed optimization method, we developed and used an experimental prototype (see Fig. 1). It is composed of the following modules and

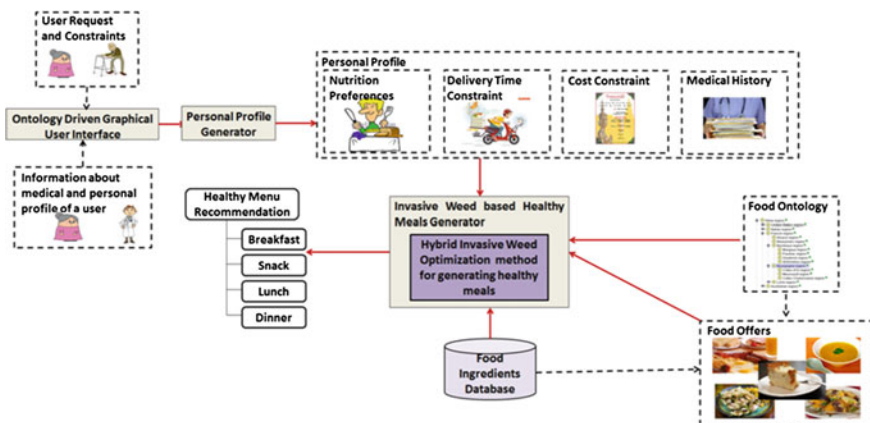


Fig. 1 Conceptual architecture of the experimental prototype

resources: *Ontology Driven Graphical User Interface*, *Personal Profile Generator*, *Food Ingredient Database*, *Food Ontology*, *Food Offer Repository*, and *Invasive Weed-Based Healthy Meal Generator*.

The *Ontology Driven Graphical User Interface* guides the user in specifying the food menu request and the constraints related to delivery time or cost. Additionally, this module allows a medical specialist to introduce information about the medical history of the users.

The *Personal Profile Generator* generates the personal profile of a person, based on the information introduced by the user/medical specialist by means of the *Ontology Driven Graphical User Interface*. The personal profile of a person is stored as an XML file and it contains information about the user's food preferences for menu, constraints related to delivery time or cost for the menu, and information about the medical and personal profile of the user. The *Food Ingredient Database* contains information about food types, food recipes, ingredients, and quantities of ingredients for each food type/recipe. This database has been developed based on the information provided in [15]. The *Food Ontology* contains information about different types of food, the medical and personal profile of a person, and the medical diets in case of some chronic diseases. All the ingredients are specified for each type of food, and the quantity of fats, vitamins, calories, carbohydrates, iron, and proteins is given for each ingredient. The medical and personal profile of a person contains information about the illnesses affecting the person, as well as the age, weight, height, and gender of the person. The ontology also describes the diet recommendation in case of some chronic diseases (e.g., diabetes, hypertension, etc.). Figures 2 and 3 present a fragment of our *Food Ontology*. It can be noticed from Fig. 2 that sour vegetable soup is a vegetable mixture which contains eight ingredients: garlic, cream, tomatoes, potatoes, sunflower oil, carrots, black pepper, and onion. The garlic ingredient (see Fig. 3) contains 20 mg sodium, 137 kcal, 0.2 mg vitamin B, 1.7 mg iron, 7.2 g proteins, 16 mg vitamin C, 26 g carbohydrates, 0.2 mg vitamin A, 0.2 g fats, and 22.1 mg calcium per 100 gram.

The *Food Offer Repository* contains food offers (in XML format) from different food providers. Figure 4 presents an example food offer for sour vegetable soup. The *Invasive Weed-Based Healthy Meal Generator* generates healthy menus using the hybrid weed-based optimization algorithm and relying on the *Food Ontology*, the *User Personal Profile*, and the available *food offers*.

5.2 Case Study

We have tested our hybrid weed optimization method on a set of user profiles, some of them suffering from hypertension, some from diabetes of type I, and some from both hypertension and diabetes of type I simultaneously. In this section, we present a case study illustrating how the hybrid weed optimization method is used for generating healthy menu recommendations for a person with hypertension. The menu is generated by considering the set of food menu offers, the personal profile,

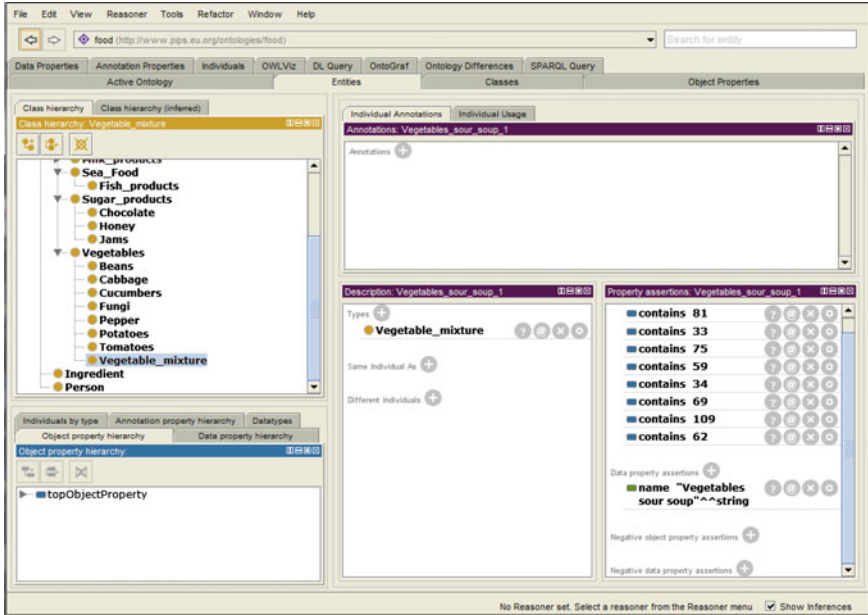


Fig. 2 Example from Food Ontology describing sour vegetable soup

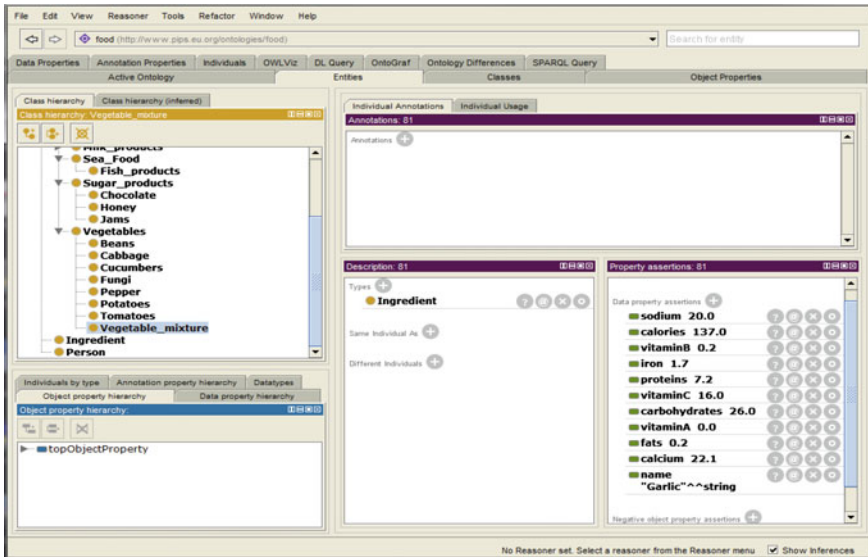


Fig. 3 Example from Food Ontology describing the garlic ingredient from sour vegetable soup

Fig. 4 Example of food offer

```
<?xml version="1.0" encoding="UTF-8"?>
<food>
  <name>Vegetables sour soup</name>
  <provider>Provider_0</provider>
  <meal>Lunch</meal>
  <type>Soup</type>
  <cost>8,12</cost>
  <time>65</time>
  <ingredients>
    <ingredient>
      <name>Carrots</name>
      <quantity>90</quantity>
    </ingredient>
    <ingredient>
      <name>Dried onion</name>
      <quantity>13</quantity>
    </ingredient>
    .....
  </ingredients>
</food>
```

Table 1 Personal profile and optimal nutritional values in the case of a user suffering from hypertension

Personal profile	Person age	69
	Person weight	55 kg
	Person height	164 cm
	Level of activity	Light active
	Favorite ingredient	Beef meat
	Disliked ingredient	Chicken meat
	Diseases	Hypertension
Optimal values	Calories	1740 kcal
	Proteins	120 g
	Fats	48.3 g
	Carbohydrates	195.6 g
	Iron	8–45 mg
	Sodium	500–1500 mg
	Vitamin A	1.2–7.5 mg
	Vitamin B1	1.6–5 mg
Vitamin C	75–1000 mg	

and the medical diet recommendation. In Table 1, we present the personal profile as well as the optimal values for the nutritional features of the menu. The values for the nutritional features of the menu are taken from [13], and they take into account the person’s diseases. Based on this information, the invasive weed-based healthy meal generator applies the hybrid invasive weed algorithm to select a food menu offer that best satisfies the user preferences related to the food and the medical diet recommendation. The solution returned (i.e., a food menu) is the cheapest and has the shortest delivery time among the set of solutions that satisfy the above-mentioned constraints (i.e., user preferences and diet recommendation).

In Tables 2, 3, 4, 5, and 6, we present some fragments of our best experimental results (in terms of average execution time (T_{avg}) and average fitness (fit_{avg})) obtained when varying the values of the adjustable parameters in the case of considered user. The adjustable parameters are the initial population of individuals pop_{init} , the number of iterations $noIt$, the maximum population size pop_{max} , the maximum number of seeds S_{max} , the minimum number of seeds S_{min} , the number of mutation points NoM , and the number of iterations It_{tb} in which a tuple of food items is tabu. Each row in Tables 2, 3, 4, 5, and 6 includes the average experimental results obtained after running the algorithm for 50 times on the same configuration for the adjustable parameters.

The experimental results have been obtained on the following versions of the algorithm:

- IWO—the classical invasive weed optimization algorithm [12].
- PRIWO—a version of the IWO algorithm as hybridized with path relinking.

Table 2 Experimental results obtained when running IWO for the user suffering from hypertension

p_{init}	noIt	p_{max}	S_{max}	S_{moin}	NoM	It_{tb}	T_{avg} (sec)	fit_{avg}
10	30	30	3	1	2	2	41.7889	0.803
10	30	20	3	1	2	2	27.7786	0.7877
10	30	30	5	1	3	2	49.8065	0.7871
5	30	20	3	1	2	2	26.913	0.7797
5	30	20	5	1	3	2	32.8974	0.768

Table 3 Experimental results obtained when running PRIWO for the user suffering from hypertension

p_{init}	noIt	p_{max}	S_{max}	S_{moin}	NoM	It_{tb}	T_{avg} (sec)	fit_{avg}
10	30	30	3	1	2	2	45.44	0.8328
10	30	20	3	1	2	2	32.498	0.8323
5	30	20	3	1	2	2	31.392	0.8303
5	30	20	5	1	3	2	38.029	0.8299
10	30	30	5	1	3	2	55.159	0.8266

Table 4 Experimental results obtained when running PRTSIWO for the user suffering from hypertension

p_{init}	noIt	p_{max}	S_{max}	S_{moin}	NoM	It_{tb}	T_{avg} (sec)	fit_{avg}
10	30	30	5	1	3	2	38.4918	0.7916
10	30	20	3	1	2	2	22.4285	0.7839
10	30	30	3	1	2	2	36.8198	0.7786
5	30	20	5	1	3	2	25.6025	0.7777
5	30	20	3	1	2	2	24.8249	0.7776

Table 5 Experimental results obtained when running PSOPRIWO for the user suffering from hypertension

p_{init}	noIt	p_{max}	S_{max}	S_{moin}	NoM	It _{tb}	T_{avg} (sec)	fit _{avg}
10	30	30	3	1	2	2	43.6375	0.7984
5	30	20	3	1	2	2	28.7828	0.7864
10	30	30	5	1	3	2	48.3846	0.7837
10	30	20	3	1	2	2	29.0498	0.7783
5	30	20	5	1	3	2	32.739	0.7696

Table 6 Experimental results obtained when running PSOPRTSIWO for the user suffering from hypertension

p_{init}	noIt	p_{max}	S_{max}	S_{moin}	NoM	It _{tb}	T_{avg} (sec)	fit _{avg}
10	30	30	3	1	2	2	36.3725	0.7558
5	30	20	3	1	2	2	24.678	0.7546
10	30	20	3	1	2	2	24.2882	0.7536
10	30	30	5	1	3	2	43.8209	0.7534
5	30	20	5	1	3	2	25.9016	0.7445

- PRTSIWO—a version of the IWO algorithm as hybridized with path relinking and tabu search.
- PSOPRIWO—a version of the IWO algorithm as hybridized with the PSO-based path relinking strategy.
- PSOPRTSIWO—a version of the IWO algorithm as hybridized with the PSO-based path relinking strategy and tabu search.

By analyzing the experimental results, it can be noticed that the best experimental results in term of fitness values, with a time penalty, are obtained in the case of variant PRIWO of the algorithm (see row colored gray in Table 3). In terms of execution time, the best experimental results are obtained in the case of variant PRTSIWO of the algorithm, with an insignificant fitness penalty. The fitness in the case of PRTSIWO is with 0.003 lower on average than in the case of IWO, while the execution time is better for PRTSIWO as compared with IWO—29.6 s versus 35.8 s on average across the various configurations of the adjustable parameters. Additionally, we have noticed that the PSO-based variants of the algorithm do not bring any significant improvement over the classical IWO algorithm. In conclusion, we can say that PRTSIWO provides the best results in what regards the fitness values achieved versus execution time (Fig. 5).

We illustrate below the best solution (i.e., menu) that is generated when running the variant PRTSIWO of the algorithm with the optimal configuration of the adjustable parameters (see row colored gray in Table 4) and by considering the user profile presented in Table 1.

Option 1	Option 2	Option 3	Option 4	Option 5	Chart
Breakfast	Scrambled eggs with mushrooms and orange juice				Provider_48
Morningsnack	Cottage cheese with cherry gem				Provider_21
Lunch - Soup	Beef sour soup with cabbage				Provider_23
Lunch - Main	Boiled potatoes with grilled sirloin beef				Provider_34
Lunch - Dessert	Pancakes with apricot jam				Provider_2
Afternoonsnack	Bananas				Provider_36
Dinner	Boiled potatoes with grilled sirloin beef				Provider_1
Food properties:		Optimum nutrients:			
Calories	1695,72 Kcal	1739,4 Kcal			
Proteins	126,47 g	119,58375 g			
Fats	46,99 g	48,3166666666667 g			
Carbohydrates	188,1 g	195,6825 g			
Iron	27,67 mg				
Sodium	633,84 mg				
Vitamin A	2,71 mg				
Vitamin B	1,98 mg				
Vitamin C	225 mg				
Total price	70,5 RON				
Maximum delivery time 75 min					

Fig. 5 The best solution (menu) obtained when running the PRTSIWO algorithm with the optimal configuration of the adjustable parameters

6 Conclusions

In this paper, we have presented a new method for generating healthy menu recommendations starting from a given user profile, a medical diet recommendation, and a set of food menu offers. Our method is based on a hybrid invasive weed optimization model, which consists of a core component and two hybridization components. The core component is based on the invasive weed optimization algorithm, while the hybrid components rely on the path relinking and tabu search algorithms. The hybrid invasive weed optimization algorithm is based on the hybrid invasive weed optimization model and it has the role of generating healthy menu recommendations starting from a given user profile, a medical diet recommendation, and a set of food offers. The method proposed here has been integrated into an experimental prototype and tested on a set of various user profiles.

Acknowledgments This work is carried out under the AAL Joint Programme with funding by the European Union (project number AAL-2012-5-195) and is supported by the Romanian National Authority for Scientific Research, CCCDI UEFISCDI (project number AAL—16/2013).

References

1. http://www.who.int/countryfocus/cooperation_strategy/ccsbrief_rou_en.pdf
2. <http://www.mhhe.com/hper/physed/clw/01corb.pdf>
3. <http://nihseniorhealth.gov/eatingwellasyougetolder/benefitsfeatingwell/01.html>
4. Willett WC (2000) Balancing life-style and genomics research for disease prevention. *Science Magazine*
5. Glover F, Laguna M (1997) *Tabu search*. Kluwer Academic Publishers, Norwell
6. Glover F, Laguna M (2004) Scatter search and path relinking: foundations and advanced designs. In: *New optimization techniques in engineering studies in fuzziness and soft computing*, vol 141, pp 87–99
7. Snae C, Brückner M (2008) FOODS: A Food-Oriented Ontology-Driven System. In: *The second ieee international conference on digital ecosystems and technologies*, pp 168–176
8. Sivilai S, Snae C, Brueckner M (2012) Ontology-driven personalized food and nutrition planning system for the elderly. In: *The 2nd international conference in business management and information sciences*
9. Kashima T, Mtsumoto S, Ishii H (2011) Decision support system for menu recommendation using rough sets. *Int J Innov Comput Inf Control* 7(5):2799–2808
10. Bing W, Fei W, Chunming Y (2010) Personalized recommendation system based on Multi_Agent and Rough Set, pp 303–307. In: *The 2nd international conference on education technology and computer (ICETC)*
11. Gaal B, Vassanyi I, Kozmann G (2005) A novel artificial intelligence method for weekly dietary menu planning. *Methods Inf Med* 44(5):655–664
12. Mehrabian AR, Lucas C (2006) A novel numerical optimization algorithm inspired from weed colonization. *Ecol Inform* 1(4):355–366
13. Harris J, Benedict F (1919) *A biometric study of basal metabolism in man*. Washington D.C, Carnegie Institute of Washington
14. Kennedy J, Eberhart R (1995) Particle Swarm Optimization. *Proc Int Conf Neural Netw* 4:1942–1948
15. Graur M (2006) *Guide for a healthly diet*. Iasi, Romania, Performatica

Therapeutic Conduct and Management of Rehabilitatee Treatment Measured with Zebris Device and Applied Using WinSpine Software

Andrei Diana, Poenaru V. Dan, Nemes Dan, Surducan Dan and Gal-Nadasan Norbert

Abstract Hereditary factors, stress, environmental factors, wrong diet, sedentary are increasingly common causes of developing degenerative lesions of the spine in young adults and beyond. This chapter aims to demonstrate the importance of good management therapeutic practices and having an appropriate therapeutic conduct. This has been demonstrated using software that extracts the flexion mobility minimums and maximums in measurements made using Zebris in both surgically untreated patients and those surgically treated. The study proves a statistically significant improvement in flexion spinal mobility at patients surgically treated (see in this paper Bonferroni test (ANOVA test: $F = 745.19$ $p < 0.001$)) compared to untreated surgical (Bonferroni test (ANOVA test: $F = 9.59$ $p < 0.001$)).

Keywords Lumbar spine · Mobility · Zebris · Flexion · Degenerative lumbar flexion · Winspine

A. Diana (✉) · P.V. Dan · N. Dan · S. Dan
University of Medicine and Pharmacy “Victor Babes”, Timisoara, Romania
e-mail: andreidiana81@gmail.com

P.V. Dan
e-mail: danvpoenaru@gmail.com

N. Dan
e-mail: nemes.dan@gmail.com

S. Dan
e-mail: surducan_dan@yahoo.com

G.-N. Norbert
Politehnica University of Timisoara, Timisoara, Romania
e-mail: norbert.gal@aut.upt.ro

1 Introduction

Intervertebral disc degeneration is characterized by dehydration of the pulpous nucleus and annulus fibrosus wear as a result of multiple mechanical and biochemical factors. A number of degenerative changes can be described as processes of destabilization followed by restabilizing processes.

Initially, the lesions of annulus fibrosus result in the loss of the pulpous nucleus contention ability. The internal concomitant changes of the pulpous nucleus lead to obstructing the joint space and to a reduced loading capacity of that vertebral segment. The nuclear material is not firmly contained within the intervertebral disc and will migrate in the direction of least resistance, which is usually toward posterior or posterolateral.

This migration leads to a “prominent” or “encapsulated hernia” of the annulus fibrosus toward the vertebral hole or root canal. If the means of the ring contention lose their stability, the nuclear material can herniate. This is the so-called “real hernia” or “non encapsulated hernia” [1].

The degenerative process is defined by structural changes, but the way the changes produce symptoms is less clear. Theories may be issued of how clinical pain occurs and shows, depending on each degenerative stage.

The examination of the patient with low back pain by specialists follows 12 steps: (after Finneson) [2]

- Observe the patient while moving, walking, and sitting (observation of spine and buttocks);
- Short-distance walking, walking on tiptoe and heels;
- Mobility of spine: extension, lateral inclination, and rotation of the body. Mobility is not expressed in degrees, as in other joints, but rather in terms like normal, slightly limited (it achieves approximately $\frac{3}{4}$ of maximum amplitude), moderately limited (about $\frac{1}{2}$ of normal amplitude), severely limited (about $\frac{1}{2}$ of amplitude);
- Mobility of spine: flexion. This mobility can be measured using the device called Zebris and this measurement represents the topic of our paper;
- Place the patient in his knees by complete flexion of the knees and hips and note any pain that occurs in the spine, knees, or hips;
- Test reflexes of the tendon, knee, and ankle compared to the right and left, to identify possible nerve damage;
- The measurement of legs length to identify a possible spinal imbalance caused by the inequality of the legs;
- Test the sensitivity of the legs;
- Test the muscle strength in the legs, comparative measurements of the thigh and calf circumference;
- Evidence of elongation of the sciatic nerve in both legs using Lasegue technique [3]. This test also shows the hamstring shortening or spasm;
- Mobilization of the coxofemoral joints, especially rotations and sacroiliac pain provocation tests to exclude an impairment at this level;

- Review the spine—the pressure on the spinous processes to identify areas of local sensitivity and reproduction of sciatic pain (“ring sign”);
- Assessment of the pulse at pedal pulses arteries, popliteal, and inguinal.

The purpose of this paper is to define an appropriate course of treatment as a more efficient management and to develop a software platform called WinSpine for determining the minimums and maximums in flexion measuring using Zebris.

2 Device Zebris Description

Zebris CMS-HS analysis system can be used for acquisition and three-dimensional (3D) analysis of all types of human and animal motion. When operating in the kinematics/dynamics of the human body, the system consists of modules specific to each type of investigation: 3D analysis of the motion, study of cervical and lumbar spine mobility, posture analysis, and analysis of plantar pressure distribution. Integration of various modules into a single system acquisition and analysis is conducted through the central unit, which acts as acquisition, digitization, and signal transmission to PC. Processing and presentation of recorded signals is by means of software dedicated to the type of analysis. The operating principle of the device is shown in Fig. 1 and is based on elapsed time from emission to reception of an ultrasonic pulse. It is used in the medical investigation. The equipment represents an additional important instrument used for diagnosis and assessment of recovery.

Examination of the head and trunk movements in recent years become a routine clinical examination of patients with spine problems. Such an examination is objective, accurate, and reproducible, which is very useful with classical methods of consultation, and to assess mobility dysfunctions manifested by a person. The

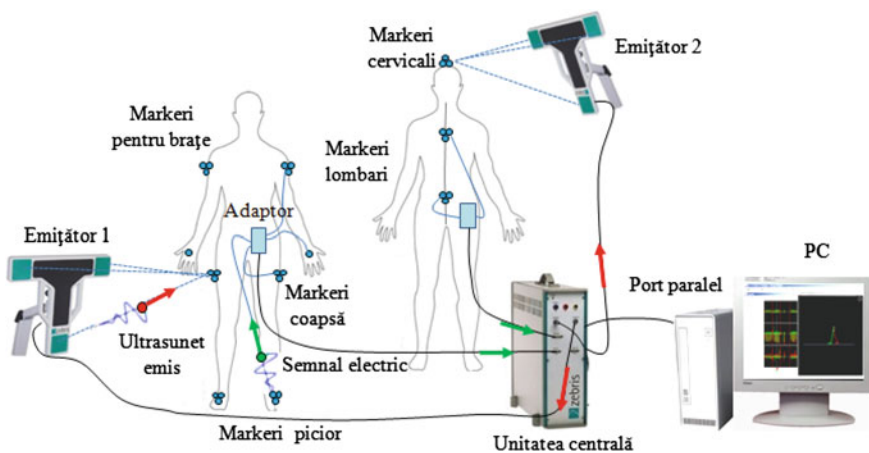


Fig. 1 Zebris CMS system scheme of the measuring principle

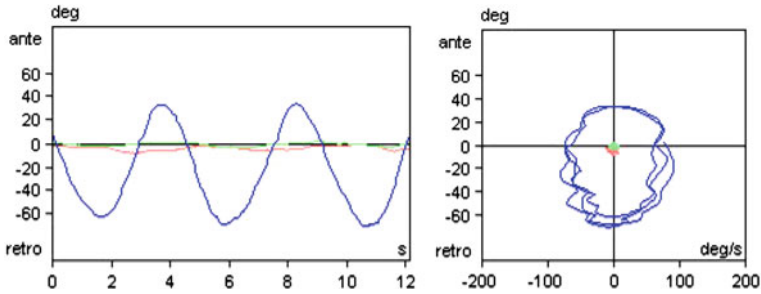


Fig. 2 Flexion sinusoid

investigation can be performed both in the case of disorders caused by pathological cases (neural, muscular, joint, and skeletal) and in assessing a person's ability to work.

Mobility analysis of one of the segments of the spine using the spine Zebris investigation system provides information such cinematic, particularly useful in determining more precisely the state of mobility and performance of motion of a subject. In recovery, the system provides real-time feedback to the medical treatment followed by a patient.

Parameters determined by this type of investigation are:

- Global angular amplitudes (degrees of mobility) of the cervical and lumbar segments, in all three anatomical planes (flexion-extension, rotation and lateral flexion);
- Instantaneous angular velocities of the movements considering the lower end of the investigated segment as fixed.

The results offered by Zebris are of a sinusoid type (see Fig. 2). We have to determine the minimums and maximums of this sinusoid in order to make a precise prediction of the degenerative lesions evolution.

After the achievement of records, the store of the results is done and the measurement report is generated. The report can be issued directly, without requiring the processing of measurements using WinSpine software. Registered parameters can be exported as text file, in order to make comparisons between different subjects [4]. The WinSpine software was developed to determine the minimums and maximums values reported by the Zebris measurements.

3 Evaluation of Flexion in Lumbar Degenerative Lesions Using WinSpine Software and Zebris Device

The WinSpine software has three components: Zebris measurements, pain questionnaires, and consumed daily calories. A detailed description of WinSpine is presented in [5]. The software can indicate a correct rehabilitee action for the questioned patient.

The reason why they determine flexion minimums and maximums with our proposed software is to find out the mobility grade of the spine. This information is not provided by the Zebris device. Considering this mobility grade of the spine, a doctor can recommend the patient a rehabilitatee program adapted for his physical capabilities.

The evaluation of the data obtained from the WinSpine software is realized using a software tool based on a fuzzy inference system [6].

The data obtained from the WinSpine software is structured in a 2D array (t, d), where t is the time stamp when the sample was taken and d is the degree of motion. Each patient has one array for each exercise. Each exercise contains several repetitions. Our software extracts from each repetition the maximum (1) and minimum (2) values and creates a mean value of the maximums and the minimums according to the following mathematical formulas:

$$F_{\max} = \frac{\sum_{i=1}^n \text{rep_max}_n}{n} \tag{1}$$

$$F_{\min} = \frac{\sum_{i=1}^n \text{rep_min}_n}{n} \tag{2}$$

where F_{\max} and F_{\min} are the mean maximums and minimums, rep_max and rep_min are the maximums and minimums of each repetition. A screenshot of the software is presented in Fig. 3.

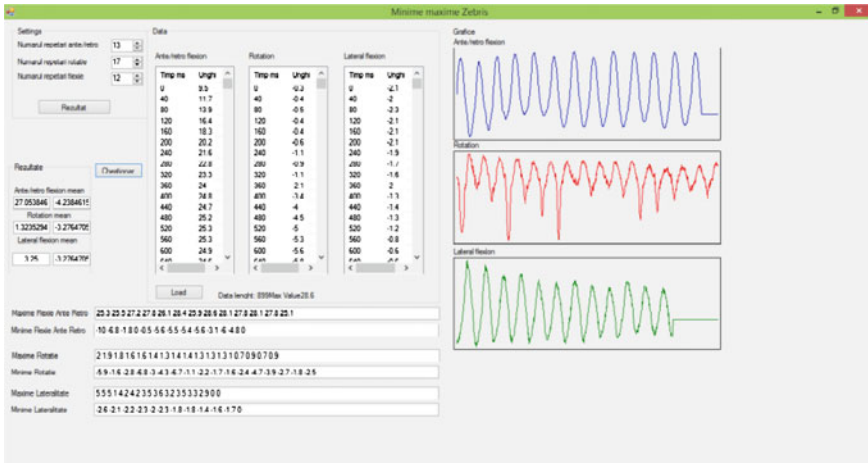


Fig. 3 Screenshot of software application for flexion evaluation

4 Results of Flexion Evaluation in Degenerative Lumbar Lesions Using Zebris Device

Values provided by the system Zebris are initially evaluated in two groups. We selected a number of 260 patients with degenerative lumbar lesions. Due to the severity of the disease, 107 patients had surgery indication and the remaining 153 subjects did not require surgery. Five evaluations were performed on each patient in the two groups with a deviation of ± 2 days. The following graph was observed:

- 1—Initial (before the adoption of surgical or non-surgical therapy management, group 1 and 2);
- 2–6 months (before applying cure 2 of therapy, group 1 and 2);
- 3–7 months (after applying cure 2 of therapy, group 1 and 2);
- 4–12 months (before applying cure 3 of therapy, group 1 and 2);
- 5–13 months (after applying cure 3 of therapy, group 1 and 2).

In group 1, 107 patients underwent surgery and three cures of ten sessions, three times in a week every 6 months (initially after surgery, at 6 months and at 12 months). In group 2, 153 patients were treated by regular medical rehabilitation: three cures of ten sessions, three times in a week every 6 months (initially, at 6 months and at 12 months).

Regarding the angle (flexion), the absence of statistically significant differences ($p > 0.05$ —unpaired t test) between the groups was recorded only in the flexion (evaluation 1) and rotation (evaluation 1 and 2). The remaining evaluations indicated more favorable values in group 1 compared with group 2, a statistically significant difference was present ($p < 0.05$). The values are presented in Table 1.

A comparison of evaluations within each group was performed by ANOVA.

The ANOVA test presented in Table 1 revealed a highly significant overall difference ($p < 0.001$) in both groups for flexion, group 1 having a more favorable evolution.

Bonferroni test confirmed favorable results in group 1 compared with group 2. Comparison between the five evaluations, using Bonferroni test, is a comparison of the following evaluations: 2 with 1, 3 with 2, 4 with 3, and 5 with 4. It results four comparisons between values, each comparison being characterized by the presence or absence of statistical significance. The presence of statistical significance represents a significant improvement of the value obtained from an evaluation compared to the value achieved from the previous evaluation.

Regarding flexion in group 1 there were highly significant differences ($p < 0.001$) between all evaluations. In group 2 there was highly statistically significant difference ($p < 0.001$) only in the evaluation of 5 versus 4 (see Table 2).

Table 1 Evaluation of the daily activity using Zebris system (flexion)—statistics in the 2 groups

Zebris (flexion)		Group 1	Group 2	
Evaluation 1	Average	8.674766	8.68366	Unpaired <i>t</i> test group 1—group 2 <i>t</i> = -0.0263 <i>p</i> > 0.05
	DS	3.267163	2.196213	
	Maximum	20.9	13.5	
	Q3	10.6	10.5	
	Median	8.4	8.9	
	Q1	6.3	6.8	
	Minimum	2.4	3.3	
Evaluation 2	Average	11.14393	9.285163	Unpaired <i>t</i> test group 1—group 2 <i>t</i> = 5.3626 <i>p</i> < 0.001
	DS	3.253073	2.336716	
	Maximum	23.3	14.31	
	Q3	13	11.24	
	Median	11.1	9.43	
	Q1	8.9	7.37	
	Minimum	4.8	3.5	
Evaluation 3	Average	20.8514	9.545621	Unpaired <i>t</i> test group 1—group 2 <i>t</i> = 31.5751 <i>p</i> < 0.001
	DS	3.372541	2.402146	
	Maximum	34	14.72	
	Q3	22.7	11.55	
	Median	20.7	9.7	
	Q1	18.6	7.57	
	Minimum	14.2	3.6	
Evaluation 4	Average	26.5486	9.211176	Unpaired <i>t</i> test group 1—group 2 <i>t</i> = 47.2875 <i>p</i> < 0.001
	DS	3.586515	2.322999	
	Maximum	41.5	14.13	
	Q3	28.4	11.09	
	Median	26.4	9.36	
	Q1	24.2	7.42	
	Minimum	19.8	3.45	
Evaluation 5	Average	28.7514	10.31183	Unpaired <i>t</i> test group 1—group 2 <i>t</i> = 48.3499 <i>p</i> < 0.001
	DS	3.548834	2.600405	
	Maximum	41.6	15.68	
	Q3	30	12.35	
	Median	28.5	10.43	
	Q1	26.4	8.48	
	Minimum	22.2	3.83	
		ANOVA group 1 <i>F</i> = 745.19 <i>p</i> < 0.001	ANOVA group 2 <i>F</i> = 9.59 <i>p</i> < 0.001	

Table 2 Assessment using Zebris system (flexion)—comparison between the values obtained from evaluations

Zebris (flexion)					
Group 1	Bonferroni test (test ANOVA: $F = 745.19$ $p < 0.001$)				
	Evaluation	1	2	3	4
	2	2.46916 $p < 0.001$	–	–	–
	3	12.1766 $p < 0.001$	9.70748 $p < 0.001$	–	–
	4	17.8738 $p < 0.001$	15.4047 $p < 0.001$	5.6972 $p < 0.001$	–
	5	20.0766 $p < 0.001$	17.6075 $p < 0.001$	7.9 $p < 0.001$	2.2028 $p < 0.001$
Group 2	Bonferroni test (test ANOVA: $F = 9.59$ $p < 0.001$)				
	Evaluation	1	2	3	4
	2	0.601503 $p > 0.05$	–	–	–
	3	0.891961 $p = 0.016$	0.260457 $p > 0.05$	–	–
	4	0.527516 $p > 0.05$	–0.073987 $p > 0.05$	–0.334444 $p > 0.05$	–
	5	1.62817 $p < 0.001$	1.02667 $p = 0.002$	0.766209 $p = 0.049$	1.10065 $p < 0.001$

5 Conclusions

A positive statistically significant ($p < 0.05$) when compared to the angle obtained by Zebris system signified an improvement in mobility.

Regarding study group 1 compared with group 2, most of the angles statistically significant improvements were observed in group 1. In the group 2 were observed angle decreases when compared (Evaluation 4 versus evaluation 3).

The common element is the presence in group 2 of an increase disability status (positive value) and a decrease in the angle (negative value) for evaluation 4 compared to evaluation 3. This element demonstrates the absence of improving the ability to perform daily activities in the presence of mobility decline.

The results are more favorable in group 1 compared with group 2.

References

1. Herbert CM, Lindberg KA, Jaysonivi I, Bailey AJ (1975) Proceedings: intervertebral disc collagen in degenerative disc disease. *Ann Rheum Dis* 34(5):467–468
2. Finneson BE, Cooper VR (1979) A lumbar disc surgery predictive scorecard. A retrospective evaluation. *Spine* 4:141–144 [PubMed]

3. Devillé WL et al (2000) The test of lasègue: systematic review of the accuracy in diagnosing herniated discs. *Spine J* 25(9):1140–1147
4. Toth-Tascau M, Stoia DI (2010) Aparate pentru investigatii medicale simple. In: Timisoara P. ISBN 978-606-554-233-4
5. Gal N, Stoicu-Tivadar V, Andrei D, Nemeş DI, Nădăşan E (2014) Computer assisted treatment prediction of low back pain pathologies. *Stud Health Technol Inform* 2014(197):47–51
6. Gal N, Stoicu-Tivadar V (2012) Knowledge representation for fuzzy inference aided medical image interpretation. In: 24th European medical informatics conference—MIE2012—in Pisa, pp 98–102 [PubMed]

A Novel Approach on the Newborns' Cry Analysis Using Professional Recording and Feature Extraction from the "First Cry" with LabVIEW

F. Feier and I. Silea

Abstract Newborn cry analysis has been a subject of interest for both the medical and engineering field together, more pronounced for the past 20 years. In this timeframe, as the acquisition instruments have developed a lot and new equipment with broader analysis spectrum arose, these studies became more and more interesting. Crying is one of the few signals that can be studied in case of a newborn, without going into invasive medical tests, in order to determine a physiological and psychological state. This paper is aimed to propose another feature extraction technique using a professional sound acquisition tool (studio recorder) and a specialized signal processing tool, LabVIEW. This new approach is tested on a newborn cry after birth and proposed for the "first cry" analysis, a novel approach in newborn cry analysis, where the first vocalizations of the newborn are recorded and analyzed.

Keywords Newborn cry analysis · Signal processing · LabVIEW · "First cry" analysis

1 Introduction

The study of newborns' cry has been a topic of increased interest for the past 20 years, as engineers work together with the medical personnel in this interdisciplinary research with still has a lot to offer. In the past decades, the idea of correlating the cry with other physical parameters (body temperature, pulse, blood saturation, fetal growth [1], and many others) in order to tie them to different types of medical conditions has been extended with the in depth analysis of the cry signal

F. Feier (✉) · I. Silea
Universitatea Politehnica Timisoara, Timisoara, Romania
e-mail: flaviu.feier@aut.upt.ro

I. Silea
e-mail: ioan.silea@aut.upt.ro

itself. Digital signal processing is more and more present in the studies performed in the past years with the purpose of obtaining information from the cry signals with the use of a numerous types of sound acquisition instruments: a large variety of microphones, tape recorders, digital video cameras, or digital Dictaphones [2, 3].

Analysis performed on the newborn cry are intended to determine a set of parameters that can be useful as indicators to determine a relationship between these and different pathologies (hypothyroidism, hypoxia, hearing disorder, asphyxia, autism) or as symptoms that could also be defining for a certain physical or psychological state (discomfort, pain, sadness, hunger, anger) [4–6]. For example, some indicators used in most of the studies for the analysis of the audio signal from the newborn cry signal are represented by:

- The fundamental frequency (F_0) [7–9];
- The melody of the cry (the changing in time of the values for the fundamental frequency, F_0) [2, 10];
- The first three formants (F_1, F_2, F_3) [8];
- The noise in the cry signal;
- The vocal tract resonance frequency [11].

From the various studies, some conclusions have been drawn, relative to parameter values and the aspect of the cry waveform. In this line of ideas, a normal or healthy infant cry is characterized by:

- Average F_0 values of 450 Hz, with range from 400–600 Hz [12, 13];
- The melody form that prevails is rising–falling [12];
- There are more sound cries [12].

The cry with a pathological tendency is defined as:

- Cries with extreme values in the F_0 .
- The melody forms that prevail are falling, falling–rising, flat, and without melody form.
- Glides and shifts are happened most [14].

Among the birth characteristics mostly used in studies are the weight, height, Apgar score at 5–10 min, head circumference or mothers' gestational age, can be mentioned. On the other hand, the physiological measurements consist of newborns' heart rate, peripheral blood saturation of the oxygen (measured with pulse oximeter), or central blood saturation (measured with NIRS spectrometer (Near Infrared Spectroscopy)) [11].

The current study is based on results and experience reported in previous articles [15, 16], where the Neonat software was presented and the results of different classifications performed, were offered as well. The Neonat software was developed by the authors was designed for cry signal acquisition, preprocessing of this, and data preparation for the Data Mining activities. The main features of the Neonat tool consist of the following:

- The cry signal from the newborn is acquired via microphone into the Neonat software, where the signal is sampled at 11 kHz after which a rectangular window function is applied before performing a Fast Fourier Transform (FFT).
- The discrete signal with the Fourier coefficient is stored in buffers for each 100 ms of the cry signal and at the end a geometric normalization is applied to the buffered elements.
- Neonat measurements capture the peak and average values of the signals from the cry waveform, with the use of an emulated Volume Unit Meter and Peak Program Meter and also present the frequency spectrum of the cry in a three-dimensional visualization (frequency, intensity, and color).

A first study [15] showed a sex differentiation from the cry signals by performing a classification with Weka, a Data Mining dedicated tool. Weka is a specialized software application developed in Java that consists of machine learning algorithms used to perform Data Mining [17, 18]. Decision tree [19, 20], lazy algorithms [21], and rule-based classifiers [22], have shown the best classification results in the performed studies.

The second study is represented by pathology studies, with the goal of obtaining a classification for newborns' that were medically determined as healthy or with some particular affection. Four lots containing newborn cries have been created after having the medical part diagnose each one in particular. These lots contain cries of babies that were evaluated as having no health problems, ones that suffered umbilical cord strangulation at birth and showed respiratory problems, others that were born premature [23] and the last lot with newborns' with normal birth and born on-time, but who had indications of health problems not related to the ones in the other categories. In order to achieve the classification goal, the Neonat software coupled with the data mining tool Weka were used.

The current study gathers the experience from previous researches and proposes another one, consisting in sound acquisition with a professional studio voice recorder (Olympus LS-100). In depth, studies of the cry signals recorded with the device are loaded into the dedicated signal processing software LabVIEW, where a large variety of methods for feature extraction can be performed. Another novelty of the current research is the acquired cry signal, which is the "first cry". There was no study identified by the authors so far, that considers in the newborns' cry analysis of the first sounds after birth. This is due to the difficulty in performing sound acquisition in a delivery room and the pre-processing activities needed to extract the cry from a recording which has a fair amount of noise over it. Our first considerations with this new approach in the study of the newborns' cry are presented in the sections below, with respect to equipment and tools to perform the analysis.

2 Cry Signal Acquisition with the Professional Recorder

As mentioned above, this new study performs the cry signal acquisition with the use of a professional sound recorder, used in audio studios for both voice and musical instrumentation recording. The device shown in Fig. 1 is an Olympus LS-100 Multi-Track Linear PCM (Pulse Code Modulation) recorder with the most relevant characteristics to the research as follows [24, 25]:

- Built in high sensitivity 90° directional two-microphone system;
- Uncompressed 24 bit/96 kHz linear PCM recording capability;
- Audio and system circuitry are separated in order to minimize sound degradation;
- Switchable low-cut filter that eliminates low-frequency sound from 100–300 Hz;
- Pre-record buffer that captures 2 s before starting the recorder;
- Possibility to start the recording when the sound reaches a certain level;
- Built in 4 GB NAND flash memory;
- Sampling frequency for PCM: 44.1–96 kHz;
- Frequency characteristics: 20–20.000 Hz.

Given the high-end capabilities of the recording system, the acquired cry signal offers undoubtedly a better quality of the signal in delivery room conditions, and the reliability of the studies performed is very high. This ensures that no cry components are lost and that the study will not oversee information which might be in fact the differentiator while performing classification studies.



Fig. 1 Olympus LS-100 multi-track linear PCM recorder [24]

3 LabVIEW

Laboratory Virtual Instrument Engineering Workbench (LabVIEW) is a development environment most commonly used for data acquisition, instrument control, and industrial automation [16]. LabVIEW provides a dedicated library for signal processing, comprised among others of waveform generators, filters, spectral analysis components, transforms, or wavelet analysis.

In this study, as a first step, LabVIEW is used for processing the cry signal recorded with the Olympus dedicated device. A simple block diagram presented in Fig. 2 allows the importing of a cry signal in a raw format (.wav), in order to store it locally and plot the waveform of the intensity over time graph.

Figure 3 presents the plot of the imported cry signal, in graph representing the waveform of an imported cry signal. The imported cry signal corresponds to a recording made with the Neonat software. Therefore, the waveform represents a cry signal with the noise eliminated in the pre-processing phase, and a windowing function applied over the first stage pre-processed signal.

The preliminary experiences with the “first cry” acquired with the dedicated recording device are represented in Fig. 4. The first challenge when dealing with the “first cry” is again the pre-processing part. In the below representation, the noise over the two cry signals is given by the medical personnel vocalization. This inconvenience, very hard to avoid during the birth procedures is unavoidable but solutions for this matter have already been given in other studies. The resolving consists of complex filtering of the entire signal, to extract only the cry, without losing any features from the newborn vocalization. Another resolution for this situation is for considering in the study only the newborn recording where no other vocalization is present. The other sources of noise easily avoidable with the enabling of the low-cut filter of the recording device, which stops the low frequencies of 100–300 Hz.

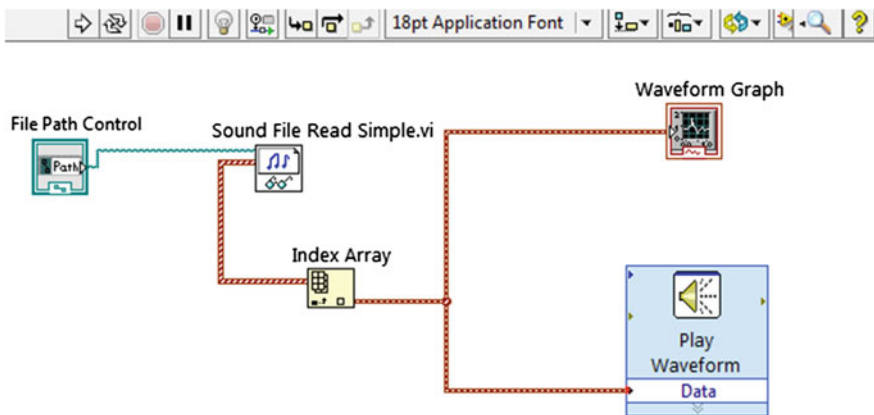


Fig. 2 LabView block diagram for processing a raw audio file

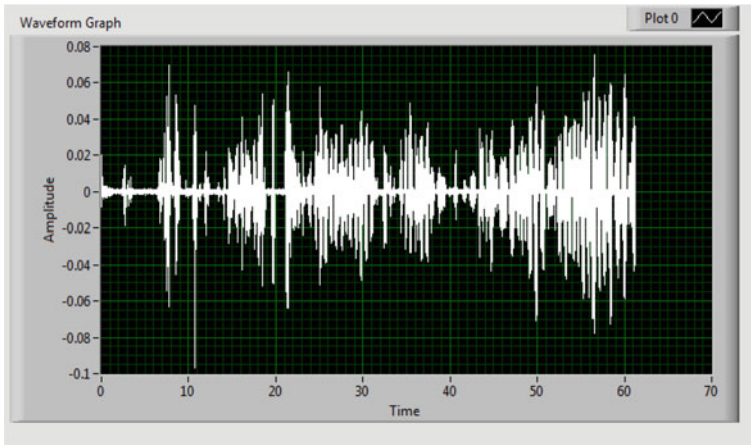


Fig. 3 Newborn cry acquired by Neonat and imported in LabVIEW

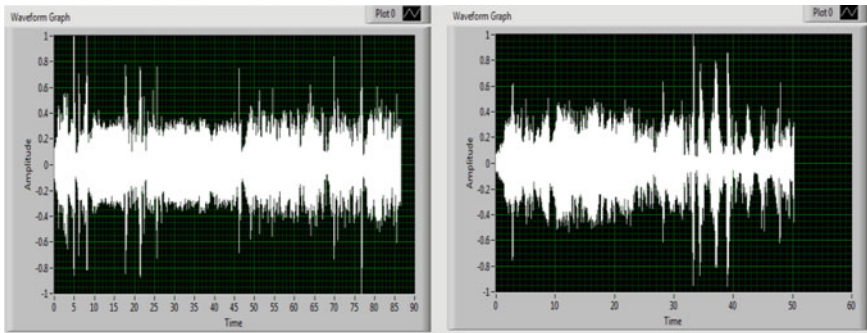


Fig. 4 “First cry” #1 and #2 in LabVIEW

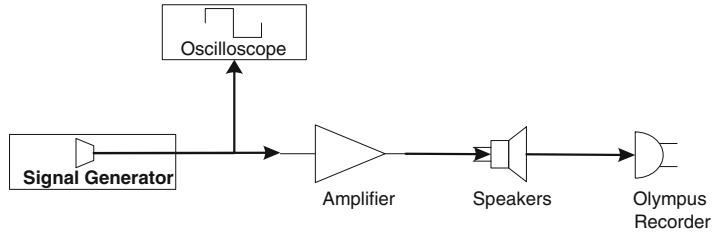
4 Equipment Preparation and Calibration

In order to correctly extract features from the cry signal, a method is proposed in order to ensure that the collected data and its interpretation is the correct one.

(A) Calibrating the cry acquisition device.

- (a) The first operation consists in generating a signal with the use of a dedicated signal generator that has the amplitude and a fundamental frequency (F_0) in the audio range (16–20 kHz).
- (b) A second operation consist in transforming the generated signal into an audible signal with the use of an amplifier which needs to be connected to high-end speakers that have a known characteristic according to their data sheet provided by their producer.

STEP 1



STEP 2

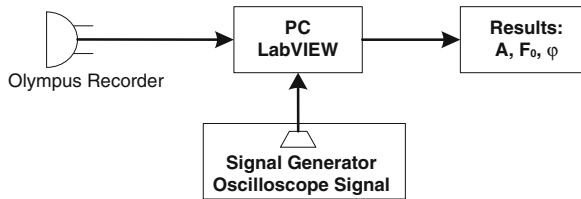


Fig. 5 Steps to prepare and calibrate the acquisition system

- (c) The resulted audio signal is recorded with the Olympus acquisition device, with its default configuration for recording. The default configuration can be modified if needed, the most important aspect here being the knowledge about the recording settings and parameters that the device uses.
- (d) The last operation performed is the transfer of the recorded information into LabVIEW and the comparison with the initially generated signal (which is stored on an oscilloscope with memory).

By comparing the parameters of the two signals, amplitude, fundamental frequency (F_0) or phase, with the use of functions offered by LabVIEW, differences in the spectrums might be encountered. This information can be very valuable for the interpretation and maybe correction brought to the “first cry” recorded signals.

Figure 5 shows the calibration system design, and the steps that need to be taken in order to validate the results of the acquired cry signals. After the parameter values of the generated signal are established, recording is done with the Olympus recorder, and the acquired signal at the recorder is compared to the generated signal with the use of components provided by LabVIEW.

(B) Cry signal acquisition

The “first cry” signal acquisition is performed via the Olympus recorder at the hospital in the delivery room.

(C) Preparing and interpreting the data

Figure 6 presents the importing of cry signals into LabVIEW, from the recording device, and the interpretation of data, the data after doing signal adjustments for parameters defined in the previous stages.

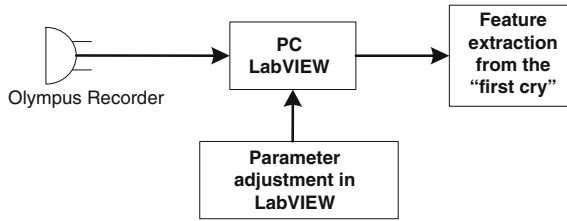


Fig. 6 Preparing and interpreting of the data

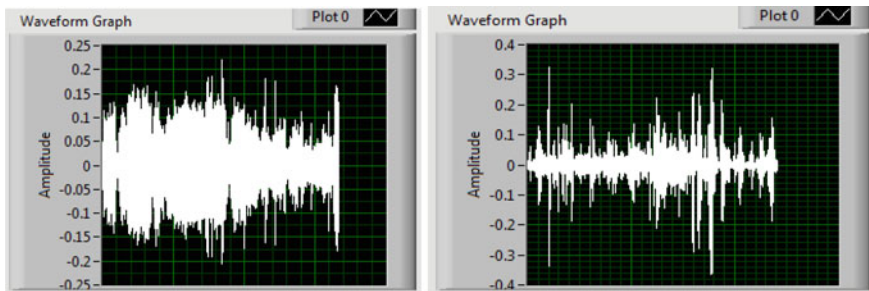


Fig. 7 “First cry” #1 and #2 after filtering with LabVIEW

The parameter adjustment performed in LabVIEW can be a result of a filtering operation, applying a window function over the signal, extracting the spectrum or other operations. In Fig. 7, a filtering is performed on the first two acquired cry signals.

5 Conclusions

This chapter is presenting a novel approach to newborns’ cry signal analysis. A professional recording tool was introduced in this study, the Olympus LS-100 Multi-Track Linear PCM recorder as opposed to conventional microphones which have been used in the previous studies. The pre-processing and feature extraction from the cry is performed by another dedicated tool, the LabVIEW development environment, which provides dedicated libraries for advanced signal processing with components like filter, waveform generators, window functions, or spectrum representations.

The analysis of the “first cry” is as well a novelty in this domain. The “first cry” represents the primal vocalization of the newborn at birth. The “first cry” can be acquired only in the delivery room aspect that makes the whole acquisition process more difficult. A pre-processing of the acquired data is necessary to extract only the cry signal.

The goal of this research is to apply already studied feature extraction techniques from this primal cry in order to perform classification studies for different pathologies. Based on the results obtained from the proposed studies, alternative feature extraction modalities or parameters can be provided in order to gain more knowledge in this area. Having already developed software for acquisition and pre-processing of the cry signal, this can be enhanced with other feature detection algorithms after the validation in LabVIEW, which allows a faster reach of results.

The final aim of the research in the newborn cry analysis is to create a screening device based on cry signal acquiring which can be able to inform the medical personnel about the high probability of a certain pathology discovered from the newborn cry. This result shall determine a more focused attention on the newborn, and specialized tests can be performed and treatment applied immediately. The screening result can also eliminate unnecessary invasive test that are being done in order to eliminate certain pathology suspicions.

Acknowledgments This work was partially supported by the strategic grant POSDRU/159/1.5/S/137070 (2014) of the Ministry of National Education Protection, Romania, co-financed by the European Social Fund—Investing in People, within the Sectoral Operational Programme Human Resources Development 2007–2013.

References

1. Wermke K, Robb MP (2010) Fundamental frequency of neonatal crying: does body size matter, Wurzburg, Germany and Christchurch, New Zealand. *J Voice* 24(4):388–394
2. Várallyay GG, Benyó Z (2007) Melody shape—a suggested novel attribute for the biomedical analysis of the infant cry. In: Proceedings of the 29th annual international conference of the IEEE EMBS cité internationale, Lyon, France, pp 4119–4121
3. Balou G (2008) Handbook for sound engineers, 4th edn. Elsevier Inc., pp 999–1005
4. Silva M, Mijovic B, van den Bergh BRH, Allegaert K, Aerts JM, Van Huffel S, Berckmans D (2010) Decoupling between fundamental frequency and energy envelope of neonate cries. *Early Human Dev* 86:35–40
5. Bocchi L, Spaccaterra L, Acciai F, Orlandi S, Favilli F, Atrei E, Manfredi C, Donzelli GP (2008) NON invasive distress monitoring in children hospital intensive care unit. In: MEDSIP 2008 4th IET international conference on advances in medical, signal and information processing, pp 2908–2911
6. Jonga J-T, Kaob T, Leec L-Y, Huanga H-H, Lod P-T, Wangc H-C (2010) Can temperament be understood at birth? The relationship between neonatal pain cry and their temperament: A preliminary study. *Infant Behav Dev* 33:266–272
7. Petronil M, Malowany AS, Johnston CC, Stevens BJ (1994) A new, robust vocal fundamental frequency (Fo) determination method for the analysis of infant cries. In: Seventh annual IEEE symposium on computer-based medical systems, pp 223–228
8. Ismaelli A, Rapisardi G, Donzelli GP, Moroni M, Bruscaiglioni P (1994) A new device for computerized infant cry analysis in the Nicu, engineering in medicine and biology society, engineering advances: new opportunities for biomedical engineers. In: Proceedings of the 16th annual international conference of the IEEE, pp 854–855
9. Petroni M, Malowany AS, Johnston CC, Stevens BJ (1995) A robust and accurate crosscorrelation-based fundamental frequency (Fo), engineering in medicine and biology society. In: IEEE 17th annual conference, pp 915–916

10. Wermke K, Mende W (1993) Variability of the cry melody as an indicator for certain developmental stages, engineering in medicine and biology society. In: Proceedings of the 15th annual international conference of the IEEE, pp 1373–1374
11. Orlandi S, Manfredi C, Bocchi L, Scattoni ML (2012) Automatic newborn cry analysis: a non-invasive tool to help autism early diagnosis. In: 34th annual international conference of the IEEE EMBS, pp 2953–2956
12. Michelson K, Todd de Barra H, Michelson O (2007) Sound spectrographic cry analysis and mothers perception of their infant's crying. Nova Science Publishers, New York, pp 31–64
13. Sasvári L, Gegesi-Kiss P, Popper P, Makói Z, Szöke Z (1975) 1st cry of newborn after vaginal and cesarean delivery. *Acta Pediatr Hung* 16(2):155–161
14. María A, Díaz R, Carlos A, García R, Luis C, Robles A, Jorge E, Altamirano X, Mendoza AV (2012) Automatic infant cry analysis for the identification of qualitative features to help opportune diagnosis. *Biomed Signal Process Control* 7(1):43–49. *Human Voice and Sounds: From Newborn to Elder*
15. Robu R, Feier F, Stoicu-Tivadar V, Ilie C, Enatescu I (2011) The analysis of the new-borns' cry using NEONAT and data mining techniques. In: 2011 15th IEEE international conference on intelligent engineering systems (INES), pp 235–238
16. Wikipedia page for LabVIEW—<http://en.wikipedia.org/wiki/LabVIEW>
17. Weka software official website. <http://www.cs.waikato.ac.nz/ml/weka/>
18. Waikato University official website. <http://www.cs.waikato.ac.nz/ml/weka/arff.html>
19. Quinlan JR (1986) Induction of decision trees. *Mach Learn* 1:81–106
20. Murthy SK (1998) Automatic construction of decision trees from data: a multi-disciplinary survey. *Data Min Knowl Disc* 2:345–389
21. Daelemans W, van den Bosch A, Weijters T (1997) IGTre: using trees for compression and classification in lazy learning algorithms. *Artif Intell Rev* 11:407–423
22. Li Q (2006) Doi K Analysis and minimization of overtraining effect in rule-based classifiers for computer-aided diagnosis. *Med Phys* 33:320–328
23. Wikipedia on preterm birth. http://en.wikipedia.org/wiki/Preterm_birth
24. On Olympus recorder. <http://www.videodirect.com/olympus/voicerecorders/olympus-ls-100.html>
25. Olympus official website. http://www.olympusamerica.com/files/oima_cckb/LS-100_Instruction_Manual_EN.pdf

Development of a Preliminary Mathematical Model to Predict the Indoor Radon Concentration in Normal and High Background Radiation Areas of Ramsar

S.M.J. Mortazavi, A. Zamani, A. Tavakkoli-Golpayegani and S. Taeb

Abstract Substantial evidence indicates that prolonged exposure to radon and its decay products in homes increases the risk of lung cancer. Indoor radon concentrations in some regions of high background radiation areas (HBRAs) of Ramsar are much higher than the recommended action level of 148 Bq/m^{-3} . This study aimed at developing simple mathematical models for prediction of radon concentration in homes located in normal and HBRAs of Ramsar. The levels of gamma background radiation and indoor radon were measured in 75 dwellings located in normal and HBRAs (30 dwellings from HBRAs and 45 dwellings from normal background radiation areas of Ramsar). Our findings showed that in normal and HBRAs of Ramsar the majority of confounding factors such as the type of building materials and ventilation in different dwellings are so close to each other that gamma radiation level can be used as a strong predictive tool for radon concentration. As radon concentration in indoor air strongly varies with time, this simple mathematical method can provide an estimate of the mean radon level in large-scale radon screening programs for homes. We are also developing mathematical models which can predict the levels of tumor markers such as CEA and CYFRA 21 based on gamma background radiation level and indoor radon concentration.

Keywords Mathematical model · Indoor radon · High background radiation areas · Ramsar · Prediction

S.M.J. Mortazavi (✉) · A. Zamani · S. Taeb
Ionizing and Non-ionizing Radiation Protection Research Center (INIRPRC) and Medical Physics & Medical Engineering Department, Shiraz University of Medical Sciences, 7134845794 Shiraz, Iran
e-mail: mmortazavi@sums.ac.ir

A. Zamani
e-mail: zamani_a@sums.ac.ir

A. Tavakkoli-Golpayegani
Standard Research Institute, Tehran, Iran
e-mail: tavakoli.golpa@gmail.com

1 Introduction

US EPA believes that radon is the second leading cause of lung cancer, after tobacco smoking. It is widely accepted that there is no threshold for lung cancer from radon inhalation. Studies performed in radon prone areas reveal that radon can accumulate in residential places at surprisingly ultra-high levels.

The United Nations Scientific Committee on the Effects of Atomic Radiation (UNSCEAR) in its 2000 report clearly confirmed that Ramsar city in northern Iran, has some inhabited areas with the highest known natural radiation levels in the world [1].

The ultra-high levels of natural background radiation in Ramsar are caused by high concentrations of radium-226 and its decay products originated from hot springs [2]. Indoor radon concentration in some regions of HBRAs of Ramsar are up to 31 kBq/m⁻³ [3], a concentration that is much higher than U.S. Environmental Protection Agency (EPA) recommended action level of 148 Bq/m⁻³ (4 pCi/L). On the other hand, the risk of lung cancer from radon inhalation in smokers is estimated to be 10–20 times greater than that of non-smokers. Considering high levels of public exposures to ionizing radiation in the residents of HBRAs of Ramsar, some experts have recently suggested that an effective remedial action program is needed [3]. Although some studies showed that individuals residing in the HBRAs of Ramsar have increased frequency of unstable chromosome aberrations, no repeatable detrimental effects caused by high levels of natural radiation in Ramsar have been detected so far [4, 5]. We have previously published reports on the health effects of exposure to elevated levels of natural ionizing radiation in Ramsar [6–10] including the first reports on the induction of adaptive response in the residents of these areas [2]. The aim of this study was to develop new mathematical models for prediction of radon concentration in homes located in normal and HBRAs. It is worth mentioning that we have also developed mathematical models which predict the levels of carcinoembryonic antigen (CEA) and cytokeratin 19 fragments (CYFRA 21) based on gamma background radiation level and indoor radon concentration. CEA and CYFRA 21 are two serologic markers for lung cancer management which are commonly measured. These results will be published in another chapter.

2 Materials and Methods

2.1 External Gamma Dose Measurements

The exact levels of gamma background radiation were measured in HBRAs and NBRAs using a calibrated RDS-110 (RADOS Technology, Finland) survey meter. This survey meter was mounted on a tripod approximately 1 m above the ground inside the 75 houses located in normal and HBRAs of Ramsar (45 houses from NBRAs and 30 houses from HBRAs). The readings were recorded every 10 min for an hour. Then, the mean of six readings was calculated.

2.2 Radon Concentration

After the tests were explained to the participants and their informed consent was taken, CR-39 dosimeters were installed in their houses to measure the indoor level of radon gas. After three months of exposure to indoor radon, the detectors were collected and sent back to the dosimetry laboratory of the National Radiation Protection Department (NRPD), Iranian Nuclear Regulatory Authority (INRA).

2.3 Data Analysis

Scatter plot was used to assess the strength of the relationship between the variables and also to graphically plot the correlations.

3 Results

Radon concentration in homes is determined by numerous factors such as uranium concentration in soil and building materials, ventilation, elevation above ground level, and living style of the residents. In spite of these confounding factors, we found a statistically significant correlation between the level of gamma exposure and indoor radon concentration in dwellings located in normal and HBRA of Ramsar. Linear least-squares fitting was carried out by using Scatter Plot software in this study. The correlation coefficient for normal and HBRA were 0.90 and 0.89,

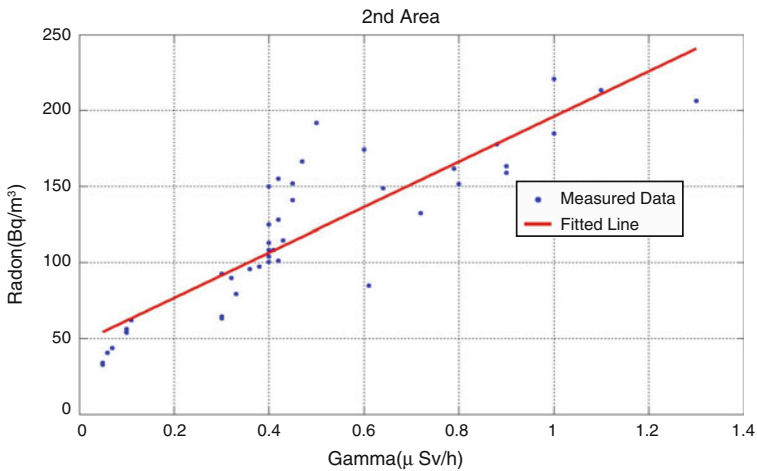


Fig. 1 Scatter plot shows the relationship between the gamma radiation level ($\mu\text{Sv/h}$) and indoor radon concentration (Bq/m^3) in normal background radiation areas (NBRAs)

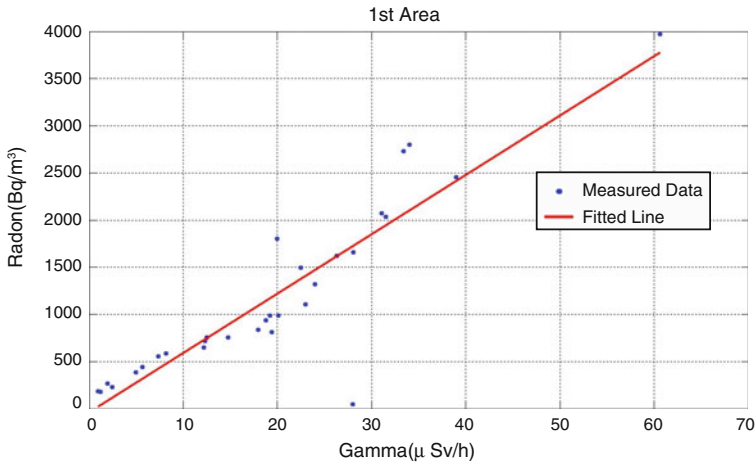


Fig. 2 Scatter plot shows the relationship between the gamma radiation level ($\mu\text{Sv/h}$) and indoor radon concentration (Bq/m^3) in high background radiation areas (HBRAs)

respectively. The data for normal background radiation areas were fit to the equation $Y = 149.1X - 46.97$ [where $Y =$ radon concentration (Bq/m^3), $X =$ Gamma exposure level ($\mu\text{Sv/h}$)]. The relationship between the gamma radiation level and indoor radon concentration in normal background radiation areas (NBRAs) is shown in Fig. 1. On the other hand, the data for HBRAs were fit to the equation $Y = 62.99X - 42.36$. Figure 2 shows the relationship between the gamma radiation level and indoor radon concentration in HBRAs.

4 Discussion

These findings clearly indicate that in normal and HBRAs of Ramsar the majority of confounding factors such as the type of building materials and ventilation in different houses are so close to each other that gamma radiation can be used as a strong predictive tool for radon concentration. It has been shown that the concentration of radon in indoor air varies widely during a day and may vary up to 300 %. Furthermore, similar fluctuations can be observed from day to day, week to week, season to season, and year to year. Therefore, as radon concentration in indoor air strongly varies with time, only long-term measurements provide a reliable picture of the radon level in a house. In this light, the simple mathematical method developed in this study, can provide an estimate of the mean radon level in large-scale screening programs for homes. The main limitation in our study was the small number of radon measurements. Further studies should be performed with a larger number of measurements to verify if this model corresponds well to larger data collected from different areas.

References

1. UNSCEAR (2000) Sources and effects of ionizing radiation. United nations scientific committee on the effects of atomic radiation (UNSCEAR)
2. Ghiassi-Nejad M, Mortazavi S, Cameron J, Niroomand-Rad A, Karam P (2002) Very high background radiation areas of Ramsar, Iran: preliminary biological studies. *Health Phys* 82(1):87
3. Sohrabi M (2013) World high background natural radiation areas: need to protect public from radiation exposure. *Radiat Meas* 50:166–171
4. Mortazavi SMJ, Mozdarani H (2013) Non-linear phenomena in biological findings of the residents of high background radiation areas of Ramsar. *Int J Radiat Res* 11(1):3–9
5. Mortazavi SMJ, Mozdarani H (2012) Is it time to shed some light on the black box of health policies regarding the inhabitants of the high background radiation areas of Ramsar? *Int J Radiat Res* 10(3):111–116
6. Mortazavi SMJ, Shabestani-Monfared A, Ghiassi-Nejad M, Mozdarani H (2005) Radioadaptive responses induced in lymphocytes of the inhabitants in Ramsar. Iran. *Int Congr Ser* 1276:201–203
7. Mortazavi S, Ghiassi-Nejad M, Rezaiean M (2005) Cancer risk due to exposure to high levels of natural radon in the inhabitants of Ramsar. Iran. *Int Congr Ser* 1276:436–437
8. Mortazavi SMJ, Abbasi A, Asadi R, Hemmati A (2005) The need for considering social, economic, and psychological factors in warning the general public from the possible risks due to residing in HLNRA. *Int Congr Ser* 1276:440–441
9. Mortazavi SMJ, Karam PA (2005) Apparent lack of radiation susceptibility among residents of the high background radiation area in Ramsar, Iran: can we relax our standards? *Nat Radiat Environ* 7:1141–1147
10. Mortazavi SMJ, Niroomand-Rad A, Mozdarani H, Roshan-Shomal P, Razavi-Toosi SMT, Zarghani H (2012) Short-term exposure to high levels of natural external gamma radiation does not induce survival adaptive response. *Iranian J Radiat Res* 10(3–4):165–170

ASD: ML Perspective for Individual Performance Evaluation

D. López De Luise, M. Fernandez Vuelta, R. Azor, M. Agüero,
C. Párraga, N. López, P. Bustamante, M. Marquez, R. Bielli,
D. Hisgen, R. Fairbain and S. Planes

Abstract There are several approaches to interact with ASD patients. Many of them do not rely on vocal abilities because of the wide spectrum of symptoms. But taking data from ML perspective may introduce new sources of information for a better interpretation of patient's behavior and helps to build new parameters to model individual performance. This paper presents some initial findings in that direction based on the automatic evaluation of real cases as a way to build a parameterized description of patients. Preliminary analysis in patients suggests that the individual performance may be compared with the universe of patients, yet it is possible to elaborate a *performance profiling* and to model evolution profiles that are present in a predefined universe of patients. The team is currently defining and testing new audio and video protocols to collect additional parameters. From these findings, it is possible to build a parametric reasoning model using MLW.

D.L. De Luise (✉) · M. Agüero · D. Hisgen · S. Planes
CI2S Lab, Pringles 10 2nd FL, C1183ADB Buenos Aires, Argentina
e-mail: daniela_ldl@eee.org; mdlldl@ci2s.com.ar

M. Agüero
e-mail: maguero@ci2s.com.ar

D. Hisgen
e-mail: dhisgen@ci2s.com.ar

S. Planes
e-mail: splanes@ci2s.com.ar

M. Fernandez Vuelta
Centro CIEL, Calle Ecce Homo, 2 Bajo Izqda, 33009 Oviedo, Spain
e-mail: manuelafv79@hotmail.com

R. Azor · C. Párraga
DICYTyV Eng. Dep.—Universidad de Mendoza, Aristides Villanueva 773,
M5502ITH Mendoza, Argentina
e-mail: dicyt@um.edu.ar

Keywords Autism spectrum disorder · Asperger · Linguistics · Reasoning model · Computational linguistic · Morphosyntactic linguistic wavelets · Language processing

1 Introduction

The autism spectrum disorder (ASD) can be defined as [7] *wide continuum of associated cognitive and neurobehavioral disorders, including the core-defining features of impaired socialization, impaired verbal and nonverbal communication, and restricted and repetitive patterns of behavior* (p. 470). It is characterized mainly by [18]:

- Qualitative impairment in communication and language
- Qualitative impairment in reciprocal social interaction
- Patterns of behavior, restricted (and stereotyped) interests and activities

Recent works denoted it as closely related to cerebral disorders in one or many brain areas, probably due to a genetic alteration [8, 22]. Regardless the cause, the typical alteration in verbal communication [23] is a real problem for the patient treatment and recovery. It usually affects also its socialization and cognitive development [24]. This is the reason that it is very important to have tools to improve communication and better understanding of the inner thoughts and feelings of the person.

C. Párraga
e-mail: dicyt@um.edu.ar

N. López · P. Bustamante
Gab. de Tecnología Médica Eng. Dep.—UNSJ, Libertador 1109 Oeste,
J5400ARL San Juan, Argentina
e-mail: nlopez@gateme.unsj.edu.ar

P. Bustamante
e-mail: pao.bustamante.011@gmail.com

M. Marquez · R. Bielli
EAndes Foundation, Cnel. Suarez 725, M5602HHO San Rafael Mendoza, Argentina
e-mail: kukenamar@yahoo.com.ar

R. Bielli
e-mail: biellibondino80@hotmail.com

R. Fairbain
Dep. de Ingeniería Traslacional (FICEyN), Universidad Favaloro, Solís 453,
C1078AAI Buenos Aires, Argentina
e-mail: rominafair@hotmail.com

BIOTECH is a proposal to apply morphosyntactic linguistic wavelets (MLW) as an intelligent system able to provide deep information of the reasoning process related to linguistics expressions. It has been applied to interpret WEB contents, automatic summarization, dialog profiling, texts and author profiling, bilingualism effects in young kids, etc. [14, 15].

In order to be able to process with MLW it is mandatory to have linguistics expressions made by the patients. To overcome the lack of language articulations, the project relies in the concept of verbal behavior [24], sensing verbal activities with specific audio and video devices and generating a metalanguage that DAISY will process, compensating the poverty of vocal production.¹

Verbal behavior is becoming widely accepted as a crucial perspective for ASD therapies. Greer [4] expresses that there is *growing evidence on the ontogenetic sources of language and its development* that derives in a *renewed interest in the theory that the verbal capability in humans is a result of evolution and ontogenetic development* (p. 363).

According to Greer and Longano [11], vocal activities like naming **appear to be a or the crucial stage in children's verbal development**. Authors like Lord et al. [19, 25], Greer [9, 10] and Ackerman [1], corroborated this and other close relations between vocal and verbal communication and cognition.

As a consequence, **it is reasonable to desire a tool-like BIOTECH to automatically evaluate verbal activities and provide help to complement those vocal activities that the patient cannot produce properly by itself**.

Another important aspect to be considered is the particularity of every individual. Experts affirm [8] that skill training should be intensive but also customized in order to get better results. The design of MLW within BIOTECH is able to gather such specific differences since it can build a specific model that represents its behavior peculiarities.

This paper aims to present the relevance of an automatic processing based on machine learning (ML), the main concepts of MLW as an approach based on ML to model linguistic reasoning, and the way it can be applied to ASD patients.

The main contribution of this approach is the application of a novel linguistic processing based on a combination of Computational Intelligence (that is, systems inspired in biological intelligence) and ML (automatic learning software).

The rest of this text is organized as follows: a global presentation of MLW and its applicability to ASD (Sect. 2), some preliminary results of application ML to a simple and much reduced dataset with real data (Sect. 3), conclusions, and future work (Sect. 4).

¹In verbal behavior theory there is a discrimination between verbal and vocal activities. The first refers to any expression of the individual (movements, sounds, gesturing, manners, etc.) while the other remains to language expressions (written or not).

2 BIOTECH Proposal

There are several approaches to treat ASD patients, ranging from diets to stimulation. Basically, they are based on a coaching process to develop certain skills in the patients. A new trend is based on technology and its application to help therapists. For instance, the Russel [20] and Nao robots [12, 21] provide mimic directives to children. There are also interactive games that use skin temperature and movement sensors to monitor reactions of the patients to certain stimulations generated from the screen [3]. Other systems monitor body symptoms of stress (*Robots Reading Autistic Kids' Minds* [5]) like cardiac rhythm, skin temperature, and muscle movements and process them in real-time to infer the emotional status of the patients, and define how to interact with him [6].

IEEE SIGHT is a Special Interest Group on Humanitarian Technology. In Argentina, it sponsors BIOTECH project, which aims to develop a model for linguistic reasoning in individuals with ASD. In order to achieve this, it uses MLW designed by CIIS Lab with the project DAISY [14], and many specific devices for acoustic and visual interaction with the patient.

Currently, the project is in its early stage, building protocols for data collection, validating them with leading experts (Ciel Argentina, Ciel Spain, TIPNEA foundation, and Burgos University), designing suitable user interfaces, and defining the best hardware architecture.

As part of this first stage, the team performed several preparatory steps described in the following subsections. The present paper summarizes also initial findings and sketches further work to be done in order to use them.

2.1 Evaluation of Video Records of Sessions with Patients

Four sessions with one of the patients were recorded. Let name him *R*. Videos have 3.25, 59.3, 22.2, and 29.55 minute.

The first evaluation aims to assess the ML information acquirable via sound and video signals. To accomplish this, all the videos are studied from two points of view: sound and images, first isolated (to extract sound and image patterns) and afterwards combined (to relate the previously extracted patters). All this processing is manual to guarantee no bugs, but using very well known free Ubuntu[®] tools as R[®] and Pitivi[®], and Audacity[®].

All the records have many clues that can be used as a basis for a systematic extraction of information relevant to build a complementary communication language. The following are some of the findings in record 3.

2.1.1 Sound Findings

Below is a description of the *answers* given by *R* upon certain stimulus:

- *R* answers *Si* (Yes) to therapist sentence *se fue papá* (dad has gone) (minute 00:35). That is the only word clearly pronounced but very softly
- *R* pronounces a kind of *yes* with the sound (minute 2:54, 4:16, among other. Figure 1 shows a spectrogram (up) and autocorrelation (down) in frequency for *yes*
- Every motorbike or car's motor sound in the background is replied with an imitation sound. In these situations, the background sound starts and then the imitation (minutes 00:30, 00:40, 02:20, 02:42, 03:18, 03:50, 04:25, 06:45, 08:10, 09:49, 12:55, 14:30, 14:35). Figure 2 presents the spectrogram (up) and autocorrelation (down) in frequency for motors
- A motorbike sound in the background is replied (record 3, minute 40), but this practice stops when *R* is commanded to stop doing it. But continued at minute 1:10 with no background sound (as finishing response). Same happens in minute 8:40 delayed to minute 9:09
- Every success is celebrated by *R* with a specific sound pattern (minutes 3:57, 4:15, 5:00, 5:12, 7:13, 7:45). When *R* is tired, he repeats the pattern but slowly (11:48, 14:46, 16:41) and once it is truncated (20:54)
- It is important to note that most of the times this sound is produced when *R* is congratulated by his success in the exercise
- Another sound replies to barking in the background (15.25, 16.00, among others). Figure 3 is the spectrogram (up) and autocorrelation (down) in frequency for celebration
- The following is the answer to birds chirping (7:24, 12:48, 13:31, 13:48, 14:11, 14:23, among others). Figure 4 has the spectrogram (up) and autocorrelation (down) in frequency for bird chirping.

In minute 9:50 when *R* was replying to birds, the therapist ask for silence and *R* gets annoyed and stops (minute 10:08) but after a while he continues answering (minute 10:12). That is, there is the ability to snooze a task within a context and to resume it afterwards.

NOTE: It is important to note that audio signals shown in the figures are the result of applying a Hamming Window² function for segmentation, and processed with autocorrelation. The spectrogram of a signal is useful to show the amount of energy spread over the different frequencies. The period-tracking is performed here by autocorrelation. The picture shows autocorrelation via frequency domain.

²Windows are mathematical functions used to avoid discontinuities in both ends of a piece of signal. This function results in a signal limited in the time. .

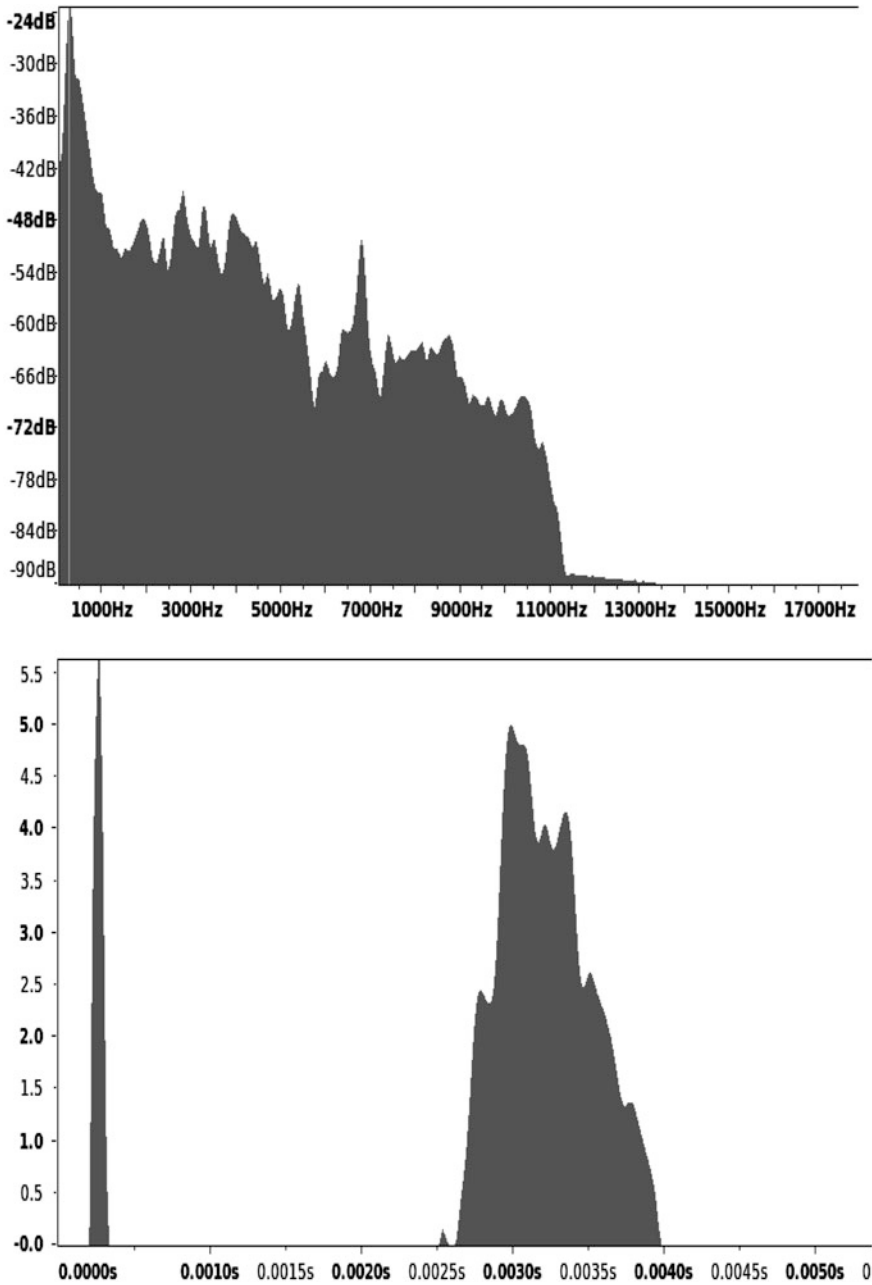


Fig. 1 Spectrogram (*up*) and autocorrelation (*down*) in frequency for *yes*

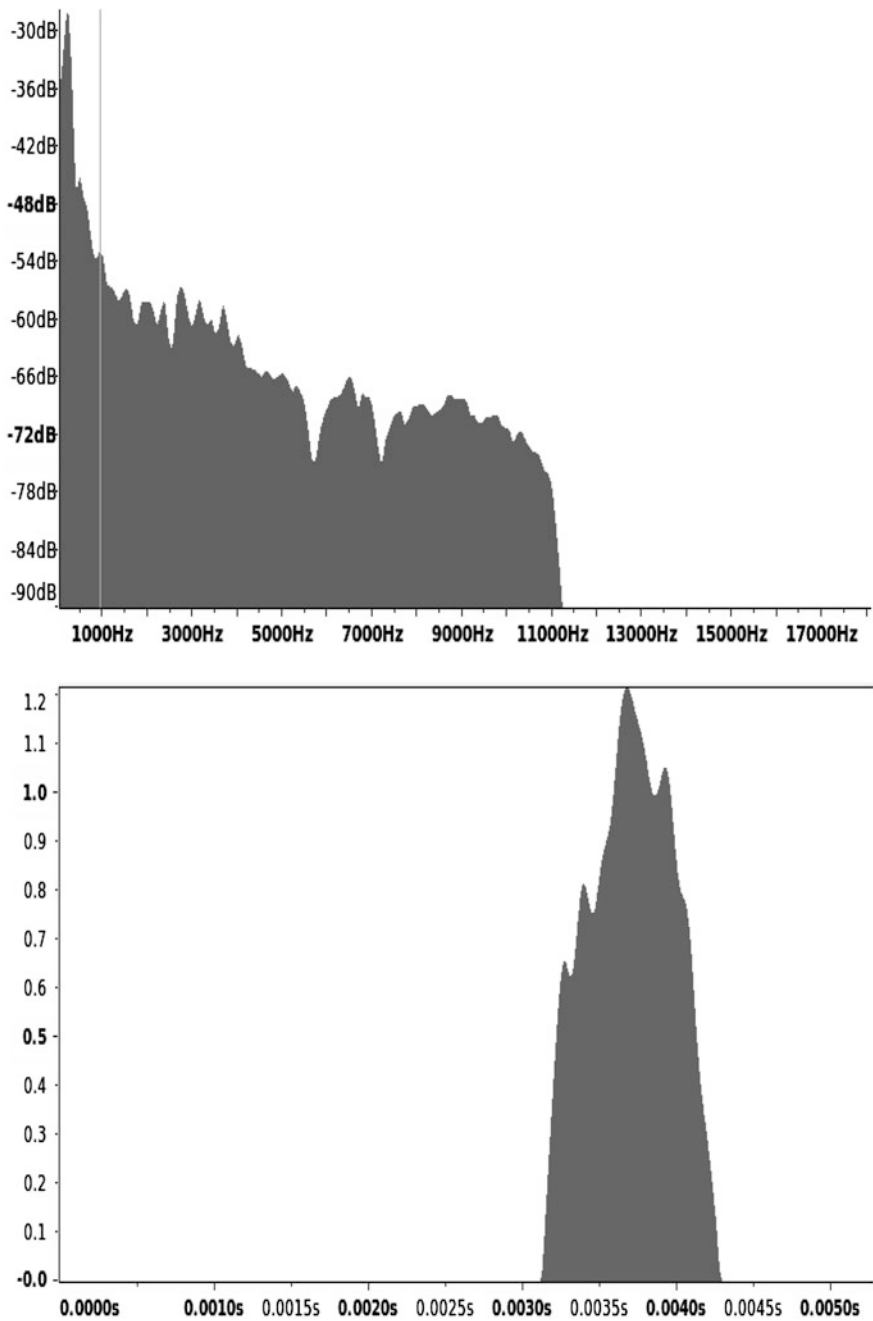


Fig. 2 Spectrogram (*up*) and autocorrelation (*down*) in frequency for motors

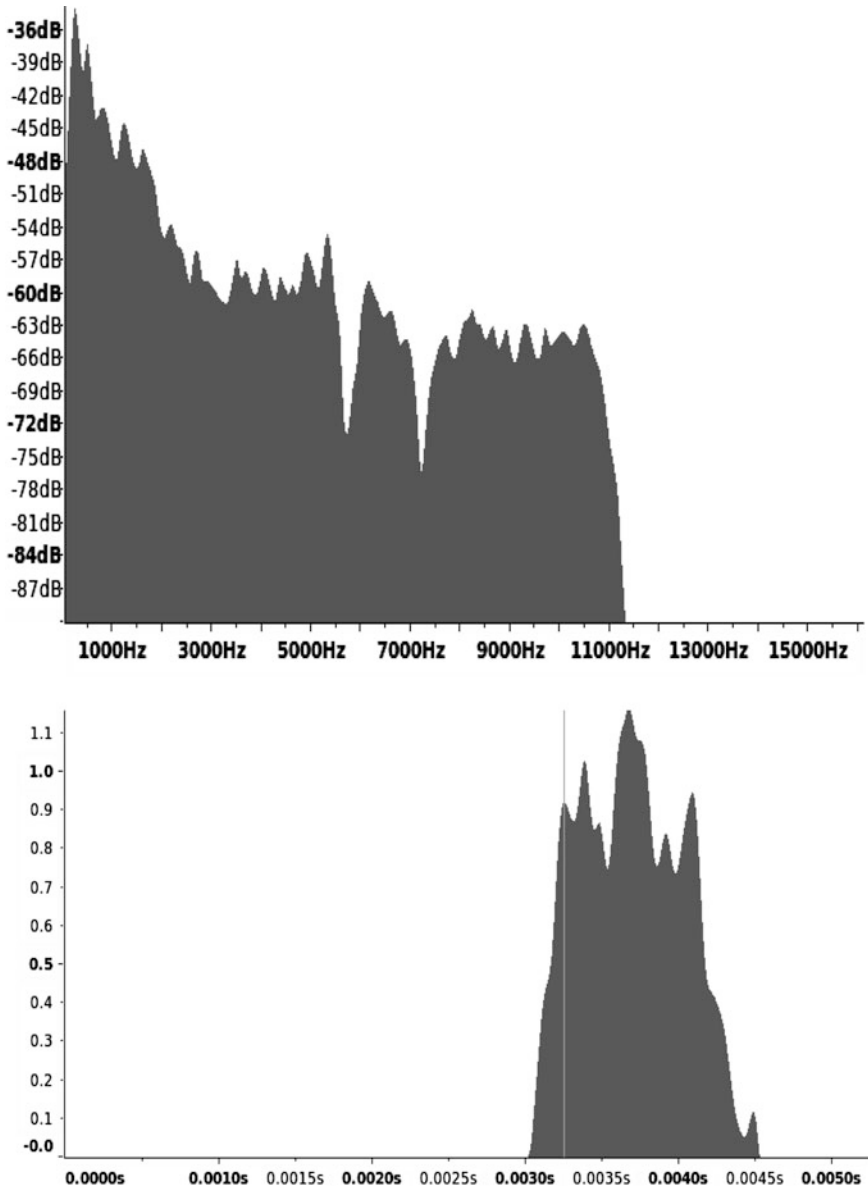


Fig. 3 Spectrogram (*up*) and autocorrelation (*down*) in frequency for motors

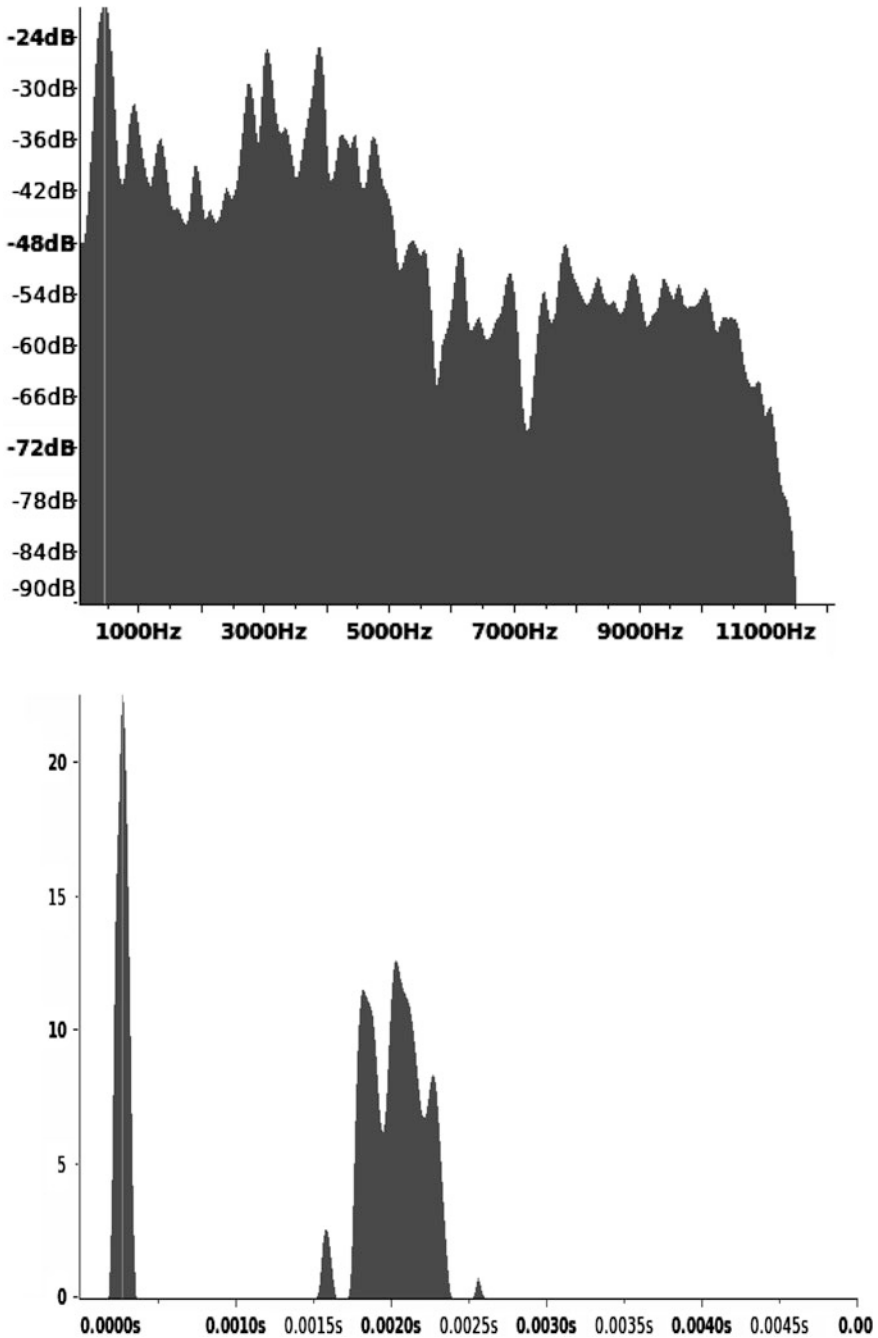


Fig. 4 Spectrogram (*up*) and autocorrelation (*down*) in frequency for bird chirping

2.1.2 Visual Findings

- A tapping with three sounds, performed with the right hand (minute 00:01, 00:04, 03:42, 06:32, 09:24, 10:31, and 16:25)
- Eyes to the left at the head level, when he puts a small purple toy into his mouth while he presses it (perhaps to feel its vibration when the toy sounds). Minutes 0:55, 1:03, 5:47, and 8:21
- Glance to backwards or lost look, when she starts listening (and sometimes when answering) birds.³ In these moments he lost the visual contact with the activity even when he is performing an activity. Minutes 07:24, 8:27 (he starts answering here in 8:36), 12:49, 13:27, 14:20 (in this moment the therapist asks him more attention)
- Glance to backwards or lost look, when she starts listening (and sometimes when answering) motors^{**}. In these moments he losses the visual contact with the activity even when he is performing an action. Minutes 00:33, 00:48, 02:00, 02:43, 06:46, 08:10, 08:50, 09:15, 09:50 (here the therapist holds his head to make him watch the target and asks for silence), 10:48 (the therapist closes his mouth with her fingers but she does not succeeds in gathering her sight. His eyes keep focused ahead), 12:59 (the therapist holds his head to catch his attention), 13:04 (the therapist holds his left hand and speaks very close to his face trying to get attention), 13:46 (the therapist put her face very close to him to get his attention), 13:56, 14:36 (the therapist challenges him), 15:12, 15:52, 18:46, 19:26, 20:46 (he is being asked for silence, but his face to the front, not the activity). In 21:03, he keeps listening a motor and does not answer to the exercise. The therapist takes this gesture as a failed answer.

2.1.3 General Findings

At minute 17:28, *R* is very tired and it is expressed by his body and sound expressions. Answers to therapist keep mostly OK, but he reduces slightly the answers to the environment. In fact, there is a moment when he keeps absolutely quiet and even lost connection to therapist.

After a short while, he reconnects with the therapist and answer to motors. But afterwards he looks tired again (in fact he stretches himself in minute 19:00) and protest (minute 19:09) making a noise that is repeated in minutes 19:15 and 20:37.

Generally speaking, the sounds appear to represent two interactions that are simultaneous:

- Interaction with the therapist
- Interaction with the surrounding

³It is important to note that many times the exercise with the therapist coexists with the interaction with the background.

Responses to both interactions are mixed; therefore certain stimulation sounds have not a response. In this record, *R* seems to perform a kind of *round robin* polling of his environment and randomly decide which one to answer regardless the sound intensity and frequency.

2.2 Evaluation of Data Records of Sessions with Patients

Therapists in Ciel Argentina keep track of every session with certain forms that collect information like date and time of session, duration, answer timings, retrials, etc. The team used a reduced dataset with the following information:

- Patient ID: a natural number to preserve biographical information of the patient
- Year/Month/Week
- HOURS: total training hours for the declared week
- UA2 and UA1: number of tasks and successful tasks
- $TPM1 = UA1/HOURS$
- $TPM2 = UA2/HOURS$
- LANGUAGE TASKS: number of tasks related to language
- OTHER TASKS: number of other tasks aside language

All this information is compiled in a database with 420 records from three children between 9- and 12-years old. All of them suffer ASD with level 3 of severity according to DSM-5 Diagnostic Criteria [2].

The dataset covers the training during several months (see Table 1).

The dataset has been evaluated with mining approaches focused in ML, in order to find out its characteristics and to determine if it makes sense an automatic approach to extract features and model ASD behavior. In Sect. 3 there is a deeper analysis.

2.3 Evaluation of MLW Reasoning Model Applicability to Individuals with ASD

Several experts in ASD agree that the disorder is originated by a biological alteration that makes the brain cells unable to select relevant from irrelevant information. Therefore a new *memory*, a new concept cannot be built with the right logic

Table 1 Therapy duration for each patient

Patient	Starting	Ending
1	Jan 2010	July 2013
2	Nov 2011	Dec 2012
3	Nov 2010	Dec 2012

and everything seems confusing. Following Scott [22], interneuron and pyramidal cells are the filters that avoid environmental distractions to be dismissed: When inhibitory interneurons are excited, pyramidal cells fire and relevant stimuli active hippo-campus and ignore irrelevant information. Both pyramidal and interneurons must be in a proper balance in order to allow the brain fine-tune which information it stores in a new memory or not.

It is therefore reasonable to conclude that the reasoning in ASD patients is distorted, mainly linguistic and conceptualization processes. As a consequence, many other derived processes are also affected: concentration, linguistic learning, ontology inner representations, verbal behavior among others. Wittgenstein said *If we spoke a different language, we would perceive a somewhat different world* and *The limits of my language means the limits of my world* [26].

As described in Sect. 3, there is a lot of information that is useful and it can be automatically extracted. It reflects many parts of the linguistic process and can be tracked using verbal behavior. From the Computational Linguistic perspective, it is possible to build a model that makes sense the verbal activities. It was previously applied to other less disruptive linguistic alterations such as in early bilingualism [15], Internet usage [13], dialog conceptualization [16], writer profiling [17], etc.

It is worth noting that MLW are not involved in procedures like tagging, translation, semantic/ontology dictionary building, etc. It is a type of leveraging information model, which makes a kind of map for linguistic processing. More details about MLW can be found in [14].

2.4 Definition and Implementation of Interfaces for MLW

In order to be able to apply MLW, it is mandatory to design and implement a convenient interface. This will gather data from specific collecting modules and the modeling device. Figure 5 depicts the overall BIOTECH architecture.

As can be seen, from the architecture figure (Fig. 5), there are three main blocks: external, virtual, and internal structure. The last two belong to DAISY project and have many internal memories (marked as cylinders) and certain processes (marked as routines symbols). The external structure collects audio and video streams taken from many intermediate outputs. That data constitute useful information to build tools to evaluate the evolution and status of the patient, the treatment, and BIOTECH as well. Biotech is currently working on the ML module that feeds with relevant information, the Inference Machine. The metalanguage is a model which maps verbal behavior of the current individual with Spanish structures and vocabulary. It is automatically inferred in the ML, deriving information with techniques similar to the ones described in the next section and some other out of the scope of this paper.

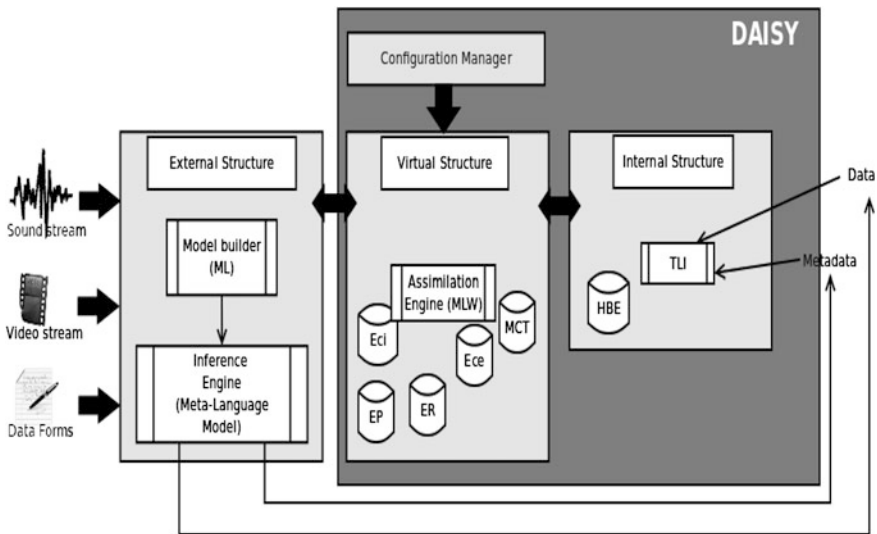


Fig. 5 Global BIOTECH architecture

3 Case Study

As mentioned in Sect. 2.1, data corresponding to three patients with ASD were analyzed. The rest of this section presents the analysis of the following findings:

- It is possible to derive a performance curve for every individual
- There is also a global performance curve.

This section presents the main statistics to show that TPM follows a Normal distribution for the global dataset. It is tested with T-Student (see Sect. 3.1), due to the number of cases. TPM Data for each individual follows the same distribution (see Sect. 3.2) with different parameters that feature every case. Kolmogorov test (Sect. 3.3) verifies these findings.

3.1 Performance for Each Individual

The specific performance for each patient does not follow exactly the global distribution. It is better described by normal distributions using specific media and standard deviation. The following table describes the parameters for each patient and the value of p-statistic (see Table 2).

Table 2 Performance statistics for each patient

Patient	Number of records	Media	Standard deviation	<i>p</i> -value (unilateral)
1	200	3.26	0.89	0.010
2	109	2.27	0.43	0.079
3	111	2.15	0.36	0.45

3.2 Global Behavior of the Performance

Distribution tested with Student (Infostat©), corresponds to Gaussian (see Table 3).

The empirical distribution is inferred using Infostat©, and the following figure shows the similarity with Normal distribution (black dots). Figure 6 shows the empirical distribution (gray) and Normal (2.66, 0.83) (in black).

The following figures compare the specific distribution for *ID* = 1, 2, and 3 with the Normal distribution derived from the global dataset and the Normal distribution for the specific individual. Figures 7, 8, and 9 is the global (up) and specific (down) curves for *ID* = 1, 2, and 3, respectively.

It is easy to observe that distributions on the left are less similar than the ones on the right, but all of them behave mainly as normal.

Table 3 Gaussian parameters for the entire dataset

Parameter	Value
N (number of records)	420
Media	2.66
Standard deviation	0.83
Confidence interval (95%):	
Lower limit	2.58
Upper limit	2.74
P statistic (bilateral)	0.991

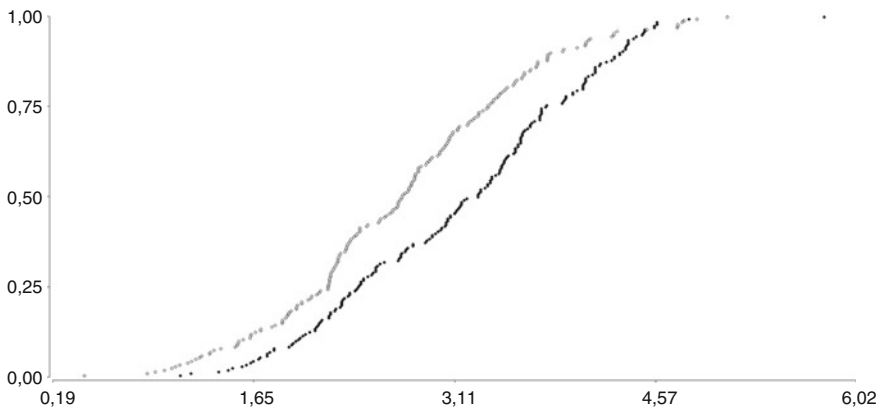


Fig. 6 Empirical distribution (gray) and normal (2.66, 0.83) (in black)

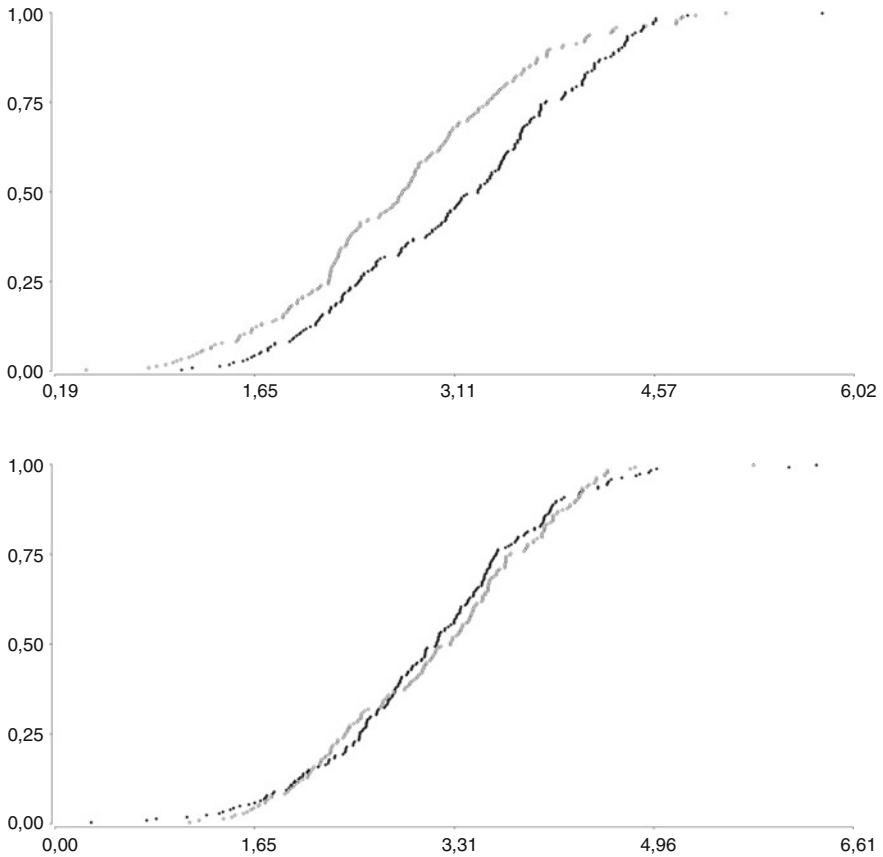


Fig. 7 Global (*up*) and specific (*down*) curves for $ID = 1$

3.3 Verification with Kolgomorov Test

Distribution validation for global dataset (Infostat©) confirms the Gaussian distribution when the distribution has specific parameters representing each individual. That is, the distribution is a good representation just when media (μ) and standard deviation (σ) are calculated for each patient at a time (see Table 4).

3.4 Variable Reduction with Principal Component Analysis (PCA)

PCA is a very well known approach to reduce a set of variables to a minimum independent number of new variables.

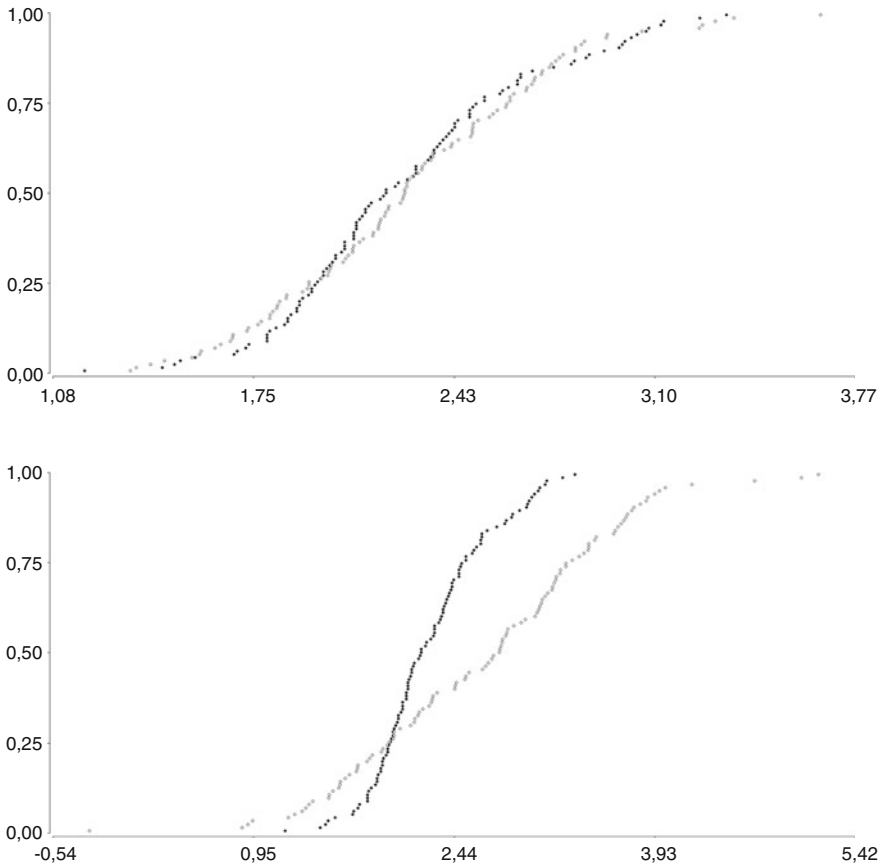


Fig. 8 Global (*up*) and specific (*down*) curves for $ID = 2$

TPM1, TPM2, HOURS, UA1, UA2, LANGUAGE TASKS, and OTHER TASKS are not independent. PCA can infer their relationship and reduces them to a minimum number by defining new variables that depends on the original ones.

Analysis with PCA results in only two variables (let say e_1 and e_2) that can be interpreted as the relation between the effort (e_1) and the time to accomplish a task, which is the efficiency (e_2). This interpretation is given by the specific combination of the original variables.

Using these new variables it is possible to model and evaluate the patient performance along the sessions and at a specific one.

When PCA is applied to global dataset (that is, merging data from all the individuals) it gives a general model to asses each person respecting the group. By splitting the dataset accordingly, each ID it is shown that every patient has a different evolution profile that is clearly defined.

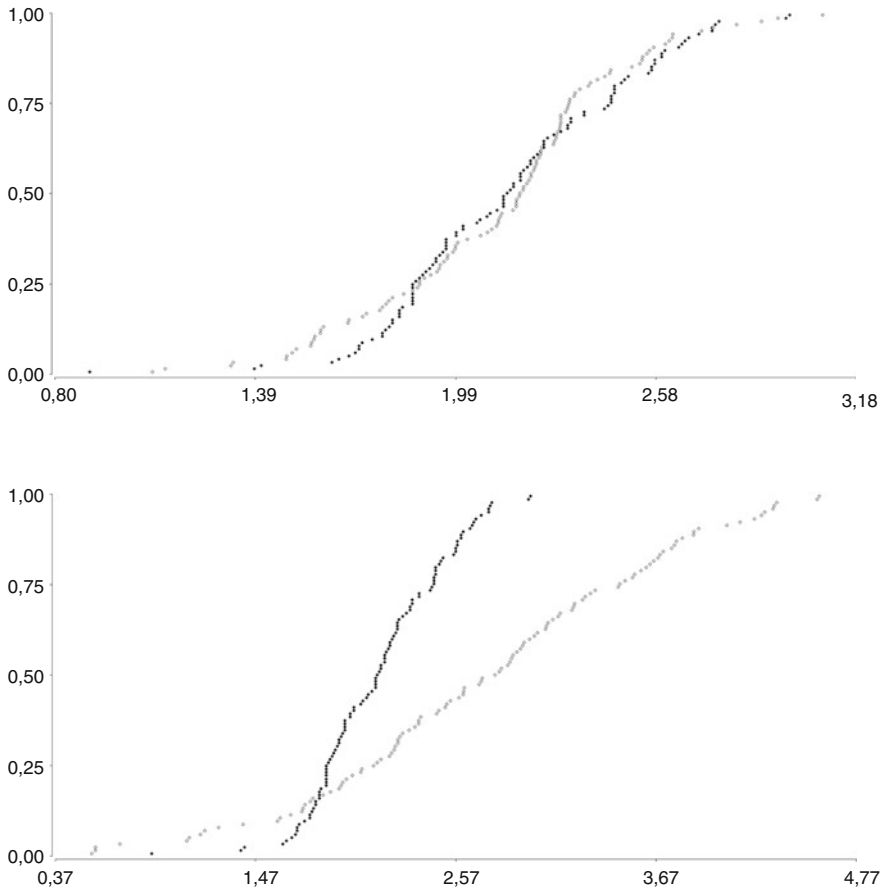


Fig. 9 Global (*up*) and specific (*down*) curves for *ID* = 3

Table 4 Gaussian parameters for the every subset

Distribution	N	Value	D statistic	p-value
global (μ, σ)	420	Normal (2.66, 0.83)	0.12	<0.0001 ^a
ID1 (μ, σ)	200	Normal (3.16, 0.78)	0.07	0.3645
ID2 (μ, σ)	109	Normal (2.27, 0.18)	0.09	0.3617
ID3 (μ, σ)	111	Normal (2.15, 0.13)	0.08	0.4881

^aNote Value with no signification

Table 5 gives specific information of the new variables for all the dataset, and each patient subset.

Note that in every case there are only two new variables (that confirms that, though each patient has distinctive parameters, the specific individual behavior

Table 5 Eigenvectors for the reduced variables

Patient	n	Representation proportion	Eigenvector: (TPM1, TPM2, UA1, UA2, HS, LAN_TASK, OTH_TASK)
All	420	0.41 0.31	$e_1:(+0.43, +0.44, +0.55, +0.52, +0.52, +0.15, +0.16)$ $e_2:(+0.51, +0.51, -0.29, -0.36, -0.26, -0.13, -0.50)$
ID1	200	0.41 0.35	$e_1:(-0.09, -0.09, +0.49, +0.52, +0.52, +0.25, +0.37)$ $e_2:(+0.62, +0.62, +0.32, +0.26, -0.22, -0.07, -0.14)$
ID2	109	0.52 0.23	$e_1:(+0.39, +0.37, +0.51, +0.51, +0.33, +0.10, +0.28)$ $e_2:(-0.51, -0.54, +0.15, +0.15, +0.59, +0.21, +0.13)$
ID3	111	0.48 0.27	$e_1:(+0.35, +0.38, +0.52, +0.52, +0.37, +0.11, +0.21)$ $e_2:(+0.50, +0.49, -0.11, -0.15, -0.49, +0.28, -0.40)$

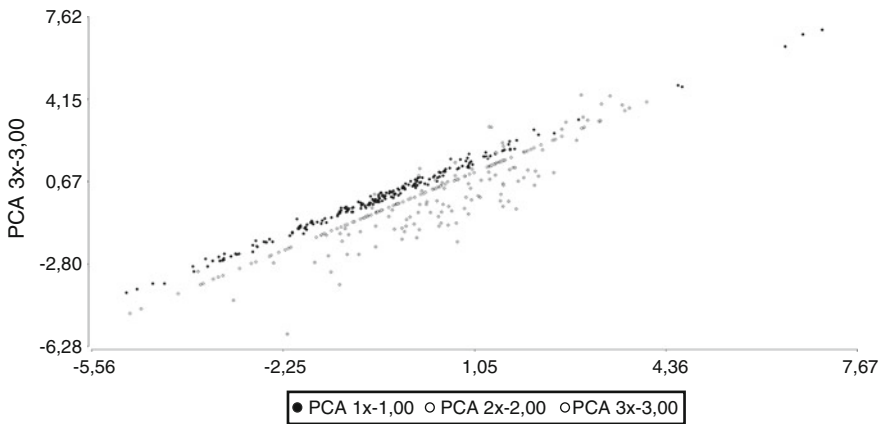


Fig. 10 Plot e_1 for $ID = 1$ (black), $ID = 2$ (white), and $ID = 3$ (gray)

follows the general distribution). The new variables have homogenous distribution that aims to represent the main features of the population and individuals.

The plots of both new variables e_1 and e_2 (see Figs. 10 and 11) explain the features of each individual related to the entire dataset. There $ID = 1$ is in black, $ID = 2$ in white, and $ID = 3$ in gray.

It is easy to observe that $ID = 1$ performs over the media in e_1 and below for e_2 . The individual 2 performs average for e_1 and over the media for e_2 . The third patient performs below the media for e_1 and average for e_2 . It can be interpreted as in Table 6, a summary of e_1 and e_2 interpretation.

Note that all the qualifications are relative to the current dataset. More data will make it possible to build a broader criterion.

Other analysis may give important information while evaluating the individual performance. That can be performed using the empirical distribution for e_1 and e_2 ,

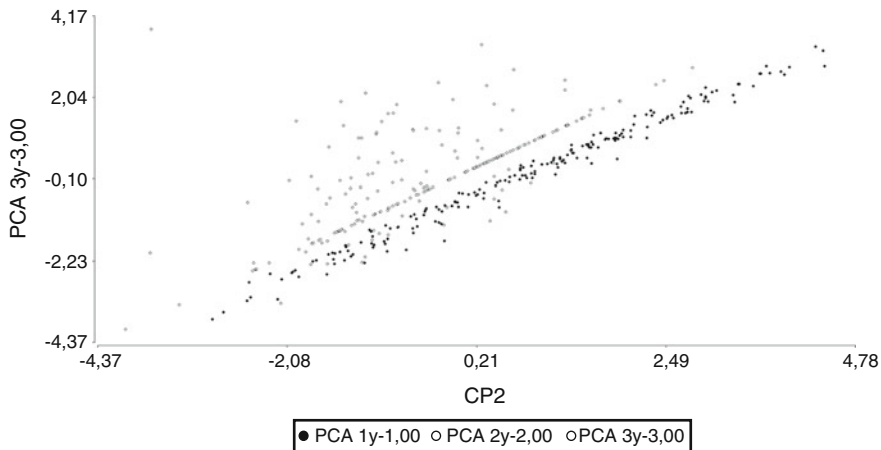


Fig. 11 Plot e_2 for $ID = 1$ (black), $ID = 2$ (white), and $ID = 3$ (gray)

Table 6 Summary of e_1 and e_2 interpretation

ID	e_1 (effort)	e_2 (efficiency)
1	High	Low
2	Average	High
3	Low	Average

There is a physical language also, that is less expressive than the one described previously

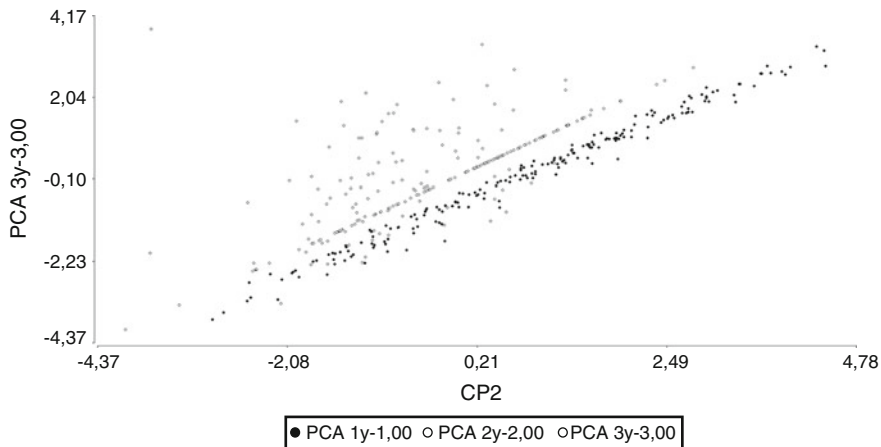


Fig. 12 Empirical distribution for $ID = 1$: e_1 (black), e_2 (white)

for each patient. Plotting the new data collected from additional sessions may allow physicians to evaluate if the current patients performance has improved or not respecting his historical performance. Figures 12, 13, and 14 are the plots of the empirical distribution for $ID = 1$, $ID = 2$, and $ID = 3$. Curves e_1 (black), e_2 (white) may be used isolated or together.

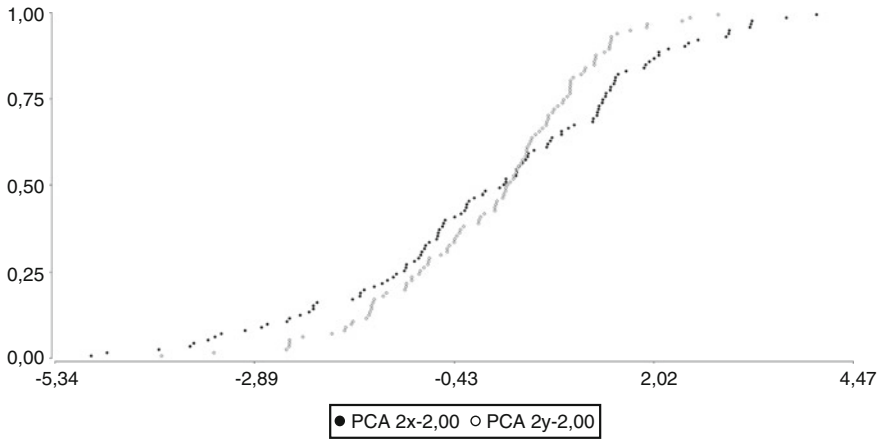


Fig. 13 Empirical distribution for $ID = 2$: e_1 (black), e_2 (white)

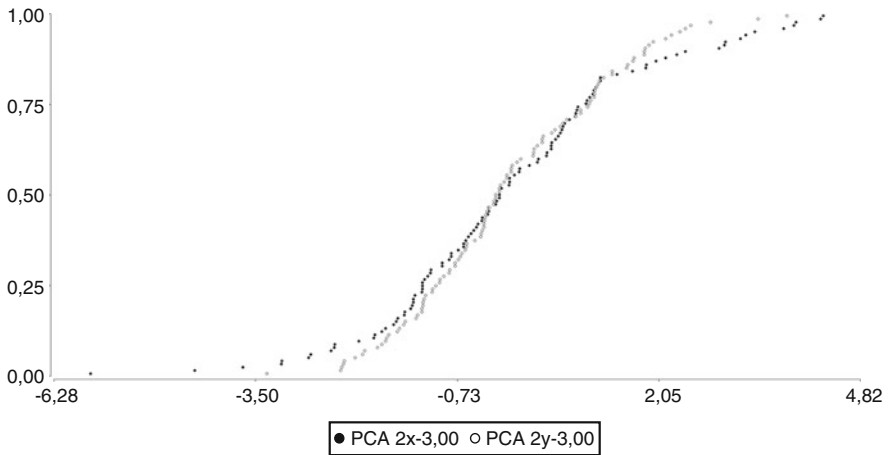


Fig. 14 Empirical distribution for $ID = 3$: e_1 (black), e_2 (white)

4 Conclusions and Future Work

Although all the findings must be confirmed with further statistics, data preliminary analysis suggest that patients have similar sessions and that training does not bias results. As a consequence, the current therapists and treatment do not make impact on the performance evolution. In other words, therapist and topic of the task make no significant bias from the statistical point of view.

The specific *TPM1* distribution for $ID = 1, 2, \text{ and } 3$ compared with the Normal distribution (derived from the global dataset), defines the performance of an individual related to the universe of patients. A study with more cases will give enough information to build a more accurate *performance profiling*.

The variables *TPM1*, *TPM2*, *HOURS*, *UA1*, *UA2*, *LANGUAGE TASKS*, and *OTHER TASKS* can be reduced to variables e_1 and e_2 using PCA. They may be interpreted as the relation between the effort (e_1) and the time to accomplish a task (e_2).

The plots of e_1 and e_2 may model the key features of each individual related to the entire dataset (here three individuals). It is useful to automatically evaluate several patients using simple clustering algorithms in order to be able to profile them. The result should be a dot cloud with different features.

These new variables may constitute a patient's performance model along with the sessions and a new parameter to evaluate each person respecting a group. It can also model evolution profiles that are present in a predefined universe of patients.

The team is currently defining and testing new audio and video protocols to collect additional parameters. This is important in order to be able to complete a parametric reasoning model using MLW.

From these findings, it may be concluded that it is possible to perform a general modeling of the skills performance and to build a specific profiling for each individual.

It remains to future work to better parameterize and evaluate outputs of the BIOTECH processing and to relate them to the status and profile of the patient.

Acknowledgments Authors thanks IEEE SIGHT for the initiative and initial sponsorship of the CIIS Lab BIOTECH project, and Universities of Mendoza, San Juan, and Favaloro for providing expertise in visual, acoustic signal processing, and mathematical knowledge. Also thank to CIIS Lab and EAndes foundation, for expert knowledge in Machine Learning, MLW, and image processing. Special thanks to CIEL in Spain and Argentina, and TIPNEA for the permanent collaboration with data, and expert knowledge in ASD.

References

1. Ackerman SA (2010) Effects of acquisition of capacity for sameness on rate learning and generalized body and object limitations. Doctoral dissertation. Columbia University, USA
2. American Psychiatric Association, APA (2013). Diagnostic and Statistical Manual of Mental Disorders, 5th Edition: DSM-5. Arlington, USA

3. Dador D (2013) Virtual-reality therapy may help with autism. Healthy living. http://abclocal.go.com/kabc/story?section=news/health/your_health&id=9190327
4. Douglas Greer D (2008) The ontogenetic selection of verbal capabilities: contributions of skinner's verbal behavior theory to a more comprehensive understanding of language. *Int J Psychol Psychol Ther* 8(3):363–386
5. Editorial: Robots Reading Autistic Kids' Minds (2011) Discoveries & breakthroughs inside science. <http://www.ivanhoe.com/science/story/2011/01/814a.html>
6. <http://www.autismomadrid.es/afanya-el-trabajo-con-ninos-con-trastorno-del-espectro-autista/>
7. Filipek PA, Accardo PJ, Ashwal S (2000) Practice parameter: Screening and diagnosis of autism. *Neurology* 55:468–479. doi:10.1212
8. Greer RD (1997) The comprehensive application of behavior analysis to schooling (CABAS®). *Behavior and Social Issues*, 7(1)
9. Greer RD (2009) The integration of speaker and listener responses. *Psychol Rec* 59:449–488
10. Greer RD (2011) The ontogenetic selection of verbal capabilities: contributions of skinner's verbal behavior theory to a more comprehensive understanding of language. *Psychol Psychol Ther*, 3(8)
11. Greer RD, Longano J (2010) The analysis of verbal behavior. A rose by naming: how we may learn how to do it. *Behav Anal Today*, 3(2), 120–132
12. Krans B (2013) Small humanoid robot helps autistic kids direct their attention. Healthline News. <http://www.healthline.com/health-news/children-small-humanoid-robot-helps-autistic-kids-direct-their-attention-032613>
13. López De Luise D (2008) Mejoras en la una estructura complementaria. PhD thesis. Universidad Nacional de La Plata. Argentina. doi:10.1007/978-90-481-9112-3
14. López De Luise D (2012) Morphosyntactic linguistic wavelets for knowledge management. *InTechOpen* 8:167–189. doi:10.5772/35438
15. López De Luise D, Hisgen D (2013) MLW and bilingualism: case study and definition of basic techniques. *IGI global: Advanced Research and Trends in New Technologies, Software, Human-Computer Interaction, and Communicability*, 568–600
16. López De Luise D, Hisgen D, Cabrera A, Morales Rins M (2012) Modeling dialogs with linguistic wavelets. *Theor Pract Mod Comput* 1:11–13
17. López De Luise D, Soffer M (2008) Automatic text processing for spanish texts. *Electronics, Robotics and Automotive Mechanics Conference*, pp 74–79. doi:10.1109/CERMA.2008.50
18. Palau M, Valls-Santasusana A, Salvadó B (2010) Aspectos neurolingüísticos en los trastornos del espectro autista [Neurolinguistic aspects in autism spectrum disorder]. *Relaciones neuroanatómicas y funcionales. Neurology* 50:69–76
19. Pereira Delgado JA (2009) The effects of peer monitoring training. *Psychol Rec* 59:407–434
20. Pranav D (2013) Meet Russell, a robot that helps autistic children develop social skills. *Fast Feed*. <http://www.fastcompany.com/>
21. Salisbury D (2013) Humanoid robot helps train children with autism. *Research news @ Vanderbilt*. <http://news.vanderbilt.edu/2013/03/robot-helps-children-with-autism/>
22. Scott F, Owen N, Tuncdemir P, Bader N, Fishell G, Tsien R (2013) Oxytocin enhances hippocampal spike transmission by modulating fast-spiking interneurons. *Nature*. doi:10.1038
23. Sotomayor J (2004) Los problemas de comunicación en niños pequeños con autismo [Communication problems in young children with autism]. *Atención temprana* 7:78–83
24. Sundberg ML (2007) A brief overview of a behavioral approach to language assessment and intervention for children with autism association for behavior analysis newsletter, 30(3)
25. Lord C, Shulman C, DiLavore P (2004) Regression and word loss in autistic spectrum disorders. *J Child Psychol Psychiatry* 45(5):936–955
26. Wittgenstein L (1922) *Tractatus logico-philosophicus*. Harcourt, Brace, New York

Part V
Neural Network and Applications

Fermat Number Applications and Fermat Neuron

V.K. Madan, M.M. Balas and S. Radhakrishnan

Abstract This chapter presents Fermat numbers, and their applications to filtering, autocorrelation, and related areas with advantages over the conventional computing. This paper discusses the basic concepts of prime numbers like Mersenne primes and Fermat primes and their comparison for computing with advantage, modulo arithmetic, Galois field, and Chinese remainder theorem. It describes and applies transforms using these concepts and their advantages like fast computation with no round off or truncation errors. It also introduces a new paradigm in neural networks (NN), about the concept of Fermat neurons. This concept needs to be developed further, as it is promising for real-life applications.

Keywords Fermat number · Modulo arithmetic · Mersenne number · Chinese remainder theorem · Galois field · Fermat neuron · XOR gate · FPGA

1 Introduction

With the advancement of silicon technology, numerous digital signal-processing techniques are being used for various applications, like space and avionics, medicine, nuclear, radar, speech processing, or sonar. In the quest for fast and efficient calculation, mathematical methods as the Fermat number transforms (FNTs) may be used. Fermat numbers have a great potential to compute efficiently and with no

V.K. Madan · S. Radhakrishnan
Kalasalingam University, Anand Nagar, Krishnankoil, Tamil Nadu 626126, India
e-mail: klvkmadan@gmail.com

S. Radhakrishnan
e-mail: srk@klu.ac.in

M.M. Balas (✉)
Aurel Vlaicu University of Arad, Arad, Romania
e-mail: marius.balas@uav.ro

errors convolutions, cross and autocorrelations, or other operations. We are interested in efficient FNTs architectures that can be implemented on FPGA.

This paper recalls some mathematical concepts that may be encountered in the FPGA field: modulo arithmetic, Fermat numbers, the Chinese remainder theorem, Galois field, FNTs, and related transforms. The authors provide a simple example, with hand calculation, for implementing convolution. Issued from these considerations, a new concept is introduced: the Fermat perceptron.

2 Fermat Numbers

The Fermat number F_n is an integer of the form

$$F_n = 2^{2^n} + 1 \quad n \geq 0 \quad (1)$$

The first five Fermat numbers are

$$3, 5, 17, 257, 65537 \quad (2)$$

If F_n is prime it is known as a Fermat prime. Fermat conjectured that all the integers expressed by the Eq. (1) are primes. However, the F_5 is composite and is divisible by 641. Up to this date, it is not known whether there is at least one Fermat prime beyond F_4 . Therefore, it is assumed that all Fermat numbers beyond F_4 are composite [1–3].

Fermat primes have a remarkable connection with the ancient problem of determining all regular polygons that can be constructed with ruler and compass alone, where the former is used to draw straight lines and the later to draw arcs. An n -sided regular polygon can be constructed if and only if n is a Fermat prime or a product of distinct Fermat primes like $F_0 F_1 = 15$ -gon, $F_0 F_2 = 51$ -gon. However, 9-gon is not constructible as it is not a product of distinct Fermat primes. Since, there are at present only five distinct Fermat primes, for odd n , the possibilities are computed as:

$${}^5 C_1 + {}^5 C_2 + {}^5 C_3 + {}^5 C_4 + {}^5 C_5 = 2^5 + 1 = 31 \quad (3)$$

Therefore, there are 31 constructible odd-sided regular polygons. Some of the possibilities are: F_0 -gon, F_1 -gon, F_2 -gon, F_3 -gon, F_4 -gon, or 3-gon, 5-gon, 17-gon, 257-gon, and 65,537-gon, respectively.

3 Number Theory and Fermat Primes

Fermat numbers play an important role in number theory. Number theory has applications in many scientific and technical areas. We are interested in particular to exploit Fermat numbers and associated orthogonal transforms for practical applications using **FPGA** programming [4]. It facilitates efficient computation in parallel programming, using small moduli. Free error results are eventually obtained by using the residue values and applying the Chinese remainder theorem (CRT).

(a) Modulo arithmetic and finite fields

Two integers, n and m , are said to be congruent modulo M if

$$N = m + kM \quad \text{or} \quad n = m \pmod{M} \tag{4}$$

Now $Z_M = (0, 1, 2, \dots, M - 1)$ constitutes a finite commutative ring with inverse defined on a ring it becomes a field and is called Galois field $GF(M)$.

We describe below some modulo arithmetic operations with $M = 7$.

addition	$5 + 4 \equiv 2 \pmod{7}$	
negation	$-5 \equiv -5 + 7 \equiv 2 \pmod{7}$	
subtraction	$9 - 5 \equiv 9 + (-5) \equiv 4 \pmod{7}$	
multiplication	$9 \times 5 = 45 \equiv 3 \pmod{7}$	(5)
inverse	$3^{-1} \equiv 5 \pmod{7}$ (this exists since $(3, 7) = 1$)	
division	$5/3 = 5 \times 3^{-1} = 5 \times 5 \equiv 4 \pmod{7}$	

(b) Primitive roots

The operation modulo M partitions the field into residue classes. The complete residue system modulo M (CRSM) forms a group. The order of each element of this group gives roots of unity. Among these roots there are special roots called primitive roots, which have maximum order of $p - 1$ where modulus is a prime p .

The particular case where modulus is a Fermat number is of special interest. There exist theorems concerning the divisors of F_t and primality of F_t . A particularly important propriety of prime F_t is the order of root modulo F_t , since it acts to generate orthogonal transform of the same length.

The transforms using Fermat prime fall under the category known as number theoretic transforms (NTTs).

According to Fermat’s theorem, if α is a integer and p a prime then

$$\alpha^{p-1} \equiv 1 \pmod{p} \tag{6}$$

Since p is a prime, α has order $p - 1$. Therefore, α is a primitive root. We see that 3 is a primitive root of all primes of F_t and also that every F_t has roots of order $d = 2^n$ with $n \leq t + 2$.

(c) The Chinese remainder theorem

The Chinese remainder theorem states that it is possible to reconstruct integers in a certain range from their residues and associated moduli. For example, the 10 integer in the range 0–9 can be reconstructed from their two residues modulo 2 and modulo 5 (the coprime factors of 10). If the known residues of a decimal digit are $r_2 = 0$ and $r_5 = 3$ then the unknown digit is 8 and is unique.

It turns out that representing numbers in a notation based on CRT has very useful applications:

- (i) fast digital computations (convolutions and Fourier transforms)
- (ii) superfast optimal transforms
- (iii) solutions of quadratic congruences.

The CRT which yields an unusual number representation is used for NTTs and for index manipulations which serve to map one-dimensional problems into multi-dimensional problems.

4 Fermat Number Transforms and Applications

The need for fast algorithms for the summation of lagged products, like convolutions and cross or autocorrelations arises in many domains of the digital signal processing (DSP): radar, sonar, nuclear spectrometry, image processing, medical applications, etc.

Operations like convolution and Discrete Fourier Transforms (DFTs) can be viewed like operations defined in finite rings and fields of integers and polynomial. The number theoretic transforms (NTTs) have DFT-like structures defined in finite rings and fields of numbers [5].

(a) Number theoretic transforms

Let (g_n) denote a discrete data sequence of length N . For example (g_n) could be a discrete-time signal denoting values of a continuous signal $g(t)$, sampled at times $t = nT$, and quantized using an analog to digital converter (ADC).

Similar to DFTs or modified DFTs, we can define a special class of Number Theoretic Transforms (NTT).

(b) Fermat and Mersenne Number Transforms

A special class of NTTs, using Fermat primes or Mersenne primes, is known as Fermat Number Transform (FNT).

FNTs have advantages over MNTs. MNTs do not have fast transform algorithm and have a rigid relation between digital signal length and computer word length in bits for processing. FNTs give much more flexibility in selecting the signal length for processing and the computer word length.

FNTs can be used to process efficiently highly composite signal length. Many of the practical signals have highly composite length like 4 and 8 K multichannel

analyzers for acquisition of gamma ray spectrum. Hence, it is possible to have an FFT-like radix-2 algorithm using butterflies, in order to compute efficiently forward and backward transforms.

The forward and backward FNT pair for a digital signal is defined below.

Let g_n be observed values of a digital signal given as:

$$\{g_n\} = (g_0, \dots, g_{N-1}) \text{ of length } N \tag{7}$$

The forward transform G_k is defined as:

$$G_k = \sum_{n=0}^{N-1} g_n \alpha^{nk} \pmod{F_t}, \quad k = 0, \dots, N - 1 \tag{8}$$

and its inverse transform g_m as:

$$g_m = \sum_{k=0}^{N-1} G_k \alpha^{-mk} \pmod{F_t}, \quad m = 0, \dots, N - 1 \tag{9}$$

where $\alpha^N \equiv 1 \pmod{F_t}$, i.e., α is a root of unity of order N . When $\alpha = 2$, it is known as Rader transform [6].

- (i) We note that FNTs only require integer arithmetic. It is easy and fast to find inverse of any number in the field
- (ii) It may be mentioned that Rader transforms using Fermat primes have significant computational advantages and they do not require multiplications and divisions, which can be achieved with left and right shifts, respectively while Fourier transform requires time-consuming complex arithmetic operations.

(c) Application of FTN to convolution

If we consider the sample convolution Y_l of two sequences h_n and x_n of N terms:

$$Y_l = \sum_{n=0}^{N-1} h_n x_{l-n}, \quad l = 0, 1, \dots, 2N - 2 \tag{10}$$

The direct calculation of Y_l requires a number of arithmetic operations which is in the order of N^2 . For large convolutions, the corresponding computational processing burden becomes rapidly excessive. Therefore, considerable effort has been devoted to devising faster computational methods. For example, for image processing the amount of data is so large that improvement in accuracy and speed are desired.

Such improvements are possible with FNTs. FNTs use only integer arithmetic, have zero truncation and zero round off errors, resulting in zero tolerance to errors in processing signals. They give efficient algorithms resulting in error free and fast convolutions, auto-correlations, and cross-correlations. For a generalized case using NTTs using Fermat numbers for convolutions, one use the following theorem:

Theorem An NTT of length N exists and implements cyclic convolutions if there exists an inverse of N and element α , which is a root of unity of order N modulo F_t .

We now consider an example of convolution of two 4-point sequences.

$$S_1 = \{2, -2, 1, 0\} = \{h_n\} \tag{11}$$

$$S_2 = \{1, 2, 0, 0\} = \{x_n\}$$

Let the modulus be $F_{n2} = 2^{2^2} + 1 = 17$. The root of unity for $\alpha^4 \equiv 1 \pmod{17} \equiv \pmod{F_2}$ are easily found to be $\alpha = 4$ (by checking $\alpha = 1, 2, 3, 4, 5, \text{ and } 6$). For S_1 the forward transform matrix can be written as:

$$[A] = \begin{bmatrix} 1 & 1 & 1 & 1 \\ 1 & 4 & 4^2 & 4^3 \\ 1 & 4^2 & 4^4 & 4^6 \\ 1 & 4^3 & 4^6 & 4^9 \end{bmatrix} \tag{12}$$

The transform is given by $AS_1 = \bar{S}_1 = \begin{bmatrix} 1 \\ 10 \\ 5 \\ 9 \end{bmatrix} \pmod{17}$ (13)

Similarly, for S_2 we have $\bar{S}_2 = \begin{bmatrix} 3 \\ 9 \\ 16 \\ 10 \end{bmatrix} \pmod{17}$ (14)

The product transform is

$$\bar{G} = \bar{S}_1\bar{S}_2 = \{3, 90, 80, 90\} = \{3, 5, 12, 5\} \pmod{17} \tag{15}$$

To compute the inverse transform we first obtain the inverse of the forward matrix as

$$A^{-1} = 13 \begin{bmatrix} 1 & 1 & 1 & 1 \\ 1 & 13 & 16 & 4 \\ 1 & 16 & 1 & 16 \\ 1 & 4 & 16 & 13 \end{bmatrix} \pmod{17} \tag{16}$$

The inverse transform is then $g = \{2, 2, 14, 2\} \pmod{17}$.

The result may be computed directly. For example, the first element of convolution is given by

$$[2 \quad -2 \quad 1 \quad 0] \begin{bmatrix} 0 \\ 0 \\ 2 \\ 1 \end{bmatrix} = 2 \tag{17}$$

There are many practical applications where FNTs have been used with advantages of fast computations, like convolutions, autocorrelation, and crosscorrelations. For example, in nuclear spectrometry it was implemented to solve an inverse problem for resolution improvement of nuclear spectrum [6].

5 The Fermat Neuron

The first artificial neural network, the Perceptron, is a simple type of single-layer feedforward network, which may be used for classification of input signal patterns that are linearly separable. Besides Perceptron, Neural Networks (NN) can use many other structures: Adaline and Madaline, Backpropagation (BP), Radial Basis Function (RBFN), Modular Neural (MNN), Learning Vector Quantization (LVQ), Kohonen’s Self-Organizing Feature Map (SOFM), Fuzzy Neural (FNN), Real-Time Recurrent Network, Elman Network, Hopfield Network, etc. Several activation (or transfer) functions are widely used: linear bipolar, threshold, signum, sigmoidal, hyperbolic tan, Gauss, etc. [7].

The neural network research has a history of implementing computer oriented research to be acceptable. For example, a single-layer perceptron was able to implement AND, OR, NOT, NAND, NOR, but was not able to implement XOR gate. The statement by Minsky and Papert in Ref. [8] implied that a single or more neurons, organized into a single layer, were incapable to implement some functions like the XOR gate. This halted the neural network research in that sense, as the authors were highly respected in their field. Later, it was found that single layers composed of several neurons, are capable to implement XOR gate [9], etc. As a matter of facts, history has many examples of propagation of such misconceptions, like Fermat conjectured that all his numbers were primes.

We are proposing now a novel concept, *the Fermat neuron*, described below, in Fig. 1, whose activation function is **mod 3**. Its basic structure has two inputs A and B and one output C. The weights for both inputs are equal to 1.

A Fermat neuron works on a finite field of Fermat primes, and it has all the advantages of the Fermat numbers, already mentioned above.

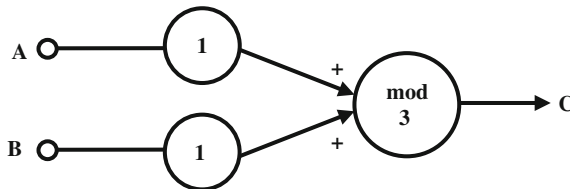


Fig. 1 The Fermat XOR neuron

Let us take the simplest case, $F_0 = 3$. The associated set for this field is $\{0, 1, 2\}$. Let us assume that the numbers represent voltages, like in a TTL circuit (transistor-transistor logic): the output logic ‘0’ represents 0–0.4 V and the input logic ‘0’ represents 0–0.8 V, whereas the output logic ‘1’ represents 2 to 5 V and the input logic ‘1’ represents 2.4–5 V. We define input logic ‘0’ as 0 V, and output logic ‘0’ as bounded between 0 V and 1 V. The logic ‘1’, for both input and output, is represented by tensions greater than 2 V. We may consider the threshold that divides the electric tensions field between ‘0’ and ‘1’, at approximately 1.5 V.

The logic and the voltage truth table for XOR are given below:

Logic			Voltage		
A	B	C = XOR	A	B	C
0	0	0	0	0	0
0	1	1	0	2	2
1	0	1	2	0	2
1	1	0	2	2	1

The voltage table is generated by applying all possible input voltages to the neuron, and the output generation is simple and self-explanatory. However, the last line may be explained, for clarity. By mod 3 addition, we get $2 + 2 = 4 \pmod{3} = 1$ V. Hence, the logic table and voltage tables match for the XOR gate.

The above example is to drive home the concept of the new paradigm. Further work is required to define identical voltage levels both for input and output for logic ‘0’ and ‘1’ and to develop the corresponding neuron. The other modifications may possibly be helpful like using other Fermat primes, using more than one neuron, and modifying weights to have additive operation rather than multiplicative to implement all logic gates. Once this is achieved, one can apply the Fermat neuron to real-life applications with the mentioned advantages.

6 Conclusions

The Fermat numbers, particularly Fermat primes, have many real-life applications. However, they are not popular and many students are not conscious about their advantages. This chapter describes theory and application of Fermat numbers to signal processing and to NN. The advantages of using Fermat primes over other primes like Mersenne are mentioned. The applications to signal processing include filtering, convolution, deconvolution, autocorrelation, etc.

The authors have proposed a new paradigm of Fermat neuron, with potential for further developing the concept and applications. They have implemented an XOR gate using a single Fermat neuron. Incidentally, the implementation of XOR gate even by using more neurons was erroneously considered as not possible in the early

stages of the neural network research. However, further research is required to develop Fermat neurons to implement all logic gates and apply them to real-life applications with advantage.

We assume that development of the perceptrons could be implemented by means of FPGA.

References

1. Burton DM (1991) Elementary number theory, Universal Book Stall, New Delhi
2. Arya SP (1989) Fermat numbers. *Math Educ* 6(1):5–6
3. Arya SP (1990) More about Fermat numbers. *Math Educ* 7(2):139–141
4. Manakov A (2010) Development of FPGA-based digital correlator using Fermat number transform, master Thesis, (supervisor: Dr. Tomsk State University, Oleg Pono-ma-rev)
5. Agarwal RC, Burrus CS (1975) Number theoretic transforms to implement fast digital convolutions. *Proc IEEE* 63(4):550–560
6. Kekre HB, Madan VK (1988) Application of rader transform to the analysis of nuclear spectral data. *Nucl Instrum Methods A* 269:279–281
7. Bose BK (2007) Neural network applications in power electronics and motor drives—an introduction and perspective. *IEEE Trans Industrial Electron* 54(1), 2007
8. Minsky M, Papert S (1968) *Perceptron*, MIT Press. Mass, Cambridge
9. Graupe D (2013) *Principles of artificial neural networks*, 3rd edn. World Scientific Publishing Company, Singapore, 19 Nov 2013

Data Clustering Using a Modified Fuzzy Min-Max Neural Network

Manjeevan Seera, Chee Peng Lim, Chu Kiong Loo
and Lakhmi C. Jain

Abstract In this paper, a modified fuzzy min-max (FMM) clustering neural network is developed. Specifically, a centroid computation procedure is embedded into the FMM clustering network to establish the cluster centroid of each hyperbox in the FMM structure. Based on the hyperbox centroids, the FMM clustering performance in undertaking data clustering problems is measured using the cophenetic correlation coefficient (CCC). A series of experimental studies using benchmark datasets is conducted. The CCC scores obtained are compared with those from other clustering algorithms reported in the literature. The empirical findings indicate the effectiveness of FMM with the centroid formation procedure for tackling data clustering tasks.

Keywords Data clustering · Fuzzy min-max neural network · Hyperbox centroid · Cophenetic correlation coefficient

1 Introduction

Clustering is a key technique for data analysis which includes statistical data analysis, data mining, data compression, and vector quantization [1]. Typically, in supervised learning methods, data are labeled with a number of specific target classes. However, being an unsupervised learning method, clustering groups data samples based on their similarity (with respect to some metric), i.e., data samples in

M. Seera (✉) · C.K. Loo
Computer Science and Information Technology, University of Malaya,
Kuala Lumpur, Malaysia
e-mail: mseera@um.edu.my

C.P. Lim
Centre for Intelligent Systems Research, Deakin University, Geelong, Australia

L.C. Jain
Faculty of Science and Technology, Data Science Institute, Bournemouth University,
Poole, UK

a cluster are more similar as compared with those in another cluster [2]. Clustering techniques are useful in many applications. Some examples include spectral clustering in recognizing freshness and adulteration levels of tomato juices [3], clustering data streams for electrical power demands in smart grids [4], an interval clustering approach for evaluating water quality [5], a hierarchical co-clustering technique for clustering music data from websites [6], as well as an adaptive fuzzy k -means clustering model for segmentation of images captured by digital cameras [7]. Some of these clustering techniques do not depend on assumptions; therefore, they are useful in situations where little or no prior knowledge is available [2].

A literature search reveals a rich body of knowledge in the domain data clustering. Typically, clustering is accomplished under a number of considerations, which include distance metric, data structure, and the number of clusters [8]. The k -means clustering [9] and fuzzy c -means [10] algorithms are popular clustering methods. Each data sample is processed and then assigned to the closest cluster center using a distance measure in k -means clustering. Many of the fuzzy clustering methods can only process spatial data samples and not nonspatial ones [10]. In regards to data-based learning, incremental learning neural networks provide several benefits, notably their robustness in handling large-scale datasets and distributed learning capabilities [11]. Being an efficient technique in knowledge discovery, incremental learning allows acquisition of additional knowledge on the fly without forgetting previously learned knowledge [12].

In this paper, the FMM clustering network [13] (hereafter refer to as FMM) is adopted for tackling data clustering tasks. FMM is able to establish connection between clusters and fuzzy sets [13]. As an incremental learning model, FMM has a number of salient features in handling data clustering problems. It does not require a predetermined number of clusters. In other words, the number of clusters grows incrementally subject to the characteristics of the incoming data samples. It has only one key parameter, i.e., the hyperbox size that needs to be fine-tuned by users [13]. Comparatively, popular clustering algorithms such as k -means and fuzzy c -means require a pre-set number of clusters to begin with, and this can be a difficult task especially when dealing with large datasets, or when the underlying data structure keeps changing in dynamic, nonstationary environments. In this regards, FMM is useful in overcoming these issues by forming a dynamic, growing network that is able to create the number of clusters incrementally based on the characteristics of the incoming data samples.

In this study, a centroid formation procedure is incorporated into the FMM network. By doing so, the performance and quality of clustering by FMM can be measured using the cophenetic correlation coefficient (CCC). Introduced by Sokal and Rohlf [14], CCC measures on how well a clustering technique is able to retain the original similarity in its data structure, whereby a higher CCC score indicates a better fitness [15]. It provides an index to indicate how much the clustering method distorts the information in its input in order to produce its output. CCC has since been widely used in numerical studies, for two main reasons, (i) as a measure of degree of fit for a set of data samples and (ii) as a criterion in efficiency evaluation of various clustering techniques [16]. In terms of applications, researchers prefer to

use the CCC indicators to assess distortions [17]. In this study, we adopt the CCC to measure the clustering quality produced by FMM. A number of benchmark datasets are used to evaluate the performance of FMM, and the CCC results are compared with those reported in the literature.

The rest of the paper is structured as follows. In Sect. 2, the FMM clustering network is first briefly described. Then, the modifications of FMM are explained. In Sect. 3, an experimental study is presented, with the results compared and discussed. Conclusions and suggestions for further work are given in Sect. 4.

2 The Fuzzy Min-Max Clustering Network

In this section, the structure of the FMM clustering neural network is briefly described. This is followed by the proposed modifications of the FMM network. Note that the detailed dynamics of the FMM clustering network can be found in [13].

2.1 Fuzzy Min-Max Clustering

The FMM clustering network [13] learns by forming hyperbox fuzzy sets in its structure. The hyperbox size is controlled by θ , which varies between 0 and 1. When θ is changed from a small to a larger value, the number of hyperboxes created increases, and vice versa. The membership function is computed with respect to the minimum (min) and maximum (max) points of a hyperbox, and to the extent in which a pattern fits within the hyperbox. The j th hyperbox fuzzy set, B_j , is defined by the ordered set of:

$$B_j = \{A_h, V_j, W_j, b_j(A_j, V_j, W_j)\} \tag{1}$$

where $A_h = (a_{h1}, a_{h2}, \dots, a_{hn}) \in I^n$ is the h th data sample with n dimensions in a dataset of m data samples, $h = 1, 2, \dots, m$; $V_j = (v_{j1}, v_{j2}, \dots, v_{jn})$ is the minimum point of the j th hyperbox, $W_j = (w_{j1}, w_{j2}, \dots, w_{jn})$ is maximum point of the j th hyperbox, and the membership function of the j th hyperbox is $0 \leq b_j(A_h, V_j, W_j) \leq 1$. Figure 1 shows the min and max points of a three-dimensional box.

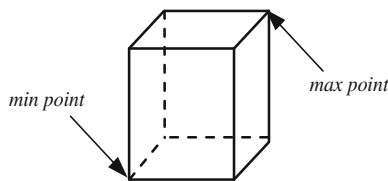


Fig. 1 A min-max hyperbox $B_j = \{V_j, W_j\}$ in I^3

The membership function measures the degree to which data sample A_h falls within a hyperbox governed by V_j and W_j . It can be seen as a measure pertaining to the extent each component is lesser (or greater) than the minimum (or maximum) point on each dimension that spills over the min and max hyperbox points. As data sample A_h approaches hyperbox B_j , $b_j(A_h, V_j, W_j)$ approaches 1. The membership function in which all the criteria are met is the average amount of the minimum and maximum point violation [13]. The resulting membership function is:

$$b_j(A_h, V_j, W_j) = \frac{1}{n} \sum_{i=1}^n [1 - f(a_{hi} - w_{ji}, \gamma) - f(v_{ji} - a_{hi}, \gamma)], \quad (2)$$

where $f(\cdot)$ is a two-parameter ramp threshold function:

$$f(x, \gamma) = \begin{cases} 1 & \text{if } x\gamma \geq 1 \\ x\gamma & \text{if } 0 \leq x\gamma \leq 1 \\ 0 & \text{if } x\gamma < 0 \end{cases} \quad (3)$$

The sensitivity parameter, γ , controls how quickly the membership function decreases when a data sample is away from the hyperbox. The fuzzy set is less crisp when γ is small and becomes crisp when γ is large. As mentioned earlier, the size of a hyperbox is constrained by $0 < \theta < 1$. For hyperbox B_j to expand and include A_h , the expansion criterion has to satisfy the following constraint:

$$\sum_{i=1}^n (\max(w_{ji}, a_{hi}) - \min(v_{ji}, a_{hi})) \leq n\theta \quad (4)$$

There is a possibility that a hyperbox overlaps with other existing hyperboxes when it starts to expand. An overlap test is introduced where a potential overlap between B_j and B_k is checked on a dimension-by-dimension basis. The overlapped region is eliminated using the hyperbox contraction process [13]. A number of cases are used to check different scenarios of the overlapped regions and to eliminate them during the contraction process.

2.2 Centroid Formation

A centroid formation procedure to compute the centroid of each FMM hyperbox is proposed. It is based on a similar investigation on FMM centroid formulation for tackling classification problems [18]. As the hyperbox structure is governed by the minimum and maximum points, no information pertaining to the centroid of data

samples contained in each hyperbox is available. As such, the centroid for each hyperbox is created, which is based on the recursive average calculation, as follows:

$$CT_{ji} = \frac{N_j - 1}{N_j} (CT_{ji-1}) + \frac{a_{hi}}{N_j} \tag{5}$$

where CT_{ji} is the centroid value of the i th dimension of the j th hyperbox, a_{hi} is the value of the i th dimension of the h th data sample, and N_j is the number of data samples encoded by the j th hyperbox. This modification is important for enabling the computation of the CCC scores in evaluating the clustering performance of FMM.

2.3 Cophenetic Correlation Coefficient

The CCC score is a useful metric to measure the quality of clustering and the associated performance of a clustering technique [1]. It is defined as follows [19]

$$CCC = \frac{\sum_{i < j} (Y_{ij} - y)(Z_{ij} - z)}{\sqrt{\sum_{i < j} (Y_{ij} - y)^2 \sum_{i < j} (Z_{ij} - z)^2}} \tag{6}$$

where Y_{ij} is the distance between objects i and j in Y , Z_{ij} is the cophenetic distance between objects i and j , from Z , and y and z are the averages of Y and Z , respectively.

In the experimental study, the average linking method is used, i.e., the average distance from the total observations in a single cluster to all points in a different cluster [20]. The pseudo-code for the overall FMM procedure with centroid formation is shown in Table 1.

Table 1 The pseudocode for FMM with centroid formation

for the first to the last data sample
determine the winning hyperbox
expand the winning hyperbox, if necessary
perform hyperbox overlap test
if hyperboxes overlap
then contract the hyperboxes
end
update winning hyperbox centroid using recursive mean estimation
end

3 Experimental Study

To evaluate the usefulness of FMM with the centroid formation procedure, four benchmark datasets from the UCI Machine Learning repository [21] were used in the experimental study, i.e., Glass, Ecoli, Iris, and Splice datasets. The background of each dataset is as follows.

The Glass dataset is motivated by criminological investigation on classification of different types of glass. The glass left at a crime scene could be used as evidence, when it could be correctly identified [21]. The dataset contains a total of 214 data samples, each with 9 features, and with 6 target classes, as listed in Table 2. The Ecoli dataset [21] is related to protein localization sites. It contains a total of 336 data samples, each with 7 features. Table 3 shows the target classes of the Ecoli dataset.

The third dataset, Iris [21], is a frequently used problem in multivariate analysis. It contains a total of 150 data samples, each with 4 features. There are four target classes, as shown in Table 4. The fourth dataset, Splice [21], is concerned with recognizing the boundaries between exons and introns in a sequence of

Table 2 Class details of the Glass dataset

Class	Description
1	Building windows float processed
2	Building windows non float processed
3	Vehicle windows float processed
4	Containers
5	Tableware
6	Headlamps

Table 3 Class details of the Ecoli dataset

Class	Description
1	Cytoplasm
2	Inner membrane without signal sequence
3	Periplasm
4	Inner membrane, uncleavable signal sequence
5	Outer membrane
6	Outer membrane lipoprotein
7	Inner membrane lipoprotein
8	Inner membrane cleavable signal sequence

Table 4 Class details of the Iris dataset

Class	Description
1	Iris Setosa
2	Iris Versicolour
3	Iris Virginica

Table 5 Class details of the Splice dataset

Class	Description
1	Neither
2	Recognizing exon/intron boundaries (ei)
3	Recognizing intron/exon boundaries (i.e.)

deoxyribonucleic acid (DNA). It is a large and complex dataset, with 2991 data samples, each with 60 features. There are a total of three target classes, as shown in Table 5.

3.1 Results and Discussion

For the Glass and Ecoli datasets, we compared the results of FMM with those from the multilayer perceptron (MLP) neural network, as reported in [22]. For the Iris dataset, we compared the results with that reported in [1]. The results from Splice dataset were compared with that from an ensemble Min-Transitive Combination of Hierarchical Clustering (MATCH) model, as reported in [23].

The overall results are shown in Tables 6, 7, 8, and 9. As stated in [22], CCC scores were not available for classes 7 and 8 for the Ecoli dataset, as there was only one cluster for both classes. The cluster numbers were not reported in [23].

From Tables 6, 7, 8, and 9, it can be seen that the CCC scores of FMM are higher than those reported in [1, 22, 23]. However, FMM creates more clusters than

Table 6 Performance comparison for the Glass dataset

Class	MLP [22]		FMM	
	CCC	Cluster	CCC	Cluster
1	0.885	5	0.936	6
2	0.974	2	0.977	2
3	0.924	2	0.936	2
4	0.986	3	0.989	4
5	0.928	2	0.931	2
6	0.977	2	0.984	3

Table 7 Performance comparison for the Ecoli dataset

Class	MLP [22]		FMM	
	CCC	Cluster	CCC	Cluster
1	0.688	7	0.705	9
2	0.772	2	0.828	3
3	0.868	3	0.932	4
4	0.658	7	0.840	8
5	0.720	14	0.910	15
6	0.998	2	0.999	3

Table 8 Performance comparison for the Iris dataset

Clustering [1]		FMM	
CCC	Cluster	CCC	Cluster
0.872	3	0.976	5

Table 9 Performance comparison for the Splice dataset

MATCH (Ensemble) [23]		FMM	
CCC	Cluster	CCC	Cluster
0.6437	–	0.813	821

those from [1, 22]. In general, FMM is able to produce a high CCC score of above 0.8 for all datasets (except Class 1 in the Ecoli dataset). As indicated in [17], a CCC score of 0.8 and above implies that the degree of distortion between the input and clustered data is not high.

The effects of the hyperbox size toward the FMM results were examined too. The respective CCC scores for different hyperbox sizes, ranging from 0.1 to 0.9 with an increment of 0.2, are shown in Table 10. In addition, the numbers of clusters are shown in Table 11. Note that owing to too few clusters, no CCC score could be produced in certain hyperbox size settings. It can be seen that when the hyperbox size was small, the number of clusters produced was high. The higher the hyperbox size setting, for instance at 0.9, the number of hyperboxes became smaller. In some cases, only one hyperbox was produced as all data samples were clustered within one hyperbox (that covered almost the entire feature space); therefore, no CCC score was produced.

Table 10 CCC comparison

Dataset	$\theta = 0.1$	$\theta = 0.3$	$\theta = 0.5$	$\theta = 0.7$	$\theta = 0.9$
Glass	0.938	0.943	–	–	–
Ecoli	0.789	0.811	0.887	0.861	–
Iris	0.872	0.966	0.976	–	–
Splice	0.542	0.813	0.664	0.531	–

Table 11 Cluster comparison

Dataset	$\theta = 0.1$	$\theta = 0.3$	$\theta = 0.5$	$\theta = 0.7$	$\theta = 0.9$
Glass	28	19	1	1	1
Ecoli	129	80	42	30	1
Iris	43	12	5	1	1
Splice	1795	821	382	171	1

4 Conclusions

In this study, a centroid formation procedure has been incorporated into the FMM clustering neural network. The key advantage of FMM is its online learning capability whereby the number of clusters can be increased online, incrementally over time. The centroid formation procedure enables performance measurement of FMM using the CCC score. CCC is a useful clustering metric, and is commonly used for evaluation of various clustering techniques. From the experimental results, the CCC scores produced FMM are higher than those reported in literature.

Further work will focus on incorporating transfer learning into FMM. This will allow FMM to be used in cross-domain problems. In addition, more experimental studies with real-world problems will be conducted, in order to ascertain the effectiveness of FMM in undertaking data clustering problems.

Acknowledgments This project is supported by UMRG Research Subprogram (Project Number RP003D-13ICT).

References

1. Erisoglu M, Sakallioğlu S (2010) An investigation of effects on hierarchical clustering of distance measurements. *Selçuk J Appl Math Special Issue*, 39–53 (2010)
2. Babuška R (2000) Fuzzy clustering algorithms with applications to rule extraction. In: Szczepaniak PS, Lisboa PJG (eds) *Fuzzy systems in medicine*, pp 139–173
3. Hong X, Wang J, Qi G (2014) Comparison of spectral clustering, K -clustering and hierarchical clustering on e-nose datasets: application to the recognition of material freshness, adulteration levels and pretreatment approaches for tomato juices. *Chemometr Intell Lab Syst* 133:17–24
4. Sancho-Asensio A, Navarro J, Arrieta-Salinas I, Armendáriz-Íñigo JE, Jiménez-Ruano V, Zaballos A, Golobardes E (2014) Improving data partition schemes in smart grids via clustering data streams. *Expert Syst Appl* 41:5832–5842
5. Wong H, Hu BQ (2013) Application of interval clustering approach to water quality evaluation. *J Hydrol* 491:1–12
6. Li J, Shao B, Li T, Ogihara M (2012) Hierarchical co-clustering: a new way to organize the music data. *IEEE Trans Multimedia* 14:471–481
7. Sulaiman SN, Isa NAM (2010) Adaptive fuzzy- K -means clustering algorithm for image segmentation. *IEEE Trans Consum Electron* 56:2661–2668
8. Abin AA, Beigy H (2014) Active selection of clustering constraints: a sequential approach. *Pattern Recogn* 47:1443–1458
9. Krishna K, Murty MN (1999) Genetic K -means algorithm. *IEEE Trans Syst Man Cybern Part B: Cybern* 29:433–439
10. Tseng VS, Kao CP (2007) A novel similarity-based fuzzy clustering algorithm by integrating PCM and mountain method. *IEEE Trans Fuzzy Syst* 15:1188–1196
11. Martínez-Rego D, Fontenla-Romero O, Alonso-Betanzos A (2012) Nonlinear single layer neural network training algorithm for incremental, nonstationary and distributed learning scenarios. *Pattern Recogn* 45:4536–4546
12. Luo C, Li T, Chen H, Liu D (2013) Incremental approaches for updating approximations in set-valued ordered information systems. *Knowl-Based Syst* 50:218–233

13. Simpson PK (1993) Fuzzy Min-Max Neural Networks - Part 2: Clustering. *IEEE Trans Fuzzy Syst* 1:32–45
14. Sokal RR, Rohlf FJ (1962) The comparison of dendrograms by objective methods. *Taxon* 11:33–40
15. Sharma V, Nandineni MR (2014) Assessment of genetic diversity among Indian potato (*Solanum tuberosum L.*) collection using microsatellite and retrotransposon based marker systems. *Mol Phylogenet Evol* 73:10–17
16. Saraçlı S, Doğan N, Doğan İ (2013) Comparison of hierarchical cluster analysis methods by cophenetic correlation. *J Inequalities Appl* 1:1–8
17. Romesburg C (2004) Cluster analysis for researchers. Lulu Press, Raleigh
18. Quteishat AM, Lim CP (2007) A modified fuzzy min-max neural network and its application to fault classification. In: *Soft computing in industrial applications*, pp 179–188
19. MATLAB Statistics Toolbox™ User's Guide (2011) The MathWorks Inc. Natick, MA
20. Schapire RE (1999) A brief introduction to boosting. *Int Joint Conf Artif Intell* 99:1401–1406
21. Bache K, Lichman M (2013) UCI machine learning repository. archive.ics.uci.edu/ml/datasets
22. Silvestre MR, Oikawa SM, Viera FHT, Ling LL (2008) A clustering based method to stipulate the number of hidden neurons of mlp neural networks: applications in pattern recognition. *Tend Mat Apl Comput* 9:351–361
23. Mirzaei A, Rahmati M (2010) A novel hierarchical-clustering-combination scheme based on fuzzy-similarity relations. *IEEE Trans Fuzzy Syst* 18:27–39

Adaptive Neuro-Fuzzy System for Current Prediction in Electric Arc Furnaces

Manuela Panoiu, Loredana Ghiormez and Caius Panoiu

Abstract This research presents an adaptive neuro-fuzzy system which is used in the current prediction through the electric arc from an electric arc furnace. Electric arc furnaces are complex systems that produce many problems, mainly harmonic currents, reactive energy, flicker effect, etc. Therefore, a prediction as good as possible is useful for the current of the electric arc. In order to do this, an ANFIS system was used which was trained using measured data from an electric arc furnace installation. ANFIS system performance is presented in this paper based on its architecture and training parameters.

Keywords Anfis · Current prediction · Electric arc furnace

1 Introduction

In order to produce steel, electric arc furnaces are widely used because they have high productivity. However, these furnaces have also some disadvantages mainly given by the nonlinearity of the electric arc: reactive power, harmonic currents, unbalanced load, flicker effect, etc. [1–10]. A prediction of the electric arc behavior is useful in order to prevent these negative effects and also to minimize their impact on the electric power quality.

M. Panoiu (✉) · L. Ghiormez · C. Panoiu
Electrical Engineering and Industrial Informatics Department,
University Polytechnic Timisoara, Timisoara, Romania
e-mail: manuela.panoiu@upt.ro

L. Ghiormez
e-mail: loredana.ghiormez@upt.ro

C. Panoiu
e-mail: caius.panoiu@upt.ro

Using ANFIS a method for the current and voltage prediction of the electric arc is proposed in this research. In order to obtain the predictive currents values, analyzed system uses measured data from an electrical installation of an electric arc furnace of 100 tones. System is based on the fundamentals of neural networks and on the Fuzzy inference mechanism. It allows the prediction of the current of the electric arc and implicitly of the voltage-current characteristic of the electric arc. It is made also a study regarding the learning algorithm and the properly structure of the ANFIS system.

2 Electric Arc Furnace Characteristics

Melting of the metals in the electric arc furnace is made by the heat that appears in the electric arc and it is transmitted by radiation for the charging material. For a corresponding electrical voltage, the electric arc burns between the solid electrodes and the molten metal in an ionized gaseous fluid. Mainly used electric arc furnaces are the one used in steel elaboration and powered, generally, at a three-phase alternative current. The scheme of an Electric Arc Furnace (EAF) is presented in Fig. 1.

During an electric arc furnace operation can be distinguished 6 important phases [11]: Furnace charging, Melting, Refining, De-slagging, Tapping, and Furnace turn-around.

The highest problems appear in the melting phase of the scrap because of their position in the furnace tank and also because during melting process the metals are changing their position so the electric arc has a random character. Electric arc length is modifying and the current through the electric arc becomes strongly distorted. Currents distortion exist also in the refining and slagging phases but the currents are not so distorted.

Fig. 1 Scheme of an electric arc furnace (EAF)

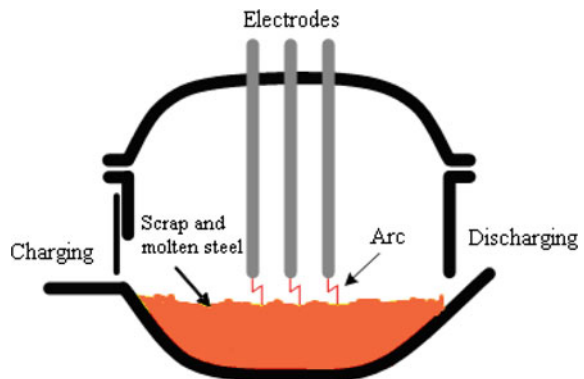


Fig. 2 Equivalent power supply circuit of the electric arc

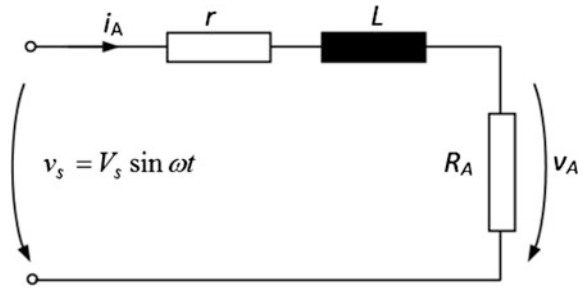
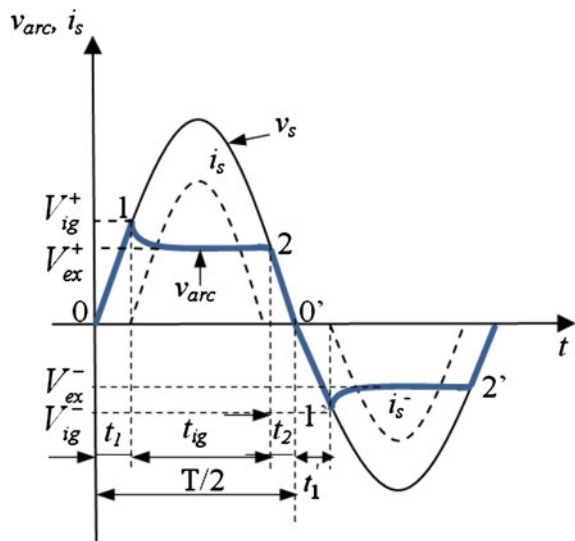


Fig. 3 Variation in time of the electric arc voltage v_{arc} , of the electric arc current i_s and of the supply voltage v_s



Equivalent power supply circuit of an electric arc with alternative current is shown in Fig. 2. In this figure R_a is the equivalent resistance of the electric arc (nonlinear), r and L are the resistance, respectively the inductance of the power supply, v_s is the alternative supply voltage, and i_A is the current of the electric arc.

Figure 3 presents variation in time for the current and voltage of the electric arc supplied with alternative current, in this case cathode and anode roll is periodically changed depending of the supply voltage frequency v_s which varies sinusoidal.

Before the ignition of the electric arc the current is null ($i_s = 0$). In this case, between the electrodes that are connected at the power supply, the voltage of the electric arc is equal to the supply voltage, v_s , and varies sinusoidal.

If the ignition conditions are met (local ionization, heating, etc.) the source voltage continues to have a sinusoidal variation on the 0–1 portion of the graph. In point 1, the source voltage reaches the ignition value V_{ig} which is large enough to

accelerate the charge carriers which produce new ions through collisions. Through this, the space between the electrodes becomes electrically conductive and the difference of electrical potential between the two electrodes decreases to the V_{ex} (extinguishing voltage) value. Since the source is capable of producing a voltage $v_s > V_{\text{ex}}$, between points 1 and 2, the arc will burn steadily through this zone.

On the 2–0' zone the supply produces a voltage, v_s , smaller than, V_{ex} , which is needed in order to burn the arc and the arc is disconnecting. Similar phenomena also take place on the negative semi-period starting from 0'. Results that the arc burns only between points 1–2, respectively 1' –2', where the current varies according to i_s curve. It can be noticed that the arc burns intermittently, having burn breaks ($t_1 + t_2$), when $i_s \rightarrow 0$.

3 Electric Arc Modeling

Many researches from the scientific literature have proposed different models of the electric arc which must allow an accurate description as possible as can for the electric arc behavior.

Here is a list of a few of the electric arc models studied so far presented in scientific literature:

- Models based on empirical relationships between the diameter or the length of the arc, the voltage, and the current flowing through the arc [12–16];
- Models that use the current-voltage characteristic of the electric arc [1, 4, 13, 17, 18];
- Models that use nonlinear and time-varying resistors [19];
- Models based on voltage sources [5, 20];
- Models that use stochastic processes [2, 21];

These classical models use a series of methods in order to simulate the electric arc behavior and are generally based on mathematical relations which use different parameters in order to describe a nonlinear element behavior and which varies chaotic in time. Even if such mathematical models are good, these cannot describe correctly the electric arc behavior in whole of the situations that appear within a complete elaboration of a charge of steel. Some studies are based on the use of models with different parameters in the two main phases of the process (melting and stable burning phases). Even in this situation classical models are not enough precisely and cannot predict a real behavior of the electric arc.

In the last period intelligent techniques were used in order to modeling the electric arc: models that are based on intelligent techniques, such as feedforward neural networks [21–24], radial basis functions neural networks [25], fuzzy logic [26] or hybrid neuro—fuzzy systems [27–30].

These intelligent techniques have a great advantage such as that is based on real data acquired from the process in real time in order to predict the electric arc behavior on a step ahead. Disadvantage for these techniques is that the prediction cannot be made accurately only for a limited number of steps above. In this research, a study regarding the possibility to predict the current of the electric arc is presented using a hybrid neuro-fuzzy system. MATLAB ANFIS system was used in order to predict the current. Measured data for the current and the voltage of the electric arc from the real installation were used in order to train the ANFIS system.

4 Adaptive Neuro-Fuzzy Inference Systems

ANFIS hybrid neuro-fuzzy systems are equivalent adaptive neural networks from the functional point of view with Takagi Sugeno fuzzy systems [31]. Compared to the classical fuzzy systems, ANFIS neuro-fuzzy systems have the capability to adapt during a learning process. In this way, applying an optimization method can be adapted to the fuzzy membership functions which appear in the premise part of the rules. The parameters of the consequences parts for the fuzzy rules can also be adapted. Criteria function of minimizing can be of the mean square error type between the actual output of a neuro-fuzzy system and the desired output of this. In order to explain the structure of a hybrid neuro-fuzzy system of ANFIS type, it a fuzzy system of Tagaki and Sugeno type of first order is considered , which has two input values, x and y , and an output value, f . Fuzzy system rules base is considered made of two rules:

Rule 1 if x is A_1 and y is B_1 then $f_1 = p_1 \cdot x + q_1 \cdot y + r_1$

Rule 2 if x is A_2 and y is B_2 then $f_2 = p_2 \cdot x + q_2 \cdot y + r_2$

In Fig. 4a, the way which is made the reasoning in a fuzzy system of Tagaki and Sugeno type of first order is intuitively shown , its output is computed as follow:

$$f = \frac{w_1 \cdot f_1 + w_2 \cdot f_2}{w_1 + w_2} = \overline{w_1} \cdot f_1 + \overline{w_2} \cdot f_2 \quad (1)$$

Figure 4b illustrates the structure of a considered neuro-fuzzy adaptive system. Equivalent ANFIS structure of the fussy system of first order is conditioned by five layers [31].

Layer 1 has the output:

$$O_{1,i} = \mu_{A_i}(x), \quad i = 1, 2, \quad \text{or} \quad O_{1,i} = \mu_{B_{i-2}}(y), \quad i = 3, 4 \quad (2)$$

Parameters of this layer are called premise parameters.

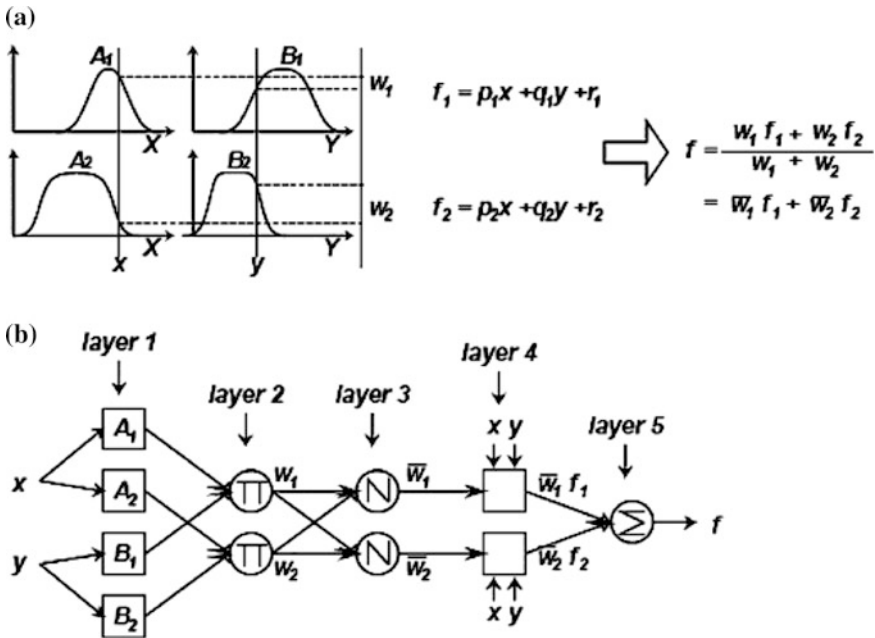


Fig. 4 **a** A two input first-order Sugeno fuzzy model with two rules. **b** Equivalent ANFIS structure [31]

If the Bell activation function is used, it is given by three parameters a_i, b_i, c_i then

$$\mu_{A_i}(x) = \frac{1}{1 + \left[\left(\frac{x-c_i}{a_i} \right)^2 \right]^{b_i}}, \tag{3}$$

$$\text{or } \mu_{A_i}(x) = e^{- \left[\left(\frac{x-c_i}{a_i} \right)^2 \right]^{b_i}} \tag{4}$$

where $\{a_i, b_i, c_i\}$ is the parameter set of the membership functions referred to as premise parameters.

Layer 2 has the output

$$O_{2,k} = w_k = \mu_{A_i}(x) \times \mu_{B_j}(y), \quad i = 1, 2, \quad j = 1, 2, \quad k = 1, \dots, 4 \tag{5}$$

Each node represents the activation value for a rule.

Layer 3 has fixed nodes with the outputs:

$$O_{3,i} = \bar{w}_i = \frac{w_i}{w_1 + w_2}, \quad i = 1, 2 \quad (6)$$

Layer 4 has adaptive nodes with the activation function

$$O_{4,i} = \bar{w}_i \cdot f_i = w_i (f_i = p_1 \cdot x + q_1 \cdot y + r_1) \quad (7)$$

Layer 5 is made of a fix node that computes the ANFIS overall output

$$f = O_{5i} = \sum_{i=1}^2 \bar{w}_i \cdot f_i = \frac{\sum_{i=1}^2 w_i \cdot f_i}{\sum_{i=1}^2 w_i} \quad (8)$$

Learning within an ANFIS system is hybrid [31].

5 Current Prediction

In this section current prediction is studied, taking into account ANFIS model parameters. In order to achieve ANFIS model, measured data in both initial melting and stable burning stages were used. Because in the initial melting stage, the currents are more distorted in this paper was present this case only. Also, were used n samples: the first $n/2$ (training data set) was used for training the ANFIS while the remaining $n/2$ (checking dataset) were used for validating the identified model.

It was demonstrated that ANFIS can be employed to predict the future values of a chaotic time series [31]. In order to make a prediction in time of the current or voltage of the electric arc, measured values for the current and voltage up to a moment t to predict a value at o moment $t + p$ were used. This can be done by creating a mapping from d sample data points, sampled every units in time with sample time s , $[x(t - (d - 1) \cdot s), \dots, x(t - s), x(t)]$ in order to predict a value of the current at moment $t + p$, i.e., $i(t + p)$.

$$x = [i(t - (d - 1) \cdot s), v(t - (d - 1) \cdot s) \dots, i(t - s), v(t - s), i(t), v(t)] \quad (9)$$

For example if it is desired a prediction for the moment $t = 4$, and 3 samples $d = 3$ are used, sample time $s = 4$, the training data vector should be formed as:

$$trn = [x(t - 8), x(t - 4), x(t)] \quad (10)$$

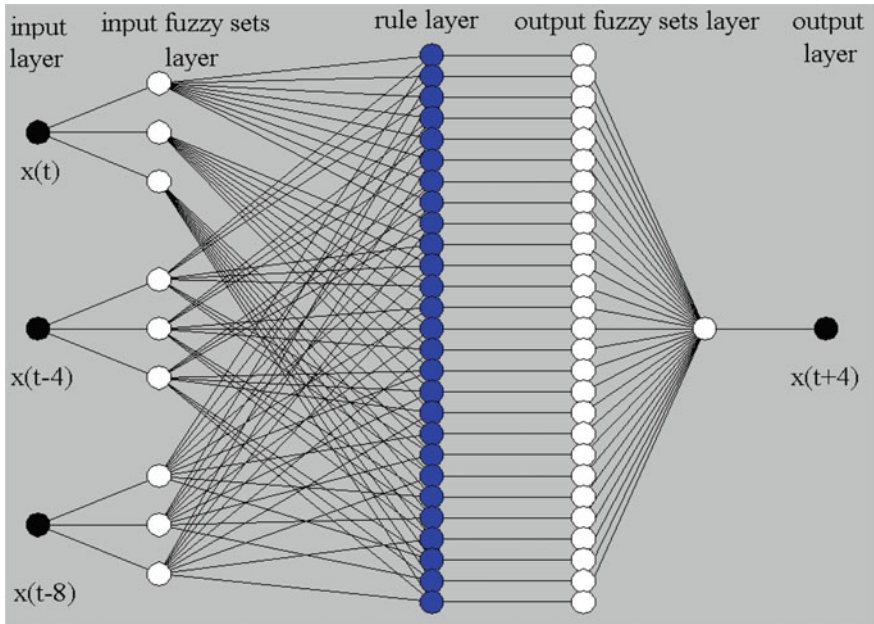


Fig. 5 The ANFIS structure for sample time $s = 4$, past samples $d = 3$ and step ahead $p = 4$

And corresponds to the prediction for the output value $y = i(t + 4)$. These elements are illustrated in Fig. 5.

For each moment t , in range $9:n$ training input/output data are represented by a structure in which the first component is the vector tn and the next component is the output y . If there are n measured data then $n/2$ can be used for training and $n/2$ for checking. For the testing was used full sample of measured data. Figure 6 presents measured data used in order to testing the performance of the ANFIS system. These data were measured in the melting phase of the charging material after approximately 12 min from the beginning of the elaboration process of charge.

In Table 1, can be noticed that was modified the number of fuzzy sets for the input data in range 2–4. Also, modified past samples number were used for the prediction. For training, ANFIS system uses Sugeno inference mechanism and a training method based on a hybrid algorithm. Grid partition is used to generate FIS. Performance of the ANFIS system was determined taking into account the error obtained at training, checking, and testing using measured data as before mentioned.

In the presented case in this research 600 samples were used. 300 samples are used for training, checking, and testing of the ANFIS system. These measured data were acquired with an acquisition frequency of 5 kHz, as presented in [6, 8, 9].

It can be noticed from Table 1 that the smaller error obtained at the system’s testing is 2.00, obtained for the sample time $s = 2$, past sample number $d = 3$ and step $p = 2$. ANFIS system has used in this case four fuzzy sets for each input and the

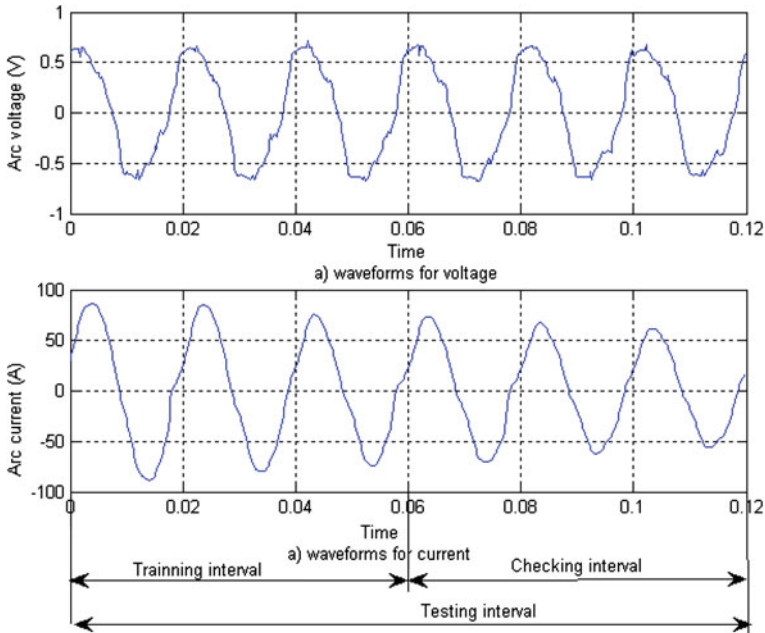


Fig. 6 The waveforms for training and checking data

training was performed for 100 epochs. Raising the number of training epochs will not obtain a smaller error contrariwise the error grows. Another good error, 2.08, was obtained for the case in which were used four steps ahead for the prediction $p = 3$, with the sample time $s = 3$. ANFIS system training parameters have been: number of epochs = 500 and the number of fuzzy sets for each input is 2. The same situation but using less training epochs carries on approximately the same result and that being a testing error of 2.75. For this case, raising the number of epochs has none advantage because even if was obtained a smaller error at training, the training time considerable grows. Also, it is not a good idea to increase the number of fuzzy sets because it can be noticed that the checking and the testing errors increased for 3 and 4 fuzzy sets, respectively. In this case, the overtraining phenomenon appears.

For a prediction of $p = 5$ or $p = 6$ steps ahead, with the same parameters above mentioned, the error increases around value 4.43, at two fuzzy sets for each input of the ANFIS system. Also, in this case, if many fuzzy sets are used the input values will obtain a better error for training but at checking and testing it will be observed the overtraining phenomenon.

Also, from Table 1 it can be noticed that in the case of using a smaller number of data $n = 300$ instead of 600, the ANFIS system does not offer better performance. These occurs because there are too less data and from these data the analyzed system characteristics cannot be extracted correctly. Therefore, it can be observed, for example, that for a prediction $p = 6$ steps ahead, the obtained error for the

Table 1 Errors variation depending on various parameters of training process

Nr. Crt.	Nr. Fuzzy sets	Error for 100 epoch			Error for 500 epoch		
		Train	Check	Test	Train	Check	Test
1. Sample $s = 2$, past samples $d = 2$, step ahead $p = 2$							
a	2	9.24	9.15	9.19	3.62	3.19	3.41
b	3	3.26	4.94	4.18	2.52	3.49	3.04
c	4	2.83	3.44	3.15	2.43	3.26	2.88
2. Sample $s = 1$, past samples $d = 3$, step ahead $p = 1$							
a	2	8.19	7.72	7.96	5.34	4.27	4.84
b	3	5.81	5.93	5.87	3.6	3.46	3.53
c	4	5.05	4.85	4.93	4.13	3.70	3.92
3. Sample $s = 2$, past samples $d = 3$, step ahead $p = 2$							
a	2	3.37	5.08	4.13	2.14	1.69	1.93
b	3	1.63	4.43	3.34	1.63	4.43	3.34
c	4	1.06	2.63	2.00	0.97	3.25	2.39
4. Sample $s = 3$, past samples $d = 3$, step ahead $p = 3$							
a	2	15.81	13.61	14.78	15.11	13.43	14.31
b	3	12.07	11.32	11.71	9.02	8.54	8.78
c	4	11.74	10.72	11.25	8.85	8.21	8.54
5. Sample $s = 2$, past samples $d = 4$, step ahead $p = 2$							
a	2	2.50	2.66	2.56	1.51	1.74	1.63
b	3	1.17	6.39	4.57	1.17	6.39	4.57
c	4	0.74	6.75	4.78	0.74	6.75	4.78
6. Sample $s = 3$, past samples $d = 4$, step ahead $p = 3$							
a	2	2.76	2.74	2.75	2.03	2.13	2.08
b	3	1.20	8.94	6.34	1.20	8.94	6.34
c	4	0.88	7.73	5.47	0.88	7.73	5.47
7. Sample $s = 4$, past samples $d = 4$, step ahead $p = 4$,							
a	2	2.98	3.38	3.18	2.62	3.67	3.18
b	3	1.25	11.41	8.06	1.23	11.27	7.96
c	4	0.91	11.14	7.85	0.9	11.15	7.85
8. Sample $s = 2$, past samples $d = 4$, step ahead $p = 4$,							
a	2	3.59	4.89	4.28	3.02	3.75	3.4
b	3	1.64	8.32	5.96	1.64	8.32	5.96
c	4	1.17	10.67	7.55	1.17	10.67	7.55
9. Sample $s = 6$, past samples $d = 4$, step ahead $p = 6$							
a	2	3.23	5.36	4.43	3.02	5.65	4.53
b	3	1.79	13.39	9.55	1.79	13.39	9.55
c	4	1.13	34.19	24.19	1.13	34.19	24.19
10. Sample $s = 5$, past samples $d = 5$, step ahead $p = 5$							
a	2	1.8	5.22	7.17	1.63	6.77	4.93
b	3	0.55	6.9	4.9	0.52	7.11	5.1

(continued)

Table 1 (continued)

Nr. Crt.	Nr. Fuzzy sets	Error for 100 epoch			Error for 500 epoch		
		Train	Check	Test	Train	Check	Test
11. Sample $s = 6$, past samples $d = 6$, step ahead $p = 6$							
a	2	1.65	5.54	4.09	1.53	5.85	4.27
b	3	0.59	17.6	12.45	0.5	18.3	13.4

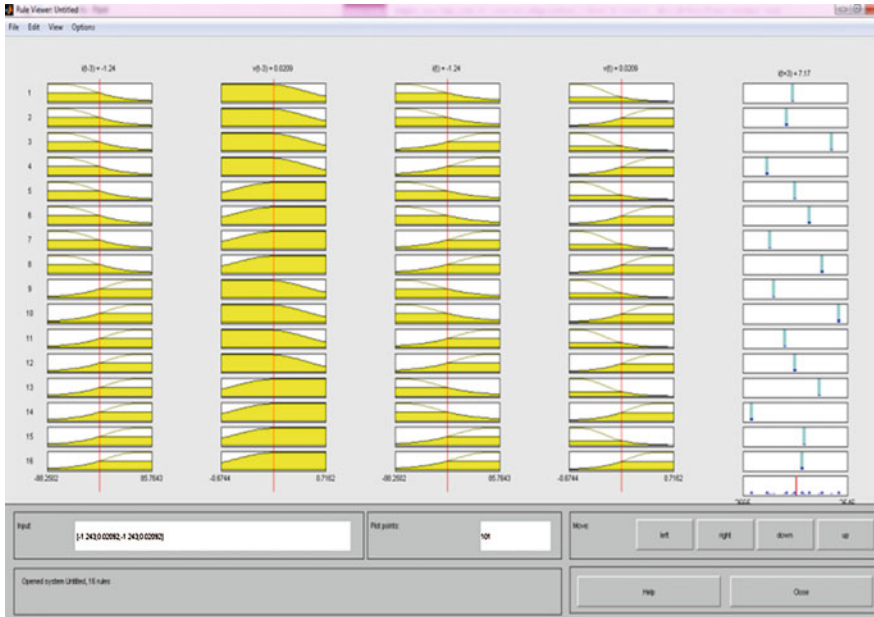


Fig. 7 The ANFIS rules for sample time $s = 3$, past samples $d = 4$, step ahead $p = 3$, and two fuzzy sets

training data is very good, 1.23, but at testing and checking it increases very much reaching up to approximately 14 at checking and approximately 9 at testing.

In conclusion, analyzing all the presented situation from Table 1 can be concluded that an admissible variant as from the obtained error point of view but even from the training time point of view is the one with the next parameters: Sample time $s = 3$, past samples $d = 4$, step ahead $p = 3$, when the obtained error at testing is 2.75 at two fuzzy sets on the input. For these data, in Fig. 7 are presented the rules for the considered case. It can be noticed in Fig. 8 that the variation of the nonlinear surface for the output depends on the two input values. Also, an error variation for a training set of 500 epochs can also be observed (Fig. 9).

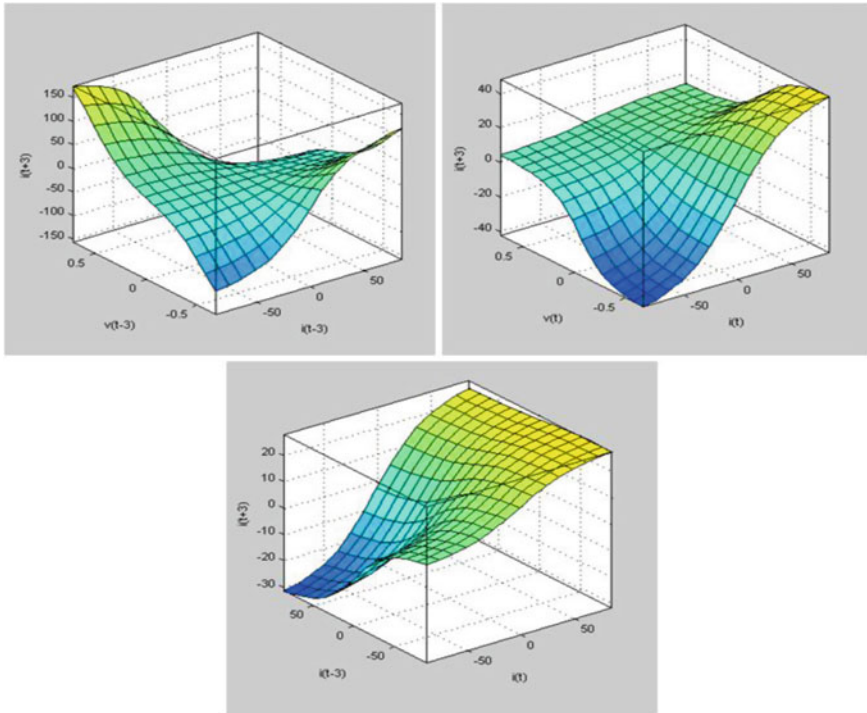


Fig. 8 Variation of system output on two system inputs for sample time $s = 3$, past samples $d = 4$, step ahead $p = 3$, and two fuzzy sets

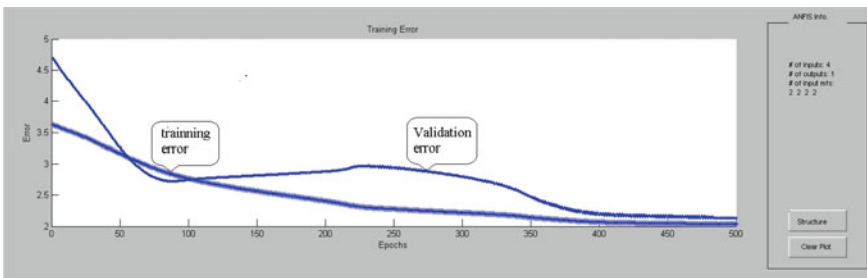


Fig. 9 Variation of training error and validation error for sample time $s = 3$, past samples $d = 4$, step ahead $p = 3$, and two fuzzy sets

Figure 10 shows the variation in time of the measured current, and of the output for the ANFIS system, i.e., for the predicted value of the current.

But for a prediction of $p = 6$ steps ahead, the error is increasing. So, when sample time $s = 6$, past samples $d = 4$, step ahead $p = 6$, are chosen with the obtained error at testing 4.43 for two fuzzy sets at each input. In this case in Fig. 11

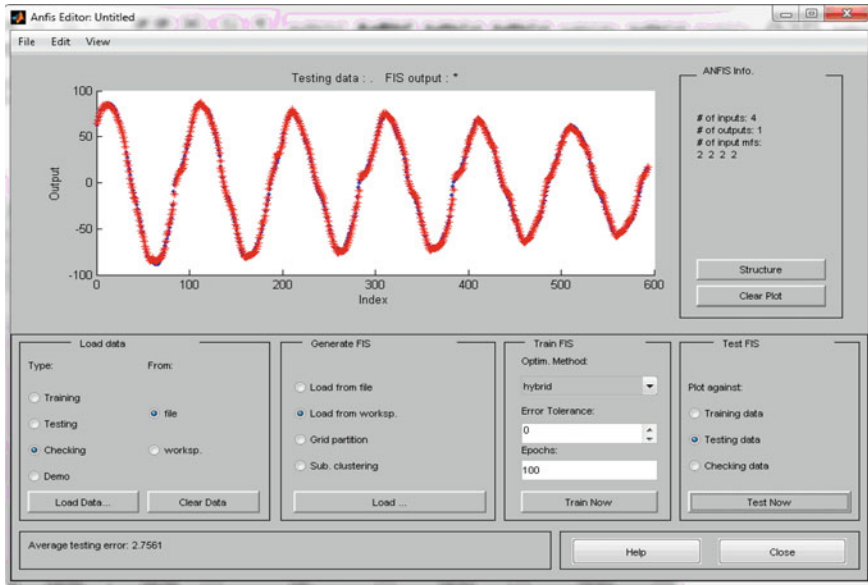


Fig. 10 The variation of the measured data (blue) and the predicted current (red) for sample time $s = 3$, past samples $d = 4$, step ahead $p = 3$, and two fuzzy sets

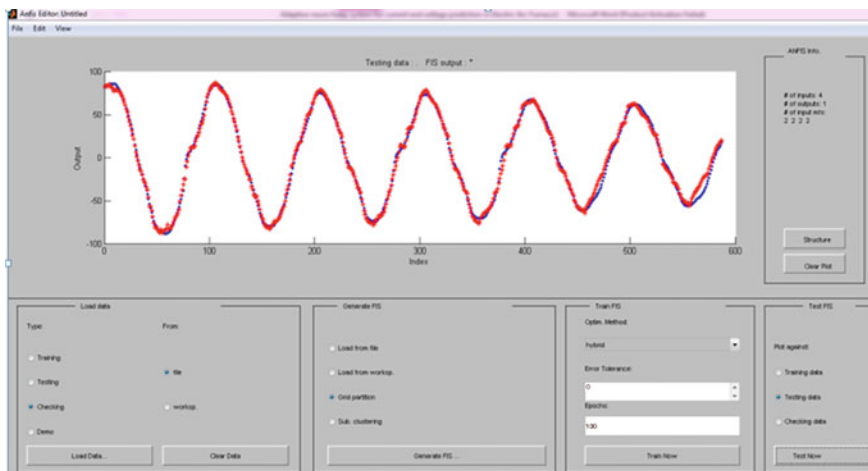


Fig. 11 The variation of the measured data (blue) and the predicted current (red) for sample time $s = 6$, past samples $d = 4$, step ahead $p = 6$, and two fuzzy sets

was presented only the variation in time of the error for 500 epochs and the output variation of the ANFIS system, i.e., for the predicted current as compared to the measured data that were used to testing the prediction accuracy.

6 Conclusions

In this paper, a detailed study regarding the possibility of using of an intelligent ANFIS system for the prediction of current in the case of an electric arc furnace was performed. This study can offer important information which are useful in order to build a system that can allow the reactive power compensation and rejection of the harmonic currents in the case of electric arc furnace. By using the prediction in real time for the electric current value, such a system used for rejection-compensation can adapt its parameters in real time such as to obtain maxim efficiency. This study was based on acquired values taken offline in the installation of an electric arc furnace with a capacity of 100 tones and a power of 100 MW. Following the study, conclusions regarding the proper structure of the ANFIS system, number of used data for the training system, and the number of steps ahead for which another correct prediction can be performed were taken.

References

1. Islam M, Chowdhury AH (2012) Comparison of dynamic resistance arc furnace models for flicker study. In: IEEE 7th international conference on electrical and computer engineering, Dhaka, pp 193–196. 20–22 Dec 2012
2. Esfahani MT, Vahidi B (2012) A new stochastic model of electric arc furnace based of hidden markov model: a study of its effects on the power system. *IEEE Trans Power Delivery* 27 (4):1893–1901
3. Chang GW, Chen CI, Liu YJ (2010) A neural-network-based method of modeling electric arc furnace load for power engineering study. *IEEE Trans Power Syst* 25(1):138–146
4. Gomez A, Durango JM, Mejia AE (2010) Electric arc furnace modeling for power quality analysis. In: ANDESCON, the bi-annual conference of the andean council of the IEEE, pp 1–6
5. Göl M, Salor Ö, Alboyaci B, Mutluer B, Çadırcı I, Ermiş M (2010) A new field-based EAF model for power quality studies. *IEEE Trans Ind Appl* 46(3):1230–1242
6. Panoiu M, Panoiu C, Şora I (2009) Modelling the electromagnetic pollution of the electric arc furnaces. *Revue Roumain des Science Techniques-serie Electrotechnique et Energetique* 54 (2):165–174
7. Xu S, Song Q, Liu W, Tong L (2006) Research on compensation for electric arc furnace using measurement field data in distribution supply system. In: 37th IEEE power electronics specialists conference, pp 1–6
8. Panoiu M, Panoiu C, Şora I, Osaci M (2007) About the possibility of power controlling in the three—phase electric arc furnaces using PSCAD-EMTDC simulation program. *Adv Electr Comput Eng* 7(1):38–43
9. Panoiu M, Panoiu C, Şora I, Osaci M, Muscalagiu I (2007) Modeling, simulating and experimental validation of the ac electric arc in the circuit of three-phase electric arc furnaces. In: 6th EUROSIM Congress, Ljubljana, 9–13 Sept 2007
10. Deaconu SI, Popa GN, Toma AI, Topor M (2009) Modeling and experimental analysis for modernization of 100 t—EAF. *IEEE Trans Ind Appl* 46(6):2259–2266
11. <http://www.steel.org/en/Making%20Steel/How%20Its%20Made/Processes/Processes%20Info/Electric%20Arc%20Furnace%20Steelmaking.aspx>
12. Hooshmand R, Banejad M, Esfahani MT (2008) A new time domain model for electric arc furnace. *J Electr Eng* 59(4):195–202

13. Golkar MA, Tavakoli Bina M, Meschi S (2007) A novel method of electrical arc furnace modeling for flicker study. *Renew Energies Power Qual* 126(7):620–626
14. Emanuel AE, Orr JA (2000) An improved method of simulation of the arc voltage-current characteristic. In: *Proceedings of the ninth international conference on harmonics and quality of power*, pp 148–154
15. Tang L, Kolluri S, Mark FMG (1997) Voltage flicker prediction for two simultaneously operated arc furnaces. *IEEE Trans. Power Delivery* 12(2)
16. Montanari GC, Loggini M, Cavallini A, Pitti L (1994) Flicker and distortion compensation in electrical plants supplying arc-furnaces. *Ind Appl Soc Ann Meet* 3:2249–2255
17. Cano Plata E, Tacca HE (2005) Arc furnace modeling in ATP-EMTP. In: *International conference on power systems transients, Montreal, Canada 19–23 June 2005*
18. Zheng T, Makram EB (2000) An adaptive arc furnace model. *IEEE Trans Power Delivery* 15 (3):931–939
19. Petersen HM, Koch RG, Swart PH, Heerden R (1995) Modelling arc furnace flicker and investigating compensation techniques. *IEEE Trans Power Delivery* 8:1733–1740
20. Hocine L, Yacine D, Kamel B, Samira KM (2009) Improvement of electrical arc furnace operation with an appropriate model. *Energy*, pp 1207–1214. Elsevier
21. O’Neill-Carrillo E, Bánfai B, Heydt GT, Si J (2001) EMTP implementation and analysis of nonlinear load models. *Electr Power Compon Syst* 809–920
22. Hui Z, Wang X (2009) Prediction model of arc furnace based on improved BP neural network. *J Inf Commun Technol* 127–130
23. Mazumdar J, Haley RG, Lambert F, Venayagamoorthy GK (2006) Predicting load harmonics in three phase systems using neural networks. In: *Twenty-first annual IEEE applied power electronics conference and exposition*, pp 1738–1744
24. Sadeghian AR, Lavers JD (2000) Application of feed forward neuro-fuzzy networks for current prediction in electric arc furnace. In: *Proceedings of the IEEE-INNS-ENNS international joint conference on neural networks, 2000. IJCNN*, pp 420–425
25. Sadeghian AR, Lavers JD (1999) Application of radial basis function networks to model electric arc furnace. In: *International joint conference on neural networks*, pp 3996–4001
26. Sadeghian AR, Lavers JD (1999) Application of adaptive fuzzy logic system to model electric arc furnace. In: *18th international conference of the north american fuzzy information processing society. NAFIPS*, pp 854–858
27. Sadeghian A, Lavers JD (2011) Dynamic reconstruction of nonlinear V-I characteristic in electric arc furnace using adaptive neuro-fuzzy rule-based networks. *Appl Soft Comput*, pp 1448–1456. Elsevier
28. Haruni AMO, Negnevitsky M (2010) An artificial intelligence approach to develop a time-series prediction model of the arc furnace resistance. *J Adv Comput Intell Intell Inf* 14 (6):722–728
29. Wiczorek T, Macza K (2008) Modeling of the AC-EAF process using computational intelligence methods. *Electrotech Rev* 11:184–188
30. Wang F, Jin Z, Zhu Z (2005) Modeling and prediction of electric arc furnace based on neural network and chaos theory. *Adv Neural Networks Lect Notes Comput Sci* 3498:819–826. Springer-Verlag
31. Jang JSR (1993) Adaptive—network—based fuzzy inference system. *IEEE Trans Syst Man Cybern* 23(3):665–685

Exact Hessian Matrix Calculation for Complex-Valued Neural Networks

Călin-Adrian Popa

Abstract In this paper, we present the full deduction of the method to evaluate the Hessian matrix of a complex-valued feedforward neural network. The Hessian matrix is composed of the second derivatives of the error function of the network, and has many applications in network training and pruning algorithms, as well as in fast re-training of the network after a small change in training data. The software implementation of the presented method is straightforward.

Keywords Complex-valued neural networks · Hessian matrix

1 Introduction

The domain of complex-valued neural networks has received an increasing interest over the last few years. This is especially due to the increasing number of applications, which include antenna design, estimation of direction of arrival and beamforming, radar imaging, communications signal processing, image processing, and many others (for an extensive presentation of the applications of complex-valued neural networks, see [5]).

A natural way to extend the power and capabilities of complex-valued neural networks is to generalize these network algorithms and methods that have been proven to be effective in real-valued neural networks. One such algorithm is the method for calculating the Hessian matrix for a feedforward neural network, which was first presented by [3], and then included in the classical book [4].

The Hessian matrix is a symmetric matrix whose elements are second-order derivatives of the error function with respect to the weights and biases of the network. There are several applications of the Hessian matrix, first of all in the

C.-A. Popa (✉)

Department of Computer and Software Engineering, Polytechnic University Timișoara,
Blvd. V. Pârvan, no. 2, 300223 Timișoara, Romania
e-mail: calin.popa@cs.upt.ro

Newton algorithm, where its inverse is used for fast training of the network. Then, in the real domain, it was used for fast re-training of a network after a small change in the training data [2], for the identification of the least significant weights as a basis for network pruning techniques [7], and for improving the speed of training algorithms [1]. The Hessian matrix was also used by [8] for Bayesian estimation of regularization parameters and for assigning probabilities to different network solutions, and has many other applications.

In this paper, we will present the full deduction of the method for calculating the Hessian matrix for a complex-valued feedforward neural network using the so-called $\mathbb{C}\mathbb{R}$ -calculus or Wirtinger calculus, see [6].

The main ideas from this type of calculus are the following. Assume that we have a function $f : \mathbb{C} \rightarrow \mathbb{R}$, which in our case will be an error function that we want to minimize. For this function, let $g : \mathbb{R}^2 \rightarrow \mathbb{R}$ be such that $g(x, y) = f(z)$, where $z = x + iy$, $i = \sqrt{-1}$, and $h : \mathbb{C} \times \mathbb{C} \rightarrow \mathbb{R}$, such that $h(z, \bar{z}) = f(z)$, where \bar{z} is the complex conjugate of z . For example, if $f_0(z) = z\bar{z} = |z|^2 = x^2 + y^2$, then $g_0(x, y) = x^2 + y^2$, and $h_0(z, \bar{z}) = z\bar{z}$, where in this last case z and \bar{z} are independent variables.

In the general case, the gradient of f with respect to z is defined as

$$\frac{\partial f}{\partial z} := \frac{\partial g}{\partial x} + i \frac{\partial g}{\partial y},$$

and in our particular case, $\frac{\partial f_0}{\partial z} = 2x + 2iy = 2z$. For the function h , we can define the \mathbb{R} -partial derivative by

$$\frac{\partial h}{\partial z} := \frac{1}{2} \left(\frac{\partial g}{\partial x} - i \frac{\partial g}{\partial y} \right),$$

and the complex \mathbb{R} -partial derivative, or $\overline{\mathbb{R}}$ -partial derivative by

$$\frac{\partial h}{\partial \bar{z}} := \frac{1}{2} \left(\frac{\partial g}{\partial x} + i \frac{\partial g}{\partial y} \right).$$

For the example, we have that $\frac{\partial h_0}{\partial z} = \frac{1}{2}(2x - 2iy) = \bar{z}$ and $\frac{\partial h_0}{\partial \bar{z}} = \frac{1}{2}(2x + 2iy) = z$, from where we can see that in the case of the \mathbb{R} -partial derivative we treat \bar{z} as a constant and derive with respect to z , and for the $\overline{\mathbb{R}}$ -partial derivative we treat z as a constant and derive with respect to \bar{z} .

We can also see that we have the following relation:

$$\frac{\partial f}{\partial z} = 2 \frac{\partial h}{\partial \bar{z}},$$

which means that in order to compute the gradient of the function f with respect to z , we can compute the $\overline{\mathbb{R}}$ -partial derivative of the function h . This is a technique that we will use in the paper.

Let us now pass to the N -dimensional case. Assume we have a function $F : \mathbb{C}^N \rightarrow \mathbb{R}$, which will also be an error function in our case, and which we want to minimize. For this function, let $G : \mathbb{R}^{2N} \rightarrow \mathbb{R}$ be such that $G(x_1, y_1, \dots, x_N, y_N) = F(z_1, \dots, z_N)$, where $z_j = x_j + iy_j, \forall j \in \{1, \dots, N\}$, and $H : \mathbb{C}^N \times \mathbb{C}^N \rightarrow \mathbb{R}$, such that $H(z_1, \dots, z_N, \bar{z}_1, \dots, \bar{z}_N) = F(z_1, \dots, z_N)$, where \bar{z}_j is the complex conjugate of $z_j, \forall j \in \{1, \dots, N\}$.

In this case, the gradient $\frac{\partial f}{\partial z}$ is replaced by the gradient vector:

$$\nabla F = \left(\frac{\partial F}{\partial z_1}, \dots, \frac{\partial F}{\partial z_N} \right)^T,$$

where $(\cdot)^T$ means transpose, because the gradient vector is a column vector, and the components of the gradient vector are the gradients of F with respect to each variable z_j , as follows:

$$\frac{\partial F}{\partial z_j} = \frac{\partial G}{\partial x_j} + i \frac{\partial G}{\partial y_j}, \forall j \in \{1, \dots, N\}.$$

For the function H , the \mathbb{R} -partial derivative with respect to z_j is given by

$$\frac{\partial H}{\partial z_j} = \frac{1}{2} \left(\frac{\partial G}{\partial x_j} - i \frac{\partial G}{\partial y_j} \right), \forall j \in \{1, \dots, N\},$$

and the complex \mathbb{R} -partial derivative, or $\overline{\mathbb{R}}$ -partial derivative with respect to \bar{z}_j by

$$\frac{\partial H}{\partial \bar{z}_j} = \frac{1}{2} \left(\frac{\partial G}{\partial x_j} + i \frac{\partial G}{\partial y_j} \right), \forall j \in \{1, \dots, N\},$$

It can now be easily seen that

$$\frac{\partial F}{\partial z_j} = 2 \frac{\partial H}{\partial \bar{z}_j}, \forall j \in \{1, \dots, N\},$$

which means that in order to compute the gradient vector of the function F , we can compute the $\overline{\mathbb{R}}$ -partial derivatives of the function H , with respect to the variables $\bar{z}_j, \forall j \in \{1, \dots, N\}$.

Another important property that we will use is the chain rule:

$$\begin{aligned}\frac{\partial h_1(h_2)}{\partial z} &= \frac{\partial h_1}{\partial h_2} \frac{\partial h_2}{\partial z} + \frac{\partial h_1}{\partial \bar{h}_2} \frac{\partial \bar{h}_2}{\partial z}, \\ \frac{\partial h_1(h_2)}{\partial \bar{z}} &= \frac{\partial h_1}{\partial h_2} \frac{\partial h_2}{\partial \bar{z}} + \frac{\partial h_1}{\partial \bar{h}_2} \frac{\partial \bar{h}_2}{\partial \bar{z}}.\end{aligned}$$

The remainder of the paper is organized as follows. Section 2 gives the detailed deduction of the method to compute the Hessian matrix of a complex-valued feedforward neural network using the above-described $\mathbb{C}\mathbb{R}$ -calculus. An example of application of this method for a three-layered neural network is given in Sect. 3. Section 4 presents the conclusions of the present paper. Software implementation is a straightforward task, and resembles the implementation of the classical back-propagation algorithm for feedforward complex-valued neural networks.

2 Hessian Matrix Evaluation

Consider a fully connected complex-valued feedforward network that has L layers denoted by $\{1, \dots, L\}$, where 1 is the input layer, L is the output layer, and the rest are hidden layers. For this network, we have the following least squares error function:

$$E^*(\mathbf{w}) = \frac{1}{2} \sum_{i=1}^c (y_i^L - t_i) \overline{(y_i^L - t_i)},$$

where \mathbf{w} represents the vector of all the weights and biases of the network, $\mathbf{y}^L = (y_i^L)_{1 \leq i \leq c}$ represent the outputs of the network, and $\mathbf{t} = (t_i)_{1 \leq i \leq c}$ represent the targets of the network. We have denoted by $E^* : \mathbb{C}^N \rightarrow \mathbb{R}$ the error function that depends upon the N weights and biases of the network. For this function, let $E : \mathbb{C}^N \times \mathbb{C}^N \rightarrow \mathbb{R}$ be such that $E(\mathbf{w}, \bar{\mathbf{w}}) = E^*(\mathbf{w})$, where $\bar{\mathbf{w}}$ represents the complex conjugate of the vector \mathbf{w} . Thus, on E we can apply the \mathbb{R} -partial derivative and $\overline{\mathbb{R}}$ -partial derivative with respect to each weight and bias of the network, which were defined above.

We will first calculate the components of the gradient vector of the error function E^* , which are gradients of the error function with respect to each weight or bias. If we denote by w_{jk}^l the weight connecting neuron j from layer l to neuron k from layer $l - 1$, we can write the gradient of the error function E^* with respect to weight w_{jk}^l as

$$\frac{\partial E^*}{\partial w_{jk}^l} = 2 \frac{\partial E}{\partial w_{jk}^l}.$$

From this relation, we deduce that it is sufficient to compute the $\overline{\mathbb{R}}$ -partial derivative of E with respect to $\overline{w_{jk}^l}$ in order to obtain the desired component of the gradient vector of the error function E^* . For this computation, we make the following notations:

$$s_j^l := \sum_k w_{jk}^l x_k^{l-1}, \quad (1)$$

$$y_j^l := G^l(s_j^l), \quad (2)$$

where $G^l : \mathbb{C} \rightarrow \mathbb{C}$ represents the activation function of the layer $l \in \{2, \dots, L\}$, $\mathbf{x} = (x_k^1)_{1 \leq k \leq d}$ are the network inputs and $x_k^l = y_k^{l-1}$, $\forall l \in \{2, \dots, L-1\}$, $\forall k$. The activation function can be a fully complex function, where the complex number is treated as a whole, for example

$$G(z) = \tanh z,$$

or a split complex function, where the real and complex parts of the complex number are treated separately, for example

$$G(x + iy) = \tanh x + i \tanh y.$$

First, we start with the output layer L , for which we can write the chain rule

$$\begin{aligned} \frac{\partial E}{\partial w_{jk}^L} &= \frac{\partial E}{\partial s_j^L} \frac{\partial s_j^L}{\partial w_{jk}^L} + \frac{\partial E}{\partial \overline{s_j^L}} \frac{\partial \overline{s_j^L}}{\partial w_{jk}^L} \\ &= \frac{\partial E}{\partial s_j^L} x_k^{L-1}, \end{aligned}$$

where $\frac{\partial s_j^L}{\partial w_{jk}^L} = 0$, because s_j^L does not depend on $\overline{w_{jk}^L}$. Further applying the chain rule

$$\begin{aligned} \frac{\partial E}{\partial \overline{s_j^L}} &= \frac{\partial E}{\partial y_j^L} \frac{\partial y_j^L}{\partial \overline{s_j^L}} + \frac{\partial E}{\partial \overline{y_j^L}} \frac{\partial \overline{y_j^L}}{\partial \overline{s_j^L}} \\ &= \frac{1}{2} (\overline{y_j^L} - \overline{t_j}) \frac{\partial G^L(s_j^L)}{\partial \overline{s_j^L}} + \frac{1}{2} (y_j^L - t_j) \frac{\partial \overline{G^L(s_j^L)}}{\partial \overline{s_j^L}}, \end{aligned}$$

and denoting $\delta_j^L := \frac{\partial E}{\partial \overline{s_j^L}}$, we have that

$$\frac{\partial E}{\partial w_{jk}^L} = \delta_j^L \overline{x_k^{L-1}},$$

where

$$\delta_j^L = \frac{1}{2} (\overline{y_j^L} - t_j) \frac{\partial G^L(s_j^L)}{\partial s_j^L} + \frac{1}{2} (y_j^L - t_j) \frac{\partial \overline{G^L(s_j^L)}}{\partial s_j^L}.$$

For a hidden layer $l \in \{2, \dots, L-1\}$, application of the chain rule yields

$$\begin{aligned} \frac{\partial E}{\partial w_{jk}^l} &= \frac{\partial E}{\partial s_j^l} \frac{\partial s_j^l}{\partial w_{jk}^l} + \frac{\partial E}{\partial \overline{s_j^l}} \frac{\partial \overline{s_j^l}}{\partial w_{jk}^l} \\ &= \frac{\partial E}{\partial s_j^l} x_k^{l-1}, \end{aligned}$$

because $\frac{\partial s_j^l}{\partial w_{jk}^l} = 0$, and then

$$\frac{\partial E}{\partial s_j^l} = \sum_r \left(\frac{\partial E}{\partial s_r^{l+1}} \frac{\partial s_r^{l+1}}{\partial s_j^l} + \frac{\partial E}{\partial \overline{s_r^{l+1}}} \frac{\partial \overline{s_r^{l+1}}}{\partial s_j^l} \right), \quad (3)$$

where the sum is taken over all the neurons r from layer $l+1$ to which neuron j from layer l sends connections.

Using the chain rule again, we have that

$$\begin{aligned} \frac{\partial s_r^{l+1}}{\partial s_j^l} &= \frac{\partial s_r^{l+1}}{\partial y_j^l} \frac{\partial y_j^l}{\partial s_j^l} + \frac{\partial s_r^{l+1}}{\partial \overline{y_j^l}} \frac{\partial \overline{y_j^l}}{\partial s_j^l} \\ &= w_{rj}^{l+1} \frac{\partial G^l(s_j^l)}{\partial s_j^l}, \end{aligned}$$

$$\begin{aligned} \frac{\partial \overline{s_r^{l+1}}}{\partial s_j^l} &= \frac{\partial \overline{s_r^{l+1}}}{\partial y_j^l} \frac{\partial y_j^l}{\partial s_j^l} + \frac{\partial \overline{s_r^{l+1}}}{\partial \overline{y_j^l}} \frac{\partial \overline{y_j^l}}{\partial s_j^l} \\ &= w_{rj}^{l+1} \frac{\partial \overline{G^l(s_j^l)}}{\partial s_j^l}, \end{aligned}$$

because again we have that $\frac{\partial s_r^{l+1}}{\partial y_j^l} = \frac{\partial \overline{s_r^{l+1}}}{\partial \overline{y_j^l}} = 0$. If we denote $\delta_j^l := \frac{\partial E}{\partial s_j^l}$,

$\forall l \in \{2, \dots, L-1\}$, Eq. (3) becomes

$$\frac{\partial E}{\partial s_j^l} = \sum_r \left(\delta_r^{l+1} \overline{w_{rj}^{l+1}} \frac{\partial \overline{G^l(s_j^l)}}{\partial s_j^l} + \delta_r^{l+1} w_{rj}^{l+1} \frac{\partial G^l(s_j^l)}{\partial s_j^l} \right),$$

and finally

$$\frac{\partial E}{\partial w_{jk}^l} = \delta_j^l \overline{x_k^{l-1}}, \forall l \in \{2, \dots, L-1\}.$$

where

$$\delta_j^l = \sum_r \left(\delta_r^{l+1} \overline{w_{rj}^{l+1}} \frac{\partial \overline{G^l(s_j^l)}}{\partial s_j^l} + \delta_r^{l+1} w_{rj}^{l+1} \frac{\partial G^l(s_j^l)}{\partial s_j^l} \right).$$

In conclusion, we have that $\frac{\partial E^*}{\partial w_{jk}^l} = 2 \frac{\partial E}{\partial w_{jk}^l}$, where

$$\frac{\partial E}{\partial w_{jk}^l} = \delta_j^l \overline{x_k^{l-1}}, \forall l \in \{2, \dots, L\}, \quad (4)$$

and

$$\delta_j^l = \begin{cases} \sum_r \left(\delta_r^{l+1} \overline{w_{rj}^{l+1}} \frac{\partial \overline{G^l(s_j^l)}}{\partial s_j^l} + \delta_r^{l+1} w_{rj}^{l+1} \frac{\partial G^l(s_j^l)}{\partial s_j^l} \right), & l \leq L-1 \\ \frac{1}{2} (y_j^l - t_j) \frac{\partial \overline{G^l(s_j^l)}}{\partial s_j^l} + \frac{1}{2} (\overline{y_j^l} - \overline{t_j}) \frac{\partial G^l(s_j^l)}{\partial s_j^l}, & l = L \end{cases}. \quad (5)$$

The elements of the Hessian matrix are the second-order derivatives of the error function with respect to any two arbitrary weights or biases of the network. Let us denote by $w_{mn}^{l_1}$ and $w_{jk}^{l_2}$ two such parameters of the complex-valued neural network, and further assume that $2 \leq l_1 \leq l_2 \leq L$. For these two parameters, we have four second-order \mathbb{R} - and $\overline{\mathbb{R}}$ -partial derivatives:

$$\frac{\partial^2 E}{\partial w_{mn}^{l_1} \partial w_{jk}^{l_2}}, \frac{\partial^2 E}{\partial \overline{w_{mn}^{l_1}} \partial \overline{w_{jk}^{l_2}}}, \frac{\partial^2 E}{\partial w_{mn}^{l_1} \partial \overline{w_{jk}^{l_2}}}, \frac{\partial^2 E}{\partial \overline{w_{mn}^{l_1}} \partial w_{jk}^{l_2}}.$$

Because the computations are similar, we will give a method to calculate the second-order $\overline{\mathbb{R}}$ -partial derivative of the error function E with respect to $\overline{w_{mn}^{l_1}}$ and $\overline{w_{jk}^{l_2}}$.

We start again with the chain rule

$$\begin{aligned} \frac{\partial^2 E}{\partial w_{mn}^{l_1} \partial w_{jk}^{l_2}} &= \frac{\partial s_m^{l_1}}{\partial w_{mn}^{l_1}} \frac{\partial^2 E}{\partial s_m^{l_1} \partial w_{jk}^{l_2}} + \frac{\partial \overline{s_m^{l_1}}}{\partial w_{mn}^{l_1}} \frac{\partial^2 E}{\partial \overline{s_m^{l_1}} \partial w_{jk}^{l_2}} \\ &= \overline{x_n^{l_1-1}} \frac{\partial^2 E}{\partial s_m^{l_1} \partial w_{jk}^{l_2}}, \end{aligned}$$

where, as above, we have that $\frac{\partial s_m^{l_1}}{\partial w_{mn}^{l_1}} = 0$. Now, using (4), we can write that

$$\begin{aligned} \frac{\partial^2 E}{\partial s_m^{l_1} \partial w_{jk}^{l_2}} &= \frac{\partial (\delta_j^{l_2} \overline{x_k^{l_2-1}})}{\partial s_m^{l_1}} \\ &= \frac{\partial \delta_j^{l_2}}{\partial s_m^{l_1}} \overline{x_k^{l_2-1}} + \frac{\partial \overline{x_k^{l_2-1}}}{\partial s_m^{l_1}} \delta_j^{l_2}, \end{aligned} \tag{6}$$

and, by the chain rule, that

$$\begin{aligned} \frac{\partial \overline{x_k^{l_2-1}}}{\partial s_m^{l_1}} &= \frac{\partial s_k^{l_2-1}}{\partial s_m^{l_1}} \frac{\partial \overline{x_k^{l_2-1}}}{\partial s_k^{l_2-1}} + \frac{\partial \overline{s_k^{l_2-1}}}{\partial s_m^{l_1}} \frac{\partial \overline{x_k^{l_2-1}}}{\partial \overline{s_k^{l_2-1}}} \\ &= \frac{\partial s_k^{l_2-1}}{\partial s_m^{l_1}} \frac{\partial \overline{G^{l_2-1}(s_k^{l_2-1})}}{\partial s_k^{l_2-1}} + \frac{\partial \overline{s_k^{l_2-1}}}{\partial s_m^{l_1}} \frac{\partial \overline{G^{l_2-1}(s_k^{l_2-1})}}{\partial \overline{s_k^{l_2-1}}} \\ &= h_{km}^{l_2-1, l_1} \frac{\partial \overline{G^{l_2-1}(s_k^{l_2-1})}}{\partial s_k^{l_2-1}} + g_{km}^{l_2-1, l_1} \frac{\partial \overline{G^{l_2-1}(s_k^{l_2-1})}}{\partial \overline{s_k^{l_2-1}}}, \end{aligned}$$

where we have denoted $h_{km}^{l_2-1, l_1} := \frac{\partial s_k^{l_2-1}}{\partial s_m^{l_1}}$ and $g_{km}^{l_2-1, l_1} := \frac{\partial \overline{s_k^{l_2-1}}}{\partial s_m^{l_1}}$. If we further denote

$b_{jm}^{l_2, l_1} := \frac{\partial \delta_j^{l_2}}{\partial s_m^{l_1}}$, Eq. (6) becomes

$$\frac{\partial^2 E}{\partial s_m^{l_1} \partial w_{jk}^{l_2}} = b_{jm}^{l_2, l_1} \overline{x_k^{l_2-1}} + h_{km}^{l_2-1, l_1} \frac{\partial \overline{G^{l_2-1}(s_k^{l_2-1})}}{\partial s_k^{l_2-1}} \delta_j^{l_2} + g_{km}^{l_2-1, l_1} \frac{\partial \overline{G^{l_2-1}(s_k^{l_2-1})}}{\partial \overline{s_k^{l_2-1}}} \delta_j^{l_2}.$$

Now, we must find a way to compute $h_{km}^{l_2-1, l_1}$, $g_{km}^{l_2-1, l_1}$, and $b_{jm}^{l_2, l_1}$. We will start with the first two. If $l_2 = l_1$, we have $h_{km}^{l_2-1, l_1} = g_{km}^{l_2-1, l_1} = 0$, because $s_k^{l_2-1}$ and $\overline{s_k^{l_2-1}}$ do not depend on $\overline{s_m^{l_1}}$. If $l_2 - 1 = l_1$, $h_{km}^{l_2-1, l_1} = 0$, $g_{km}^{l_2-1, l_1} = \delta_{km}$, because $s_k^{l_2-1}$, $\overline{s_k^{l_2-1}}$, and $\overline{s_m^{l_1}}$ are now on the same layer, and δ_{km} is the Kronecker delta symbol: $\delta_{km} = 1$ if

$k = m$ and $\delta_{km} = 0$ if $k \neq m$. For $l_2 \geq l_1 + 2$, (in which case we must have $L \geq 4$) we can again apply the chain rule

$$\begin{aligned} \frac{\partial s_k^{l_2-1}}{\partial s_m^{l_1}} &= \sum_r \left(\frac{\partial s_r^{l_2-2}}{\partial s_m^{l_1}} \frac{\partial s_k^{l_2-1}}{\partial s_r^{l_2-2}} + \frac{\overline{\partial s_r^{l_2-2}}}{\partial s_m^{l_1}} \frac{\overline{\partial s_k^{l_2-1}}}{\partial s_r^{l_2-2}} \right) \\ &= \sum_r \left(h_{rm}^{l_2-2, l_1} w_{kr}^{l_2-1} \frac{\partial G^{l_2-2}(s_r^{l_2-2})}{\partial s_r^{l_2-2}} + g_{rm}^{l_2-2, l_1} \overline{w_{kr}^{l_2-1}} \frac{\overline{\partial G^{l_2-2}(s_r^{l_2-2})}}{\partial s_r^{l_2-2}} \right), \end{aligned}$$

where we have used the fact that

$$\begin{aligned} \frac{\partial s_k^{l_2-1}}{\partial s_r^{l_2-2}} &= \frac{\partial s_k^{l_2-1}}{\partial y_r^{l_2-2}} \frac{\partial y_r^{l_2-2}}{\partial s_r^{l_2-2}} + \frac{\overline{\partial s_k^{l_2-1}}}{\overline{\partial y_r^{l_2-2}}} \frac{\overline{\partial y_r^{l_2-2}}}{\overline{\partial s_r^{l_2-2}}} \\ &= w_{kr}^{l_2-1} \frac{\partial G^{l_2-2}(s_r^{l_2-2})}{\partial s_r^{l_2-2}}, \end{aligned}$$

and

$$\begin{aligned} \frac{\partial s_k^{l_2-1}}{\partial s_r^{l_2-2}} &= \frac{\partial s_k^{l_2-1}}{\partial y_r^{l_2-2}} \frac{\partial y_r^{l_2-2}}{\partial s_r^{l_2-2}} + \frac{\overline{\partial s_k^{l_2-1}}}{\overline{\partial y_r^{l_2-2}}} \frac{\overline{\partial y_r^{l_2-2}}}{\overline{\partial s_r^{l_2-2}}} \\ &= w_{kr}^{l_2-1} \frac{\partial G^{l_2-2}(s_r^{l_2-2})}{\partial s_r^{l_2-2}}, \end{aligned}$$

and the sum goes over all the neurons r from layer $l_2 - 2$ that send connections to neuron k in layer $l_2 - 1$.

Similarly, we have that

$$\begin{aligned} \frac{\overline{\partial s_k^{l_2-1}}}{\partial s_m^{l_1}} &= \sum_r \left(\frac{\overline{\partial s_r^{l_2-2}}}{\partial s_m^{l_1}} \frac{\overline{\partial s_k^{l_2-1}}}{\overline{\partial s_r^{l_2-2}}} + \frac{\overline{\partial s_r^{l_2-2}}}{\partial s_m^{l_1}} \frac{\overline{\partial s_k^{l_2-1}}}{\overline{\partial s_r^{l_2-2}}} \right) \\ &= \sum_r \left(h_{rm}^{l_2-2, l_1} \overline{w_{kr}^{l_2-1}} \frac{\overline{\partial G^{l_2-2}(s_r^{l_2-2})}}{\partial s_r^{l_2-2}} + g_{rm}^{l_2-2, l_1} w_{kr}^{l_2-1} \frac{\partial G^{l_2-2}(s_r^{l_2-2})}{\partial s_r^{l_2-2}} \right), \end{aligned}$$

where, like above, we used

$$\begin{aligned} \frac{\overline{\partial s_k^{l_2-1}}}{\partial s_r^{l_2-2}} &= \frac{\overline{\partial s_k^{l_2-1}}}{\overline{\partial y_r^{l_2-2}}} \frac{\overline{\partial y_r^{l_2-2}}}{\partial s_r^{l_2-2}} + \frac{\overline{\partial s_k^{l_2-1}}}{\overline{\partial y_r^{l_2-2}}} \frac{\overline{\partial y_r^{l_2-2}}}{\partial s_r^{l_2-2}} \\ &= \overline{w_{kr}^{l_2-1}} \frac{\overline{\partial G^{l_2-2}(s_r^{l_2-2})}}{\partial s_r^{l_2-2}}, \end{aligned}$$

and

$$\begin{aligned} \frac{\overline{\partial s_k^{l_2-1}}}{\overline{\partial s_r^{l_2-2}}} &= \frac{\overline{\partial s_k^{l_2-1}}}{\overline{\partial y_r^{l_2-2}}} \frac{\overline{\partial y_r^{l_2-2}}}{\overline{\partial s_r^{l_2-2}}} + \frac{\overline{\partial s_k^{l_2-1}}}{\overline{\partial y_r^{l_2-2}}} \frac{\overline{\partial y_r^{l_2-2}}}{\overline{\partial s_r^{l_2-2}}} \\ &= \overline{w_{kr}^{l_2-1}} \frac{\overline{\partial G^{l_2-2}(s_r^{l_2-2})}}{\overline{\partial s_r^{l_2-2}}}. \end{aligned}$$

In conclusion, we have obtained the following recurrence relations for computing $h_{km}^{l_2-1, l_1}$ and $g_{km}^{l_2-1, l_1}$:

$$h_{km}^{l_2-1, l_1} = \sum_r \left(h_{rm}^{l_2-2, l_1} \overline{w_{kr}^{l_2-1}} \frac{\overline{\partial G^{l_2-2}(s_r^{l_2-2})}}{\overline{\partial s_r^{l_2-2}}} + g_{rm}^{l_2-2, l_1} \overline{w_{kr}^{l_2-1}} \frac{\overline{\partial G^{l_2-2}(s_r^{l_2-2})}}{\overline{\partial s_r^{l_2-2}}} \right), \quad (7)$$

$$g_{km}^{l_2-1, l_1} = \sum_r \left(h_{rm}^{l_2-2, l_1} \overline{w_{kr}^{l_2-1}} \frac{\overline{\partial G^{l_2-2}(s_r^{l_2-2})}}{\overline{\partial s_r^{l_2-2}}} + g_{rm}^{l_2-2, l_1} \overline{w_{kr}^{l_2-1}} \frac{\overline{\partial G^{l_2-2}(s_r^{l_2-2})}}{\overline{\partial s_r^{l_2-2}}} \right). \quad (8)$$

Now, let us turn our attention to $b_{jm}^{l_2, l_1}$. We will first treat the case in which $l_2 \leq L-1$. From the formula for δ_j^l given in relation (5), we have that

$$\begin{aligned} \frac{\partial \delta_j^{l_2}}{\partial s_m^{l_1}} &= \sum_r \left(\frac{\overline{\partial \delta_r^{l_2+1}}}{\overline{\partial s_m^{l_1}}} \overline{w_{rj}^{l_2+1}} \frac{\overline{\partial G^{l_2}(s_j^{l_2})}}{\overline{\partial s_j^{l_2}}} + \delta_r^{l_2+1} \frac{\overline{\partial w_{rj}^{l_2+1}}}{\overline{\partial s_m^{l_1}}} \frac{\overline{\partial G^{l_2}(s_j^{l_2})}}{\overline{\partial s_j^{l_2}}} \right. \\ &\quad + \delta_r^{l_2+1} \overline{w_{rj}^{l_2+1}} \frac{\overline{\partial^2 G^{l_2}(s_j^{l_2})}}{\overline{\partial s_m^{l_1} \partial s_j^{l_2}}} + \frac{\overline{\partial \delta_r^{l_2+1}}}{\overline{\partial s_m^{l_1}}} \overline{w_{rj}^{l_2+1}} \frac{\overline{\partial G^{l_2}(s_j^{l_2})}}{\overline{\partial s_j^{l_2}}} \\ &\quad \left. + \frac{\overline{\delta_r^{l_2+1}}}{\overline{\partial s_m^{l_1}}} \frac{\overline{\partial w_{rj}^{l_2+1}}}{\overline{\partial s_m^{l_1}}} \frac{\overline{\partial G^{l_2}(s_j^{l_2})}}{\overline{\partial s_j^{l_2}}} + \frac{\overline{\delta_r^{l_2+1}}}{\overline{\partial s_m^{l_1}}} \overline{w_{rj}^{l_2+1}} \frac{\overline{\partial^2 G^{l_2}(s_j^{l_2})}}{\overline{\partial s_m^{l_1} \partial s_j^{l_2}}} \right) \\ &= \frac{\overline{\partial G^{l_2}(s_j^{l_2})}}{\overline{\partial s_j^{l_2}}} \sum_r b_{rm}^{l_2+1, l_1} \overline{w_{rj}^{l_2+1}} + \frac{\overline{\partial^2 G^{l_2}(s_j^{l_2})}}{\overline{\partial s_m^{l_1} \partial s_j^{l_2}}} \sum_r \delta_r^{l_2+1} \overline{w_{rj}^{l_2+1}} \\ &\quad + \frac{\overline{\partial G^{l_2}(s_j^{l_2})}}{\overline{\partial s_j^{l_2}}} \sum_r a_{rm}^{l_2+1, l_1} \overline{w_{rj}^{l_2+1}} + \frac{\overline{\partial^2 G^{l_2}(s_j^{l_2})}}{\overline{\partial s_m^{l_1} \partial s_j^{l_2}}} \sum_r \overline{\delta_r^{l_2+1}} \overline{w_{rj}^{l_2+1}}, \end{aligned}$$

where we have denoted $a_{jm}^{l_2, l_1} := \frac{\overline{\partial \delta_j^{l_2}}}{\overline{\partial s_m^{l_1}}}$, the sum goes over all neurons r in layer l_2+1

to which neuron j in layer l_2 sends connections, and $\frac{\overline{\partial w_{rj}^{l_2+1}}}{\overline{\partial s_m^{l_1}}} = \frac{\overline{\partial w_{rj}^{l_2+1}}}{\overline{\partial s_m^{l_1}}} = 0$. This means

that we have to find a formula for calculating $a_{jm}^{l_2, l_1}$, also. Like in the case of $b_{jm}^{l_2, l_1}$, we can write that

$$\begin{aligned}
\frac{\overline{\partial \delta_j^{l_2}}}{\overline{\partial s_m^{l_1}}} &= \sum_r \left(\frac{\overline{\partial \delta_r^{l_2+1}}}{\overline{\partial s_m^{l_1}}} w_{rj}^{l_2+1} \frac{\partial G^{l_2}(s_j^{l_2})}{\partial s_j^{l_2}} + \frac{\overline{\delta_r^{l_2+1}}}{\overline{\partial s_m^{l_1}}} \frac{\partial w_{rj}^{l_2+1}}{\partial s_m^{l_1}} \frac{\partial G^{l_2}(s_j^{l_2})}{\partial s_j^{l_2}} \right. \\
&\quad + \frac{\overline{\delta_r^{l_2+1}}}{\overline{\partial s_m^{l_1}}} w_{rj}^{l_2+1} \frac{\partial^2 G^{l_2}(s_j^{l_2})}{\overline{\partial s_m^{l_1} \partial s_j^{l_2}}} + \frac{\partial \delta_r^{l_2+1}}{\partial s_m^{l_1}} \frac{\overline{\partial G^{l_2}(s_j^{l_2})}}{w_{rj}^{l_2+1} \overline{\partial s_j^{l_2}}} \\
&\quad \left. + \delta_r^{l_2+1} \frac{\overline{\partial w_{rj}^{l_2+1}}}{\overline{\partial s_m^{l_1}}} \frac{\partial G^{l_2}(s_j^{l_2})}{\partial s_j^{l_2}} + \delta_r^{l_2+1} \frac{\overline{\partial^2 G^{l_2}(s_j^{l_2})}}{\overline{\partial s_m^{l_1} \partial s_j^{l_2}}} \right) \quad (9) \\
&= \frac{\partial G^{l_2}(s_j^{l_2})}{\partial s_j^{l_2}} \sum_r a_{rm}^{l_2+1, l_1} w_{rj}^{l_2+1} + \frac{\partial^2 G^{l_2}(s_j^{l_2})}{\overline{\partial s_m^{l_1} \partial s_j^{l_2}}} \sum_r \overline{\delta_r^{l_2+1}} w_{rj}^{l_2+1} \\
&\quad + \frac{\overline{\partial G^{l_2}(s_j^{l_2})}}{\partial s_j^{l_2}} \sum_r b_{rm}^{l_2+1, l_1} w_{rj}^{l_2+1} + \frac{\partial^2 \overline{G^{l_2}(s_j^{l_2})}}{\overline{\partial s_m^{l_1} \partial s_j^{l_2}}} \sum_r \delta_r^{l_2+1} \overline{w_{rj}^{l_2+1}}.
\end{aligned}$$

The expressions for the second-order \mathbb{R} - and $\overline{\mathbb{R}}$ -partial derivatives of the activation functions follow easily by applying the chain rule:

$$\begin{aligned}
\frac{\partial^2 G^{l_2}(s_j^{l_2})}{\overline{\partial s_m^{l_1} \partial s_j^{l_2}}} &= \frac{\partial^2 G^{l_2}(s_j^{l_2})}{\partial s_j^{l_2} \partial s_j^{l_2}} \frac{\partial s_j^{l_2}}{\overline{\partial s_m^{l_1}}} + \frac{\partial^2 G^{l_2}(s_j^{l_2})}{\partial s_j^{l_2} \partial s_j^{l_2}} \frac{\overline{\partial s_j^{l_2}}}{\overline{\partial s_m^{l_1}}} \\
&= \frac{\partial^2 G^{l_2}(s_j^{l_2})}{\partial s_j^{l_2} \partial s_j^{l_2}} h_{jm}^{l_2, l_1} + \frac{\partial^2 G^{l_2}(s_j^{l_2})}{\partial s_j^{l_2} \partial s_j^{l_2}} g_{jm}^{l_2, l_1},
\end{aligned}$$

$$\begin{aligned}
\frac{\partial^2 G^{l_2}(s_j^{l_2})}{\partial s_m^{l_1} \partial s_j^{l_2}} &= \frac{\partial^2 G^{l_2}(s_j^{l_2})}{\partial s_j^{l_2} \partial s_j^{l_2}} \frac{\partial s_j^{l_2}}{\partial s_m^{l_1}} + \frac{\partial^2 G^{l_2}(s_j^{l_2})}{\partial s_j^{l_2} \partial s_j^{l_2}} \frac{\overline{\partial s_j^{l_2}}}{\partial s_m^{l_1}} \\
&= \frac{\partial^2 G^{l_2}(s_j^{l_2})}{\partial s_j^{l_2} \partial s_j^{l_2}} h_{jm}^{l_2, l_1} + \frac{\partial^2 G^{l_2}(s_j^{l_2})}{\partial s_j^{l_2} \partial s_j^{l_2}} g_{jm}^{l_2, l_1},
\end{aligned}$$

and the analogous ones for $\frac{\overline{\partial^2 G^{l_2}(s_j^{l_2})}}{\overline{\partial s_m^{l_1} \partial s_j^{l_2}}}$ and $\frac{\partial^2 \overline{G^{l_2}(s_j^{l_2})}}{\overline{\partial s_m^{l_1} \partial s_j^{l_2}}}$.

Next, we have to deal with the case in which $l_2 = L$. Then, from expression (5), it follows that

$$\begin{aligned}
\frac{\partial \overline{\delta_j^{l_2}}}{\partial \overline{s_m^{l_1}}} &= \frac{1}{2} \frac{\partial (y_j^{l_2} - t_j)}{\partial \overline{s_m^{l_1}}} \frac{\partial \overline{G^{l_2}(s_j^{l_2})}}{\partial \overline{s_j^{l_2}}} + \frac{1}{2} (y_j^{l_2} - t_j) \frac{\partial^2 \overline{G^{l_2}(s_j^{l_2})}}{\partial \overline{s_m^{l_1}} \partial \overline{s_j^{l_2}}} \\
&\quad + \frac{1}{2} \frac{\partial (y_j^{l_2} - t_j)}{\partial \overline{s_m^{l_1}}} \frac{\partial \overline{G^{l_2}(s_j^{l_2})}}{\partial \overline{s_j^{l_2}}} + \frac{1}{2} (y_j^{l_2} - t_j) \frac{\partial^2 \overline{G^{l_2}(s_j^{l_2})}}{\partial \overline{s_m^{l_1}} \partial \overline{s_j^{l_2}}} \\
&= \frac{1}{2} \frac{\partial \overline{G^{l_2}(s_j^{l_2})}}{\partial \overline{s_m^{l_1}}} \frac{\partial \overline{G^{l_2}(s_j^{l_2})}}{\partial \overline{s_j^{l_2}}} + \frac{1}{2} (y_j^{l_2} - t_j) \frac{\partial^2 \overline{G^{l_2}(s_j^{l_2})}}{\partial \overline{s_m^{l_1}} \partial \overline{s_j^{l_2}}} \\
&\quad + \frac{1}{2} \frac{\partial \overline{G^{l_2}(s_j^{l_2})}}{\partial \overline{s_m^{l_1}}} \frac{\partial \overline{G^{l_2}(s_j^{l_2})}}{\partial \overline{s_j^{l_2}}} + \frac{1}{2} (y_j^{l_2} - t_j) \frac{\partial^2 \overline{G^{l_2}(s_j^{l_2})}}{\partial \overline{s_m^{l_1}} \partial \overline{s_j^{l_2}}},
\end{aligned} \tag{10}$$

and

$$\begin{aligned}
\frac{\partial \overline{\delta_j^{l_2}}}{\partial \overline{s_m^{l_1}}} &= \frac{1}{2} \frac{\partial (y_j^{l_2} - t_j)}{\partial \overline{s_m^{l_1}}} \frac{\partial \overline{G^{l_2}(s_j^{l_2})}}{\partial \overline{s_j^{l_2}}} + \frac{1}{2} (y_j^{l_2} - t_j) \frac{\partial^2 \overline{G^{l_2}(s_j^{l_2})}}{\partial \overline{s_m^{l_1}} \partial \overline{s_j^{l_2}}} \\
&\quad + \frac{1}{2} \frac{\partial (y_j^{l_2} - t_j)}{\partial \overline{s_m^{l_1}}} \frac{\partial \overline{G^{l_2}(s_j^{l_2})}}{\partial \overline{s_j^{l_2}}} + \frac{1}{2} (y_j^{l_2} - t_j) \frac{\partial^2 \overline{G^{l_2}(s_j^{l_2})}}{\partial \overline{s_m^{l_1}} \partial \overline{s_j^{l_2}}} \\
&= \frac{1}{2} \frac{\partial \overline{G^{l_2}(s_j^{l_2})}}{\partial \overline{s_m^{l_1}}} \frac{\partial \overline{G^{l_2}(s_j^{l_2})}}{\partial \overline{s_j^{l_2}}} + \frac{1}{2} (y_j^{l_2} - t_j) \frac{\partial^2 \overline{G^{l_2}(s_j^{l_2})}}{\partial \overline{s_m^{l_1}} \partial \overline{s_j^{l_2}}} \\
&\quad + \frac{1}{2} \frac{\partial \overline{G^{l_2}(s_j^{l_2})}}{\partial \overline{s_m^{l_1}}} \frac{\partial \overline{G^{l_2}(s_j^{l_2})}}{\partial \overline{s_j^{l_2}}} + \frac{1}{2} (y_j^{l_2} - t_j) \frac{\partial^2 \overline{G^{l_2}(s_j^{l_2})}}{\partial \overline{s_m^{l_1}} \partial \overline{s_j^{l_2}}}.
\end{aligned}$$

The expressions for calculating the second-order \mathbb{R} - and $\overline{\mathbb{R}}$ -partial derivatives of the activation functions are the same as above. Thus we only have to give the expressions for calculating the $\overline{\mathbb{R}}$ -partial derivatives of the activation functions used in the above expressions. They are also deduced by applying the chain rule:

$$\begin{aligned}
\frac{\partial \overline{G^{l_2}(s_j^{l_2})}}{\partial \overline{s_m^{l_1}}} &= \frac{\partial \overline{G^{l_2}(s_j^{l_2})}}{\partial \overline{s_j^{l_2}}} \frac{\partial \overline{s_j^{l_2}}}{\partial \overline{s_m^{l_1}}} + \frac{\partial \overline{G^{l_2}(s_j^{l_2})}}{\partial \overline{s_j^{l_2}}} \frac{\partial \overline{s_j^{l_2}}}{\partial \overline{s_m^{l_1}}} \\
&= \frac{\partial \overline{G^{l_2}(s_j^{l_2})}}{\partial \overline{s_j^{l_2}}} h_{jm}^{l_2, l_1} + \frac{\partial \overline{G^{l_2}(s_j^{l_2})}}{\partial \overline{s_j^{l_2}}} g_{jm}^{l_2, l_1},
\end{aligned}$$

and analogously for $\frac{\partial \overline{G^{l_2}(s_j^{l_2})}}{\partial \overline{s_m^{l_1}}}$.

It can be observed that the expressions for $h_{km}^{l_2-1,l_1}$ and $g_{km}^{l_2-1,l_1}$ are calculated by forward propagation, and the expressions for $b_{jm}^{l_2,l_1}$ and $a_{jm}^{l_2,l_1}$ are calculated by backward propagation. Finally, putting it all together, we obtain the following formula for a component of the Hessian matrix of the error function E :

$$\begin{aligned} \frac{\partial^2 E}{\partial w_{mn}^{l_1} \partial w_{jk}^{l_2}} &= \overline{x_n^{l_1-1}} b_{jm}^{l_2,l_1} \overline{x_k^{l_2-1}} + \overline{x_n^{l_1-1}} h_{km}^{l_2-1,l_1} \frac{\partial \overline{G^{l_2-1}(s_k^{l_2-1})}}{\partial s_k^{l_2-1}} \delta_j^{l_2} \\ &+ \overline{x_n^{l_1-1}} g_{km}^{l_2-1,l_1} \frac{\partial \overline{G^{l_2-1}(s_k^{l_2-1})}}{\partial s_k^{l_2-1}} \delta_j^{l_2}. \end{aligned} \quad (11)$$

3 Three-Layered Complex-Valued Feedforward Neural Network

In this section, we will consider the special case of a network with only one hidden layer, in which case $L = 3$. We will denote by i, i' neurons from the input layer, by j, j' neurons from the hidden layer, and by k, k' neurons from the output layer. With these conventions, Eqs. (1) and (2) become

$$s_j^2 := \sum_i w_{ji}^2 x_i^1,$$

$$x_j^2 := G^2(s_j^2),$$

$$s_k^3 := \sum_j w_{kj}^3 x_j^2,$$

$$x_k^3 := G^3(s_k^3).$$

The expression (11) for the second-order $\overline{\mathbb{R}}$ -partial derivative of the error function E , in the case $l_1 = l_2 = 3$, is

$$\frac{\partial^2 E}{\partial w_{k'j'}^3 \partial w_{kj}^3} = x_j^2 \frac{\partial \delta_k^3}{\partial s_{k'}^3} x_j^2,$$

because $h_{jk'}^{2,3} = g_{jk'}^{2,3} = 0$. Now, we only need to compute $\frac{\partial \delta_k^3}{\partial s_{k'}^3}$ using Eq. (10):

$$\begin{aligned} \frac{\partial \delta_k^3}{\partial s_{k'}^3} &= \frac{1}{2} \frac{\partial G^3(s_k^3)}{\partial s_{k'}^3} \frac{\overline{\partial G^3(s_k^3)}}{\partial s_k^3} + \frac{1}{2} (y_k^3 - t_k) \frac{\overline{\partial^2 G^3(s_k^3)}}{\partial s_{k'}^3 \partial s_k^3} \\ &\quad + \frac{1}{2} \frac{\overline{\partial G^3(s_k^3)}}{\partial s_{k'}^3} \frac{\partial G^3(s_k^3)}{\partial s_k^3} + \frac{1}{2} \overline{(y_k^3 - t_k)} \frac{\partial^2 G^3(s_k^3)}{\partial s_{k'}^3 \partial s_k^3} \\ &= \delta_{k'k} \left[\frac{\partial G^3(s_k^3)}{\partial s_k^3} \frac{\overline{\partial G^3(s_k^3)}}{\partial s_k^3} + \frac{1}{2} (y_k^3 - t_k) \frac{\overline{\partial^2 G^3(s_k^3)}}{\partial s_k^3} + \frac{1}{2} \overline{(y_k^3 - t_k)} \frac{\partial^2 G^3(s_k^3)}{\partial s_k^3} \right], \end{aligned}$$

where we used expression (5) for δ_k^3 , and $\delta_{k'k}$ is the Kronecker delta symbol defined above. The final expression for the second-order $\overline{\mathbb{R}}$ -partial derivative is

$$\begin{aligned} \frac{\partial^2 E}{\partial w_{k'j}^3 \partial w_{kj}^3} &= \overline{x_j^2 x_j^2} \delta_{k'k} \left[\frac{\partial G^3(s_k^3)}{\partial s_k^3} \frac{\overline{\partial G^3(s_k^3)}}{\partial s_k^3} \right. \\ &\quad \left. + \frac{1}{2} (y_k^3 - t_k) \frac{\overline{\partial^2 G^3(s_k^3)}}{\partial s_k^3} + \frac{1}{2} \overline{(y_k^3 - t_k)} \frac{\partial^2 G^3(s_k^3)}{\partial s_k^3} \right]. \end{aligned}$$

Now, we consider the case in which $l_1 = l_2 = 2$. We also have $h_{ij}^{1,2} = g_{ij}^{1,2} = 0$, so expression (11) becomes

$$\frac{\partial^2 E}{\partial w_{j'j}^2 \partial w_{ji}^2} = \overline{x_j^1} \frac{\partial \delta_j^2}{\partial s_j^2} \overline{x_j^1}.$$

We have to compute $\frac{\partial \delta_j^2}{\partial s_j^2}$, for which we use formula (9):

$$\begin{aligned} \frac{\partial \delta_j^2}{\partial s_j^2} &= \frac{\overline{\partial G^2(s_j^2)}}{\partial s_j^2} \sum_r b_{rj'}^{3,2} \overline{w_{rj}^3} + \frac{\partial^2 \overline{G^2(s_j^2)}}{\partial s_j^2 \partial s_j^2} \sum_r \delta_r^3 \overline{w_{rj}^3} \\ &\quad + \frac{\partial G^2(s_j^2)}{\partial s_j^2} \sum_r a_{rj'}^{3,2} w_{rj}^3 + \frac{\partial^2 G^2(s_j^2)}{\partial s_j^2 \partial s_j^2} \sum_r \overline{\delta_r^3} w_{rj}^3. \end{aligned}$$

The above relation shows that we also need expressions for $a_{rj'}^{3,2}$ and $b_{rj'}^{3,2}$. Using again Eq. (10), we have that

$$\begin{aligned} \frac{\partial \delta_r^3}{\partial s_j^2} &= \frac{1}{2} \frac{\partial G^3(s_r^3)}{\partial s_j^2} \frac{\overline{\partial G^3(s_r^3)}}{\partial s_r^3} + \frac{1}{2} (y_r^3 - t_r) \frac{\overline{\partial^2 G^3(s_r^3)}}{\partial s_j^2 \partial s_r^3} \\ &\quad + \frac{1}{2} \frac{\overline{\partial G^3(s_r^3)}}{\partial s_j^2} \frac{\partial G^3(s_r^3)}{\partial s_r^3} + \frac{1}{2} \overline{(y_r^3 - t_r)} \frac{\partial^2 G^3(s_r^3)}{\partial s_j^2 \partial s_r^3}, \end{aligned}$$

and

$$\begin{aligned} \frac{\overline{\partial \delta_r^3}}{\partial s_j^2} &= \frac{1}{2} \frac{\overline{\partial G^3(s_r^3)}}{\partial s_j^2} \frac{\partial G^3(s_r^3)}{\partial s_r^3} + \frac{1}{2} \overline{(y_r^3 - t_r)} \frac{\partial^2 G^3(s_r^3)}{\partial s_j^2 \partial s_r^3} \\ &+ \frac{1}{2} \frac{\partial G^3(s_r^3)}{\partial s_j^2} \frac{\overline{\partial G^3(s_r^3)}}{\partial s_r^3} + \frac{1}{2} (y_r^3 - t_r) \frac{\overline{\partial^2 G^3(s_r^3)}}{\partial s_j^2 \partial s_r^3}, \end{aligned}$$

where the first- and second-order \mathbb{R} - and $\overline{\mathbb{R}}$ -partial derivatives have the following expressions:

$$\frac{\partial G^3(s_r^3)}{\partial s_j^2} = \frac{\partial G^3(s_r^3)}{\partial s_r^3} h_{rj'}^{3,2} + \frac{\partial G^3(s_r^3)}{\partial s_r^3} g_{rj'}^{3,2},$$

and analogously for $\frac{\partial \overline{G^3(s_r^3)}}{\partial s_j^2}$, and

$$\begin{aligned} \frac{\partial^2 G^3(s_r^3)}{\partial s_r^3 \partial s_j^2} &= \frac{\partial^2 G^3(s_r^3)}{\partial s_r^3 \partial s_r^3} h_{rj'}^{3,2} + \frac{\partial^2 G^3(s_r^3)}{\partial s_r^3 \partial s_r^3} g_{rj'}^{3,2}, \\ \frac{\partial^2 \overline{G^3(s_r^3)}}{\partial s_r^3 \partial s_j^2} &= \frac{\partial^2 \overline{G^3(s_r^3)}}{\partial s_r^3 \partial s_r^3} h_{rj'}^{3,2} + \frac{\partial^2 \overline{G^3(s_r^3)}}{\partial s_r^3 \partial s_r^3} g_{rj'}^{3,2}, \end{aligned}$$

and the analogous ones for $\frac{\partial^2 G^3(s_j^2)}{\partial s_r^2 \partial s_j^2}$ and $\frac{\partial^2 \overline{G^3(s_j^2)}}{\partial s_r^2 \partial s_j^2}$.

Finally, the expressions for $h_{rj'}^{3,2}$ and $g_{rj'}^{3,2}$ can be deduced using Eqs. (7) and (8):

$$\begin{aligned} h_{rj'}^{3,2} &= \sum_j \left(h_{jj'}^{2,2} w_{rj}^2 \frac{\partial G^2(s_j^2)}{\partial s_j^2} + g_{jj'}^{2,2} w_{rj}^2 \frac{\partial G^2(s_j^2)}{\partial s_j^2} \right) \\ &= w_{rj'}^2 \frac{\partial G^2(s_j^2)}{\partial s_j^2}, \\ g_{rj'}^{3,2} &= \sum_j \left(h_{jj'}^{2,2} \overline{w_{rj}^2} \frac{\partial \overline{G^2(s_j^2)}}{\partial s_j^2} + g_{jj'}^{2,2} \overline{w_{rj}^2} \frac{\partial \overline{G^2(s_j^2)}}{\partial s_j^2} \right) \\ &= \overline{w_{rj'}^2} \frac{\partial \overline{G^2(s_j^2)}}{\partial s_j^2}, \end{aligned}$$

where we used the fact that $h_{jj'}^{2,2} = 0$, $g_{jj'}^{2,2} = \delta_{jj'}$.

The last case is the one in which $l_1 = 2, l_2 = 3$. In this case, we have $h_{ij}^{2,2} = 0$, $g_{ij}^{2,2} = \delta_{ij}$, so expression (11) becomes

$$\frac{\partial^2 E}{\partial w_{j'i'}^2 \partial w_{kj}^3} = \overline{x_i^1} b_{kj}^{3,2} \overline{x_j^1} + \overline{x_i^1} \delta_{ij'} \frac{\partial \overline{G^2(s_j^2)}}{\partial s_j^2} \delta_k^3,$$

in which the expression for $b_{kj}^{3,2}$ was deduced above.

4 Conclusions

The detailed deduction of the algorithm to calculate the Hessian matrix for feed-forward complex-valued neural networks using $\mathbb{C}\mathbb{R}$ -calculus was presented. First, we made a short introduction in the domain of the $\mathbb{C}\mathbb{R}$ -calculus or Wirtinger calculus, emphasizing what is needed for the calculation of the elements of the Hessian. Then, we started with the deduction of the classical backpropagation algorithm for complex-valued neural networks, which provided the components of the gradient vector of the error function necessary for the calculation of the elements of the Hessian matrix. Afterward, the method for calculating these elements was shown step by step, emphasizing that it has both forward and backward propagation stages, much like the classical backpropagation algorithm used for gradient descent training.

An example showing the detailed steps for a simple three-layered feedforward complex-valued neural network was given, in which we could observe that many steps of the general algorithm were not necessary, thus greatly simplifying the general algorithm in this case. It can be easily seen from this simple example that the algorithm resembles the gradient descent algorithm, making its software implementation a straightforward adaptation of the implementation of the backpropagation algorithm.

References

1. Becker S, LeCun Y (1989) Improving the convergence of back-propagation learning with second-order methods. In: Touretzky D, Hinton G, Sejnowski T (eds) Proceedings of the 1988 connectionist models summer school. Morgan Kaufman, San Mateo, pp 29–37
2. Bishop CM (1991) A fast procedure for retraining the multilayer perceptron. *Int J Neural Syst* 2 (3):229–236
3. Bishop CM (1992) Exact calculation of the hessian matrix for the multi-layer perceptron. *Neural Comput* 4(4):494–501
4. Bishop CM (1995) *Neural networks for pattern recognition*. Oxford University Press, Inc., New York

5. Hirose A (2013) Application fields and fundamental merits of complex-valued neural networks. In: Hirose A (ed) Complex-valued neural networks, Wiley, Hoboken, pp 1–31
6. Kreutz-Delgado K (2009) The complex gradient operator and the CR-calculus. arXiv preprint arXiv:0906.4835
7. LeCun Y, Denker JS, Solla S, Howard RE, Jackel LD (1990) Optimal brain damage. In: Touretzky D (ed) Advances in neural information processing systems (NIPS 1989), vol 2. Morgan Kaufman, Denver
8. Mackay DJC (1992) A practical Bayesian framework for backpropagation networks. Neural Comput 4(3):448–472

Functioning State Estimator of Pump-Motor Group of MOP-Type Drive Mechanisms Using Neural Networks

V. Nicolau and M. Andrei

Abstract The oleo-pneumatic mechanism (MOP) presents the highest fault rate of all the components of IO-type high-voltage circuit breaker. Hence, estimating the functioning states of MOP-type mechanism is important to maintain full switching capabilities of circuit breaker. In this paper, aspects of functioning state estimation using neural networks are discussed. Several neural network architectures are studied. Neural estimator makes good state estimations, and it can deal with false malfunctions. Also, simulation results are presented.

Keywords Neural networks · Estimation · MOP mechanism · Circuit breaker

1 Introduction

In power networks, circuit breakers (CB) are very important for network stability and security. The functioning states of circuit breakers, which characterize their switching capabilities, are critical elements for optimal planning and operations of large-scale power grids. Due to their importance, the circuit breakers must be checked periodically to ensure that they have full switching capabilities. Maintenance practices, replacement, and utilization of circuit breakers can be optimized using diagnostic and monitoring techniques, which must be selected with realistic expectations [1]. Estimation of CB functioning state can improve the control law and overall performance, like reliability and availability of the power network. Hence, an intelligent diagnostic system should include techniques for prediction of CB life expectancy and detection of their potential failures [2].

V. Nicolau (✉) · M. Andrei
Department of Electronics and Telecommunications “Dunarea de Jos”,
University of Galati, 47 Domneasca St., Galati 800008, Romania
e-mail: viorel.nicolau@ugal.ro

M. Andrei
e-mail: mihaela.andrei@ugal.ro

In national power network, changing the old circuit breakers with new ones is not an easy task, due to the cost of the breaker and station equipment, which becomes prohibitive at high voltages [3]. There are still many IO-type oil-based high-voltage circuit breakers in use, which are operated by oleo-pneumatic mechanisms (MOP). Their behavior analysis pointed out that the MOP-type drive mechanism presents the highest fault rate [4].

In the MOP-type drive mechanism, the acting energy needed for switching the mobile contacts of IO-type oil-based high-voltage CB is stored into an accumulator with nitrogen under pressure. From there, the energy can be transmitted through a hydraulic system. The main drawback of this acting mechanism is the accumulator, which loses in time the internal pressure, meaning that it loses the stored energy. Pressure loss is a natural process and it cannot be avoided. When this is detected, a pump actuated by a motor restores the pressure. The good functioning state of pump-motor group is very important, because its failure goes to the impossibility of switching the circuit breaker.

In general, the artificial intelligence methods are used intensively to improve the overall performances of high-voltage circuit breakers from power networks. Neural networks (NN) are widely applied for classification and prediction problems, due to their universal approximation and generalization capabilities. Mechanical condition recognition of vacuum CB was studied using feedforward neural networks (FFNN) in [5] and RBF neural networks in [6]. Artificial neural networks were used in [7] for characteristic analysis of the circuit breaker kinematics, in order to diagnose their technical state. Also, a monitoring system of circuit breakers based on NN is presented in [8]. Other NN approaches were studied for the intelligent control of circuit breaker operation in [9], and to identify multiple failures of protection relays and circuit breakers in [10]. In addition, multiple artificial intelligence methods can be used simultaneously. In [11], an intelligent fault diagnosis system for high-voltage circuit breakers is studied, based on neural network and expert system integration. Nozzle optimization of SF6 circuit breaker based on artificial neural network and genetic algorithm is studied in [12].

In this paper, aspects of functioning state estimation using neural networks are discussed. The goal is to find a FFNN model to estimate the degree of functioning state of MOP-type drive mechanism of IO high-voltage circuit breakers. Several neural network architectures are studied. Neural estimator gives good results. It can deal with false malfunctions, and it can be used for early detection of the fault tendencies of MOP mechanisms.

The paper is organized as follows. Mathematical models are presented in Sect. 2. In Sect. 3, aspects of neural estimation are studied. Neural networks are proposed as state estimator and simulation results are presented in Sect. 4. Conclusions are pointed out in Sect. 5.

2 Mathematical Models

The pump-motor group of the MOP-type drive mechanism restores the nitrogen pressure into the accumulator, every time significant pressure loss is detected. In normal operation, the pump-motor group starts several times every hour, functioning few seconds for every start.

The pressure recovery circuit has two parameters as malfunction indicators: the number of starts per hour (N_S) and the total functioning time per hour (T_F). If the number of starts is too big, this means that the accumulator loses the internal pressure too quickly and the recovery circuit is working too often. By contrary, if the motor does not start during 1 h, this can indicate a malfunction of pressure variation sensing. In addition, if the motor is functioning for long time periods every hour, this means that the pressure is restored too slowly due to a failure in the pump-motor circuit.

The two parameters are affected by internal disturbances w_i (e.g., wear and tear of various components, such as valves and electro-valves), and external disturbances w_e (e.g., weather conditions, especially temperature which affects the high pressure oil circuits). Regarding the normal operation in time in the presence of internal and external disturbances, the pump-motor group of every MOP mechanism should fulfill two performance conditions:

$$N_S(t, w_i, w_e) \in [N_{Smin}, N_{Smax}] \quad (1)$$

$$T_F(t, w_i, w_e) \in [T_{Fmin}, T_{Fmax}] \quad (2)$$

The performance conditions are indicated in the technical specifications, and they are defined as boundary ranges of the two parameters. From Eq. (1), it results that the motor must start at least N_{Smin} times in an hour, but not too often, no more than N_{Smax} . Similar results are obtained from Eq. (2). The minimum value, T_{Fmin} , is not specified, but it must be nonzero value, being correlated with N_{Smin} .

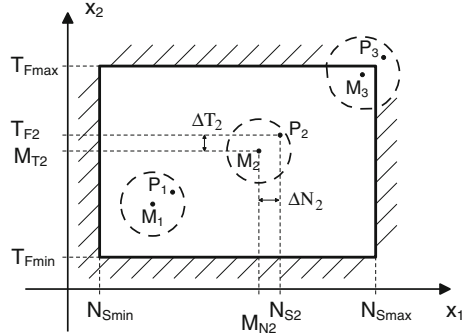
The normal operation point of MOP-type drive mechanism, denoted P , can be characterized in \mathfrak{R}^2 by a pair of coordinates changing in time, $(x_1(t), x_2(t)) \in \mathfrak{R}^2$:

$$x_1(t) = N_S(t, w_i, w_e), x_2(t) = T_F(t, w_i, w_e) \quad (3)$$

For the model of MOP-type mechanism, perturbations can be considered as additive. Depending on the time horizon, perturbations have three different influences on the MOP operating point: short-term, which refers to days and weeks, medium-term, which extends from months to 1 year, and long-term time period, referring from several years to life cycle.

In the presence of internal and external disturbances, the point P is shifting in \mathfrak{R}^2 within the permitted area, as shown in Fig. 1. Short-term perturbations are of random nature and produce variations of P point around the mean value M , computed over a predefined time horizon. The mean value includes medium- and long-term components, and it is also varying in time. In Fig. 1, the restriction

Fig. 1 Shifting operating point in \mathfrak{R}^2 within the permitted area



boundaries are illustrated with shaded areas, and the boundaries of short-term random variations are represented as circles with dashed lines around mean values.

For every operating point P_i around the mean value M_i , the point coordinates can be written as follows:

$$\begin{cases} x_1(t) = M_N(t) + \Delta N(t) \\ x_2(t) = M_T(t) + \Delta T(t) \end{cases} \quad (4)$$

where $\Delta N(t)$ and $\Delta T(t)$ are the short-term components, considered as random variables with normal distribution and zero mean. The mean values, $M_N(t)$ and $M_T(t)$, are functions of time t , including medium- and long-term components.

The MOP behavior analysis is based on variations in time of medium- and long-term components of mean values from Eq. (4). On medium-term components, during 1-year period, the mean value of normal operating point has a cyclic movement, as the temperature is changing from one season to another. During life cycle, the aging process of circuit breakers leads to worsening performance. As a result, both parameters, number of starts and functioning time, increase. The mean value of operating point is slowly changing from lower-left to upper-right corner, as illustrated in Fig. 1 for three different situations. In addition, the variations of P point on short- and medium-term can increase.

3 Aspects of Neural Estimation

Many applications with neural networks, including estimation problems, reduce the problem of approximating unknown functions of one or more variables from discrete noisy measurements. In addition to the conventional notion of approximation, neural networks are valued especially for their ability to generalize. But an accurate approximation of a function can lead to poor generalization capability of the network. Therefore, both approximation and generalization are desired properties under different circumstances, being taken into account when a neural network is designed and trained.

There are many aspects which must be solved when using neural networks, regarding the optimal network topology, learning algorithms to deal with local minima, the conditions to achieve good generalization, and efficacy in scaling to larger problems [13]. The most practical concerns are the network size, time complexity of learning, and network ability to generalize.

Neural estimation of functioning state of MOP drive mechanism is a case of approximation problem, with big dimension of the input space, as illustrated in Fig. 2. Considering the approximation with NN, the main design objective is to find a neural network which can make good approximation of an unknown function f , which represents some desired input–output mapping.

At every k moment of time, the network inputs are N consecutive samples of input dataset, denoted by $x(k), \dots, x(k - N + 1)$, and the output represents the desired estimated value:

$$\hat{y}(k) = f(x(k), x(k - 1), \dots, x(k - N + 1)) \tag{5}$$

The time series prediction is a special case of approximation problem, where the inputs and the output are samples of the same observed dataset. In this case, the output represents the predicted value for m time steps ahead:

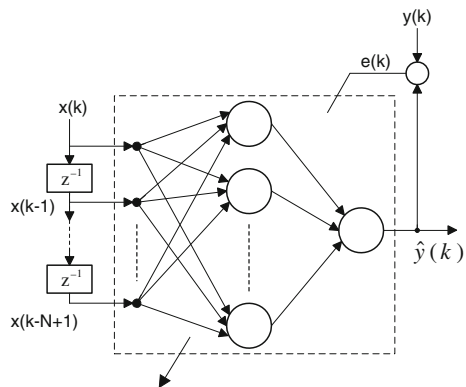
$$\hat{x}(k + m) = f(x(k), x(k - 1), \dots, x(k - N + 1)) \tag{6}$$

For every step k , the estimation error $e(k)$ is computed based on the desired and estimated values of MOP functioning state. The performance goal has to be small enough to assure good estimation performance, but not too small to avoid loss of generalization. The mean squared error (mse) was chosen as performance function:

$$\text{mse} = E[e^2(k)] = \frac{\sum_{i=1}^M e^2(k)}{M} \tag{7}$$

where M is the number of vectors in datasets.

Fig. 2 General estimation problem using neural networks



The more complex the estimation problem is, the more information about the past is needed, and the size of the input layer and the corresponding number of weights are increased. The more the hidden nodes are used, the more accurate the approximation is. However, when the datasets are affected by noise, determination of the number of hidden units becomes more complicated [14]. To build an efficient neural estimator, an optimum number of hidden units must be determined by testing several neural architectures.

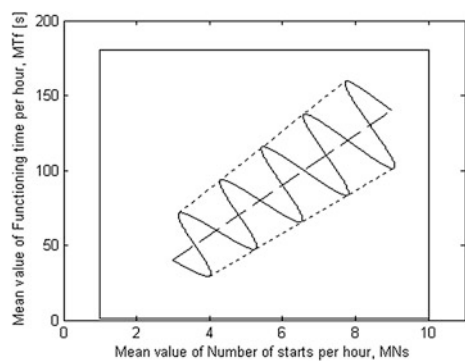
It can generally be assumed that any real data will have some degree of uncertainty, generated by systematic or random errors. The estimates take into account the uncertainty in the target data or the uncertainty in the input data. Therefore, it is necessary for any learning system to be able to cope with such uncertainty, producing valid estimates based on real datasets [15]. In this paper, it is assumed that there is noise on the input datasets, generated by measurement system.

4 Simulation Results

For simulations, a large input dataset is generated using the pump-motor model from Eq. (4). It contains hourly records of operating points, $(x_1 = N_S, x_2 = T_F) \in \mathfrak{R}^2$, for a time horizon of five years. Both coordinates are positive integers, with first coordinate containing only few discrete values. The mean values from Eq. (4), $M_N(t)$ and $M_T(t)$, are functions of time t and include medium- and long-term components. Their time variations are shown in Fig. 3. Medium-term component has a cyclic movement, depending on temperature variations during 1-year period, and the long-term is slowly changing in time to bigger values of both coordinates. The short-term components are considered as random variables with normal distribution and zero mean.

The resulting dataset contains 43,800 points. The coordinates of operating points, $x_1 = N_S$ and $x_2 = T_F$, are represented as functions of time in Fig. 4, with different gray colors for every year in the time horizon. Two points are placed intentionally outside the permitted area, being represented with 'o' mark.

Fig. 3 Variations of mean values $M_N(t)$ and $M_T(t)$



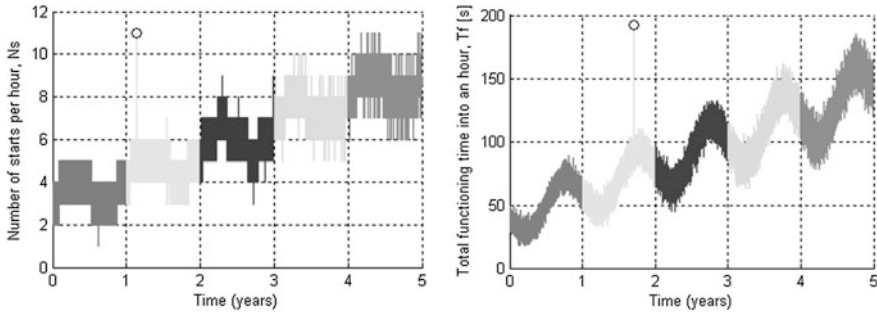


Fig. 4 Variations in time of coordinates N_S and T_F

They represent short abnormal functioning states, without meaning a malfunction of the pump-motor group. A classical monitoring system would classify them as malfunction points.

The operating points of dataset are illustrated in Fig. 5, with different gray colors for every year. In the left figure, the operating points are represented separated as single dot. Because the variable N_S has few discrete values, it is difficult to observe the point shifting during every year. Therefore, in the right figure, there are drawn the surfaces generated by variations of operating points each year. It can be observed that the operating points shift slowly toward higher values, moving to upper-right corner of the permitted area.

For state estimation, several architectures of feedforward neural networks are studied. The FFNN estimator receives N time-delayed samples of input dataset, denoted by $x(k), \dots, x(k - N + 1)$, as shown in Fig. 2. Each sample x characterizes the operating point, $(x_1 = N_S, x_2 = T_F) \in \mathfrak{R}^2$. The FFNN output represents the estimation of degree of functioning state on a scale from 0 to 10. The output decreases to 0 when the operating point shifts from good functioning state to malfunction.

The FFNN has one hidden layer with N_{hn} neurons, being trained using Levenberg–Marquardt back-propagation algorithm. The output layer has one linear

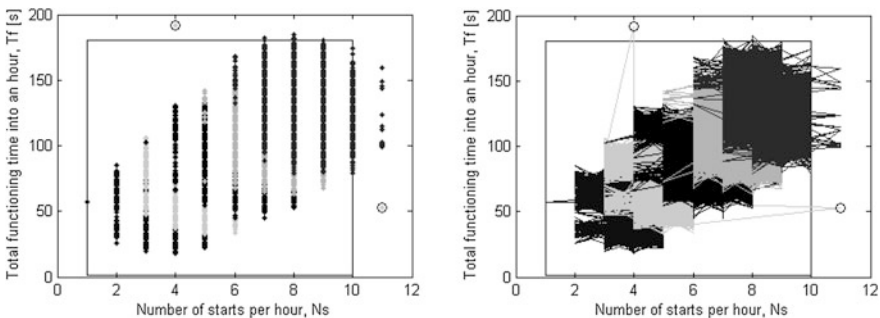


Fig. 5 Variations of operating points

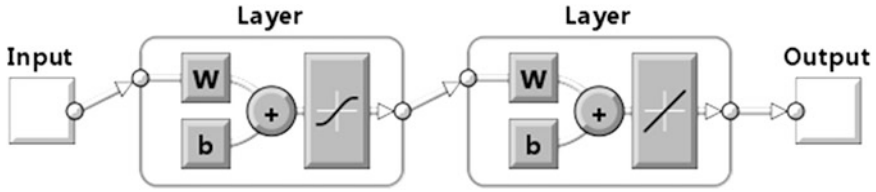


Fig. 6 FFNN architecture

neuron. The neurons in hidden layer have tansig transfer functions, and the output neuron has purelin transfer function. The architecture of feedforward neural network is illustrated in Fig. 6.

The performance function is mse, the mean squared error of estimated state related to real functioning state. During learning and testing of NN, the same performance criterion is used, denoted msel and mset, respectively. The performance goal has to be small enough to assure good estimation performance, but not too small to avoid loss of generalization.

The training datasets are chosen uniformly from the entire input dataset, with different numbers of learning vectors, N_{lv} . During training, a maximum of 500 epochs are allowed. For network testing, the entire dataset with 43,800 samples is used. The numbers N , N_{hn} , and N_{lv} are parameters, generating different network architectures. The training and testing results for different parameter values are represented in Table 1. The number of samples N for each coordinate has two different values: 4 and 8. The number of learning vectors N_{lv} has also two values: 1095 and 4380, from a total of 43,800 vectors in dataset. The number of hidden neurons N_{hn} is determined by testing three neural architectures with different values of N_{hn} : 8, 16, and 32 hidden neurons.

If the training dataset is small ($N_{lv} = 1095$), then the training errors are small, but the testing errors are bigger. The network is a good approximator for training dataset, but has poor generalization capabilities. In addition, if the number of hidden neurons is bigger, the testing errors are bigger. This means that the training dataset is too small to make good training of the network.

Increasing the number of training vectors ($N_{lv} = 4380$), the network continues to learn, producing better approximation for testing datasets. Therefore, the second training dataset was chosen for training of the estimator. The chosen architecture for

Table 1 Network performance for different neural estimators

N	N _{lv}	FFNN, N _{hn} = 8		FFNN, N _{hn} = 16		FFNN, N _{hn} = 32	
		msel	mset	msel	mset	msel	mset
4	1095	0.0596	0.0810	0.0405	0.0808	0.0276	0.1661
	4380	0.0685	0.0723	0.0533	0.0623	0.0412	0.0555
8	1095	0.0382	0.0729	0.0270	0.1128	0.0046	0.2397
	4380	0.0473	0.0527	0.0321	0.0426	0.0235	0.1377

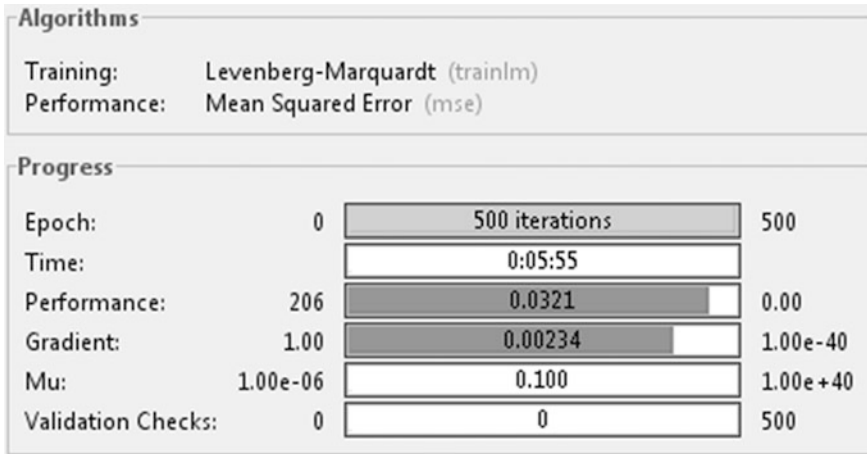
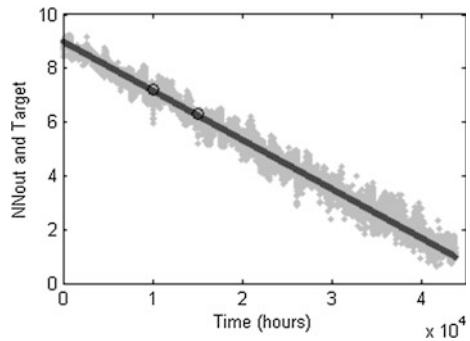


Fig. 7 Training conditions and performance for the selected FFNN

Fig. 8 FFNN output and the target values



the FFNN estimator was marked as italics in the table. For the selected neural architecture, the training conditions and performance are shown in Fig. 7.

The FFNN output and the target values are represented in Fig. 8, with gray and black color, respectively. Also the two operating points outside the permitted area are illustrated. It can be observed that the operating points crossing the border of permitted area for short time periods do not affect the network estimation.

5 Conclusions

In this paper, aspects of functioning state estimation using neural networks are discussed. Different FFNN architectures, with different input dimensions, number of hidden neurons, and training conditions, are analyzed. The network output is not

perturbed by operating points crossing the border of permitted area for short time periods. Neural estimator makes good state estimations, and it can deal with false malfunctions.

References

1. Sweetser C, Bergman WJ, Montillet G, Mannarino A et al (2002) Strategies for selecting monitoring of circuit breakers. *IEEE Trans Power Deliv* 17(3):742–746
2. Nguyen TC, Chan S, Bailey R, Nguyen T (2002) Auto-check circuit breaker interrupting capabilities. *IEEE Comput Appl Power* 15(1):24–28
3. Eisa MM (2002) Automating motor-operated air-breaker switches. *IEEE Comput Appl Power* 15(2):52–56
4. Manea I, Ionescu E, Irimia D (2003) Modern methods to diagnose the oleo-pneumatic operating mechanisms type MOP. In: The 5th International Power Systems Conference. Timisoara, Romania
5. Snyman T, Nel AL (1993) Mechanical condition monitoring of impulsively loaded equipment using neural networks. In: Proceedings of IEEE South African symposium on communications and signal processing, pp 96–102
6. Meng Y, Jia S, Rong M (2005) Mechanical conditions monitoring of vacuum circuit breakers using artificial neural network. *IEICE Trans Electron E88-C(8):1652–1658*
7. Adam M, Baraboi A, Pancu C, Pispiris S (2009) The analysis of circuit breakers kinematics characteristics using the artificial neural networks. *J. WSEAS Trans Circ Syst* 8(2):187–196
8. Hou Y, Liu T, Lun X, Lan J, Cui Y (2010) Reasearch on monitoring system of circuit breakers based on neural networks. In: International conference on machine vision and human-machine interface (MVHI 2010), pp. 436–439. ISBN: 978-1-4244-6595-8
9. Chen X, Siarry P, Ma Z, Huang S (2004) Fitting of a neural network to control the intelligent operation of a high voltage circuit breaker. *IEEE Proc-Gener Transm Distrib* 151(6):761–768
10. Negnevitsky M, Pavlovsky V (2005) Neural networks approach to online identification of multiple failures of protection systems. *IEEE Trans Power Deliv* 588–594
11. Niu X, Zhao X (2012) The study of fault diagnosis the high-voltage circuit breaker based on neural networks and expert systems. In: International workshop on information and electronics engineering, vol 29, pp 3286–3291. Published by Elsevier, Procedia Engineering
12. Cao Y, Liu Y, Li J, Liu X (2008) Nozzle optimization of SF6 circuit breaker based on artificial neural network and genetic algorithm. In: IEEE International conference on electrical machines and systems (ICEMS 2008), pp 222–225. ISBN: 978-7-5062-9221-4
13. Hush DR, Horne BG (1993) Progress in supervised neural networks. *IEEE Signal Process Mag* 10(1):8–39. doi:[10.1109/79.180705](https://doi.org/10.1109/79.180705)
14. Leung H, Lo T, Wang S (2001) Prediction of noisy chaotic time series using an optimal radial basis function neural network. *IEEE Trans Neural Netw* 12(5):1163–1172
15. Wright WA (1999) Bayesian approach to neural-network modeling with input uncertainty. *IEEE Trans Neural Netw* 10(6):1261–1270

Part VI
Knowledge-Based Technologies for Web
Applications, Cloud Computing, Security,
Algorithms and Computer Networks

Self-organizing System for the Autonomic Management of Collaborative Cloud Applications

Bogdan Solomon, Dan Ionescu and Cristian Gadea

Abstract Cloud computing has become an integral technology both for the day-to-day running of corporations, as well as for people life as more services are offered which use a back-end cloud. For the cloud providers, the ability to maintain the systems' Service Level Agreements and prevent service outages is paramount since long periods of failures can open them to large liabilities from their customers. These are the problems that autonomic management systems attempt to solve. Autonomic computing systems are capable of self-managing themselves by self-configuring, self-healing, self-optimizing, and self-protecting themselves, together known as self-CHOP. In this paper, an autonomic computing system which manages the self-optimizing function of a cloud collaborative application is presented. The autonomic control system itself uses self-organizing algorithms based on the leaky bucket flow model inspired from network congestion control.

1 Introduction

The growth in complexity of the company's IT infrastructure has made it nearly impossible for humans to manage and maintain it in a good and safe state. Cloud computing provides the ability for companies to subscribe to services such that the company pays only for the required resources and to scale up or down those resource usage based on company computational needs. Due to this capability, there is a need for a solution according to which cloud computing users can intelligently decide when to request more servers and when to release used servers. From the point of view of cloud computing providers, there is a need to move server loads via virtualization such that only the required CPU power is used for a certain demand. Ensuring that the appropriate number of virtual machines is deployed on a hardware

B. Solomon (✉) · D. Ionescu · C. Gadea
NCCT Laboratory, University of Ottawa, 161 Louis Pasteur Room B-306,
Ottawa, ON K16N5, Canada
e-mail: bsolomon@ncct.uottawa.ca

platform, such that the hardware is neither underutilized nor the virtual machines starve each other for resources, is not a trivial administrative task. The issue becomes even more complex when the end user's location is taken into consideration. In order to achieve better response times and latency, it is preferable to offer services as close as possible to the end user. Such approaches can be seen in content delivery networks (CDN) [1], which cache web data in datacenters across the world in order to be closer to the end users.

Autonomic computing has been proposed by the industry and researched by academia since its launch [2]. The management of the complexity problem is what autonomic management systems attempt to solve. Autonomic systems must be able to analyze themselves at runtime, determine its state, determine a desired state, and then if necessary attempt to reach the desired state from the current state. Normally, the desired state is a state that maintains the system's service level agreement (SLA) [3]. For a self-configuring system for example, this could include finding missing libraries and installing them with no human intervention. A self-healing system would be able to determine errors in execution and recover to a known safe state. A self-optimizing system example would be a cluster of servers that dynamically adds and removes servers at runtime in order to maintain a certain utilization and client response time. Finally, a self-protecting system example would be a server that detects a denial of service (DoS) attack and prevents it by refusing requests from certain internet protocol (IP) addresses.

The goal of this paper is to develop a self-organizing autonomic computing system capable of managing a geographically distributed collaborative cloud application. The control loop of each of the servers is based on the leaky bucket model frequently used in network congestion control as presented in [4]. While the work in [4] is used as a starting point, the model is modified in order to be better applied to the architecture and behavior of the media server used for the collaboration application.

The remainder of the paper is organized as follows. Section 2 introduces related work and background on the collaboration application which is controlled by the autonomic system. Section 3 introduces the self-organizing and leaky bucket model through which the autonomic behavior is achieved. Section 4 presents some metrics obtained from a test bed. Finally, Sect. 5 reflects on the contributions of this paper and proposes topics for future research.

2 Related Work

In cloud systems, a very important requirement is the ability of the cloud infrastructure user to automatically scale the systems up and down in order to deal with spikes in user numbers. All major cloud vendors Amazon [5], Rackspace [6], etc. provide reactive scaling abilities. Such systems allow cloud users to set up thresholds or periodic jobs for scaling the system up and down. Generally, the reactive scaling solution is fairly simple and only monitors one parameter—the

CPU utilization. Rackspace's solution differs in which it allows integration with Nagios monitoring, thus theoretically allowing scaling based on any other parameter. All autoscaling systems provided in industry allow the use of a cooling period after an autoscaling decision. The cooling period is used to avoid conflicts or repeated actions and allow the system to settle after an autoscaling decision is applied. The problem with reactive scaling is that the decision to autoscale the system is performed either after the SLA has already been breached, or before the SLA has been breached but with a possibility of the SLA never being breached. For example, in the case of an application which starts responding too slowly after the CPU utilization passes 70 %, a reactive autoscaling system can either add new servers when the CPU passes 70 %—which leads to a period before the server is started during which the SLA is breached. The other solution is to add servers when CPU utilization passes 65 %. However, a decision performed when the utilization breaches 65 % will be incorrect if the utilization settles at 66 % for example and then drops.

Recently, research has focused on building hybrid systems, which combine reactive scaling with predictive scaling [7, 8], in order to maintain the SLA goals in the face of unpredictable demand spikes. Such systems either use one of the approaches (reactive/predictive) during out scaling and the other approach during in scaling, or use a base reactive system in which the predictive system uses to learn the behavior and in the future predict necessary scalings. Such approaches have advantages over predictive systems in which they can make decisions before the SLA is breached in some circumstances [8]. The approach taken in this paper is a fully predictive system for both in scaling and out scaling of the system. While not included, a reactive scaling system is very easy to add to the system as a fallback decision making.

2.1 Background on the Controlled Application

The application to be controlled is a web-based collaboration application, which includes the ability of users to communicate with each other via text or video/audio chat while viewing synchronized content. The system's architecture is presented in [9]. This section will present some of the characteristics of the application that are relevant to the autonomic system which will self-optimize it in a self-organizing manner. The application is developed as a client-server architecture, with the server side being deployed in a cloud in order to scale up and down based on demand. The cloud-based server side of the application is also designed to be deployable in multiple clouds in separate geographic locations, in order to allow clients to connect to the best location available. This design leads to a client-server system in which clients connect to a server, while messages sent between clients go through the server. The server then distributes the messages to the appropriate destination clients. Clients connect to a cluster of virtualized servers, and clients communicating with each other connect to different server instances in the cloud. The system

(servers in collaboration with the clients) ensures that clients in the same collaboration session view the same state of the shared “workspace.” The system is made out of a geographically distributed application—clients connect to one of multiple clouds which are distributed in various locations. Clients from different clouds can still communicate with each other.

Due to the fact that the cloud sizes are not static in order to scale up and down based on demand, a very important ability for the servers is to discover new servers when servers come online and for servers to broadcast when they leave the cluster. In order to achieve this goal, the cluster architecture uses a group membership service (GMS) to create a group which the servers can join and leave. The servers then use the group created by the GMS system to communicate with each other. Using a GMS for such communication instead of an approach like broadcasting messages in the network ensures that multiple clusters can be co-located in the same network and not interfere with each other’s inter-server communication. In order to deal with group members crashing, members periodically send a refresh message to update the status of their group membership. If a long enough period passes without a refresh from a group member, then member is considered dead and removed from the group. If a group member attempts to join a group with a name that does not exist, then a group with that name is created.

3 Self-organizing Control Model

One of the most important steps in developing an autonomic computing system, whether the system is controlled via machine learning, control theory, or any other method, is the development of an abstract model for the system to be controlled usually named as plant or controlled object. This is a compulsory step to take in any control problem at hand as once the model is developed, various control methods can be devised and tests can then be applied to determine if specific properties of the control system are met such as its stability, sensitivity which shows how responsive the control system is to various parameter, input, or disturbance variations. The model presented in this paper is a control theoretic model which will use equations in matrix form to represent the model structure. The self-organizing model is based on the work in [10] and was presented in [11].

As mentioned previously, the control system developed for the cloud of servers uses a decentralized self-organizing architecture. The autonomic control model is composed of two parts: a leaky bucket model which is the control model being executed at each server’s control loop and a self-organizing model, which is the model of how the server control loops are combined to create a control system for the entire cloud. The self-organizing system uses a structure similar to that of Ashby’s homeostat [12], as shown in Fig. 1. Each of the four control loops output, one for each server, in turn is used to control the state of the other servers.

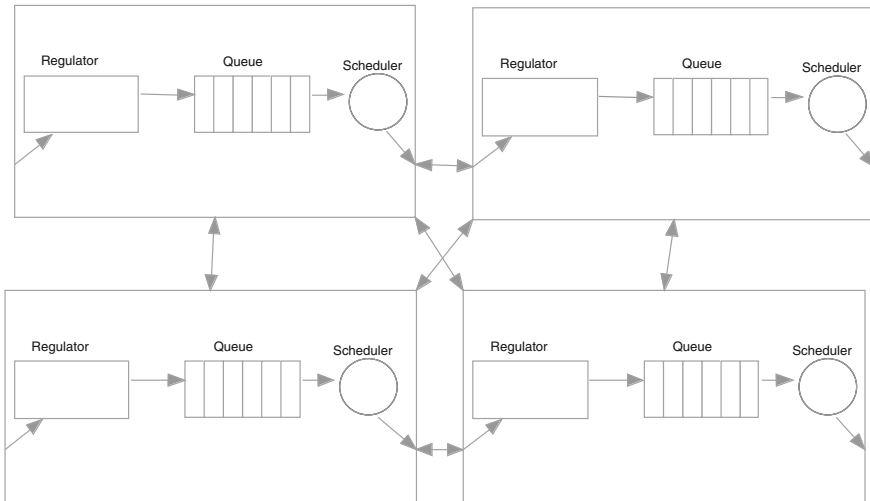


Fig. 1 Homeostat-like structure

3.1 Leaky Bucket Model

The leaky bucket model is commonly used in network congestion control and is based on a fluid flow model.

In the fluid flow model, a stochastic process of first order is modeled as a single-server queuing system with constant service rate, as in Fig. 2, where u is the rate of packets arriving at the queue, x is the state of the queue represented by the number of packets in the queue, and v is the rate at which packets are processed and released from the queue.

The leaky bucket model is built on top of the fluid flow model, in order to ensure that the network equipment is not jammed when large bursts of traffic are created. The control is performed by dropping packets once a certain condition is met. The leaky bucket model is created by adding a “token bucket” to the queue. The token bucket is filled at a constant rate and whenever a packet is removed from the queue, a packet is also removed from the token bucket. At the same time, the service rate of the queue is controlled by the amount of tokens in the token bucket. The model of the system is shown in Fig. 3. The token bucket is filled at a constant rate $R > 0$. Logically, the leaky bucket model can be interpreted as follows. When the token bucket is full, the network equipment has to process fewer packets than R , which represents a target of how many packets the system can process without problems. When the token bucket is empty or nearly empty, the network equipment is processing many more packets than R and some of the packets have to be dropped. In such a case, the network equipment will process R packets, and the rest will be dropped.



Fig. 2 Single-server queuing system

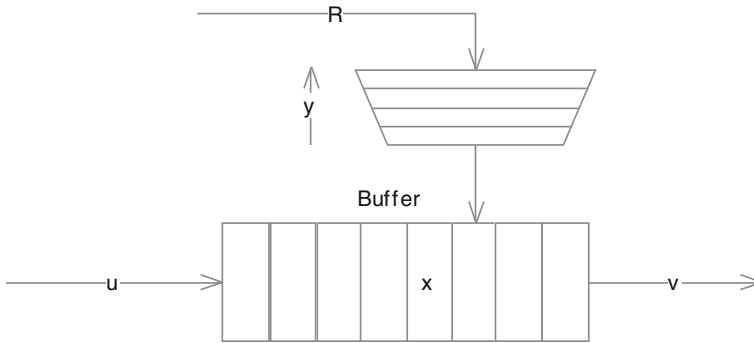


Fig. 3 Token leaky queuing system

The full model and how it is applied to the problem at hand can be found in [11] and is given below. A continuous time fluid flow model of the buffer dynamics is as follows:

$$\frac{dx(t)}{dt} = u(t) - v(t) \tag{1}$$

where $u(t)$ denotes the rate at which the users’ requests are released to the network such that they are eventually queued by the servers and finally processed and represent the input to the system model described by Eq. (1), while the output of the system is $v(t)$. A series of researches have been undertaken for the study of the $u(t)$ in various technical incarnations. In [7], the authors provide an empirical model for it considering a single link of capacity c (the total amount of traffic/fluid of the link).

For the fluid flow model of the autonomic computing, the assumption is that there is no round-trip delay as in the case of the model developed by Katabi et al. The state of the system is denoted by $(i; x)$, where $i = \{0, 1, \dots, N\}$ is the number of up nodes and x , with $0 \leq x \leq c$ where x is the total amount of fluid in the system which in this case comprises only the up servers, while c denotes the total amount of fluid in the universe or in more layman words, the total capacity of the processing.

The set of virtual servers under the control of the Autonomic Computing system is considered to contain i servers which are processing the queue of processes activated by users’ requests for information. There are also other virtual servers

which are down due to the lack of users's requests. The users' requests occur at rate σ and responses to users' requests are processed at rate θ . The fluid arrival process is defined as follows: in $(T_n; T_{n+1})$, the fluid arrival rate is $\sigma(1 - X(t)/c) - r(X(t))$ if $N_n \in \{1, 2, ..N\}$ and is equal to 0 if $N_n = 0$. In the above description of the fluid arrival process, $r(X(t))$ is the processing rate function. Assuming that the buffer storing all users' requests operates under a standard FIFO basis, the processing rate function is further defined by the ratio between the load $X(t)$ and the residence time $\theta(X(t))$.

With the above notations, the fluid model for the virtual server system is described by the following equation:

$$\begin{aligned} \frac{d}{dt}X(t) &= \sigma \left(1 - \frac{X(t)}{c} \right) - r(X(t)) \\ r(X(t)) &= \frac{X(t)}{\theta(X(t))} \end{aligned} \tag{2}$$

Equation (2) has to be interpreted as an averaged description of a wide class of buffers depending on the particular form of the residence time function $\theta(x)$. For instance, if a linear form for $\theta(X(t))$ is

$$\theta(X(t)) = \frac{X_0 + X(t)}{\mu_X} \tag{3}$$

where $X_0 > 0$ is the initial load in the queue buffer and $\mu_X > 0$ is the average service rate of the stochastic process $X(t)$, Eq. (2) can be written as

$$\frac{dx(t)}{dt} + \frac{\mu_X X(t)}{X_0 + X(t)} = \sigma \left(1 - \frac{X(t)}{c} \right) \tag{4}$$

$$v(t) = \frac{\mu_X X(t)}{X_0 + X(t)} \tag{5}$$

The set of Eqs. (4) and (5) can be further linearized around the nominal value of $X(t)$ where the queue works in a permanent regime, be it X_S in order to bring the set of equations to an ordinary differential equations:

$$\frac{dX(t)}{dt} + \frac{\mu_X X_0}{(X_0 + X_S)^2} X(t) = \sigma \left(1 - \frac{X(t)}{c} \right) - \frac{\mu_X X_S^2 + \mu_X X_0 X_S - \mu_X X_0^2}{(X_0 + X_S)^2} \tag{6}$$

$$v(t) = \frac{\mu_X X_S^2 + \mu_X X_0 X_S - \mu_X X_0^2}{(X_0 + X_S)^2} + \frac{\mu_X X_0}{(X_0 + X_S)^2} X(t) \tag{7}$$

Using the following notations,

$$a_1 = \frac{\mu_X X_0}{(X_0 + X_S)^2} \quad (8)$$

$$b_1 = \frac{\mu_X X_S^2 + \mu_X X_0 X_S - \mu_X X_0^2}{(X_0 + X_S)^2} \quad (9)$$

Eqs (6) and (7) can be written as

$$\frac{dX(t)}{dt} + a_1 X(t) = \sigma \left(1 - \frac{X(t)}{c} \right) - b_1 \quad (10)$$

$$v(t) = b_1 + a_1 X(t) \quad (11)$$

Using a block diagram representation, the fluid flow model for computing processes can be represented as

$$\frac{dx(t)}{dt} + a_1 X(t) = \sigma \left(1 - \frac{X(t)}{c} \right) - b_1. \quad (12)$$

3.2 Self-organizing Model

For a router or switch, the leaky bucket model is used in order to determine when to start dropping packets such that the network equipment maintains a predefined SLA with regards to the time it takes for the network to process packets. While dropping packets in a network is not desired as in most cases it will require retransmission, it is necessary in the face of bursts. If packets were not dropped, the buffer size would continue to increase and the processing time of packets would also increase.

For the collaboration application described in this paper, the control problem is that of managing the number of server instances deployed in the cloud such that instances do not get overloaded and neither are instances underutilized. Logically, the system adds servers when the leaky bucket models of the servers show that token buckets are empty—thus having to process too many computing processes, and remove servers when the token buckets are full—showing that the servers are processing few processes. The addition/removal of servers is achieved by adding self-organizing capabilities to the cloud, similar to the work in [10].

In order to reach a self-organizing state for the collaboration cloud, the server control loops exchange data with each other as well as with the cloud control subsystem in order to determine if a new server is required or if servers should be stopped. Section 4 presents results obtained from a cloud of servers which are used in order to communicate between servers to achieve the self-organizing state. The self-organizing control is achieved in four steps.

- **First Step**—In the first step, a server which reaches a state where it is overloaded based on the state of its leaky bucket model sends a request to the load balancer subsystem demanding that no new client connections be redirected to the server.
- **Second Step**—In the second step, servers periodically vote on whether new servers are required or not. One of the servers is responsible for counting the votes and if more than a predefined percentage of servers vote in favor for the creation of new servers, new servers are added to the pool.
- **Third Step**—In the third step, a server which is not accepting new connections and whose token bucket model is showing that the server is not overloaded anymore sends a message to the load balancer subsystem notifying it that new client connections can be redirected to the server.
- **Fourth Step**—Finally, servers also vote on whether to remove servers from the pool of active servers or not. A server cannot at the same time vote to add and remove servers. Similar to the addition of servers, if more than a predefined percentage of servers vote for the removal of servers, some of the servers will be removed from the pool.

The above four steps ensure that no single server will be overloaded by receiving too many requests compared to its peers. While it can be argued that such a system is not necessary if an efficient load balancer is used, the specifics of the collaboration application do not guarantee that properly balanced client connections will lead to properly balanced server loads. Consider a case where the cloud contains two servers, called Server 1 and Server 2 with 20 users connected to each server. The 40 users are grouped into two collaboration sessions—Session 1 and Session 2, with each of the two sessions having 15 users connected to one server and 5 users connected to the other server. Due to the fact that collaboration sessions are created dynamically by users, it is impossible to know at the time when users connect to the system how sessions will be created and which servers sessions will span. Furthermore, assume a case in which each of the two servers receives a video/audio stream from users and which is to be broadcasted to all other users inside the session. Both streams are sent in Session 1. In such a case, both servers would have two incoming streams, but Server 1 would have 29 outgoing streams, while Server 2 would only have nine outgoing streams. Depending on the capabilities of the two servers, it is possible that even though both servers are having the same number of users connected, Server 1 is overloaded in this example while Server 2 is not.

Also, using the state of the token bucket to decide when to add/remove servers to/from the cloud, it can be ensured that the number of servers in the cloud does not fluctuate sporadically and exhibit oscillations. Servers vote on whether new servers should be added or removed by looking at their own token bucket and making a

voting decision. The voting decision is based on comparing the token bucket level with predefined thresholds. A server can vote for one of the three options: add server, remove server, or no change. A server whose token bucket has its level above the higher threshold votes for removal of servers, a server with a token bucket level below the lower threshold votes for addition of servers, and a server with a bucket level between thresholds votes for no change. Note that a server does not change its previous vote as soon as one of the thresholds is passed, but waits a certain amount of time in order to ensure that the observed behavior is not a single spike. One of the servers is chosen to gather the votes from the other servers, count them, and pass any decision to the actuator of the system. The choosing of the server which gathers the vote and counts them is done using a distributed lock mechanism. Whenever servers start, one of the servers acquires the distributed lock and is the server in charge of gathering votes. If that server goes down, another server will acquire the lock and become the new server which gathers the votes and counts them.

A control system which scales a cloud of servers has to deal with two problems.

- The system has to ensure that servers are added only as needed and that a breach of SLA does not trigger multiple server additions without a change in the system. For example, the SLA is breached and a new server is created. The new server will take time to be deployed and properly started. While the new server is being deployed, if there is no change in the behavior of the system and traffic of the system is constant, the control system should not add more servers.
- Removal of servers does not exhibit the same problem, as stopping a server can be seen to be nearly instant with the server simply stopping to receive requests and removing itself from the server group. At the same time, if traffic continues to increase while the new server is added, the control system should add new servers as needed and should not wait until the new server is started to make a new decision.
- The control system should not exhibit oscillations by continuously adding and removing servers. Both of these problems are solved in commercial cloud implementations by adding a cooling or cooldown period, during which time the autoscaling condition is not reevaluated in order to allow the system to settle down. A cooling period does not, however, allow the system to make modifications if the traffic situation worsens during the cooling period.

In order to deal with the above two problems, the vote counter stores both the state of the system the last decision was based on as well as the desired state of the system based on the last control decision taken. The decision regarding the addition of new servers is based on the percentage of servers voting for addition of servers—which can be seen as the percentage of servers which are not accepting new connections or which are moving toward not accepting connections. If the percentage of servers voting for addition passes a predefined threshold, then the system starts the process of adding as many servers as required to bring the percentage back under the predefined threshold. At the same time, the system stores the current percentage that the decision was based on, as well as the percentage that the server

addition will cause once the server is fully started. For example, assuming the case of a cloud which has five total servers out of which three servers are not accepting new connections and which has a threshold of 80 % votes for adding new servers, in which one of the two accepting servers sends a vote in favor of server addition. Once the vote is received, the controller computes how many servers should be added in order to bring the vote percentage under 80 %. In this case, the system would add a single server bringing the percentage of servers voting for addition to 66 % (4/6). The control system would also store the reason the change decision was taken (4/5 voting for addition) and the target of the decision (4/6 voting for addition). Once the new server is started and the control system receives information about the new server, the control system discards the reason the change decision was taken as well as the target goal and resumes normal processing.

While the new server is being deployed, one of three situations can arise:

1. There is no change in the voting of the servers. Without any other change in the system, the control system takes no other action and the system is stable.
2. The server which was voting for no change modifies its vote to server addition. Such a modification results in the target system having a percentage of 83 % (5/6) of the servers voting for addition of servers. As such, the control system again computes how many servers it should add—which is again one, leading to a current state of 100 % (5/5) voting for addition and target state of 71 % (5/7) voting for addition.
3. One of the servers which was voting for addition modifies its vote to no change. Note that it is actually possible for multiple of the servers to change their vote to no change. Such a modification results in the target system having a percentage of 50 % (3/6) of the servers voting for addition. The system, however, uses a different threshold for removing servers, and as such it will not remove servers unless the percentage of servers voting for removal passes that threshold. Furthermore, since the last decision which is still in progress was of adding servers, the control system waits until the new servers are added and it has resumed normal execution before performing any removal actions.

The removal of active servers from the cloud is achieved similarly to the process of adding servers; however, as mentioned previously it does not present the same challenges due to the fact that stopping a server is nearly instant from the view of system. Once the percentage of servers voting for removal passes a predefined threshold, the control system computes how many servers have to be removed in order to bring the percentage of voters under the threshold and stops the computed number of servers. Unlike in the case of addition of servers, once a decision is taken, the control system continues normal execution since removal of servers is achieved instantly.

It should be noted that if both addition and removal thresholds are sufficiently larger than 50 %, the system will not exhibit oscillations due to the fact that servers voting for addition, servers voting for no change, and servers voting for removal are equal to 100 %, while the decision of adding or removing servers is done in such a way as to bring the new percentage right under the threshold. At the same time, it is

possible to add or remove multiple servers if multiple servers change their previous vote at the same time. If only one server modifies its vote, then adding/removing one server will almost always result in the respective percentage being under the threshold again. Finally, the usage of percentages assures that a system with a large number of servers will respond properly when traffic increases.

The communication between self-organizing components is achieved using a GMS system to broadcast messages among the control peers in order to reach the control decisions. The control messages will be to either accept or reject new clients' messages sent by the servers to instruct the load balancing system of their ability or voting messages gathered by the server peer which holds the distributed lock and used to determine when to add/remove servers.

4 Results

A test bed was created in order to test the behavior of the collaborative application under various loads. Figure 4 shows the physical topology of the infrastructure, which was used to simulate various deployment scenarios and run tests on how the collaborative system behaves. The test bed uses five servers connected via a switch to one of the four routers with a fifth router providing outside internet connection. Figure 5 displays how routing will be done within the network and the various VLANs used to create the separate clouds. The server names are cloud1 through cloud5, with cloud4 and cloud5 being in the same VLAN, while cloud1, cloud2, and cloud3 are each in their own VLAN. Cloud1 also acts as the cloud controller running all the various services necessary for a cloud-like virtual image storage, network management, and cloud computing fabric controller. Each of the virtual machines was given 2 GB RAM, 1 VCPU, and 20 GB hard drive storage. The network connections are 100 Mbps with some of the router connections being 10 Mbps. While such connection speeds would be too low for a datacenter, it is fine for these tests as the low speeds can be used to simulate overloaded internet connections with low throughput. Each of the five servers has its own control loop, similar to the design in Fig. 1 and each server communicates with all other ones just as in Fig. 1.

A separate computer not shown in the diagrams is responsible for simulating client requests. In order to test audio/video streaming, a prerecorded webcam video is streamed whenever the client simulator decides to start streaming. The stream used for testing is a 64×64 video stream at 25 frames per second with a bit rate of 180 Kbps. The client simulator is written in Java and can simulate various client distributions by varying the amount of clients, the number of clients in every session, the number of clients streaming in each session, and the time delay between messages being sent in a session. The simulator initially creates a number of sessions and a number of clients in each session. Each client is created with a given time to live. Periodically, the session calculates how many clients should be streaming in the session at that point in time. If more clients are required to stream

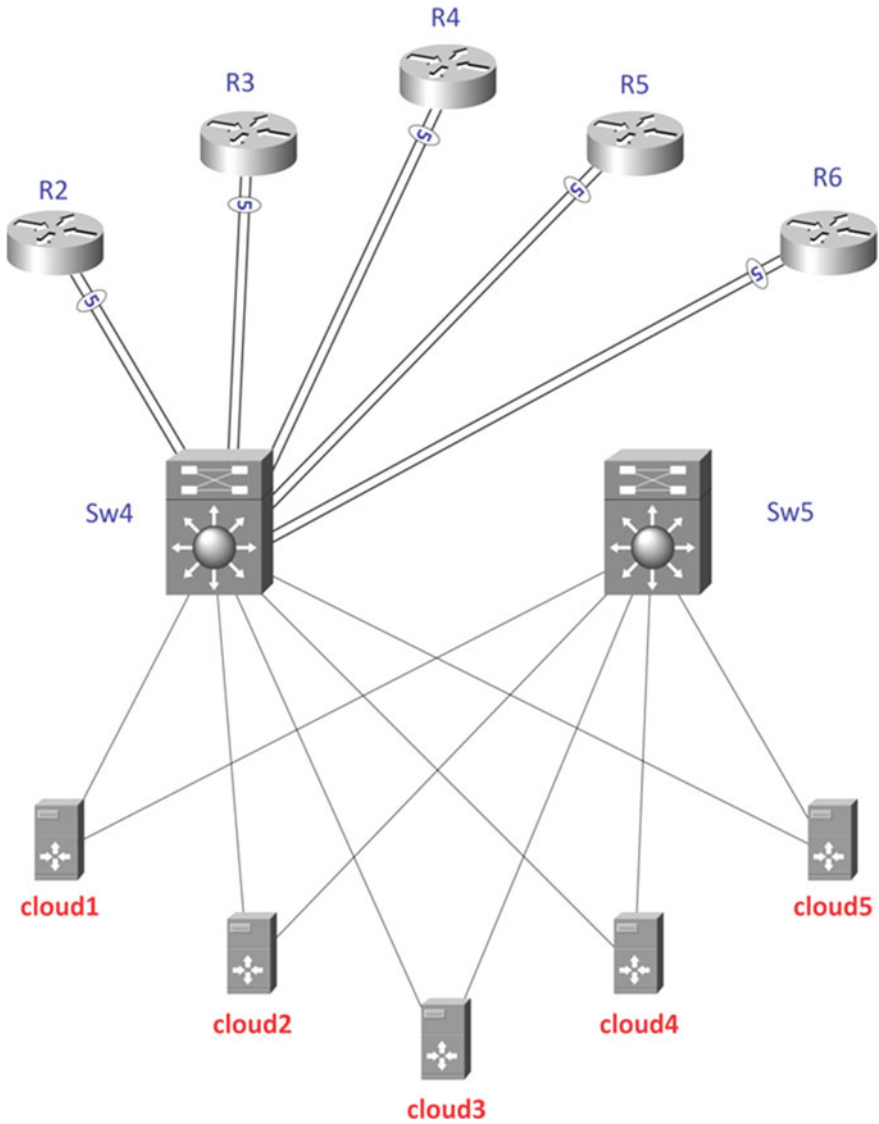


Fig. 4 Physical topology

than are currently streaming, the session simulator instructs a number of clients to start streaming also. If less clients are required to stream than are currently streaming, the session simulator instructs a number of clients to stop streaming. If there is no change in the number of clients needed to stream, then no change is made in which clients are streaming. Whenever a client reaches its time to live, the client is put to sleep and given a time after which it should wake up and reactivate.

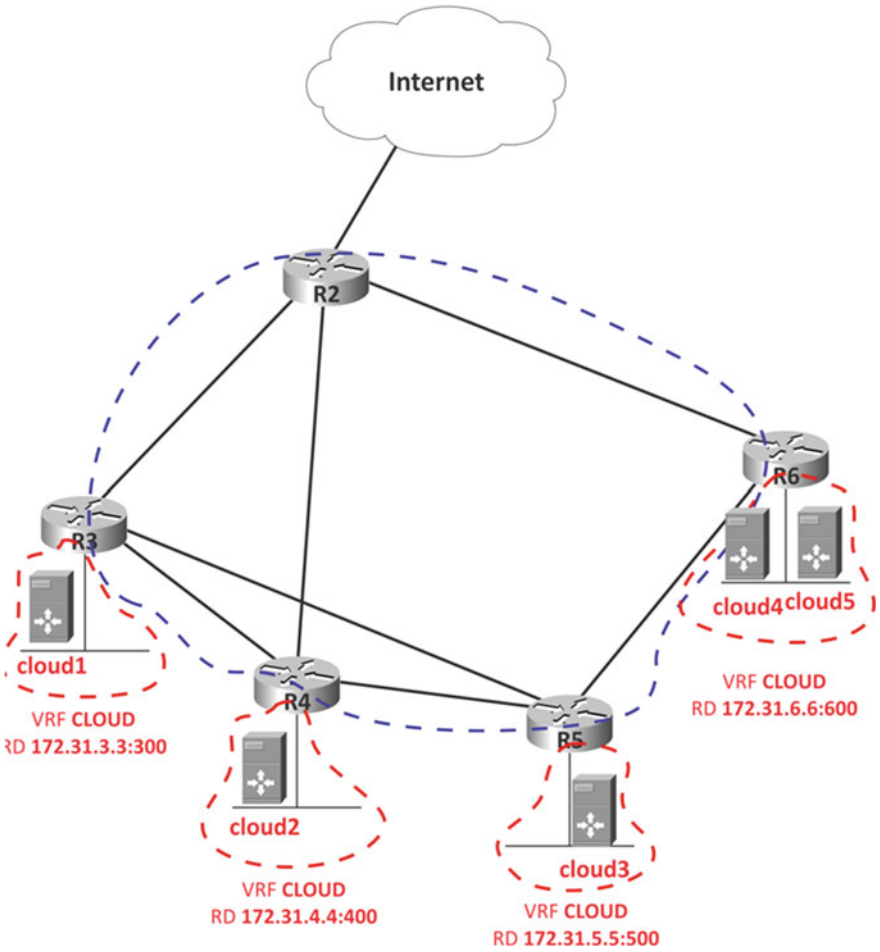


Fig. 5 Logical topology routing

When a client reactivates, it joins again the same session it was a member of, before going to sleep. The amount of time clients is awake and sleep is randomized thus generating various session sizes over time. Three variables can be varied in order to determine how they affect the measured data obtained from the collaboration servers. For each of these tests, one variable was modified gradually, while all other variables were kept constant. The data is measured from all the servers every 30 s, and is composed of bandwidth received, bandwidth sent, latency, and CPU usage. Since the tests are run at different moments in time, the timescale is normalized to the period from when each test was started.

4.1 1 Server, 1 Collaborative Session, 1 Streams Per Session

The first test was run with a single server, one collaborative session, and a single user audio/video streaming and is used as a base for comparison with all other tests. The number of clients was varied from 5 to 40, where the 10 Mbps network link was saturated, in increments of 5.

These results show the average latency steadily increasing as more clients are in the session. Interestingly, the CPU usage increases faster in the beginning and slows down as latencies start increasing faster. Figures 6, 7, 8, and 9 show the latency results, while Figs. 10, 11, 12, and 13 show the CPU usage results. The spikes in all figures happen when a stream ends and another stream is started to replace it. The rest of the tests will be presented only in tabular form, to save space (Table 1).

4.2 1 Server, 1 Collaborative Session, 2 Streams Per Session

The number of clients for this test was varied from 5 to 25, where the 10 Mbps network link was saturated, in increments of 5.

Similar to previous tests, the CPU and latency are not directly related. The test for 25 users is an outlier due to the network link becoming overloaded. Looking at the median CPU usage, the increase is constant between 5 and 20 users. At the same time, median latency increases faster as more users are in the session, with a small increase between 5 and 10 users and a large increase between 15 and 20 users. Comparing the results of this test with the previous results for 1 server, 1 session, and 1 stream based on the number of outgoing streams, the results for 8, 18, and 28 outgoing streams are similar in term of latency but fairly different in term of CPU usage. Comparing 39 outgoing streams for 1 server, 1 session, 1 stream with the

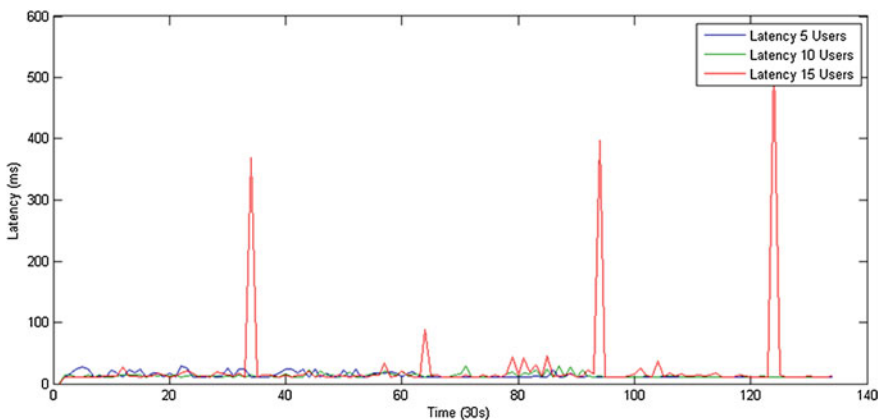


Fig. 6 Latencies for 5, 10, and 15 clients—1 server, 1 session, 1 stream

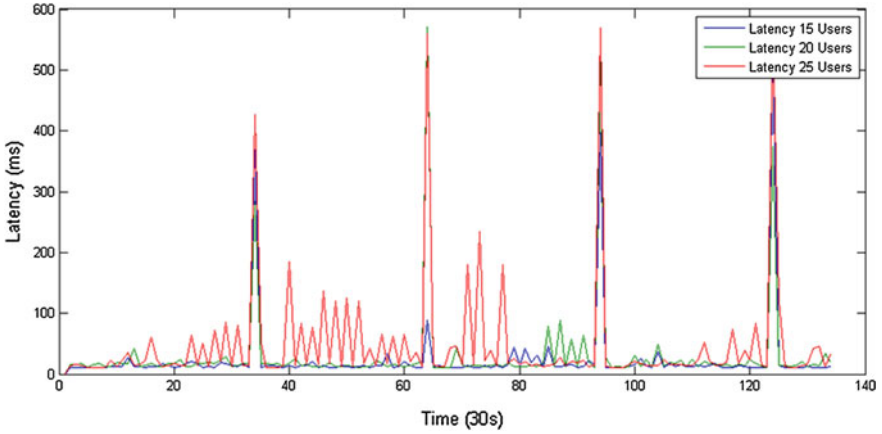


Fig. 7 Latencies for 15, 20, and 25 clients—1 server, 1 session, 1 stream

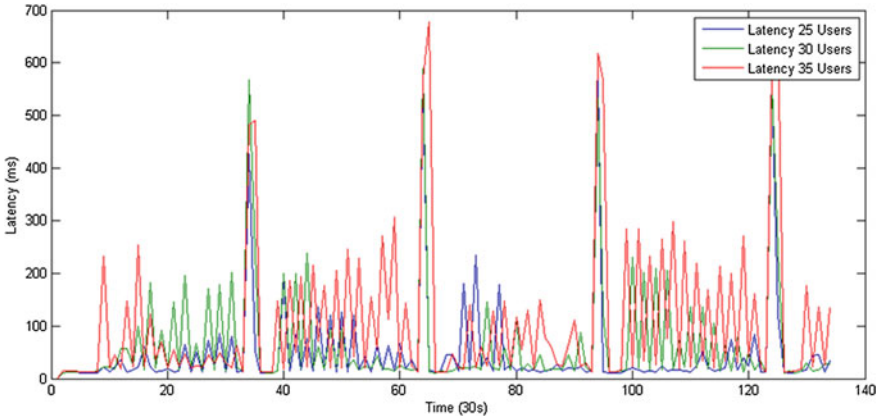


Fig. 8 Latencies for 25, 30, and 35 clients—1 server, 1 session, 1 stream

result for 38 outgoing streams for 1 server, 1 session, and 2 streams, it can be seen that the latency for 2 streams is much lower than the latency for 1 stream. This suggests that latency is not dependent only on the number of outgoing streams, but also on either the number of clients or on the multiplicity of incoming streams to outgoing streams (for example, a stream that goes from one source to 39 destinations shows higher latency than 2 streams each of them going to 19 destinations) (Table 2).

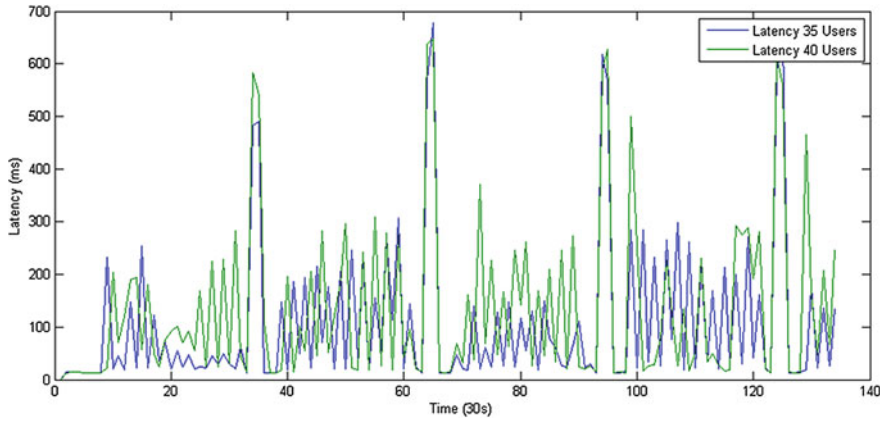


Fig. 9 Latencies for 35 and 40 clients—1 server, 1 session, 1 stream

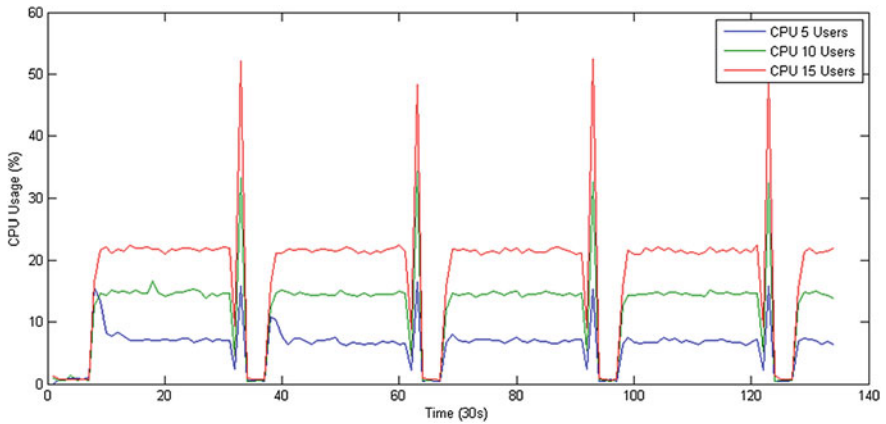


Fig. 10 CPU for 5, 10, and 15 clients—1 server, 1 session, 1 stream

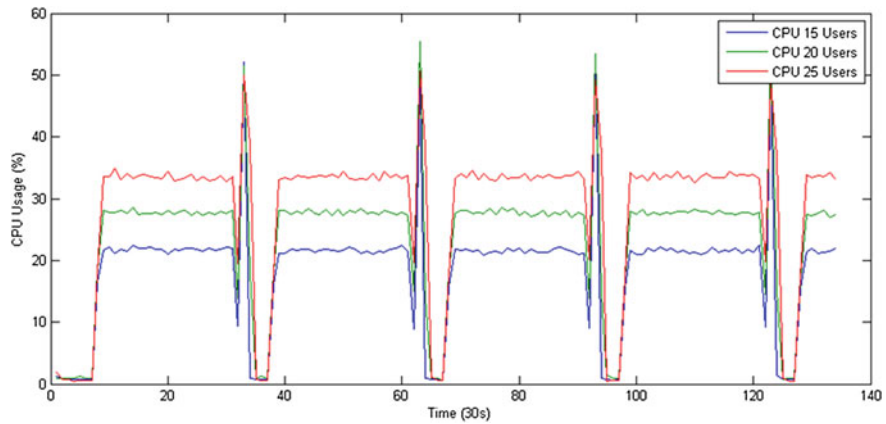


Fig. 11 CPU for 15, 20, and 25 clients—1 server, 1 session, 1 stream

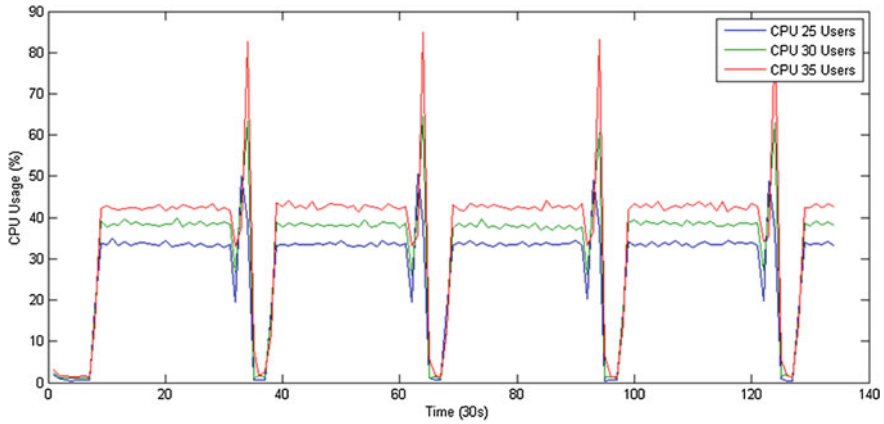


Fig. 12 CPU for 25, 30, and 35 clients—1 server, 1 session, 1 stream

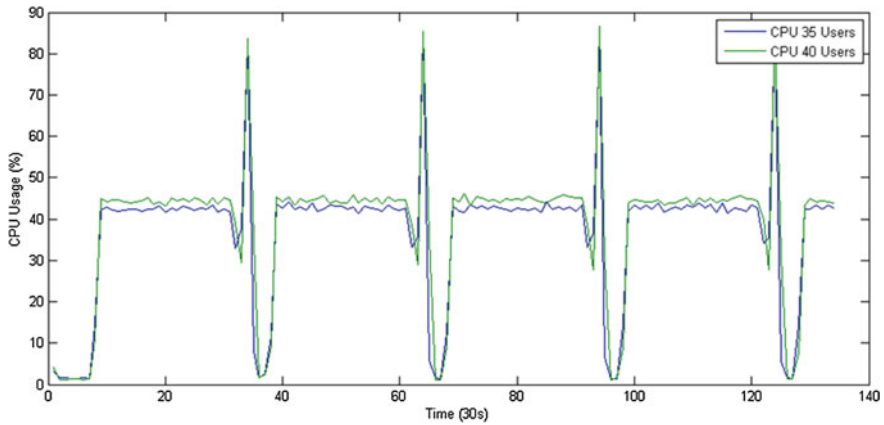


Fig. 13 CPU for 35 and 40 clients—1 server, 1 session, 1 stream

Table 1 Median and mean CPU, latencies for 1 server, 1 session, 1 stream

Number of users	Median latency (ms)	Mean latency (ms)	Median CPU (%)	Mean CPU (%)	Outgoing streams
5	10.40	13.16	6.86	6.16	4
10	11.60	13.20	14.51	12.41	9
15	12.03	24.08	21.49	18.32	14
20	14.90	30.43	27.56	23.57	19
25	16.48	48.05	33.41	28.50	24
30	20.02	65.88	38.15	32.79	29
35	34.80	109.41	42.27	36.64	34
40	59.75	135.60	44.22	38.62	39

Table 2 Median and mean CPU, latencies for 1 server, 1 session, 2 streams

Number of users	Median latency (ms)	Mean latency (ms)	Median CPU (%)	Mean CPU (%)	Outgoing streams
5	10.20	11.92	13.56	11.33	8
10	12.70	21.65	22.95	19.12	18
15	20.03	64.12	31.87	27.29	28
20	33.95	95.57	40.15	31.35	38
25	277.84	274.80	35.31	32.29	48

4.3 1 Server, 1 Collaborative Session, 3 Streams Per Session

Increasing the amount of streaming clients to three saturates the 10 Mbps network link after 20 clients—the 20-client test is not shown. The same patterns as before can be seen again in this test:

1. CPU and latencies do not directly correlate.
2. Latency for 5 clients is very close to latencies for 5 clients in all tests.
3. As the number of outgoing streams and sent bandwidth increases, latencies also increase.
4. Latencies for similar numbers of outgoing streams are lower when the multiplicity of incoming streams to outgoing streams is lower (Table 3).

4.4 1 Server, 2 Collaborative Sessions, 1 Stream

In this test, 2 collaborative sessions of equal size are created, but only one session contains a streaming client. In the second session, clients only exchange text/synchronization messages. The goal of this test is to determine if there are other factors in the application outside video/audio streaming impacting latencies and CPU usage. If this test was compared to the test in Sect. 14.a, it would be expected that latencies are very similar for equal numbers of clients. This expectation is met for most data points, with the main differences being shown by the 25, 30, and 35 clients latency values. CPU usage values are very close for all tests. While generally different, due to the fact that both ends of the test (5, 10, 15, 40 clients) show similar

Table 3 Median and mean CPU, latencies for 1 server, 1 session, 3 streams

Number of users	Median latency (ms)	Mean latency (ms)	Median CPU (%)	Mean CPU (%)	Outgoing streams
5	10.40	19.77	19.86	16.45	12
10	14.55	35.68	34.44	28.76	27
15	66.53	120.21	38.82	33.46	42

Table 4 Median and mean CPU, latencies for 1 server, 2 sessions, 1 stream

Number of users	Median latency (ms)	Mean latency (ms)	Median CPU (%)	Mean CPU (%)	Outgoing streams
5	11.40	12.77	6.99	6.36	4
10	12.48	13.75	14.62	12.48	9
15	14.35	25.29	22.04	18.96	14
20	15.41	42.44	27.69	23.75	19
25	22.58	62.11	33.92	29.16	24
30	29.72	87.54	38.73	33.34	29
35	40.48	122.10	42.18	36.44	34
40	61.64	143.27	44.24	38.84	39

results, the differences can be assumed to be due to variability inside the system. This assumption can be tested in the next tests (Table 4).

4.5 2 Servers, 1 Collaborative Session, 1 Stream Per Session

In order to test the behavior when multiple servers are present, sessions were created with 10, 20, 30, etc. clients. By doing this, it can be ensured that each of the two servers will receive 5, 10, 15, etc. clients per session since clients are distributed to the servers in a round-robin fashion.

First of all, the results are compared for the same client load on both servers, in order to ensure that similar loads show similar results as shown in Table 5. Overall, the two servers show similar latencies for a certain client load, with some variance existing, however. Between 80 and 100 users, the difference between the latencies for the two servers varies significantly. CPU usage, however, varies clearly between the two servers with Server 2 having lower CPU usage than Server 1.

Table 5 Median and mean, latencies for 2 servers, 1 session, 1 stream

Number of users per session	Median latency server A (ms)	Median latency server B (ms)	Mean latency server A (ms)	Mean latency server B (ms)	Outgoing streams per server
10	11.00	10.60	12.02	11.58	5
20	11.50	11.30	20.30	20.49	10
30	12.46	13.17	16.31	33.10	15
40	14.68	16.05	47.37	43.23	20
50	16.58	19.24	48.99	90.13	25
60	21.10	22.05	52.05	70.06	30
70	43.40	43.77	103.13	113.71	35
80	113.88	64.68	170.83	132.31	40
90	305.22	192.82	291.45	200.33	45
100	489.42	411.70	419.02	390.21	50

Table 6 Median and mean CPU for 2 servers, 1 session, 1 stream

Number of users per session	Median CPU server A (%)	Median CPU server B (%)	Mean CPU server A (%)	Mean CPU server B (%)	Outgoing streams per server
10	7.91	6.26	6.64	5.73	5
20	15.81	12.39	12.68	10.79	10
30	24.44	18.41	19.40	15.97	15
40	30.46	23.96	24.11	20.63	20
50	35.94	29.51	28.23	25.41	25
60	40.26	34.00	31.89	28.61	30
70	38.49	37.93	30.59	32.73	35
80	36.53	37.03	31.13	32.51	40
90	34.64	37.65	29.52	32.82	45
100	31.52	34.64	26.15	32.20	50

Comparing these results with those of Table 1, while taking into account the fact that the number of outgoing streams for this test is slightly higher than that for a single server due to the proxy between servers, it can be seen that the results are very similar for similar numbers of users per session per server.

These results show that basing the scaling decision on the CPU usage of the server is not enough to accurately predict the latency experienced by clients (Table 6).

5 Conclusions

This paper has presented a self-organizing autonomic system used for the control of a collaborative application deployed in a cloud. The system uses a leaky bucket model previously developed to control the server's admission rate combined with a self-organizing voting system to decide when to add or remove servers.

Future work will focus on testing the behavior of the autonomic system, determining how fast the system adapts to changes and how well the cloud resources are used.

References

1. Akamai. Akamai CDN. <http://www.akamai.com>. Accessed May 2014
2. Horn P (2009) Autonomic computing: IBM's perspective on the state of information technology, October 2001. Accessed May 2009
3. Ionescu D, Solomon B, Litoiu M, Mihaescu M (2008) A robust autonomic computing architecture for server virtualization. In: INES 2008 international conference on intelligent engineering systems, pp 173–180, Feb 2008

4. Guffens V, Bastin G (2005) Optimal adaptive feedback control of a network buffer. In: Proceedings of the 2005 American Control Conference, vol 3, pp 1835–1840, June 2005
5. Amazon. Auto Scaling. <http://aws.amazon.com/autoscaling/>. Accessed Jan 2014
6. Rackspace. Easily Scale Your Cloud With Rackspace Auto Scale. <http://www.rackspace.com/blog/easily-scale-your-cloud-with-rackspaceauto-scale/>. Accessed Jan 2014
7. Iqbal W, Dailey MN, Carrera D, Janecek P (2011) Adaptive resource provisioning for read intensive multi-tier applications in the cloud. *Future Gen Comput Syst* 27(6):871–879
8. Moore LR, Bean K, Ellahi T (2013) Transforming reactive auto-scaling into proactive autoscaling. In: Proceedings of the 3rd international workshop on cloud data and platforms, CloudDP'13, pp 7–12. New York, NY, USA, ACM
9. Solomon B, Ionescu D, Gadea C, Litoiu M (2013) Migrating legacy applications: challenges in service oriented architecture and cloud computing environments, Chapter Geographically Distributed Cloud-Based Collaborative Application, IGI Global
10. Solomon B, Ionescu D, Litoiu M, Iszlai G (2011) Self-organizing autonomic computing systems. In: 2011 3rd IEEE international symposium on logistics and industrial informatics (LINDI), pp 99–104, Aug 2011
11. Solomon B, Ionescu D, Gadea C, Veres S, Litoiu M (2013) Self-optimizing autonomic control of geographically distributed collaboration applications. In: Proceedings of the 2013 ACM cloud and autonomic computing conference, CAC'13, pp 28:1–28:8. New York, NY, USA, ACM
12. Ashby WR (1954) Design for a brain. Wiley New York
13. Katabi D, Handley M, Rohrs C (2002) Congestion control for high bandwidth-delay product networks. *SIGCOMM Comput Commun Rev* 32(4):89–102

An Architecture and Methods for Big Data Analysis

Bogdan Ionescu, Dan Ionescu, Cristian Gadea, Bogdan Solomon and Mircea Trifan

Abstract Data production has recently witnessed explosive growth, reaching an insurmountable amount (larger than 4 ZB in 2013). This includes data sources such as sensors used to gather climate information, reports on household parameters, posts to social media sites containing digital pictures and videos, purchase transaction records, and cell phone GPS signals, to name a few. Not yet having more than an intuitive and ad hoc definition, big data is challenging the IT infrastructure of companies and organizations, forcing them to look for viable solutions leading to data processing such that enterprises can deploy a better business strategy. In essence, big data implies collecting, extracting, transforming, transporting, loading (ETL), classifying, analyzing, interpreting, and visualizing, among many other operations, on large amounts of structured, semi-structured, and unstructured data, in the order of a few petabytes per day, executed and terminated in critical time. This paper will introduce the architecture and the corresponding functions of a platform and tools implementing part of these challenging operations, while others are being obtained via composing elementary operations. The architecture is built around a distributed network of virtual servers called “agents,” which can migrate around a network of hardware servers whenever available resources are provided or created. A control center makes decisions on moving the agents based on the availability of resources when needed. An example from the telecommunications industry will illustrate how the platform is applied to this domain of big data.

1 Introduction

Everyday, an amount of 2.5 quintillion bytes of data is created around the world. At this rate, it is estimated that more than 90 % of the data in the world existing today has been created in the last 2 years alone. Recent reports of market research

B. Ionescu (✉) · D. Ionescu · C. Gadea · B. Solomon · M. Trifan
NCCT Laboratory, University of Ottawa, 161 Louis Pasteur Room B-306,
Ottawa on K16N5, Canada
e-mail: bogdan@ncct.uottawa.ca; ionescu@site.uottawa.ca

companies, such as International Data Corporation (IDC) [1], mention that there is a tremendous increase in the rate of data creation, which from a rate of production of 1.8 ZB (1.8×10^{21} B) per year in 2011 arrived at a rate of more than 4 ZB per year in 2013. A doubling of the amount of data every other 2 years was also predicted. It is no surprise that data-intensive computing, search, and information storage, all done in almost real-time, have generated a new trend in the computing landscape. The spread of cloud computing and data storage options at low or acceptable costs for hosting server farms, as well as the rush for interpreting large amounts of data for predicting the advent of events of interest for business, politicians, social behaviors, or endemics, all have changed the way that data was regarded and produced in the last decade.

“Big data,” as it was called, is being touted as a critical challenge. It includes the processing of data to obtain analytics results, as well as its management. The term first appeared in 2011 in a gartner report about emerging technologies [2].

Most definitions of big data focus on the size of data in storage, although a more comprehensive definition shall encompass the variety and the velocity of data being acquired and processed. Thus big data is defined merely by its volume, variety, velocity, and value—the four “V”s. Each of them has ramifications. The *volume* is defined by terabytes, records, transactions, tables and files; the *velocity* of dealing with large amounts of information can be defined as batch, near time (soft real-time), or real-time streams, while the *variety* is defined by the character of the data such as structured, unstructured, semi-structured, or all of the above, and the *value* is defined by the revenue or the results brought into the enterprise using a big data application.

The term “big data” was created to define the collection of large amounts of data in structured, semi-structured, or unstructured formats in large databases, file systems, or other types of repositories, and the processing of this data in order to produce an analysis and synthesis of the trends and actions in real or almost real-time. Out of the above amounts of data, the unstructured data needs more real-time analysis and bears more valuable information to be discovered, providing a more in-depth understanding of the researched subject. It is also the unstructured data which incurs more challenges in collecting, storing, organizing, classifying, analyzing, as well as managing.

The successes registered by Narwhal and its team, namely, the big data analytics used by the winner of the 2012 presidential elections in the US, demonstrated that it is not enough to have or host a huge amount of data; rather, there is a need to know how to use it, too [3].

Industries have implicated themselves in a strong competition for providing a big data solution which can take advantage of the high potential of big data. Tier 1 companies are having products which address the challenges above by providing products based on the popular Hadoop framework [4]. Many government agencies, especially within the United States, have announced major plans to accelerate big data research and applications [5]. Despite the availability of commercially available big data storage devices and tools available from Google, Facebook, Baidu, Taobao, and Cisco (among others), the field of big data is still relatively new and requirements for big data, as well as the analytics associated with it, are not yet

formalized. A good definition for big data is still being debated between main players in the field, with academia and the industry still discussing this subject. However, it is unanimously agreed that the value chain of big data consists of the following big categories of operations: data generation, data acquisition, data storage, and data analysis [6].

Many solutions for big data storage and processing have been experimented with. As such, permanent storage and management of large-scale disordered datasets, distributed file systems, and NoSQL databases are mentioned as good choices for approaching big data projects. Presently, there is a collection of technologies and tools available to experiment with various big data applications. Cloud computing infrastructures, Amazon AWS, Microsoft Azure, and data processing frameworks based on MapReduce, Hadoop, and Microsoft DryadLINQ, allow running domain-specific parallel applications. For example, Gunarathne et al. [7] used available cloud resources to assemble genome segments and reduce the dimension in the analysis of their chemical structure such that the analysis of 166-D datasets, which consisted of 26,000,000 data points, was accomplished.

This paper presents a cloud-based architecture and methods for a platform designed to acquire, index, collect, interpret, process, transport and store structured, unstructured, and semi-structured data in order to provide the user with a customizable platform that is able to extract data and information from large data sources, as well as stream various repositories and resources. The platform is easily programmed via a graphical language using simple concepts such as data source, data destination, data converters, and data transformers. These primitive concepts allow for the establishment of a data flow which starts from data sources and moves to storage locations through data analytics interpreters, the latter being included in the data transformer group. Initially, the platform is discovering and collecting data and then indexes it in order to locate it quickly. A Hadoop mechanism is used for indexing and location. The final goal of the platform is to present the user with the results of the data analysis in an easy-to-read format such that the user can engage in decision-making across many domains without difficulty.

The platform was designed to enable the following:

- indexing and classifying static and dynamic data from structured, unstructured, and semi-structured data repositories;
- mining through statistical identification and discovery of complex events through analyzing and predicting data evolutions from structured, unstructured, and semi-structured data repositories;
- integration and unification of large-scale data from disparate resources and streams;
- analysis while maintaining data integrity and data cleansing;
- controlling the cloud environment for accomplishing data auditing while reporting changes of data in the controlled repositories;
- scalability and elasticity on discovery of new data sources;
- effective and meaningful decision support;
- continuous quality control of results.

The remainder of the present paper is organized as follows: Sect. 2 is dedicated to a review of existing technologies for building big data. Section 3 briefly introduces the requirements which are at the heart of the big data platform architecture described in this paper. Section 4 outlines the proposed architecture for a big data platform and briefly discusses key functions of such a platform. The core of the big data platform is also presented in more detail. In Sect. 5, the architecture components are discussed in more detail. In Sect. 6, an application of the big data platform is given. Section 7 provides the conclusions of the paper.

2 Related Work

The globalization of the economy brought with it a huge amount of information which companies, at all levels of their structural and organizational complexity, had to digest in order to set-up a well-defined business plan, as well as marketing and production strategies. The immediate impact on the company IT infrastructure was overwhelming. The increasing data volumes of the early 2000s caused the storage and processing technologies to be stretched over their limits by the numerous terabytes of data, thereby resulting with a scalability crisis. Enterprises had to make sound and solid business decisions to cope with the big data avalanche, as data is nowadays the new raw material of business. Today, big data is a “must have,” and so are the corresponding hardware and software technologies which can deal with it. No longer ignoring such information, companies nowadays rely on the newly discovered facts from real-time big data analysis.

Big data projects were initially derived from decision support systems, which, in an industrial wording, are known as business intelligence applications. As a consequence, a large spectrum of commercial and open source tools and libraries have been built. On the other hand, academia has produced a rich theoretical basis for big data analysis using the strong theoretical background offered by statistics and operations research, as well as associated libraries that laid a solid foundation for data mining [8], data analytics [9], and decision-making systems [10]. One of the results of the R project (among other projects) was the generation of specific languages and models, such as the R statistical language [10] or the Predictive Model Markup Language (PMML) [11], which allowed researchers to combine statistical methodologies (along with ready-to-use packages) in order to process massive amounts of data collected from various repositories, eventually feeding the decision support system. Forced by the nature of its business, Google had to develop hardware and software infrastructure to deal with data discovery, collection, storage, and processing. On the software side, the MapReduce programming model [12] was designed and implemented. The Open Software movement reacted and produced Hadoop. The industry has also dedicated time and effort to produce big data platforms which enterprises can buy or pay to use on-the-cloud.

Tier 1 companies, such as EMC, Oracle, IBM, Microsoft, Google, Amazon, and Facebook, along with several startup companies, offer big data solutions. Big data is

presently one of the important strategic technologies. The US government produced their “Big Data Research and Development Plan” in 2012, along with a May 2014 study entitled “Big Data: Seizing Opportunities, Preserving Values” [5]. The European Community and Japan produced similar works and even the United Nations issued a “big data for development” report in which big data is seen as an efficient source of information for better protection and governing of the people [13].

Currently, the majority of big data projects, which are either financed by the industry or initiated in academic circles, rely on Hadoop. At the industrial level, Hadoop is used in applications such as spam filtering, network searching, click-stream analysis, and social recommendation. Companies including IBM [14], MapR, EMC, Cloudera, and Oracle offer commercial Hadoop execution and/or support, as well as parts or solutions for various applications. There is also a rich list of open source projects among which Hadoop is widely used [15].

Hadoop is an open-source software framework for storage and large-scale processing of datasets on clusters of hardware or virtual servers, partially inspired by Google’s MapReduce and Google File System (GSF) papers. Its framework consists of the following modules:

- Hadoop common, containing libraries and utilities of the framework;
- Hadoop Distributed File System (HDFS), a distributed file system that stores data on commodity machines, providing very high aggregate bandwidth across the cluster;
- Hadoop YARN, the resource management platform responsible for managing compute resources in clusters and using them for scheduling of users’ applications;
- Hadoop MapReduce, a programming model for large-scale data processing.

Hadoop modules were designed to be insensitive to failures. It has been successfully deployed by Yahoo, Facebook, IBM, EMC, Oracle, and other big data analytics providers. The Hadoop “platform” also consists of a number of related projects such as Pig, Hive, HBase, Spark, Drill, D3.js, and HCatalog, among others.

Hadoop is deployable in an on-site datacenter, as well as in the cloud. The Hadoop cloud deployment avoids companies being trapped in specific set-up expertise. The cloud solution of Hadoop is available from Microsoft, Amazon, and Google.

As big data analysis implies setting up a mathematical environment for the application of statistical analysis methods (among which one can also include prediction), the R project [10] was developed. R is a language and environment containing modules for linear and nonlinear modeling, classical statistical tests, time-series analysis, classification, clustering, and graphical display of results. R provides facilities for data manipulation, calculation, and graphical display, including:

- an effective data handling and storage facility,
- a suite of operators for calculations on arrays, in particular matrices,
- a large, coherent, integrated collection of intermediate tools for data analysis,

- graphical facilities for data analysis and display, and
- a programming language which includes primitives for conditionals, loops, user-defined recursive functions and input and output facilities.

The R system was written in R, a language which combines C, C++, and Fortran assets in the statistical analysis of real-time data. The R language was designed as to allow users to add functionality on an as needed basis for each application component.

PMML [11] is an open source XML-based language designed to provide the means to describe models related to predictive analytics and data mining. PMML was developed to allow applications to define and exchange models produced by data mining and machine learning algorithms. It supports common models such as logistic regression and feedforward neural networks. Models are described via an XML Schema. One or more mining models can be contained in a PMML document. A PMML document is an XML document with a root element of type PMML and is a valid XML document.

Other languages such as WEKA [8] allow users to build state-of-the-art machine learning algorithms and data preprocessing tools. In combination with KNIME [9], it allows for building using visual assembly of data and data mining pipelines.

The combination of WEKA and KNIME provides a solid platform and tools for visually building complex and massive data analysis applications. Apache Mahout [16] is another Java-based open source project dedicated to the creation of a machine learning library, to be used in conjunction with Hadoop, thereby providing a solid basis for algorithms for data clustering, data classification, pattern mining, dimension reduction, and more.

A comprehensive survey of big data and related technologies is given in [6].

3 Requirements for the Architecture of a Big Data Platform

Increasing amounts of data flooding the IT infrastructure have created serious challenges in data acquisition, storage, management, and analysis. As relational databases only apply to structured data, traditional RDBMSs could not handle the huge volume and heterogeneity of big data. As big data applications encompass a complex combination of computing and networking infrastructures, a main set of requirements will consider the implementation of big data infrastructures so as to provide cost efficiency, elasticity, and smooth upgrading/downgrading solutions.

Based on the result analysis of several use cases, the following series of functional requirements have been determined as being crucial for the implementation of big data platforms:

- (a) Heterogeneous data discovery and collection tools: the platform has to be capable of programmatically connecting with real-time data flows produced by

databases, file systems, web pages, web sources, web services, emails, HTTP and FTP servers, data streaming sources, and specific applications such as CRP, ERP, and others.

- (b) Data unification and integration tools: the platform must be able to access, collect, unify, cleanse, and store data from multiple and different data sources, and to deal with inconsistent or noisy data. The platform shall implement data preprocessing tools which shall unify the data and integrate the various data sources.
- (c) Data indexing, tagging, mining, and classification tools: the platform has to be capable of providing tools for data indexing, both statically and dynamically, to extract patterns, and to classify the information contained in massive amounts of data.
- (d) Statistical analysis tools: the platform must support different data types to be fed to statistical data analysis algorithms for calculating key statistic and stochastic parameters and provide results from a set of statistic functions such as the correlation coefficients, state estimation and prediction, and other statistical and stochastic analysis.
- (e) Self-provisioning and self-optimization: the platform shall implement at least the self-provisioning and self-optimization functions of the set of self-management functions of an autonomic computing environment, as the complexity of the computing and networking infrastructure of any big data platform can very quickly reach the limits of human manageability.
- (f) Interactive exploration: the platform has to provide a set of visualization techniques for visual analysis and easy interaction with the data.
- (g) Intelligent decision support: the platform shall have the ability to incorporate/plug-in algorithms and corresponding mechanisms for domain-specific data interpretations required by the decision-making systems.
- (h) Manual operation: the platform shall provide facilities for manual analysis, semiautomated decision support or fully automated systems from case-to-case.

The nonfunctional requirements shall include scalability and real-time or near real-time performance.

4 An Architecture for a Big Data Platform

This section describes the architecture of a big data platform which fulfills the requirements listed in Sect. 3. The architecture is sketched in Fig. 1.

The architecture shown in Fig. 1 has, at its core, a data mining, monitoring, and management platform henceforth referred to as “M3Data”. M3Data provides a series of components which are interconnected by the big data platform.

As represented in Fig. 2, M3Data is endowed with connectors for various sources of information (either structured, semi-structured, or unstructured). It collects the data and puts it in a data flow object. It performs various processing

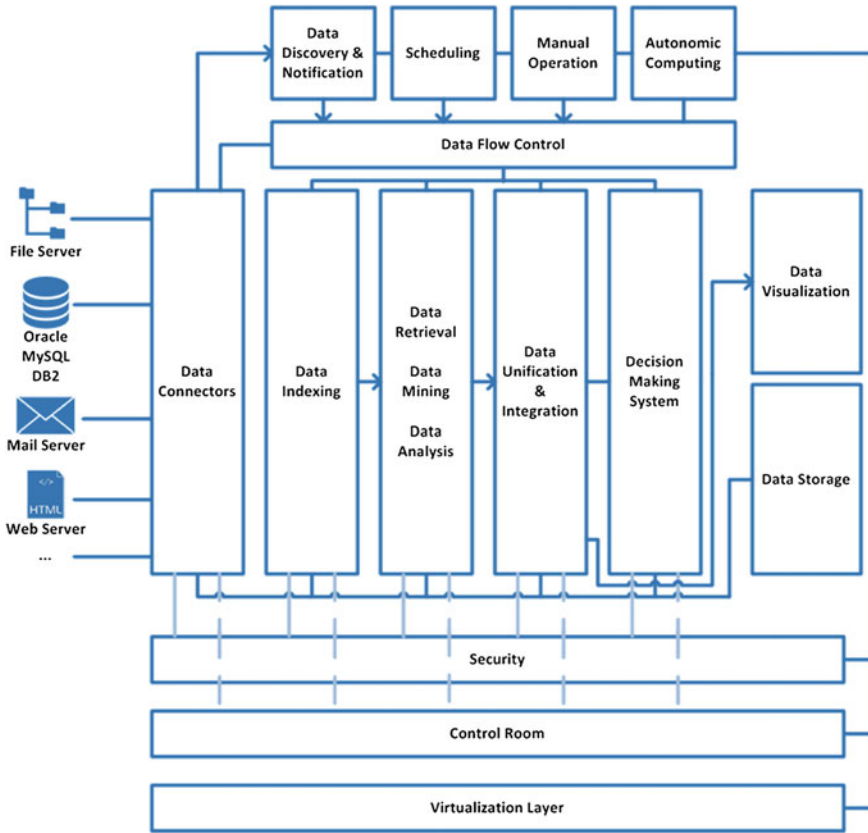


Fig. 1 Architecture of big data platform

operations on the data, from mining and analytics to extraction, integration, cleansing, and distribution of it. During all of these processes, it is monitoring and logging all modifications of the data.

The architecture of M3Data consists of six layers of software packages, as shown in Fig. 3.

The layers of the core of the big data platform assure the following functionality, all of which are essential to any big data application, and thus to the big data platform presented in this paper:

- (a) platform control: all control functions are implemented in the control layer of M3Data;
- (b) platform security: specifically, M3Data uses the role-based access control security principles implemented in a security layer, which can also be coupled with an external security mechanism;
- (c) platform communication: the communication layer implements all protocols needed to communicate with the data sources and inside the building blocks,

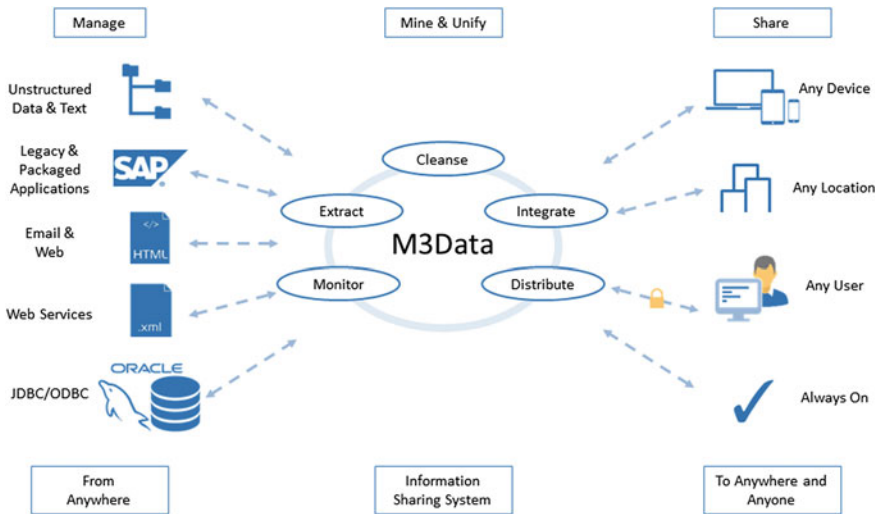


Fig. 2 What M3Data Is

- referred to as “agents,” of an M3Data application, as well as the internal platform communications, like the communication between agents for notification, processing, and control of data and the platform;
- (d) platform processing: a series of mining, unification, and analysis of the data are included in the processing layer. The platform implements also algorithms specific to transactional capabilities such as the roll-back of data flows from all destinations and sources.
 - (e) platform event notification: M3Data notification layer implements functions for trapping, recording, and passing to the control and processing layer all events generated by the database triggers, OS events, emailers, etc.
 - (f) data transfer: data transfer from source to destination among all data resources of the platform is implemented in the data transfer layer.
 - (g) data storage: the platform implements all basic functions for creating, retrieving, modifying/updating, deleting, and searching large amount of data

The above layers all concur to the collection, transformation, and transfer of data from source to destination.

One of the key modules of M3Data is a graphical programming language which allows users to cut the development time by an order of magnitude. This is extremely useful in cases when large sources of data lie onto a very large distributed system with a very large number of applications such as the case of health care systems. This functionality is embedded in the Data Flow Programming Studio (DFPS) component, which contains all the graphical programming primitives and operators needed to ease the programming burden of designing and implementing a specific big data application. The user therefore only needs to translate the business

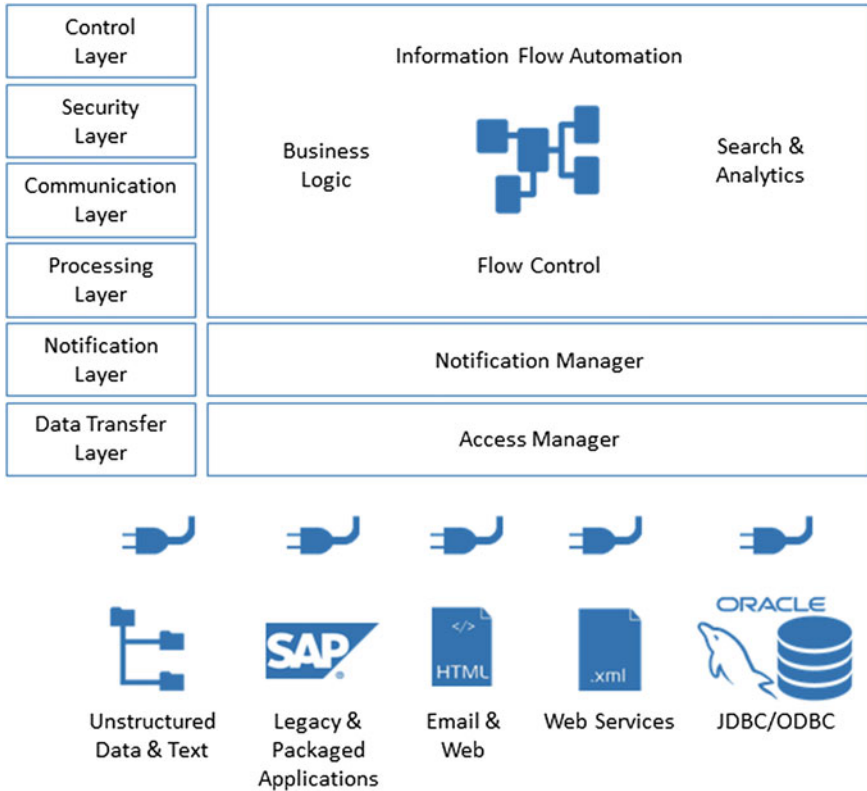


Fig. 3 How M3Data works

rules of the application into a data flow describing the path which the data has to traverse while various business tasks of the application run and then implement the business logic in a DFPS diagram. The look and feel of the iconic programming language, called Data Flow Programming Language (DFPL), is given in Fig. 4.

The graphical language was implemented by following the rules and premises of graph grammar theory. The data flow control is intrinsically contained in a DFPS diagram. A diagram can be built using the following block diagram:

- (a) resource blocks, which are iconic representations for the data repositories which sources of data for the overall application. The supported resources are DB2, Informix, any JDBC database, MSSQL, Oracle, Lucene, as well as web services, IMAP, and files from a file system. Any of these resources can be either source or target for the data flow.

The platform provides support for other repositories by extending its integration tools via a plug-in implementation framework

- (b) converters, which can be simple or cycled. A simple converter implements a very simple data manipulation operation, while a cycled converter defines a

5 Main Components of the Big Data Platform

This section presents a high-level overview of the main components of the architecture of the big data platform, as previously introduced in Sect. 4. Namely, it describes components for data flow control, data connectors, data discovery, data notification and scheduling, data indexing and search, data mining and analysis, data unification and integration, decision support, data security, data control, data storage, data visualization, and autonomic computing.

5.1 Data Flow Control

As big data platforms are required to constantly manipulate massive amounts of data (where the data often has a complex structure), the platform has to be endowed with tools that permit the administrators and users to program it in a very flexible way, thereby allowing them to interact with the data flow at every step of the operations which the data has to experience. Data is collected via the connectors of the platform and is then prepared to be analyzed, stored, and displayed. The DFPS diagrams therefore provide arrows that originate at the source of data and point toward the target repository of the data, and link together various blocks of the diagrams.

However, when data synchronization has to be done among many repositories, it is sometimes possible for two or more databases or repositories to hold the same data and which therefore have to be kept synchronized while data is changed in one of the databases. This is made possible via triggers and the logic around them. Using the DFPS, the following big data operations can simply be inherited from the library of implemented blocks:

- (a) accessing,
- (b) cleansing and processing,
- (c) distributing and migrating,
- (d) monitoring and synchronizing,
- (e) unification and reporting,
- (f) monitoring, notifying, and scheduling,
- (g) searching and retrieving,
- (h) classifying,
- (i) logging.

Based on the above existing diagrams, more complex diagrams for big data processing can be built as shown in Fig. 5.

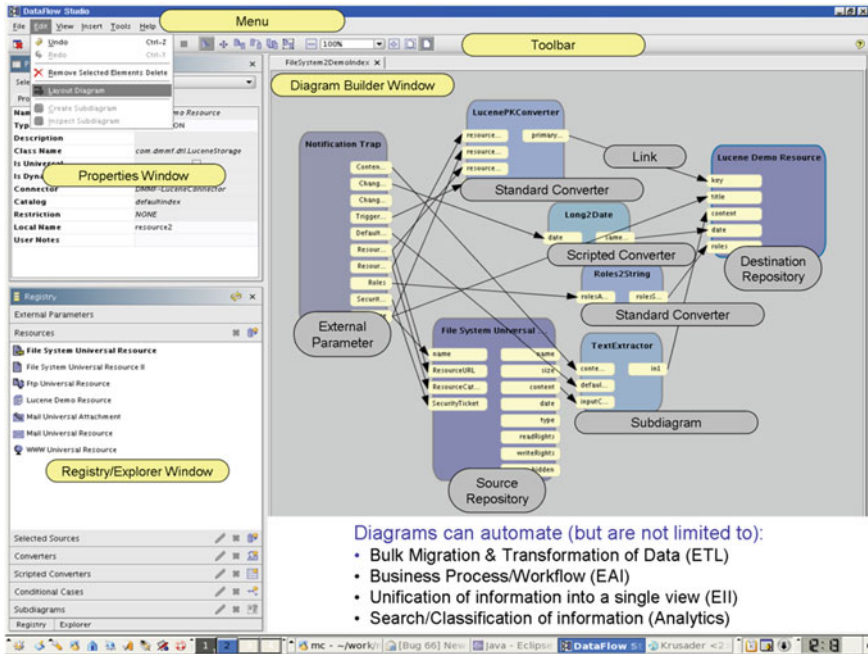


Fig. 5 Using the data flow programming studio to build complex diagrams

5.2 Data Connectors

Big data applications require a platform that is properly connected to various sources of information which are to be analyzed by the analytics module of the platform such that predictions can be made in regards to the business course that an enterprise has to adopt in order to be successful in a global competitive environment. A big data platform therefore has to provide all the connectors to the above sources of information such that any new information is acquired and interpreted in real-time or near real-time.

The big data platform described in this paper contains connectors to various databases such as Oracle, DB2, Informix, Sybase, and other databases which have Java-based APIs. A series of connectors are provided for additional legacy databases, some of which were programmed in the database’s native programming language (usually C). There are also connectors to file systems specific for Windows, Linux, and Unix/Solaris/AIX operating systems, as well as for email servers, web servers, web services, FTP servers and connectors for CRM, ERP, and BI applications. Any other connectors can be created and inserted in the data flow diagram, where they will reside at the source level of the diagrams, as was shown in Fig. 4.

5.3 Data Discovery, Notification and Scheduling

The platform contains modules which are in charge of data discovery of all existing sources of data, such as data streamers, file systems, databases, emailers, HTTP or FTP servers, and more. Connectors are available in the DFPS as basic blocks and are programmed using simple drag-and-drop operations on the block symbol of a diagram. The platform has to be authorized to connect with the sources of data using corresponding access credentials to the database, file system, emailer, or other data source. A notification system prompts the platform when new data has been inserted in the repository and indexes it accordingly. The notification can trigger an action for validating the data modification or can place the notification and data in a batch mode. The latter functionality is contained in the Scheduling module of the platform.

A notification diagram can be used in the context of any data source and destination to trigger a runtime action of the big data platform functions in regards to unification, mining, analytics, and others. This is summarized in Fig. 6.

5.4 Data Indexing and Search

The platform has powerful indexing capabilities and provides a search engine for crawling and indexing the massive data repositories supported by the big data

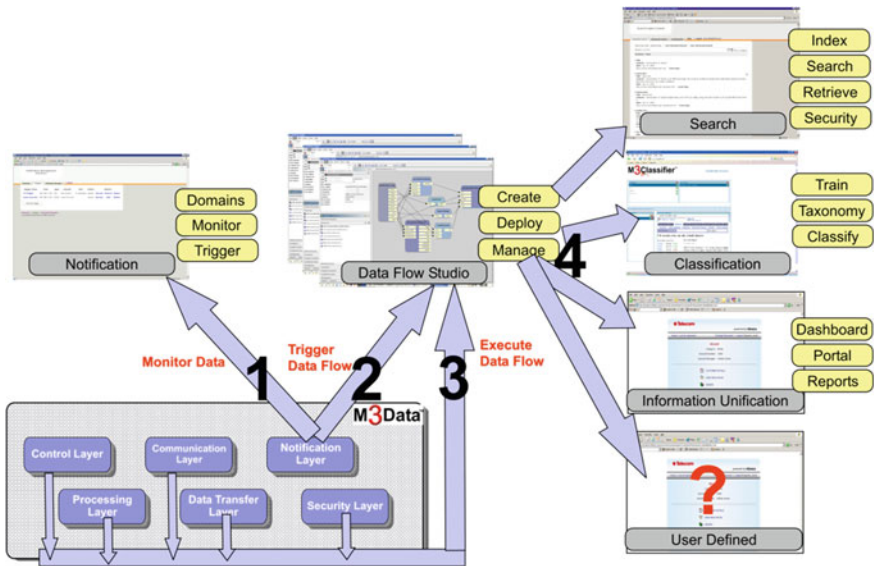


Fig. 6 Trigger a notification on a big data application; an example

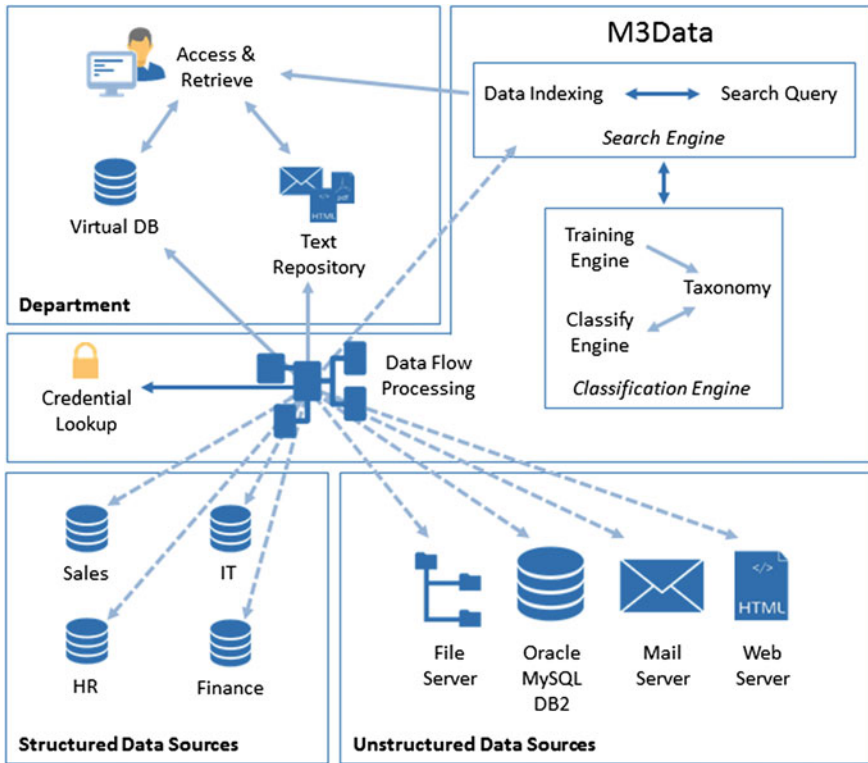


Fig. 7 Data indexing and search module

platform. The indexing and search engine provides real-time web-style full-text search, as well as more advanced SQL-like querying capabilities. The indexing engine allows for more complex indexing of the data which accelerates the search and helps in the data classification. Data from distributed heterogeneous relational databases is retrieved along with other types of data such as files, web pages, and emails. It is then indexed and displayed as needed based on search inputs or automated reports. Figure 7 illustrates the indexing and search features of the big data platform. Data can be also indexed using multiple indexes which can be customized to support whatever combination of fields, types, and related content is need.

5.5 Data Mining and Analysis

Based on the platform’s flexible search engine, a large variety of data can be inspected and explored for hidden information. The platform is capable of combining SQL-based searches and results, providing flexible search with support for

partial matches. In the case of partial matches, the results are statistically classified according to the confidence factor obtained.

The platform allows to create multiple and customized indexes in order to adapt the search solution to the specific needs of the data mining strategies. In this way, the platform provides for high flexibility in selecting and tuning the search on particular queries and search strategies.

5.6 *Data Unification and Integration*

The platform provides tools for the unification and analysis of massive amounts of data culled from a variety of structured, semi-structured, and unstructured data sources. For unstructured data, an automatic XML schema matching tool is provided. At the XML level, a transformation of the XML schema takes place automatically for unifying data from two different text forms. For example, column items are mapped semantically into each other using a rule-based mapper. If a similarity of the items defined in the two XML description of the form are discovered, uniform values are produced (e.g., for salutations, name suffixes, street abbreviation, etc.). The unification tool of the platform is designed to be flexible in terms of the addition of new *transformer* blocks in the data flow programming diagram (Fig. 4). The functionality of these new blocks can be programmed in Java or C/C++. By following the above procedures, WEKA-style mining modules and elements of the R language were integrated in the system.

5.7 *Decision Support*

The platform contains a Business Rule Management System (BRMS) with a forward and backward chaining inference-based rules engine. The BRMS module is based on Drools, which implements the Rete algorithm, and is a component of the JBoss Application Server. JBoss was used as the platform's distributed Java middleware. The decision support system of the big data platform presented in this paper is therefore based on the Drools version included in the JBoss community edition server. This version of JBoss contains the Drools Guvnor (the business rules manager), the Expert (the rule reasoning engine), the Flow (process/workflow), the Fusion (event processing/temporal reasoning) and the Planner (the automated planning).

5.8 *Data Security*

The security module of the platform implements a restricting system to control access for authorized users via RBAC. The platform allows users to access the

information in the system if the users belong to a certain group of users, which is defined by certain roles for various job functions. The platform allows for the creation of roles, role assignment, and role and permission authorization. RBAC allows users to have differentiated access to the objects of information. If the role of the user does not have role/access privileges to obtain a specific object of information, the object is defined as nonexistent for that user.

RBAC is also applied on various operations required by various platform services, some of which may need elevated privileges, e.g., updating an index versus searching it.

5.9 Data Control

A necessary module of a distributed system is related to the control of all aspects of storing and executing various actions by the platform on the distributed data. This resource management module is responsible for managing compute resources in clusters. It allows platform administrators to install, deploy, and upgrade all platform components. The control module keeps track of computational processes, their distribution in the system, as well as automatically redistributing them if some processes do not terminate in due time, or are interrupted. It allows platform administrators and application designers to locate, in real-time, the components (agents) of the big data application and to get information about their state. It also records all operations that take place in the system and logs them in a Journalizer for further investigation. In this way, users can audit all data movement and transformations in a big data application as needed. Figure 8 shows the main components of the control center of the big data platform.

The following components make up the control center package:

- The deployment component, which provides tools for the installation, deployment, and upgrading of the Big Data Platform at run time;
- The security module, which was described in Sect. 5.8;
- The queue management module, which keeps track of all processes, and their status, and implements resilience methods such that the big data platform is reliable and avoids failures;
- The Journalizer module, which keeps logs of all big data platform operations for use in auditing the activities of the big data platform and for debugging the big data functionality.

5.10 Data Storage

Although a very important component of a big data application, the data storage module is conditioned by the existence of the necessary hardware foundation that

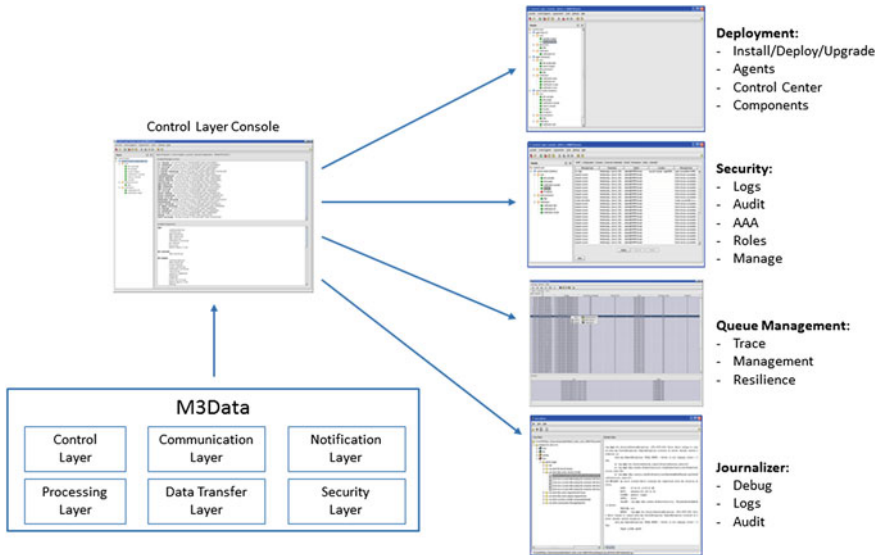


Fig. 8 M3Data control center

can handle very large amounts of structured, semi-structured, and unstructured datasets while remaining capable of scaling in real-time in order to keep up with the growth of the data volume. It must also provide the Input/Output Operations Per Second (IOPS) necessary to deliver data to the mining/analytics tools. This module comprises vast amounts of commodity servers with direct-attached storage (DAS). Redundancy is at the level of the entire compute/storage unit, and if a unit suffers an outage of any component, it is replaceable in its entirety (data included). Such a hardware/software combination is typically running Hadoop, along with NoSQL or cassandra as analytics engines, and typically have PCIe flash storage instead of (or in addition to) regular hard drives so as to keep storage latency at a minimum. Due to the large volume of data, there is usually no shared storage in the configuration of all storage units.

A recent trend in the industry has been to use *hyperscale* computing environments which are very well known from the implementations of the largest web-based operations of Google, Amazon, Facebook, Apple, and others.

An alternative for big data storage is represented by a *scale-out or clustered NAS*. It uses parallel file systems that are distributed across many storage nodes. These systems can handle billions of files without the performance degradation experienced with ordinary file systems as they grow.

Another storage unit format which can handle a very large numbers of files is *object storage*. Object storage tackles the same challenge as scale-out NAS, namely, that traditional tree-like file systems become unwieldy when they contain a large number of files. Object-based storage gets around this by giving each file a unique identifier and indexing the data and its location. Rather than the typical

kinds of file systems, this method is more similar to how the internet's Domain Name System (DNS) operates. Object storage systems can scale to very high capacity and large numbers of files (in the billions), and are therefore another option for enterprises that want to take advantage of big data. Object storage, however, is a less mature technology than scale-out NAS.

In general, big data storage needs to be able to handle large capacities and to provide low latency for data retrieval, thereby feeding the analytics module with data.

5.11 Data Visualization

Any big data platform has to provide a visual conclusion to the data extracted and interpreted by the analytics module. Data visualizations are sets of valuable tools in a variety of settings, allowing the creation of a visual representation of data points, reports on progress, or even the visualization of concepts for the customer segments. This module is also external to the big data platform whose architecture is presented in this paper. By taking advantage of modern web-based graphic toolsets, open source projects (as well as companies that have this as their business model) exist that offer flexible visualization tools that are capable of handling big data. Another model for big data visualization is represented by interactive data visualization. Interactive visualization addresses the use of computers and mobile devices to drill down into charts and graphs for additional details, thereby interactively (and immediately) changing the data displayed, as well as the processing flow.

The big data field benefits from its own visualization tools and patterns. The platform, however, can integrate with any of the existing dash-boards or infographic tools presently available, as well it can be endowed with a specific interface as in the examples given below.

5.12 Autonomic Computing

Autonomic computing is one of the vital modules of the architecture. Autonomic computing is now a more mature technology and mainly addresses problems related to large and very large systems. It is meant to apply a supervised control of the computing environment. Autonomic computing is organized in a form of a control system for real-time processes. Using a control loop, it implements functions such as self-provisioning/configuration, self-healing, self-optimization, and self-protection, effectively simulating the behavior of a system administrator.

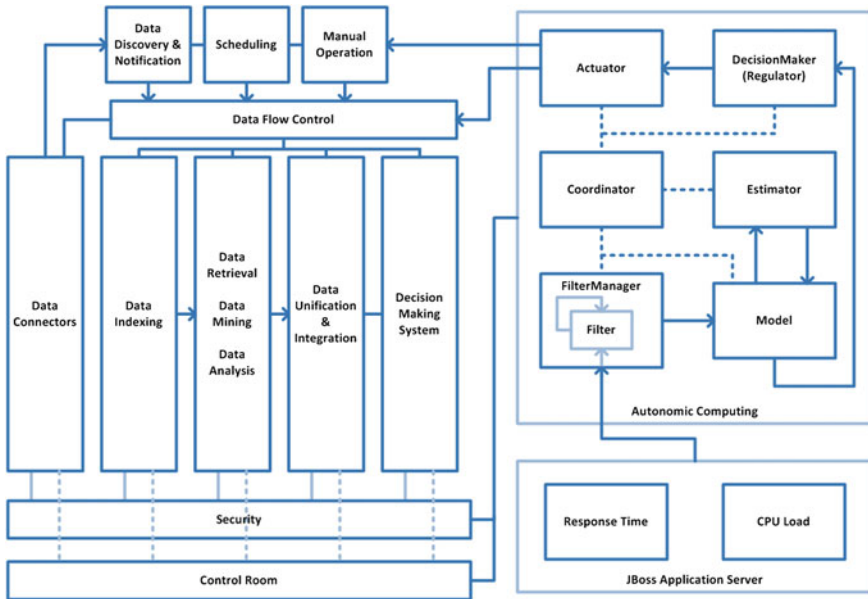


Fig. 9 Autonomic computing environment for a big data platform

The autonomic computing module of the platform described in this paper is based on an autonomic computing platform proposed in [17]. The IT infrastructure of the big data platform is the controlled object of the autonomic computing loop shown in Fig. 9, which resolves the automated provisioning of the system over the virtual layer, taking into account constraints related to the optimal usage of computing resources, while the big data platform is resolving external requests.

In the big data platform of this paper, the autonomic computing architecture is mapped into a real-time control loop whose elements or blocks are transducers, which include software transducers for CPU load, task response time, or think-time, all of which are provided by the middleware application server. The central decision-making system of the autonomic computing module makes decisions based on state estimation and resource availability. A controller which establishes the opportunity of provisioning yet another copy of the whole big data server, or using another computing resource for an agent of the big data platforms, transmits this decision to an actuator which contains the entire set of deployment and configuration via regular expressions and which puts these commands into an execution list. Through the above process, the autonomic computing applied to the big data architecture presented in Fig. 1 takes care of the automatic provisioning and of the optimization of the resource usage of the big data application.

6 Applications of the Big Data Platform

In a typical application, any big data platform has to provide services for three types of users: the big data platform administrator, the big data architect and/or designer, as well as for the final user/consumer of the big data platform results (who usually is not a savvy computer professional). This is represented in Fig. 10.

The first deployment of the various components of the big data platform presented in this paper is done by the administrator of the Platform, as shown in Fig. 11. From that point on, the Autonomic Computing System takes control of the entire operation of the system in cooperation with the M3Data internal mechanisms, which take care of the distribution of agents and of processes within the entire distributed system onto which the big data platform is deployed.

A test deployment of the big data platform was created for a military system which implemented complex data acquisition, indexing, retrieval, unification, and analysis of data collected from a series of databases, documents from a specific file system, emails, and web services. This deployment is summarized in Fig. 12.

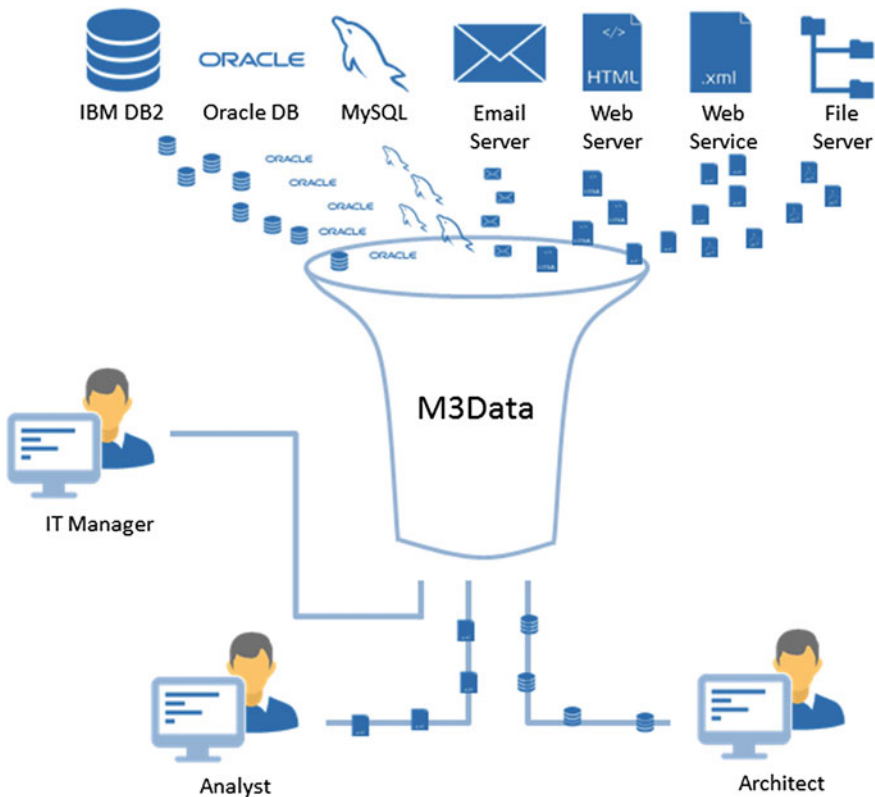


Fig. 10 M3Data users

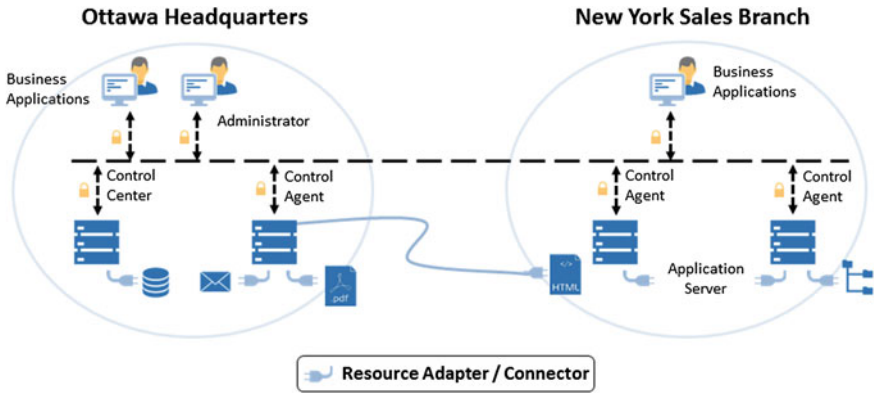


Fig. 11 Deploying a big data platform

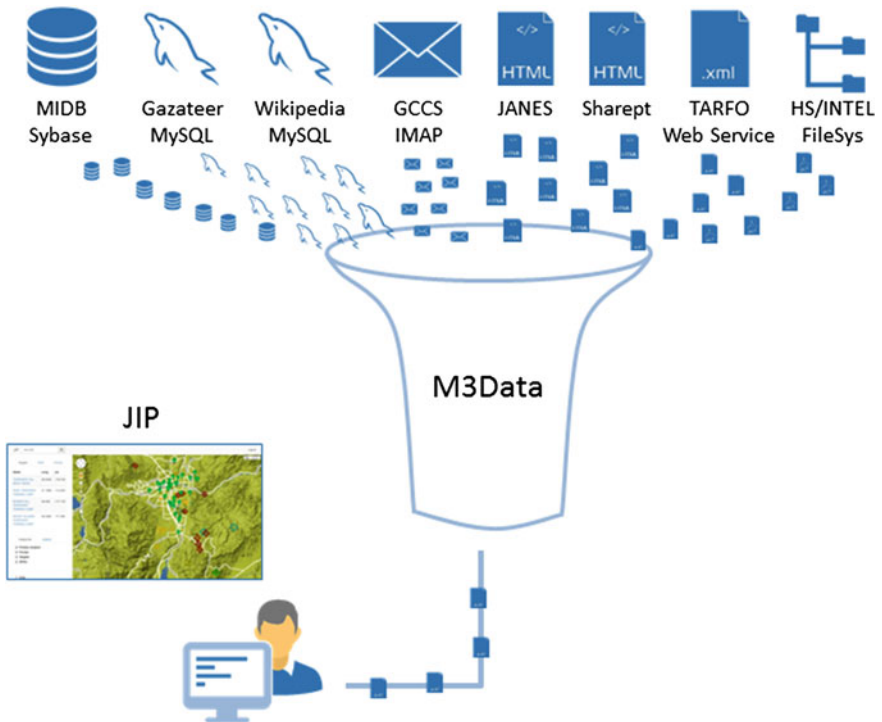


Fig. 12 An application of the big data platform in the military domain

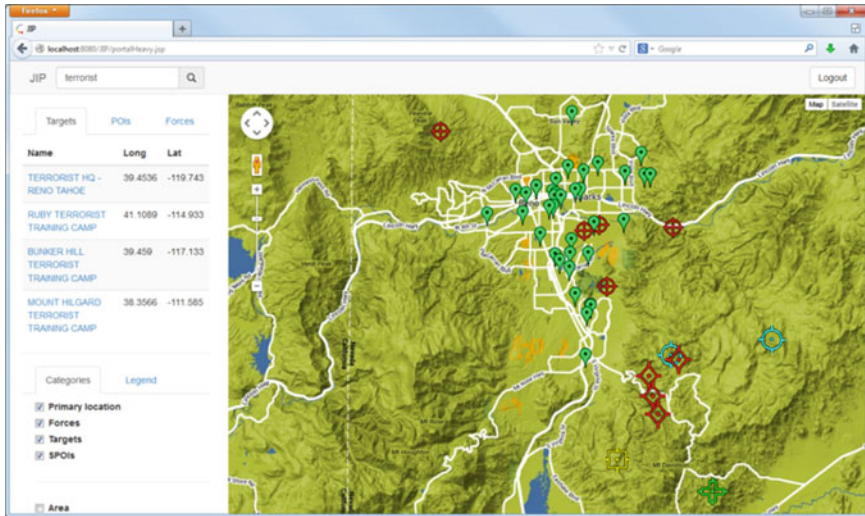


Fig. 13 Visualizing the results of a big data application

The visualization of the results obtained from the big data application is overlaid on top of a geographic map as shown in Fig. 13.

7 Conclusions

In this paper, the requirement and corresponding architecture for a big data platform have been introduced. The resulting platform is built around an information sharing platform and comprises data collection components, data processing, analysis, as well as transport and visualization tools. The platform is also endowed with a graphical programming environment, a control center of the distributed system application, and automated provisioning and optimization systems. The graphical programming environment allows users to interactively modify the functionality and work flow of various modules and functions of the big data platform, thereby making it applicable for a series of applications which require collecting massive amounts of data from which hidden data has to be inferred and visualized. For an example deployment, the big data platform was applied to the military domain. The flexibility, ease-of-use, robustness, and other characteristics of the big data platform introduced in this paper are therefore of significant value as big data continues to grow in importance in the IT industry.

References

1. Reinsel D, Gantz J (2011) Extracting value form chaos. <http://www.emc.com/collateral/analyst-reports/fdc-extracting-value-from-chaos-ar.pdf>. Accessed Feb 2015
2. B. M. 2011 hype cycle special report (2011) <http://www.gartner.com/newsroom/id/1763814>. Accessed Feb 2015
3. Amazon. AWS Case Study: Obama for America Campaign 2012 (2012) <http://aws.amazon.com/solutions/case-studies/obama>. Accessed Feb 2015
4. White T (2009) Hadoop: the definitive guide. 1st edn. O'Reilly Media, Newton
5. Podesta J, Pritzker P, Moniz E (2014) Seizing opportunities, preserving values, 1st edn. White House Publishing, Washington
6. Chen M, Mao S, Liu Y (2014) Big data: A survey. *Mob Netw Appl* 19(2):171–209
7. Gunarathne T, Wu T-L, Choi JY, Bae S-H, Qiu J (2011) Cloud computing paradigms for pleasingly parallel biomedical applications. *Concurr Comput: Pract Exp* 23(17):2338–2354
8. Hall M, Frank E, Holmes G, Pfahringer B, Reutemann P, Witten IH (2009) The weka data mining software: an update. *SIGKDD Explor Newsl* 11(1):10–18
9. Beisken S, Meinel T, Wiswedel B, de Figueiredo L, Berthold M, Steinbeck C (2013) Knimecdk: workflow-driven cheminformatics. *BMC Bioinf* 14(1):257
10. R. D. C. Team (2011) R: a language and environment for statistical computing. R Development Core Team, 1st edn
11. PMMLorg. Pmml 4.2—general structure (2014) <http://www.dmg.org/v4-2-1/GeneralStructure.html>. Accessed Feb 2015
12. Jeffrey D, Sanjay G (2004) Proceedings of usenix osdi '04: Operating systems design and implementation. In: ICSOC, pp 107–111, Oct 2004
13. Big Data for Development: Opportunities Challenges (2012) <http://www.unglobalpulse.org/projects/BigDataforDevelopment>. Accessed Feb 2015
14. Eaton C, Deutsh T, Deroos D, Lapis D, Zikopoulos, P (2012) Understanding big data, analytics for enterprise class; hadoop and streaming data. McGraw-Hill, 1st edn 2012
15. Hadoop (2015) Hadoop Wiki: PoweredBy <http://wiki.apache.org/hadoop/PoweredBy>. Accessed Feb 2015
16. Apache. Apache Mahout Project (2014) <https://mahout.apache.org/>. Accessed Feb 2015
17. Solomon B, Ionescu D, Litoiu M, Mihaescu M (2007) Towards a real-time reference architecture for autonomic systems. In: SEAMS '07: proceedings of the 2007 international workshop on software engineering for adaptive and self-managing systems, pp. 1–10

Process Mining Functional and Structural Validation

Maria Laura Sebu and Horia Ciocârliu

Abstract Current study proposes solutions for functional and structural validation of business process models extracted after mining the event log dataset with several process mining algorithms. Structural validation (verification) assesses the quality of the business processes using conformance analysis techniques and computed statistical results. Cross-validation for structural validation is also presented as a methodology used for evaluating business processes. Furthermore we propose extending verification of process models with functional validation with the scope of aligning business processes with business objectives. Functional validation starts with process requirement definition, split of process requirements on clear use cases, and generating event log data capturing the use case functionality. Functional validation is applied on real event log data generated during one software release in automotive industry, tools development area. Structural and functional validation techniques are captured in a proposal for a framework.

Keywords Process mining · Functional validation · Conformance analysis · Process discovery

1 Introduction

Business process management (BPM) includes a set of techniques and methods designed to produce better processes. Business processes as the base in any organization are composed of all the activities executed inside an organization with the scope of producing business results. BPM takes independent processes and

M.L. Sebu (✉) · H. Ciocârliu
Computer and Software Engineering Department, Politehnica University
of Timisoara, Timisoara, Romania
e-mail: laura.sebu@student.upt.ro

H. Ciocârliu
e-mail: horia.ciocarlie@cs.upt.ro

transforms them into flexible, orchestrated business services that work together to create substantial business value.

Process analysis as the first important phase of BPM includes discovery of business processes. Once the business process is available, further analysis could be performed with the scope of redesigning the business process by correcting possible flaws and enhancing the process models. Identifying the most consuming activities, bottlenecks, rework, and obsolete activities are possible actions performed with the scope of improving business processes and increasing the quality of the business results. After the improvements are put in practice, the organization is able to measure the progress of the enhancements proposed in the monitoring phase. Management of improvements and full process automation represents the last phases in BPM lifecycle as presented in Fig. 1.

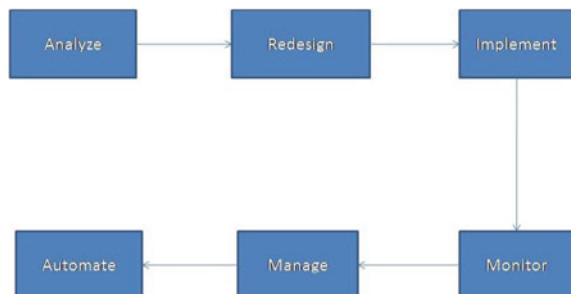
As several process models could be available such as the ones retrieved in the analysis phases or the ones resulted after performing corrections and enhancements, the identification of the most suitable one for accomplishing business objectives becomes a priority. We propose an approach for validating the most suitable process model from structural perspective, how compliant the model is with the event log dataset and from functional perspective, black box validation, if the business expectations are achieved.

A good BPM solution put in place inside an organization offers functionality to reduce costs by performing the management of processes automatically. BPM allows the process analyst to correctly model and iteratively improve the business process.

The resulting systems constructed on business process models are called process-aware management systems (PAIS). A PAIS can be defined as a software system that manages and executes operational processes involving people, applications, and information sources based on process models [1]. PAIS systems are based on abstractions of process definition. Execution is automated and directed by process models. If process models are not available as abstraction, process mining techniques could be used to extract them.

Process mining includes techniques and tools for discovering, monitoring, and enhancing process models used inside an organization [2]. Process mining as abstract is part of the process modeling and analysis area and uses data mining to obtain results. Data recorded during the execution of a process is used to extract

Fig. 1 Business process management phases



knowledge: discover real process models, organizational structure, and additional information about internal processes.

Complex organizations managing complex business processes are the perfect candidate for process mining techniques. Due to the complexity of the results, validation of the resulted process models is of critical importance. This would increase the confidence in the resulting process models and could aid identifying the areas which need corrections or redesign. This theoretical approach for the validation in PAIS is proposed for implementation in a functional and structural validation framework described in Sect. 4.

The illustration of this approach is performed by considering a software development process, the change control board process model used in several organizations and described and analyzed in [3]. A component of the software configuration management (SCM) in charge of handling changes required by users of different types (change requests, feature requests, problem reports, and information requests) is called change control board (CCB).

For exemplification, process mining discovery algorithms are applied on a real event log dataset created during one release of a software product in automotive industry.

The current study uses implementations of process mining tools and methods captured in ProM Framework 6.3, an academic project of Eindhoven Technical University. ProM provides a wide variety of algorithms and supports process mining in the broadest sense [4]. It can be used to discover processes, identify bottlenecks, analyze social networks, and verify business rules.

2 Process Mining

PAIS systems are constructed on process models. Process mining area solves the problem of the unavailability of process models. Data available from process tracking systems is used to extract knowledge: real process models, organizational structure, and additional information about internal processes.

Process mining could be split into 3 major phases [2] resumed in Fig. 2 [5].

First phase, data preparation, includes the actions performed to prepare the input for process mining algorithms. Input data could be provided by different sources in different formats. In this phase, the data must be transformed into extensible event stream (XES) format recognized by process mining implementations available on the market. XES data is flexible, being able to capture event log data from any background, it provides a simple way of representing the information, and it is



Fig. 2 Change control board process

transparent, intuitive, and extensible for specific domains. Due to these advantages, XES becomes the standard for process mining event log data representation [6]. Once the input data is available, the next step is defining the objectives of the process mining analysis: discovery of business process, analysis of business process, performance improvement, identify bottlenecks, and identify the most time consuming activities (Fig. 3). Once the objectives are stated, the dataset could be adapted to increase the visibility of the targets. Filtering after specific values of attributes is one technique used for this purpose.

As soon as the event log dataset is prepared and the targets for the analysis are identified, in the second phase, pattern discovery, the process mining algorithms are applied on the input data. Several mining algorithms for extracting process models are currently available on the market in different process mining implementation. Assessing the quality of the obtained process models from functional and structural perspective is the subject of the current study.

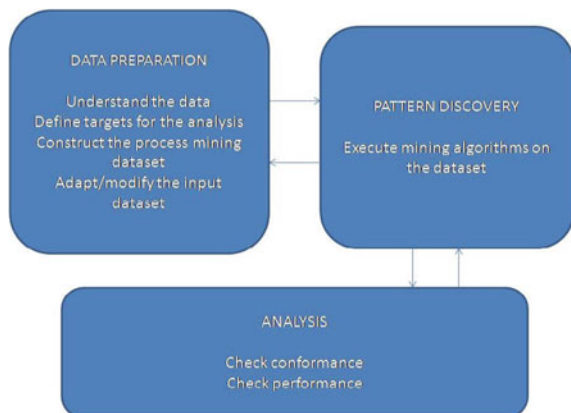
Once the most suitable process model is available, an analysis of the results could be performed further. This includes checking the statistical results for calculating process performance indicators, verifying the conformance of the resulted process model, retrieving other relevant information internal to organizations, and identifying bottlenecks.

Process Mining operates with the following concepts [5]:

- A process is an abstract representation of a set of activities logically ordered with the scope of accomplishing a business objective
- An event corresponds to an activity executed in the process and is composed of attributes with specific values
- Events are linked together in cases

Event log dataset represents the start point for mining from different perspectives [2]:

Fig. 3 Process mining phases



- Process perspective focused on identifying all possible paths an item could follow to reach a close state
- Organizational perspective focused on checking which is the resources involved in the activities and how they interact
- Case perspective focused on analyzing specific behavior due to specific values of the attributes.

3 Business Process Structural Validation

Process Mining analyzes event process logs generated during the execution of a process and covering the process lifecycle. The scope is to discover real process models. Even if in some cases a reference process model is available as it was the one used for illustration in this study, in most cases where process mining is applied, the process model represents the output of process discovery algorithms applied on event log data.

Below a brief comparison of process mining algorithms is presented. The α -algorithm is the most known process mining algorithm and it is the first process discovery algorithms that could deal with concurrency. But it is not the most suitable choice for real life data with noise, different granularity, coming from different sources. Heuristic Miner algorithm was the second process mining algorithm proposed after the α -algorithm having the advantage of overcoming the limitations of the α -algorithm. Heuristic Miner can also abstract exceptional behavior and noise and it is suitable for real log data. The Fuzzy Miner algorithm is included in the new generation of process mining algorithms and as improvement, the Fuzzy Miner is able to deal with event log data with very high granularity.

As many process mining algorithms are available in academic and commercial implementations, assessing the quality of the obtained process model represents an important step for making the right choice in identifying the most suitable business process model. For this purpose, the resulted process models are analyzed using conformance checking techniques on the event log dataset. The event log is replayed on the process model and several useful metrics are calculated [2]. Fitness metric informs about the percentage of the log traces that could be replayed by the process model from beginning to end. This could be calculated at case and event level. Precision (Behavioral Appropriateness) is another useful metric describing how accurate the model describes the process (the model should not be too generic). Structure (Structural Appropriateness) captures the level of details of the process model; the simplest model capturing all possible execution paths represents the best process model choice.

Another useful approach for assessing the structural quality of process models is the usage of a common technique in data mining, separation of data into training and test dataset. The training set is used as input for process discovery algorithms. The test data set and process model obtained after discovery is applied on the

training set is used as input for conformance analysis of the process models. This approach could be extended in a k -fold cross validation: partitioning the data into k subsets, process discovery is applied on one subset and validating the analysis results on the other subsets. A description of this technique applied in process mining could be found in [7].

4 Business Process Functional Validation

Functional validation is the software testing process used within software development in which software is tested to ensure it conforms to all requirements. Functional testing of a business process implies checking if the process model is compliant with the process requirements representing business objectives. Business process functional testing involves evaluating and comparing each process with business requirements.

The first step is determination of the business process expectations. Our proposal is to capture the expectations in use cases with step by step scenarios. The use cases could be defined from 3 different perspectives: process perspective, case perspective, and organizational perspective. The second step is represented by the creation of test data based on use case definition. Once the test dataset is available, the next step includes checking the conformance of the obtained process models with the generated test data at previous step. The output of the conformance analysis step is considered the result of the test. In the last phase, several testing metrics could be calculated for assessing the functional validity of process models (Fig. 4).

5 Functional Validation on CCB Process Model

Theoretical approach described in previous chapter is exemplified on a real event log dataset. The base business process is the one described in Sect. 1. CCB business process is followed to implement and include in deliveries a set of changes proposed by users.

The event logs recorded are exported from IMS in csv format:

- users.csv—containing all users having permissions to access and update the items in IMS
- items.csv—containing all requirements (change requests, feature requests, problem reports, information requests)
- events.csv—containing all operations performed by the users to update the state of the items

Once data is prepared in XES format as process mining algorithms require, the process models are extracted from the event log data. The algorithms chosen are Heuristic Miner algorithm as it is the most suitable for real life data like in the

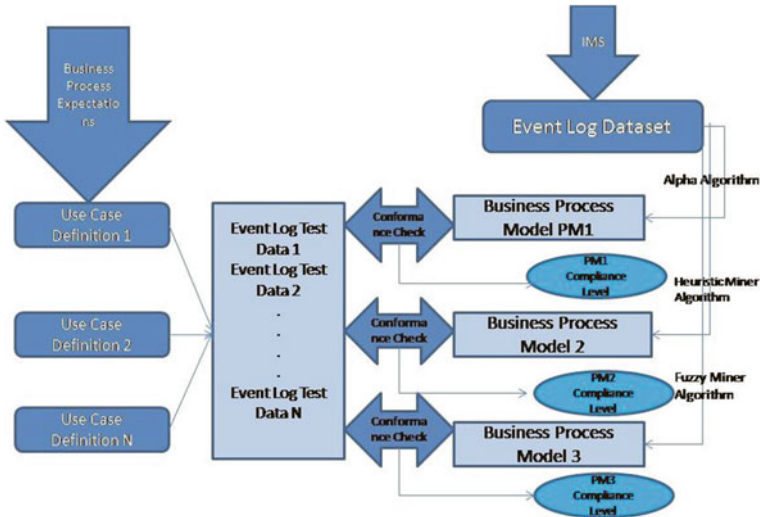


Fig. 4 Process mining functional validation framework

current situation and α algorithm as it is the most widely known process mining algorithms (Figs. 5 and 6).

The first step in functional validation of the resulted process models obtained is the definition of business expectations from the process model captured in use cases (Table 1).

Each of the following use cases could be split into one or more test scenarios. For each scenario, a dataset is created. The complete dataset and process models obtained with different process mining algorithms are the input for a conformance checking phase. The compliance of each process model with the test dataset represents the factor for deciding which of the business process is the most suitable for

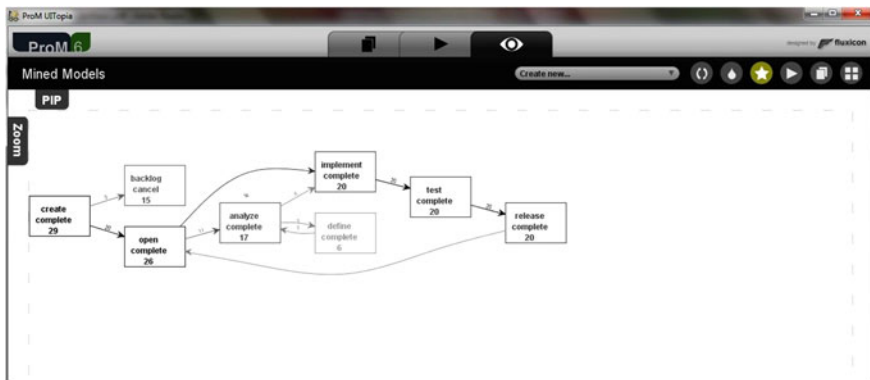


Fig. 5 CCB process model extracted with Heuristic Miner algorithm

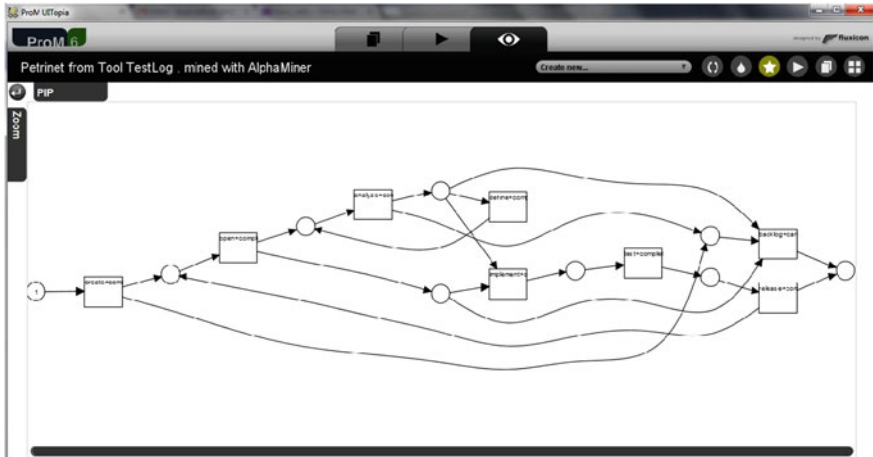


Fig. 6 CCB process model extracted with α Miner algorithm

Table 1 Use case definition

Use case no.	Description
Use case 1	The items could be created by support team, opened, analyzed, implemented, tested and released by engineering team and accepted by support team
Use case 2	The items could be created by support team, opened, analyzed and canceled by engineering team and accepted by support team
Use case 3	Items could be created by support team, opened, implemented, tested, and released by engineering team
Use case 4	Items should always be tested after implementation
Use case 5	Items should always be canceled only after an analysis is performed
Use case 6	Items should always be created by users within group "Support"
Use case 7	Items should always be implemented by users within Group "Engineering Team"
Use case 8	Items should always be analyzed after delivery

accomplishing the business objectives and should be used in practice and for further analysis.

The use case approach is an efficient technique for collecting essential requirements from stakeholders, helping to focus on the real needs. It will help business analysis and project teams to arrive at a common, shared vision of what the process should do. In Fig. 7 a global image of the complete validation flow is captured.

Fig. 7 Business process validation flow

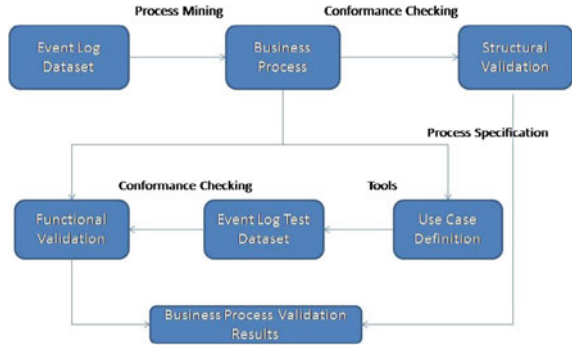
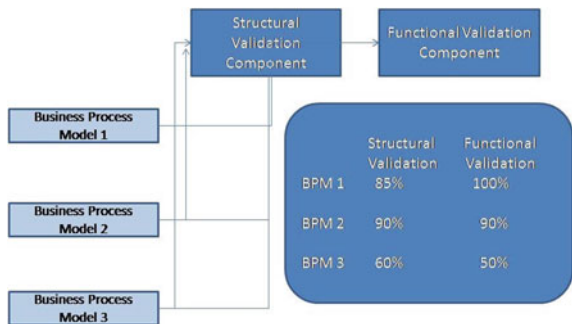


Fig. 8 Functional and structural validation framework



We propose the implementation of structural and functional validation of process models in a framework. For evaluating the compliance of a process model, specific metrics are used in case of structural and functional validation. These metrics represent the output results of the proposed framework (Fig. 8).

6 Conclusions

The benefits of introducing BPM in any organizations are undoubtful. BPM enables organizations to align business objectives with internal processes and has the capacity to reduce costs, improve efficiency, and minimize errors and risks. When a business process is not available, process mining techniques allow retrieval of process models from internal event log traces. Applying process mining on a dataset requires a thorough understanding of the data and a lot of expertise in interpreting the results and finding solutions to enhance the process. In this context, validation of process models becomes an important step as the process models represent the base for any further analysis.

In this study, we proposed validation from different perspectives. A structural approach identifies the correctness of process models by checking the compliance of the model with the full event log trace, precision of the model to capture the scenarios in the event log, and the simplicity of the model.

The functional approach on the other hand validates a business process based on a set of business objectives defined as use case scenarios.

Validation is an important part in any business for ensuring good results and it should be applied in all the areas inside an organization. Validation of business processes inside an organization which produces results by executing internal processes is even more important as the quality of process models could impact all business areas.

Validation of process models could also increase the confidence in process mining results as the organizations will have the insurance that the process reflects the expectations and it was extracted correctly from the event log dataset.

References

1. Dumas M, van der Aalst WMP, Hofstede AHM (2005) Process aware information systems: bridging people and software through process technology. Wiley & Sons, Chichester
2. van der Aalst WMP (2011) Process mining : discovery, conformance and enhancement of business processes. Springer, Berlin-Heidelberg
3. Urena Hinojosa E (2008) Process mining applied to the change control board process. Discovering real processes in software development process. Master's Thesis. Technische Universiteit Eindhoven, Eindhoven, The Netherlands
4. Verbeek MW, Buijs JCAM, van Dongen BF, van der Aalst WMP (2010) ProM6: the process mining toolkit BPM 2010 Demo, Sept 2010
5. Sebu ML, Ciocarlie H (2014) Applied process mining in software development. Case study
6. <http://www.xes-standard.org/>
7. Rozinat A, Alves de Medeiros AK, Gunther CW, Weijters AJMM, van der Aalst WMP (2011) Towards an evaluation framework for process mining algorithms. Eindhoven University of Technology, Eindhoven

Evaluating the Performance of Discourse Parser Systems

Elena Mitocariu

Abstract In this paper are analyzed two different methods for comparing discourse tree structures. The aim is to identify the best technique to evaluate the output of discourse parser system. The first, is a traditional method and is based on quantifying the similarities between the parser output and a reference discourse tree (gold tree). It uses three scores: Precision, Recall, and F-measures. The second one examines the discourse tree representations in qualitative terms. Like first one, three scores are computed: Overlapping score, for analyzing the similarities in terms of topology, Nuclearity scores which take into account the type of nodes, and Veins scores which measure the coherence of discourse. By evaluating discourse tree structure resulted from a parser, the performance of discourse parser systems can be measured. A comparative survey is realized aiming to present assessment methods for discourse tree structures.

Keywords Discourse parser · Evaluating methods · Discourse trees

1 Introduction

Discourse parsing systems are developed in order to obtain automatically discourse tree. They can be grouped into three classes, depending on the architecture used in their development. First are discourse parsing systems based on symbolic or probabilistic grammars. In Langer [1] a set of recursive rewriting rules are the starting point for context-free grammars (CFG). Soricut and Marcu [2] also have

E. Mitocariu (✉)

Faculty of Computer Science, “A.I.Cuza” University of Iasi, 16, General Berthelot St.,
700483 Iasi, Romania
e-mail: elena.mitocariu@info.uaic.ro

E. Mitocariu

SOP HRD/159/1.5/S/133675 Project, Romanian Academy Iasi Branch
(POSDRU/159/1.5/S/133675), Iasi, Romania

developed a statistical discourse parser based on probabilistic grammars. The issue is that the grammars cover only the basic aspect of a language system. The second class uses learning methods in developing the parsing systems. The learning method is split into two categories: handwritten rules and automatic learning. Both learning methods are dependent of grammar corpus. The corpus is created according to the grammar rules of a specific language. To use the parser for another language it is necessary to align the corpus to the specific grammar language.

The third group uses complete online analysis with no pre-query annotation [3]. Eckle-Kohler [4] developed a pattern-matching approach which makes use of complete online analysis.

Driven by one or another approach, the differences between the discourse tree structures can vary widely. Further, the same discourse can be represented by many discourse tree structures, all performed properly. In order to evaluate the performance of discourse parser system, in most of the cases are compared two discourse tree structures: one is the parser output and the other is a reference tree. This is not easily performed because it must be necessary for the use of the same corpus. The process to achieve the corpus is often complex. This is not always free and available. In order to evaluate a parser, different scores were computed for comparing discourse tree structures.

In this paper are presented two methods used in the evaluation of discourse trees. The first is proposed by Marcu [5] and is focused on three scores: Precision, Recall, and F-measures. The second was developed by Mitocariu et al. [6] and like first, use three scores: Overlapping score, Nuclearity score, and Veins score. The purpose of this paper is to evaluate their efficiency, taking into account tree features: the topology of tree, the type of the nodes, and the coherence of the text. In order to perform this, a discourse is parsed and three discourse tree structures are compared: first is the gold (the reference tree), second is the output of a discourse parser system, and third is developed by an expert in NLP. To all these three trees are applied the scores proposed by Marcu [5] and Mitocariu et al. [6] and their results are analyzed.

The paper is organized as follows: in Sect. 2 are described two main theories in discourse analysis: rhetorical structure theory (RST) developed by Mann and Thompson [7] and veins theory (VT) whose founders were Cristea et al. [8]. In Sect. 3 methods for evaluating a discourse parser are presented. Conclusions are presented in Sect. 4.

2 Discourse Theories

It is unnecessary to develop a discourse parser system, without evaluating its performance. The evaluation methods vary from each other according to the verified discourse tree structure. Further, each discourse parse system is build according to one or more discourse theories. The discourse theory catches different features of

a discourse. One is centered on the attention features, other on the informational and intentional features. In this paper are presented two main discourse theories: RST and VT.

2.1 *Rhetorical Discourse Theory (RST)*

The central principle of RST is the notion of relation between two adjacent elementary discourse units (*edus*). These can be either clauses or propositions. According to the role that occurs in the text, *edus* can be *nuclei* or *satellites*. The *nucleus* represents the most important spans of discourse. Without them the coherence of text is wasted. *Satellites* are not as important as *nuclei* are. They supplement *nucleus* with additional information. Without *satellites* the coherence of the text is kept. Each node has the type *nucleus* or satellite.

Based on the notion of *nucleus* and satellite, two main relations are computed: **paratactic** and **hypotactic**. **Paratactic** relations link *edus* of the same importance (*nucleus* with *nucleus*). **Hypotactic** relations link *edus* with different importance (satellite with *nucleus*). These are divided into subset of other relations, each of them having an exclusive name.

2.2 *Veins Theory(VT)*

Veins theory uses binary tree representation of discourse structure. Each node may be a *nucleus* or a *satellite*. The discourse tree has two types of nodes: leaves which are *edus* and inner nodes which denote a relation between his children. An inner node has two children. At least one of him must be a *nucleus*.

Taking from RST the type of relations but ignoring their name, VT extends the links between adjacent *edus* to ones which are not necessarily closer. In order to do this, two new expressions are considered: **head** and **vein**. The **head** and **vein** expressions are computed over the discourse structure trees and contain the labels of *edus* which can be accessed from a specific node.

Head expressions are an ordered list of the most important *edus* of discourse. In a discourse structure tree, the **head** expressions are computed bottom-up considering the following algorithm:

```

If the node is leaf
  Head expression = his own label
Else (if it is an inner node)
  Head expression = the concatenation of his nuclear
  child

```

Starting from the leaves, which represent *edus* in discourse, the head expressions are computed bottom-up. Each leaf has the *head* as his own label. An inner node has the head computed from the concatenation of the head expressions of his *nuclear* child.

The *vein* expressions for a binary discourse tree structure are subsets of sequences of discourse and are computed top-down according to the following algorithm:

```

If the node = root
  Vein expression = his own head expression
Else
  If is a nuclear node
    If has a left satellite sibling
      Vein expression = concatenation of the vein
      expression of his parent with the head expression of
      his sibling marked
    Else (it has a nuclear sibling)
      Vein expression = vein expression of his par-
      ent
  Else
    If is a satellite node
      If is a left child
        Vein expression = concatenation of vein ex-
        pression of his parent with his own head expression
      Else (if it is a right child)
        Vein expression = concatenation of vein ex-
        pression of his parent without marked units with his
        own head expression

```

The vein expressions are computed top-down starting with the root of the discourse structure tree. The root of the discourse structure tree has the *vein* expression identical with his own *head* expression. For the rest of the nodes the *vein* expressions are computing depending on their type and location (right or left) and the sibling type and location (right or left).

3 Methods for Evaluating Discourse Parser Output

Discourse parser systems are built different and thereby the output differs. Because the heuristics in developing parser systems are very various, it is difficult to find a precise method for comparing the efficiency of parsers. The majority approaches make use of the same corpora in the evaluating process. If the same corpus is not used, the evolution of parser is not precise. A commonly used method was proposed by Black [9] and represents a traditional approach for evaluating tree structures. It is PARSEVAL. PARSEVAL has been criticized for not representing “real” parser quality [10–12].

Leaf-Ancestor (LA) developed by Sampson et al. [12] takes into consideration the path from each terminal node to the root in the tree obtained by parser and the same path calculated in the gold tree, according to Levenshtein distance.

Maziero and Pardo [13] have developed the RSTeval tool, which does compare rhetorical trees. This is an online tool for the automatic comparison of RST rhetorical trees (human and automatically built trees), based on the Precision, Recall, and F-measures. They test the similarity between spans, nuclearity, and relations between two rhetorical trees.

In this paper we are evaluating the methods proposed by Marcu [5] and the approach developed by Mitocariu et al. The first one represents a reference unit in evaluating a parser. The second one is a different method, in terms of not using the same corpus, for evaluating discourse parsing systems.

3.1 Precision, Recall, and F-measures

The same discourse can be represented by many discourse tree structures. This number is computed according to Catalan number to which is added different type of nuclearity for inner nodes. Thus, the same discourse can have, a number given by (1) of different discourse tree structure, where n represents the number of clauses.

$$\text{Number of trees} = \frac{(2 * n - 2)!}{n! * (n - 1)!} * 3^{n-1} \quad (1)$$

The high number of representations of discourse structure trees is the main reason of finding proper methods for evaluating discourse tree structures correctly. In incremental discourse parser systems it is necessary to find the best trees for future development, instead of considering all of them to be equal. To exemplify this better let us consider the sample of text from Example 1 and the three discourse tree structures. The text is from MUC corpus (Message Understanding Conference). It contains 30 newspaper texts. Fig. 1 is the gold representation, extras from corpus, Fig. 2 represents the output of a discourse parser system, and Fig. 3 depicts the discourse structure developed by an expert in NLP area. The trees are developed according to RST and VT standards. The label N_N or N_S denotes the nuclearity type of the left and right child. N_N means that both child are *nucleus* and N_S means that left child is *nucleus* and right child is *satellite*.

Example 1

0. *Business Brief*
1. *Petrie Stores Corp.*
2. *Losses for Fiscal 2nd Period, Half Seen Likely by Retailer*
3. *Petrie Stores Corp., Secaucus, N.J., said*
4. *An uncertain economy and faltering sales probably will result in a second-quarter loss and perhaps a deficit for the first 6 months of fiscal 1994*

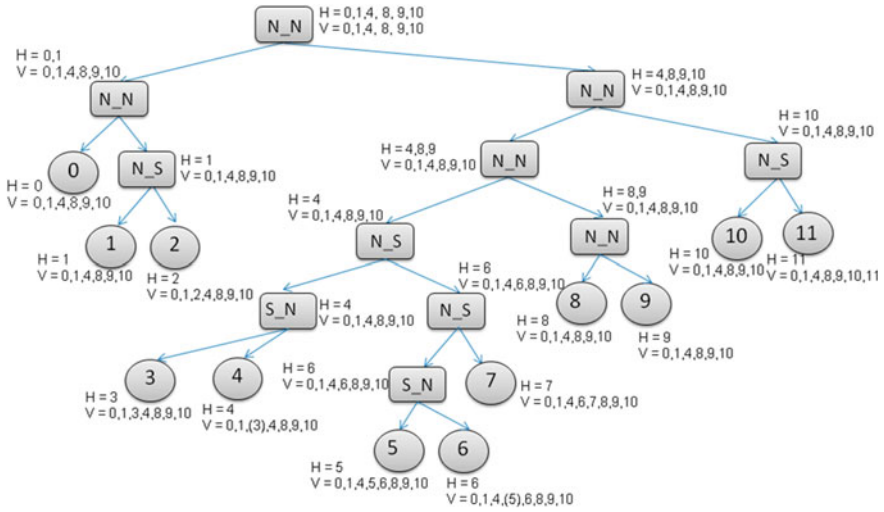


Fig. 1 Gold discourse tree representation

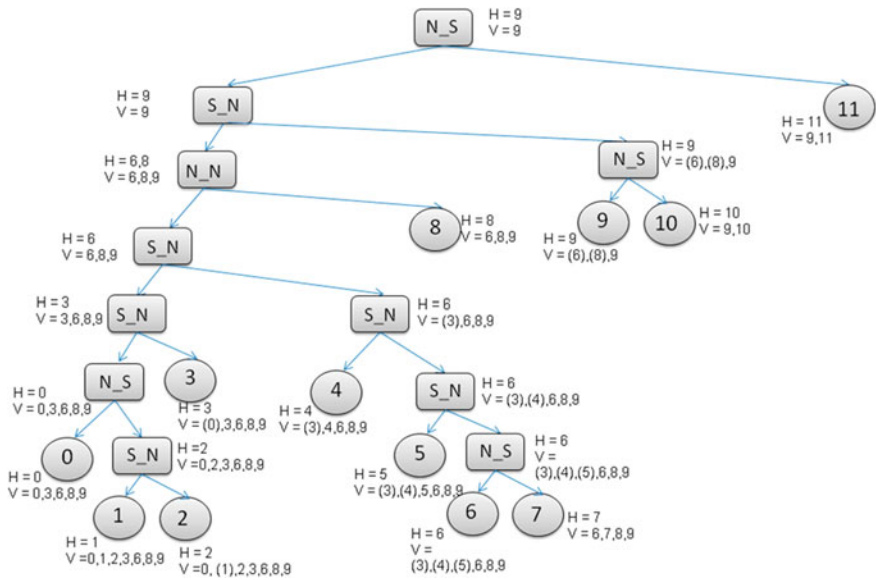


Fig. 2 Discourse tree representation of the parser output

- 5. The women's apparel specialty retailer said
- 6. Sales at stores open more than 1 year, a key barometer of a retail concern's strength, declined 2.5 % in May, June, and the first week of July.
- 7. The company operates 1,714 stores.

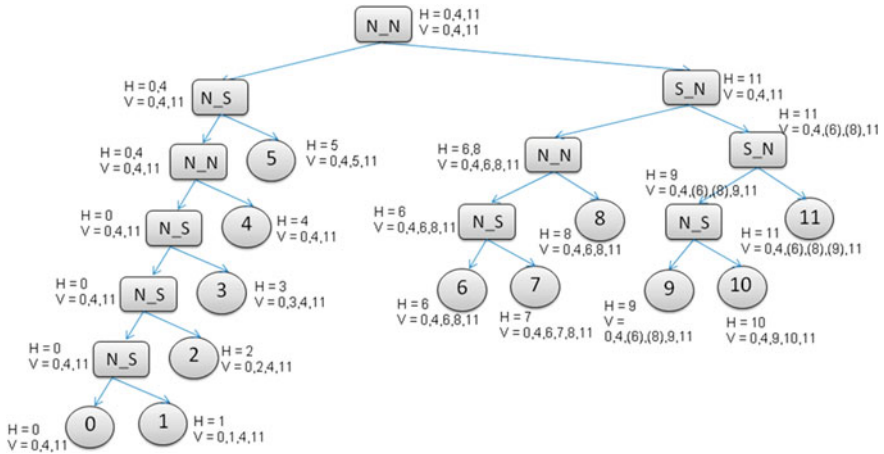


Fig. 3 The discourse tree representation developed by an expert in NLP domain

8. In fiscal 1993's second quarter, ended last August 1, the company had net income of \$1.5 million, or 3 cents a share, on revenue of about \$355 million
9. In the first 6 months of fiscal 1993, net was \$8.4 million, or 18 cents a share, on revenue of about \$678 million
10. Directors also approved the election of Allan Laufgraben, 54 years old, as president and chief executive officer and Peter A. Left, 43, as chief operating officer
11. Milton Petrie, 90-year-old chairman, president, and chief executive officer since the company was founded in 1932, will continue as chairman

According to Marcu [5] the “best” discourse trees are those which are skewed to the right. The same discourse can be represented by many discourse structure trees. Some of them convey to the same meaning as one from gold (the reference tree; the tree with which are compared the observed trees). These are the best trees from all. The best means those discourse trees which are closer to the gold discourse trees.

To analyze how much the tree is skewed to the right, Marcu [5] proposes a weight score (w). This is computed as follows:

```

If the node is a leaf w = 0
Else
w = w(left) + w(right) + depth(right) - depth(left)
    
```

After computing the weight score for the tree from figures presented above, it was obtained the scores given in Table 1.

After analyzing the score resulted, it can be observed that the best discourse tree is the gold one, second is the result of parser, and on the last is one realized by an

Table 1 Weight scores for the discourse tree representation from figures

Figures	Weight score
Figure 1. Gold discourse tree representation	-1
Figure 2. Discourse tree representation of the parser output	-12
Figure 3. The discourse tree representation developed by an expert in NLP domain	-14

expert in NLP area. This means that the parser system is closer to the gold than the discourse structure tree developed by an NLP expert.

With these scores it can be easily predicted which tree is the best tree for future development. To complete the weight score, Marcu [5] developed another three: Precisions, Recall, and F-measures. These scores reflect:

Precision the number of correctly labeled *edus* in analyzed tree and gold tree with respect to the total number of labeled *edus* identified in the analyzed tree.

Recall the number of correctly labeled *edus* in analyzed tree and gold tree with respect to the number of labeled *edus* in the corresponding gold tree

$$FMeasures = \frac{2 * Precision * Recall}{Precision + Recall}$$

The parser output and the discourse tree realized by a human expert are compared with the gold tree. In these paper are analyzed the segmentation process and the type of nuclearity. Features like Units (how many leaves are in the discourse tree), Spans which reveals the inner nodes and which leaves they cover, and Nuclearity which reveals the types of *edus* according to RST (*nucleus* or *satellite*), are observed.

Thus, after computing the scores, the results are depicted in Table 2.

The results are very relevant. The score 1 for Units reveals that the parser output and the gold have the same number of leaves. The same case is for the discourse tree developed by a human expert and the gold tree. The score 1 for Units means that all three discourse structure trees have the same segmentation (have the same number of *edus*).

Table 2 Precision, Recall, and F-measures for the trees from figures

The scores	The parser output versus gold tree			The human expert representation versus gold tree		
	Units	Spans	Nuclearity	Units	Spans	Nuclearity
Precision	1	0.36	0.58	1	0.18	0.75
Recall	1	0.36	0.58	1	0.18	0.75
F-measures	1	0.36	0.58	1	0.18	0.75

Even if the scores for Units are equal, when the Spans are considered, the parser output has a better score than the human expert. The difference is significant. This means that for inner nodes only two nodes from eleven covers the same *edus* in the case of human expert. These are the ones which cover the *edus* 0, 1, 2 and the root (which cover the whole tree). The parser deals much better. It has four inner nodes identical with the gold tree.

Precision and Recall scores are the same because if the number of leaves is equal these means that the number of inner nodes is also equal. Nuclearity scores reveal that the tree developed by an expert is better than the parser output. As in previous case, the difference is significant (0.58–0.75). The results present a better representation of discourse tree developed by an expert compared with the gold tree. The Nuclearity scores establish the importance of *edus* in discourse. The human expert considers the most of the *edus* to have the same importance as the gold tree reveals.

All the scores proposed by Marcu [5]: weight, Precision, Recall, and F-measures, confirm that between the parser output and the tree managed by an expert, the second one is closer to the gold representation, but in case of Spans analyses the tree from parser output is better than the one developed by human expert.

3.2 *Overlapping Score, Nuclearity Score, and Veins Score*

The aim of comparing the measures proposed by Marcu [5] with scores developed by Mitocariu et al. [6], is to analyze which are more relevant in comparing discourse tree structure.

A discourse tree can be described as a set of tuples of the form $R_k[i,m,j]$. This notation represents a text span consisting of two arguments and the relation between them. The two arguments are the left one spanning between *edus* i and m and the right one spanning between the *edus* $m + 1$ and j . The tuples are computed only for the inner nodes. A discourse structure tree has the number of tuple equal to the number of inner nodes.

For example, in Fig. 1, the set of tuples are: [0,2,11] for the root, [0,0,2], [1,1,2], [3,9,11], [3,7,9], [3,4,7], [3,3,4], [5,6,7], [5,5,6], [8,8,9], [10,10,11], [0,0,2].

3.2.1 *Overlapping Score*

Based on tuple representation, three scores are computed. First, Overlapping score (OS) measure the topology of tree. It is computed as follows:

$$OS = \frac{\text{Number of Overlapping tuples}}{\text{Number of Total tuples}} \quad (2)$$

The Overlapping tuples are the one which have the identical i and j in the tuple representation. For example, if considering the set of tuples for Fig. 2 compared with the set of tuples for Fig. 1, the Overlapping tuples are: [0,10,11] with [0,2,11]; [0,0,2] with [0,0,2]; [1,1,2] with [1,1,2]; and [5,5,7] with [5,6,7].

The total number of tuples is equal to the number of leaves decreasing by one and denotes the number of inner nodes.

3.2.2 Nuclearity Score

According to Mitocariu et al. [6], Nuclearity score (NS) analyzes the type of nuclearity for the tuples which overlap. Thus, the trees are observed in terms of the similarities between their structures.

$$NS = OS * \frac{\text{Number of Nuclearity Overlapping tuples}}{\text{Number of Overlapping tuples}} \quad (3)$$

From (3) it can be observed that none of Overlapping tuples in comparing Fig. 2 with Fig. 1 has the same nuclearity. But if the discourse tree structures from Fig. 3 is compared with the discourse structure tree from Fig. 1, in terms of nuclearity, there is a nuclearity Overlapping tuple: the one of the root. Both trees have the root N_N .

3.2.3 Veins Scores

Veins scores were computed to measure the coherence of text. More precisely, two different discourse tree structures can convey to the same meaning even if they are different in terms of topology. Veins scores are based on Precision, Recall, and F-measures as have been described by Marcu [5]. The starting point represents VT and the scores are applied on the veins expressions of each *edu*. Observing the labels from veins expression for each *edu*, can analyze the coherence of the text. The scores are presented below:

$$VSPrecision = \frac{\sum_{i=1}^N \frac{ll_i}{Ti}}{N} \quad (4)$$

$$VSRecall = \frac{\sum_{i=1}^N \frac{ll_i}{Gi}}{N} \quad (5)$$

$$VSFMeasure = \frac{2 * VSPrecision * VSRecall}{VSPrecision + VSRecall} \quad (6)$$

Table 3 The results after applying the scores proposed by Mitocariu et al.

The scores	The parser output versus gold tree	The human expert representation versus gold tree
OS	0.36	0.18
NS	0	0.5
VSPrecision	0.78	0.72
VSRecall	0.49	0.48
VSF-measures	0.59	0.57

where,

IL_i represents the number of identical labels from the vein expression of the *edu i* in the analyzed tree and the gold tree;

T_i represents the total number of labels of the vein expression for *edu i* in the analyzed tree;

G_i represents the total number of labels of the vein expression for *edu i* in the gold tree;

N represents the total number of *edus*

A score nil represents that the analyzed trees are totally different, and a score equal to 1, represents identical discourse trees.

Thus, after applying the score proposed by Mitocariu et al. [6], was obtained the following results (Table 3).

The scores present, in terms of topology, the parser output as a better one than discourse tree created by an expert. Also, by analyzing the veins expressions of the *edus* the parser output is closer to the gold than the tree developed by a human expert. But the difference is not significant. In terms of topology, the Overlapping score is equal to the Precision and Recall on Spans proposed by Marcu [5]. This equality proves that the score proposed by Mitocariu et al. [6] returns the same results as those proposed by Marcu [5]. Further, the Nuclearity score is applied to inner nodes whereas the Precision and Recall on Nuclearity are applied only to the *edus*. Both methods return the same results. In terms of nuclearity, the human expert is closer to the gold than the discourse parser output. The Veins scores reveal the labels from the vein expressions of *edus* from parser output and human expert contains nearly the same labels as the *edus* from the gold tree.

4 Conclusions

The paper aims to compare two methods of evaluating discourse parser systems. The first is a traditional one and is developed by Marcu [5]. The second one is developed by Mitocariu et al. [6]. To evaluate them was used Message Understanding Conference corpus (MUC-7) which includes 30 newspaper texts

whose lengths vary widely (average of 408 words and standard deviation of 376 words).

The scores proposed by Mitocariu et al. [6] were compared to measures developed by Marcu [5]. In order to realize the comparison between methods of evaluating discourse structure tree, three discourse tree structures were used. A gold discourse tree was the referential tree for both methods. In order to evaluate a discourse tree structure it is necessary to compare the tree obtained by system with one that is known to be right. For this, an expert in NLP area manually annotated a corpus and reveals its discourse trees. Gold files are prepared by hand. The evaluation of a discourse parser is usually done by comparing the parser output against this gold representation. This comparison specifies how performance the parser is (how closely is the parser output to the gold representation).

The comparison reveals that Overlapping score, Nuclearity score, and Veins score are defined correctly and can be used as an alternative way for Precision, Recall, and F-measures. Overlapping score analyzes the spans of text. In this case, both measures present the parser output better than the tree developed by human. Nuclearity scores present the tree created by expert closer to the gold, as the Precision and Recall.

This means that both measures are correctly defined. It is better to remember that Precision, Recall, and F-measures, most of the time need the same corpus to evaluate the discourse parser systems, while the scores developed by Mitocariu et al. [6] need only the gold discourse structure tree to test the parser performance. Also, in the method proposed by Mitocariu et al. [6] the type of inner nodes is observed. However, the method proposed by Marcu [5] considers only the nuclearity of *edus*. Another advantage of using the score proposed by Mitocariu et al. [6] is that the scores are language independent. If a discourse parser for a foreign language is developed, it can be evaluated using the scores proposed by Mitocariu et al. [6] even if a referential corpus is missing.

Acknowledgments This paper is supported by the Sectoral Operational Programme Human Resources Developed (SOP HRD), financed from the European Social Fund and by the Romanian Government under the contract number POSDRU/159/1.5/S/133675.

References

1. Langer H (2001) Syntax and parsing. In: Carstensen K-U, Ebert C, Endriss C, Jekat S, Klabunde R, Langer H (eds) Computerlinguistik und Sprachtechnologie. Eine Einführung, pp 203–245. Heidelberg, Berlin: Spektrum Akademischer Verlag
2. Soricut R, Marcu D (2003) Sentence level discourse parsing using syntactic and lexical information. In: Proceedings of the HLT/NAACL, pp 228–235
3. Kermes H (2003) On-line text analysis for computational lexicography. Ph.D. thesis, IMS, University of Stuttgart. Arbeitspapiere des Instituts für Maschinelle Sprachverarbeitung (AIMS), vol 9, number 3
4. Eckle-Kohler J (1999) Linguistisches Wissen zur automatischen Lexicon-Akquisition aus deutschen Textcorpora. Ph. D. thesis, Universität Stuttgart: IMS

5. Marcu D (2000) The rhetorical parsing of unrestricted texts: a surface-based approach. *Comput Linguist* 26(3):395–448
6. Mitocariu E, Anechitei DA, Cristea D (2013) Comparing discourse tree structures. In: Gelbukh A (ed) *Computational linguistics and intelligent text processing 1*, vol 7816
7. Mann WC, Thompson SA (1998) Rhetorical structure theory: toward a functional theory of text organization. *Text* 8(3):243–81
8. Cristea D, Ide N, Romary L (1998) Veins theory: a model of global discourse cohesion and coherence. In: *Proceedings of the 17th international conference on computational linguistics*
9. Black E (1992) Meeting of interest group on evaluation of broad-coverage grammars of English. *LINGUIST List* 3.587. <http://www.linguistlist.org/issues/3/3-587.html>
10. Carroll JA, Briscoe E, Sanlippo A (1998) Parser evaluation: a survey and a new proposal. In: *Proceedings of the 1st international conference on language resources and evaluation*, Granada, Spain, pp 447–454
11. Briscoe EJ, Carroll JA, Copestake A (2002) Relational evaluation schemes. In: *Proceedings workshop beyond parseval—towards improved evaluation measures for parsing systems*, 3rd international conference on language resources and evaluation, pp 4–38. Las Palmas, Canary Islands
12. Sampson Geoffrey, Babarczy Anna (2003) A test of the leaf-ancestor metric for parse accuracy. *Nat Lang Eng* 9(4):365–380
13. Maziero EG, Pardo TAS (2009) Metodologia de avaliação automática de estruturas retóricas [methodology for automatic evaluation of rhetorical structures]. In: *7th Brazilian symposium in information and human language technology (STIL)*, São Carlos, Brazil

Considerations Regarding an Algebraic Model for Inference and Decision on Heterogeneous Sensory Input

Violeta Tulceanu

Abstract In this paper, we outline the foundations for a model for reasoning on images based on abstract concept and action representation via concept algebra. On performing object detection and recognition on image streams, the instances are mapped to ontology. Concept algebra rules and definitions of abstract notions, permit expressing image semantic and the making of further assumptions. This enables abstract reasoning on knowledge extracted or resulted from a cascade of deductions obtained from sets of images processed with different detection and recognition techniques. It also becomes possible to corroborate knowledge extracted from the image stream with information from heterogeneous sources, such as sensory input. Concept algebra reasoning aims to emulate human reasoning, including learning, but remains quantifiable, making way for verifiability in deductions.

1 Introduction

Image understanding is important in fields such as medicine, aerospace, security, and semantic web. Classic approaches rely on stochastic methods involving feature classification and clustering, as in [1], where protein subcellular distributions are interpreted using various sets of subcellular location features (SLF), combined with supervised classification and unsupervised clustering methods. Earlier approaches use artificial neural network [2]. Another approach is case-based reasoning, as described in [3], where two creek type case-based reasoners operate within a

V. Tulceanu (✉)

SOP HRD/159/1.5/S/133675 Project, Institute of Computer Science,
Romanian Academy, Iasi Branch, Iasi, Romania
e-mail: violeta.tulceanu@infoiasi.ro

V. Tulceanu

“Al.I.Cuza” University of Iasi, General Berthelot Street no. 16,
700483, Iasi, Romania

propose-critique-modify task structure to combine low-level structure analysis with high-level interpretation of image content. Case-based reasoning (CBR) has been steadily expanding in the last 20 years and is widely applied in health sciences [4]. The subject is extensively covered in Perner's 2008 book [5].

Apart from health sciences, image understanding has generated extensive work in security areas such as iris biometrics, as described in [6], where techniques are based on statistical analysis, starting with the work of Flom and Safir [7], Daugman [8] and Wildes [9], with subsequently inspired models such as neural networks, Gaussian mixture models, wavelets, fusing quality scores, etc. We find it also necessary to mention the model-based approach of the DARPA image understanding benchmark for parallel computers [10]. Among the probabilistic approaches, we also note Bayesian reasoning on qualitative descriptions for images [11].

However, more recent work tends toward a higher level of abstraction layer for image reasoning, using syntactic reasoning models such as [12], which employ a LALR type grammar and description languages [13]. Drawing from this and Knauff's article [14] on a neuro-cognitive theory of deductive relational reasoning with mental models and visual images, we notice a direction in image understanding that can be successfully further expanded, namely providing a fully quantifiable model with a high-degree of expressiveness for human-like reasoning.

Thus, providing a formal language (or equivalent structure) that can capture abstract concepts, actions, and complex syllogisms about images, without necessarily mentioning the detected, but rather the semantic of the relationships between them.

This prompted us to revert to our work in brain-computer interfacing that led us to model human thought processes using concept algebra. The recent work performed by Feldman [15], Wang [16–19], Hu [20], and Tien [21] strengthened our assumption that the model would fit well the need to express abstract relations between objects, as well as allow learning. This means that the model can use previous knowledge in addition to current observations in order to make deductions, resulting in better image comprehension across different image streams.

Using concept algebra produces the basis for a framework that allows reasoning on images, and can be further combined with epistemic logic to produce a reasoning and communication framework that can be used by heterogeneous (mobile) sensor agents.

2 Concept Algebra for Formal Ontology and Semantic Manipulation

Let us assume that we are provided with an image input stream, on which application-specific object detection and recognition have been performed, resulting in mapping of the objects to an informal static ontology. Our goal is to provide a denotational mathematical structure that is formal, dynamic, and general in order to rigorously model and process knowledge, thus obtaining a formal ontology fit for

semantic manipulation and further use for inference and machine learning. Operational semantics for the calculus of concept algebra are formally elaborated using a set of computational processes in real-time process algebra (RTPA), as proposed by [19]. According to [19], we have the following definitions:

Definition 1 *Denotational mathematics* is a category of expressive mathematical structures that deals with high-level mathematical entities, with hyperstructures on HS beyond numbers on R with a series of embedded dynamic processes (functions).

Definition 2 A hyperstructure, HS , is a type of mathematical entity that is a complex n-uple with multiple fields of attributes and constraints, as well as their interrelations.

Wang employs the OAR (object-attribute-representation) model in order to extend classic ontologies such as WordNet (which is purely lexical) and ConceptNet (that adds complex concepts and higher-order concepts that compose verbs with arguments such as events and processes) as to distinguish between concept relations and attribute relations, thus facilitating machine learning and causal reasoning. Thus, he defines his language knowledge base, LKBUDM (UDM being a type suffix of RTPA).

Wang’s model heavily relies on RTPA, and views concepts as sets of IDs, attributes, objects, internal relations, and external input and output relations, whereas knowledge in general adds synonym and antonym relations to concepts.

In the following section, we propose an alternative to Wang’s model. We simplify by removing the RTPA notation, producing our own definition of concepts. From Wang’s model, we maintain the semantic environment Θ and the sets of relational and compositional operators $OP = \bullet_r, \bullet_c$.

Namely, we use the compositional operators as described by Wang [17]: inheritance, tailor, extension, substitute, composition, decomposition, aggregation, instantiation, and specification. We maintain the same semantic, only replacing concept representation. Thus, it remains possible to derive new concepts from previous ones. However, our approach relational operators differ, as alternative definitions of concepts co-exist, and translation from a syntactic representation to any semantic representation will lead to the same abstract concept. Thus, instead of relating synonyms, antonyms, etc., the relational operator links concrete concepts and abstract ones; be it pure abstractions (“good”, “beautiful”) or verbs.

3 Our View of Knowledge Representation

Remark 1 A concept may represent a concrete object (*table, tree*), a measurable phenomenon (*wind, pressure*), an abstract notion (*task, gain, self*), or an action (*return, take off, beacon*).

Remark 2 Auditory stimulation using words results in brain activation patterns that consist of simultaneously increased activity on a subset of the monitored brain

locations. The set of monitored brain locations is finite, but can be arbitrarily chosen. Potentially infinite number of concepts can be defined on a set if you include PSDs (location and intensity, which is a real number).

Remark 3 One such brain location corresponds to a semantic dimension of the concept described by the stimulus word. The set of all semantic dimensions B , forms our working alphabet.

Definition 3 The definition of a concept C is the disjunction of the definitions of all its known synonyms S_i : $C = S_1 \vee S_2 \vee \dots \vee S_n$ (Building = House \vee Hut \vee Tower \vee Shed).

Remark 4 Two distinct concepts, C_1 and C_2 may share semantic dimensions and one synonym may belong to one or more concepts (Ex.: “castle” may be in “house” or “fortification”).

Definition 4 A syntactic definition $SintD$ of a concept synonym is a conjunction of free variables $X_1 \dots X_k$, each variable X_i corresponding to a feature in the agent-specific data model. The set of all syntactic definitions $SintD$ is $SintD$.

Definition 5 A semantic definition $SemD$ of a concept synonym is a conjunction of free variables $Y_1 \dots Y_m$, each variable Y_j corresponding to a semantic dimension in the abstract layer representation of the concept. The set of all semantic $SemD$ definitions is $SemD$.

Definition 6 Translation between syntactic and semantic definitions of concept synonyms are performed by applying a bijective, invertible, and non-commutative function $tsl: SintD \rightarrow SemD$, where $tsl(X_1 \dots X_k) = Y_1 \dots Y_m$. Its inverse $tsl^{-1}: SemD \rightarrow SintD$, $tsl^{-1}(Y_1 \dots Y_m) = X_1 \dots X_k$ performs semantic-to-syntactic translation.

Definition 7 The translation function $tsl: SintD \rightarrow SemD$ can be extended to function $Tsl: SintD^n \rightarrow SemD^n$, Tsl having variable arity. Function Tsl allows translating concepts, as tsl allows translating concept synonyms.

Definition 8 A basic sentence F_i is a conjunction of concepts occurring simultaneously at a given moment t .

Definition 9 Basic inference is obtained by applying rules over basic sentences $I = F_1 \dots F_n$, $R_1 \leftarrow R_1^1 \dots R_1^{k_1}$, where R is constant according to the domain—Horn clauses.

Definition 10 An agent is a mobile entity equipped with sensory input (denoted SI), such as an UAV, radiosonde, ground vehicle with thermocam, etc. The set of agents, $Agents = \{agent \mid agent = \{self, resources, vocabulary, concept representation mechanism, inference mechanism, epistemic logic, learning mechanism, querying mechanism, game theory strategies, group, trusted agents, friends, enemies, task, current action, intention, gain, visible universe, invisible universe, knowledge\}\}$.

Remark 5 The agent's definition of self is a unique identifier (Self, rank) where Self is a word over an alphabet $A, A \cap B = \Phi, B = \{\cup b_i\}$ and b_i is a semantic dimension, and rank is an indicator of the agent's position in the group hierarchy.

Remark 6 The resource set R is formed by the semantic definitions of the concepts, denoting the resource to which weights are attached: $R = \{(SemD(C), w)\}$.

Remark 7 The vocabulary D is initially a predefined set D_0 of semantic concept definitions, which is further extended by learning or deduction. Thus, when an agent needs to learn a new concept C, it can ask several trusted agents and select the most frequent definition, query through a question/answer mechanism, or deduce the definition himself from web queries and ontology. The vocabulary becomes $D_i = D_0 \cup C$.

Remark 8 The sets for group G, trusted agents TA, friends Fr, and enemies E are apriorically defined, and can be updated by learning, reasoning, or communication with trusted sources. They consist of agent definitions as in 3.

Definition 11 An observation O is obtained by an agent by translating the sensory input (SI), which it receives as syntactic definitions into the corresponding semantic definitions and applying the inference rules to them $F_1 = tsl(SI_1) \dots F_n = tsl(SI_n), R_1 \leftarrow R_1^1 \dots R_1^{k_1} \dots$

Remark 9 The knowledge K of an agent is initially aprioric K_0 , and further updated by adding to it the validated inferences from observations and knowledge shared by trusted agents $K_{i+1} = k_i \cup VI \cup TF$, where $TF = \{\cup F, F \in \{\text{TrustedAgent}\}\}$ and $VI = \cup I, I = \{\{\cup O_i\}, K_i R_1 \leftarrow R_1^1 \dots R_1^{k_1} \dots\} \wedge I = \text{True}$.

Remark 10 Common knowledge K is the intersection of knowledge of agents in a given group $K = \cap K_i$, where $i \in \text{Agents}$.

Definition 12 The visible universe V is the sum of the agent's current observations via sensory input corroborated with the inferences, obtained by applying rules on the observations and its aprioric knowledge restricted to the current setting $V = \{\cup O_i\} \cup I, I = \{\{\cup O_i\}, K_{set}, R_1 \leftarrow R_1^1 \dots R_1^{k_1} \dots\} x$, where $K_{set} \subseteq K$ ($K_{set} = K \cap \{\cup O_i\}$).

Definition 13 The invisible universe Inv represents everything that cannot be inferred from knowledge K and current observations O_i .

4 Reasoning Mechanism

Thus, let us assume an agent that has acquired an image input stream. First, the agent will produce a syntactic representation of the objects it detects, which it translates to the semantic definition over the space of semantic dimensions (Fig. 1).

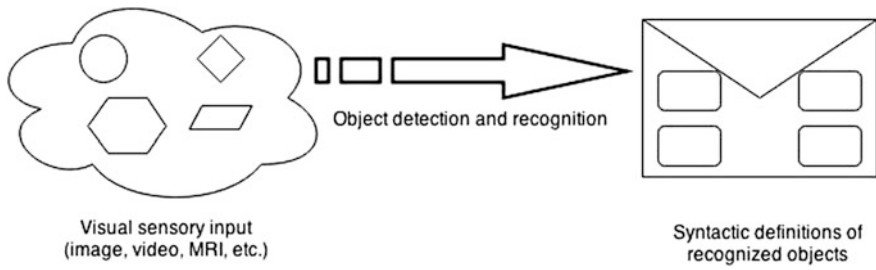


Fig. 1 Sensory input is expressed syntactically

Once detected, sentences are being formed by applying rules to sequences of observations and extracting the abstract concepts. For instance, if in one image a tree is standing and whereas in the following it is down, the inference rule applied should introduce the abstract concept “fell” in the sentence, which is related through an relational operator to the concept “tree”. Each agent will have a set of abstract concepts to operate with, as described in the previous section (Fig. 2).

Cascading application of inference rules should eventually describe the action that occurs in the image stream. The inference rules are applied recursively on the basic sentence and agent’s knowledge; the deductions in each step being added to the knowledge, until the targeted level of deduction is reached. In case of a multi-agent system, the inference rules will also apply to knowledge from trusted agents. All new sentences are added to the agents’ knowledge, which it can share with other agents. In other words, if another agent does not possess the semantic definition of the “tree”, it can obtain it and the related abstract concepts from another agent, along with sample syntactic definitions. Learning means adding or replacing the order of the semantic definitions in the concept definitions. The most common, thus most likely, definition will be first. Rules can also be shared, since they are at the same abstraction level.

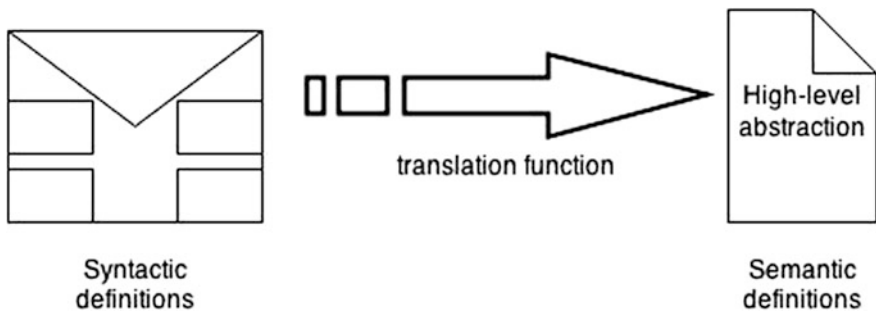


Fig. 2 Agents will process visual input and produce agent-specific syntactic representations of the detected objects. These are further translated to algebraic semantic representations

Thus, we have so far outlined a mechanism for inference on sensory input that allows action understanding and is representation-independent. It becomes possible for agents that have different input, in terms of dimensionality and significance, to learn concepts from one another and to corroborate their knowledge (Fig. 3).

Also, having formal representations for abstract concepts (such as gain, intention, trust, etc.) makes way for communication and cooperation in groups of agents, with the possibility to negotiate group strategies that are adequate in the given context.

The agents complete their vision of the visible universe by communicating, and use an epistemic logic on top of the algebraic formalism. Strategies are decided via a game-theoretic approach, whereas queries for learning new information are made by extending concept algebra with query algebra. Each agent is aware of both self and group interests, and will act according to what the situation requires (Figs. 4 and 5).

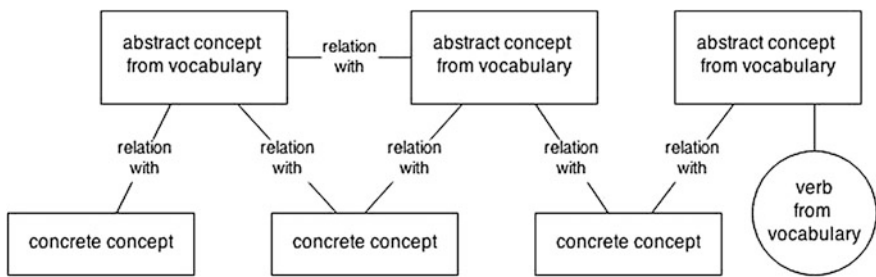


Fig. 3 Basic sentence: object identification and first-level abstractions and verb

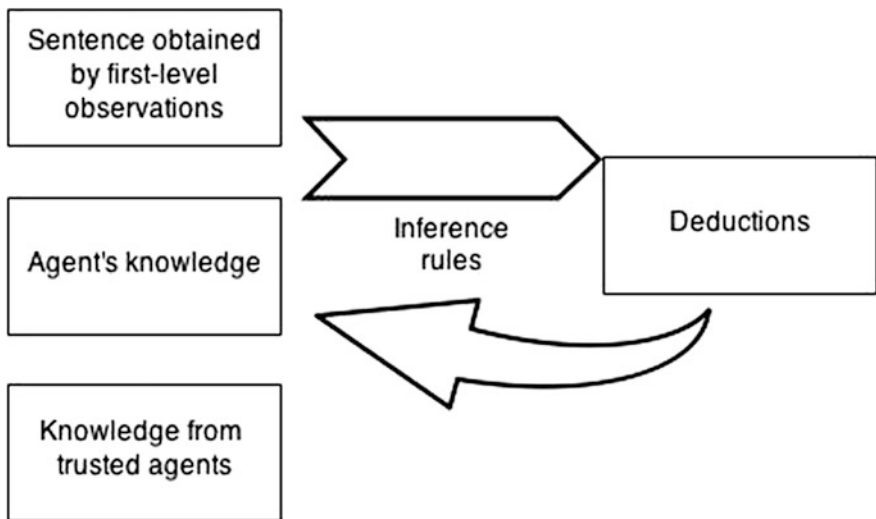


Fig. 4 Inference loop with multiagent knowledge

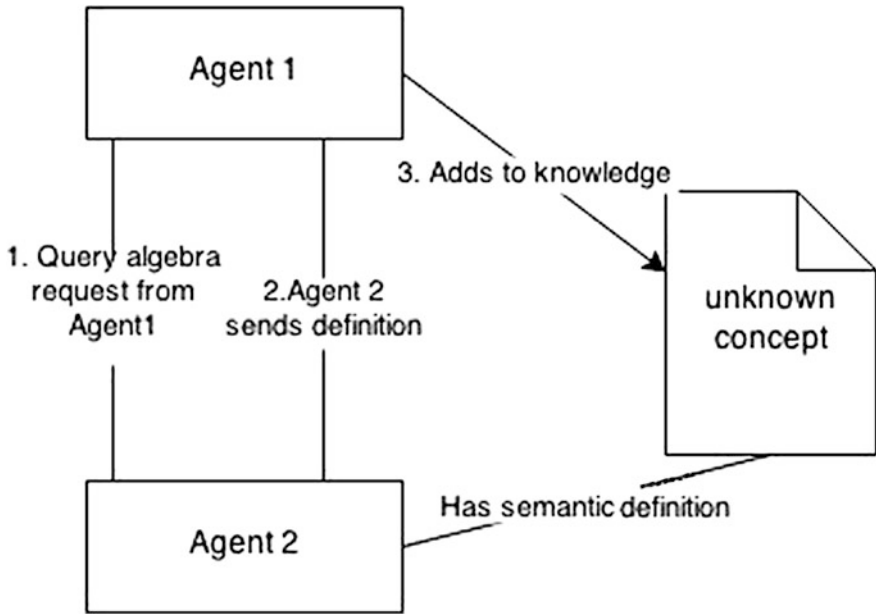


Fig. 5 Requesting semantic definition of unknown concept from another agent using query algebra

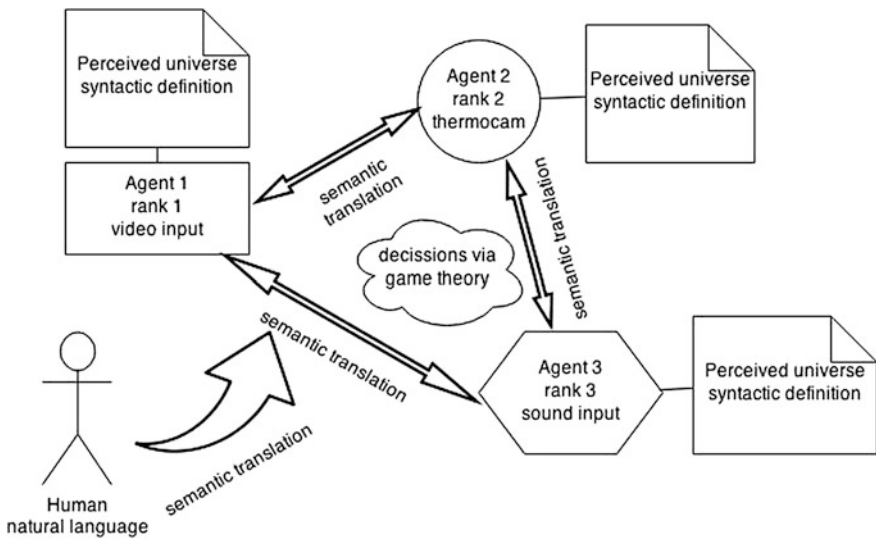


Fig. 6 Group decisions with human interaction

Finally, as the formalism is compatible with natural language makes it possible to send voice queries or commands simultaneously to different members of heterogeneous mobile agent groups (as each agent is aware of its identity and role) (see Fig. 6).

5 Conclusions and Future Work

In this paper, we have outlined the building blocks for a framework based on concept algebra that can provide an abstraction layer for reasoning on images from different sources, regardless of specific data representations. Our approach to knowledge representation makes way for extensions to various logics, and for combining with query algebra for rigorously formalized searches in the input. The result is the possibility for agents with heterogeneous knowledge and representations to communicate and learn, develop strategies, and define intentions within a multi-agent group, and can interface with natural language. Future work involves the concrete definition of the inference rules and the deduction of abstract concepts and of actions. Also, implementation is required in order to assess the practical efficiency of the proposed reasoning mechanism. Finally, once the formalism is completely implemented and a high-level reasoning mechanism is thoroughly defined, extending the concept algebra with epistemic logic and implementing game theory decision-making strategies, would allow for intelligent sensing agents that can cooperate.

References

1. Huang K, Murphy RF (2004) From quantitative microscopy to automated image understanding. *J Biomed Opt* 9(5):893–912
2. Kulkarni AD (1993) *Artificial neural networks for image understanding*. John Wiley Sons Inc, New York
3. Grimnes M, Aamodt A (1996) A two-layered case-based reasoning architecture for image understanding. *Adv Case-Based Reasoning, Lect Notes in Computer Science* 1168:164–178
4. Bichindaritz I (2012) Research themes in the case-based reasoning in health sciences core literature. In: *Advances in data mining, applications and theoretical aspects. Lecture notes in computer science, vol 7377*, pp 9–23
5. Perner P (2008) *Case-based reasoning for signals and images*. Springer, Berlin Heidelberg
6. Bowyer KW, Hollingsworth K, Flynn PJ (2008) Image understanding for Iris biometrics: a survey. *Comput Vis Image Underst* 110(2):281–307
7. Flom L, Safir A (1987) Iris recognition system. U.S. Patent 4,641,349
8. Daugman J (1994) Biometric personal identification system based on iris analysis. U.S. Patent No. 5,291,560
9. Wildes RP (1997) Iris recognition: an emerging biometric technology. *Proc IEEE* 85(9):1348–1363
10. Weems C, Riseman E, Hanson A (1991) The DARPA image understanding benchmark for parallel computers. *J Parallel Distrib Comput* 11(1):1–24

11. Sochera G, Sagerer G, Perona P (2000) Bayesian reasoning on qualitative descriptions from images and speech. *Image Vis Comput* 18(2):155–172
12. Ogiela MR, Tadeusiewicz R (2002) Syntactic reasoning and pattern recognition for analysis of coronary artery images. *Artif Intell Med* 26(1–2):145–159
13. Tadeusiewicz R, Ogiela MR (2004) *Medical image understanding technology: artificial intelligence and soft-computing for image understanding*. Springer-Verlag, Berlin Heidelberg
14. Knauff M (2009) A neuro-cognitive theory of deductive relational reasoning with mental models and visual images. *Spat Cogn Comput: Interdisc J* 9(2):109–137
15. Feldman J (2006) An algebra of human concept learning. *J Math Psychol* 50(4):339–368
16. Wang Y (2008) On concept algebra: a denotational mathematical structure for knowledge and software modelling. *Int J Cogn Inform Nat Intell* 2(2):1–19
17. Wang Y (2006) On concept algebra and knowledge representation. In: 5th IEEE international conference on cognitive informatics, vol 1, pp 320–331
18. Wang Y (2010) On concept algebra for computing with words (CWW). *Int J Seman Comput* 4(3):331
19. Wang Y, Tian Y, Hu K (2011) Semantic manipulations and formal ontology for machine learning based on concept algebra. *Int J Cogn Inform Nat Intell* 5(3):1–29
20. Hu K, Wang Y (2007) A web knowledge discovery engine based on concept algebra. In: Canadian conference on electrical and computer engineering, pp 1255–1258
21. Tian Y, Wang Y, Hu K (2009) A knowledge representation tool for autonomous machine learning based on concept algebra. *Trans Comput Sci V, Lecture Notes in Computer Science* 5540:143–160

Integrated Design Pattern for Intelligent Web Applications

Zsolt Nagy

Abstract Nowadays, it is impossible to develop web applications without proper design patterns, as developers must serve both rich client-side programming tasks and usual server-side engineering and coding. The most popular design pattern is model–view–controller (MVC). In this paper, we are searching for the answers to whether the classic MVC is suitable for today’s web engineering needs, or whether it is possible to suggest a new, integrated design pattern for modern web development.

Keywords Design pattern · Web development · MVC · Software engineering · Intelligent web

1 Introduction

The development of a web-based system is much more work for a software engineer than traditional software development. The life cycle of a web system, development process, tracking, and maintenance is just some concepts that differ significantly in classic software engineering. It is comprehensible why traditional development methods are not suitable for web-based systems, and why they usually need corrections and extensions to make them usable for web development.

2 Design Patterns

In the case of large-scale projects, design pattern usage is essential. There are numerous design patterns, and both in desktop and web environments, the most popular one is model–view–controller (MVC).

Z. Nagy (✉)
College of Nyiregyhaza, Nyiregyhaza, Hungary
e-mail: info@nagyzsolt.hu

2.1 MVC

The MVC design pattern is not a new invention. In 1979, Trygve Reenskaug saw the need to create a pattern which he called “Thing-Model-View-Editor.” A revised version of it was implemented in Smalltalk-80, with its new name, MVC [1].

The MVC design pattern assigns one of three different roles to an object in an application. These roles are: model, view, and controller. This assignment defines not only the role of an object, but also the way it can communicate with other objects. A group of similar MVC objects is usually called a layer; for instance, a group of models is called model layer.

MVC has many benefits for web development. Objects of MVC-based applications are more reusable; their interfaces are more precisely defined, and the application itself is much more expandable than other applications.

Model The model encapsulates data specific to an application and defines the logic and computational process that modifies, manipulates, or processes this data. A simple example: a model object can represent a player in a computer game, or a contact in a phonebook. A model object is obviously able to connect to another model, with one-one or one-many relations. Model objects represent knowledge and experience related to a specific domain, and thus they can be used again in the future if there are similar problems to be solved.

Generally, a model object does not have a direct connection with view objects. This is an important requirement as data and view are normally in close relation. View objects present data, while a view object makes it possible to update or modify these data on a user interface.

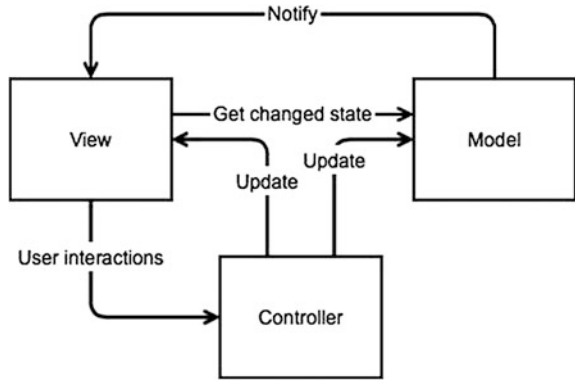
However, the correct process is if operations in the view layer, which create or modify data, are communicated through a controller object and result in the creation or updating a model object. In the reverse direction, the situation is the same, whereby a model object changes (i.e., data arrives over the network connection), it notifies a controller object, which updates the appropriate view object.

View A view object is an object that users are able to see in their application. View object knows how to react with the user actions and how to draw itself. The main purpose of view objects is to display data from model objects and to make it possible to edit those data. Despite this, view object is not in direct relation with model objects in the MVC application.

View objects receive information about model data changes via controller objects and communicate user-initiated actions (i.e., an email address entered in a text field) through controller to model objects.

Controller As shown previously, the controller object plays an intermediary role between a model and a view object. The major purpose of the controller layer is to broadcast and transmit View and model layer changes in both directions. A controller can serve setup and coordinate tasks in an application and manage the lifecycle of other objects.

Fig. 1 Traditional MVC architecture



A controller object interprets user actions made in view objects and transmits new or changed data to the model layer. When model objects change, a controller object communicates the new model data to the view objects, so that they can display them. The big advance in MVC architecture is that multiple views can belong to a similar model or controller. This can be used efficiently in web-based environment, whereas we would like to display the same content in different resolution displays (i.e., notebooks, tablets, and smartphones). This advantage also appears in the area of the latest mobile application development. For example, in the case of iOS (operating system of Apple mobile devices) development, the integrated development environment (IDE) called Xcode creates views simultaneously for iPad and iPhone devices by default. Xcode calls views “Storyboards,” whereas the model and controller that serve those storyboards remain the same.

Nevertheless, we should take into consideration that the original smalltalk MVC architecture allows certain communications between model and view objects (Fig. 1).

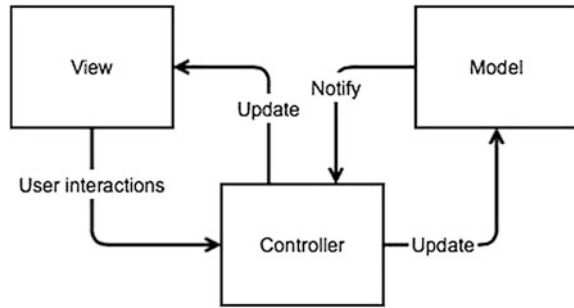
Many publications describe and apply this traditional MVC structure that truly meets the basic requirement. The view does not modify the model and the model cannot reach the view directly; those are the tasks of the controller.

3 Limitations of the Original MVC Pattern

However, a problem still arises in relation with this design pattern, regarding reusability.

In an MVC application, model and view objects are the most reusable components of an application. A user only meets with the view in most cases, and thus a view is equal to the application itself from this point of view. A consistent, predictable, and familiar behavior is essential, which requires an excessive reusability of the application’s view components.

Fig. 2 Cocoa framework MVC design pattern



Model objects encapsulate domain-specific data and related processes, and it is even more worthy if we can reuse our well-prepared models in other applications.

Regarding these remarks, the best design principle is if we decouple model and view objects, which greatly enhances the flexibility of our application, and the reusability of its components.

Therefore, we should consider using a new, objective-C Cocoa framework version of MVC design pattern, alongside current modern web engineering. In the age of a responsive, intelligent web, hundreds of views based on the same model and controller can exist, or the same view can even belong to more than one model [2] (Fig. 2).

A quick example of multiple views with the same model and controller is if we consider an intelligent web portal that is capable of serving different user interfaces (UI) for its individual users, based on the visitor's device type, geographical location, or language preferences. In another case, a smartphone booking application (such as Kayak¹ or SkyScanner²) collects the best cheapest offers onto a single view from different and continuously expanding models, from separate booking systems all over the world.

It should be noted that in the original smalltalk MVC concept, the controller's main purpose is to respond to user events, as it participates as a mediator between the user and the application; updating the model is only a side effect. Nevertheless, we use controller as a separator between model and view in most implementations today, whereas it was originally the observer's task.

Thirty-five years have passed since the introduction of the MVC pattern. Therefore several new and modified versions of this method have appeared that fit the needs of present software engineering. One of its modified, slightly renamed design patterns is the model-view-presenter (MVP).

¹<http://www.kayak.com>.

²<http://www.skyscanner.com>.

4 Model–View–Presenter

The MVP is a revised version of MVC, although highlighting the differences is not so easy as multiple different design patterns exist with the name of MVP.

Mike Potel, CTO (Chief Technology Officer) of Taligent Inc. described the original MVP pattern in 1996. The original name was Taligent Programming Model, which became popular from its structural architecture and was called MVP [3].

4.1 Taligent MVP

Potel took the original smalltalk MVC pattern, where a text typed in a text entry field is the model. The view component receives data from the model and determines how that data from the model will be presented on the screen.

It is the controller’s task to determine how user interactions, in a form of gestures and events, cause data changing in the model. Such a user action is typing into a text entry field, thus changing the underlying string. The loop closes when model notifies the Vview that its state has changed, and the view needs to be redrawn.

Potel’s approach was to break down the original MVC architecture into its constituent parts and refine them, and to assist and support programmers in developing more complex applications successfully.

In the first step, he formalized the separation between the model and the view–controller, which is referred to as the presentation. There are two fundamental concepts that programmers have to deal with: how to manage and how to present data.

Since data management is quite a complex process, it is necessary to generalize and extend the model concept in Potel’s model.

He drew up three main questions that can be answered with different objects and data management layers created inside the model:

- What is the data?—model answers this question.
- How do I specify that data?—selection layer gives the answer.
- How do I change that data?—command layer is suitable for this.

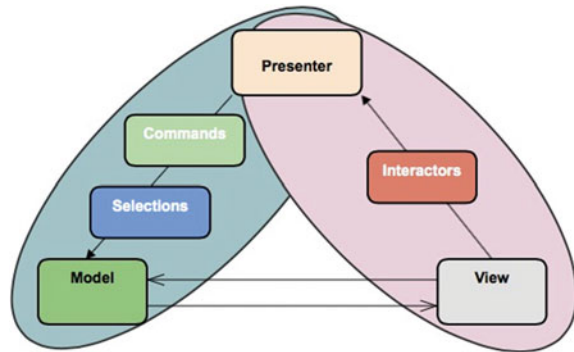
In this case, a model contains the business logic and the data itself.

The selection components determines with which slice of data we consider working with. Its result could be a row of data, a column, or a single element that meets a given criteria.

A command then defines an operation that can be executed on a given data. Some commands are: delete, insert, modify, or print.

The other fundamental phase of the programming work is to develop, maintain, and connect the user interface to the model. Therefore, some questions arise on the user side, which must be also answered by programmers.

Fig. 3 Taligent MVP



- How do I display data?—view
- How do user interactions map into changes in that data?—interactor
- How do I connect the whole system all together?—presenter

View is the visual representation of the model and consists of the user interface, graphical user interface (GUI) elements, displayed on the screen. However, a view does not necessarily have graphical representation (Fig. 3).

Interactors are components that specify how to map user events into data-changer operations. For example, an interactor can be a mouse movement, a keyboard keystroke, a drag and drop action, or a checkbox selection.

The presenter controls the operations of all components in an application. It represents and elevates the function of the traditional smalltalk controller to an application level. The role of the presenter is to create the appropriate model, selection, command, view, or interactor and manage the application workflow.

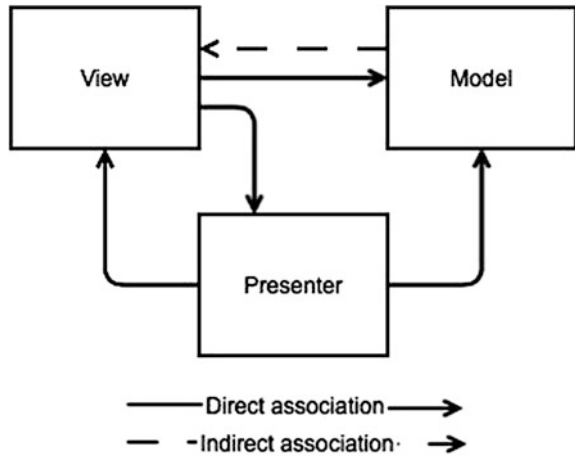
The most obvious differences between Taligent MVP and classic MVC are the presenter and interactors. A presenter is a kind of a general manager, although the interactors rather than the presenter are responsible for capturing user events. Thus, there is no need to create separate presenters for each view element (widgets), as it was in the case of smalltalk controllers. Generally, a given view owns only one presenter, although in certain cases, a presenter can even manage more than one view.

Actually, interactors are similar to smalltalk-80 controllers and respond to user events and call the suitable commands and selections of the model [4].

4.2 Dolphin Smalltalk MVP

The Dolphin smalltalk team simplified the original MVP pattern in the sense that they removed interactor, command, and selector elements from the definition of the architecture, and even the function of the presenter was simplified. It was transformed from a subsystem management component into a mediator, whose purpose is to update the model, based on information received from the view.

Fig. 4 Dolphin Smalltalk MVP



They recognized that the concept of an MVC Controller falls short of the requirements of modern software development frameworks. Its main characteristic is to respond to user interactions, although nowadays, native widgets can handle those events directly. However, it should be noted that the functionality of those GUI elements could be described by and mapped according to the original MVC architecture. Today’s deservedly popular client-side JavaScript/Ajax frameworks do exactly that.

Therefore, view is the component that captures user-generated events in the Dolphin MVP design pattern. The view then delegates these events to the appropriate part of the presenter, who, afterward, modifies the model upon receiving data. An important difference exists between MVC and Dolphin MVP; namely, that the model modification is the fundamental task of the presenter, whereas capturing user events is only a secondary function; a side effect [5] (Fig. 4).

4.3 *Model-View-ViewModel (MVVM)*

Finally, we cannot forget the MVVM design pattern, which is the one used mostly among Microsoft platform developers.

MVVM is a Microsoft-implemented version of Martin Fowler’s presentation model [6] and became popular by its wide use in Microsoft Presentation Foundation (MPF) and silverlight frameworks [7]. MVVM’s main objective is to separate the user interface from the underlying business logic. Using MVVM patterns, components of an application can be tested more easily and can be developed separately. The MVVM pattern consists of the following elements:

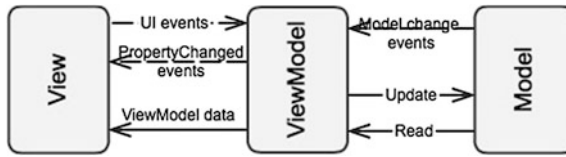


Fig. 5 MVVM design pattern

- Model: traditional MVC Model concept.
- View: the user interface itself displays information for users and triggers events based on user interactions.
- ViewModel: a bridge between the view and the model.

Each view owns its own ViewModel. A ViewModel receives data from a model, then transforms them into an appropriate format for the view, notifies the view if underlying data have changed, and updates model data based on user interface events [8] (Fig. 5).

Although the structure is similar to the MVP architecture in many respects, Microsoft says MVP is quite suitable for traditional server-generated web pages and the request/response paradigm, whereas MVVM is an optimized design pattern for creating rich client applications, where client-side business logic and application state are maintained through interactions between users or services.

Using this pattern, one can easily create two-way data bindings. For example, programmers can use declarative data binding to connect the view to the ViewModel, rather than writing code to connect the two together. Thus by connecting view properties to ViewModel, we do not need to write any code for the ViewModel to update the view when it is necessary; it happens automatically.

Unlike MVP's presenter, ViewModel does not need a reference to the view. Connecting the view and the ViewModel makes it possible: if a property value in the ViewModel changes, the new value is transferred to the view automatically.

For example, if a user presses a button on the view, then a command is executed in the ViewModel and performs the requested action. The ViewModel does this, and so a view never modifies model data.

Some developers doubt whether this pattern or, more specifically, the practical usage of this pattern is correct. The problem is that many software engineers want to compress the business and application logic into the ViewModel.

They cannot put it into the view, as it is only a simple user interface. It does not know where the data comes from; it only knows how to display that data.

The model contains the data itself; this is obviously also not the right place for the application logic.

There is nothing left other than the ViewModel, which already contains a subset of model data, and those commands that are connected to the view. Therefore, if we put the application logic into it, the ViewModel is going to become very complex, so bug fixing and testing will be very difficult in the future.

That is why it is necessary to supplement the MVVM model with a controller element; its name in the industry is model–view–controller–viewmodel (MVCVM) architecture.

The controller’s main task is to implement the application logic and to gather independent components into a whole application. This functionality could be familiar to us even if its name was not the same. Indeed, the presenter component of Taligent MVP had exactly the same purpose.

It is clear now that the original MVC architecture has been changed several times in the past, depending on the requirements of the age or the technology. Even experts interpret the same design pattern in different ways; Josh Smith’s following sentence characterizes the situation very well: “If you put ten software architects into a room and have them discuss what the MVC pattern is, you will end up with twelve different opinions [9].”

5 Our New Design Pattern

The idea of working out a new design pattern as a reaction to the developers’ requirements came from the IT industry. Based on our experience, our goal is to formalize current ad hoc style solutions and offer a new design pattern.

5.1 *Initial Problem*

During our previous introduction to different design patterns, one could recognize that both MVP and MVVM systems differ from the classic MVC pattern in one important fact: they both substitute the controller. However, it is clear that it is impossible to create complex applications without controller roles, or controller functionality.

In addition, we like the original MVC architecture, or more precisely, its modified, Cocoa version, where view and model do not communicate with each other directly, but through the controller. Furthermore, our choice is verified by the fact that MVC frameworks are the most popular development environments, both on the client and the server side.

Software engineers have better experience with server-side solutions; they usually use MVC tools for development. The following example describes the MVC triage, with the most common server-side programming language, PHP.³

The model is responsible for maintaining the connection with the database, while the model reads and writes table data, and contains those PHP classes that were written for data management and data representation. Such a class can be a person,

³<http://www.php.net>.

whose properties are name, address, email, and phone, whereas its methods can be `getName()`, `setName()`, etc. Obviously, methods are clearly detailed, in order to implement, for example, data validation before database actions.

The controller's task is to prepare data received from the model for the view, or to request data from the model upon user interactions generated on view. These interactions arrive typically in the form of HTTP (GET or POST) requests.⁴ As we noted previously, application logic will also be the function of the controller component and is now an extension of the concept, compared to the traditional MVC architecture.

The view is responsible for generating and displaying the current HTML content, and is typically a template in a PHP environment. Templates contain standard HTML and so-called template (`{tag}`) tags. These tags could be simple variables, methods, loops, or selections that are compiled to a PHP code by the template engine. Although PHP codes and HTML tags can be combined during native PHP coding, template tags make our code shorter, more transparent and, in optimal cases, they are independent of the underlying programming language.

Using templates, decoupling view and model became much easier. However, as client-side content is getting richer, the work with them is also getting more and more difficult. As long as it was far enough in the past to attach a JavaScript library to a template and call for some of its methods, but nowadays, heavy codes may vary today's complex view components. Client-side programmers' work has increased dramatically; they use their own tool collections, and use a separate framework, which does not fit in with the services of today's server-side MVC systems.

Furthermore, client and server-side development tasks can hardly be parallelized with current technologies, and it would be optimal if we could provide a suitable structure, where client-side and server-side programmers can work independently.

We need a recommendation, where a server-side developer does not need to understand JavaScript language, and a client-side developer is even allowed to not know anything about PHP or Smarty templates.⁵

5.2 *MVC Integration*

Thus the real question is how can we connect a JavaScript MVC with a PHP MVC framework in such a way that the new, integrated system also fits into the MVC architecture.

Approaching from the server side, it is clear that a view component needs further segmentation, as view complexity makes the development work harder. If we change the view component to a whole client-side MVC, our new system becomes an M(MVC)C.

⁴<http://www.w3.org/Protocols/rfc2616/rfc2616.html>.

⁵<http://www.smarty.net>.

Fig. 6 Server-side MVC

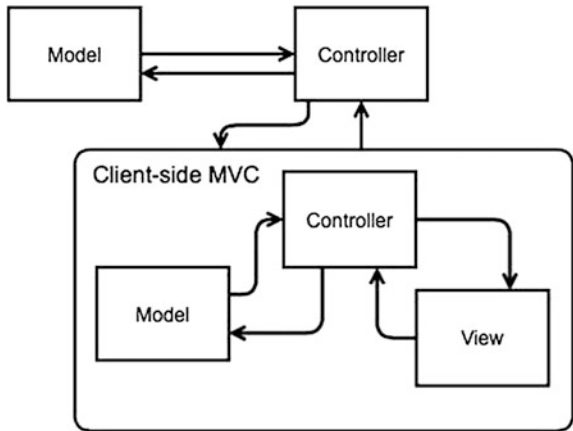
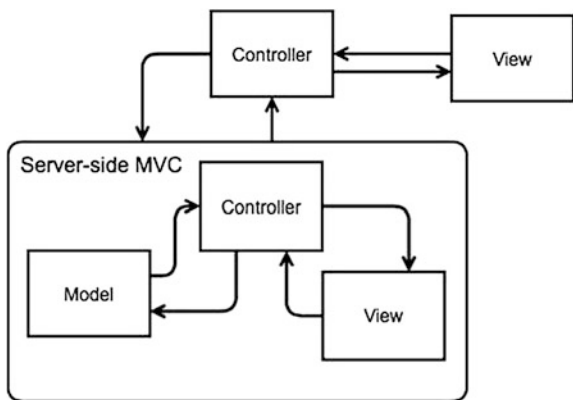


Fig. 7 Client-side MVC



In the case of client-side MVC, the model component of an MVC pattern is a simple HTML code, and the view is a CSS file,⁶ (one CSS file means one View), whereas the controller is the browser itself that assigns HTML with CSS.

From another approach, view is a user interface born from a combination of an HTML, CSS, and data. JavaScript classes and methods play the role of a controller, and the model is the data coming from the web server.

Whichever aspect we take, the model is the interface where a server-side MVC system could be attached.

It seems to be a reasonable solution the server-side system considers serving the client-side, just like its view component (Fig. 6), whereas the client-side MVC considers data coming from the server side as its model's data source (Fig. 7).

One can presume that we should throw out both the client MVC model and the server MVC view, but the answer is no.

⁶<http://www.w3.org/Style/CSS/>.

Fig. 8 Integrated MVC

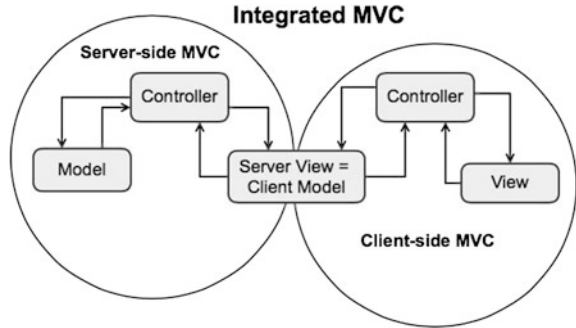
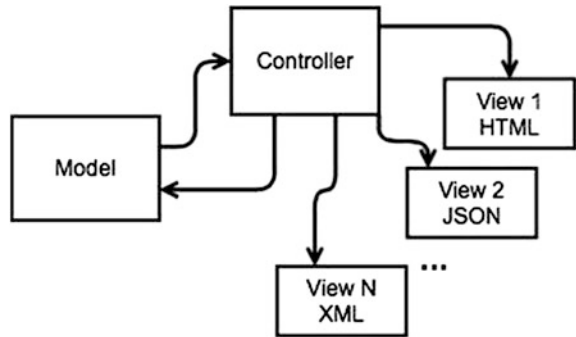


Fig. 9 Server MVC: multiple views



Our goal is to leave the two existing frameworks untouched and establish a bridge between them. The bridge, the solution, is a common interface that maps client-side model to the server-side view (Fig. 8).

The new architecture also supports multiple connections of client-side MVCs to the same PHP system, even if each client requires different data formats.

Since this design pattern supports multiple views, the number of server-side view components can be easily extended. Thereby we made it possible to serve not only HTML pages, but also arbitrary formats such as JSON⁷ or XML⁸ (Fig. 9).

6 Conclusions

Whether our new, integrated system still meets the MVC design pattern requirements is an important question. Since we can examine the system from any directions, the Cocoa-style architecture still exists here; there were no changes. Only an output format (View) and the input source (Model) have been changed.

⁷<http://www.json.org>.

⁸<http://www.w3.org/XML/>.

Therefore, this new pattern has many benefits, not only for rich internet application (RIA) development, but also for mobile platforms, where an Android or an iOS developer could work independently of the PHP engineer, even though they use the same design pattern; our new integrated MVC.

References

1. Reenskaug T The original MVC reports. http://heim.ifi.uio.no/~trygver/2007/MVC_Originals.pdf
2. Apple Developer: Cocoa Core Competencies: Model-View-Controller (2013) <https://developer.apple.com/library/mac/documentation/general/conceptual/devpedia-cocoacore/MVC.html>
3. Potel M (1996) MVP: model-view-presenter the taligent programming model for C++ and Java. Taligent Inc.
4. Greer D (2007) Interactive application architecture patterns. <http://aspiringcraftsman.com/2007/08/25/interactive-application-architecture/>
5. Bower A, McGlashan B (2000) Twisting the triad: the evolution of the dolphin Smalltalk MVP application framework. Tutorial Paper for ESUG
6. Fowler M (2004) Presentation model. <http://martinfowler.com/eaDev/PresentationModel.html>
7. Smith J (2009) WPF apps with the model-view-viewmodel design pattern. <http://msdn.microsoft.com/en-us/magazine/dd419663.aspx>
8. Microsoft developer network: implementing the model-view-viewmodel pattern. <http://msdn.microsoft.com/en-us/library/ff798384.aspx>
9. Smith J (2008) Using MVC to unit test WPF applications. <http://www.codeproject.com/Articles/23241/Using-MVC-to-Unit-Test-WPF-Applications>

Energy Performance Optimization of Wireless Sensor Networks

Cosmina Illes, Cristian Vasar and Ioan Filip

Abstract This paper describes a case scenario regarding the energy consumption in a wireless sensor network consisting of many sensors which monitor a large area, such as a forest. The sensors are distributed in environments with challenging radio conditions (with obstacles, attenuation, or perturbation) and the transmission of data from the monitoring sensor to destination is very difficult due to the large distance between the sensors. Because of the distance between the sensors are required multihop algorithms to optimize the energy consumption. Also data aggregation techniques and multiple base stations are used for optimizing the energy consumption and to increase the battery and the entire network's lifetime.

1 Introduction

Wireless sensor networks are based of sensors that are distributed on a large area for monitoring physical or environmental conditions. Nowadays applications require that the sensors should be autonomous. The wireless sensor networks are equipped with sensors, which are battery powered, and have a radio communication and cooperatively pass their data through the network to a main location. Although the first studies of the wireless sensor networks were made for military purposes, they impose in large ranges of applications: military, industrial, medical, domestic automations, environment monitor, transports because of their reliability, precision, flexibility, and low cost materials [1].

C. Illes (✉) · C. Vasar · I. Filip
Department of Automation and Applied Informatics, University Politehnica Timisoara,
Bvd. V. Parvan, No.2, 300223 Timisoara, Romania
e-mail: cosmina.illes@fih.upt.ro

C. Vasar
e-mail: cristian.vasar@aut.upt.ro

I. Filip
e-mail: ioan.filip@aut.upt.ro

The main constraints of wireless sensor networks are:

- **Nodes distribution:** the location of the nodes can be distributed deterministic or stochastic and is strictly depending on the application, the nodes distribution affects directly the networks communication performances.
In the deterministic distribution case, the nodes are placed manually, while in the stochastic distribution case the nodes are placed randomly.
- **Energy consumption:** a very important issue is minimizing the energy consumption without affecting the data accuracy. The nodes have their own limited source of energy that is why we need communication and data processing techniques that minimize the local energy consumption.
- **Scalability:** the number of the nodes placed in the monitoring area is very large. In some application, it can reach hundreds or thousands of nodes.
- **Coverage:** a networks sensor obtains and provides some specific information of the monitored environment.
- **Fault tolerance:** some times some networks nodes temporary interrupt working because of an energy lack, a physical fault, or because of the environment inferences, but the global functionality of the network does not need to suffer.
- **Connectivity:** It is said that a wireless sensor network is strongly interconnected due to the large density of the nodes which prevent nodes to isolate one from another.
- **The transmission environment:** due to the fact that in the multihop wireless sensor networks the communication between two nodes is realized wireless the problems that appear in the wireless communication may affect the functionality of the entire network.
- **Data aggregation:** due to the fact that more sensors are placed in a large area and monitor the same physical parameters, they can provide redundant data [2].

In case of a forest fire detection system, wireless sensor networks are used for monitoring temperature, humidity, smoke, and gas detection. The main advantage of using wireless sensors network in a forest fire detection system is the possibility of maximizing the energy harvested within the environmental, financial, and technical limitations.

Forest fire monitoring can be made using wireless sensor network and GPRS network. This system has the design of a wireless sensor network and its software implementation, but uses GPRS modules to send the data to the monitoring center [3].

The temperature and humidity of a particular forest location can be measured in real-time using the large number of sensors placed in the forest, and the measured data can be transmitted to the fire-fighting monitoring center in real-time [4].

A system used to know precisely and almost in real-time the risk of forest fires is presented in paper [5]. The paper presents a range-based protocol for detecting and localizing the fire in the forest and control the entire environment.

Forest fire detection can also be made using medium access control (MAC) protocols in wireless sensor networks [6].

More and more applications require wireless connection due to the disadvantages that wired connections have: wired devices cannot be placed very close to the monitored phenomenon, limited devices mobility, and high maintenance costs because of the large number of sensors that must gather data from large areas. However, in the specialized literature, it is state that sending a single bit over radio is at least three orders of magnitude more expensive than executing a single instruction locally, so the wireless communication can have a higher cost in comparison with the local data processing [7].

2 Wireless Sensor Network

A forest fire detection system based on wireless sensor networks consists of the monitoring nodes which are usually distributed on the large areas. The monitoring sensors receive data from the monitored environment using the sensing unit, perform basic calculations using the processing unit and transmit the data to the monitoring center using the radio communication unit. Figure 1 presents a monitoring sensor's block diagram. A monitoring sensor is made by a sensing unit, a processing unit, a radio communication unit, and a battery unit.

The battery unit is used to supply energy to the other units of the sensor. Because it does not exist a constant power supply there must be used batteries. Today some sensors are equipped with photovoltaic cells to recharge their batteries.

The sensing unit consists of sensors or actuators that observe and monitor the physical parameters of the environment in which they are distributed.

The sensing unit's energy consumption depends on the sampling rate and on the duty cycle [8].

The processing unit performs basic calculations based on the information received from the sensing unit. It consists of a processor and external memory.

The radio communication unit is used for data communication in a wireless sensor network but it has a reduced range of communication because of the energy limitations.

In a simple wireless network, a periodically communication is made between sensors and a control center called base station. The base station stores and processes the measured data [9]. The battery of the nodes is very limited and it is very

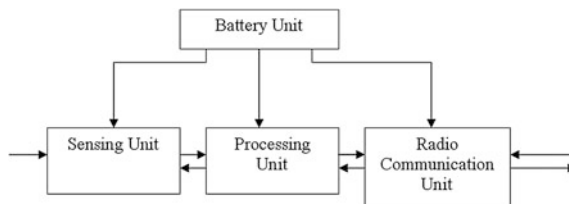


Fig. 1 Monitoring sensor's block diagram

difficult to replace it frequently due to the large number of the nodes in the network but also due to the large area in which the nodes are distributed. Due to the energy limitation of the radio communication, the distance between the source and the destination is limited. Is not always possible a direct communication between the source and the destination in a forest fire detection system because of the large area in which the nodes are distributed. In order to solve this problem are used relay stations where the data packages take multihops from the source to the destination. The value of the transmission range affects the network's topology and the energy consumption. The distance progress of the data packages from source to the destination is bigger if the transmission range is larger. This is possible only with higher energy consumption per transmission. However, if the transmission range is shorter it is needed less energy consumption to forward the data packages to the next hop although a larger number of hops is needed for the data packages to reach to their destination.

The methods that are usually used for reducing the number of data packages that travel through the network, involve data aggregation techniques.

Data collected from the network's sensors is merged together and rerouted to the base station for reducing the data packages that travel through the network. The base station is the root of the routing tree and the network's sensors are the tree's branches and the information travels from the sensors to the base station along this routing tree [10].

The distance between the sensors is maximized, but without exceeding the radio communication range. A wireless sensor network with one base station like in Fig. 2 was considered in the simulations for this paper. The sensors can communicate directly only with the closest neighbors. For example, node 75 can communicate directly only with nodes 85, 74, 76, and 65. The base station communicates with node N(100), the base station is used to prevent the node N (100) to run out of energy. If it was not used a base station all the network's nodes will use N(100) as a repeater. So the N(100) nodes battery will be the one who runs out first.

Fig. 2 Network's sensors distribution

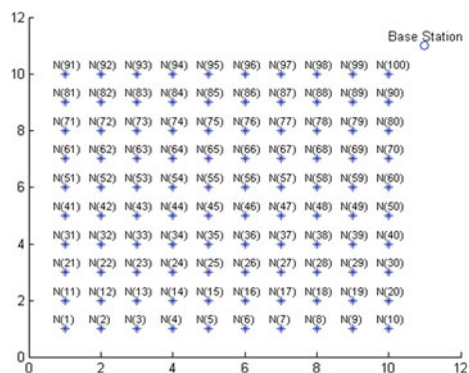
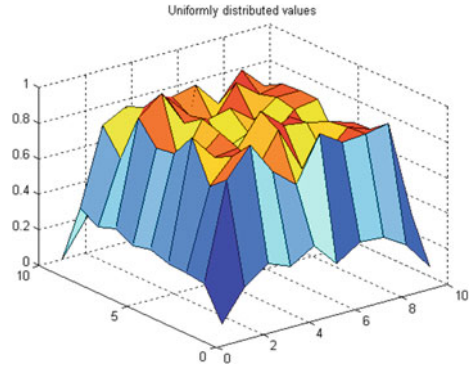


Fig. 4 Uniform distribution for 100 nodes



A wireless sensor network with 100 nodes placed in a 10 by 10 matrix, which normalized values have a uniform distribution is presented in Fig. 4. The total number of communications is 715.

We have considered the following:

- The sensors are placed in nonsquare matrices and their position is static. We studied nonsquare matrices from 1 by 10 to 10 by 10 nodes.
- The sensor's measurements are covered into per units.
- The wireless sensor network is used to detect and extract data from the monitored area.

A wireless sensor network with 60 nodes placed in a nonsquare 6 by 10 matrix, which normalized values have a uniform distribution is presented in Fig. 5. The total number of communications is 245.

The number of communications for the nodes placed in square matrices from 1 by 1 to 10 by 10 is presented in Fig. 6 with solid line and the number of communications for the nodes placed in nonsquare matrices from 1 by 10 to 10 by 10 is presented in the same figure with dotted line.

Fig. 5 Uniform distribution for 60 nodes

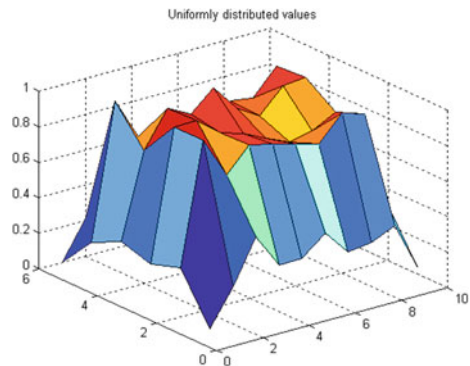
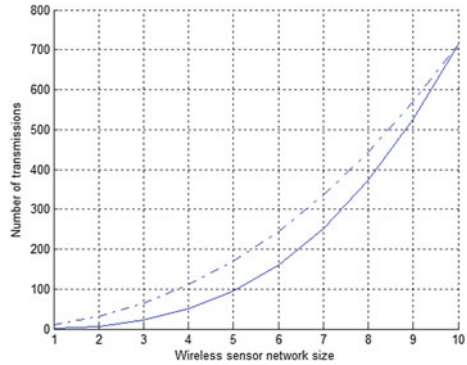


Fig. 6 Number of transmissions



The studies were performed to see how the number of communications is influenced by an additional base station. For reducing the number of communications without affecting the determination of the global and local peaks, we considered the following:

- The communication is starting from the farthest node from the base station.
- The communication is realized on the lines of the matrix in the base station’s direction.
- A node receives and stores the data that are forwarded from his closest neighbors and will send his own value in the network only if his value is larger than the maximum value from the received and stored data from his neighbors otherwise the node will wait the next sampling period.

This rule realizes the data aggregation using a solution which calculates the maximum value.

For example, if the network is like the one presented in Fig. 3 the total number of communications is 715.

In Fig. 7, it is presented an example regarding the number of transmissions from the network’s sensor to the base station for 100 nodes arranged in a 10 by 10 matrix

Fig. 7 Number of direct transmissions for every node when two base stations are used

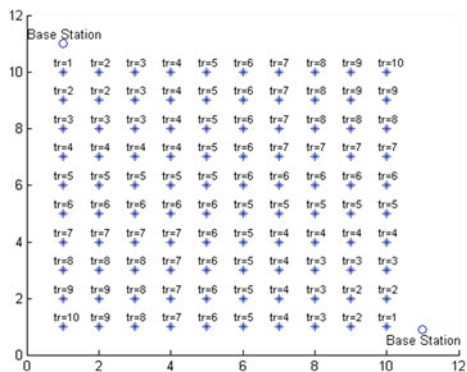
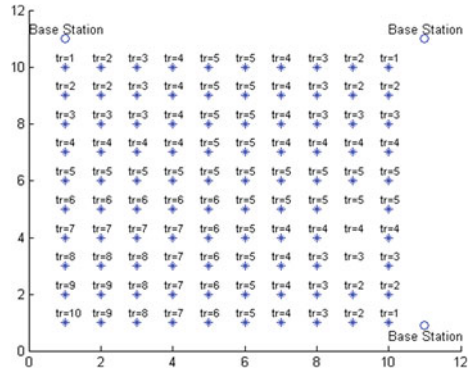


Fig. 8 Number of direct transmissions for every node when three base stations are used



when two base stations are used. Taking into consideration the rule which realizes the data aggregation, the total number of communications for the network presented into Fig. 7 is 550.

In Fig. 8, it is presented an example regarding the number of transmissions from the network's sensor to the base station for 100 nodes arranged in a 10 by 10 matrix when three base stations are used. Taking into consideration the rule which realizes the data aggregation the total number of communications for the network presented into Fig. 8 is 465.

In Fig. 9, it is presented an example regarding the number of transmissions from the network's sensor to the base station for 100 nodes arranged in a 10 by 10 matrix when four base stations are used. Taking into consideration, the rule which realizes the data aggregation the total number of communications for the network presented into Fig. 9 is 380.

The studies were made for square matrices from 1 by 1 to 10 by 10 nodes and even for nonsquare matrices from 1 by 10 to 10 by 10 nodes, using one, two, three, and four base stations.

The number of communications in every case is presented in Fig. 10, with dotted line are presented the number of communications for the nodes placed in nonsquare

Fig. 9 Number of direct transmissions for every node when four base stations are used

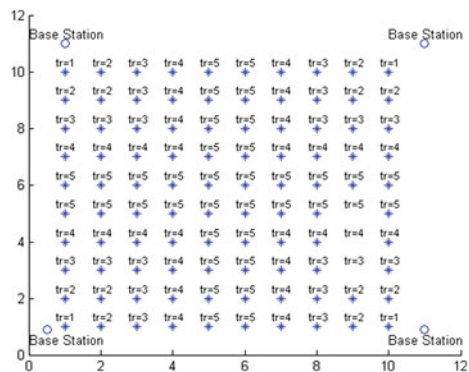
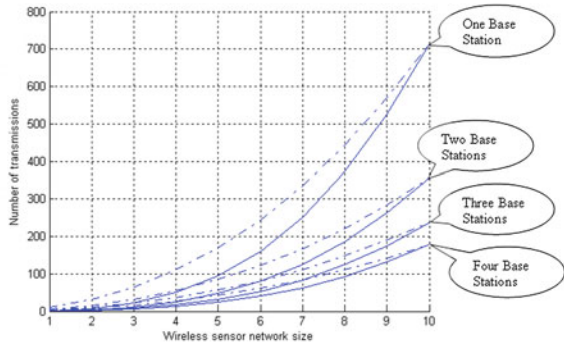


Fig. 10 Number of transmissions using one, two, three, and four base stations



matrices using one, two, three, and four base stations and in the same figure with solid line are presented the number of communications for the nodes placed in square matrices also using one, two, three, and four base stations.

4 Conclusions

In this paper, some cases of reducing the battery consumption using data aggregation are presented. Switching nodes in active or sleep modes and using multiple base stations can reduce the number of communications. This cases lead to an important energy saving without affecting the network’s connectivity. The cases were studied because in case of forest fire detection the nodes are distributed in large areas where the frequently change of the node’s battery is a time and money consumer. Also the nodes cannot always be placed in a square matrix form due to the large number of nodes and the large area that they have to cover. The number of communications has an exponential growth in both cases even if the square matrix form is the ideal form.

In case of using multiple base stations, the number of communications is decreasing. Using two base stations instead of one decreases the number of communications with 50 %. Using three base stations instead of two also decreases the number of communications with 50 %. This rule is available for four base stations instead of three and also for multiple base stations. The main advantage of using one, two, three, or four base stations is the possibility of reducing the number of communications between the nodes with low costs. But adding more base stations in the network will make the network’s structure be more complicated. So adding base stations to the network can be a good thing but also a bad one, because using more base stations makes the network to do not be viable.

A problem that can occur in this wireless sensor networks is related to the fact that we have used a static routing three. In case one node fails the entire network communication is affected, this is the main disadvantage. But this can be avoided using a dynamic routing tree.

Redefining a proper routing tree and adding multiple base stations, we can reduce the number of communications and increase the fault tolerance of the network.

Future research directions will be using routing techniques for reducing the number of communications.

References

1. Vasar C, Prostean G, Filip I, Szeidert I (2011) Above increasing autonomy of wireless sensor networks used for windmill monitoring. *Applied computational intelligence and informatics (SACI)*, pp 607–610, Timisoara, Romania
2. Al-Karaki JN, Kamal AE (2004) Routing techniques in wireless sensor networks: a survey. *IEEE Wirel Commun* 6–28
3. Zhu Y, Xie L, Yuan T (2012) Monitoring system for forest fire based on wireless sensor network. In: 10th world congress on intelligent control and automation (WCICA), pp 4245–4248. Beijing, China
4. Tunca C, Isik S, Donmez MY, Ersoy C (2013) Performance evaluation of heterogeneous wireless sensor networks for forest fire detection. In: 21st signal processing and communications applications conference (SIU), pp 1–4. Haspolat, Cyprus
5. Sabri Y, Najib EK (2012) A prototype for wireless sensor networks to the detection of forest fires in large-scale. *Next generation networks and services (NGNS)*, pp 116–122. Faro, Portugal
6. Al-Habashneh A, Ahmed MH, Husain T (2009) Adaptive MAC protocols for forest fire detection using wireless sensor networks. In: *Canadian conference on electrical and computer engineering (CCECE)*, pp 329–333. St. John's
7. Rabaey JM, Ammer MJ, da Silva JL, Patel D, Roundy S (2000) PicoRadio supports ad hoc ultra-low power wireless networking. *IEEE Comput* 42–48
8. Popa M, Prostean O, Popa AS (2013) A classification of solutions for the energy limitation in wireless sensor networks. In: *IEEE 9th international conference on computational cybernetics (ICCC 2013)*, pp 293–297. Tihany, Hungary
9. Shrivastava N, Buragohain C, Agrawal D, Suri S (2004) Medians and beyond: new aggregation techniques for sensor networks. In: *Proceedings of the second ACM conference on embedded networked sensor systems (SenSys 2004)*, pp 239–249. New York, U.S.A., August 2004
10. Vasar C, Prostean O, Filip I, Szeidert I, Robu A (2008) Using data aggregation to prolong the lifetime of wide-area wireless sensor networks. In: *4th international conference on intelligent computer communication and processing, ICCP 2008*, pp 247–252. Cluj-Napoca, Romania

Jigsaw Inspired Metaheuristic for Selecting the Optimal Solution in Web Service Composition

Viorica Rozina Chifu, Ioan Salomie, Emil Șt. Chifu,
Cristina Bianca Pop, Petru Poruțiu and Marcel Antal

Abstract This paper presents a new metaheuristic for selecting the optimal or near-optimal solution in semantic web service composition. The metaheuristic proposed here is inspired from the jigsaw cooperative learning strategy, which was successfully applied in the student learning process. The search space is modeled as an enhanced planning graph structure which encodes all the web service composition solutions for a given user request. To evaluate the quality of a solution, we use a fitness function that considers as evaluation criteria the QoS attributes and the semantic quality. We evaluated our jigsaw inspired metaheuristic on a set of scenarios with different complexities.

1 Introduction

Web services are software components that expose their functionalities over the Internet. There are situations in which it is necessary to combine a set of existing atomic web services in order to satisfy a complex request. Due to the large number of services, offered by different providers and having the same functionality, a large number of composition solutions can be obtained for the same composition request.

V.R. Chifu (✉) · I. Salomie · E.Șt. Chifu · C.B. Pop · P. Poruțiu · M. Antal
Technical University of Cluj-Napoca, Barițiu 26-28, Cluj-Napoca, Romania
e-mail: Viorica.Chifu@cs.utcluj.ro

I. Salomie
e-mail: Ioan.Salomie@cs.utcluj.ro

E.Șt. Chifu
e-mail: Emil.Chifu@cs.utcluj.ro

C.B. Pop
e-mail: Cristina.Pop@cs.utcluj.ro

M. Antal
e-mail: Marcel.Antal@cs.utcluj.ro

In this situation, the selection of the best web service composition solution according to the functional requirements and nonfunctional requirements (i.e., QoS attributes) becomes a combinatorial optimization problem. Optimization problems can be solved using suitable optimization techniques, such as metaheuristics that are able to produce good solutions (i.e., near-optimal solutions) in a short time and without processing the entire search space.

In the last years, a great interest has been manifested in developing new metaheuristics as powerful techniques for solving optimization problems. Most of these metaheuristics are inspired from the processes occurring in nature, such as the foraging behavior and the breeding process of birds [1, 2], the river formation process [3], or the water life cycle [4]. Others metaheuristics are inspired from the physical and chemical processes [5] or from the musical improvisation [6]. Nature has been considered as a good source of inspiration, since biological systems or processes in nature exhibit self-optimization and self-organization capabilities in a de-centralized way.

In this paper, we propose a new metaheuristic for selecting the optimal or near-optimal solution in semantic web service composition. The metaheuristic proposed here is inspired from Jigsaw, a cooperative learning strategy [7] that was successfully applied in the student learning process. We followed two main steps when developing the jigsaw-inspired metaheuristic: (i) analyzing jigsaw learning strategy [7], and modeling the resulting concepts and processes so as to fit to the optimization problem; (ii) elaborating a jigsaw-inspired optimization algorithm for solving optimization problems, based on the above. We have applied the new algorithm in the context of selecting the optimal or near-optimal solution in semantic web service composition. In our case, the search space of possible web service compositions is represented as an enhanced planning graph (EPG) dynamically built for a given user request. To identify the optimal or near-optimal composition solution encoded in the EPG, we have defined a fitness function which uses the QoS attributes and the semantic quality as selection criteria. To validate the jigsaw inspired metaheuristic, we have implemented an experimental prototype and carried out experiments on a set of scenarios of different complexities.

The paper is organized as follows. Section 2 presents related work. Section 3 briefly describes the EPG structure. Section 4 presents our jigsaw-inspired metaheuristic, while Sect. 5 illustrates the experimental results. We end our paper with conclusions and future work proposals.

2 Related Work

This section reviews some bio-inspired methods for selecting the optimal or near-optimal solution in web service composition.

In [8], the authors present a hybrid particle swarm-based algorithm for selecting the near-optimal solution in web service composition based on QoS attributes. The algorithm proposed combines the particle swarm optimization (PSO) with a

chaotic mutation operator and a local search method to improve the convergence of the classical PSO algorithm. The chaotic mutation operator is used in order to avoid the stagnation of the particles into a local optimum in the early stage of evolution, whereas the local search method aims to improve the diversity of the algorithm. To evaluate the quality of a particle, a QoS-based fitness function is defined.

The authors of [9] present a genetic-based algorithm for selecting a near-optimal solution in web service composition that uses as evaluation criteria the QoS attributes and user constraints. The novelty of this approach consists in defining a new type of chromosome encoding and two types of crossover operators: one in which the genes of a child are inherited from one or the other of the parents alternatively, and another one in which a certain percentage of the genes are inherited from one of the parents and all the remaining genes are inherited from the other parent [9]. Additionally, this approach defines a QoS model that considers the following QoS attributes: response time, execution cost, availability, reputation, and successful execution rate. The QoS model proposed takes into account the following types of execution patterns between the services involved in a composition solution: sequence, cycle, XOR-parallel, and AND-parallel.

In [10], the authors propose a hybrid algorithm that combines genetic algorithms with the simplex method for selecting a near-optimal solution in web service composition. The simplex method is used for improving the local search capabilities of the genetic algorithms. The algorithm proposed considers as selection criteria the QoS attributes and has been tested on a cloud service environment.

The paper [11] proposes a new algorithm for selecting a near-optimal solution in web service composition based on QoS attributes. The algorithm proposed is inspired from the foraging behavior of animals in nature. In this approach, the population of individuals is partitioned into clusters, and there are four types of individuals: cluster heads, producer, scroungers, and rangers. A cluster head is the best individual in its cluster (i.e., the individual that has the highest fitness value in the cluster). There is only one producer, which is the individual that has the best fitness value among the whole population. The rest of the individuals are partitioned into scroungers and rangers. The producer searches the environment for resources using a specific searching strategy. Every scrounger tries to find resources by moving toward its cluster head. The cluster head of each cluster moves toward the producer, and the rangers perform random walks in the search space to look for resources.

In [12], the authors propose a genetic-based algorithm for selecting a near-optimal solution in multipath web service composition based on QoS attributes. In this type of composition, different topologies of solutions may provide the same output. A genetic individual is a composition solution of variable length, which includes: (i) the input and output parameters of the corresponding task, (ii) whether the task is inside a parallel/choice structure, and (iii) the associated concrete service. The evolution of the population is ensured by applying a crossover-based operator and a mutation operator.

3 Web Service Composition Search Space

We represent the web service composition search space on which we apply the jigsaw-inspired metaheuristic as an EPG [13]. The EPG structure is built by mapping the AI planning graph problem [14] to the semantic web service composition and by also enhancing the mapped concepts with new abstractions such as service cluster and parameter cluster. A service cluster groups together services with the same functionality. The functionalities of the services in the same cluster are annotated only with ontological concepts, which are arranged in an **is-a** hierarchy. A parameter cluster groups together input and output parameters of services, annotated in their turn with ontological concepts, which are arranged in an **is-a** hierarchy as well. The EPG construction is an iterative process which operates at the semantic level. At each step, a new layer consisting of a tuple (A_i, L_i) is added to the graph, where A_i represents a set of service clusters and L_i is a set of clusters of input/output parameters. In the tuple (A_0, L_0) of layer 0, A_0 is an empty set of services, and L_0 contains the user provided input parameters. For each layer $i > 0$, A_i is a set of clusters of services for which the input parameters are in L_{i-1} , and L_i is a set of clusters of parameters obtained by adding the outputs of the services in A_i to the set L_{i-1} . The EPG construction ends either when the requested outputs are contained in the current set of parameters or when the sets of service and parameter clusters are the same on two consecutive layers. A web service composition solution as encoded in the EPG is defined as a set of web services, each service in the set being selected from one different service cluster of the EPG (one web service is selected from each service cluster on each layer of the EPG). To evaluate a composition solution sol , we defined a fitness function QF as:

$$QF(sol) = \frac{w_{QoS} * QoS(sol) + w_{Sem} * Sem(sol)}{(w_{QoS} + w_{Sem}) * |sol|}, \quad (1)$$

where: (a) $QoS(sol)$ is the QoS score of sol [13]; (b) $Sem(sol)$ is the semantic quality score of sol [13]; (c) w_{QoS} and w_{Sem} are weights representing the relevance of the QoS and semantic quality respectively.

4 The Jigsaw-Inspired Selection Method

For finding the optimal or near-optimal composition solution in web service composition, we have developed a new metaheuristic, inspired from the jigsaw cooperative learning strategy. This strategy was successfully applied in the student learning process [7]. Our Jigsaw inspired metaheuristic is applied on the *EPG* structure. A multicriteria fitness function that considers the QoS and the semantic quality is used to evaluate the quality of a composition solution.

4.1 Mapping the Jigsaw Cooperative Strategy to the Problem of Selecting the Optimal Solution in Web Service Composition

The jigsaw method is a cooperative learning strategy that was successfully applied in the student learning process (see Fig. 1).

According to the method, a group of students that need to learn a course material is divided into smaller subgroups (which are termed *home groups*). The number of members in a subgroup is equal to the number of parts in which the course material is divided. Within a home group, a separate part of the course material is assigned to each student. Since the same course material as a whole is assigned to each home group, one particular student in any home group has the same material part to study as one other specific student in any other home group. To increase the learning accuracy for each material part, the students across home groups who have learned the same part of the course material will get together into an *expert group*. The students of each expert group will do a brainstorming at the expert group level and will share their knowledge, so that each member becomes an *expert* on the part of the material he/she studied. Finally, each expert will go back into his/her home group and will teach the other members of the home group about the part of the

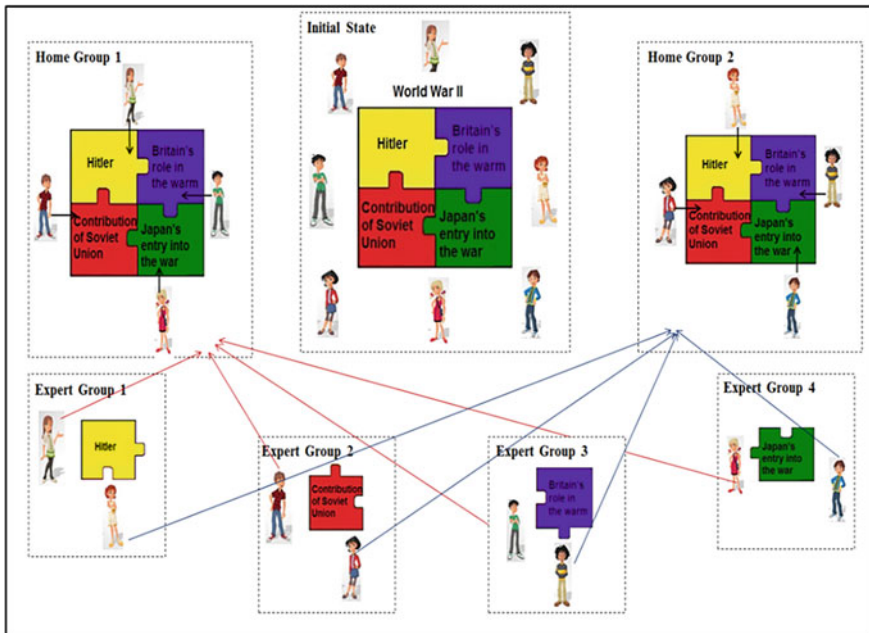


Fig. 1 Example of learning by applying the jigsaw method

Table 1 Mapping the jigsaw learning strategy onto the optimization problem

Jigsaw learning strategy	Optimization problem
The whole material to be studied	A set of solutions to the optimization problem, representing the initial population of individuals
Part of the course material to be studied by one student	A solution to the optimization problem
Student	Agent with a solution associated
Home group	Set of agents
Expert group	Set of agents with similar solutions
Brainstorming at the expert group level	Combine the solutions associated to the agents from the expert group by means of crossover
Learning at the home group level	Each agent enhances its solution based on the experience of the other agents in the home group, experience already achieved in the expert group

material he/she studied. The main benefit of this learning approach stems from the fact that students need to work together as a team in order to learn the course material assigned. Each member of the team contributes to the established goal.

Starting from this cooperative learning strategy, we have developed a new metaheuristic that can be applied for selecting the optimal or near-optimal solution in semantic web service composition. As such, we have mapped the concepts of the jigsaw cooperative learning method [7] onto the problem of selecting a near-optimal solution in semantic web service composition, as in Table 1.

4.2 The Jigsaw-Inspired Algorithm

The jigsaw-inspired optimization algorithm (see **ALGORITHM 1**) takes the following parameters as input: the number of home groups ($noHG$), number of agents in each home group ($noAHG$), the number of agents in each expert group ($noAEG$), the search space (EPG), and the number of iterations (it). The algorithm returns the optimal or near-optimal solution according to the fitness function.

The algorithm consists of an initialization stage and an iterative stage. In the initialization stage, a number $noAHG$ of composition solutions are randomly generated. This set of solutions will be assigned to each home group, one distinct solution for each group member and the same set of solutions for each group. Then the solutions associated to the agents in each home group will be submitted to a perturbation process (i.e., a mutation) in order to simulate the process of learning a separate part of the course material for each student in one home group. In the iterative stage, the following steps are performed until the stopping condition is met:

ALGORITHM 1: JIGSAW-INSPIRED OPTIMIZATION ALGORITHM

Inputs: *noHG*, *noAHG*, *noAEG*, *it*, *EPG*

Output: sol_{opt} – optimal or near-optimal solution

Comments: *itr* – current iteration

Begin

HomeGroups = \emptyset ExpertGroups = \emptyset ; *itr* = 0; BestSolutions = \emptyset AgentsHG = \emptyset ;

for *j* = 1 **to** *noAHG* **do**

 agent_{*j*} = **ASSIGN_RANDOM_SOLUTION**(*EPG*)

 AgentsHG = AgentsHG \cup agent_{*j*}

endfor

for *i* = 1 **to** *noHG* **do**

 HomeGr_{*i*} = **BUILD_HOME_GR**(AgentsHG);

PERTURB_EACH_SOLUTION_IN_HOMEGR(HomeGr_{*i*})

 HomeGroups = HomeGroups \cup HomeGr_{*i*}

endfor

for *i* = 1 **to** *noHG* **do**

 BestAg_{*i*} = **EXTRACT_BEST_AGENTS**(HomeGr_{*i*}, *NoAEG*)

 ExpertGr_{*i*} = **BEST_AGENT**(BestAg_{*i*})

 BestAg_{*i*} = BestAg_{*i*} – **BEST**(BestAg_{*i*})

 BestAgents = BestAgents \cup BestAg_{*i*}

 ExpertGroups = ExpertGroups \cup ExpertGr_{*i*}

endfor

foreach BestAg **in** BestAgents **do**

foreach ag_{*j*} **in** BestAg

IDENTIFY_THE_MOST_APPROPRIATE_ExpertGR(ExpertGroups, ag_{*j*})

endfor

endfor

while(*itr* < *it*)

foreach ExpertGr **in** ExpertGroups

 sol_{*best*} = **EXTRACT_BEST_SOLUTION**(ExpertGr)

 BestSolutions = BestSolutions \cup sol_{*best*}

 noBest = **COMPUTE_NO_BEST**(*itr*, *it*, |ExpertGr|)

 ExpertGr = **UPDATE_SOLUTIONS**(ExpertGr, noBest, BestSolutions)

endfor

GO_BACK_TO_HOME_GROUPS(ExpertGroups, HomeGroups)

for *i* = 1 **to** *noHG* **do**

COMBINE_KNOWLEDGE(*itr*, HomeGr_{*i*})

endfor

itr = *itr* + 1

endwhile

return **GET_BEST_SOLUTION**(HomeGroups)

End

Step 1 This step creates a number of expert groups equal to the number of home groups. The steps followed to create the expert groups are: (i) from each home group, a number $noAEG$ of agents are selected as the best agents in the home group (i.e., agents having associated solutions with the highest fitness values); (ii) the very best agent in each home group is assigned to each expert group, (iii) for the remaining best agents (i.e., the best agents identified at step (i) except the very best one) the most appropriate expert group into which each of them should be placed is identified; the most appropriate expert group is selected based on computing the similarity between each expert group and each agent to be placed, as follows:

$$\text{Sim}(\text{ag}_i, \text{ExpertGr}_k) = \sum_{j=1}^n |\text{Fitness}(\text{ag}_i) - \text{Fitness}(\text{ag}_{kj})|, \quad (2)$$

where (a) $\text{Fitness}(\text{agent}_i)$ represents the fitness of the agent that needs to be placed into an expert group; (b) $\text{fitness}(\text{agent}_{kj})$ represents the fitness of an agent which is already in the k th expert group (agent placed in previous iterations in step (iii); initially only the agent placed in step (ii)); and (c) n represents the number of agents already in the k th expert group.

Step 2 For each expert group, the following operations are performed:

- A one point crossover operation is performed between every two agents in the expert group, where the crossover point is randomly chosen. As a result of crossover, two new solutions are obtained. This process is similar to the jigsaw learning process, in which each student borrows part of the knowledge from other students (brainstorming).
- The solutions resulted by applying crossover between the agents in the expert group are ranked according to their fitness value, and the best solution is kept to be used in the next iterations. Half of the total number of solutions, actually the best ones, are kept in the expert group, and the other half are replaced with new solutions, as follows:
 - A number $noBest$ of solutions are replaced with the best solutions kept from the previous iterations, where $noBest$ is computed according to the following formula:

$$noBest = r * \frac{|\text{ExpertGr}|}{2}, \quad (3)$$

where: (a) $|\text{ExpertGroup}|$ represents the number of elements from the expert group, and (b) r is computed as the ratio between the current iteration and the total number of iterations.

- The remaining solutions are replaced with new randomly generated solutions.

Step 3 The agents in the expert groups return to their home groups and share their new solutions with the other members of the home group. The sharing is performed

using a one point crossover operator. The crossover operator is applied between every two agents in the home group (similar to the learning process in which each student borrows part of the knowledge from other students (brainstorming)). As a result of crossover, two new solutions are obtained, which will replace the old solutions of the two agents on which the crossover was applied.

5 Experimental Results

The convergence of the jigsaw inspired metaheuristic toward the optimal solution is influenced by a set of adjustable parameters specific to this algorithm, namely: the number of home groups (*noHG*), the number of agents in each home group (*noAHG*), the number of iterations (*it*), and the number of agents in each expert group (*noAEG*). To establish the optimal values for the adjustable parameters, we followed three steps: (1) performing an exhaustive search in the EPG in order to find the optimal composition solution together with its score—this optimal score will be used when we will adjust the parameter values for our jigsaw inspired metaheuristic so as to obtain the optimal or near-optimal solution; moreover, our algorithm is able to hit such an optimal solution in a short time, since it does not need to process the entire search space; (2) establish an initial configuration of the adjustable parameters based on a set of preliminary assumptions that will be validated experimentally; (3) iteratively fine-tune the initial configuration of the parameters in order to identify their optimal values. We applied these three steps when testing our jigsaw inspired metaheuristic on three different scenarios with various complexities. Table 2 illustrates the experimental results of step (1) (the exhaustive search) for each scenario, as follows: (i) *code* of scenario; (ii) the structure of the *EPG*, illustrating the number of layers (on table, each layer is represented as a mathematical set), the number of clusters on each layer (given by the cardinality of each set), and the number of services per cluster (given by the value of each element in a set); (iii) the number of solutions encoded in the EPG

Table 2 EPG configurations and other additional information

Scenario code	EPG configuration	Search space complexity	Global optimal fitness	Time (min:s)
S	Layer 1:{4 5 6} Layer 2:{6 4 6} Layer 3:{4 6 5}	2073600	6.456	3:08
M	Layer 1:{3 5 4 6} Layer 2:{6 4 6 5} Layer 3:{4 6}	6220800	7.482	15:47
L	Layer 1:{6 5 3 3} Layer 2:{4 6 4 3} Layer 3:{6 5 6}	13996800	8.024	56:18

(illustrated as column 3, *Search Space Complexity*, in Table 2); (iv) the global optimal fitness value (*Global Optimal Fitness* in Table 2); and (v) the execution time (*Time*). Tables 3, 4, and 5 present some fragments of our best experimental results (in terms of average optimal fitness (*fitOpt*), average standard deviation (*STD*), and average execution time *Time*) obtained when varying the values of the adjustable parameters in running the jigsaw inspired metaheuristic. Each row illustrates the average results of running the algorithm for 100 times on the same configuration of the adjustable parameters. For each table, there is only one row colored gray to indicate the optimal configuration of the adjustable parameters, as they led to the very best result. We have also assessed our jigsaw-inspired metaheuristic by comparing it with the state of the art genetic-inspired algorithm for selecting the optimal solution in web service composition, proposed in [15]. For the jigsaw-inspired metaheuristic we have considered the optimal configuration of the adjustable parameters, as highlighted for each of the three scenarios in Tables 3, 4, and 5. The comparative analysis has been made on the same three scenarios

Table 3 Experimental results for scenario S when running the Jigsaw-inspired metaheuristic

<i>noHG</i>	<i>noAHG</i>	<i>it</i>	<i>noAEG</i>	<i>Fitness</i>	<i>STD</i>	<i>Time</i> (s)
10	30	15	10	6.374	0.082	0.111
20	15	12	10	6.372	0.084	0.109
20	15	13	11	6.368	0.088	0.100
16	30	10	10	6.342	0.114	0.163
15	30	10	10	6.34	0.116	0.15
10	30	10	10	6.327	0.129	0.108
20	15	10	10	6.31	0.146	0.99
20	15	15	11	6.287	0.169	0.99
20	15	12	8	6.264	0.192	0.102
10	35	10	12	6.231	0.225	0.127

Table 4 Experimental results for scenario M when running the Jigsaw-inspired metaheuristic

<i>noHG</i>	<i>noAHG</i>	<i>it</i>	<i>noAEG</i>	<i>Fitness</i>	<i>STD</i>	<i>Time</i> (s)
20	15	13	11	7.360	0.122	0.147
16	30	10	10	7.35	0.132	0.267
20	15	15	11	7.313	0.169	0.156
10	30	15	10	7.292	0.19	0.161
15	30	10	10	7.276	0.206	0.236
20	15	12	8	7.249	0.233	0.156
20	15	12	10	7.221	0.261	0.144
20	15	10	10	7.186	0.296	0.158
10	30	10	10	7.176	0.306	0.161
10	35	10	10	7.141	0.341	0.194

Table 5 Experimental results for scenario L when running the jigsaw metaheuristic

<i>noHG</i>	<i>noAHG</i>	<i>it</i>	<i>noAEG</i>	<i>Fitness</i>	<i>STD</i>	<i>Time (s)</i>
10	30	15	10	7.953	0.071	0.241
16	30	10	10	7.937	0.105	0.410
20	15	13	11	7.932	0.11	0.241
20	15	12	10	7.903	0.139	0.238
20	15	10	10	7.865	0.177	0.234
15	30	10	10	7.855	0.169	0.369
10	30	10	10	7.83	0.194	0.250
20	15	15	11	7.83	0.194	0.227
20	15	12	8	7.807	0.217	0.233
10	30	12	6	7.797	0.227	0.291

Table 6 Experimental results for scenarios S, M, and L

Scenario/algorithm		Fitness	STD	Time (s)
S	Jigsaw inspired metaheuristic	6.374	0.082	0.111
	Canfora	6.056	0.4	0.241
M	Jigsaw inspired metaheuristic	7.292	0.19	0.161
	Canfora	7.275	0.207	0.340
L	Jigsaw inspired metaheuristic	7.953	0.071	0.241
	Canfora	7.36	0.664	0.344

(S, M, and L) as described in Table 2. Moreover, we have used the same stopping condition, i.e., 100 iterations, for both algorithms under comparison.

Table 6 presents the experimental results obtained by the two algorithms.

The experimental results in Table 6 show that our jigsaw-inspired metaheuristic provides better fitness values in a shorter execution time as compared to the genetic-inspired algorithm of Canfora et al.

6 Conclusion

In this paper, we have presented a new metaheuristic for selecting the optimal or near-optimal solution in semantic web service composition. The metaheuristic proposed is inspired from jigsaw, a cooperative learning strategy that has been successfully applied in the student learning process. The main steps in developing our jigsaw-inspired metaheuristic were the following: (i) analyzing the jigsaw learning strategy and modeling the resulting concepts and processes so as to fit to the optimization problem; (ii) elaborating a jigsaw-inspired optimization algorithm

for solving optimization problems, based on the above. The new algorithm has been tested in the context of selecting the optimal or near-optimal solution in web service composition. In our approach, the web service composition has been modeled as an EPG which was dynamically generated for each user request. The quality of a web service composition solution has been evaluated via a fitness function that uses the QoS attributes and the semantic quality as evaluation criteria. As future work, we intend to test the metaheuristic proposed here on other optimization domains.

Acknowledgments This work is carried out under the AAL Joint Programme with funding by the European Union (project number AAL-2012-5-195) and is supported by the Romanian National Authority for Scientific Research, CCCDI UEFISCDI, (project number AAL-16/2013).

References

1. Kennedy J, Eberhart R (1995) Particle swarm optimization. In: The international conference on neural networks, vol 4, pp 1942–1948
2. Yang XS, Deb S (2009) Cuckoo search via Levy flights. In: The world congress on nature and biologically inspired computing, pp 210–214
3. Rabanal P, Rodríguez I, Rubio F (2007) Using river formation dynamics to design heuristic algorithms. *Unconventional Comput J*, vol 4618, pp 163–177
4. Eskandar H, Sadollah A, Bahreininejad A, Hamdi M (2012) Water cycle algorithm—A novel metaheuristic optimization method for solving constrained engineering optimization problems. *Comput Struct J* 110–111:151–166
5. Kirkpatrick S, Gelatt CD, Vecchi MP (1983) Optimization by simulated annealing. *Sci, New Ser* 220(4598):671–680
6. Geem ZW, Kim JH, Loganathan GV (2001) A new heuristic optimization algorithm: harmony search. *Simul J* 76(2):60–68
7. Jigsaw—a cooperative learning strategy. <http://www.jigsaw.org/>
8. Zheng K, Xiong H (2012) A particle swarm-based web service dynamic selection algorithm with QoS global optimal. *JICS* 9(8):2271–2278
9. Amiri MA et al (2013) QoS-based web service composition based on genetic algorithm. *J AI Data Mining* 1(2):63–73
10. Zhang C et al (2013) A hybrid algorithm based on genetic algorithm and simplex method for QoS-aware cloud service selection. In: International conference on parallel and distributed processing techniques and applications
11. Hassina B, Sathya M (2013) An optimization algorithm for QoS-aware web service selection based on animal scavenging behavior. *Int J Adv Res Comput Sci Soft Eng* 3(4):70–78
12. Jiang H, Yang X, Yin K, Zhang S, Cristoforo JA (2011) Multi-path QoS-aware web service composition using variable length chromosome genetic algorithm. *Inf Technol J* 10:113–119
13. Pop CB et al (2010) Immune-inspired method for selecting the optimal solution in web service composition, LNCS, vol 6162, pp 1–17. Springer, Heidelberg
14. Russell S, Norvig P (2003) Artificial intelligence: a modern approach. Upper Saddle River, NJ, Prentice Hall/Pearson Education
15. Canfora G, Di Penta M, Esposito R, Villani ML (2005) An approach for QoS-aware service composition based on genetic algorithms. Conference on genetic and evolutionary computation, pp 1069–1075

Multimedia as a Tool for Learning Engineering

D. López de Luise, J. Gelvez, N. Borromeo, L. Maguet and L. Dima

Abstract Certain subjects in Engineering cover complex concepts. Multimedia may provide a simple, short and effective way to explain them. This paper aims to describe a virtual learning environment named MIDA. It has been designed to train and evaluate a set of tips to improve teaching in that area. LEARNITRON is an offspring of the project. It is a sub project for automatic modelling learning profile of students according to the combination of students profile, topics to be taught and current set of multimedia tools. The goal of this paper is to sketch LEARNITRON and how to improve multimedia tools for teaching, based on basic machine learning techniques. The resulting model may be useful to define specific features for better educational videos, and to acknowledge the right scope of multimedia as a way to teach or train students in Engineering subjects based not on personal opinion but on statistical findings.

Keywords Multimedia language · Audiovisual techniques · Engineering education · Video-games · Automatic learning

1 Introduction

Audiovisual tools and new technologies are recent acquisitions of modern classrooms. They became an interesting question for current academy [1]. The main goal of this paper is to introduce an approach based on multimedia to help teaching in complex Engineering subjects, and better explanation of the real world implementations, main benefits and common usage.

From Neuroscience point of view creativity and originality are processes that create specific patterns in the brain [2] and it is possible the enhancement of creativity by training [3]. But creativity and academic achievement sometimes are

D.L. de Luise (✉) · J. Gelvez · N. Borromeo · L. Maguet · L. Dima
CI2S Lab, Pringles 10-2nd FL, C1183ADB Buenos Aires, Argentina
e-mail: mdldl@ci2s.com.ar; daniela_IdI@ieee.org

independent among higher levels of intelligence [4], this because The dramatic change in learners should be balanced by an equal change in teachers' instruction especially among high achievers [5].

There are multiple intelligences and each one may be accessed using different stimulus. There is close relation between the musical intelligence with the right hemisphere and the logical intelligence with the left hemisphere. It is also clear that there is an equal relation between both of (the bodily and the linguistic intelligences) with the left hemisphere and the spatial intelligence with the right hemisphere [6].

Furthermore, intelligence and creativity are interrelated and they are separate constructs based on meta-analytic findings. Genetics research review shows a prevalent view of the power of the environment impacting genetic potential [7]. This proposal takes multimedia as a tool to improve Engineering topics understanding, uses and real world applications of its principles. Many authors based their studies on technical and theoretical hints, discarding other sources of information like text articulation. That is the case of [8], that includes a historical introduction of Control Systems. Information is complete but static. Marton defines a general hard coded multimedia learning profile [9] that helps identify topics to be improved. The current proposal takes some of its principles but adds a plastic learning approach for the profiles.

Paper [10] presents a list of simple and didactic available media for teaching. Among others:

- Sound as a source of information (for instance radio)
- Visual information (a photograph, a poster, etc.)
- Light audiovisual (proyectors, interactive whiteboard, etc.)
- Audiovisual (Cinema and television)

The paper [10] also agrees that audio is an important element for education, since it usually represents half of the communication in multimedia. They have inherent features that make them adequate for teaching in classrooms.

The contents to be covered by LEARNITRON prototype are pretty abstract and close to mathematics. Therefore they require pedagogic tools simpler and self-explanatory [11]. Audiovisual communication may be useful to engage student with a game with images, sound and underlying abstract concepts. Albert [12] affirms that it is relevant to take them as part of the future society. In fact, multimedia plays an important role in any Engineering applications as they constitute a set of techniques that make it possible a deeper and faster understanding [13] of complex ideas. The efficiency relies in the usage of many human senses. Experiences in [14] indicates that it allows to a more concrete, clear and precise explanation of the topics. In [15] teachers used photographs, collage, paintings, role playing, etc., resulting in a better response and increased interest and enthusiasm by students. In [16] military instruction was improved on topics like survival and strategy efficiency using slides, and films.

Those are proof of a cognitive theory [17] that considers every learning process as a three-layered human psyche. First level describes what and why of a concept.

Second is how (known as technical dimension). Third relates with making or not decision. The first two define the efficiency and efficacy of the learning process.

There must be also a step from Information and Control Theory (ICT) towards pedagogy [11], supported by educational regulations and compliant with social and organizational environments. Thus, it is mandatory to engage a well use of ICTs prior to broadly incorporate new technologies. Many other authors have proposed multimedia utility in learning process [18, 19], and implemented certain alternatives [20–25].

Section 2 presents the global architecture of the MIDA prototype, the multimedia application that feeds LEARNITRON model. Section 3 has initial test cases and statistics. Finally, Sect. 4 describes conclusions and future work.

2 Project Architecture

LEARNITRON is a learning model automatically built using trace data taken from a virtual museum named MIDA. The museum has a set of ancient devices that implement certain engineering principles. Every object has also video, text and photo information. During a visiting, a user can interact with the device, assemble/disassemble it, learns basic or advanced information from videos and texts. All the knowledge is tested in a sandbox where the visitor must solve puzzles using the concepts just learned.

Taking trace data from logs and log-in forms, the prototype applies machine learning to understand the visitor's behaviour and infers the relationship of each multimedia tool and feature with learning process and the inherent abstraction process.

Among others, LEARNITRON project have these main goals:

1. Trace behavioural information to be able to discriminate junior from senior visitors and their abilities.
2. Show ancient devices as a way to introduce complex concepts from the physics, mathematics, chemical, hydraulics, mechanics, etc.
3. Provide a confident and efficient tool to assess the impact of certain multimedia artefacts to learning and conceptualization processes. Among other usages of such model, could be custom advice for a specific classroom about which are the best suited sequence of concepts, multimedia approaches, learning speed and reinforcement requirements.
4. Show and explain real world applications of abstract concepts that are usually hard to visualize.
5. Promote Engineering careers, as it can be visited by anyone that takes time to play with devices, read/listen information and play in the sandbox.
6. Track and evaluate certain factors in the dramatic decrease of the Engineering students, and high desertion in firsts levels. This is done by indirect tracking the persistence, motivation, and other clues.

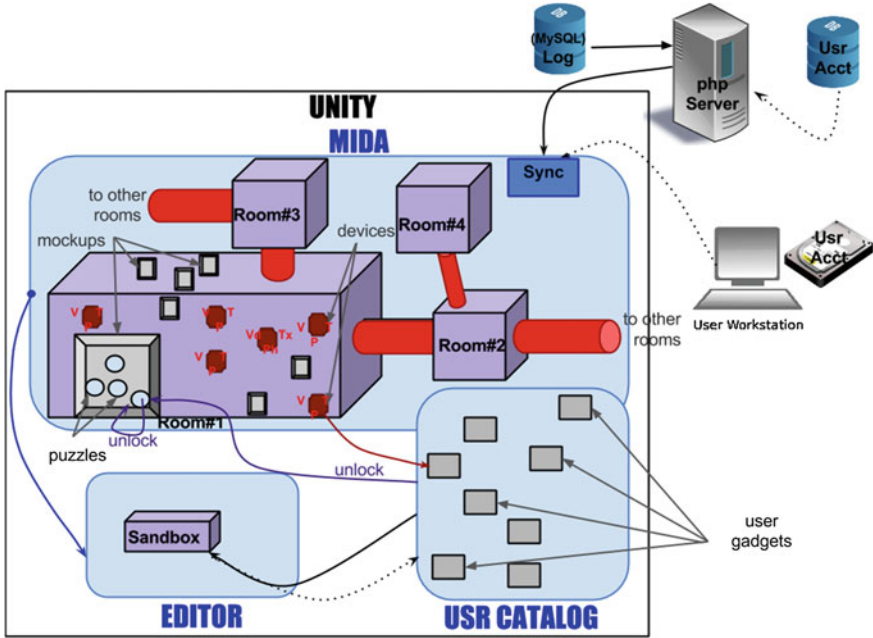


Fig. 1 MIDA architecture

All these goals rely on the association between education and ICTs [11], since it is well known they impact positively making the student more creative and self-sufficient.

The architecture of MIDA (Museo de la Ingeniería Desde la Antigüedad, museum for ancient engineering artefacts) is in Fig. 1. The museum components are built using platform UNITY (c), and many others are in a data server and/or in a end user terminal.

The museum starts with a welcome screen and ask the visitor certain minimal data to be able to hold together all the information of a single user along different sessions.

Figure 2 shows the mentioned first screen, that also has the option of navigate controls, which are multi-platform.

Following is a short summary of the main components sketched in the global diagram.

2.1 Core

The three following components of the museum’s core are in UNITY(c) platform: MIDA, device catalogue of the user and editor.

Fig. 2 Welcome screen



MIDA is a museum designed as a set of interconnected rooms connected through ports (marked as red pipelines).

Every room has two components:

1. *Mock-ups* holding many puzzles that may or may not be activated according to the learning degree of the user. The more puzzles are successfully completed, the more ones will be unlocked. This is because a puzzle is a mini test of certain tip or concept. Figure 4 shows a typical mock up.

2. *Device* are ancient objects selected by its features (among others poles, lever, vessels, Da Vinci's screw, etc.). Every object in the showroom has videos (introductory or function's demo), texts (introductory or technical), and images or photos. Besides it is possible to assemble and disassemble the device to understand its architecture.

Figure 3 shows a mock-up with a set of locked puzzles. It is important to note that whenever a user solves a problem, the objects related to the game are added to the user's stock. The system checks the stock to determine which games are



Fig. 3 Typical showroom



Fig. 4 Mock-up

available. Accumulated objects may also be used to build new devices and to compete in a IEEE tournament named TRIC, a bi-annual student competition that started in 2006. Figures 4 and 5 show a sample object with its complements.

There is no restriction to the number of complements associated to the device, but it is expected that every one has at least one video, one picture, one introductory text, one technical text and a handler to assemble/disassemble it (see Fig. 6).

The handler also allows the user to manipulate the device, changing the point of view, perspective, rotating it, zooming-in/out or providing further information.

Although the objects in the exposition are ancient devices, the main goal is to provide insight on basic engineering principles that make it work and perform certain activity. That is why showrooms are organized by degrees of knowledge and types of knowledge. Ludic learning is inside the game, the principle of try and error, the self-exploratory approach. To understand the object it is required to understand its working principle from a practical point of view, to understand the “tricks” that make it possible to accomplish certain function.

Any time a game is selected from a mock, what really happens is a selection of the set of concepts to be evaluated. In the system the knowledge is represented by the set of artefacts acquired in the user stocks during game playing as a consequence of the successfully resolution of the problems. It is expected that the concepts are then available for expand the visitor’s creativity. This is a new instance to test the ability to reuse and apply the knowledge in a new free context. To do so there is the “sandbox”, a free environment that allows the composition of a new device taking the objects in the private stock of the user. This way each visitor may create its own invent with functionalities at wish. It is implicit in this new stage of MIDA that the ability to make such compositions require deeper understanding of the engines [7].

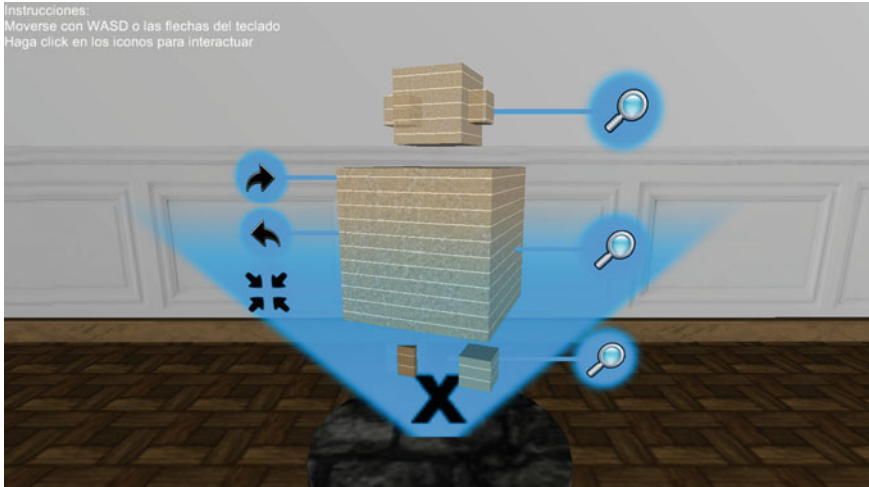


Fig. 5 Sample device and its complements

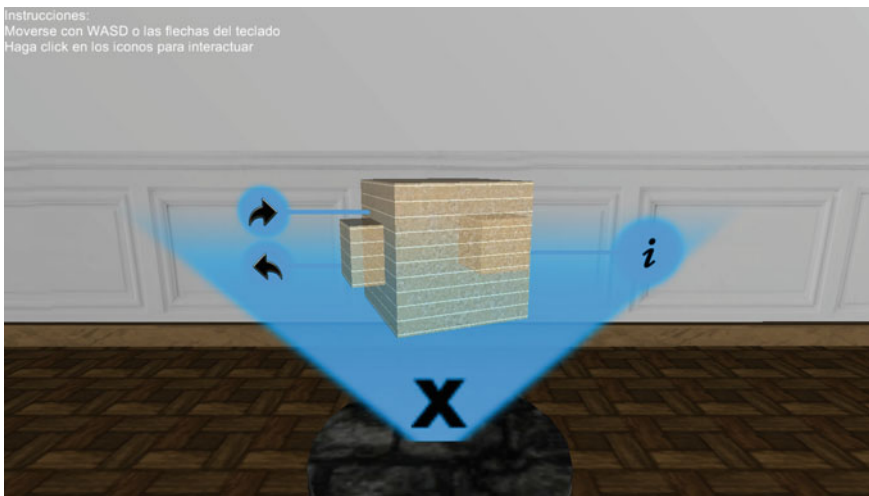


Fig. 6 An object assemble/disassemble

Figure 7 is a sandbox outline. The tools and physics available to build devices are variable but there is a general distribution that holds in any case: a tool bar, test and edit buttons and the blackboard.

Note that the figure has a number of simple objects. There are four different cameras to view the engine from four perspectives (upper tool-bar), and more buttons to test, restart from scratch and to save the device (for future use or export).

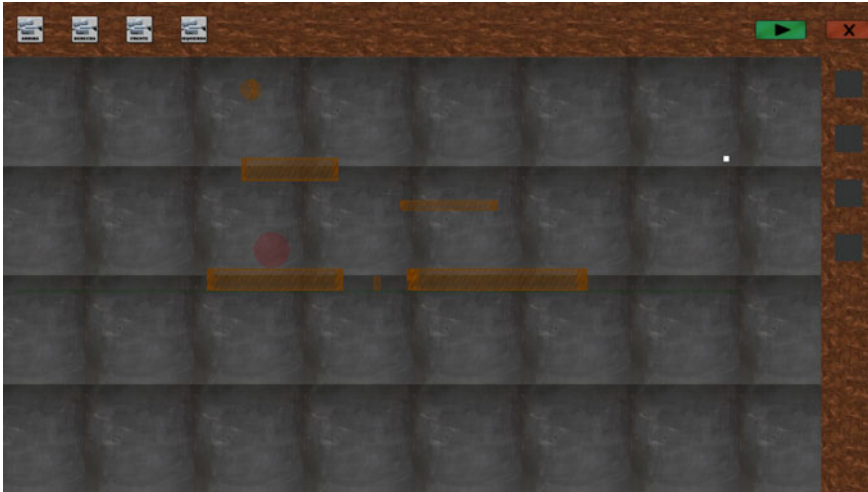


Fig. 7 Outline of a sandbox

As sandbox's editor is expected to be inventively used, there are certain details to guarantee the easy understanding of the phases of the object's construction. For instance, the global outlook of the edition mode is quite different from the one during test mode (Fig. 8) where the device is working under real laws of physics, chemical, mechanical, etc. Other minor changes are for example the buttons ability to function according to parts rotations, enlarging or composition.

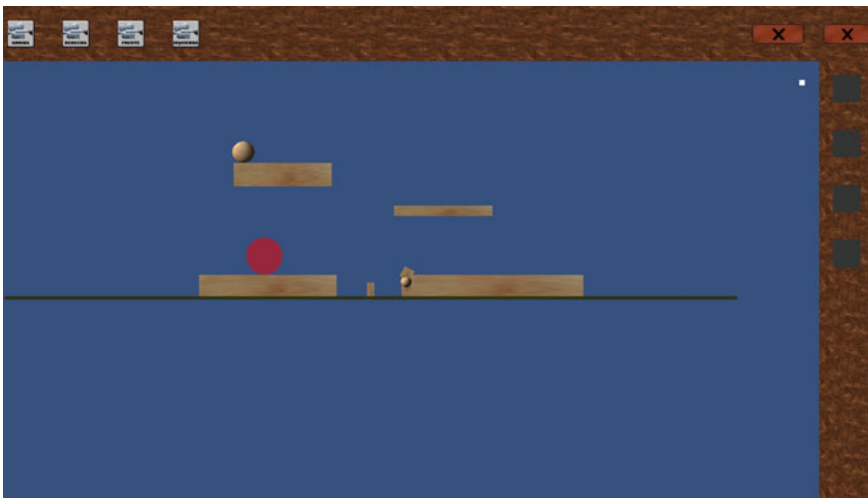


Fig. 8 Sandbox during test phase

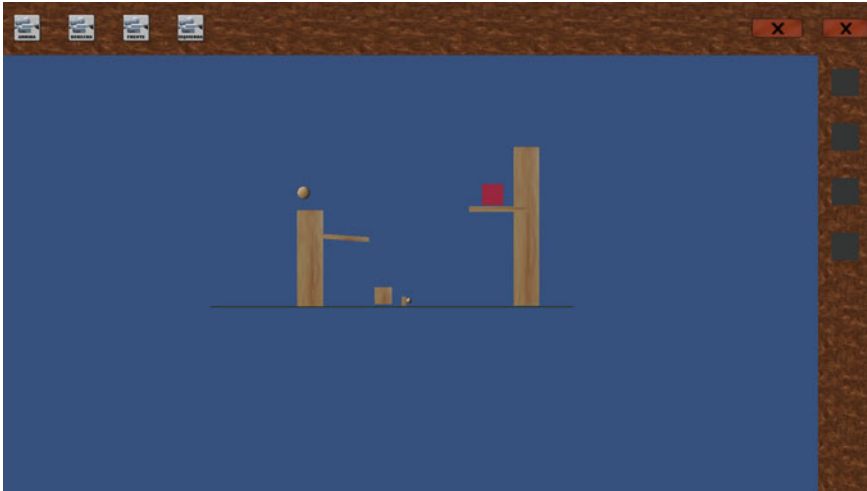


Fig. 9 First puzzle

Other important tip built in the sandbox's evaluation mechanism is the hypothesis that better knowledge relates to efficient use of resources [3, 7]. Many problems could be associated to a single object in the showroom. Each one requires a different interpretation of the applicability of the same concept. But in order to reach the highest scores it is mandatory to solve puzzles with the minimum required of pieces, otherwise the problem is solved but with a lower score, reflecting a lower degree of understanding.

Due the complexity of certain devices, the exposition has a specific organization that graduate the speed and amount of concept incorporated. Earlier devices are typically very simple, later ones require a high degree of expertise.

Figures 9, 10, 11 and 12 show some of the diverse games in the current set of puzzles designed just for inclined plane and lever.

2.2 *Server Modules*

The server has a module connected to a MySQL (c) database that holds the visitor's records and logs. All this information is used to profile performance of learning process for each individual and globally. The first tracking is useful to help understand and advice a student about the best practices suitable for his/her case. The second one allows a deeper understanding of the effects of certain multimedia tools and its specific configuration for certain concepts. Statistical analysis and modelling based on machine learning are the main activities of LEARNITRON ad part of this project, in order to evaluate and infer performance, and to develop a list of recommendations and best practices in the usage of multimedia for Engineering

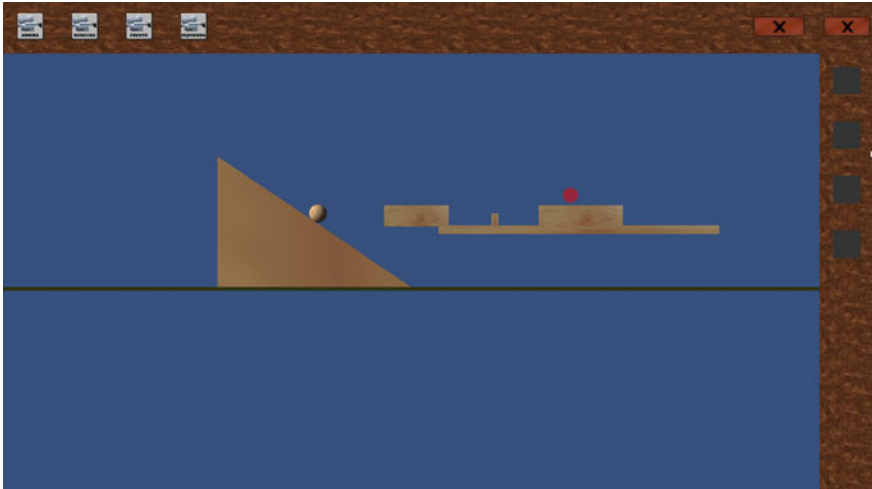


Fig. 10 Puzzle 2

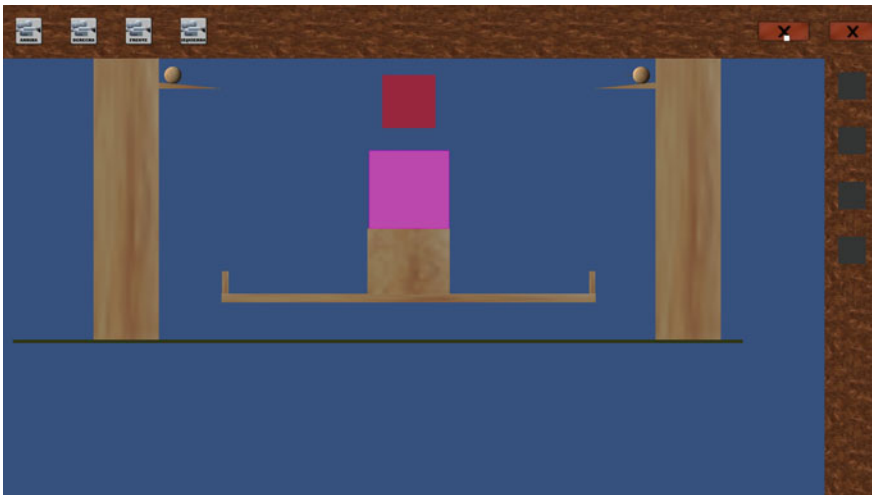


Fig. 11 Puzzle 3

education. Section 4, covers detailed information about statistical processing of part of the tracking data, and an explanation of its utility to understand how to manage to convert them into academic helpful hints.

Along the LEARNITRON model and tracking data, there is also user session information, to allow visitors to come back from other terminals, and keep playing, navigating the museum from the last session, and to hold the devices added to the private stock (this last feature is under implementation).

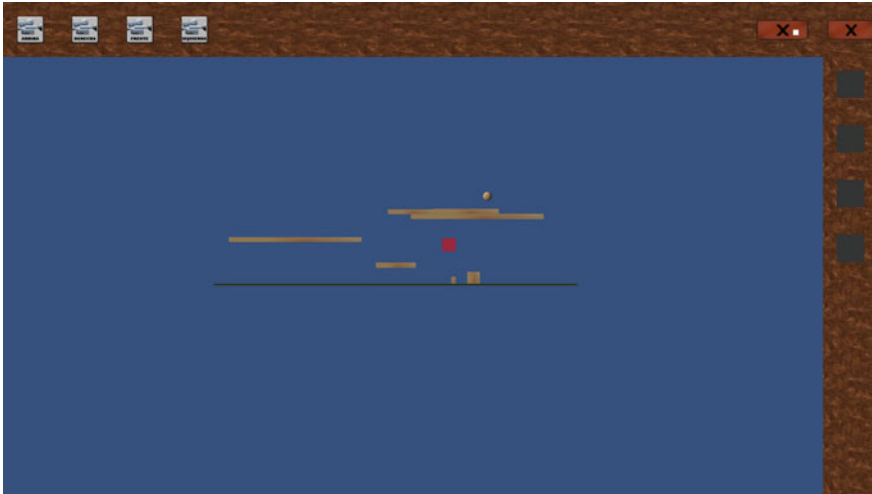


Fig. 12 Puzzle 4

2.3 User Modules

The user may log in from a PC or a mobile (if it has the software to connect and navigate in Internet, and to run Unity).

There is an option to keep session information locally, avoiding the requirement to improve performance and provide fault tolerance.

3 Tests and Statistics

Activity of any visitor is recorded in a log like the one in Fig. 13. This log file corresponds to only 2 min of a basic interaction with an object, and one puzzle. The user is identified as ID 10.

This section shows how the LEANTRON statistical evaluation finds out the expertise and part of the user learning preferences. It also has another module that models the learning profile but is under construction and out of the scope of this paper.

The logs and user information hold implicit information that may be turned explicit by statistical analysis and machine learning approaches. The only data required to do that are object identification, timestamps and activity performed.

At this point it is important to note that object in this context is not only a device part of the showroom but any software component or event from a programmer's point of view. This is so, because it constitutes the simplest approach to cover a wide range of activities (each one with custom properties) with a uniform notation.

	id	userid	date	actionId	objectId	value
<input type="checkbox"/> Editar Copiar Borrar	1	10	2014-03-17 00:36:30	0	10000	1
<input type="checkbox"/> Editar Copiar Borrar	2	10	2014-03-17 00:36:31	0	20001	1
<input type="checkbox"/> Editar Copiar Borrar	3	10	2014-03-17 00:36:32	0	40001	1
<input type="checkbox"/> Editar Copiar Borrar	4	10	2014-03-17 00:36:37	0	50001	1
<input type="checkbox"/> Editar Copiar Borrar	5	10	2014-03-17 00:36:39	0	50002	1
<input type="checkbox"/> Editar Copiar Borrar	6	10	2014-03-17 00:36:40	0	50001	1
<input type="checkbox"/> Editar Copiar Borrar	7	10	2014-03-17 00:36:41	0	60001	1
<input type="checkbox"/> Editar Copiar Borrar	8	10	2014-03-17 00:36:44	0	50001	1
<input type="checkbox"/> Editar Copiar Borrar	9	10	2014-03-17 00:36:51	0	40001	1
<input type="checkbox"/> Editar Copiar Borrar	10	10	2014-03-17 00:36:55	0	40002	1
<input type="checkbox"/> Editar Copiar Borrar	11	10	2014-03-17 00:37:01	0	40001	1
<input type="checkbox"/> Editar Copiar Borrar	12	10	2014-03-17 00:37:03	0	120001	1
<input type="checkbox"/> Editar Copiar Borrar	13	10	2014-03-17 00:37:03	0	130001	2
<input type="checkbox"/> Editar Copiar Borrar	14	10	2014-03-17 00:37:05	0	20001	1
<input type="checkbox"/> Editar Copiar Borrar	16	10	2014-03-17 00:37:06	0	80001	1
<input type="checkbox"/> Editar Copiar Borrar	17	10	2014-03-17 00:37:11	0	20001	1
<input type="checkbox"/> Editar Copiar Borrar	18	10	2014-03-17 00:37:21	0	80001	1
<input type="checkbox"/> Editar Copiar Borrar	19	10	2014-03-17 00:37:22	0	130001	1
<input type="checkbox"/> Editar Copiar Borrar	20	10	2014-03-17 00:37:22	0	90000	1
<input type="checkbox"/> Editar Copiar Borrar	21	10	2014-03-17 00:37:25	0	100000	1
<input type="checkbox"/> Editar Copiar Borrar	22	10	2014-03-17 00:37:27	0	90000	1
<input type="checkbox"/> Editar Copiar Borrar	23	10	2014-03-17 00:37:30	0	110001	1
<input type="checkbox"/> Editar Copiar Borrar	24	10	2014-03-17 00:37:42	0	110001	0
<input type="checkbox"/> Editar Copiar Borrar	25	10	2014-03-17 00:37:43	0	110001	1
<input type="checkbox"/> Editar Copiar Borrar	26	10	2014-03-17 00:37:43	0	110002	1
<input type="checkbox"/> Editar Copiar Borrar	27	10	2014-03-17 00:38:01	0	100000	1
<input type="checkbox"/> Editar Copiar Borrar	28	10	2014-03-17 00:38:04	0	90000	1
<input type="checkbox"/> Editar Copiar Borrar	29	10	2014-03-17 00:38:08	0	100000	1
<input type="checkbox"/> Editar Copiar Borrar	30	10	2014-03-17 00:38:10	0	90000	1
<input type="checkbox"/> Editar Copiar Borrar	31	10	2014-03-17 00:38:25	0	100000	1
<input type="checkbox"/> Editar Copiar Borrar	32	10	2014-03-17 00:38:26	0	130001	3
<input type="checkbox"/> Editar Copiar Borrar	36	10	2014-03-17 00:38:26	0	20001	1
<input type="checkbox"/> Editar Copiar Borrar	37	10	2014-03-17 00:38:29	0	10000	0

Marcar todos Para los elementos que están marcados: Cambiar Borrar Exportar

Mostrar : Fila de inicio: Número de filas: Cabeceras cada filas

Fig. 13 Trace log

As the object itself is well known, it is part of LEARNITRON task to use specific information about every object feature and user’s behaviour.

The trace covers the exact moment of every action, the component (objectId) and the type of activity (value).

Figure 13 shows the trace of an user that logs in into the showroom (objectID 20001), goes around and manipulates an invent (objectID 40001), reads its texts (objectID 50001 y 50002), assembles and disassembles the device, doesn't watch its video, and observes its photograph (objectID 60001). Then starts a game in the mock-up (objectID 80001), builds a device within the sandbox (objectID 90000), tests it (objectID 100000) and fails. Afterwards, he/she changes parts of the object, sorting of the pieces, resizes and reshapes them during its activity in the sandbox, and finally he/she wins the game (130001, value 3).

Data collected expresses the way the user accesses to the implicit concepts within each invent. That is the reason separated evaluations are performed for skills, learning profile and effective approach. Following subsections describe statistics obtained from Infostat (c) and Weka (c) for each one.

3.1 Skills Evaluation

Table 1 shows the absolute frequencies (FA), relative frequencies (FR) and mean value (MV) for objectID organized into 5 binds.

It is obvious that bin [52001-78001] has the lowest score. That means a reduced trend to text reading and photo watching (in fact, observers of the test noted that the visitor did not use the video).

Figures 14 and 15 are the histogram and pie graphic respectively.

Observe that objects in bin [78001-104001] were most frequently used. That bin represents editor and tests for functioning for the devices created in the sandbox. It is curious that despite the number of trials, a few number of elements from the stock were used to solve the puzzle (the frequency is very low).

From the previous findings, it can be asserted that the visitor is expert (a minimum number of components used very efficiently) and provided an adequate solution to the problem.

It can also be said that, for some unknown reason, the user is not interested in additional information (a good explanation could be his high knowledge in the device). The skilled management of the items shows a user that has good knowledge of the topic.

Table 1 Frequencies for objectID

ObjectID	FA	FR	MV
[1-26001]	7	0.21	13001
[26001-52001]	7	0.21	39001
[52001-78001]	1	0.03	65001
[78001-104001]	10	0.3	91001
[104001-130001]	8	0.24	117001

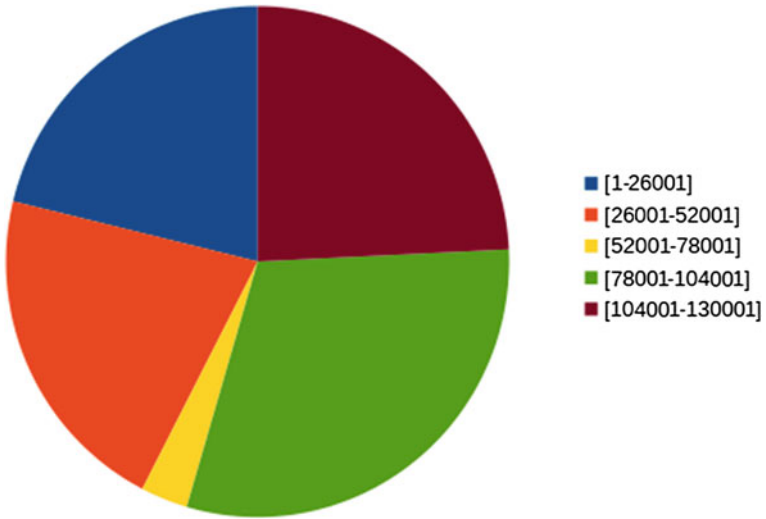


Fig. 14 Histogram of object usage

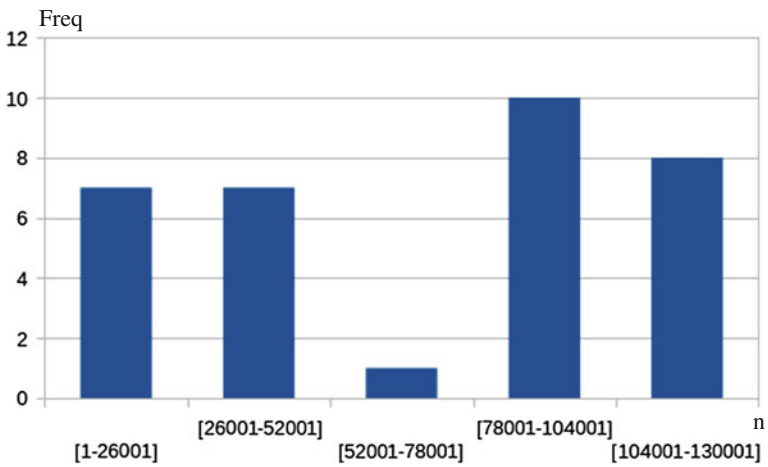


Fig. 15 Usage frequencies

3.2 Learning Profile

Although the accumulated relative frequencies polygon is useful to insight the empirical distribution shape for certain set of samples from a population [26], this usually requires a big number of samples in order to be a good approximation to the real population distribution.

There are a lot of graphics for single variable empirical distribution. This project uses the graphic built by InfoStat (c), that calculates the dots in the drawing following the algorithm depicted in Fig. 16.

The dots generated using Eq. (1) integrate a graphic presentation of the observed values for variable X and its empirical evaluation for every dot long Y axis.

The empirical distribution found for variable objectID can be used to evaluate the differences among its behaviour and big data, which is usually related to a normal distribution. Figure 17 shows the current values.

Empirical distribution is quite different to normal plots (see Fig. 18). This exhibits an object manipulation with an intentional behaviour, far away to an arbitrary manipulation.

The shape of Fig. 16, shows the user learning profile. More data could confirm the specific typical curve for this and similar visitors.

- 1 Let $x(1), x(2), \dots, x(n)$
Be samples of a population with size n
- 2 $x(1), x(2), \dots, x(n)$ sorted in ascending order
- 3 Calculate empirical distribution function for sample $x(i)$ to be:

$$F(x(i)) = \frac{(i - 0.375)}{(n + 0.25)} \quad (1)$$

Fig. 16 Empirical distribution for InfoStat (c)

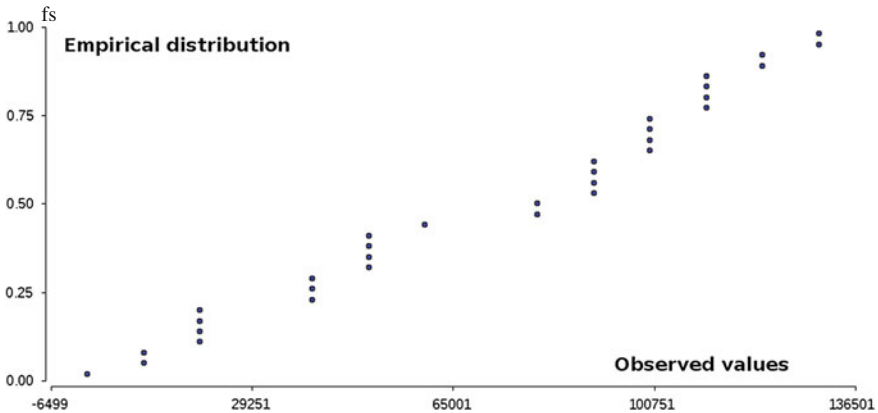


Fig. 17 Empirical distribution for objectID

Fig. 18 Empirical distribution for a typical normalized population

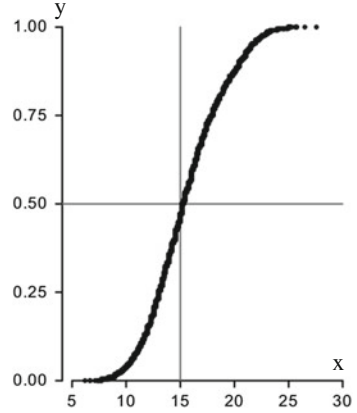


Table 2 Time distribution

ObjectID	Variable	n	Media	S.D.	Min	Max
10000	Time	2	2	1.41	1	3
20001	Time	4	2	2.16	0	5
40001	Time	3	18	24.43	1	46
40002	Time	1	4	0	4	4
50001	Time	3	3	2	1	5
50002	Time	1	2	0	2	2
60001	Time	1	1	0	1	1
80001	Time	2	5.5	6.36	1	10
90000	Time	4	1.75	1.26	0	3
100000	Time	4	20	25.91	3	58
110000	Time	2	7.5	6.36	3	12
110001	Time	1	1	0	1	1
110002	Time	1	0	0	0	0
120001	Time	2	1	1.41	0	2
130001	Time	2	1	0	1	1

Table 2 shows the mean value, Standard deviation (D.E.), minimum and maximum quantity of seconds for each objectID.

3.3 Effective Approach

For this evaluation it is important to relate the type of component and the time spent by the student with each one (see Table 2).

The highest time spent is for objects type 10000 (editor of the sandbox), followed by 110000 (parts of the invented device). All this suggests that the user spent

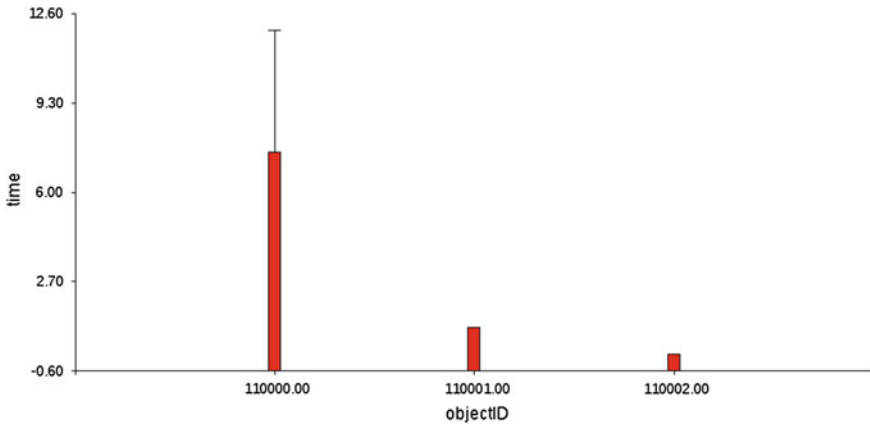


Fig. 19 Empirical distribution from data

more time manipulating components than visiting the showroom's objects. The behaviour can be summarized as a pragmatic person (preference for doing instead of reading, watching or listening).

Besides the type of components selected, timings describe pretty much about the user preferences. Figure 19 exposes more visually these characteristics.

The graphic shows a big prevalence of objects type 11000, with more time than the rest. It is important to note that the puzzle selected intends the usage of the three objects in the picture, but only object 11000 is very much most used than the rest.

It is interesting the specific characteristics of the problem. When the user gets into the sandbox, he has the following objects available: 11000, 11001, 11002, and 11003, from which the optimal solution just requires objects 11000 and 11001.

Whenever the user understands the related device, he can use this expertise to optimize the solution. Otherwise, he will require at least three objects. The visitor selects object 11002, but less time than the usual, suggesting that he realized that it should not be part of the solution. Then, he changes the object by 11001, and managed it until the successful building of the solution.

4 Conclusions and Future Work

This paper presented the global architectures and appearance of the MIDA interface. From the information presented in Sects. 1–3, it can be said:

- User activity is represented in times, type and number of objects manipulated
- It is possible to infer the activity performed using trace data
- It is possible to infer expertise and difficulties experienced by the visitor, using simple statistics on tracking data

- It is possible to know the expertise tracking the time spent with every object
- It is possible to define preferences for a set of users and customize sequence of learning
- The shape of Fig. 17 can be used as a user profile but with more data it can be a characterization of subsets of students. From the previous analysis, it is possible to define learning trends and therefore teaching approaches.

It remains to improve many technical details (hybrid persistency, portable scoring tables, social media communications, and more ancient devices and showrooms).

Other future activities are:

- Increase the tracking to specific object information (colour, size, sounds)
- Evaluate individual characteristics VS typical profiles, and its uses in education improvement
- Make comparative tracking of an individual along time (several sessions)
- Develop a reporting module to let people access to meaningful information and summaries

Regarding the statistics and the learning modelling, the machine learning that uses this statistical information is under construction and will be fully tested using an extensive testing.

References

1. Fernández M, Kumpel D (1992) Pedagogy and Multimedia (Multimedia y Pedagogía). CIIIE 2
2. Rodríguez Muñoz F (2011) Contributions of neuroscience to the understanding of human creativity. *Arte, Individuo y Sociedad* 23(2):45–54. doi:10.5209/rev_ARIS.2011.v23.n2.36253
3. Barron F, Harrington D (1981) Creativity, Intelligence, and Personality. *Annu Rev Psychol* 32:439–476
4. Palaniappan A (2008) Influence of intelligence on the relationship between creativity and academic achievement: a comparative study. In: Learning Conference 08. Ref: L08P0484
5. Foong L, Shariffudin R, Mislan N (2012) Pattern and relationship between multiple intelligences, personality traits and critical thinking skills among high achievers. In: 3rd international conference on e-education, e-business, e-management and e-learning. IACSIT Press, IPEDR vol 27
6. Ghraibeh A (2011) Brain based learning and its relation with multiple intelligences. *Int J Psychol Stud* 4(1):103–113. Canadian Center of Science and Education. doi:10.5539/ijps.v4n1p103
7. Kim K, Cramond B, VanTassel-Baska J (2010) The relationship between creativity and intelligence. Cambridge University Press, Cambridge, Chapter 21, pp 395–412. <http://dx.doi.org/10.1017/CBO9780511763205.025>
8. Fridman L (1999) Introduction to control system technology, 6th edn
9. Marton P (1996) Educational profiles (Perfiles Educativos) RedALIC 72
10. Porcher L (1980) Audiovisual media. CINCEL S. A, Madrid
11. Valverde J, Garrido M, Sosa M (2010) Educational regulations for TICs in Extremadura (Políticas educativas para la integración de las TIC en Extremadura). *Educación*. 352:77–98

12. Albert Gómez MJ (1997) Multimedia and social pedagogy (Medios audiovisuales-multimedia y pedagogía social). *Educación Social* 7
13. Aguaded J, y Martínez E (1998) Media, resources and didactic technology for professional education. *Comunicara* (11)
14. Postman L (1961) Human learning and audiovisual education. *Audiov Commun Rev* 9(5):68–78
15. Díaz M, Gutierrez R (1999) Resources and audiovisual techniques (Recursos y técnicas audiovisuales). *Enseñanza universitaria* 1:361–368. ISSN 1131-5245
16. Cabrero J (1999) University technology (Tecnología educativa). Universidad de Sevilla, Madrid
17. Adame Tomás A (2009) Audiovisual media in classroom (Medios Audiovisuales En El Aula). DEP. LEGAL: GR 2922/2007 No 19. ISSN 1988-6047
18. Lucero F, Gonzalez JJ, Cubo S (2009) Pedagogic perspective for multimedia (Perspectiva pedagógica de los multimedia). *Revista Española de Pedagogía* 225(61):309–336
19. González Castlán Y (2013) Tutorial videos as a tool for pedagogy (El Video Tutorial como Herramienta de Apoyo Pedagógico). *Vida científica* 1
20. Zambrano J (1998) Multimedia: pedagogic functionality translator (Multimedia: Traductor de Funcionalidades Pedagógicas). *RIBIE IV*
21. Jimenez A (1996) A pedagogy of multi-literacies: designing social futures. *Harvard Educ Rev* 66:60–92
22. Way E (2007) Ethics and multimedia pedagogy (Ética y pedagogía multimedia). *PUPC* 16(31)
23. Alonso R (1995) Pedagogic documentation (La documentación pedagógica). *Revista Complutense de Educación* 6(1)
24. Delgado S (2003) Pedagogic perspective for multimedia (Perspectiva pedagógica de los multimedia). *Revista Española de Pedagogía* 225:309–336
25. Castellanos M (2003) Project based learning: a methodology for the meaningful learning of high-school physics. *Pedagogy v.* 24:69
26. Zambrano F (2012) *Infostat Manual*

Educational Assessment Engineering: A Pattern Approach

Paul Hubert Vossen

Abstract In this paper we will propose a pattern approach to educational assessment. To begin with, the context of classroom-based assessment will be described in order to set the stage. Then the ingredients of a so-called reference model for assessment rating and scoring in education will be presented. This reference model is based on theoretical concepts and techniques borrowed from discrete mathematics and fuzzy logic. It is the result of 8 years of research and development, including classroom experimenting with preliminary versions of the reference model. Finally, we will propose a visual pattern language which will help assessors to design their own assessment schemes compatible with the assessment task at hand.

Keywords Educational assessment · Assessment engineering · Assessment design · Pattern · Scheme · Profile · Scale · Measuring · Counting · Rating · Scoring · Grading

1 Problem Statement

In contrast to high-stakes, large-scale, standards-based testing on a (inter)national level, for *classroom-based assessment*¹ (CBA) there isn't an engineering approach to *educational assessment* based on a mathematical theory of *rating* and *scoring*. This is the more astonishing as *assessment* for educational purposes has a very long tradition [1, 2]. The lack of an adequate full-blown theory and method of *educational assessment* design for CBA has profound negative consequences for us as

¹Terms or phrases in *italics* refer to concepts which have a specific meaning in or for the reference model proposed in this paper and which may more or less deviate from their use in other contexts.

P.H. Vossen (✉)
Research Center SQUIRE, Niederstetten, Germany
e-mail: p.h.vossen@googlemail.com

teachers and *assessors*. For instance, even after an extensive literature research we couldn't find a suitable principled solution to the *team-mate dilemma* (TMD), i.e. how to assign *scores* to individual students who work in teams on larger projects, as implied and practiced by so-called problem-based learning (PBL), an approach often seen in (software) engineering courses [3].

Starting from this well-known *assessment* problem, we successively developed a comprehensive *assessment reference model* (cf. [4] for an explanation of the term *reference model*), which not only solves the *Team-Mate-Dilemma*, but a host of other practical problems typically encountered in the context of CBA and similar authentic learning and training contexts. This paper is not meant to delve into all those issues solved by our approach [5]. Here it suffices to note, that by design the *reference model* (aka as meta-model, or generic model) is applicable to many teaching and learning contexts, to any kind of *assignment* with its specific response type, to *holistic assessment* [6] on an arbitrary ordinal scale without explicit *assessment criteria*, to *analytic assessment* with an arbitrary number and type of *assessment criteria*, to *assessment* with a single *assessor* or with multiple *assessors*, with a binary quality scale (e.g. correct vs. incorrect) or a quality scale with an arbitrary number of levels (e.g. a 3-point scale, a 5-point scale, etc.) [7].

We have dubbed this generic approach to *educational assessment* PASS, short for performance assessment scoring system. Indeed, the system is *prima facie* concerned with *assessment rating* and *scoring*, however, the main goal of a sound and complete *performance rating* and *scoring* system is ultimately to be able to give students timely and accurate feedback about their learning performance on given *assignments* (i.e., *assessment tasks*) in the spirit of *formative assessment* [8, 9]. Thus it is a crucial link in TLA, the *Teaching-Learning-Assessing* cycle of education.

The outline of this paper is as follows. First, we will explain the important distinction between *assignment types* and *assessment types*. Then we will discuss basic and complex *assessment rating and scoring procedures* and how these can be specified by precisely defined mathematical functions (for technical details about these functions, see our website www.scoring.de.vu). Given the underlying *assessment* functions of PASS it is possible to introduce *assessment patterns* as building blocks for *assessment design*, both simple and complex. We will introduce a highly visual representation of such *assessment patterns* so that a concise textual explanation will suffice to understand how *assessment schemes* of arbitrary complexity can be built up using a single construction principle. In order to show the overall *assessment structure and flow* depicted by any such scheme we will present an example *glass-box assessment scheme* showing a variety of *assessment patterns* and how they are related in a *cluster of assignments*. Finally, we will propose a preliminary *assignment-assessment matching table* as a simple device (still under development) to select an appropriate *assessment scheme* for any given *assignment type*.

2 Assignment Types

As part of a comprehensive TLA process, students will be assessed with respect to progress towards and achievement of their learning goals. *Assignments* are the explicit, concrete means by which teachers try to make this learning progress observable, analyzable and understandable. *Assignments* can be very simple, e.g. consisting of a sequence of yes-no-questions or multiple-choice items at an end-of-course examination, but may also be set up as complex interactive class exercises, in-class group projects or individual homework projects.

As long as *assignments* are only of a more or less primitive question-answering or apply-the-rules type, aimed at certifying what students know or can do, *rating* and *scoring* is not much of an issue [2]. However, nowadays, more and more teachers adopt much more realistic and challenging learning objectives and learning tasks under the banner of *authentic learning* [8].

In such a context, *assignments* may be larger tasks, taking many hours, days or even weeks, both within class and at home, and the overall task may be split up into several component subtasks, all to be assessed separately at first and then combined in a single *end score*, possibly mapped onto an overall course grade if needed. For such situations, more elaborate *assessment schemes* are needed, which weren't available when we started up our research on PASS in 2007, and which are still not available today.

3 Assessment Types

We are primarily interested in so-called *formative assessment* [9, 10], which considers *assessment* to be an integral, crucial part of the *Teaching-Learning-Assessing* cycle. Thus, *assessment rating* and *scoring* are not only considered ends in themselves as in *summative assessment* [11], though a means of reflection, communication, documentation and instruction aimed at improving both teaching and learning.

Relevant *assessment types* should be able to deal with quite distinct *assessment* contexts, modes and parameters. Also, the role of the *assessor* is becoming much more important and critical, because most often *authentic tasks* have a complexity, variety and openness which doesn't allow simple *scoring* modes which just count the number of items done correctly within a prescribed amount of time (by and large the paradigm of classical test theory [12]). On the contrary, it is not uncommon for *authentic assessment* to deal with dozens if not hundreds of independent or interdependent *indicators* of learning progress and learning outcomes. Hence, the question looms large, how to structure the entire *assessment* component of the TLA cycle in a meaningful and effective way.

For instance, *performance quality indicators* come mainly in two forms: either *scores* on a bounded ordinal quality scale (best represented by the unit interval) or

rates on an *ordinal scale* with a single lower bound (best represented by the nonnegative real number line). A non-trivial issue is, how such different *indicators* can be merged in a systematic, meaningful way. It turned out that a satisfactory answer was to be found in the field of fuzzy logic [13, 14], especially in a recent paper on so-called *Tied Adjointness Algebra* [15].

Behavioral observation and its modern variant learning analytics [16] however aren't yet assessing. Assessing also implies, in our view, expressing what one has observed and analyzed in a way that enables adequate feedback and comparison over time or across students. PASS is also meant to support such assessment reporting and analysis as part of the TLA cycle.

4 Basic Assessment

Basic to our *educational assessment reference model* are so-called *scores*: quality judgments on a scale from 0 to 1, usually represented as percentages. Such judgments can be made by an experienced assessor in a *holistic* manner [6], i.e. without explicitly using *quality criteria*, although one may assume, that the *assessor* has tacitly applied relevant *quality criteria* before giving a personal judgment in the form of a single *score*. More often, however, such judgments will be the result of an explicit procedure of applying and aggregating several *quality criteria* of a simple nature, so-called *n-point ordinal scales*, where n is called the *granularity* of the *quality scale* (cf. [17] for a typical example). This is the approach we adopted for PASS too, but we extended it in several fundamental ways.

First, we assumed that an *assessor* will be able to specify for each *quality criterion* a distribution of a given number of *credit points* over the levels of the adopted *n-point scale*, instead of just selecting one single level of it. Secondly, we assumed that it usually makes sense to add the number of *credit points* per quality level to arrive at a *quality mass distribution* aggregated over all *quality criteria*. This distribution may then be standardized by dividing through the total number of *credit points* over all criteria to arrive at a kind of probability distribution over the *n-point ordinal scale*. This is what we have called a *quality profile* for a given *assignment*. Such quality profiles may be totally ordered using the function **rank** or its quasi-complement **rank** from which one may calculate a *score* somewhere in between, representing the personal *tolerance* of the *assessor* (Fig. 1; here, B signifies the well-known Beta-function: cf. http://en.wikipedia.org/wiki/Beta_function).

This then is the general *profile-based standardized scoring* formula of *basic assessment*. There are three special cases of this *scoring formula*: if the degree of *granularity* is two, one has classical tests and examinations with just two levels of quality: correct/incorrect, good/bad, etc.; if no explicit *quality criteria* are used, one has classical *holistic assessment* using a *quality distribution* (instead of a point); if both degree of *granularity* is two and no explicit criteria are given, then one has the special case mentioned above in which a *score* (percentage) is directly specified.

Scoring : Tolerance \times Probability Granularity \rightarrow Score

$$\text{Scoring}(\tau, \mathbf{p}) \cong \tau \cdot \max(\text{rank}(\mathbf{p}), \overline{\text{rank}}(\mathbf{p})) + (1 - \tau) \cdot \min(\text{rank}(\mathbf{p}), \overline{\text{rank}}(\mathbf{p}))$$

$\mathbf{p} = (p_1, \dots, p_n) : \text{Granularity} \rightarrow \text{Probability}$ with $\sum_{k=1}^n p_k = 1$

$$\text{rank}(\mathbf{p}) = \frac{1}{n-1} \sum_{i=1}^{n-1} \frac{1}{i \cdot B(i, \sum_{k=n+1-i}^{n-1} p_k)}$$

$$\overline{\text{rank}}(\mathbf{p}) = 1 - \frac{1}{n-1} \sum_{i=1}^{n-1} \frac{1}{i \cdot B(i, \sum_{k=1}^i p_k)}$$

Fig. 1 Profile-based standardized scoring

5 Complex Assessment

Once one has calculated *scores* for *assignments* belonging to an *assignment cluster*, the question arises how to combine those multiple *scores* into a single *score*. For this, we developed a *scoring formula* called *combining*, which can be viewed as a generalization of the geometric mean. Indeed, the *scores* s will be combined by multiplying factors of the form s^w where the weights w add up to 1. Alternatively, one may take powers w of the 1-complements of s , multiplying through and then taking the 1-complement of the resulting product. It turns out, that the former product is always smaller than the latter complement [18], so that a parameter *lenience* is required, to pick a combined *score* between both extremes (Fig. 2).

Another approach is required to increase or decrease a given *score* based upon the nonnegative value of an indicator of type *rate*, which results from counting or measuring some aspect of learning performance. We have called such a procedure *refining a given score*, because it starts from a given *score* (e.g., a *profile-based score*) and takes a single *rate* indicator to adjust that initial *score* (Fig. 3). The parameter *impact* determines, how much the *rate* indicator will influence the given

Combining : Lenience \times Weight^m \times Score^m \rightarrow Score

$$\text{Combining}(\lambda, w_1, \dots, w_m, s_1, \dots, s_m) \cong \lambda \cdot \overline{s^w} + (1 - \lambda) \cdot s^w$$

$$s^w \cong \text{Combining}(0, w_1, \dots, w_m, s_1, \dots, s_m) \cong \prod_{i=1}^m s_i^{w_i}$$

$$\overline{s^w} \cong \text{Combining}(1, w_1, \dots, w_m, s_1, \dots, s_m) \cong 1 - \prod_{i=1}^m (1 - s_i)^{w_i}$$

$$s^w \leq \overline{s^w}$$

Fig. 2 Combining several scores into a single overall weighted score (exhibiting a single configuration parameter *lenience*)

$$\begin{aligned}
 &\mathbf{Refining} : \mathit{Impact} \times \mathit{Rate} \times \mathit{Score} \rightarrow \mathit{Score} \\
 &\mathbf{Refining}(\delta, \sigma, s) \stackrel{\text{def}}{=} \frac{1 - (\delta \cdot (1-s))^\sigma}{1 - \delta \cdot (1-s)} \times s \\
 &\mathbf{Refining}^{-1} : \mathit{Impact} \times \mathit{Score} \times \mathit{Score} \rightarrow \mathit{Rate} \\
 &\mathbf{Refining}^{-1}(\delta_0, s_0, s) \stackrel{\text{def}}{=} \begin{cases} 1 & \text{if } \delta_0 = 0 \text{ or } s_0 = 0 \text{ or } s_0 = 1 \\ \frac{\ln\left(1 - \left(\frac{s}{s_0}\right)(1 - \delta_0(1 - s_0))\right)}{\ln \delta_0(1 - s_0)} & \text{if } \delta_0 \neq 0 \text{ and } s_0 \neq 0 \text{ and } s_0 \neq 1 \text{ and } s < \frac{s_0}{1 - \delta_0(1 - s_0)} \\ \infty & \text{if } \delta_0 \neq 0 \text{ and } s_0 \neq 0 \text{ and } s_0 \neq 1 \text{ and } s \geq \frac{s_0}{1 - \delta_0(1 - s_0)} \end{cases}
 \end{aligned}$$

Fig. 3 Refining a score by using a rate to get a new score, and its inverse (exhibiting a single configuration parameter *impact*)

score. The resulting new score may be used again as the starting point for further refinement, hence the alternative name *iterative scoring* for this procedure.

A third function called *benchmarking*, is based on the same formula as *refinement*, but goes into the other direction (hence *inverse refining*): it takes a *profile-based* or other single score, compares it with a so-called *benchmark score* and calculates the *rate* which would transform the *benchmark score* into the *observed score*. In this way it is possible to use a normal *profile-based score* to act as a *rate* working on another *score*.

6 Grading Systems

At the end of a possibly complex chain of *scoring*, *refining*, *benchmarking* and *combining* one will be left with a single *score* which represents in a well-defined way all the *assignments* and *assessments* that should be taken into account. Now the last step can be done: converting this *final score* into an alphanumeric or symbolic *grade* of a given *grade system*. *Grades* aren't usually meant for further calculation, rather they will be used for documenting, reporting and communicating the learning achievements, i.e. knowledge and skills, of a student or trainee. Thus, *grades* are best thought of as literals denoting ordered categories of competence, even when they come across in the form of numbers, i.e., as numerals.

Many different *grading systems* exist all over the world, and the way that *scores* are related to *grades* may be all but trivial or intuitive [19, 20]. Fortunately, this conversion problem is mostly solved on an institutional level, i.e. *assessors* are provided with a *conversion formula* or *conversion table* along with further rules how to do the conversion. In this paper we will not deal with any of those institutional *conversion schemes and practices*, as this would seriously put in question the generality of our approach. Instead, we will propose a general *parameterized*

$$\begin{aligned}
 \text{Grading} &: \text{Curvature} \times \text{Polarity} \times \text{Score} \rightarrow [\underline{G}, \overline{G}] \\
 \text{Grading}(r, p, s) &\cong \gamma_{rps} \cdot \underline{G} + (1 - \gamma_{rps}) \cdot \overline{G} \\
 \gamma_{rps} &\cong p\sqrt{1 - s^r} + (1 - p)(1 - \sqrt{1 - s^r}) \\
 \text{standard polarity: } &\gamma_{r10} = \underline{G} \quad \gamma_{r11} = \overline{G} \\
 \text{reverse polarity: } &\gamma_{r00} = \overline{G} \quad \gamma_{r01} = \underline{G}
 \end{aligned}$$

Fig. 4 Grading as a mapping from the score scale onto some grade scale (exhibiting two configuration parameters *curvature* and *polarity*)

conversion formula (Fig. 4), which takes into account the allowed range of the *grades* (minimum and maximum), the *curvature* of the *conversion relationship* (linear or not) as well as the *polarity* of the *conversion relationship* (does higher *scores* lead to higher *grades* or the reverse?). As it turns out, a broad variety of quasi-numerical grading practices can be covered in this way.

7 Assessment Patterns

In the previous sections we have introduced the basic concepts and constructs out of which all *assessment patterns* may be built up. Patterns are a well-known concept in software design [21] as well as educational design [22]. *Assessment patterns* define in a data-driven way, how an *assessor* arrives at his appraisals of observed responses to *assignments* (i.e., the *assessment inputs*) in terms of *assessment rates* and *scores*. Following the logic of the previous three sections we distinguish 8 *assessment patterns*: 4 basic *assessment patterns* (together known as *profile-based scoring*), 3 complex *assessment patterns* (relating *rates* and *scores*) and one *assessment pattern* for *grading* (Fig. 5). Definitions and short explanations follow now.

Pattern H₂ (holistic two-level scoring). This is the simplest form of *assessment*: specifying a *score* as a number between 0 and 1, inclusively. Often such a score will be expressed as a percentage. Implicitly, two quality levels are assumed: good/bad, correct/incorrect, etc. Intuitively it means, that the *assessor* gives an estimate of the degree of quality (fuzzy interpretation) or of the chance that the overall quality of the assessed object or aspect is good (probabilistic interpretation). As simple as it looks, this kind of direct numerical *assessment* has some serious drawbacks. People aren't very good in doing such kind of direct judgments of quality or probability. Thus reliability and validity may be at stake. Also having only two levels of quality is severely restricting, forcing one to a very coarse statement, notwithstanding the apparent (but mostly illusory) precision of the score given.

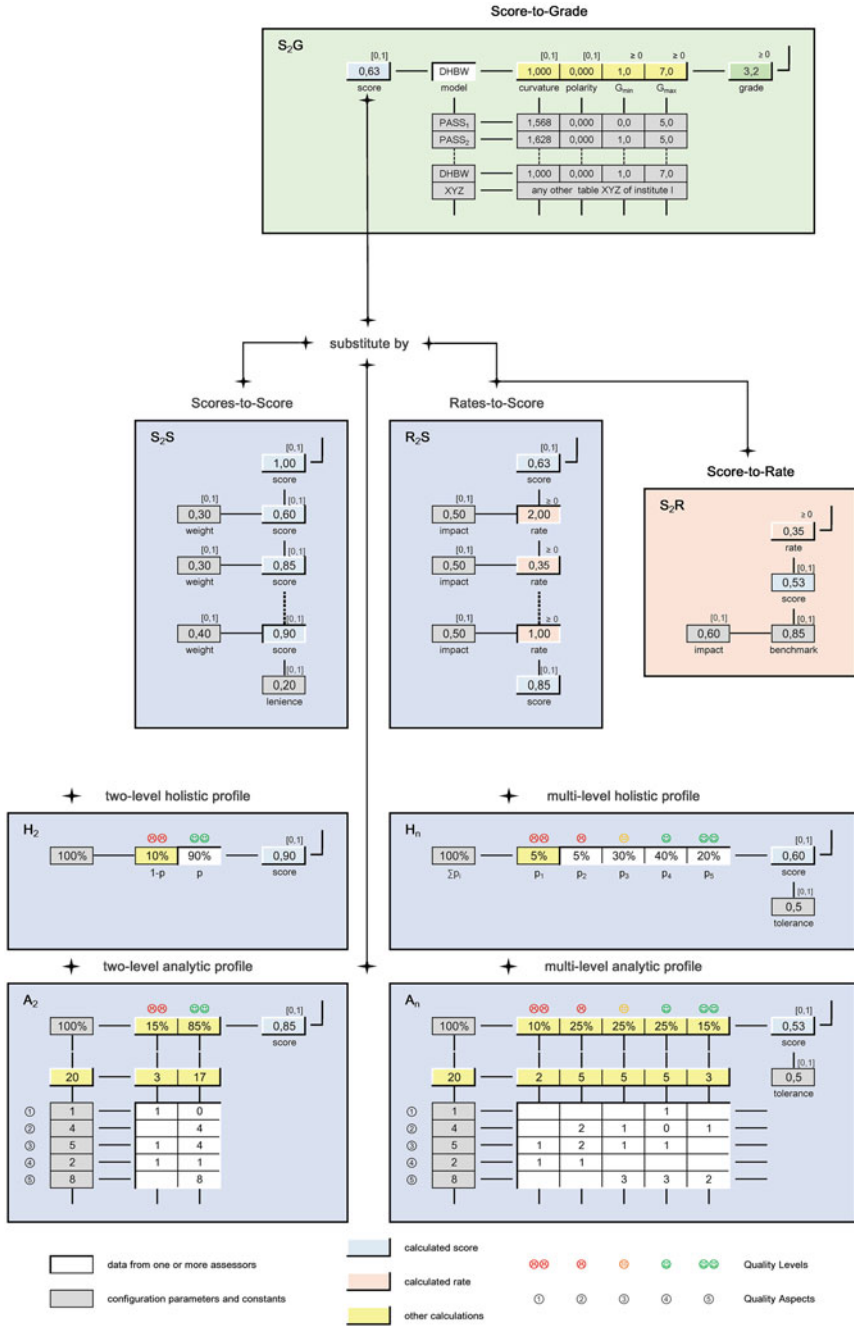


Fig. 5 Assessment patterns

Pattern H_n (holistic multi-level scoring). This *pattern* addresses the latter objection of having only two quality levels to choose from. Instead, this *pattern* offers more than two quality levels and thus enables *assessors* to express a finer scaled opinion or judgment about the overall quality. This will be done by distributing a total of 100 % (or any other total quantity) over the n quality levels, i.e. the *assessor* acknowledges different levels of quality in the observed evidence of competence from learner's responses. From this so-called *scoring profile* the basic *scoring formula* calculates a unique overall score, taking *assessor's tolerance* into account. However, the *pattern* doesn't force or enable the *assessor* to explicate the reasons (i.e., criteria) for his differentiated profiling.

Pattern A_2 (analytic two-level scoring). Here one has a *pattern* which can be observed very often in daily practice of CBA and beyond. For instance, this *assessment pattern* is applied to *assignments* which are composed of two or more items, e.g. questions or exercises, which can be checked individually for correctness and completeness, and which may be awarded a maximum number of (*credit*) *points*. If p points are given on the positive side, the rest of the maximum points will be automatically allotted to the negative side. The total number of points on the positive side over all items will then be divided by the sum of all maximum points per item, in order to get a percentage. This will be the *score* generated by this *pattern*. There are many variants of *assessments* which follow this *assessment pattern*. It is easy to implement, and the *score* is easy to calculate, which makes it so popular, however, it only uses two very coarse quality levels.

Pattern A_n (analytic multi-level scoring). Like H_2 , the weak point of A_2 is that only two quality levels are distinguished. *Pattern A_n* , the most general of the *profile-based scoring patterns*, allows any number n of quality levels. Moreover, the difference with H_n is that the quality distribution is not directly estimated by entering probabilities at the respective quality levels, but instead those probabilities are calculated from the distributions of points over all (m) distinguished *quality criteria*. Thus the *quality profile* has a strong empirical basis which also serves as a justification of the overall *assessment*. The calculation of the *score* proceeds in exactly the same way as with H_n .

Pattern S_2S (scores-to-score, aka weighted scores). This *weighted scores pattern* has already been defined in Sect. 5 under the label *combining scores*. It is the generalization of the geometric mean (GM), which is more appropriate for *scores* on the unit interval than a common arithmetic mean (AM). The generalization comes from introducing different weights for the respective *scores* such that the sum of weights is 1. If all weights are set equal to $1/k$, k being the number of *scores* to be merged, then the geometric mean is back. There is both an optimistic and a pessimistic variant of such a generalized GM, which gives the *assessor* a bit of freedom to express how *lenient* he or she wants to be when applying this *assessment pattern*. This *pattern* enables the *assessor* for instance to aggregate multiple *scores* for the *assignments* within an *assignment cluster*.

Pattern R_2S (rate-to-score, aka iterated scores). The *iterated scores pattern* has been initially invented to solve TMD, the *Team-Mate-Dilemma* mentioned at the beginning of this paper (for a more general treatment on group assessment see [23]). However, its use in PASS has got a much broader significance, as it is the dedicated *pattern* which converts *rates* (resulting from counting or measuring) into *scores*. The underlying idea is to calculate a kind of bonus-malus-factor on the basis of a given *score*, the *rate* in question and a so-called *impact* parameter (defined on the unit interval, like all PASS parameters), which determines how strong the influence of the *rate* on the *score* might be. An *impact* of 0 implies that the *rate* won't have any influence at all on the *score*, an *impact* of 1 implies that the *score* can be increased up to 1 depending upon the value of the *rate*. The given *score* will be multiplied by the *bonus-malus-factor*, which is defined in such a way, that the product will again be a *score* on the unit interval. A *bonus-malus-factor* of 1 has a special meaning: it implies that the *score* will not change at all. A *bonus-malus-factor* below 1 acts as a *malus* (the *score* will be decreased), a *bonus-malus-factor* above 1 acts as a *bonus* (the *score* will be increased). Finally, a special role is played by a *binary bonus-malus-factor* (corresponding to a *rate* of either 0 or 1) as it acts as a knock-out criterion, e.g. plagiarism or not.

Pattern S_2R (score-to-rate, aka benchmarked scores). Sometimes one wants a profile-based *score* to act on another *score* as if it were a *rate* (see preceding *pattern R_2S*) in order to get the advantages of a *bonus-malus-factor*. Thus one needs a mechanism to convert a *score* into a *rate*. This can be accomplished easily by “inverting” the refining formula already introduced in Sect. 5: assume a *benchmark score* (serving as a kind of standard or norm, because the *rate* will turn out to be 1 if the observed *score* equals the *benchmark score*) and a given degree of *impact*, and then calculate the *rate* which would produce the given *score*. Thus one has in fact a well-defined *rate* that can be used in another application of the previous *pattern* (R_2S).

Pattern S_2G (score-to-grade, grading for short). Finally, the *pattern S_2G* is PASS owns *grading formula* introduced in Sect. 6 or any other procedure (*conversion function* or *conversion table*) adopted by the educational institution issuing *grades*. We will not further dwell on this here (cf. explanation in Sect. 6).

8 Assessment Schemes

With the *assessment patterns* (Sect. 7) at hand, we are able to construct any convoluted *assessment schemes* we like. Of course, for practical purposes *assessment schemes* should be as simple as possible, however, as the *assignment* structure and *assessment* design force us to take complex relationships into account, we want our *assessment patterns* to support and not hinder us in this respect. It turns out that there is a simple *construction principle* for any *assessment scheme*:

Construction Principle for Assessment Schemes

Start with the grading pattern S_2G . Substitute for the score in S_2G any assessment pattern which has a score as output: S_2S , R_2S , or any of the four *profile patterns*. Then, in S_2S , substitute for any input score any assessment pattern which produces a score as output. Otherwise, in R_2S , replace any calculated rate into an instance of the score-to-rate pattern S_2R . Finally, repeat this process until no substitution or replacement can be made any more.

How this works can be seen in Fig. 6. From the construction principle above and the example on the next page it will be clear, that any *assessment scheme* can be represented by a *tree of assessment patterns* starting with S_2G , having any number of non-terminal nodes S_2S or R_2S , and ending with one or more *profile-scoring assessment patterns* H_2 , H_n , A_2 or A_n , which constitute the leaves of the tree. This fictitious *assessment scheme* has been specially constructed to show various *assessment patterns*. Actually, all *assessment patterns* are represented, making the scheme itself rather unrealistic, although formally entirely correct. The structure and flow of *assessment* can be easily followed. There are four *assignments*, one of which is a sub-*assignment* acting within a R_2S pattern. The other three *assignments* yield *scores*, based on some *profile-based scoring pattern*, which are then merged by means of the S_2S pattern. At the end, the *final score* is converted into a grade using the S_2G pattern with the generic PASS formula.

9 Choosing Assessment Patterns for Given Assignment Types

Existing *assignment types* are usually based on preconceived ideas about what kind of *assessment type* will be adequate and practical. Thus one may expect to find one or more *assessment patterns* closely associated with existing *assignment types*. We have worked out this hypothesis for a number of familiar *assignments*. The result is shown in Table 1. Although this table is far from complete, it already shows clearly, that indeed all *assessment patterns* can be found in practice, and also that some *assessment patterns* are more frequently used than other ones. More importantly, up to now we have found **no** example of an *assignment-assessment type* which can't be covered by a combination of the 8 *assessment patterns* introduced in this paper. This empirical fact confirms our belief that our set of *assessment patterns* is—for all practical purposes—indeed a complete set.

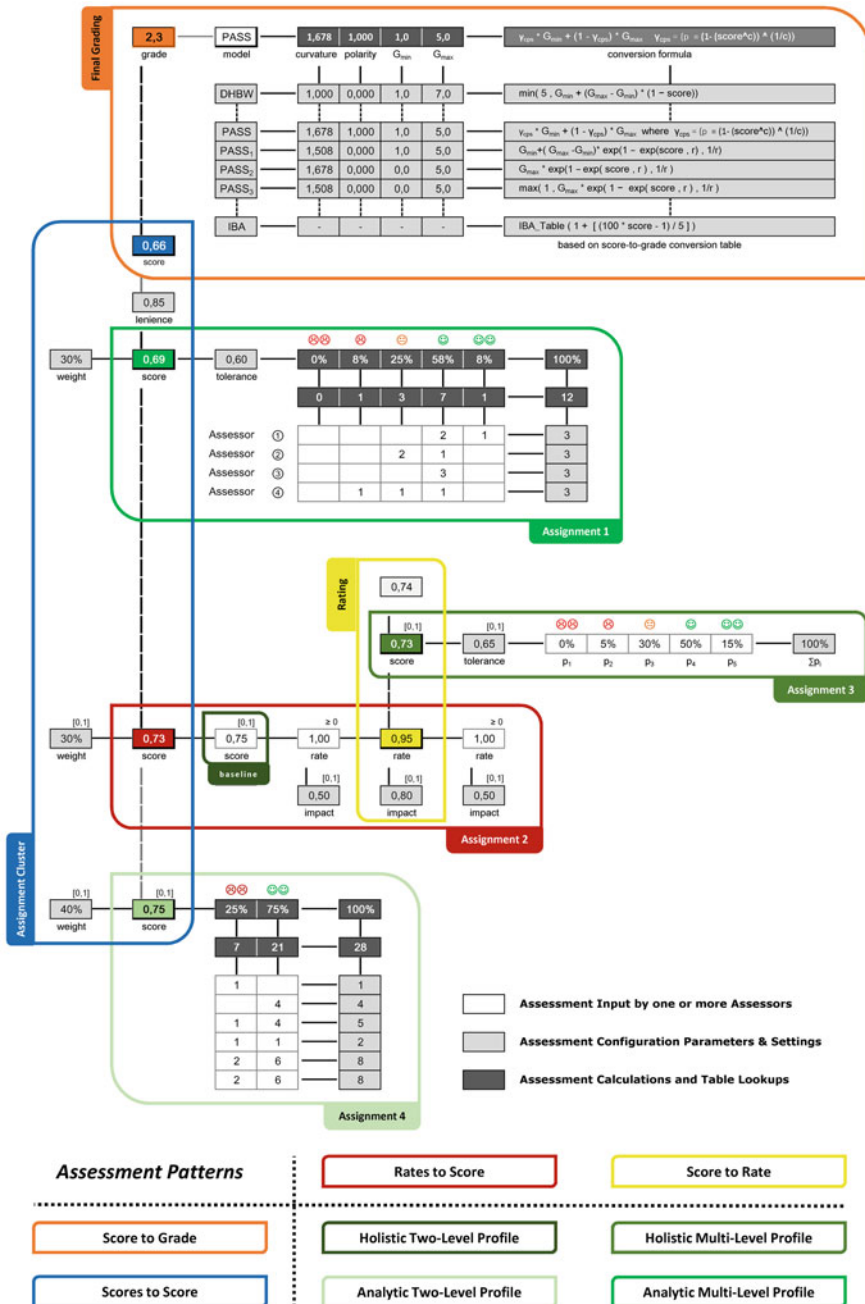


Fig. 6 Glass-box assessment scheme showing various assessment patterns

10 Implementation Issues

Currently, *assessment schemes* are implemented using Microsoft Excel together with VBA (the latter in order to provide the basic PASS functionality). This is possible, because all *assessment types* are made up of only 8 basic building blocks, the *assessment patterns* we have introduced in Sect. 7. For ease of use, any concrete *assessment scheme* will hide most or all configuration details and will be designed in such a way, that it supports the *assessor* optimally while assessing the outcome of *assignments*. This is a highly creative part of *assessment design* so that in practice each *assessment scheme* will probably look differently.

Using this low level form of implementation makes only sense for someone who is thoroughly familiar with the formal details of PASS, who has a good working knowledge of Excel VBA, and who has a lot of experience in interaction design.

For successful dissemination of the system, however, an interactive software application is needed, preferably based on modern web technology, which enables teachers to set up arbitrary *assessment schemes* targeted to the chosen *assignments*, *assessors* to use these predefined *assessment schemes* for entering their *assessment* data and students to retrieve the results of *assessment* of their *assignment* work. This software development effort is now going on at several places. The most challenging part of the development effort is to find out which kind of user interface will be the most satisfying for the respective stakeholders and user roles [21].

Acknowledgments Without the generous support of the educational institutions we are working for and the many cohorts of students who have suffered as well as profited from our unbridled belief in the necessity and feasibility of a genuine *assessment engineering* approach, the *performance assessment scoring system* PASS would not have seen the daylight. Thanks to all, including many who didn't even know that they were gently being used as subjects in an ongoing system development project. Many of the features offered by the current reference model emerged as necessary enhancements to previous versions of the system, covering certain unexpected complications (e.g. students leaving or entering a course in between) of real-life *assessment* in higher education, especially in the context of *authentic* TLA.

References

1. Madaus GF, O'Dwyer LM (1999) A short history of performance assessment—lessons learned. *Phi Delta Kappan* 80(9):688–695
2. Johnson RL (2009) *Assessing performance: designing, scoring, and validating performance tasks*. Guilford Press, New York
3. Hsieh C, Knight L (2008) Problem-based learning for engineering students—an evidence-based comparative study. *J Acad Libr* 34(1):25–30
4. Fettke P, Loos P (2007) *Reference modeling for business systems analysis*. Idea Group Publications, North Carolina
5. Vossen PH (2011) A truly generic performance assessment scoring system (PASS). In: *Proceedings of the INTED 2011 Conference, Valencia, Spain, 7–9 March 2011*

6. Schuwirth L, Ash J (2013) Assessing tomorrow's learners—in competency-based education only a radically different holistic method of assessment will work—six things we could forget. *Medical teacher* (Early Online)
7. Brookhart SM (2003) Developing measurement theory for classroom assessment purposes and uses. *Educ Meas Issues Pract* 22(4):5–12
8. Herrington J, Oliver R (2000) An instructional design framework for authentic learning environments. *Education Tech Research Dev* 48(3):23–48
9. Yorke M (2003) Formative assessment in higher education—moves towards theory and the enhancement of pedagogic practice. *High Educ* 45:477–501
10. Bennett RE (2011) Formative assessment: a critical review. *Assess Educ Principles Policy Pract* 18(1):5–25
11. Taras M (2009) Summative assessment—the missing link for formative assessment. *J Further Higher Educ* 33(1):57–69
12. Goldstein H (1989) Psychometric test theory and educational assessment. In: Simons H, Elliott J (eds) *Rethinking appraisal and assessment*, Open University Press, pp 140–148
13. Bergmann M (2008) *An introduction to many-valued and fuzzy logic—semantics, algebras, and derivation systems*. Cambridge University Press, Cambridge
14. Johanyák ZC (2009) Survey on four fuzzy set theory based student evaluation methods. In: *Proceedings of Kecskemét College, Faculty of Technology (GAMF), Kecskemét, vol XXIII*, pp. 121–130
15. Morsi NN, Lotfallah W, El-Zekey MS (2006) The logic of tied implications, part I—properties, applications and representation. *Fuzzy Sets Syst* 157:647–669
16. Suthers D, Verbert K (2013) Learning analytics as a “middle space”. In: *Proceedings of the 3rd LAK Conference, 08–12 April 2013*, 4p
17. Lalla M, Facchinetti G, Mastroleo G (2004) Ordinal scales and fuzzy set systems to measure agreement—an application to the evaluation of teaching activity. *Qual Quant* 38:577–601
18. Vossen PH (2013) Educational assessment engineering—a matter of quality assurance. *Workshop with Chinese Teachers at International Vocational Academy, Darmstadt*
19. Guskey TR, Bailey JM (2000) *Developing grading and reporting systems for student learning*. Corwin Press, Thousand Oaks
20. Yorke M (2007) *Grading student achievement in higher education: signals and shortcomings*, Routledge
21. Borchers J (2001) *A pattern approach to interaction design*. Wiley (Series in Software Design Patterns)
22. Bergin J et al (2012) *Pedagogical patterns—advice for educators*, CreateSpace Independent Publishing Platform
23. Roberts TS (2006) *Self, peer and group assessment in E-learning*. Information Science Publishing, New York

Feasibility of Extracting Unique Signature for Each User Based on Analysing Internet Usage Behaviours

Rozita Jamili Oskouei

Abstract This paper presents the results of our study about feasibility of extracting unique web signature for each user by exploring Internet usage behaviors. Proxy server access log files of one engineering college are collected for 32 months continually for this study. Behaviors of users are compared with each other in various aspects including their time spend on Internet per day. Further the relationships between visited websites by users and time of connection per day, relationships between number of hits (number of visited webpages in a day) and time of connection and gender of users is explored. The results of this study confirm the feasibility of having unique web signature for users and the length of extracted web signature in our study was 1–78. Approximately for 82 % of total users in our study, we extract unique web signature. In an average analyzing the access log files of proxy servers for 15–20 continues days is sufficient for extracting signature of users. *k*-means and DBSCAN clustering methods are used for creating clusters of users based on the similarity of their web signatures. Some applications of Web-signature are:

- Help to administrators for predicting the more overload timing per day and plan for that.
- Grouping users based on their similarity of contents of Web-Signatures and establishing intelligent social network between those users based on their similar behaviors.

Keywords Web signature • Internet usage behavior • Access log files • Proxy server • *k*-means • DBSCAN

R.J. Oskouei (✉)

Department of Computer Science and Information Technology,
Institute for Advanced Studies in Basic Sciences (IASBS), Zanjan, Iran
e-mail: rozita2010r@gmail.com; r_jamili@iasbs.ac.ir

1 Introduction

Technical institutions have made significant investment in Internet and computing infrastructure with objective to make quantum jump in academic productivity and its quality. But based on the results of several studies which are done by re-researcher in all around of the world, this infrastructure is dominantly used for non-academic purposed and has not contributed to academic productivity and quality.

In this paper, we present results of our investigations conducted to generate unique and stable Web Signature for each individual user with extracting his/her Internet usage behavior and exploring relationships between the extracted Web Signature with other behavioral features of users.

Our investigation results are summarized on:

- Stable and unique Web Signature is generated with analyzing Web access log files for continues 20 days.
- Dominant use of Internet is for social network Websites based on analyzing Web Signature several of users.

This paper is organized in six sections. The second section includes related works. Section third presents our algorithm for detecting Web Signatures. Section fourth shows the process of updating Web Signatures. Section fifth presents applications of Web Signatures. Finally section sixth includes conclusions.

2 Related Works

Several research efforts [1–5] have been made to predict user behavior based on history of Internet usage. They have used data mining techniques such as classification, clustering, association mining for detecting patterns from large number of data for predicting students' future performances.

In [2, 3], a model has been proposed to predict the performance in a Web based management course based on their on-line Internet activities. In [4] authors discovered pedagogical relevant knowledge contained in databases obtained from Web-based educational systems.

Gezy and Izumi [6] have been studied the human behavior on Internet with the help of Web usage mining. Authors on [7] made a framework for exploration of knowledge workers' browsing behavior on a large corporate Intranet. Complex browsing patterns have been revealed and it has been concluded that users effectively utilized only small amount of avail-able resources and a large number of resources have been occasionally accessed. In [8] authors discovered the browsing patterns with exploring pages visited by them. They made an algorithm for exploring users' dynamic patterns based on association mining.

Different studies related to extracting users' behaviors on Internet are established. Analyzing users' behaviors by extracting the contents of visited Web pages

are studied on [9–12]. User navigation behavior mining (UNBM), mainly studied the problems of extracting the interesting user access patterns from user access sequences (UAS), which are usually used for user future access prediction and web page recommendation [13–21]. Different application of behavior mining including the fraud detection [22] or predicting users future behaviors are discussed by [23–28].

Our research is an extension of these works, with the help of sequence and behavior mining of users for extracting unique Web Signature for each individual user and creation of different clusters of users based on their Web signatures length or contents.

3 Web Signature

We analyzed proxy server access log files of one engineering college for a period of 32 months continually. This institute is one of the premier technical institutes and offers 4 years under-graduate degree programs, 2 years post-graduate pro-grams and PhD program in all major disciplines of physical and social sciences and of engineering. Total students population was approximately five thousand and majority of them resided in hostels inside of campus. Internet facilities were available in computer center, different laboratories and also in hostels. Yearly academic calendar was divided in three semesters: first, second and summer semester. The first semester generally started in the second week of July and ended by second week of December. Similarly, the second semester started in the first week of January and continued till second week of May. The summer semester was of smaller duration. It started in second week of May and ended by second week of July. Log files, which had been analyzed for generation of signature, were for the duration varying from 5 to 35 continues days. These intervals of continues days were during normal semester working days without/with tests and examinations weeks. For our analysis, we extracted a small subset of fields from each record of log files. Fields extracted by us included Username, Data/Time and URL. The Username was an artificially generated identifier for each user. This has been done to protect the identity of individuals.

This section presents the results of our investigation regarding feasibility of Web-Signature for Internet users and its strength and stability over a period of time. We made these investigations by analyzing log files for a period of 30 months continually. Since these files contained voluminous data, we decided to create aggregated views on these. Our aggregated views are included session, and day history for each user. The ER diagram, given on Fig. 1 describes the attributes of entity types User, Websites, Category, Session and Day-History. Figure 2 models the relationship between users, day history, sessions, visited Web sites and their categories.

The key attribute of User, VUserID which is a virtual ID given to students. This ID is related one-to-one to Registration-ID given by Dean (Academic Affairs) Office and User-ID given by computer center authority. Registration-ID and User-ID are not explicitly store in the database to protect the privacy of individual users.

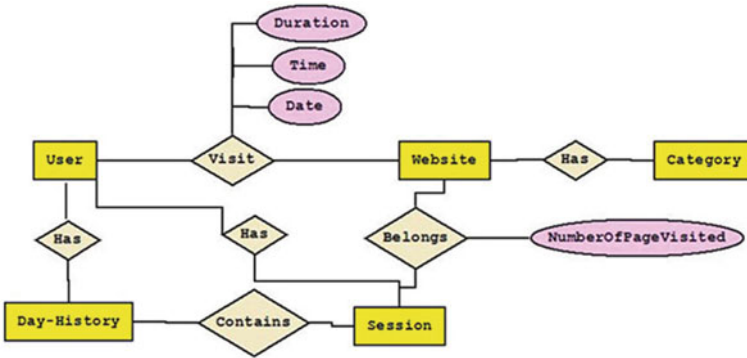


Fig. 1 ER diagram for our entities

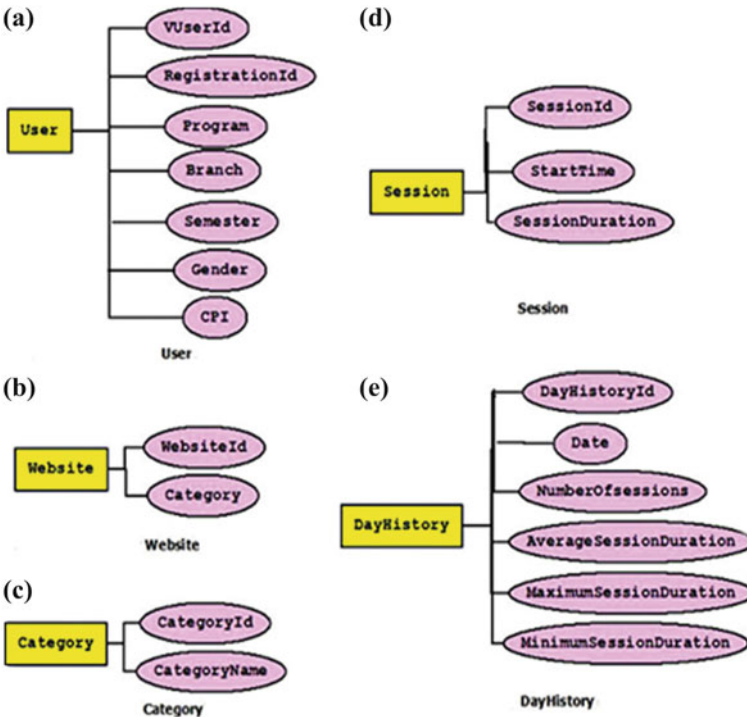


Fig. 2 Entities and their attributes

To define a session, we analyzed time stamps of records of students who belonged to Regular users group (users who connected dairy to Internet named as Regular users in this study) and connected to Internet more than one time per day. The number of such students was 2730 out of 5000 total users in our study. In the other words, we had not considered records of students who never connected to Internet

(named as Internet Absentees) or those who did not connect every day (named as Non-Regular). We computed the average time difference between consecutive records of these students for a period of one month. Based on analysis of these averages, we decided to define beginning and end of a session if two consecutive records of one user have difference between the time stamps more than 15 min.

Similarly Day-History entity type represents the history of Sessions in a day. It saved the number of sessions for a day, their average, minimum and maximum time duration. Further, Session-Website table contains Website-Id and Session-Id as keys along with number of visited pages of each Website in a session by one user.

Other entity types of Fig. 1 have key attributes which are created by the systems.

Figure 2 describes the relationships between entity types of Fig. 1. Visit relationship type has three attribute: Duration, Time and Date. These are required for our analysis.

To filter out Web sites which are not visited frequently by user, we defined a support value, for each Website.

$$\text{Support}_{(i)} = \frac{\text{NVD}}{\text{TND}} * 100$$

where:

NVD: Number of Days on which a Website has been visited

TND: Total Number of Days which are selected for calculating Support.

This research work, computed support value for Web sites visited by students for different number of days such as 5, 10, 15, 20, 25 and 30 continuous days. It may be noted that a Web site might have been visited several times in a day by one user but we have counted it as one for calculating the support value.

It is evident from the results of this analysis that support values more than 50 % are relatively more stable if they are computed on the basis of records of more than 15 days and the support values less than 50 % are not stable even if they are computed on the basis of the larger number of days. Further, it is concluded that number of Web sites having support value more than 50 % and computed for more than 15 days, provide relatively stable set of Web sites visited by an individual user.

3.1 Algorithm for Extracting Web Signature

In this section, the results of our study for establishing a Web signature are presented. As a first step, we focused only on Regular users and extracted the Web sites visited by them with support value more than 50 %. The average, maximum and minimum cardinality of such sets of Web sites were (31, 188 and 1) respectively. This research work attempts to generate unique set of Web sites for each Regular user from these sets of Web sites.

A set is a gathering together into a whole of definite, distinct objects of our perception and of our thought which are called elements of the set [29]. The elements

or members of a set can be anything: numbers, people, letters of the alphabet, other sets, and so on. Sets are conventionally denoted with capital letters. Sets A and B are equal if and only if they have precisely the same elements. When we say “order” in sets we mean the size of the set. Two sets are equal [30] if they have precisely the same members. And the equals sign ($=$) is used to show equality, so you would write: $A = B$.

The proposed algorithm first sorts elements of sets, then group them based on the cardinality and test for equality between the sets in each group. If a set is not equal to any other sets in the group, then it is identified as a unique signature.

The algorithm for identification of unique subsets of Web sites is given below.

Alg. 1 Web-Signature Extraction

Require: Sets of Websites identified with unique integer Id and having support value more than 50 for regular users

Ensure: Unique sets of Websites for regular users

- 1: Start
 - 2: Sort elements of each set on the basis of their integer Ids
 - 3: Group sets based on their cardinality
 - 4: For each group and
 - 5: For each set $S_{(i)}$ in this group
 Test whether $S_{(i)} = S_{(j)}$ where $j \neq i$ and $S_{(j)}$ also belongs to same group with $S_{(i)}$
 - 6: If $S_{(i)} = S_{(j)}$, it is not unique set
 - 7: Remove $S_{(j)}$ from group
 - 8: Increment j and go to step 5
 - 9: Exit
-

The proposed algorithm is demonstrated with a set of Websites for a small number of users on (Table 1). Further Table 2 is tested the equality, by computing Euclidean distance between two sets.

In Table 2 the Euclidean distance between set for User-ID ca0901 with other sets of the group is presented. Since distance with it0817 is equal to zero these sets are equal. Therefore both of these users have not unique Web-Signature. Similarly the distance with other sets are given on Table 3. Six sets with cardinality of 6 for users (it0813, fe0904, fe0905, it0843, st0904 and ce0718) are unique whereas two sets for users (ca0901, it0817) are not unique. In other words, these six sets can be used as unique Web-Signature of these users.

Other distance based formulas are existing which we can apply and the results almost would be similar such as:

- Mahalanobis distance normalizes based on a covariance matrix to make the distance metric scale-invariant.

Table 1 The samples of users with their sets of visited websites

User-Id	Cardinality of sets	Set's elements
it0648	5	{1, 4, 33, 92, 157}
cs0866	5	{1, 12, 33, 92, 259}
cs0813	5	{1, 19, 23, 33, 82}
pe0907	5	{1, 19, 23, 33, 82}
co0980	5	{1, 33, 47, 48, 208}
ch0602	5	{1, 6, 12, 33, 92}
el0966	5	{1, 4, 12, 19, 33}
cs0894	5	{1, 19, 28, 33, 97}
st0904	6	{1, 19, 28, 29, 33, 82}
ca0901	6	{1, 19, 28, 33, 82, 92}
it0813	6	{1, 12, 19, 33, 82, 250}
it0817	6	{1, 19, 28, 33, 82, 92}
fe0904	6	{1, 6, 9, 11, 12, 33}
fe0905	6	{1, 12, 19, 28, 33, 92}
it0843	6	{1, 4, 19, 28, 33, 92}
ce0718	6	{1, 4, 11, 33, 92, 173}

Table 2 Applying euclidean distance for set belongs to user ca0901

Detecting uniqueness of signature for user ca0901	
$d(\text{ca0901}, \text{it0817}) = 0$	$d(\text{ca0901}, \text{fe0904})! = 0$
$d(\text{ca0901}, \text{fe0905})! = 0$	$d(\text{ca0901}, \text{it0843})! = 0$
$d(\text{ca0901}, \text{st0904})! = 0$	$d(\text{ca0901}, \text{ce0718})! = 0$
Sign user ca0901—not unique, $\text{sign}(\text{ca0901}) = \text{sign}(\text{it0817})$	

- Manhattan distance measures distance following only axis-aligned directions.
- Chebyshev distance measures distance assuming only the most significant dimension is relevant.
- Minkowski distance is a generalization that unifies Euclidean distance, Manhattan distance, and Chebyshev distance.

The proposed algorithm is applied for all regular 3496 users’ sets of visited Websites and obtained unique Web-signature for 3002 users. In other words, 86 % of Regular users had unique Web signature.

This research work also computed such unique Web-Signature with sets of Websites having different support values above 50 %. Table 4, shows the results of this analysis. It is evident from this table that number of unique Web-Signatures decreases with increase in support values. For Support value of 100, the percentage of unique Web-Signatures comes down to 67 %.

The results of other related studies show that, there is no gender bias for unique sets of visited Web sites. All of these results bring to focus available trade-off. Elements of unique sub-sets of Web sites are relatively more stable for higher support value but the number of unique subsets decreases with higher support

Table 3 Detecting uniqueness of sets with applying euclidean distance

<i>Applying euclidean distance</i>	
<i>Search for user-id it0813</i>	
$d(it0813, fe0905) = ! = 0$	$d(it0813, it0843) = ! = 0$
$d(it0813, st0904) = ! = 0$	$d(it0813, ce0718) = ! = 0$
$d(it0813, fe0904) = ! = 0$	
<i>Sign of user (it0818) is unique</i>	
$d(fe0904, fe0905) = ! = 0$	$d(fe0904, it0843) = ! = 0$
$d(fe0904, st0904) = ! = 0$	$d(fe0904, ce0718) = ! = 0$
<i>Sign for user (fe0904) is unique</i>	
<i>Search for user Id (fe0905) or user Id (fe0905)</i>	
$d(fe0905, it0843) = ! = 0$	$d(fe0905, st0904) = ! = 0$
$d(fe0905, ce0718) = ! = 0$	
<i>Sign for user (fe0905) is unique</i>	
<i>Search for user id (it0830)h for set(it0843)</i>	
$d(it0843, st0904) = ! = 0$	$d(it0843, ce0718) = ! = 0$
<i>Sign for user(it0843) is unique</i>	
<i>Search for user(st0904)</i>	
$d(st0904, ce0718) = ! = 0$	
<i>Sign for user(st0904) is unique</i>	
<i>other user, with the length 6, user(ce07 18) has unique signature</i>	

Table 4 Web signature for different support values

Different supports (%)	50	60	70	75	80	85	90	95	100
Unique sign number	3002	2970	2840	2695	2551	2511	2443	2399	2326
(%)	86	85	81	77	73	72	70	69	67

values. To use these unique sub-sets as Web-Signatures of students, one may have to take a middle path between support value and number of Web-Signatures. In our view, we should focus on number of unique Web signatures even if they are based on Web sites having lower support value. Consequently, we decided to use, support value of 50 for Web-Signature.

Further, to study the stability of Web-Signature, we divided each signature in 2 parts:

- Static part: contains those Web sites which have support value equal to or more than 80 ($80 \leq \text{Support-Value}$).
- Dynamic part: contains those Web sites which have support values between 50 and 80 ($50 \leq \text{Support-Value} < 80$).

To check the stability of Web-Signature over a period of time, we computed the Web Signatures from log records of 15, 30, 45, 60, 75, 90, 105, 120, 135 and 150 continues days. Exploring gender based variations on length of static and

Table 5 Average distribution of websites based on their support values

Support	Gender		
	Female (%)	Male (%)	Total (%)
50 <= Support < 60	10	8	9
60 <= Support < 70	5	6	6
70 <= Support < 75	10	10	10
75 <= Support < 80	10	9	9
80 <= Support < 85	5	5	5
85 <= Support < 90	10	10	10
90 <= Support < 95	10	10	10
95 <= Support <= 100	40	42	41

dynamic parts of Web-Signature based on their stability during 150 continuous days shows that:

- Female users almost had stable Static part even during 150 continues days whereas for male users this period was 120 continues days. Further, female users had almost up to 135 continue day’s stability on dynamic part of Web-Signature, whereas stability of male users’ dynamic part of Signature is shown maximum up to 105 days. There-fore, if the signature is computed on the basis of records of 15 days, it can be used for entire semester of 14 weeks.

Since we have included only those Web sites which are having support more than 50 in their signature, there would be a sub-set of Web sites which are more likely to change over a period of time. For example, a Web site having support value equal to 50 would be less stable in compare with Web sites with support value of 90 or 100. Table 5 gives the average percentage of the visited Web sites with different support ranges for total Web sites which are part of Web-Signature of students.

From this table it is evident that 66 % (80 <= Support <= 100) of the Web sites for all Web-Signatures are responsible for static-part of Web-Signature and remaining 44 % (support < 50) contribute to dynamic-part of Web-Signature.

3.2 How Many Days Need for Making Stable Signature?

The other challenge regarding identifying signature would be assigning the minimum number of days for detecting signature for each user. Our analysis shows the best number of connection days would be 15–25 continues days.

Whenever we define a signature for each individual user, the main requirement of this signature would be uniqueness on that Signature for each user. Therefore we have to be able to design a domain for the length of signature which would be making us able to define uniquely identification for each user.

3.3 Web-Signature Updating

It is clear from previous section that our extracted Web-Signatures are stable for a period of 100 days on an average. These Web-Signatures may be updated again with repeating the process studied earlier. We explored the possibility of obtaining the Web-Signature only by partial updating of only dynamic-part as static-part is unlikely to change.

This investigation compared the Web-Signature computed after expiry of 100 days based on access log files for 5, 10 and 15 days for few students. The update period concerned 5, 10 and 15 days. The results show, the update would be complete after 10 days. Further, these results indicate that there are many changes in the dynamic-part of Web-Signatures compare to the static-part. From these analyses we conclude that Web-Signature needs to be recomputed by identifying only dynamic part of the Web-Signature and replacing this new dynamic-part in Web-Signature would be obtain new Web-Signature of each individual user.

For similarity detecting and identifying the users with unique Web-Signature, we proposed Algorithm 2.

Alg. 2 Web-Signature Update

Require: Sets of Websites which identified with unique integer-number and having support value more than or equal to 50 and less than 80

Ensure: Unique Sets of Websites for each regular user

- 1: Start
 - 2: Obtain sets of Websites with $50 \leq \text{Support-value} < 80$ for each user and named as dynamic-part of Web-Signature
 - 3: Add this extracted dynamic-part to the previous Web-signature static-parts
 - 4: Compile (create) new sets
 - 5: Sort elements of new sets
 - 6: Run Algorithm1 for identifying unique sets
 - 7: Get number of unique sets along with individual users which are having unique set as Web-Signature
 - 8: Exit
-

4 Clustering Based on Signature

Different clusters based on length of signatures and total time spent and total visited websites by each user are made. k -means and DBSCAN [31] clustering methods are used for modeling different clusters based on their signatures length, time spent and academic performance of users. One of the main advantages of this clustering would be help for identifying and analyzing outliers in different aspects.

4.1 Relationship Between Web-Signature and Average Time Spent

This research work, analyzed the relationship between Web-Signature length and average time spent on Internet and number of visited Web sites per day. These results show that, maximum number of users had Web-Signature length in the range of (10–30). Further, the minimum number of users had Web-Signature length >50.

Figure 3 shows relationship between average times spent on Internet per day by both female and male users and their Web-Signature length. Vertical axis shows the average time spent in minutes and horizontal axis shows the Web-Signature length.

Based on the results of Fig. 3, it is evident that minimum time spent on Internet belongs to users with Web Signature length of “1” and maximum time spent belongs to users with the length of Web Signature more than 55. Our analysis shows that, there is a strong correlation between Web-Signature length and average time spent per day on Internet. Table 6 shows gender based correlation between time-spent on Internet with Web Signature length.

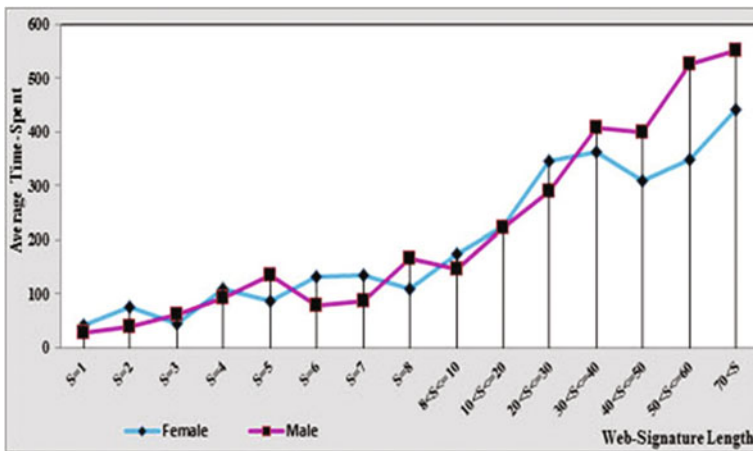


Fig. 3 Average time spent versus signatures’ length

Table 6 Correlation between the lengths versus average time spent on internet

Correlation between web-signaturelength versus average time spent on internet	
Total-users	0.81
Female	0.83
Male	0.80

In the other words, Web-Signature length can be a good indicator for relative measure of time spent on Internet. Further, outliers in terms of Signatures length are also outliers in terms of average time spent on Internet.

Analyzing the distribution of the Web sites which are part of Web-Signature of students in terms of their category shows that when the Web-signature length increase, the percentage of Websites belonging to curricular category decrease and the category of Websites belonging to co-curricular and ex-curricular increase. In other words, the users having Web-signature length less than 5 visit Internet more for academic purposes compare to those users which are having the Web-Signature length of 40.

4.2 Relationship Between Web-Signature Length and Academic Performance

Academic performance of students in terms of cumulative performance index (CPI) can be varied and affected based on their social interactions or Internet usages. We explored for all Regular users the academic performance (CPI) relation-ships with their Web Signature length and average time spent on Internet per a day. The results of analyzing distributions of users based on their CPI are:

- Majority of users in both female and male students had CPI in the range of $7.5 = < \text{CPI} < 9$.
- Both female and male academically weak students with $\text{CPI} < 5$ had minimum average Web Signature length. Whereas, in male users, in and average the maximum Web Signature length belongs to academically excellent students with the CPI in the range of more than or equal to 9 ($9 \leq \text{CPI}$). However, this is not true for female users. Since in female users maximum average Web Signature length belongs to students with the CPI ranges $6.5 < \text{CPI} < 7$.

5 One Application of Extracted Web Signature

One of the main problems in educational environments is searching for useful resources through the Internet for helping students for solving problems or learning some difficult tasks. But unfortunately this is not an easy task to find expert per-son who can help or who is interested to help for solving problems. For solving this problem we proposed a model which is extension of our previous proposed model [32].

Our proposed modeling scheme has the following steps:

- Extract the categorization of Websites based on our specified Website's categorization scheme [33] from Web signature. Based on this scheme, all visited

Websites categorized under two categories based on content and structure of those Websites.

- Make different clusters of users based on similarity of Websites' categories in their Web Signature.
- Make a database for recording those users' Information including their user name and email-id.
- Finally start to create online community or social network within the users in each cluster.
- Send an invitation for all users in same cluster by attaching other users' email id from the created data-base.
- If a user is interested for communication, s/he can send an email to other user and start for discussion about any interested solutions for solving problems.

With this approach, two individual users possibly may get several invitations based on similarity of visited Websites in their Web Signature, from each other. For example, different users are having similar Websites in their Web Signature such as Ja-va.com and ieee.org, so academically exchanging knowledge or data within these users would be desirable and helpful for beginners or fresher students whenever it is possible to make easily a social network group with all seniors or professors for solving problems or discussing about solutions.

The primary focus in this research work was to detect communities based on their academic related category of Websites visiting behaviors. We used invitation sending method for privacy and security issues. Extracting community can be done on offline or online model. In the form of offline, access log files are used and invitation to join the network would be sent. For example, an invitation would be sent every 12 h. In online method, whenever a user opened a website, her/his information would be saved in our server's database and invitation will be sent immediately for all visitors of that Website in same time. Our future work will be considered on establishing dynamic social network among students of different colleges and other environments.

6 Conclusion

This research work attempt to explore the feasibility of creating a unique Web Signature for each Internet user with analyzing access log files. We proposed an algorithm for extracting unique Web-Signature. The main challenge which occurred during this analysis was: What is the average length (cardinality) of Signature? And how long our extracted Web-Signature would be stable? Our results declared that cardinality of Web-signatures were 1 to 188 and the extracted Web-Signatures were stable in an average for 3 months.

In another step, we used k -means and DBSCAN clustering methods for grouping users based on their Web-Signature length, time spent on Internet and CPI. We used the results of these clustering for creating groups of users with similarity of their

Internet usage behaviors especially in academic environments for communicating between professors or senior students with fresher students based on their similarity of interests.

References

1. Al-Radaideh QA, Al-Shawakfa EM, Al-Najjar MI (2006) Mining students data using decision trees. In: International Arab conference on information technology (ACIT'2006)
2. El-Halees A (2014) Mining students data to analyze learning behavior: a case study/ <http://eref.uqu.edu.sa/files/eref2/folder6/f158.pdf> Accessed 1 Aug 2014
3. Romero C, Ventura S, Gracia E (2014) Data mining in course management system : model case study and tutorial. <http://sci2s.ugr.es/docencia/doctoM6/Romero-Ventura-Garcia-CE.pdf> Accessed on 1 Aug 2014
4. Merceron A, Yacef K Educational data mining : a case study. <http://citeseerx.ist.psu.edu/viewdoc/download?doi=10.1.1.137>
5. Cortez O, Silva A (2014) Using data mining to predict secondary school student performance. <http://repositorium.sdum.uminho.pt/bitstream/1822/8024/1/student.pdf>. Accessed on 1 Aug 2014
6. Gezy P, Izumi N, Akho S, Hasida K (2007) Human Web behavior mining. In: IADIS international conference WWW/Internet
7. Eytan Adar G, Weld DS, Bershad BN, Gribble SD Why web search: visualization and predicting user behavior
8. Maheswara Rao VVR, Kumari VV, Raju K (2010) Understanding user behavior using web usage mining. In: 2010 international journal of computer applications (0975-8887) vol 1, no. 7
9. Butakov S, Odinma A (2009) Web content usage behaviors. In: Proceedings of the fifteenth Americas conference on information systems, San Francisco, California 6–9 Aug 2009
10. Oskouei RJ (2010) Behavior mining of female students by analyzing log files. In: IEEE, ICDIM 2010
11. Oskouei RJ Differential internet behaviors of students from gender groups. IJCA Internet J Comput Appl 7. ISBN:978-93-80746-46-3
12. Suneetha KR, Krishnamoorthi R (2009) Identifying user behavior by analyzing web server access log file. IJCSNS Int J Comput Sci Netw Secur 9(4):327–332
13. Xue L, Chen M, Xiong Y, Zhu Y (2010) User navigation behavior mining using multiple data domain description. In: 2010 IEEE/WIC/ACM international conference on web intelligence and intelligent agent technology
14. Iwazume M, Shirakami K, Hatsudani K, Takeda H, Nishida T (2014) IICA: an ontology-based internet navigation system. AAAI Technical Report WS-96-06. www.aaai.org. Accessed 1 Aug 2014
15. Berendt B (2014) Web usage mining, site semantics, and the support of navigation. <http://robotics.stanford.edu/ronnyk/WEBKDD2000/papers/berendt.pdf>. Accessed 1 Aug 2014
16. Marques E, Garcia AC, Ferraz I (2014) RED: a model to analyze web navigation patterns. www.research.ibm.com/fui-workshop/.../marques-redcadui.pdf. Accessed 1 Aug 2014
17. Dong Y, Zhang H, Jiao L (2006) Research on application of user navigation pattern mining recommendation. In: Proceedings of the 6th World Congress on intelligent control and automation, Dalian, China, 21–23 June 2006
18. Borzemski L (2007) Internet path behavior prediction via data mining: conceptual framework and case study. J Univ Comput Sci 13(2):287–316
19. Yuan Lin I, Huang XM, Chen MS (2014) Capturing user access patterns in the web for data mining. <http://www.computer.org/portal/web/csdl/doi/10.1109/TAI.1999.809818>. Accessed 1 Aug 2014

20. Jalali M, Mustapha N, Mamat A, Sulaiman NB (2008) A new clustering approach based on graph partitioning for navigation patterns mining. In: IEEE
21. Ling H, Liu Y, Yang S (2007) An ant colony model for dynamic mining of users interest navigation patterns. In: IEEE international conferences on control and automation
22. Xu J, Sung AH, Liu Q (2014) Behavior mining of fraud detection. <http://jrpit.acs.org.au/jrpit/JRPITVolumes/JRPIT39/JRPIT39.1.3.pdf>. Accessed 10 Aug 2014
23. Hao MC, Ladisch J, Dayal U, Hsu M, Krug A (2014) Visual mining of E-customer behavior using pixel bar charts. <http://www.hpl.hp.com/techreports/2001/HPL-2001-144.pdf>. Accessed 5 Aug 2014
24. Manavoglu E, Pavlov D, Lee C Giles Probabilistic, "User Behavior Models" In: 3rd IEEE international conference on data mining (ICDM03)
25. Yada K, Motoda H, Washio T, Miyawaki A (2004) Consumer behavior analysis by graph mining technique. Springer, Berlin, pp 800–806
26. Adar E, Weld DS, Bershad BN, Gribble SD (2007) Why we search: visualizing and predicting user behavior. www 2007/Track: Datamining
27. Zhou B, Hui SC, Fong ACM (2005) Discovering and visualizing temporal-based web access behavior. In: Proceedings of the 2005 IEEE/WIC/ACM international conference on web intelligence (WI05)
28. Hu J, Zeng HJ, Li H, Niu C, Chen Z (2007) Demographic prediction based on users browsing behaviors behavior. www 2007/Track: Data Mining, session: Predictive Modeling of Web Users
29. Cantor G (1918) Set theory. http://www-history.mcs.st-and.ac.uk/HistTopics/Beginnings_of_set_theory.html and <http://www.math.vanderbilt.edu/~schectex/courses/infinity.pdf>. Accessed 11 Aug 2014
30. Arasu A, Ganti V, Kaushik R (2006) Efficient exact set-similarity joins. <ftp://research.microsoft.com/users/datacleaning/papers/vldb06.pdf>. Accessed 1 Aug 2014
31. BoydHawkins DM (1980) Identification of outliers. Chapman and Hall, London
32. Oskouei RJ (2011) Establishing social network communities between students based on their internet usage patterns. In: International Conference on Computer and Communication Technology (ICCT), Allahabad, UP, India
33. Oskouei RJ, Sajja PRP (2012) Mining gender affinity to social networking. Inderscience, Int J Soc Netw Min (IJSNM)

Privacy Preserving Data Mining Survey of Classifications

Mahdi Aghasi and Rozita Jamili Oskouei

Abstract With the rapid progress of data mining, protecting sensitive information is a critical issue before sharing to outside parties. Association rules become a powerful tool in discovering hidden sensitive information among parties, whereas some of them try to protect their own sensitive information by blocking inference channels. For instance, two parties are selling same products in different markets. After sharing their sale information to each other, one tries to analyze the adversary sale information (that we call it data mining). So, after analyzing and accessing to adversary's beneficial information, the party changes the arrangement of his products in his market since it helps the customers to access products more easily and quickly. However the rate of selling in his market will increase, the other party is analyzing the information which has been censored (that what we call it privacy preserving in data mining). The methods that the parties has been trying to hide before sharing sensitive information and the characteristics of the algorithms have been discussed in this paper.

Keywords Data mining · Privacy preserving data mining · Censor sensitive information · Association rules

Motivation—Protecting sensitive mined data has become an important issue in privacy preserving in data mining. Classification of different methods and approaches which have been proposed in data mining and privacy preserving data mining is the aim of this paper by the researchers who want to have an acquaintance to brief classifications of privacy preserving data mining.

M. Aghasi
Department of Computer, Science and Research Branch,
Islamic Azad University, Zanzan, Iran
e-mail: mahdi.aghasi@gmail.com

R.J. Oskouei (✉)
Department of Computer and Information Technology,
Institute for Advanced Studies in Basic Sciences (IASBS), Zanzan, Iran
e-mail: rozita2010r@gmail.com

1 Introduction

The advancement of information technology leads us to protect information before sharing it. Understanding the limitations of accessing to the amount of data is the most important part of Privacy Preserving in Data Mining; that means who should access to how much of the data.

In this paper, it has been tried to focus on data-mining background in advance, while the important part of the paper has been focusing on introduction of different approaches of data-mining and algorithms of data mining privacy preserving for sanitizing sensitive knowledge in context of mining association rules or item sets with brief descriptions. It has been tried to concentrate on different classifications of data mining privacy preserving approaches.

2 Basic Concepts

2.1 Data Mining Concepts

Data Mining classification based on activities and algorithms [1–3]. The practice of examining large databases in order to generate new or useful information or pattern is *Data Mining*.

2.2 Privacy Preserving Data Mining Concepts

Today as the usage of data mining technology has been increasing, the importance of securing information against disclosure of unauthorized access is one of the most important issues in securing of privacy of data mining [4]. The state or condition of being isolated from the view or presence of others is *privacy* [5] which is associated with data mining so that we are able to conceal sensitive information from revelation to public [4]. Therefore to protect the sensitive rule from unauthorized publishing, *privacy preserving data mining* (PPDM) has focused on data mining and database security field [6].

Support and Confidence Let $I = \{i_1, i_2, \dots, i_m\}$ be a set of items and let D is the dataset of transactions that the goal of sanitization is its modification in order to no sensitive rule disclosed. Any $X \subseteq I$ is an item set. Each item set which contains k items called k -item set. Let $D = \{T_1, T_2, \dots, T_n\}$ be a set of transactions. The well-known measure in frequent item set mining is support of item set. The support measure of an item $X \subseteq I$ in database D , is the count of transactions contain X and denoted as Support count (X). An item set X has supported measures in dataset D if $s\%$ of transactions support X in dataset D . Support measure of X is denoted as Support (X):

$$\text{Support}(X) = \frac{\text{Support_count}(X)}{n} \times 100 \tag{1}$$

where n is the number of transactions in dataset D .

Item set X is a frequent item set when $\text{Support}(X) \geq \text{MST}$ where MST is Minimum Support Threshold that is predefined threshold. After mining frequent item sets, the association rule is an implication of the form $X \rightarrow Y$, where $X, Y \subset I$, and $X \cap Y = \emptyset$. The Confidence measure for rule $X \rightarrow Y$ in dataset D is defined:

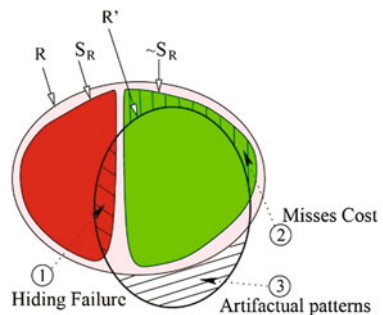
$$\text{Confidence}(X \rightarrow Y) = \frac{\text{Support}(XY)}{\text{Support}(X)} \times 100 \tag{2}$$

Note while the support is a measure of the frequency of a rule, the confidence is a measure of the strength of the relation between set of items. Association rule mining algorithms scan the database of transactions and calculate the support and confidence of the candidate rules to determine if they are considerable or not. A rule is considerable if its support and confidence is higher than the user specified minimum support and minimum confidence threshold [7].

Set of metrics In this part, we preface the set of metrics to evaluate not only how much sensitive knowledge has been disclosed, but also to quantify the effectiveness of the suggested algorithms in terms of information loss and in terms of non-sensitive rules removed as a side effect of the translation procedure. We classify these metrics into two major groups: Data sharing-based metrics and Pattern sharing-based metrics.

Data sharing-based metrics As it is presented in Fig. 1, R is denoted as all association rules in the database D , as well as S_R for the sensitive rules, the none sensitive rules $\sim S_R$, discovered rules R' in sanitized database D' . The circles with the numbers of 1, 2, and 3 are possible problems that respectively represent the sensitive association rules that were failed to be censored, the legitimate rules accidentally missed, and the artificial association rules created by the sanitization process.

Fig. 1 Data sharing-based metrics



- Problem No. 1 occurs when some sensitive rules in sanitized database are discovered, which is denoted as *Hiding Failure (HF)* and it is measured in terms of the percentage of sensitive association rules that are discovered from D' . In the best case, HF should be 0% and it calculates as follows:

$$HF = \frac{\#S_R(D')}{\#S_R(D)} \quad (3)$$

where $\#S_R(X)$ denoted as the number of sensitive association rules discovered from the database X .

- Problem No. 2 happens when some legitimate association rules are hidden as a side effect of the sanitization process. This occurs when some non-sensitive association rules support decrease in the database due to the sanitization process. We call this problem *misses cost (MC)*, and it is measured in terms of the percentage of legitimate association rules that are not discovered from D' . In the ideal condition it should be 0%. The misses cost is calculated as follows:

$$MC = \frac{\#\sim S_R(D) - \#\sim S_R(D')}{\#\sim S_R(D)} \quad (4)$$

where $\#\sim S_R(X)$ represents the number of non-sensitive association rules discovered from the database X .

- Problem No. 3 happens when some artificial rules are generated in database D' as a product of sanitizing process, which is called as artifactual patterns or artificial patterns (AP). It is measured in terms of the percentage of the discovered association rules that are artifacts, i.e., rules that are not present in the original database. AP is measured as follows:

$$AP = \frac{|R'| - |R \cap R'|}{|R'|} \quad (5)$$

where $|X|$ denotes the cardinality of X .

Dissimilarity could be measured by the difference of the original and sanitized databases by computing the difference between their sizes in bytes. However, dissimilarity should be measured by comparing their contents instead of their sizes [5, 8–11].

Pattern sharing-based metrics As it is presented in Fig. 2, $\sim S_R$ conveys the non-sensitive rules which are removed as a side effect of the sanitization process (RSE), which is known as *Side Effect* (Problem No. 1). It is related to the misses cost problem in data sanitization (Data sharing-based metrics). Problem No. 2 occurs in an adversary try to recover some sensitive by using some non-sensitive through inference channels. We refer to such a problem as *Recovery Factor*.

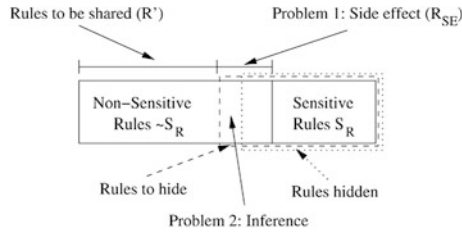


Fig. 2 Pattern sharing-based metrics

- Side effect factor (SEF) measures the number of non-sensitive association rules that are removed as a side effect of the sanitization process. The measure is calculated as follows:

$$SEF = \frac{(|R| - (|R'| + |S_R|))}{(|R| - |S_R|)} \tag{6}$$

where R , R' , and S_R represent the set of rules mined from a database, the set of sanitized rules, and the set of sensitive rules, respectively, and $|S|$ is the size of the set S .

- Recovery factor (RF) expresses the possibility of an adversary recovering a sensitive rule based on non-sensitive ones. In the case that, all the subset of sensitive association rules could be mined from the database the recovery factor will assign to 1, otherwise it will assign to 0. However, the recovery factor is never certain, i.e., an adversary may not learn an item set even with its subsets [5, 8–10].

3 Different Approaches Sin PPDM

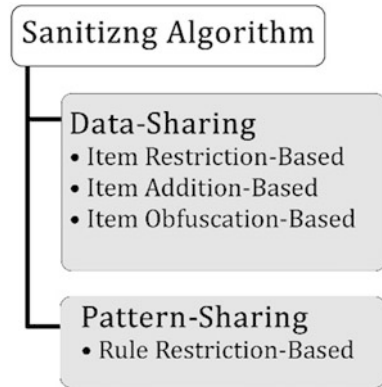
Many approaches have been proposed in PPDM in order to censor sensitive knowledge or sensitive association rules. In this paper two classifications in existing sanitizing algorithm of PPDM have been mentioned.

3.1 Classification 1

In this classification there are two techniques that the findings are discussed in detail as follow:

- Protecting sensitive information (data-sharing techniques).
- Protecting sensitive rules which contain sensitive information (pattern-sharing techniques) [10].

Fig. 3 Sanitizing algorithm based on sharing method



In data-sharing technique, without analyzing or any statistical techniques, data will be communicated between parties. In this approach, the algorithms suppose change database by producing distorted data in the data base. In pattern-sharing technique, the algorithm tries to sanitize the rules which are mined from the data set [5] (Fig. 3).

Data-Sharing techniques

- **Item Restriction-Based:** in this approach the methods reduce the support or confidence, below the given disclosure threshold (ψ) by deleting items or transaction from a database in order to hide the sensitive data that can be disclosure to public [5, 9]. Disclosure threshold basically shows how relaxed the privacy preserving mechanism should be. In the case of $\psi = 0\%$, no sensitive association rule should be discovered. In the case of $\psi = 100\%$, there is no restriction on discovering sensitive association rules [8].
- **Item Addition-Based:** unlike the previous algorithm, this approach modifies transactions by adding some items which are not presented in transactions. The addition process affects items in an antecedent part of rule, which the confidence reduction will be resulted. This issue produces some new and fake rules in sharing knowledge [5, 8, 12].
- **Item Obfuscation-Based:** in this approach sensitive rule will be hidden by replacing “?” (Unknown) in items of transaction with sensitive rules instead of deleting them. Opposite the Item Addition-Based there is no false rule to share between the parties [5, 8, 12].

Pattern-Sharing technique

- **Rule Restriction-Based:** in this technique the algorithms try to censor the mined rule from the database instead of the data itself. In these approaches the algorithm tries to sanitize either all sensitive rules which make no party to access to sensitive rules or sanitize no rule which no party is able to identify or learn anything about the owner of sensitive rules [5, 8, 13].

Fig. 4 Sanitizing algorithm based on operation



3.2 Classification 2

In this class there are five approaches that the findings are discussed in detail as follow (Fig. 4):

Heuristic Base Approach

- **Data distortion techniques:** In this technique the algorithm tries to sanitize sensitive rule by increasing or decreasing the support or confidence of the rule. In these algorithms, it operates by changing 0s to 1s or vice versa in selected transactions from database, although undesirable side effects will be produced in the new database which introduces some optional solution of algorithm’s efficiency [6, 11, 13, 14]. Atallah et al. first proposed the heuristic algorithm [15]. Some of heuristic-based data distortion techniques sanitization strategies include Algo1a, Algo1b, Algo2a [16], Algo2b, Algo2c [17], Naïve, MinFIA, MaxFIA, IGA [10, 12], RRA, RA [18], and SWA [10, 19].
- **Data blocking techniques:** in this technique, the 0’s and 1’s will be replaced by “?”(Unknown) in sensitive items of selected transaction instead of inserting or deleting them [6, 11]. Saygin et al. were the first proposed blocking based techniques for sensitive rule hiding. Also the safety margin introduced to show how much below the minimum threshold new support and confidence it should be [20]. Verykios et al. accept that the user decide how much the safety zone should be [14].

Border Based Approach In this approach by the concepts of borders, the algorithm tries to preprocess the sensitive rules, so the minimum number of them will be censored. Afterward, Database quality will maintain as well while side effects will be minimized [4, 6, 13].

Exact Approach In this approach it tries to formulate the hiding problem to a constraint satisfactory problem (CSP). The solution of CSP will provide the minimum number of transactions that have to be sanitized from the original database. Then solve it by helping binary integer programming (BIP), such as ILOG CPLEX,

GNU GLPK or XPRESS-MP [6, 13]. Although this approach presents a better solution among other approaches, high time complexity to CSP is a major problem. Gkoulalas and Verykios proposed an approach in finding an optimal solution for rule hiding problems [21].

Reconstruction Based Approach In this approach the algorithm generates a database which is reconstructed from the sanitized knowledge base which is extracted from the original data. Side effects in database is lesser than heuristic approaches [6, 11, 13]. Chen et al. were the first who proposed this approach [11, 22].

Cryptography Based Approaches This approach will be used in multiparty computation. If the database is distributed between several sites in an organization, securing computation is vital. So, it tries to encrypt database (with an input privacy) instead of distortion for sharing [4, 6, 10]. Although this technique minimize shared information, there is a little overhead on minimize tasks [12].

4 Related Works

Atallah et al. [15], tried to deal with the problem of limiting disclosure of sensitive rules. They attempt to selectively hide some frequent item sets from large databases with as little as possible impact on other, non-sensitive frequent item sets. They tried to hide sensitive rules by modifying given database so that the support of a given set of sensitive rules, mined from the database, decreases below the minimum support value.

Oliveira and Zaiane [18] tried to develop a mechanism that will enable data owners to select an appropriate balance between privacy and precision in discovering association rules. By use of Round Robin and Random algorithms, they tried to hide information by reducing support of some items. That makes a smaller impact on database with less generation of artifact rules.

Lee et al. [24] presented a new algorithm that provides a sanitized database by multiplying the original data base by sanitization matrix which has been produced by observing the relationship between sensitive patterns and non-sensitive patterns. They tried to prove that their algorithm (HPCME) by the introduction of the new factor (restoration probability) is more efficient and accurate in comparison with the former algorithms (NHF and HF).

Oliveira et al. [8] presented a framework to protect sensitive knowledge before sharing association rules. The framework includes (a) a sanitizing algorithm called downright sanitizing algorithm (DSA) which sanitizes sensitive rules while blocks some inference channels, (b) a set of metrics to evaluate attacks against sensitive knowledge and the impact of sanitization. Inference channels are the ways that adversary tries to reconstruct sensitive hidden rules by non-sensitive ones which called as forward-interface attack and backward-interface attack.

Jafari and Wang [23] proposed an algorithm that modifies the transaction in the database in order to hide sensitive association rules by reducing the confidence of them. They proposed two algorithms named ISL and DSR. The first algorithm tries

to increase the support of left hand side of the rule, while the second one tries to decrease the support of the right hand side of the rule.

Natwichai et al. [24] focus the problem of classification rules privacy preservation or classification rules hiding. They proposed a new algorithm to hide sensitive classification rules for categorical data sets. By using the more extracted characteristics information from the dataset with regard to classification issue, they improved decision tree building, and make the reconstruction process better.

Amiri [25] proposed three approaches in sanitizing algorithm. (a) The Aggregate approach tries to decrease the support of sensitive item set greedily below the support threshold; (b) The Disaggregate approach opposite to the pervious algorithm, instead of deleting item set from data base, it tries to modify the sensitive transactions in data base individually by deleting some items to reduce the support of sensitive item below the support threshold; (c) The combination of former approaches that called The Hybrid approach tries to identify sensitive item set as in Aggregate approach in advance, and then instead of deleting the whole item set, it tries to delete some items of item set as in Disaggregate approach.

Guo [11] proposed a framework with three phases: mining frequent set, performing sanitation algorithm over frequent item sets, and generate released database by using FP-tree-based inverse frequent set mining.

Duraiswamy et al. [26] proposed an algorithm named SRH that modifies the database transaction. So the confidence of association rules will be reduced. They proposed that the efficiency of their algorithm will be analyzed and improved by reducing the side effects.

Weng et al. [27] proposed that their algorithm (FHSAR) hides sensitive association rules by scanning database once and the side effects generated are minimized. FHSAR scans database one time while collects information about the correlation between each transaction and sensitive rules.

Moustakides and Verykios [28] presented max–min algorithm which hides sensitive item sets and minimizes the impact of hiding process to non-sensitive information. The aim of max–min is the optimization criterion as this is applied to the hiding sensitive item sets by reducing the support of sensitive item sets while at the same time it tries to maintain the support of non-sensitive item sets intact, if possible.

Duraiswamy [29] proposed an algorithm called ISSRH which is based on modifying database transactions so that the confidence of the association rules can be reduced. ISSRH after indexing database, identify sensitive items and generate sensitive rules, after clustering rules the hiding process perform.

Dehkordi et al. [7] have introduced a novel method for concealing sensitive association rules, the algorithm which implements the distortion technique based on the Genetic Algorithm approach.

Chandrakar et al. [30] proposed a hybrid algorithm based on modifying the database transactions which it tries to decrease not only its support below the support threshold, but also its confidence smaller than a pre-specified minimum confidence.

Hong et al. [31] proposed a greed-based approach for inserting newly transactions into the database. So it can easily make good trade-offs between privacy preserving and execution time.

Jain et al. [4] proposed two algorithms called increase support of left hand side (ISL) and decrease support of right hand side (DSR) to hide useful association rule from transaction data. In ISL method, confidence of a rule is decreased by increasing the support value of left hand side (L.H.S.) of the rule, so the items from L.H.S. of a rule are chosen for modification. In DSR method, confidence of a rule is decreased by decreasing the support value of right hand side (R.H.S.) of a rule, so items from R.H.S. of a rule are chosen for modification. Their algorithm prunes number of hidden rules with the same number of transactions scanned, less CPU time and modification.

Jain et al. [32] proposed an algorithm based on data distortion technique, where the position of the sensitive items change, but its support and the size of database remain the same as before. This approach results in a significant reduction of the number of rules generated. The proposed heuristics use the idea of representative rules to prune the rules first and then hides the sensible rules.

Radadiya [6] proposed an algorithm called ADSRRC which tried to improve DSRRC algorithm. DSRRC could not hide association rules with multiple items in the antecedent (L.H.S) and consequent (R.H.S.), so it uses a count of items in consequence of the sensible rules and also modifies the minimum number of transactions to hide maximum sensitive rules and maintain data quality.

5 Proposed Solution and Algorithm

The proposed algorithm in this paper hides sensitive rules based on infrequent insensitive rules which is called censorship based on infrequent insensitive rules (CBIIR). This algorithm tries to identify the right item (victim item) in selected transactions, in advance, and then it hides the victim items in order to minimize the side effects of hiding process. CBIIR decreases support of sensitive rules by removing the victim items from selected transactions.

In Step 1, for each sensitive rule which includes k -items, it tries to find similar $k + 1$ items' infrequent insensitive rules. Being similar means having the same items in the antecedent (LHS) as all items in the antecedent of victim rules and same items in consequent (RHS) of victim rules' in addition of some different items in rules consequent. Then CBIIR focuses on finding different item.

In Step 2, CBIIR focuses on finding all infrequent $k - 1$ item rules which Different item exists in LHS or RHS in order to find Known items. Different item is the one that exists in similar rule, but it doesn't exist in sensitive rule. (Imagine, $X \rightarrow Y$, Y is different item which doesn't exist in sensitive rule and X is known item as exists in sensitive rule). Then it tries to extract victim item, so it tries to find all $k - 1$ items frequent rules except $X \rightarrow Y$ and then sorts them in ascending order. The LHS first item of the first rule in sorted list known as victim item.

In Step 3, it tries to remove victim item in transactions which X (the known item) exists and Y (the different item) doesn't exist.

CBIIR Algorithm

Input D, S_R, ψ

Output D'

begin

```

R ← Extract all rules from D
//Step 1: find similar infrequent insensitive
rules and different items for each similar rules
foreach sensitive k-item rules  $sr_i \in S_R$  do
    SimR ← find k+1-item similar rule to  $sr_i$  in R
    if  $sup(SimR) < \psi$  then
        D ← SimR -  $sr_i$ 
    end
end

```

//Step 2: find known items and victim items

```

foreach different  $d_i \in D$  do
foreach k-1-item  $r_m \in R$  do
    if  $d_i \in r_m$  then
        //select infrequent rules
        if  $sup(r_m) < \psi$  then
            K ← select Max-Sup( items( $r_m$ ) -  $d_i$  )
        end
        //select frequent rules
        if  $sup(r_m) > \psi$  then
            V ← select Min-Sup( items( $r_m$ ) -  $d_i$  )
        end
    end
end

```

K_i ← select the Max-Sup(items(K))

V_i ← select the Min-Sup(items(V))

K ← null

V ← null

end

//Step 3: Remove victim items

```

foreach sensitive k-item rules  $sr_i \in S_R$  do
foreach transaction  $t_j \in D$  do
    if  $K_i \in items(t_j)$  and  $D_i \notin items(t_j)$  then
        // remove victim item
        D' ← items( $t_j$ ) -  $V_i$ 
    end
end

```

end

end

end

6 Conclusion and Future Work

In this paper, we presented to classifications of different methods and approaches of privacy preserving data mining. First classification focuses on techniques of protecting either data or pattern after mining the data, whereas the second classification describes several approaches that are used in different fields of working. While the algorithm of hiding sensitive rules is different, it has been tried to overview each algorithm briefly.

Eventually, after evaluating several approaches in privacy preserving data mining it will be concluded that Heuristic Base Approach and Reconstruction Based Approach are the most authentic and efficient approaches that have been proposed.

In some practical field which data is sensitive and vital part of human life, like medical background and information about a patient, data blocking techniques won't be used, due to the changes that the algorithm does on data or the false rules that it might produce to hide the mined rules.

Although some other algorithms have been focusing on removing the selection of victim items without any concern on side effects, CBIIR tries to accentuate deleting the right victim item among nominated victims. So, theoretically we are on the verge of decreasing side effects of hiding operation, especially decreasing production of artificial patterns. The aim of this paper is to improve preserving privacy precisely based on a new proposed algorithm to protect it from disclosure.

In this work there is need to implement the provided algorithm in advance and then compare it with a well-known algorithm with similar operation like item-grouping algorithm (IGA) in order to illustrate the differences of hiding process on graphs.

References

1. Concepts M, Kantardzic M (2011) Data-mining concepts 1.1. Data Min Concepts, Model Methods, Algorithms, 2nd edn, 1–25
2. Hand DJ (2007) Principles of data mining. *Drug Saf* 30:621–622
3. Fayyad U, Piatetsky-shapiro G, Smyth P (1996) From data mining to knowledge discovery in databases. *AI Mag* 17:37
4. Jain YK, Yadav VK, Panday GS (2011) An efficient association rule hiding algorithm for privacy preserving data mining. *Int J Comput Sci Eng* 3:2792–2798
5. HajYasien A (2007) Preserving privacy in association rule mining. Ph. D Thesis, University of Griffith
6. Radadiya NR, Prajapati NB, Shah KH (2013) Priv Preserv Assoc Rule Min 2:208–213
7. Dehkordi MN, Badie K, Zadeh AK (2009) A novel method for privacy preserving in association rule mining based on genetic algorithms. *J Softw* 4:555–562
8. Oliveira SRM, Za OR, Zaiane OR, Saygin Y (2004) Secure association rule sharing. *Adv Knowl Discov Data Min* Springer, pp 74–85
9. Verykios VS, Gkoulalas-Divanis A (2008) A survey of association rule hiding methods for privacy, Chap. 11. In: *Privacy-Preserving Data Mining*, pp 267–289

10. Oliveira SRM, Zaiane OR (2006) A unified framework for protecting sensitive association rules in business collaboration. *Int J Bus Intell Data Min* 1:247–287
11. Guo Y (2007) Reconstruction-based association rule hiding. In: Proceedings of SIGMOD2007 Ph.D. Workshop on Innovative Database Research, pp 51–56
12. Oliveira SRM, Zaiane OR (2002) Privacy preserving frequent itemset mining. *Proc IEEE Int Conf Priv Secur Data Mining* 14:43–54
13. Gkoulalas-Divanis A, Verykios VS (2010) Association rule hiding for data mining. Springer, New York
14. Verykios VS, Pontikakis ED, Theodoridis Y, Chang L (2007) Efficient algorithms for distortion and blocking techniques in association rule hiding. *Distrib Parallel Databases* 22:85–104. doi:[10.1007/s10619-007-7013-0](https://doi.org/10.1007/s10619-007-7013-0)
15. Atallah M, Bertino E, Elmagarmid A et al (1999) Disclosure limitation of sensitive rules. In: Proceedings 1999 workshop on knowledge and data engineering exchange (Cat. No. PR00453)
16. Dasseni E, Elmagarmid AK, Bertino E, Verykios VS (2001) Hiding association rules by using confidence and support. In: *Information Hiding*, pp 369–383
17. Verykios VS, Elmagarmid AK, Bertino E et al (2004) Association rule hiding. *Knowl Data Eng IEEE Trans* 16:434–447
18. Oliveira SRM, Zaiane OR, Tg C (2003) Algorithms for balancing privacy and knowledge discovery in association rule mining. In: Seventh international proceedings database engineering and applications symposium, pp 54–63
19. Oliveira SRM et al (2003) Protecting sensitive knowledge by data sanitization. In: Proceedings of the IEEE international conference on data mining, p 613
20. Saygin Y, Verykios VS, Clifton C, Saygm Y (2001) Using unknowns to prevent discovery of association rules. *ACM SIGMOD Rec* 30:45–54
21. Gkoulalas-Divanis A, Verykios VS (2006) An integer programming approach for frequent itemset hiding. In: Proceedings of the 15th ACM international conference on Information and knowledge management. ACM Press, New York, pp 748–757
22. Chen X, Orlowska M, Li X (2004) A new framework of privacy preserving data sharing. In: Proceedings of the 4th international workshop private security aspiration data mining, IEEE Press, pp 47–56
23. Jafari A, Wang S-L (2005) Hiding sensitive predictive association rules. In: IEEE international conference on systems, man and cybernetics, pp 164–169
24. Natwichai J, Li X, Orlowska ME (2006) A reconstruction-based algorithm for classification rules hiding. *Proc 17th Australas Database Conf* 49:49–58
25. Amiri A (2007) Dare to share: protecting sensitive knowledge with data sanitization. *Decis Support Syst* 43:181–191. doi:[10.1016/j.dss.2006.08.007](https://doi.org/10.1016/j.dss.2006.08.007)
26. Science I, Duraiswamy K, Manjula D, Maheswari N (2008) A new approach to sensitive rule hiding. *Comput Inf Sci* 1:P107
27. Weng C-C, Chen S-T, Lo H-C (2008) A novel algorithm for completely hiding sensitive association rules. *Eighth Int Conf Intell Syst Des Appl* 2008:202–208. doi:[10.1109/ISDA.2008.180](https://doi.org/10.1109/ISDA.2008.180)
28. Moustakides GV, Verykios VS (2008) A maxmin approach for hiding frequent itemsets. *Data Knowl Eng* 65:75–89. doi:[10.1016/j.datak.2007.06.012](https://doi.org/10.1016/j.datak.2007.06.012)
29. Duraiswamy K, Manjula D, Maheswari N, Science MA (2009) Advanced approach in sensitive rule hiding. *Mod Appl Sci* 3:P98
30. Science C, Publications S, Chandrakar I et al (2010) Hybrid algorithm for privacy preserving association rule mining. *J Comput Sci* 6:1494–1498
31. Hong T-P, Lin C-W, Chang C-C, Wang S-L (2011) Hiding sensitive itemsets by inserting dummy transactions. In: *GrC IEEE*, pp 246–249
32. Jain D, Khatri P, Soni R et al (2012) Hiding sensitive association rules without altering the support of sensitive item (s). *Adv Comput Sci Inf Technol Netw Commun* 3:75–84

A Formal Analysis for RSA Attacks by Term Rewriting Systems

Mohammad Kadkhoda, Anis Vosoogh and Reza Nourmandi-Pour

Abstract The high security for RSA cryptosystem depends on the less power of attacks broken it. This subject can be reduced to find the prim numbers and integer factors. Any attack besides the brute force attack, may succeed and obtain plaintext or private key. So, it is necessary to keep the RSA cryptosystem security against attacks. In this paper, we proposed a formal cryptanalysis for RSA cryptosystem, by term rewriting systems (TRS) and termination proving. We have embedded one RSA attack in a TRS model, such that attack has been successes on the RSA cryptosystem if and only if its TRS model has been terminated. Since the automated termination proving of TRSs has been grown in the last years, our work will promise.

Keywords RSA cryptosystem · Attack analysis · Formal verification · Term rewriting system · Termination proving

1 Introduction

The RSA cryptosystem [1] is one of the mathematical public key encryption. By some algebraic assumptions such as prime number and integer factoring computation, which are important in RSA cryptosystem, any attack ways are faced with hard problem and high complexity of computation [2]. When security of RSA tied

M. Kadkhoda
ACECR, Tarbiat Modares University, Tehran, Iran
e-mail: kadkhoda@chmail.ir

A. Vosoogh (✉)
Science and Research Branch, Islamic Azad University, Sirjan, Iran
e-mail: anisvosoogh@yahoo.com

R. Nourmandi-Pour
Department of Computer Engineering, Sirjan Branch,
Islamic Azad University, Sirjan, Iran

with factoring modulus n , i.e., finding prime numbers p and q when multiple of them equal to n , it is not surely impossible and may find an effective attack to break it. On the other hand many attacks are developed where are based on careless in RSA implementation and supported by high processing computers. Therefore, we need to analyze RSA attacks that increase RSA resistant when tackle with them.

An attack uses the variation analysis during cryptographic operation to get the information about message or secret key [3]. It can also use a difference of the operations execution time [4] and may mathematical analysis of RSA. It can be vulnerable to analyze RSA and prevent of attacks.

In this paper, we proposed a formal analysis of RSA attacks. First, we transform the algorithm of RSA attack to a term rewriting system (TRS) as a formal language on functional terms of first-order logic. This transform consists of a special computation on ciphertext or public key to a TRS, where decoding the message or private key is tied with termination of this TRS. Therefore, we have an attack algorithm that is embedded in a TRS such that the security analysis of the RSA attack is replaced with termination proving of its TRS. Since we know there are many automated termination proving tools, this transform is supported attack analysis for keep secure of RSA cryptosystems. In other words, in our work success of RSA attack has redefined by termination, where RSA is not secure or attack is successful, if correspond TRS for it terminated. This helps us to increase security of RSA cryptosystems by attack analysis and avoid when it is happened.

The remainder of this paper is organized as follows: in Sect. 2, we review previous analysis methods for RSA attacks. Next in Sect. 3, we review the RSA cryptosystem and some of its variants. In Sect. 4, we present some basic notations and facts on rewriting system. In Sect. 5, we discuss the attack analysis by term rewriting system and present one example. Section 6 consists of the result of our work and comments on some future works.

2 Related Works

The analysis and the verification security of cryptosystem in the some research have recently received more attention [3, 5]. Number of methods has been applied specifications of RSA to formally prove various properties of variant attacks, because they can deal with them [6].

There are many attacks against brute force that are developed successfully. In [4] OAEP is proposed as an appropriate padding scheme. It required ensuring the security of the cryptosystem and when a cryptographic algorithm is secure from a theoretical point of view, we cannot guarantee that it is also secure when it is implemented.

At RSA cryptosystem, the private key is always mathematically linked to the public key [3]. This linked operation is easier to do in one direction and its converse is very difficult when we do not have additional information; although it is possible that a mathematical attack broke it by driving the private key [7]. Especially, by

Table 1 Comparison of time for broken and length of private key

Time of broken	Length of key (Bit)
Fast	256
Fast, for especial state	384
Fast, with full equipment	512
For short-term	768
The near future	1024
For several days	2048
For several years	4096

factoring the modulus into their prime numbers, the private key is detected and hence, the security of the cryptosystem is broken.

A new algorithm for RSA deals with two opposite problems, data security degree and computing processes speed. If the RSA key size grows increase, running their algorithms needs lots of time and memory. Practically, we should balance the key size and security degree. When an attack faces to key size grow, it may be weekend. However in application it may not occur strongly [8]. The comparison of time for broken and length of private key in the original RSA cryptosystem has been shown in Table 1.

A fast variant of RSA is considered by getting public or private key significantly smaller than $\varphi(n)$ that create RSA-small- e or RSA-small- d , respectively. In RSA-small- e the encryption costs can be reduced and in RSA-small- d the decryption costs can be reduced [9]. While the encryption costs are reduced in RSA-small- e , the decryption costs remain the same as original RSA. It is similar for RSA-small- d because public and private key are inverse in the other modulo $\varphi(n)$. Unlike the small public exponent scenario RSA-Small- e , it is not safe to use very small private exponents. Boneh and Durfee [10] have shown that any private exponent $d < n^{0.292}$ should be considered unsafe.

Factoring is a hard computation problem. Pomerance [11] has an interesting introduction into what clever methods can do. May or may not an attack can be conducted in a reasonable amount of time on a correctly implemented RSA. However, there are many attacks on poor or naïve implementations. Peter Shor [12] has shown that a quantum computer has a polynomial time algorithm for factoring integers. Nevertheless, engineering a quantum computer has still a way to go, so RSA is safe for now.

3 RSA Cryptosystem

The reader referred to [13] for the basics of RSA cryptosystem and some of its variants that recently come in [3]. However, we review main points of RSA methods.

The cryptography by RSA has three algorithms for key generation, encryption, and decryption. First, we select two distinct prime numbers p and q randomly, then

compute their multiply n and select integer e that is relatively prime to $\varphi(n)$ where $\varphi(\cdot)$ is Euler's phi function, and finally obtain integer d by e and $\varphi(n)$ such that $ed \equiv 1 \pmod{\varphi(n)}$. The pair (e, n) is our public key and (d, n) is our private key. Second, a plaintext $M \in \mathbb{Z}_n$ is encrypted by e th power modulo n to ciphertext $C = M^e \pmod{n} \in \mathbb{Z}_n$. Third, a ciphertext $C \in \mathbb{Z}_n$ is decrypted by d th power modulo n . It follows from Lagrange's theorem that:

$$C^d \pmod{n} = M^{ed} \pmod{n} = M \pmod{n} = M.$$

From the key relation, it follows that there exists a unique positive integer k satisfying $ed = 1 + k\varphi(n)$. We call this RSA key equation or simply the key equation.

4 Term Rewriting System

The definitions and symbols of TRS are somewhat coherent as [14]. Let F be a finite signature where each symbol $f \in F$ has a nonnegative integer, $r > 0$ as arity. The set of symbols in F having arity r is denoted by $F(r)$. $F(0)$ contains at least one member. The set of terms over F and the enumerable set of variables V , where $F \cap V = \emptyset$, is denoted by $T(F, V)$. A term containing no variables is closed, and $T(F)$ is the set of closed terms. The symbol or variable u occurs $|s|_u$ times in the term s , and $|s|$, the size of s , is the sum of all $|s|_u$. $\text{Fun}(t)$ denotes the set of all function symbols occurring in the term t and $\text{Var}(t)$ is set of its variables. In this paper, TRS is defined as a pair (F, R) , where R is a finite set of rewrite rules on the signature F . The rewrite relation induced by R , is denoted by \rightarrow_R , its transitive closure is \rightarrow^+R , and its transitive and reflexive closure is \rightarrow^*R . $D(R)$ is one or the set of defined symbols R where $f \in R$ if $f = \text{root}(l)$ where $l \rightarrow r \in R$. A strict order $>$ is not reflexive and transitive binary relation and a partial order \geq , is reflexive, transitive, and asymmetric binary relation. A quasi-order \succeq , is transitive and reflexive binary relation. A subterm ordering on $T(F, V)$ define $s D t$, when there is a context P where $s = P[t]$.

A partial order on a set A is well founded if the infinite descending sequence a_1, a_2, \dots of elements of A does not exist. A rewrite relation which is also a partial order is called a rewrite order. A well-founded rewrite order is called reduction order. A TRS R is compatible with partial order $>$ if $R \subseteq \geq$. A TRS R is terminates if it is compatible with a reduction order \geq . Otherwise, TRS (F, R) is terminating if there is no infinite rewrite sequence for one term $t \in T(F, V)$.

4.1 Termination Property

Termination is important property in theory of rewriting. This property is preserved when computation process has been finished for all start terms. For example, let us consider the following TRS with seven rewrite rules:

1. $odd(s(x)) \rightarrow if(g(x), s(x), p(x))$
2. $odd(0) \rightarrow 0$
3. $g(s(s(x))) \rightarrow true$
4. $g(0) \rightarrow false$
5. $if(false, s(x), p(x)) \rightarrow x$
6. $if(true, s(x), p(x)) \rightarrow odd(p(x))$
7. $p(s(x)) \rightarrow x$

This system calculates that the given number x is odd or not. To prove the termination of this system we need to define a well-founded order. For example, the weight function for operations and constants helps us to compare terms of system and confirm whether it is terminated or not. For this, we require the determination of each of the following maps:

$$W : \{odd, if, g, s, p, true, false, 0\} \rightarrow N$$

$$\tau : \{odd, if, g, s, p, true, false, 0\} \rightarrow \{null, identity, min, max\}$$

A possible solution for W and τ of the above TRS is as follows:

$$(W, w_0 = 1) \quad odd \rightarrow 3, if \rightarrow 2, g \rightarrow 2, s \rightarrow 2, p \rightarrow 2, true \rightarrow 1, false \rightarrow 1, 0 \rightarrow 1$$

$$\tau : odd \rightarrow identity, if \rightarrow max, g \rightarrow null, s \rightarrow null, p \rightarrow null, true \rightarrow null, false \rightarrow null, 0 \rightarrow null.$$

So, the following inequalities must be used to preserve the condition of termination of these rewriting rules.

$$\begin{aligned} W_g &> 1, W_{odd} + 2 > 1, W_p > 1, \\ W_{odd} + i + 1 &> W_{if} + \max(a, i + 1, i - 1), \\ W_{if} + \max(a, i + 1, i - 1) &> W_{odd} + i - 1 \\ W_{if} + \max(0, i + 1, i - 1) &> i \end{aligned}$$

The set of these constraints are satisfied. This subject can be shown by Torpa [15], a tool of automated termination proving or any automated SAT solver tools. In this paper, we have focused on termination property as a technique for attack analysis and verify security of RSA cryptosystem that is one of general cryptography methods.

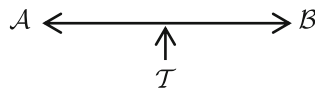
5 Attack Analysis by Termination of Rewrite System

New methods of attacks other than RSA brute force attack and factoring modulus have been establishing to recede of exponential hope. So, we need an effective analysis method for ensuring to able or unable of the attack to obtain plaintext or private key. In this section, RSA algorithm is analyzed to find its weaknesses about

attacks. This work is done by termination analysis on attack rewrite system. In the following we define a RSA attack and its structure for broken key.

5.1 Attacks against RSA

The RSA function which is defined at section, is an example of a one-way function, in role play, entity \mathcal{A} (sender) may wish to send entity \mathcal{B} (recipient) encrypted information C that malicious attacker entity \mathcal{T} (enemy) will try to attack, as bellow:



It is not known as an invertible without the d . General attacks on RSA involve trying to compute d , or some other ways to get to M . Entity \mathcal{T} may know only $\langle e, n \rangle$, or C and $\langle e, n \rangle$. The decryption key can assign an M that only the encryption key can be verified. Knowing $\langle e, n \rangle$, if entity \mathcal{T} can factor n then d can be computed in a reasonable time interval. Likewise, knowing e, d and n then entity \mathcal{T} can factor n . These two known properties will be used to show some unsafe RSA implementations. So we have three main attacks: brute force, factoring n , computing e th root modulo n .

If entity \mathcal{T} has access to C , then e and n can do a brute force search to find M . But factoring n involves a much smaller search space and thus, more efficient to do. Security of RSA depends on the computation of factoring of n and the e th roots modulo n . The first is fairly well researched, and its complexity is understood. However, the second is an open question. It has not yet been proven that taking the e th roots modulo n is at least as hard as factoring n . This means RSA security has not been proven to be at least as hard as factoring. But it has a large amount of research, which encourages that it will stay secure well into the future.

RSA will be shown to hold up to all known attacks. We write a list of variant of RSA attacks; however summaries of new research findings are not complete (Table 2). We divide RSA attacks in three groups: blind attacks, math-based attacks, and run-based attacks.

Table 2 List of RSA attacks

Group	Attack	Against
Blind attacks	<ul style="list-style-type: none"> • Brute force • Random method 	Search space Near of M or d
Math-based attacks	<ul style="list-style-type: none"> • Factoring n, • Root modulo n • Find d directly 	Small- d (Wiener) Small- e (Coppersmith) Plaintext M
Run-based attacks	<ul style="list-style-type: none"> • Timing and error message • Interactive 	Running time of cryptographic operation (Kocher) Chosen ciphertext (Bleichenbacher, Manger)

Now, instead of reviewing the several attacks where has been come in the many old researches [2, 6], a major and known attacks is selected among them.

5.2 Transform RSA Attacks to a TRS

We define original RSA cryptosystem with triple (K, E, D) where K is key generation process, E is encryption structure on $\langle e, M \rangle$ and D is decryption structure on $\langle d, C \rangle$ for message M .

For an $RSA = (K, E, D)$, the RSA attacks can be treated as a rule-based system. Since term rewriting system is a nondeterministic computation model, so it is equipped for embedding any complex computing as well as attack algorithms. Follow, we proposed a new formal description for RSA schema by TRS model.

Definition 1 Transform RSA attack to a TRS start with defining the set of signatures F and $T(F, V)$ set of terms where V consist of variables x, y, z , and set of rules R for coverage all process in computing attacks. Now, TRS (F, R) is defined as:

$$F = \{Attack(\cdot), Encrypt(), Decrypt(), Public(), Private(), New(), e, d, \dots\}$$

and,

$$R = \left\{ \begin{array}{l} Attack(x, a) \rightarrow New(Attack(x, a), x), \\ Encrypt(e, x) \rightarrow y, \\ Decrypt(d, y) \rightarrow x, \\ Public(e, y) \rightarrow e, \\ Private(d, x) \rightarrow d, \quad \dots \end{array} \right\}$$

where, three dots consist of other process of attacks for broken private key d or obtained message M .

Initial term $Attack(x, a)$ has been successful if and only if (F, R) is terminated and we access to M the encoded message or d key of decryption. An elementary definition of $Encrypt(e, M)$ and $Decrypt(d, C)$ is $e \oplus M$ and $d \oplus C$, respectively, where \oplus is power function. Now, we can show (F, R) is terminated when attack process has been finished in the sufficient time.

Theorem 1 Let consider entity T is a RSA attack when \mathcal{A} and \mathcal{B} are receiver and sender entities, respectively. If TRS (F, R) has defined as well as Definition 1, with three set of rewrite rules based on $RSA = (K, E, D)$, then termination of (F, R) is equals attack occurred.

Proof (Sketch) An attack is successful if their process has been completed in the optimal time, absolutely. When attack is tackled with M and C as a data and K, E , and D as cryptosystem protocols, it is finally stopped and presents their result. When all of these processes are embedded in a rewrite rules, our result is present as a term where it has data or structure either or both. These facts prove RSA is successful and can be considered while their (F, R) is terminated.

Next, an example of this transform is presented. We ensure attack occurs hen termination test is to be approved.

5.3 Attack other than factoring n

In the following, we select the attack algorithm in [5] as attack other than factoring n . We propose a new presentation of this attack in terms of rewriting system and prove its termination by Torpa, a termination tool. We show that security of RSA can be broken by this attack.

Table 3 Transform the attack to a TRS

$Attack(Public(e, n), c) \rightarrow mod(power(c, Public(e, n)), n)$ $Public(e, n) \rightarrow Private(0, gilotet(div(e, n)), min(div(e, n), gilotet(div(e, n))))$ $Private(x, y, z) \rightarrow f(y, private(s(x), gilotet(div(1, div(z, y))), div(1, div(z, y))))$ $if(true, y, x, y', z) \rightarrow f(y, s(x))$ $if(true, y, x, y', z) \rightarrow$ $\quad f(y:y', private(s(x), gilotet(div(1, z)), min(div(1, z), gilotet(div(1, z))))$ $f(y, private(x, y', z) \rightarrow if(y = y', y, x, y', z)$ $f(y, s(x)) \rightarrow if-o-e(odd(proj(y, s(x)), y, s(x))$ $if-o-e(true, y, s(x)) \rightarrow recons(y, s(x))$
--

Table 4 Verify termination for RSA attack

<p>TORPA 1.6 is applied to</p> <pre> Attack (Public (e , -> n) , , Public (e , -> n) , Private (x , -> y , , if (true , -> y , , if (true , -> y , , f (y , -> private , f (y , -> s (x)) , if -> o - , Choose polynomial interpretation A: lambda x.x+1, rest identity remove: Attack (Public (e , -> n) , Choose polynomial interpretation c: lambda x.x+1, rest identity remove: Public (e , -> n) Choose polynomial interpretation (: lambda x.x+1, rest identity remove: Private (x , -> y , remove: if (true , -> y , remove: if (true , -> y , remove: f (y , -> private Choose polynomial interpretation i: lambda x.x+1, rest identity remove: if -> o - Choose polynomial interpretation ,: lambda x.x+1, rest identity remove: f (y , -> s (x)) Terminating since no rules remain.</pre>

Let entity \mathcal{A} be public key $\langle e, n \rangle = \langle 2621, 8927 \rangle$ where entity \mathcal{A} private key $d = 5$, $p = 113$ and $q = 79$. Then entity \mathcal{B} encrypts the message M so the ciphertext $C = 6948$ can be sent it to entity \mathcal{A} . Suppose the attack entity \mathcal{T} obtain the encrypted message $C = 6948$. By using the following algorithm entity \mathcal{T} will recover the original message M . The term rewriting model is (Table 3).

Obviously, this attack has encouraged computational work for computing the private key or plain text. This TRS description of attack helps us to detect that the process is finished or not. So, we applied Torpa, a termination tool for detecting the resistance RSA cryptosystem. Result of termination test for this attack is shown below (Table 4).

The ongoing research that might bring in new security issues and challenges to RSA will be referred to in our proposal that uses termination tools as Torpa for attack analysis and enhances the degree of security of RSA cryptosystems by preventing them.

6 Conclusion

Our aim in this paper is to develop powerful termination analysis of the term rewriting systems and to prove security of RSA cryptosystem against attacks except brute force attack. Due to increased attacks especially run-based attacks on RSA we need to make sure whether they are able or not, to obtain plaintext or private key.

We defined a transform of RSA attack to a term rewriting system, and termination proving tools verify relevant TRS is terminated or not. While we have embedded algorithm of RSA attacks in a rewriting system, these attacks are successful if and only if their rewrite system is been terminated. Any attack that occurred referred to keep termination and to stop attack computation. However, this is not considered a great success, because proof termination method for TRSs is relatively difficult. But, some termination proof tools may be suitable for automated attack analysis and this embedding will be promising. Our result shows that termination analysis can be used for this cryptanalysis problem. This idea is first introduced and needs more study for many protocols and encryption ways.

References

1. Rivest R, Shamir A, Adelman L (1978) A method for obtaining digital signature and public key cryptosystem. *Commun ACM* 21:120–126
2. Bonte S (1999) Twenty years of attack on the RSA cryptosystem. *Not Am Math Soc* 46 (2):203–213
3. Itoh K, Kunihiro N, Kurosawa K (2008) Small secret key attack on a variant of RSA. In: Malkin T (ed) *CT-RSA'2008*. LNCS, vol 4964, pp 387–406
4. Bellare M, Rogaway P (1995) Optimal asymmetric encryption—how to encrypt with RSA. In: Santis AD (ed) *ERUOCRYPT'94*, LNCS, vol 950, pp 92–111

5. Aboud SJ (2009) An efficient method for attack RSA scheme. In: IEEE, No 978, pp 587–592
6. Yan SY (2008) Cryptanalytic attacks on RSA, Springer, New York
7. Boneh D, Durfee G, Frankel Y (1998) An attack on RSA given a small fraction of the private key bit. In: Ohta K, Pei D (eds) ASIACRYPT'98, LNCS, vol 1514, pp 25–34
8. Mousa A (2005) Sensitivity of changing the RSA parameters on the complexity and performance of the algorithm. In: Journal of Applied Science, Asian Network for Scientific Information, pp 60–63
9. Wiener M (1990) Cryptanalysis of short RSA secret exponents. IEEE Trans Inf Theory 36:553–558
10. Boneh D, Durfee G (2000) Cryptanalysis of RSA with private key d less than $N^{0.292}$. IEEE Trans Inf Theory 46(4):1339–1349
11. Pomerance C (1996) A tale of two sieves. Not Am Math Soc 43:1473–1485
12. Shor P (1997) Polynomial-time algorithms for prime factorization and discrete logarithms on a quantum computer. SICOMP 26(5):1484–1509
13. Menezes AJ, Oorschot PV, Vanstone S (1997) Handbook of applied cryptography. CRC Press, Boca Raton
14. Baader F, Nipkow T (1998) Term rewriting and all that. Cambridge University Press, Cambridge
15. Zantema H (2004) Torpa: termination of rewriting proved automatically. In: Oostrom V (ed) RTA'11, LNCS, vol 3091, pp 95–104

Part VII
Knowledge-Based Technologies

Heuristic Optimization of Wireless Sensor Networks Using Social Network Analysis

Alexandru Iovanovici, Alexandru Topirceanu, Cristian Cosariu,
Mihai Udrescu, Lucian Prodan and Mircea Vladutiu

Abstract A rapidly rising number of civilian and military real-world applications require deployments of large sensor networks. However, problems like limited energy supply, tough environments, data latency, and integrity cause adverse effects on large topologies of sensors. This paper presents a novel approach in designing the placement of relay nodes in a sensor network. By using concepts from the area of social network analysis and mapping them to the already classical field of sensor networks we succeed to add improvements to the costs implied with deploying the infrastructure. By socializing the topology with the concepts of centrality and community structure, our research is focused around a flexible design space exploration algorithm that we have devised, which offers a balance between the performance and cost of deploying relays in a sensor network. As a result, our WSN design achieves a relevant improvement over the state of the art solutions.

Keywords Wireless sensor network topology · Social network analysis · Design space exploration algorithm

A. Iovanovici (✉) · A. Topirceanu · C. Cosariu · M. Udrescu · L. Prodan · M. Vladutiu
Politehnica University Timisoara, 300077 Timisoara, Romania
e-mail: iovanalex@cs.upt.ro

A. Topirceanu
e-mail: alexandru.topirceanu@cs.upt.ro

C. Cosariu
e-mail: cristian.cosariu@cs.upt.ro

M. Udrescu
e-mail: mudrescu@cs.upt.ro

L. Prodan
e-mail: lprodan@cs.upt.ro

M. Vladutiu
e-mail: mvlad@cs.upt.ro

1 Introduction

The recent years were the witness of an almost explosive development in the area of sensor networks in general, and wireless sensor networks in particular, in the civilian fields [1]. Much because of the miniaturization and integration of the hardware, combined with the low cost associated, more applications are devised which employ some kind of networked sensors. These applications—such as disaster management, forest fire detection, plant automation—require the deployment of an array of nodes which have to operate unattended for long time, on limited power supply. Major deployments consist of hundreds of nodes interconnected at a logical level, in accordance to topologies, and also at a physical level, wirelessly. One of the major issues that can be identified is the depletion of the battery's energy [2–4]. Such situations can cause issues with the network's topology because some of the relaying nodes are not able to forward data causing partitioning of the network and disruption of the services [5].

Applying social network analysis principles in order to analyze and optimize sensor networks is nothing but natural as the social perspective provides an innovative means of analyzing the structure of entities with a social-like structure [6]. Thus, we can detect influential nodes, patterns of communication and also study dynamics inside the network. This strongly relates to wireless sensor networks as it is important to disseminate the sensor nodes that are critical for the data throughput, which are more central so that relays can be placed at those positions, and also model growth as the network coverage spreads in time.

Much of the research in the field of sensor networks was oriented in the recent years to maximize what is called “functional requirements,” such as data latency [7], real time-ness and “non-functional requirements” such as data integrity [7]. Minimizing energy requirements is often the top priority, but most of the sensor network deployment is in tough and adverse environments where there are many more hazards than just energy loss [3].

In our discussion, we are going to differentiate between regular nodes responsible for gathering data and/or acting upon received commands and relay nodes which collect data from the nodes in the direct area of coverage and send them upstream to the network sink. The scope of this paper is to propose an optimization solution for choosing the number of required relays and their optimal position so that we maximize the performance of the network while keeping the overhead at a minimum.

In the design of a WSN, the practitioner has to balance the costs involved with the solution, with the performance, and one of the key performance metrics is the average delay from node to sink. Our research is part of a larger endeavor of designing and deploying a near real-time sensor network for monitoring and reporting data regarding road traffic conditions and consequently dynamically adapt the state of the traffic lights.

2 State of the Art Sensor Deployment

2.1 Background

Mostly dependent on the task of the network there are two major strategies in placing the nodes of a sensor network: deterministic and random. The first one can ensure great coverage with careful placement [8], but due to the adverse conditions on the field there are situations in which the distribution has to be done in a random manner, with adverse effects on the network metrics [7]. Rich literature exists on the topic of optimal node placement [8], which is considered an NP-hard problem [9] and some nondeterministic approaches were proposed, which provide suboptimal results.

One interesting approach, which is also the starting point of our investigations, is the one presented by Xu et al. in [8]. The authors take into consideration a two-tiered topology in which nodes are clustered around relaying nodes which further communicate directly with the sink. Further, they discuss a multiple-hop hierarchy of relay nodes, connected in a tree manner to the sink. One of the issues identified is that the random distribution can leave some parts of the network disjoint, actually partitioning the network.

Another practical application is the exploration of the issues arising while scaling the network. From an economic perspective, much of the sensor network deployments consist of incremental stages with more nodes being added. Related to the issue of low-power operation, there is a growing interest in the area of network connectivity [9]. Early work has considered the coverage as being the paramount of the research [8], but because modern sensor nodes are running at the threshold of the energy requirements their coverage is largely diminished. Flat 2D sensor networks usually consider relay nodes to be simply another node, but with higher transmission power and/or energy autonomy. The problem is getting interesting in two-and multi-tier sensor networks where sensors are usually clustered in what can be called subnets, as presented by Chen et al. in [10].

2.2 Social Network Approach

The novelty introduced in this paper is the usage of social network analysis (SNA) principles to enhance the properties of a wireless sensor's network topology. Through measurements performed over raw state of the art sensor networks, our goal is to propose an optimal coverage of physically-linked relays over any given network so that we maximize the throughput and reliability and minimize the number of relays and cost of cable. We have measured the basic network metrics: network size (nodes and edges), average path length, clustering coefficient, average degree, network diameter, density and modularity, and also the distributions of the degrees, betweenness, closeness, and (eigenvector) centrality [11]. After performing social network analysis, we have concluded that an optimal way to leverage the

relay placement is through community detection and centrality algorithms. We define the basic set of SNA principles further used in this paper. The average path length of a network is the mean distance between two nodes, averaged over all pairs of nodes [11]. The degree of a node is defined as the total number of its (outgoing) edges. Thus, the average value of the degrees, measured over all nodes, is called the average degree of the network. Modularity is a measure that shows the strength of the division of a network into communities [12]. High-modularity means a strong presence of well-delimited communities. Similar to the Pagerank algorithm, (Eigenvector) centrality measures the influence a node has in the network.

Algorithm 1 SIDeWISE pseudocode for a cost-throughput-optimal network

Input: raw wireless sensor network with $|V|$ nodes with positional data (x_i, y_i) , and wireless coverage range r .

- 1 : Create edges between all pairs of nodes in range: $\text{dist}(n_i, n_j) \leq r$
- 2 : Measure centrality on obtained graph $G = \{V, E\}$
- 3 : Assign the sink s as the node in V with centrality 1 (maximal)
- 4 : Detect communities com_i in G using resolution
- 5 : Discard communities with $\text{size}(\text{com}_i) < \lambda \times |V|$ (5% of population)
- 6 : Measure centrality on each community com_i independently
- 7 : Assign the node with centrality 1 in each com_i as the local relay r_i
- 8 : Create a fully connected graph $\text{GR} = \{R, \text{ER}\}$ of relays r_i and s
- 9 : Using GR , create a Kruskal-MST graph $\text{MST GR} = \{R, \text{MST ER}\}$
- 10: **while** (sink s does not have centrality 1)
- 11: pick each edge from GR and temporarily add it to MST GR
- 12: fitness of added edge is equal to new centrality of s
- 13: pick edge with best fitness and keep it in MST GR

Output: wireless sensor network G with cost-optimal overlapping relay and sink physical network MST GR

3 Methodology

In order to generate our input data, we use a WSN topology generator which produces a topology of nodes (sensors) with 2D geographical data. We convert the information into gdf file format which can be imported in Gephi [13], a leading tool in large graph data visualization. Any layout of sensors in a geographic space can be processed by our algorithm by importing it in Gephi, where our developed plugin can be used from. Further, our enhancement algorithm, called SIDeWISE, processes the topological data. The result is the initial sensor network with an additional overlapping layer of optimally placed relays which are all connected to a sink through a heuristically obtained minimum cost spanning.

We further present the SIDeWISE (SocIally enhancedD WIREless Sensor nEtwork) algorithm step by step. We start with a topology of given sensors $|V|$

which all have positional data attached. Also, a wireless coverage range r is given, and a resolution parameter which controls the density of required relays to be placed. A graph $G = \{V, E\}$ is formed by connecting each of the two sensors that are within each other's coverage range r . Once the graph is obtained, the Eigenvector centrality algorithm is run on G [14]. The Eigenvector centrality was chosen as it is considered a well predictor of a node's influence in a network [11, 15]. The centrality algorithm is defined in such a way that only one node—the most central—has a centrality of 1.0. All other nodes have their centralities between 0 and 1. Consequently, we define node s with maximal centrality as the sink for G . Next, a community detection algorithm is run on G , a graph measure which is designed to measure the strength of division of a network into communities. This is achieved using the modularity algorithm [16] with a corresponding default resolution of 1.0 [17]. Depending on the input resolution one can decide to detect few larger communities (resolution > 1), or multiple smaller ones (resolution < 1). This affects the total number of placed relays. For efficiency purposes, all resulting communities with a population less than λ (5 %) than the total population are discarded, being considered irrelevant for throughput. On the remaining (significant) communities, com_i , centrality is measured again independently, and the nodes with centrality 1 are chosen as the local relays r_i . The relays r_i and the sink s are organized into a fully connected graph $GR = \{R, ER\}$ with point-to-point links between all relays. Further, graph GR is filtered using Kruskal's algorithm and a minimum spanning graph $MST GR$ is obtained. It consists of all relays and the sink, connected by a minimum cost tree.

At this point we have a cost-optimal overlapping tree of relays and $MST GR$, but from a throughput perspective it may result as highly latent. This problem is depicted in Fig. 1. The next optimization tries to heuristically lower the average

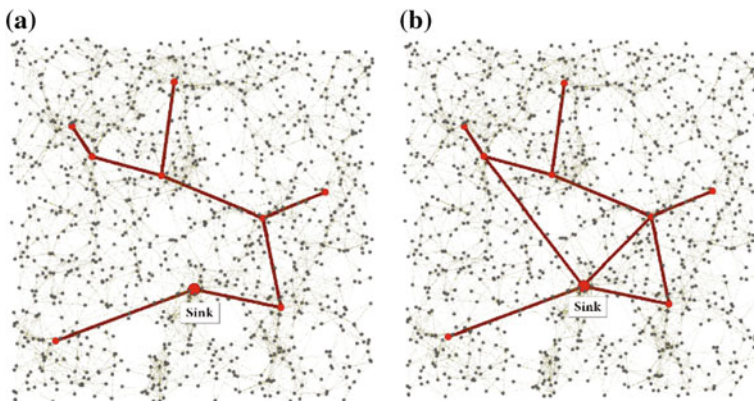


Fig. 1 Heuristic optimization of the MST to increase throughput of relays (red nodes). **a** A relay network connected with an MST. **b** The same MST but with additional two edges so that the sink (bigger red node) becomes the central node of the network

number of hops required for relays to reach the sink. As such, an iterative process of maximizing the sink's centrality is proposed. Even though the ideal result would be to connect all relays with the sink directly, this would alter the cost-optimality. Thus, a trade-off solution like the one depicted in Fig. 1b is preferred. Most relays now have a distance of one or two hops with the addition of only two edges to the MST. The algorithm tries to add another edge to the MST, measures the sink's new resulting centrality and keeps this as a fitness for the added edge. It does this for all candidates. After one iteration, the edge with the best fitness is kept in the MST. This is repeated until the centrality of the sink becomes 1.

4 Simulations and Results

The started research comprises multiple stages of parameter analysis and optimization using real-world validation, and in this paper we exemplify the functionality of SIDEWISE on realistic networks by explaining how the algorithm's parameters affect the results. The previously described topology depends on two ad hoc parameters: the resolution of the modularity, and the wireless coverage radius. We highlight the impact of these two parameters in regard to the number of assigned relays.

Setting the resolution is equivalent to finding an ideal trade-off between the number of terms in a sum and the value of each individual term. The experimental results depicted in Fig. 2 show that as the resolution increases from the default value, (i.e., 1.0) the total number of detected communities (red) decreases slowly and converges toward a minimal value. In the chosen example, a 1000 node network can be divided into not less than nine communities, regardless of how much the resolution is increased. As the resolution is decreased from 1 toward 0, the number of detected communities increases exponentially, but their actual size decreases steadily. Because the SIDEWISE algorithm neglects communities smaller

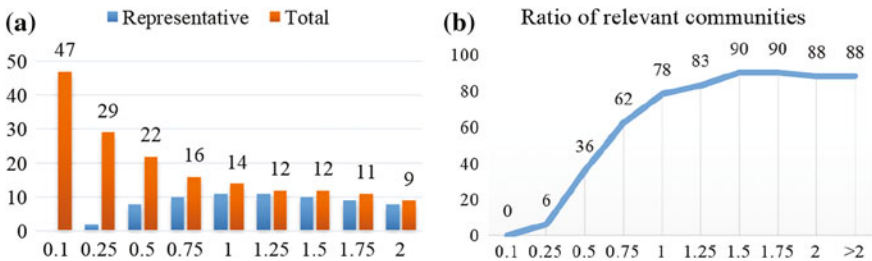


Fig. 2 **a** The impact of using a custom resolution (OX-axis) for the community detection algorithm, expressed in number of representative (*blue*) versus total (*red*) communities (OY-axis). The default value for the resolution is 1. **b** The ratio between relevant (size $> \xi$ %) and total detected communities on a network based on resolution. A low resolution yields poor mapping results (<50 % relevance), and high-resolutions all converge toward the same result (~ 90 % relevance)

than λ % (5 %) of the total population, the number of relevant communities (blue) decreases to a state in which not a single community is considered relevant to have its own relay. Figure 2a shows the numerical values of the relevant versus total number of communities depending on the resolution, and Fig. 2b shows the increasing ratio of the two numbers. As a conclusion to this experiment, we consider that applying SIDeWISE requires understanding the impact a custom set resolution has on the overall structure of relays. If the real-world conditions require sparse relay placement, one can consider lowering the resolution, so that only the truly most relevant communities of sensors receive a relay in their vicinity. Based on the observation, we suggest working with resolutions between 0.5 and 1.25.

Measurements confirm the fact that the number of required relays does not grow linearly with the number of nodes, but logarithmically. Our proposal has the same property as the small-world network described by Watts and Strogatz [11]. This is a very important feature of the SIDeWISE algorithm because it manages to keep the number of relays relatively low, thus the cost remains low, as the overall network propagation delay is rapidly decreased. Making an analogy with the small-world property that represents an ideal balance between the characteristics of a regular network and a random network [11], Fig. 3 suggest the same principle: the socially enhanced wireless sensor networks lie at the ideal crossroads between cost and performance. One the left side is a network with just one sink and no relays. While being cost-optimal ($1r$), it offers the worst performance as the propagation delay is maximal (6.98τ). On the right side is a network fully covered by relays. In this case, the delay is optimal (1τ) but the cost is maximized ($100r$). As the graphics of the delay and cost show, there is a window in which we can create a network with the best possible trade-off: a relatively low delay, (i.e., high performance) and a low cost. This is the type of enhancement which the SIDeWISE algorithm facilitates. Experimentally we prove that our proposed solution has a cost of $7r$ with a delay of only 3.62τ . This yields a 92 % performance improvement over (a) and only uses 7 % of the relays required for (b).

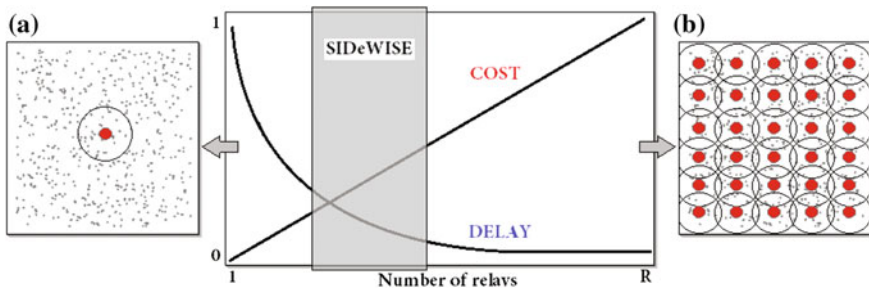


Fig. 3 The SIDeWISE algorithm balances cost and propagation delay by optimizing the placement of the relays in a WSN. The two extreme cases are represented by a single-sink network (a) and a network fully covered by relays (b)

5 Conclusions and Future Work

To the best of our knowledge, our work represents a novel approach in designing the placement of relay nodes in a sensor network. By using concepts from the area of network analysis and mapping to ad hoc sensor networks, we succeed to add improvements to the costs implied with deploying the infrastructure. Our research is focused around the algorithm we have devised, called SIDEWISE.

We consider our research as a framework for a much in depth analysis involving detailed physical characteristics of the network. The logarithmic behavior of SIDEWISE is of particular importance for the demanding applications of modern day sensor network with large number of nodes and still growing. Taking two classical reference examples, (single central relay/sink and a regular mesh of sinks) we have shown the location of our algorithm in the design space. In regard to the central sink placement SIDEWISE provides an improvement of 92 % in terms of performance while using only 7 % of the cost required for the mesh placement.

Our future work is focused toward real-world testing of the algorithm and a more insightful analysis of the functional requirements of the network with proven simulation tools.

References

1. Mainwaring A, Culler D, Polastre J, Szewczyk R, Anderson J (2002) Wireless sensor networks for habitat monitoring. In: Proceedings of the 1st ACM international workshop on wireless sensor networks and applications. ACM, pp 88–97
2. Chong C-Y, Kumar SP (2003) Sensor networks: evolution, opportunities, and challenges. *Proc IEEE* 91(8):1247–1256
3. Cheng P, Chuah C-N, Liu X (2004) Energy-aware node placement in wireless sensor networks. In: Global telecommunications conference GLOBECOM'04. IEEE, vol 5. pp 3210–3214
4. Cui S, Ferens K (2011) Energy efficient clustering algorithms for wireless sensor networks. In: Proceedings of ICWN, pp 18–21
5. Khelifa B, Haffaf H, Madjid M, Llewellyn-Jones D (2009) Monitoring connectivity in wireless sensor networks. In: IEEE symposium on computers and communications, ISCC 2009. IEEE, pp 507–512
6. Wasserman S, Galaskiewicz J (1994) *Advances in social network analysis: research in the social and behavioral sciences*. Sage
7. Li LE, Sinha P (2003) Throughput and energy efficiency in topology-controlled multi-hop wireless sensor networks. In: Proceedings of the 2nd ACM international conference on Wireless sensor networks and applications. ACM, pp 132–140
8. Younis M, Akkaya K (2008) Strategies and techniques for node placement in wireless sensor networks: a survey. *Ad Hoc Netw* 6(4):621–655
9. Bari A, Chen Y, Jaekel A, Bandyopadhyay S (2010) A new architecture for hierarchical sensor networks with mobile data collectors. In: Distributed computing and networking. Springer, Heidelberg, pp 116–127
10. Chen G, Cui S (2013) Relay node placement in two-tiered wireless sensor networks with base stations. *J Comb Optim* 26(3):499–508

11. Wang XF, Chen G (2003) Complex networks: small-world, scale-free and beyond. *Circuits Syst Mag IEEE* 3(1):6–20
12. Newman ME (2006) Modularity and community structure in networks. *Proc Natl Acad Sci* 103(23):8577–8582
13. Bastian M, Heymann S, Jacomy M (2009) Gephi: an open source software for exploring and manipulating networks. In: *ICWSM*, pp 361–362
14. Newman ME (2008) The mathematics of networks. *New Palgrave Encycl Econ* 2:1–12
15. Langville AN, Meyer CD (2011) *Google's page rank and beyond: the science of search engine rankings*. Princeton University Press, Princeton
16. Blondel VD, Guillaume J-L, Lambiotte R, Lefebvre E (2008) Fast unfolding of communities in large networks. *J Stat Mech: Theory Exp* 2008(10):P10008
17. Lambiotte R, Delvenne J-C, Barahona M (2008) Laplacian dynamics and multi-scale modular structure in networks. arXiv preprint arXiv:[0812.1770](https://arxiv.org/abs/0812.1770)

Interactive Applications for Studying Mathematics with the Use of an Autostereoscopic Display

Monica Ciobanu, Antoanela Naaji, Ioan Virag and Ioan Dascal

Abstract The abstract character of mathematical concepts can often discourage students who need to assimilate new materials. In order to help them overcome this problem, we developed a set of interactive teaching tool packages (ITTPs) consisting of theoretical modules and applications. A pseudo-holographic display was used for visualizing 3D objects and the outcome of modifications of the parameters inside mathematical formulas. One of the starting ideas was to develop the software using open-source libraries capable of manipulating 3D models like Java 3D. We extended the concept to work inside a web browser as well, in order to make the applications available on mobile devices and eliminate the need to install any other software.

Keywords Autostereoscopic display · Teaching tools · Pseudo-holographic images

1 Introduction

In today's scientific world, the use of holographic-like images for developing applications in various fields such as medical imaging, industry, military applications, entertainment, advertising, or computer game development represents a cutting-edge technological approach.

The main goal of our research was to use this technology to improve the quality of education by developing new visual-interactive methods for teaching mathematics.

Our team further developed an idea started by Wolfgang Schlaak from the Fraunhofer Institute for Telecommunications, Heinrich Hertz Institute [1]. In their research, they built an application that allowed physicians to study the patients' CT scans by visualizing them in 3D, with the possibility of rotating the image by means of hand gestures (called noncontact image control). The display they used was an

M. Ciobanu · A. Naaji (✉) · I. Virag · I. Dascal
Department of Computer Science, "Vasile Goldis" Western University of Arad,
96 Liviu Rebreanu St. Arad, Satu Mare, Romania
e-mail: anaaji@uvvg.ro

autostereoscopic multiview display, which involved tracking the user's eyes by means of a set of cameras mounted on top of the display and adjusting the image accordingly, to produce a sensation of depth.

In our research, we used the latest technology in the field of image visualization consisting of HoloVision aerial image display, produced by the Provision company [2]. This new type of autostereoscopic display does not require any cameras for tracking the viewers' eyes, being based on Pepper's Ghost technique, and allows a larger number of persons to visualize the projected 3D models without the use of special glasses.

For the time being, the HoloVision display was only used for marketing purposes; to our knowledge, we are the first scientific team that used the aerial image display for educational purposes.

The main differences between the two technologies is that the monitor we used does not have the 3D image attached to the display, but rather exhibits similarity to an actual hologram. The monitor uses a special mirror in order to focus and display the pseudo-3D holographic image.

Another key objective was to use available open-source libraries in order to allow other teams to further develop the applications or to adapt the existing ones to different fields of study.

The applications were developed to run on both classical computer architecture and holographic display for an enhanced user experience.

In Fig. 1, we can see that the user interface developed for the 2D monitors is different from the one developed to display the images on the autostereoscopic

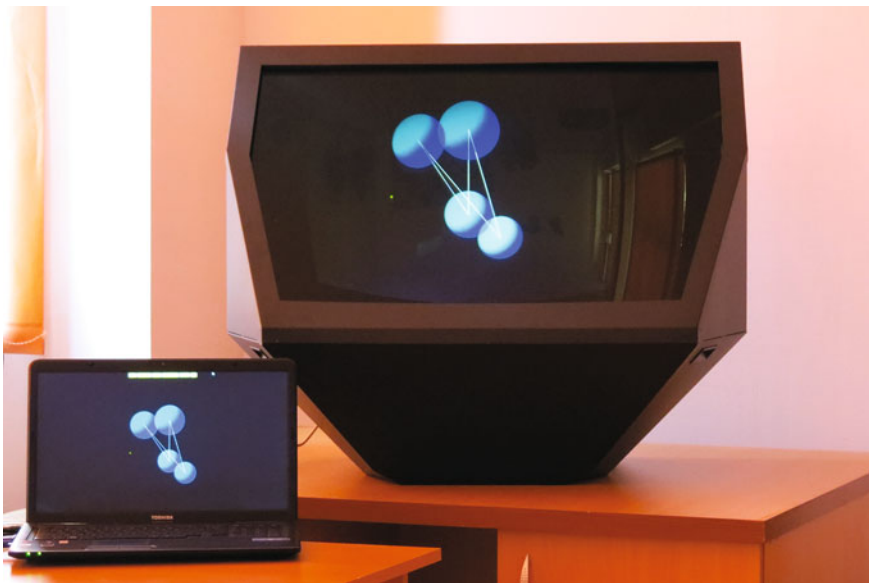


Fig. 1 Interfaces developed for laptop and holographic display

device. It was necessary to create two types of interfaces because, the HoloVision display is optimized to render 3D models focusing the image outside of the display area, providing the illusion that the image floats in midair in front of the monitor. The 3D image cannot be rendered in the same way on a 2D monitor, but the 3D model keeps its details on the HoloVision display even if it is scaled.

The two versions of the software were needed for individual study on a 2D monitor and for presenting the subjects to a group of students using the 3D display, as the viewing angle and distance allow this. The HoloVision holographic display that we used is able to display a 30 cm image focused at approximately 90 cm in front of the monitor, viewable at a 60-degree angle from the center and does not require the user to wear any kind of special glasses.

2 The Software Developed for Interactive Teaching Tool Packages Using Open-Source Libraries

The autostereoscopic display was used for ITTPs related to linear algebra and analytical geometry. We developed the programs based on Java 3D API and JavaScript because of their open-source nature. This was necessary in order to allow others to contribute with similar applications for different fields of study where visualization plays an important role such as architecture or medicine.

2.1 The Applications Developed by Using Java 3D API

The Java 3D API is an application programming interface used for creating portable 3D applications and applets. It provides a library for creating and manipulating 3D models and for constructing the structures used in rendering the scene. A scene graph is used to construct the scene, which is structured as a tree that contains the elements necessary to display the 3D objects. Developers can easily describe very large virtual worlds using this approach. Java 3D delivers Java's famous "write once, run anywhere" benefit to developers. Reference [3] presents a very detailed description regarding the mathematical concepts used behind the scenes in Java 3D.

Using Java 3D API, we developed applications for vectorial spaces, straight lines, and planes in three-dimensional Euclidean space, sphere and circle in space and conics in Euclidian plane.

The first application refers to the calculus of the expression of a vector with the help of its coordinates with respect to a base, solved using elements of matrix calculation. The graphical interface of the developed software can be seen in Fig. 2.

The second application solves problems related to elements of vector calculation and implement basic algebraic operations such as scalar multiplication, vector addition, and vector product. The created program allows the representation and rotation around axis of the vectors obtained by the addition of vectors using the

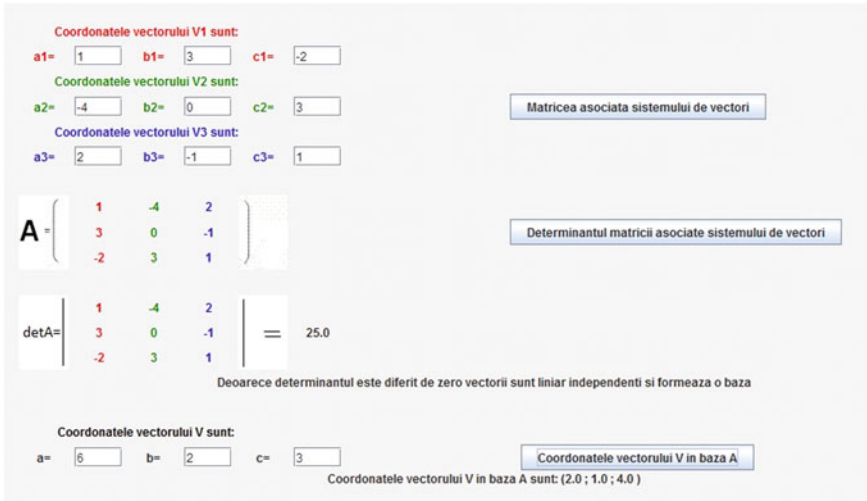


Fig. 2 Interface for the calculus of coordinates of a vector

parallelogram or the triangle rule, by multiplication of vectors by scalars, or by vector product calculation (Fig. 3).

Other applications are used to determine the intersection between two lines, two planes, a plane and a line, a line and a sphere, and a plane and a sphere (Fig. 4). They allow the calculus of the angle between lines and planes, the power of a point with respect to a sphere and draw the radical plane of two spheres, the radical axis of three spheres, and the radical center of four spheres.

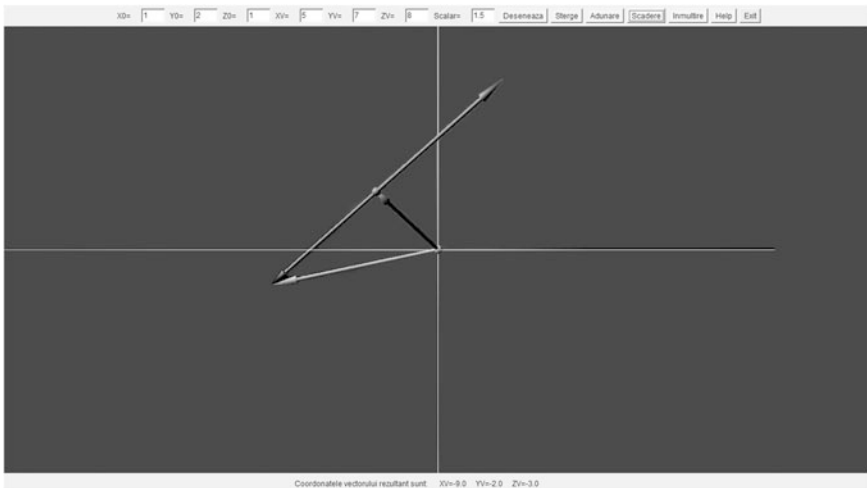


Fig. 3 Interface for vector calculus

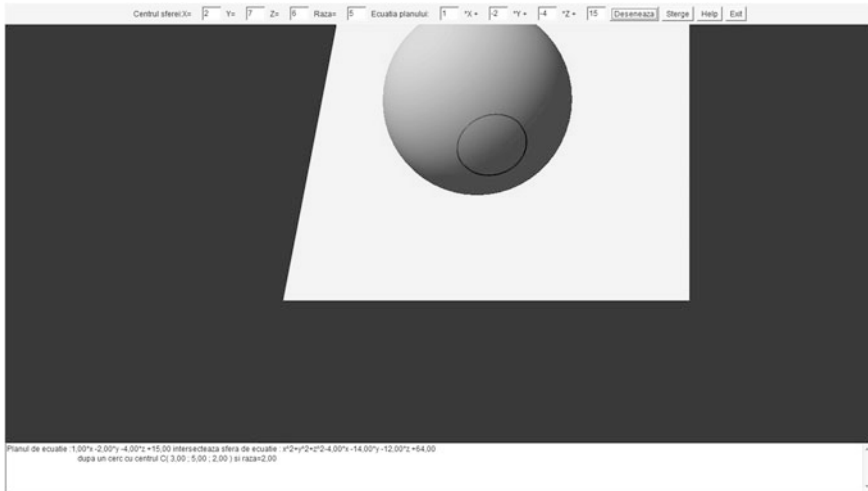


Fig. 4 Interface for visualizing the intersection between a sphere and a plane

In Fig. 4 is shown the circle obtained as the intersection of a sphere and a plane. The application also can illustrate the circle as intersection of two spheres and analyze all possible situations regarding the distance between the centers of the two spheres or from the sphere to the plane.

Another application draws conics starting from their general equation (Fig. 5). For the graphic representation of the nondegenerate conic, with or without center, the canonical equation of the conic, the center of the conic, and the axis of symmetry are determined. Thus, the invariant orthogonals are calculated and, based on their values, different types of conics are represented (ellipses, hyperbolas, parabolas as well as degenerate conics), along with complete solutions.

2.2 The Applications Developed by Using JavaScript

For the visualization part of the conic sections, we decided to use a JavaScript-based solution [4]. This approach, besides the fact that can be run inside any up to date browser, will also allow, if there is needed, to extend the applications to be run on mobile devices.

Using JavaScript, we developed applications for representations of conics as intersection of a cone surface and a plane. The user interface is a simple one and allows the movement of the plane on the Ox and Oy axes or the rotation of it around the Ox axis. It is also possible to rotate the whole 3D model for viewing the intersection of the plane with the cones from different angles (Figs. 6 and 7).

Conic sections, as the circle, ellipsis, parabola, or hyperbola, can be viewed in real time by adjusting the cursors.

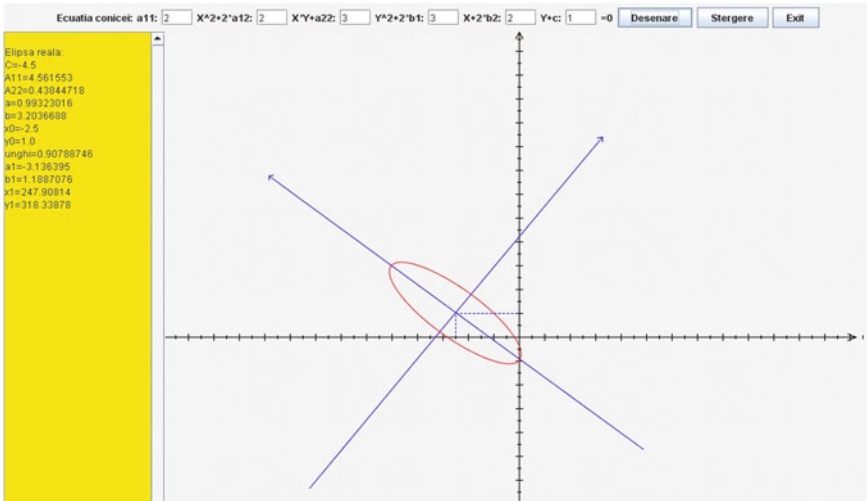


Fig. 5 Interface for the representation of conics in euclidian plane

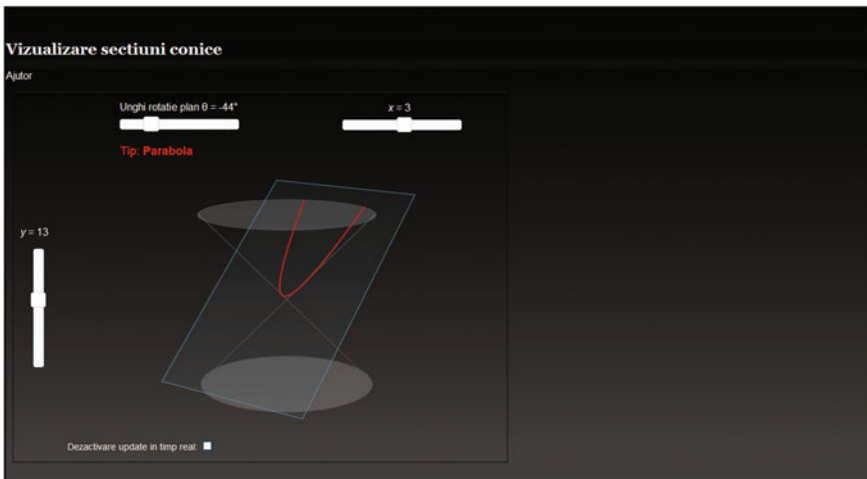


Fig. 6 Interface for visualizing a parabola

The source code for all the applications is based on standards like HTML5, CSS, the jQuery API [5] for the user interface, the Raphael library [6] for working with vector graphics, and the conics3D JavaScript extension written by Lodewijk Bogaards [7] for the visualization of the conic sections.

It is also possible to deactivate the real-time update of the image if the application runs on older browsers.

The applications also have a help section where the different options are explained to the user.

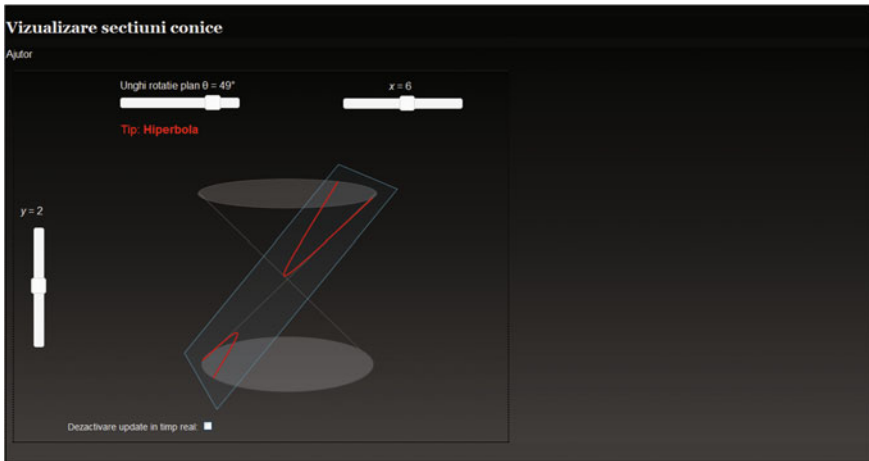


Fig. 7 Interface for visualizing a hyperbola

3 Conclusions

The IITPs designed with the help of software are an illustration of the ability to study, research, and develop, facilitating the learning of mathematical subjects.

The interactive applications conceived for the topics of IITPs facilitate the understanding of abstract notions, following the perception gained by the student from direct interaction with the three-dimensional geometric object. The programs created within our research provide the possibility to regard this object from different angles.

The use of autostereoscopic display provides a new approach, both from the technical point of view and teaching methods.

Acknowledgments The presented results were financially supported by the Hungary-Romania Cross-Border Co-operation Program 2007–2013, under the grant no. HURO/1001/040/2.3.1., entitled: Development of Open-Source Software and Interactive Teaching Tools for Mathematics —SOFTMAT (<http://softmat.uvvg.ro>).

References

1. Fraunhofer Institute of Research webpage (<http://www.fraunhofer.de/archiv/pi-en-2004-2008/EN/press/pi/2007/11/ResearchNews112007Topic3.html>)
2. Provision Company (<http://www.provision.tv/>)
3. Ammeraal L, Zhang K (2007) Computer graphics for java programmers, Wiley, Hoboken

4. Osmani A (2014) Learning JavaScript design patterns, available online at <http://addyosmani.com/resources/essentialjsdesignpatterns/book/>
5. jQuery API Documentation <http://api.jquery.com/>
6. The Raphaël JavaScript library home page <http://raphaeljs.com/>
7. Bogaards L, Conic Sections app, <http://www.mrhobo.nl/>

Determining the Similarity of Two Web Applications Using the Edit Distance

Doru Anastasiu Popescu and Dragoş Nicolae

Abstract This paper presents a method for measuring the similarity of two web applications using the algorithm for determining the Levenshtein distance. The web pages used in the measurement of similarity have the source code made of tags. After presenting the algorithm for determining the similarity of two web applications, we present the results obtained with its implementation in Java using various websites. The final part of the paper presents the definition of fuzzy sets, using the degree of similarity of a web page with a web application as a membership function.

Keywords HTML · XML · Tags · Similarity · Measurement

1 Introduction

The problem of determining the similarity between different concepts is current. At the moment, there are many papers each using different formulas, algorithms, and mathematical concepts depending on the particular domain. The notion of similarity appeared lately, related to documents written using different languages: HTML, XML, Latex, or images. To measure the similarity there are used various mathematical formulas that rely on processing algorithms, particularly using strings. In [1–3], there are shown ways to measure the similarity for HTML files, in [4, 5] for XML documents, in [6] for mathematical documents, and in [7] for files that contain images.

In this paper, we present a new way of defining the similarity of web pages in HTML format, using the edit distance (also called Levenshtein distance) together

D.A. Popescu (✉)

Faculty of Mathematics and Computer Sciences, University of Pitesti, Pitesti, Romania
e-mail: dopopan@yahoo.com

D. Nicolae

Faculty of Automatic Control and Computer Science, Politehnica University of Bucharest, Bucharest, Romania
e-mail: dragosnicolae23@gmail.com

with the algorithm that calculates the degree of similarity. For this algorithm, the results obtained for various sites and set of tags used to define this notion are presented. In the last part, there are explained some results using fuzzy sets.

2 Edit Distance

The edit distance, also called Levenshtein distance, refers to the two strings s_1 of m characters and s_2 of n characters and the way by which one can turn into the other using three possible operations

- i. deletion of a single character
- ii. insertion of a single character
- iii. substitution of a single character with a different one

The minimum number of operations i–iii to convert the string s_1 to s_2 is called the edit distance of s_1 and s_2 . The determination of this distance can be achieved by an algorithm of complexity $O(m \cdot n)$ that uses dynamic programming, [8]. Let $d(i, j)$ be the edit distance of the string consisting of the first i characters from s_1 and the string formed with the first j characters of s_2 . The edit distance of s_1 and s_2 will be $d(m, n)$ and it is determined using the following recurrence formulas:

- $d(i, 0) = i, i = 0, m$
- $d(0, j) = j, j = 1, n$
- $d(i, j) = \begin{cases} d(i-1, j-1), & \text{if } s_1(i) = s_2(j) \\ \min \begin{cases} d(i-1, j) + 1 \\ d(i, j-1) + 1 \\ d(i-1, j-1) + 1 \end{cases} & \text{if } s_1(i) \neq s_2(j), i = 1, m, j = 1, n \end{cases}$

The algorithm is as follows:

```

for i=0,m do
    d(i,0)=i
endfor
for j=1,n do
    d(0,j)=j
endfor
for i=1,m do
    for j=1,n do
        if s1(i)==s2(j) then
            d(i,j)=d(i-1,j-1)
        else
            d(i,j)=min(d(i-1,j), d(i,j-1), d(i-1,j-1))+1
        endif
    endfor
endfor

```

3 Defining the Degree of Similarity of Two Web Applications

Below, we present a definition of similarity of a web page with another web page using Levenshtein distance; afterwards we define the degree of similarity between a web page and a web application and then the degree of similarity between two web applications. In calculating the degree of similarity, there are used only web pages that are generated by HTML files. We mention that the results in this section remain valid for other types of files using tags in the source code.

We consider two web applications, WA1 and WA2, that contain the web pages p_1, p_2, \dots, p_m , respectively, q_1, q_2, \dots, q_n and a set of HTML tags denoted with TG. The code source of the web pages consists of HTML tags.

For a web page p_i , consisting of HTML tags, from WA1 we note with $T1_i$ the sequence of tags of p_i , which are not found in the set TG. The same for the WA2's q_j page: we denote with $T2_j$ the sequence of tags of q_j , which are not found in the set TG.

Definition 1 For two sequences of tags $T1_i$ and $T2_j$, we define the degree of similarity as the Levenshtein distance between the strings of tags $T1_i$ and $T2_j$, denoted by $DL(T1_i, T2_j)$.

Example For $T1_i = \langle BR \rangle \langle B \rangle \langle I \rangle$ and $T2_j = \langle BR \rangle \langle U \rangle$, we have $DL(T1_i, T2_j) = 2$. From the first string, we delete the tag $\langle I \rangle$ and substitute $\langle B \rangle$ with $\langle U \rangle$, thereby we made two operations.

Definition 2 For two web pages p_i of WA1 and q_j of WA2, we define the degree of similarity between p_i and q_j as being the number denoted by $d(p_i, q_j)$ and given by the relation

$d(p_i, q_j) = 1 - DL(T1_i, T2_j) / \max(\text{len1}, \text{len2})$ where len1 and len2 represent the number of tags from $T1_i$, respectively, from $T2_j$.

Definition 3 Let p_i be a web page from WA2. We define the degree of similarity between p_i and the web application WA2 as being the number denoted by $d(p_i, WA2)$, calculated as follows:

$$d(p_i, WA2) = \max\{d(p_i, q_j), j = 1, n\}$$

Definition 4 The degree of similarity between the web applications WA1 and WA2 is denoted by $d(WA1, WA2)$ and we define it using the relation

$$d(WA1, WA2) = \sum_{i=1}^m d(p_i, WA2) / m$$

The algorithm's steps to determine the number $d(WA1, WA2)$ is described below.

Input data

- the paths of the web applications
- the path of the TG file
- a sub unitary value, eps , used to group the web pages in pairs where $d(p_i, q_j) < \text{eps}$

Output data

- the similarity degree for pair of web pages (p_i, q_j)
- the similarity degree for every page p_i from WA1 with WA2
- the similarity degree of WA1 and WA2
- pairs of pages (p_i, q_j) with the property that $d(p_i, q_j) < \text{eps}$

Steps

- recursively determine the HTML files of each web application
- determine the sequence of tags for each page by eliminating the argument tags and the tags that are in the TG set
- calculate $DL(T1_i, T2_j)$ using the Levenshtein distance, determine $d(p_i, q_j)$, and find the pairs (p_i, q_j) with $d(p_i, q_j) < \text{eps}$, $i = 1, m$ and $j = 1, n$
- calculate $d(p_i, \text{WA2})$, $i = 1, m$
- calculate $d(\text{WA1}, \text{WA2})$

Example Let us consider two web applications WA1 and WA2 consisting of three, respectively, two web pages.

p1.html

```
<HTML>
<HEAD></HEAD>
<BODY><U>Conference</U></BODY>
<B> Day 1 </B><BR>
<I> Day 2 </I><BR>
</HTML>
```

p2.html

```
<HTML>
<HEAD></HEAD>
<BODY>
<B> Day 1 </B><BR>
<I> Day 2 </I><BR>
</BODY>
</HTML>
```

p3.html

```
<HTML>
<HEAD></HEAD>
<BODY>
<BODY><U>Conference</U></BODY>
<B> Day 1 </B><BR>
</BODY>
</HTML>
```

```

q1.html
<HTML>
<HEAD></HEAD>
<BODY><I>Conference</I></BODY>
<BR><<BR>
<U> Day 1 </U><BR>
<I> Day 2 </I><BR>
</HTML>
q2.html
<HTML>
<HEAD></HEAD>
<BODY>
<BODY><U><B>Conference</B></U></BODY>
<B> Day 1 </B><BR>
</BODY>
</HTML>

```

Let TG be, {<HTML>,</HTML>,<HEAD>,</HEAD>,<BODY>,</BODY>}

We obtain

$$\begin{aligned}
 T11 &= \langle U \rangle \langle /U \rangle \langle B \rangle \langle /B \rangle \langle BR \rangle \langle I \rangle \langle /I \rangle \langle BR \rangle \\
 T12 &= \langle B \rangle \langle /B \rangle \langle BR \rangle \langle I \rangle \langle /I \rangle \langle BR \rangle \\
 T13 &= \langle U \rangle \langle /U \rangle \langle B \rangle \langle /B \rangle \langle BR \rangle \\
 T21 &= \langle I \rangle \langle /I \rangle \langle BR \rangle \langle BR \rangle \langle U \rangle \langle /U \rangle \langle BR \rangle \langle I \rangle \langle /I \rangle \langle BR \rangle \\
 T22 &= \langle U \rangle \langle B \rangle \langle /B \rangle \langle /U \rangle \langle B \rangle \langle /B \rangle \langle BR \rangle \\
 DL(T11, T21) &= 6; \quad DL(T11, T22) = 4; \quad DL(T12, T21) = 6; \quad DL(T12, T22) = 4; \\
 DL(T13, T21) &= 7; \quad DL(T13, T22) = 2; \\
 d(p1, q1) &= 0.4; \quad d(p1, q2) = 0.5; \quad d(p2, q1) = 0.4; \quad d(p2, q2) = 0.4286; \quad d(p3, q1) = 0.3; \\
 d(p3, q2) &= 0.7143; \\
 d(p1, WA2) &= 0.5; \quad d(p2, WA2) = 0.4286; \quad d(p1, WA2) = 0.7143; \\
 d(WA1, WA2) &= 0.5476.
 \end{aligned}$$

4 Implementation and Results

Using the algorithm from Sect. 2, we realized an implementation in Java. The program generates a window like the one in Fig. 1, which allows us to introduce the data described above as input data.

For testing the program, there were used various web applications. For the websites of SOFA conferences from previous editions, we have obtained the results in Table 1.

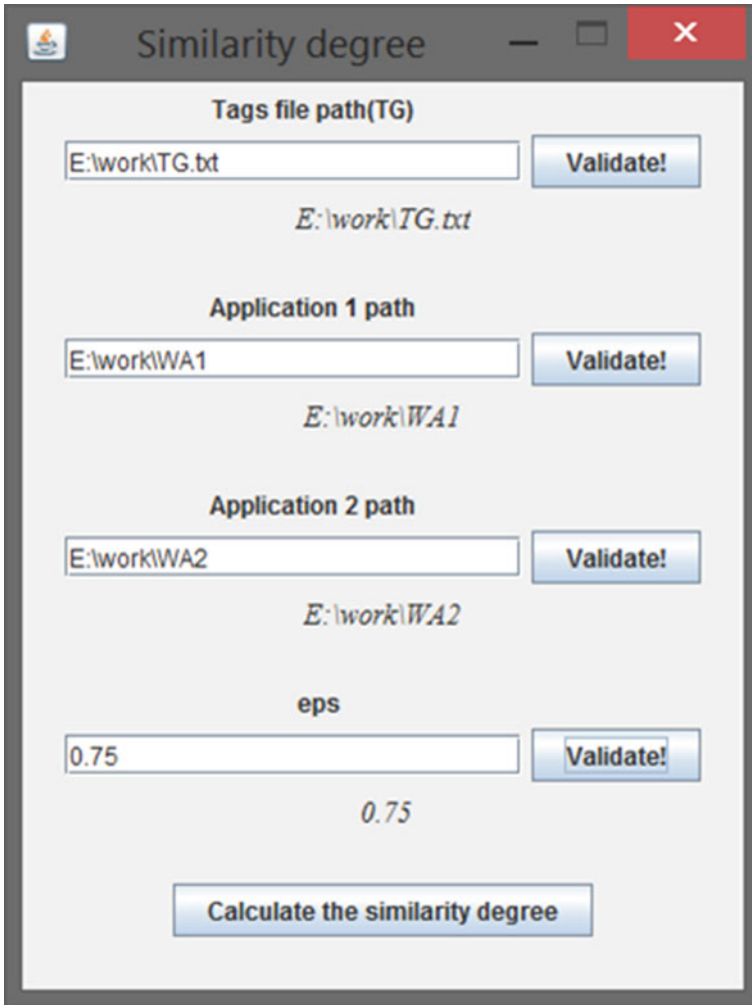


Fig. 1 Similarity degree program

Table 1 Results obtained with the Levenshhein distance

	2005	2007	2009	2010	2012
2005	1	0.641023	0.639442	0.625897	0.623278
2007	0.598694	1	0.851363	0.817743	0.815373
2009	0.622923	0.894149	1	0.897198	0.883024
2010	0.656366	0.903183	0.924772	1	0.92688
2012	0.619693	0.857521	0.879404	0.894534	1

Table 2 Results obtained with the maximum length of a common subsequence

	2005	2007	2009	2010	2012
2005	1	0.790159	0.814117	0.796022	0.824284
2007	0.777402	1	0.935187	0.925461	0.938187
2009	0.797082	0.928973	1	0.947101	0.953915
2010	0.840778	0.970579	0.982854	1	0.99105
2012	0.791578	0.914627	0.929161	0.935078	1

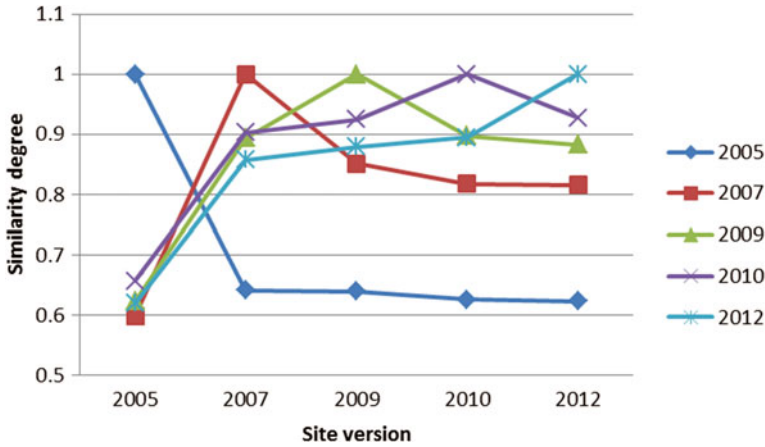


Fig. 2 Results obtained with the Levenshtein distance

In [2], it is presented another way of defining the degree of similarity between two web applications based on the maximum length of a common subsequence of tags. An implementation using Java, for the same input, leads to the results in Table 2.

The graphs that show the comparison between the two ways of calculating the degree of similarity is shown in Figs. 2 and 3. The first graph, from Fig. 2, contains the results of the method presented in this paper, while the second one (Fig. 3) illustrates the results of the method described in [2].

5 Defining the Fuzzy Sets Using the Web Pages of a Web Application and the Degree of Membership

The notion of similarity degree is very suitable to measure as to what extent a web page is similar to the web pages of a web application. For this, we use fuzzy sets.

Further, we denote by X the set the web pages created using tags, $WA1$ and $WA2$ two web applications as in the previous sections, but considered as sets of the web pages created only using tags, thus $WA1$ and $WA2$ are subsets of X .

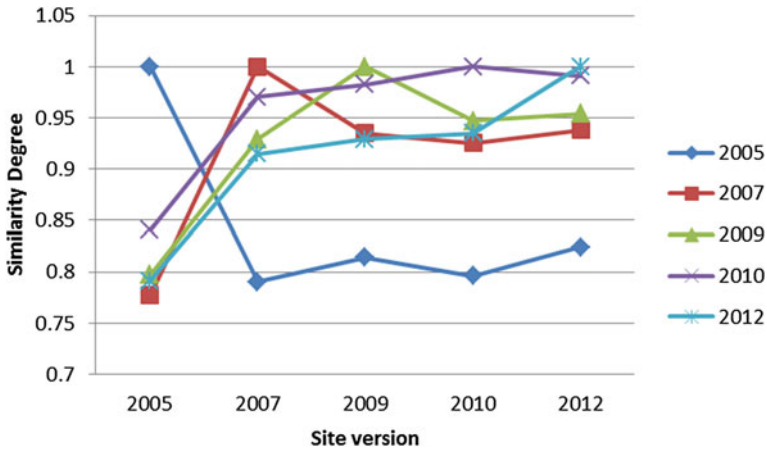


Fig. 3 Results obtained with the maximum length of a common subsequence

The membership function is defined as follows:

$f_{WA2}: X \rightarrow [0, 1], f_{WA2}(p) = d(p, WA2)$, where p is from X

The fuzzy set associated to WA1 is $M1 = \{(p_i, f_{WA2}(p_i)), i = 1, m\}$.

We can achieve a classification of the web pages according to the degree of similarity as follows:

1. For any $i = 1, m, p_i$ is *similar* to the web pages from WA2, if the degree of similarity is greater than or equal to 0.75;
2. For any $i = 1, m, p_i$ is *nearly similar* to the web pages from WA2, if the degree of similarity is greater than or equal to 0.5 and less than 0.75;
3. For any $i = 1, m, p_i$ is *slightly similar* to the web pages from WA2, if the degree of similarity is greater than or equal to 0.25 and less than 0.5;
4. For any $i = 1, m, p_i$ is *not similar* to the web pages from WA2, if the degree of similarity is less than 0.25.

6 The Similarity Using the Discrete Cosine Transform

Another method to check the similarity of two web applications is to use notions of converting tag sequences in frequencies. Below, we present a way of representing the tag sequences from $T1_i$, respectively, $T2_j$ from Sect. 2, for the web pages p_i in WA1 and q_j in WA2, $i = 1, 2, \dots, m, j = 1, 2, \dots, n$, based on the discrete cosine transform (DCT).

Having a sequence of tags T consisting of the characters t_0, t_1, \dots, t_{r-1} , we divide it into sequences of eight characters and determine their conversions, using [9], with the following formulas for the DCT coefficients:

$$g_i = \frac{1}{2} c_i \sum_{k=0}^7 x_i \cos\left(\frac{(2k + 1)i\pi}{16}\right)$$

where

$$c_i = \begin{cases} \frac{1}{\sqrt{2}}, & i = 0 \\ 1, & i > 0 \end{cases}, \text{ where } i = 0, 1, \dots, 7$$

and x_i , from the set $\{0, 1, \dots, 255\}$, is the ASCII code of the character t_i .

The reverse operation of getting the numbers x_i , [9] (and thus the characters t_i) is defined by the formulas

$$x_k = \frac{1}{2} \sum_{i=0}^7 c_i g_i \cos\left(\frac{(2k + 1)i\pi}{16}\right), \text{ where } k = 0, 1, \dots, 7$$

After obtaining the coefficients with the indices $0, 1, \dots, 7$, for each group of eight characters from T , we reconstitute the indices with values $0, 1, \dots, r - 1$, obtaining the DCT coefficients: g_0, g_1, \dots, g_{r-1} .

The method for measuring the similarity of images represented by the discrete cosine transform [10] can be used in the case of web pages using

- Manhattan Distance
- Euclidean Distance
- Cosine Similarity

7 Conclusions

Nowadays, an important issue is related to the comparison of two objects, applications, files, etc. depending on the elements used in their construction. In this class of problems is also situated the similarity of web pages and documents which use tags in the description. The method to measure the similarity can be achieved using algorithms that compare different source code for files that generate the web pages, documents, or images. This paper presents such an algorithm in addition to the existing ones [1, 4, 6, 7]. Besides the testing done on the web applications presented in the paper, we wish to conduct a study on a sample of more complex applications in order to highlight the Java implementation of the algorithm presented in Sect. 2.

In the following period, we wish to take over some concepts used in the images and signals processing to obtain new ways of measuring the similarity of web applications and to compare them with the existing ones.

References

1. Popescu DA, Danauta CM (2011) Similarity measurement of web sites using sinkweb pages, TSP2011. IEEE, pp 24–26
2. Popescu DA, Nicolae D (2012) Similarity measurement of web site. In: SOFA 2012, 5th international workshop soft computing applications. Proceedings LNCS, Springer, pp 349–356
3. Lerman K, Getoor L, Minton S, Knoblock C (2004) Using the structure of web sites for automatic segmentation of tables. In: SIGMOD 2004 June 13–18, Paris, France, ACM (2004)
4. Korn F, Saha B, Srivastava D, Ying S (2013) On repairing structural problems in semistructured data. *Proc VLDB Endow* 6(9):601–612
5. Pawlik M, Augsten N (2012) RTED: a robust algorithm for the tree edit distance. In: The 38th international conference on very large data bases, August 27th–31st 2012, Istanbul, Turkey. Proceedings of the VLDB Endowment, vol 5, no 4
6. Wolska M, Grigore M, Kohlhase M (2011) Using discourse context to interpret object-denoting mathematical expressions. *Towards a Digital Mathematics Library*. Bertinoro, Italy, July 20–21st, 2011. Masaryk University Press, Brno, Czech Republic, pp 85–101 (2011)
7. Benjamin O, Sigrid E, Ian S (2013) Determining image similarity from pattern matching of abstract syntax trees of tree picture grammars. PRASA Johannesburg, pp 83–90
8. Jain AK, Dubes RC (1988) *Algorithms for clustering data*. Prentice Hall, New Jersey
9. Vladimir B (2001) Discrete cosine and sine transforms. In: Rao KR et al (ed) *The transform and data compression handbook*. Boca Raton, CRC Press LLC
10. Remani NVJM, Rachakonda SR, Kurra RSR (2011) Similarity of inference face matching on angle oriented face recognition. *J Inf Eng Appl* 1(1) (2011)

Generative Learning Object Assessment Items for a Set of Computer Science Disciplines

Ciprian-Bogdan Chirila

Abstract Learning objects with static content are good for learning and practice, but not much recommended for assessment. The main problem is with content repetition which enables mechanical answer memorization by the student and replication of answers from class neighbors which is considered as an examination fraud. The generative learning object (GLO) is an evolved concept of learning objects (LO) based on reusing the learning patterns. Enhancing GLOs with dynamic content could increase their reusability even more.

Keywords Blended learning · Generative learning objects · Generative techniques

1 Introduction

Generative learning objects [5] are learning objects with dynamic content, where the learning pattern can be easily reused [4]. Learning objects usually contain content items, practice items, and assessment items. In this paper, we will present the main principles in the implementation of experimental GLO assessment modules created for different computer science disciplines like: (i) data structures and algorithms (DSA); (ii) fundamentals of programming languages (FPL); (iii) compiling techniques (CT); (iv) operating systems (OS).

The first discipline contains two modules DSA1 and DSA2, where the following are handled: (i) search algorithms, sorting algorithms, linked lists, and hash tables in the former; (ii) trees and graphs in the latter, using random data sets. The second discipline contains one module FPL that deals with basic functional programming concepts, namely list exercises based on generative trees. The third discipline contains one module named CT, which basically deals with the generation of grammars with lexical rules and syntactical rules. The fourth discipline has one OS

C.-B. Chirila (✉)
University Politehnica Timișoara, Timișoara, Romania
e-mail: chirila@cs.upt.ro

named module, which facilitates the learning of Unix commands. All the GLO items presented can be used for both practice and assessment purposes.

The motivations behind our approach are multiple: (i) students tend to use more gadgets like smartphones, tablets, tablet PCs, and laptops thus becoming “digital students” [3]; (ii) the IT industry nowadays is more expending so that computer science disciplines are more important in this context; (iii) the number of students delivered by universities for the IT industry is quite low, especially in eastern-European countries, loosing contracts, thus affecting the national economy.

The objective of this paper is to present an experimental set of assessment items with dynamic content based on several generative models, and to try to extend it to a higher level of generalization for the learning of computer programming.

This paper is structured as follows: Section 2 presents a set of assessment items for the Data Structures disciplines. In Sect. 3, we will show how basic commands can be assessed in the context of Unix [13] operating system. In Sect. 4, we will analyze several types of generative learning items applied on the Fundamentals of Programming Languages discipline. Section 5 presents a generative pattern for grammar generation. In Sect. 6, we will describe the prototype implementation. In Sect. 7, we will present related works. Section 8 concludes and sets the future work.

2 Assessment Items for Data Structures and Algorithms Discipline

In this section, we will present the DSA1 [10] and DSA2 [15] modules containing GLO items. For starters, we decided to address the data structure discipline because we consider that it has a decent level of complexity, higher than computer programming disciplines and also lower than compiler techniques or other more complex computer science disciplines.

We will consider the following general data structures and their accompanying algorithms: (i) searching algorithms on arrays; (ii) sorting algorithms on arrays; (iii) linked lists; (iv) general and binary trees; (v) graphs, representations, and related algorithms.

Firstly, we will present the DSA1 module where the student must write the steps of the some proposed algorithms. For each step, the student has to detail: index values, comparisons with their result, array value exchanges, and matches.

The first exercise proposes a search in a generated integer array of the middle element. The search algorithm is randomly selected from a list of three algorithms: (i) linear search; (ii) binary search; (iii) interpolation search. For the first search, the array can be unsorted but for the second and the third searches they cannot. The variability in this item consists of: (i) the size of the array; (ii) the sorting order of the array with the constraint that for linear search is unsorted while for binary and interpolation is sorted; (iii) the position of the searched element.

For this parameter, several interesting particular cases from the learning point of view can be considered: (i) the middle position when the array size is odd; (ii) the two middle positions when the array size is even and when there is not only one middle position; (iii) the first position; (iv) the last position; (v) the second position; (vi) the penultimate position.

The second exercise is about writing the steps of sorting by insertion algorithm. The variability of this item consists of: (i) the size of the array; (ii) the order of the array elements (ordered, random, and reversely ordered); (iii) the direction of sorting (ascending or descending); (iv) the use of linear insertion or binary search insertion as subcomponent of the algorithm.

The third exercise deals with sorting by selection and shares the same variability as the second exercise except for the (iv) which is replaced by using simple implementation or performance implementation. The two choices are just two algorithm variants which are presented in the face-to-face lecture by the discipline tutor.

The fourth exercise is about bubble sort and shaker sort which are related sorting algorithms and where we keep the same variability as in the last sorting algorithm.

The fifth exercise is about merge sorting algorithms applied on files. The variability is completed with different variants: (i) 3 files merge; (ii) 4 files merge; (iii) natural merge; (iv) the size of the array (8–12); (v) the integer range of each element (from 0 to 1000).

The sixth exercise is direct substring search. The variability items are: (i) the alphabet used for the characters (small or big caps, from A to Z); (ii) the size of the string (usually 10–16 characters); (iii) the size of the model (5–8 characters).

The seventh exercise is substring search based on several algorithms: (i) Knuth-Morris; (ii) Knuth-Morris-Pratt; (iii) Boyer-Moore. This exercise is based on random generation of a string and the identification of a substring model inside it. The variability items in this case are the following: (i) the alphabet used for the characters (small or big caps, from A to Z); (ii) the size of the string (usually 10–16 characters); (iii) the size of the model (5–8 characters); (iv) the position of the searched model; (v) with or without overflow on the searched string.

Secondly, we will present the DSA2 module dealing with trees and graphs, where we started another set of generic exercises.

The first one deals with the general tree representation based on parent index array. A parent index array is generated randomly and the student has to draw the equivalent diagrammatic tree representation and to write the first-descendant and right-sibling arrays. The generation of the array is based on taking one parent index and to replicate it in the parent array starting at an index higher than the parent index. Thus, no circular references are created between the tree nodes. Of course, the first node will have no parent since it is the root node. The variable parameters are: (i) the size of the array “ n ”, which we limited to a maximum of 18 nodes; (ii) the name of the nodes, which are continuous letters from A to Z; (iii) the index values in the parent array; (iv) the maximum number of consecutive equal parents in the array, which will reflect the tree degree, limited to a maximum of $n/3$.

The second generic exercise is about inserting keys in a binary tree. We need to generate a set of random integer keys, which will allow the creation of a balanced binary tree. In order to achieve this goal, one simple solution is to define three integer partitions from where equal number of keys will be selected. The variable parameters are: (i) the number of keys in the tree, which we limit to a maximum of 12; (ii) the extent of the partitions, where we set the value of 30. Thus, the keys will be provided from 0 to 29, 30 to 59, and from 60 to 89; (iii) the three extraction probabilities from the partitions, which we consider to be equal to 1/3 with the constraint so that the first key should be from the second partition. As an improvement to this exercise, we could consider that the keys could be selected from a word file repository where all words are sorted alphabetically.

The third generic exercise deals with drawing a graphical diagram based on a randomly generated adjacency matrix. The variable parameters are: (i) the size of the adjacency matrix having six rows and six columns; (ii) the elements which can be 0 or 1, except the main diagonal which is all 0; (iii) the grade of the graph; (iv) the name of the nodes which are random alphabets, big capital letters. After the graph diagram is drawn, then the grade of the graph is asked. Two answers can be easily verified in an automatic manner when the assessment is performed on a computer. The graphical diagram can be created using a diagram editor, and the node names help us to check the correct links between the nodes. The graph grade is calculable out of the generated adjacency matrix.

The fourth generic exercise deals with node graph searches: (i) depth-first search and (ii) breadth-first search. The matrix generation algorithm is the same. The variable parameter is the starting node for both searches.

The fifth generic exercise is about determining the minimum coverage of tree in a weighted graph. The graph generation algorithm is the same as the previous one, except the values which are not only 0 or 1 but from 0 to 100. In order to have a balanced number distribution, the values are generated with the formula

```
rand()\%2? 0 : rand()\%100.
```

3 Assessment Items for Operating Systems Discipline

The proposed exercises will test the writing of some Unix [13] commands: (i) to create three directories with different random names; (ii) to enter one of the three directories; (iii) to create and edit a few files by writing some lines in them; (iv) to copy a randomly selected file in some random target directory; (v) to move some files with a random extension specification into a random target directory; (vi) to assess the size of a file with a random name; (vii) to change the access rights of an existing random file with a random set of given rights; (viii) to delete recursively a given folder. These assessment items can be automatically evaluated by a simple parsing for white space eliminations. The presented assessment items can also be

reused in the context of system calls where the student must write programs to fulfill the generated tasks. The answer program checking involves a more complex parsing and pattern recognition.

4 Assessment Items for Fundamentals of Programming Languages Discipline

For the Fundamentals of Programming Languages discipline, we created four assessment items dedicated to its Lisp [11, 16] laboratory. The first exercise item generates a multilevel list based on random dictionary words where the student has to apply the CAR and CDR primitives in order to extract the first occurrence of a certain letter from that word. The variable parameters in this assessment item are: (i) the word selected randomly from a dictionary, which has a certain length; (ii) the extracted letter which will be selected randomly from the second half of the word. This exercise is more complex since we have to generate a tree where the inner nodes are nonimportant, marked by stars * and the leaf nodes must contain, in order, the word letters. Such a generated result is presented in Fig. 1.

A different assessment item was designed in order to stimulate student creativity. The exercise generates randomly a multilevel list and the student has to write a Lisp expression creating that list and using three primitives (i) append; (ii) list; (iii) reverse. The word proposed for the exercise is (A B) expressed as a list. The variant parameters are: (i) the word used in the exercise; (ii) the number of nodes in the tree—equivalent with the multilevel list; (iii) the degree of the tree; (iv) the height of the tree. In Fig. 2, we present an example of the generated multilevel list based on the word (A B). Unless the word is not a palindrome the response expression is unique for each tree and thus can be assessed automatically.

In Fig. 3, we can see a generated simple expression based on a binary tree containing arithmetic operators and one letter identifier operands, implemented by an array with left child at $2 * i$ and right child at $2 * i + 1$ if the parent is at index i . These expressions must be implemented as Lisp functions by students. The variable parameters are: (i) the number of operators that we set between four and six; (ii) the name of the identifier operands.

```
(( (P) (O)) ( ( ( ( (L I) (T)) (E)) (H)) (N)) ((I C) (A))))
```

Fig. 1 Generated multilevel list

```
((B A (A B) (A B A B) (A B) (A B A B)) ((A B) (B A B A)))
```

Fig. 2 Generated multilevel word list

$$F3 = ((n + g) - (p + r))$$

Fig. 3 Generated simple expressions

$$F4 = (((g * p) * (q - b)) * ((g - i) - x)) + ((e * x) - (j * e))$$

Fig. 4 Generated complex expressions

For the complex expression, we use the same generation idea but the number of operators will be between seven and 12. In Fig. 4, we can see a generated complex expression.

5 Assessment Items for Compiling Techniques Discipline

For the compiling techniques [2] discipline, we designed one complex exercise which has the goal of generating randomly a variable grammar made of a lexical analyzer and a syntactic analyzer having a limited difficulty level. We designed a generic program structure described by a grammar having a lexical analyzer which contains: (i) the identifier rule with different set of letters, digits, and name; (ii) keywords for starting and ending program blocks having fixed semantics, but variant synonym names; (iii) separators selectable randomly from a given set; (iv) operators selectable randomly from a given list; (v) delimiters selectable randomly from a given set; (vi) integer constants in different forms; (vii) real constants in different forms (Fig. 5).

In the syntactical analyzer rule set, we created: (i) left-recursive expressions with randomly selected operators and operands, the operands can randomly be identifiers or integer constants or real constants; (ii) instruction lists; (iii) different instructions like assignments, calls, etc.; (iv) starting grammar rule built with random keywords. An example of a generated set of syntactic rules is presented in Fig. 6.

Fig. 5 Generated lexical rules

```

letter ::= a..z | A..Z
dig ::= 0..7
operator ::= +
separator ::= ,
del1 ::= [
del2 ::= ]
identifier ::= (letter|dig)*
int_literal ::= dig+
nr_real ::= dig+.dig+
start_keyword ::= ON
stop_keyword ::= OFF

```

```

programs ::= programs start_keyword ListaInstr stop_keyword
           separator | start_keyword stop_keyword
InstrList ::= InstrList Instr | Instr
Instr ::= identifier := E | identifier dell E del2 := E
E ::= E operator int_literal | E operator identifier
     | int_literal | identifier

```

Fig. 6 Generated syntactic rules

The skeleton of our compiler is quite simple, but following these ideas we can build a larger compiler skeleton. Briefly, the variable parameters are: (i) the names for the lexical and syntactical rules; (ii) the right-hand side of the lexical rules with variations for each token class; (iii) the randomly included subtrees in the right-hand side of syntactical rules.

6 Prototype Implementation

The prototype is implemented in *C* and has two versions: (i) the first one generating HTML code so that the components behave as CGIs; (ii) the second one generating LaTeX code for transforming into PDF format, ready to print. The former result is good for online posting of free exercises, while the latter is good for written exams. Regarding the balance between the server and client side, we can mention that the current implementation based on CGIs runs on the server side. We consider that is not a difficult task to translate the code into JavaScript [12] or Flash ActionScript [1], which runs on the client side in order to enable a better graphical representation.

The action results can be memorized into the learning record store (LRS) using the Experience API (xAPI) [14].

7 Related Works

According to [6], a GLO is “an articulated and executable learning design that produces a class of learning objects.” Our approach adheres fully to these ideas.

In [4] are presented the design principles for creating dynamic and reusable LOs. The principles are based on a set of distilled ideas from pedagogy and software engineering. The case study is made on a Java learning discipline. With our approach we showed that GLOs can be used for several other computer science disciplines to a certain extent.

In [5] are presented design and development tools for the GLOs as second generation learning objects underpinning pedagogical patters. In our approach we reuse pedagogical patterns in a competence-oriented learning and assessment.

In [7] they consider that GLOs are generic and reusable LOs from which specific content can be generated on demand. GLOs are characterized by variability which can be modeled using feature diagrams and they also need specification languages, parameterization languages, metaprogramming techniques for generation. In our approach the parameters are expressed through program variables, their values are set by random values within a certain range, so LO instantiation is automatic.

In [8] GLO generated LO sequences by metaprogramming are expressed using sequence feature diagrams. In our approach the metamodel is not explicit but it is embedded into the prototype modules code.

8 Conclusions and Future Work

In this paper, we presented five modules containing generic learning assessment items dedicated to a set of disciplines that we consider belonging the core for computer programming. In our approach, we identified a number of problems that must be considered as challenges for future work.

The assessment items test only the good understanding of the data structure or algorithm functioning which are essential for programming, but not programming itself with that data structure. The generative assessment items seem to cover only a small part of the content that a student must know. The part which is not covered involves the application of the data structures and algorithms in industrial strength programs.

Regarding the operating system discipline, we consider the following challenges: (i) to generate script specifications to work with files and processes, and to combine safely the possible operations; (ii) to assess automatically the correctness of the written scripts. Using repeatedly the same generative assessment items, it may transform the evaluation into a tedious activity.

The items are quite complex in creation and implementation, because they require programming knowledge for the values generation so that the authors must have programming skills. Another challenge derived from this idea is to simplify the implementation of such GLO items by using specialized templates or generative wizards constructing the output step-by-step.

As future work, we consider integrating the designed GLOs into a Learning Management System like Moodle [9]. Thus, the GLOs will be available to a larger number of tutors and implicitly students.

For the motivational part, we can think of integration with social networks. Thus, the learning activity result can be posted online and get support and approval by the other members of the community. They may try themselves some interesting e-learning topics.

Another future work is related to gamification, namely to use gaming mechanics to transform some GLOs into games. DSA modules are more likely to be able to be gamified, since it involves lots of diagrams and interactions between nodes.

In order to support learning and training together with evaluation, some assessment items could be equipped with assistance and feedback in order to be reused as training items.

Acknowledgments This paper is supported by the sectorial operational program human resources development (SOP HRD), financed from the European Social Fund and by the Romanian Government under the project number POSDRU/159/1.5/S/134378 initiated in 2014.

References

1. Adobe Systems (1998) Flash ActionScript. <http://www.adobe.com>
2. Aho AV, Lam MS, Sethi R, Ullman JD (2006) Compilers, principles, techniques and tools, 2nd edn. Pearson Education
3. Andone D, Dron J, Pemberton L, Boyne C (2007) E-learning environments for digitally-minded students. *J Interact Learn Res* 18(1):41–53
4. Boyle T (2003) Design principles for authoring dynamic, reusable learning objects. *Aus J Educ Technol* 18(1):46–58
5. Boyle T (2006) The design and development of second generation learning objects. In: *Proceedings of world conference on educational multimedia, hypermedia & telecommunications*
6. Centre for Excellence for the design, development and use of learning objects (2014) Reusable learning objects cetl-rlo-cetl. <http://www.rlo-cetl.ac.uk/whatwedo/glos/glodevelopment.php>
7. Damaeviius R, Vytautastuikys (2008) On the technological aspects of generative learning object development. *Lecture Notes Comput Sci* 5090:337–348
8. Damaeviius R, Vytautastuikys (2009) Using sequence feature diagrams and metaprogramming techniques. In: *2009 Ninth IEEE international conference on advanced learning technologies*
9. Dougiamas M (2002) Modular object-oriented dynamic learning environment (Moodle). <http://www.moodle.org>
10. Knuth DE (1998) *Art of computer programming, vol 3: sorting and searching*, 2nd edn. Addison-Wesley Professional, 800 p. ISBN-10:0201896850, ISBN-13:978-0201896855
11. McCarthy J (1979) *History of lisp*. History of programming languages. Artificial Intelligence Laboratory Stanford University
12. Mozilla Foundation (2011) JavaScript. <https://www.mozilla.org>
13. Ritchie D, Thompson K (1974) The UNIX time-sharing system. *Commun ACM* 17(7): 365–375
14. Rustici Software (2014) Tin can api. <http://tincanapi.com/>
15. Sedgewick R, Flajolet P (2013) *An introduction to the analysis of algorithms*, 2nd edn. Addison-Wesley Professional, 592 p. ISBN-10:032190575X, ISBN-13:978-0321905758
16. Touretzky DS (2013) *Common LISP: a gentle introduction to symbolic computation* (dover books on engineering)

Performance Metrics for Persistent Routing

S.N. Orzen

Abstract The work presented in this paper is focused on the persistent routing feature of real-time data communications that form logical understanding of how the computer network's function is designed with performance measurement tools and their respective characteristics. The tools which have the most essential impact on network performances are represented in section two of this paper, as having a concise representation of their composing elements through simulation. While section two introduces the understanding of the elements that form the routing problem, its representation in performance modeling of organization structures is exemplified in section three as imposing a random network workload, and utilization generation, having a good degree of realism equivalent to real-world scenarios and cases, is concluded in section four.

Keywords Definition · Design · Metric · Performance · Persistent · Routing

1 Introduction

The performance of routing technology in computer networks and communication mediums are widely researched on various cases and contexts [1]. Techniques for communicating data correctly are designed in network protocols as a strategy that is adopted from an administration possibility point of view, but in certain levels of utilization and load magnitude the strategy poses a problem.

Methodical solutions that are presented throughout this paper are tightly linked with the communication problem representation as a phenomenon, being mostly corrections to a design negative facet that has existed in networks for two centuries, namely the distributed workload in end-to-end communication. The following

S.N. Orzen (✉)
“Politehnica” University of Timisoara, Timisoara, Romania
e-mail: niko.orzen@cs.upt.ro

paragraphs, present the problem description and the methods that solve it, with a good degree of usefulness.

Logically transmitting data from one end to another, in a given criteria of time, is solved in a correctly functioning environment, but in an overloaded system, delays appear in the communication process which can disturb the overall protocol performance and lead to an interrupted transmission [1].

The solution to the time criteria based transmission problem is to constrain routers to synchronize their internal clocks on a time-to-transmit level and agree to re-route data if overloaded links appear. Feasibility is a consideration which is met only in the case when an established path fails, and there are neighboring routers that can handle the transmission load, continuing the communication process. Most network routers have performance measurements attached to them, and there is no need to interrupt a process if a link fails, because neighboring routers have the mandatory protocol agreement tools available.

The overall functioning medium is currently suppressed to establish a path and carry only on that path the persistent route, as long as it is needed by the communication process.

Tools such as time to live for transmitted packets between links, synchronized internal clocks in UTC, checksums for packet integrity, hamming code for data reconstruction on failure, priority flags for types of services, data fragmentation units for transmission capacity and timely distributed information, fall into the category of queuing theory design and permit an instant failure tolerance that is described in the next sections.

In order to make the problem observable, the persistent routing mechanized process is presented in the following points:

- (a) Fragment data and attach to it a given time limit to be received;
- (b) Transmit data and verify its time stamp throughout the network (traceroute achieves a similar performance track);
- (c) Re-assemble data and present it to the recipient.

For a correct understanding of the problem in itself, I have to mention that its focus is on transmitting data in a specific time interval which is dynamically agreed upon, while the performance of the routing protocol is handled by its speed of computing the algorithm in the hardware–software medium.

In dynamic routing agreement, there is always the minimum level of resources available, but having online conversation and video chat as examples, there is the problem of disrupting data frames communication, even if some data packets arrive earlier at the system [2].

2 The Persistent Routing Problem Elements Analysis

Persistent routing is the path which is chosen for the communication between two communicating parties (Fig. 1). As data is fragmented into packets each being allowed to take alternate network segments along the transmission lines, its logical existence can be viewed as a performance constraint for the data packets to reach their destination [2].

Most technologies that need streaming and bi-directional flows of data are dependent of opened connections and their duration, a need that in the presence of overloads is a difficulty or sometimes even impossible.

Most conditions that hold streaming services for real-time communication are developed partially in technologies that must obey shortest paths rules and designed intermediate systems crossing policies. The most consistent technologies that capture fault-tolerance efforts and are able to maintain connections are enumerated as follows:

- (a) Label Switching: a method which is designed to contain multipaths for multiprotocols (three highest levels of the OSI model stack), taking the data packets into its own capability. The MPLS protocol is designed to minimize the dynamics of the internet and reduce the routing facet by making routers respond to its need in order to establish the path first [3]. MPLS paths aren't subjected to packet collisions and re-routing given router algorithm decisions, because once a path is chosen, it can only be replaced by backup paths that tolerate the appeared flaws;
- (b) IS-IS: a communication agreement for rules that have the sole purpose of making existent systems interconnected, having in mind that even though hardware and software components forming them might differ [4]. As a communication protocol it is focused on requirements that should be made

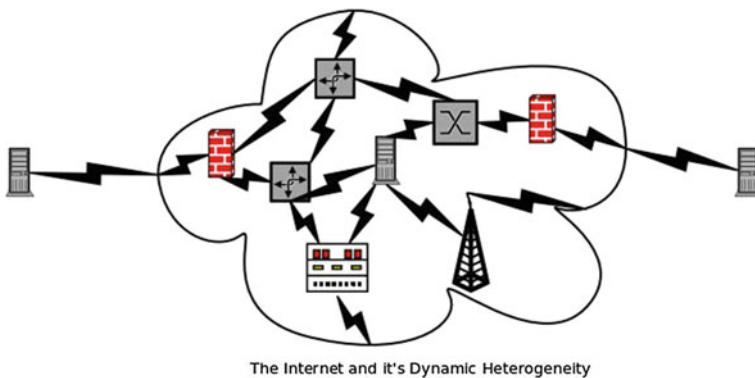


Fig. 1 End-to-end communication with transparent transportation

available for each system that should be traversed, on the first three layers of the OSI model;

- (c) BGP: a networking interconnection protocol, focused on systems that transport large volumes of data. Being a network border forwarding protocol, it has the control on choosing which paths to use for communication between defined networks [5].

These enumerations have presented the most essential technologies that sustain persistent routes and give their usefulness. As for real-time sessions its time-to-transmit feature is dependent on the performances which sustain accuracy and effectiveness.

The problem can be described from queuing theory as measuring arrival rates throughput for completed jobs.

The tool used to present the problem is the Java Modelling Tools that allows the observation of delay intervals and successful task completions. The elements that form a real-time communication session are seen in this work as having the following notions:

- (a) Arrival Rates: the measure of requests which are received by servers handling the real-time communication sessions;
- (b) Queue Time: the measure of waiting intervals at server's stations for solicited tasks;
- (c) Residence Time: the actual time that is necessary to process requests one by one;
- (d) Response Time: the measure of responsiveness on considering tasks and routing decisions;
- (e) Throughput: how many requests are successfully processed;
- (f) Utilization: the workload level of nodes, components and subsystems of the designed network;
- (g) Drop Rate: the amount of unsuccessful jobs that were registered in the network, but were not solved.

Persistence of connections is a routing feature that needs an actual view of how the performances between components comply with one another, in order to give a reliable route as a result.

Being based on measurement of delays, the computed persistent routes are based on system arrivals completions, having Little's Law as a focus for modeling performance [6].

The above illustration (Fig. 2) has the following elements forming its logical expression for routing:

- (a) $n(t)$: the number of request in the system at time t ;
- (b) T : a period of time;
- (c) $A(T)$: the area under the curve $n(t)$ over the time interval T ;
- (d) $N(T)$: the number of arrivals in the time period T .

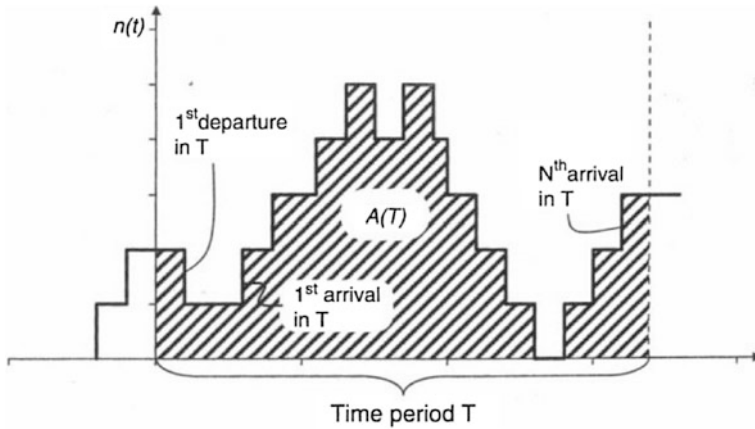


Fig. 2 Little’s law request representation in a queuing system [6]

As it is known, the performance laws of computing design the new generations of technologies, and the Amdahl parallelization and Gunther scalability laws make medium performances manageable.

Focusing on the distribution of the data packets transportation throughout the networking environment, it brings the following characteristics into attention, because the analysis of the system is viewable only when packets are doped and processes fail to execute.

Persistent routing model analysis of characteristics:

- (a) Drop Rate: the view of the conditions in which the system has failed, given the fact that overload represents the cause and bottlenecks can be identified;
- (b) Residence Time: the view of wait time for requests needing to be processed, having the purpose to allow the view of the distribution’s behavior and its variation given the element response time tuning.

Persistent routing device and algorithm analysis:

- (a) Device analysis: an analysis of the routing devices behavior, knowing that capabilities such as reconstruction of network data in case of failure are available and also that path choices are made given the graph decisions (the distributed graph vertex coloring being a method for helping to shape the workload available);
- (b) Algorithm analysis: an analysis of the actual routing in time fashioned distributions. Algorithms that implement persistent routing have the decision-making process as a central feature, whether they probabilistically compute the forward depth of the network, or learn from past experience looking backwards at initial performances obtained.

Finalizing this section, is the remark that data packets’ time to transmit successfully given the time criterion’s, has many elements with various functionalities

for given network designs. As a concise explanation of the problem is only available aside with its solution, section three describes the problem given the analysis characteristics for performances of elements degrading the stability of the communication processes.

3 Experimental Results

The experimental results presented throughout this section have the purpose of representing an insight through tests developed in the Java Modelling Tools system for the persistent routing aspect of real-time communication sessions.

Persistence of paths can be seen as a service residing on a server that has a scalable rate of signaling its traffic (Fig. 3). The previous illustration presents the basic reduction of the problem to its functioning elements, having the source to destination, as the elements forming an end-to-end communication process, while the problem is reduced to the queue time of the server which creates the traffic volume.

Being a simplistic model, the values present the available analysis tool, considering that the actual flow of data may vary given intermediate system performances.

The tuning of a system for performance is an availability of parameters facet. As described in the work of [6], Little’s Law can make a third parameter to be calculated, given that two parameters are measured from three as a whole(the number of items in a system, the average waiting time in the system for an item known as the data flow and the average arrival rates of items to the system).

An expanded model was chosen (Fig. 4) to capture the effect of performance metrics that help in adapting a distribution’s flow and the variable behavior it can

Fig. 3 Problem reduction to functioning elements

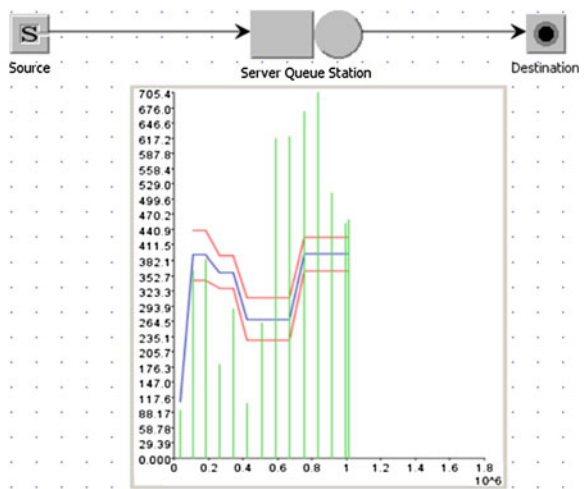
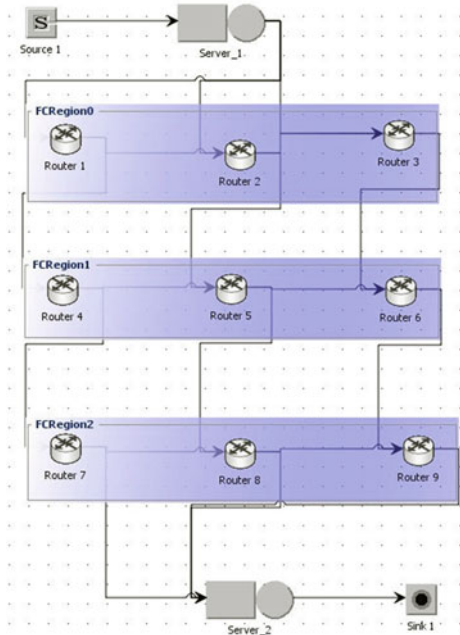


Fig. 4 Performance metrics with intermediate capacity networks



have. The model consists of two classes that generate jobs for the system and contain performance variability. In the following figures the focused class is the source of requests which necessitate accurate requirements while the second class is used to act on the system’s overall performance affecting a behavior which otherwise would be idealistic, not reflecting real-world situations and dynamics.

The utilization law that is illustrated next, designs flows for data traffic, being a result of calculating the product between throughput and service times.

The throughput and utilization laws are expressed in the following enumeration, as being variable parameters with measures fluctuation given workload volume and system stability, having also a comparable description in the work of [7].

- (a) Throughput: $X = N/R$, where X is the throughput notation, N represents the number of jobs and R stands for the response time;
- (b) Utilization: $U = X \cdot S$, where U is the utilization notation, X is the throughput and S represents the service time of the station.

A context worth noting in this section is that if routers carrying on their tasks would fail, the drop rate of the system could increase and allow the identification of an initial design flow from the elements presented in section two. Depicted in the following diagram is the captured drop rate of the expanded model, having an almost even measure during the simulation time.

Having the distribution generated randomly, the residence time and response time of server 1 and server 2, respectively, are presenting an availability feature that

is varying given the overall system workload composed of the two classes which generate requests.

The experiment presented through this section was focused on helping a design perspective to be viewable for persistent routing, making an assumption of how realistic scenarios of network distributions as described in the work of [8] perform with accurate functioning implemented equipment.

While the model is constructed from subsystems and intermediate nodes, the exemplified experiment has been concentrated on the routing behavior bringing insight of the process itself, not being fixed on proxy constraining methods which limit the routing functionality.

Modeling the performances of computer networks is a task carrying with itself more than a software–hardware correlated design. Being the most effective way of viewing the problem, the modeled metrics can be compared with CAIDA performance data, that logs network utilizations from around the world (Figs. 5, 6, and 7).

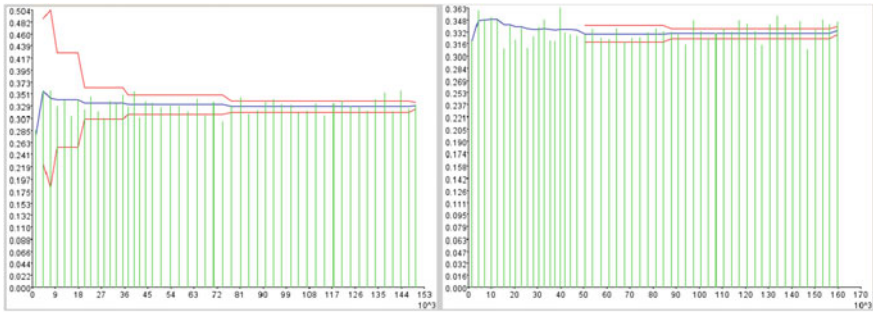
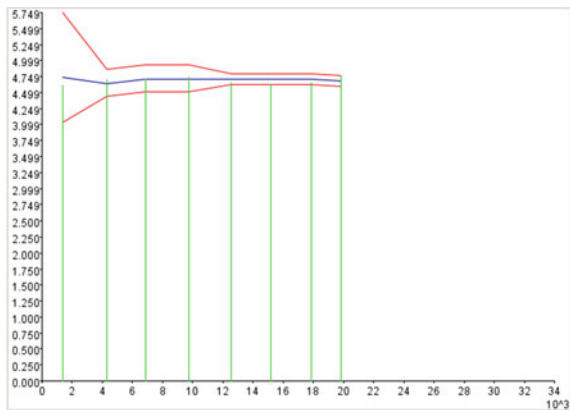


Fig. 5 Utilizations from servers 1 and 2 from the expanded model

Fig. 6 Drop rate fluctuation



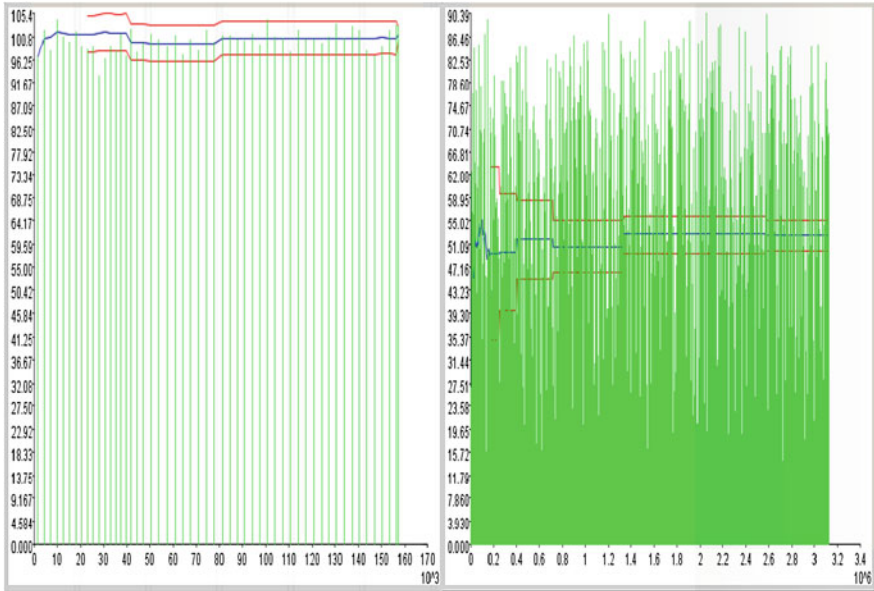


Fig. 7 Residence time (left graph) and response time (right graph)

The following graphs (Fig. 8), present the utilizations of existing network infrastructures, all having percentages at per protocol basis attached, and at four time scales, namely daily, weekly, monthly and yearly.

CAIDA has as a data analysis organization the focus of making accurate estimations on yearly, quarterly, monthly and daily basis for network information volumes. As the process of reliability is made to ensure proper analysis, performance modeling through the metrics presented has a framework-ed flow, which can be introduced to CAIDA datasets on future work.

All the metrics presented throughout sections two and three, have applicability in sustaining features such as dependability, fault-tolerance, and systems interconnection.

The session layer of the OSI model deals with helping the design of high requirement protocols and the future work for session communication has guidance from information such as the protocol utilization graphs presented below.

Long-term designs, as mentioned in the simulated experiment, can help shaping the internet functioning space and its capacity for transmitting information securely, as seen in the work of [9], a technical measurement of communication responsiveness and transmission delay.

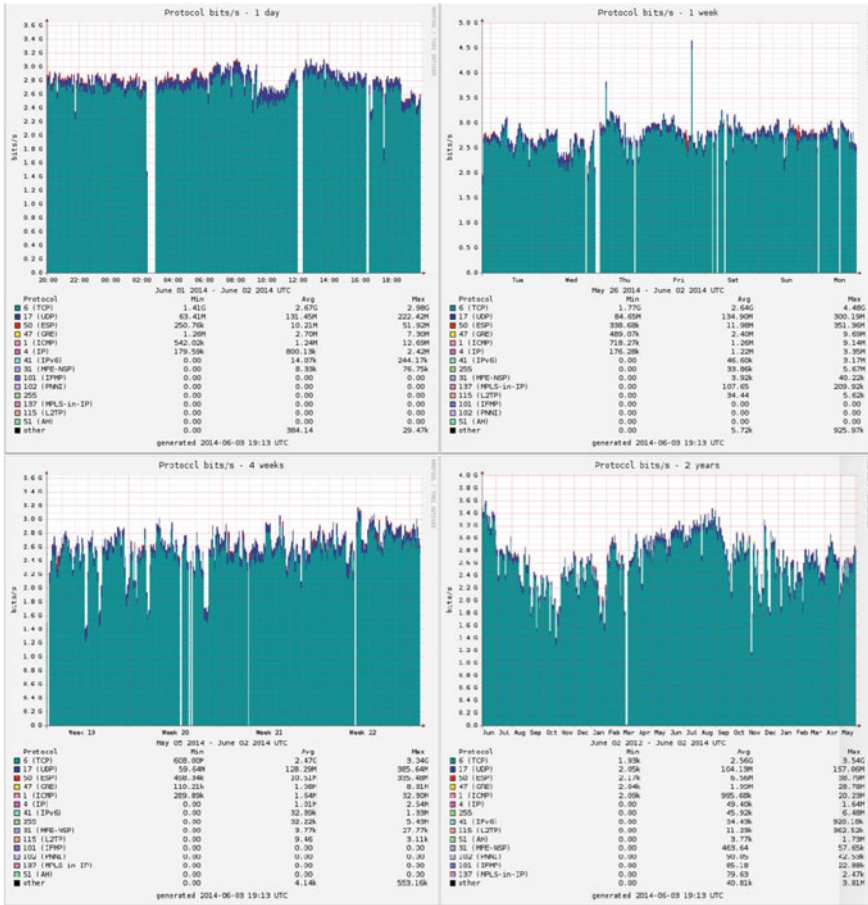


Fig. 8 CAIDA network utilizations

4 Conclusions

The work presented in this article has as central focus the engineering aspect requirements necessary to make persistent routes dependable.

Research on persistent routing is defined by quality of service and priority services, features that are mostly created through planning and speed of execution. As the delays offer the view of limits from data transmissions, the experiment created in this paper offers the queuing theory tools necessary to design reliable systems which can be scalable and functional, having high mean times between failures.

As a last mention, the affirmation that the aim toward achieving persistent real-time route administration is made possible through queuing theory, which makes the dynamic routing through Internet simplified and expressible.

References

1. Tanenbaum AS (2003) Computer networks, 4th edn. Prentice Hall
2. Alesso HP, Smith CF (2008) Connections: patterns of discovery. Wiley
3. Rodoplu V, Gohari AA (2008) Challenges: automated design of networking protocols. MobiCom'08, San Francisco, California, USA
4. Eastlake D, Banerjee A, Dutt D, Perlman R, Ghanwani A (2011) Transparent interconnection of lots of links (TRILL) use of IS-IS. Internet engineering task force (IETF), request for comments: 6326, category: standards track. ISSN:2070-1721
5. Vissicchio S, Cittadini L, Vanbever L, Bonaventure O (2012) iBGP deceptions: more sessions. Fewer Routes, INFOCOM
6. Chhajed D, Lowe TJ (2008) Building intuition: insights from basic operations management models and principles. In: Little JDC, Graves SC (eds) Little's law. Springer Science+Business Media, LLC
7. Serazzi G (2008) Performance evaluation modelling with JMT: learning by examples. In: Technical report, n 2008.09, Politecnico di Milano
8. Murphy KE, Carter CM, Brown SO (2002) The exponential distribution: the good, the bad and the ugly. A practical guide to its implementation, proceedings annual reliability and maintainability symposium, IEEE
9. <http://www.caida.org/projects/ark/statistics/>

Parity-based Concurrent Error-detection Architecture Applied to the IDEA NXT Crypto-algorithm

Andreea Bozesan, Flavius Opritoiu and Mircea Vladutiu

Abstract This paper presents a hardware architecture for online self-test in the context of the IDEA NXT crypto-algorithm. From the many techniques and solutions presented in the literature for increasing built-in self-test (BIST) capabilities, after a careful analysis of these approaches, we decided to focus our attention towards solutions based on parity-based error-detection. In this sense we designed and implemented a complete parity-based test architecture for IDEA NXT. The solution we propose doesn't interfere in any way with the algorithm's structure, as there is a complete separation between the functional and testing channels. The proposed solution is the first of this kind for the IDEA NXT crypto-algorithm. We evaluated the performance of the proposed test strategy with different redundancy levels and, formulated recommendations for the concurrent detection strategy based on the obtained experimental results.

Keywords Cryptography · IDEA NXT · Crypto-algorithm · LFSR · Concurrent-testing · Parity-based verification

1 Introduction

The Cryptographic domain is continuously trying to find ways for strengthening the means for obtaining the security of sensitive information. More and more attacks showing the weaknesses of existing algorithms were published in the past with most of the attacks on block cipher algorithms operated with just simple key

A. Bozesan (✉) · F. Opritoiu · M. Vladutiu
University "Politehnica" of Timisoara, Timisoara, Romania
e-mail: andreea.bozesan@cs.upt.ro

F. Opritoiu
e-mail: flavius.opritoiu@cs.upt.ro

M. Vladutiu
e-mail: mircea.vladutiu@cs.upt.ro

programmers and algebraic substitution boxes, so these crypto-algorithms' structure constituted merely an aid for algebraic attacks. The new trend in cryptographic algorithms is a family of symmetric encryption algorithms, flexible and scalable, called IDEA NXT, which was theoretically proven to combine the speed of IDEA and security of AES crypto-algorithms [1].

The IDEA NXT family is composed of two block ciphers (NXT64, NXT128) which essentially have the same algebraic structure but differ in block sizes, key lengths and number of rounds.

The NXT crypto-algorithms can be generalized by implementing a common version with variable parameters.

2 Mathematical Structure of IDEA NXT

The IDEA NXT algorithm, which takes an input block of 64 or 128 bits and a key of 128, 192 or 256 bits, depending on the chosen algorithm version, is based on a Lay-Massey scheme combined with two orthomorphisms. The round functions are of type substitution-permutation networks based on the Feistel scheme [1]. As stated in [1], "the orthomorphism represents a Feistel scheme on a single round which has the identity function as a round function. IDEA NXT consists of ' $n - 1$ ' iterations of a round function called *Imor64*, followed by applying a slightly modified function called *Imid64*, which is the same as *Imor64* just without the orthomorphism. The decryption process is similar to the encryption one, the only difference is that *Imio64* is used instead of *Imor64*". In this paper we focused our effort towards the 64-bit version of IDEA NXT.

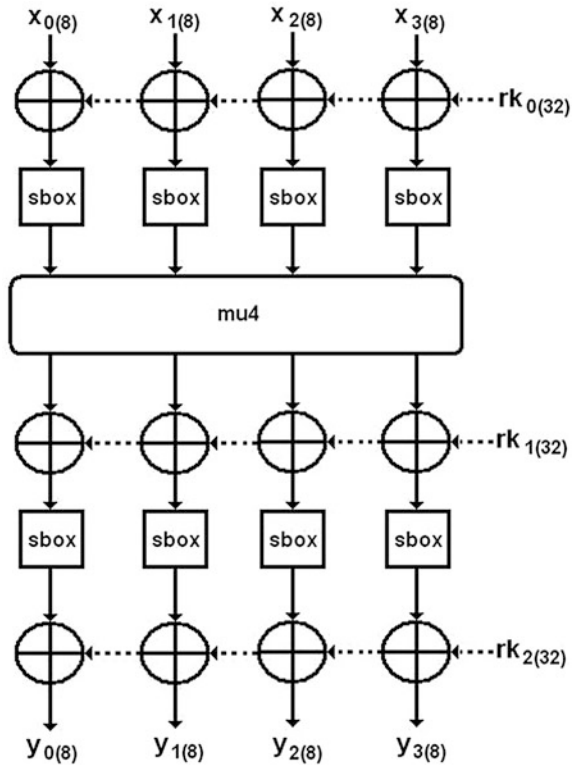
Function *f32* stays at the base of *Imor64* and also constitutes the foundation of the entire encryption algorithm. It is composed of three parts: substitution, diffusion and a round key addition part, as can be observed from Fig. 1. The substitution part uses a substitution box (*sbox*) which essentially is a look-up table filled with predefined values. The diffusive part *mu32* is a linear multipermutation defined over the Galois Field $GF(2^8)$ associated with the IDEA NXT [2].

The key is processed by a key scheduler module which performs a four-layer encryption of its own before providing obtained round the key to the data encryption process itself. This process represents the very core of IDEA NXT, which gives the algorithm its security strength [1].

The key scheduler's constituting parts are: padding, mixing, diversification and the non-linear part called *NL64*.

The non-linear step is made of multiple parts: substitution (which uses four parallel *sigma4* processes that are each composed of four substitution boxes operating in parallel), diffusion, composed of four *mu4* functions (each being a linear (4,4) multipermutation defined over algorithm's $GF(2^8)$ field) followed by successive layers of addition in the Galois Field of the algorithm, complementation and a final layer of substitution whose result drives the final, successive, layers of

Fig. 1 The f32 function, main component of lmor64 [2]



lmor64 and *lmid64*. The initial, diversification, part of the key scheduler takes as inputs the encryption’s input key block having ek bits length, and adds to it, repeatedly, the content of six 24-bit linear feedback shift registers (LFSR). In our implementation, the six LFSR components were specifically designed to generate the next sequence each new clock cycle, unlike the algorithm definition form the standard [2], in order to achieve a higher throughput.

3 Concurrent Error-detection Architectures

After an encryption algorithm is starting to be used in the field, integrated in a chip or used as a dedicated security core, it has to be checked periodically for correct functioning [3]. The possible reasons for its malfunction are varied: from system faults to intruder attacks on the implementation. As has already been proved in various papers [4–7], there are many different types of attacks that can compromise the encryption process for hardware implementations of cryptographic algorithms [8]. Attackers can inject faults into crypto-chips and cryptographic cores [9], which can lead to permanent faults by modifying the underlying semiconductor layer [10,

11]. With respect to these observations, we can mention both linear and differential cryptanalysis as well as the fault attacks [12–16].

In order to check for existing errors and faults during cryptographic system's normal operation, a dedicated testing architecture is constructed, according to the algorithm's structure, allowing the verification for correct functioning at every stage of the algorithm. With respect to the normal operation of the design under test (DUT), there are two types of error-detection principles: offline and concurrent-testing. In the first case, the testing process is performed when the system is in a dedicated test mode of operation, whereas in the second case testing is done while the system is in normal operating mode.

Concurrent checking schemes are designed to detect a high percentage of all the possible errors that can occur during DUT's normal operation, which can be of various types: single errors, double errors, unidirectional errors, transient defects. Typically, faults are modelled at the logic level by means of stuck-at defects since the failure (effect of fault activation and propagation) can be easily detected in terms of logic levels, unlike path delay defects that affect the propagation latency of the signals through the DUT. Moreover, a single fault can cause different types of errors to occur [17] and therefore, the designer is expected to design the test architecture as general as possible.

To the best of our knowledge no verification mechanisms have been implemented for the IDEA NXT crypto-algorithms family, nor offline or concurrent. Our goal was to increase the reliability of crypto-systems in which this algorithm is used, by creating a class of concurrent, self-testing architectures.

The fault detection principle we used is the non-intrusive concurrent error-detection mechanism from [19] based on the output's parity prediction. A parity detection mechanism is constructed around a DUT's module for which the output parity is checked against a predicted parity bit for that respective unit. The mechanism is similar to the one used in the AES algorithm [20] in [3]. In our implementations, as revealed in the experimental results chapter, we evaluated different levels of redundancy with respect to the number of parity bits. The two extreme cases for the number of parity bits are single-bit parity and duplication. In single-bit parity, all output bits of the circuit are protected collectively by a single parity line. Duplication leaves the original circuit intact, incurring the additional cost of circuit's duplication for verifying the correctness of the original copy. In this context, the single-bit parity case is relatively inexpensive, as no redundancy is introduced. We used a reduced number of parity bits for our parity-checking architecture, analysed in three distinct scenarios: 1 bit of parity associated with 4 bytes of the data processed by all units of the algorithm, 1 bit of parity protecting 2 bytes from the unit and 1 bit of parity associated with each byte.

The output parity prediction for a particular module consists of a mechanism for anticipating the parity of the output based solely on the module's input. By verifying the equality between the predicted parity and the actual parity of the output the architecture will detect any odd number of errors affecting the result of the protected module, while remaining completely independent from the DUT. This type of error detection fits well with the notion of integrated circuits that are

designed to be totally self-checking with respect to a set of faults, as we can verify each stage and component of a cryptographic algorithm in the proposed manner.

As mentioned before, we constructed two concurrent architectures—for the datapath and the key scheduler of the IDEA NXT algorithm in order for the whole algorithm to be checked for possible errors. The error-detection mechanism will be described in detail in the following section.

4 Proposed Concurrent Architectures

4.1 Error-Detection Mechanism for IDEA NXT's Datapath

As already described in the second chapter of the paper, IDEA NXT's datapath implement the $(r - 1)$ iterations of the round function denoted as *lmor64*, followed by the application of a slightly modified version of it called *lmid64*. The concurrent architecture for the datapath's *lmid64* is shown in Fig. 2. Both the IDEA NXT datapath and the key schedule unit are designed to incorporate parity prediction modules. Ideally, the parity prediction channel would be completely decoupled from the modules it protects. In this manner, based only on input parity, the predictor is

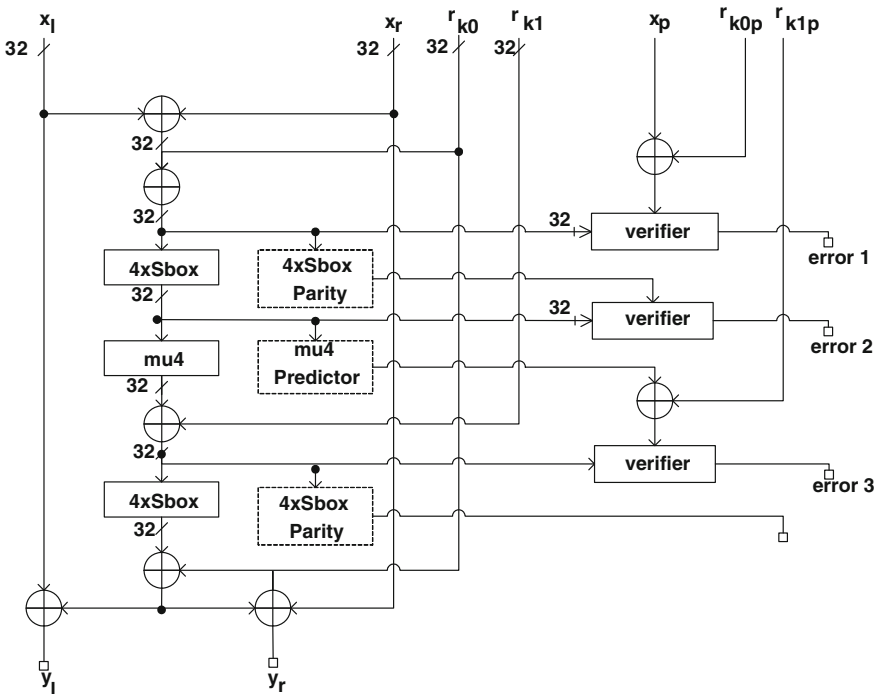


Fig. 2 Parity-based test architecture for IDEA NXT's *lmid64*, part of datapath and key scheduler

capable of anticipating the output parity. However, the completely decoupled solution is not always achievable as a reasonable tradeoff between error detection and complexity. The concurrent-testing scheme was constructed by adding two parity bits to the data block, denoted x_{1p} and x_{rp} each associated to the two 32-bit halves of the data block (denoted x_1 and x_r in the diagram). Similarly, two parity bits were added to the 64-bit round keys used in the encryption process, denoted by r_{k0p} and r_{k1p} .

The difficulty of predicting the output parity appears in the case of the more complex operations, like *sigma4*, which consists of substitution boxes, and *mu4*, respectively, which uses complex operations in the $GF(2^8)$. Regarding the parity prediction for the *sbox* instances, this is a complex problem due to operation's non-linearity. The same observation is valid also for the orthomorphism (*ortho*) used in the *lmor64* function of the encryption as well as the inverse orthomorphism used by the *lmio64* function of the decryption process.

For these complex operations we created a series of parity prediction modules which re-compute the value of the parity bits after operation's execution. A custom solution, tailored to the operation's specific implementation needed to be built for each of the prediction modules and will be presented in the following paragraphs. The prediction units are represented with dashed lines in Figs. 2 and 4 and their purpose pertains to generating the parity bits after execution of an operation for which the output parity cannot be predicted from the input parity. In such a case, we are investigating the input of the respective module for predicting the output parity. However, we are to assure that no error occurred along the datapath affecting the input to the respective module, and thus, we are to verify module's input correctness using the parallel parity channel. For this reason are added verifier modules whose error indicator are combined together for allowing to signal any discrepancy between the data lines and their associated parity bits.

As can be seen in Fig. 2, we created a testing scheme which operates in parallel with the algorithm's structure. The parity channel follows the exact same operations of the protected architecture as long as the output parity can be predicted from the input parity. It is the case for the XOR modules.

The parity prediction of the *sigma4* module and of the *sbox* unit introduces irregularity into the parity-based verification architecture. *Sigma4* is composed of four *sbox*-es, taking as inputs 8 bits of data, and in consequence, for the case of using one parity bit associated to 4 bytes of data, calculating the parity of the operation reduces to calculating the parity of each substitution box. Due to transformation's non-linearity, the output parity bit cannot be expressed in terms of *sbox* input bits and thus is realized by embedding an additional look-up table inside the module. The *sigma4* output parity bit is obtained by summing up all the individual parity outputs. Since the parity bit is generated by predictors, as already explained, the *sigma4* inputs are to be checked against errors by means of a *verifier* unit. Inside *verifier*, *sigma4* input parity is computed by operating all 32 bits with an XOR tree, obtaining a single parity bit which is then checked against the predicted parity bit run through the parity channel. After *sigma4* execution, the parity bits must be re-computed from the current state in order for them to be reinserted into the parity channel.

The prediction for *mu4* requires a dedicated output parity prediction unit as it is an irregular operation. However, since the transformation can be described in terms of the linear XOR operators, unlike the case for *sbox*, the output parity of the *mu4* module can be expressed mathematically in terms of the input bits, based on function's internal transformations. The calculation of its parity bit was obtained by XOR-ing the bits from the four 8-bit-length outputs operation takes four 8-bit inputs. The scheme of the parity predictor we constructed is shown in Fig. 3. The *xalpha* unit multiplies the degree-8 polynomial associated with its input *i*, by the monomial *x*, operation performed modulo $P(x)$, where $P(x)$ is

$$P(x) = x^8 + x^7 + x^6 + x^5 + x^4 + x^3 + 1 \tag{1}$$

The *xc* unit is similar to *xalpha*, the only difference is that it is using a different polynomial for multiplication, multiplication performed modulo $P(x)$ from Eq. (1):

$$c(x) = x^7 + x^6 + x^5 + x^4 + x^3 + x^2 + 1 \tag{2}$$

Another parity prediction module was implemented for the orthomorphism. The irregularity of this operation is visible in its defining equation from [2]:

$$\begin{aligned} y_{(64)} &= \text{Imor64}(x_{1(32)} || x_{r(64)}) \\ &= \text{OR}(x_{1(32)} \text{XOR } f32(x_{1(32)} \text{XOR } x_{r(32)}, rk_{(64)})) || (x_{r(32)} \text{XOR } f32(x_{1(32)} \text{XOR } x_{r(32)}, rk_{(64)})) \end{aligned} \tag{3}$$

When employing one parity bit or more for each half of the *ortho* input, the output parity can be predicted right from the input parity due to operation's simple linear expression. Nevertheless, if using a single parity bit for the units input, the

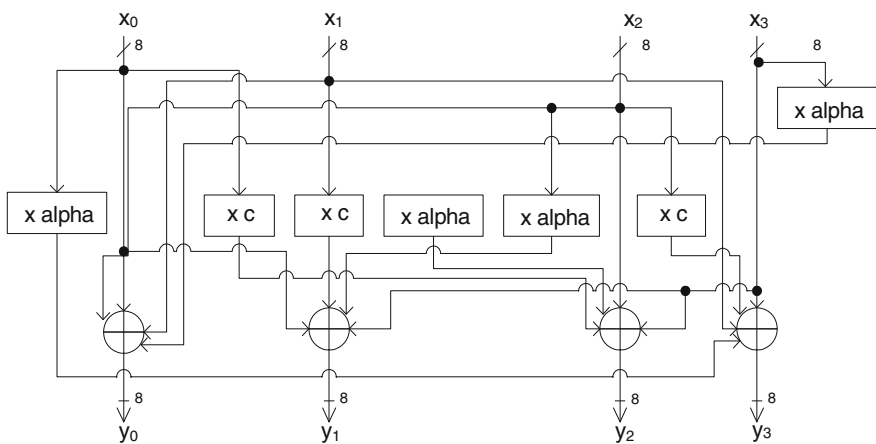


Fig. 3 Parity check scheme for the *mu4*

parity of the output cannot be predicted from input parity, requiring a dedicated predictor that generates the parity of the output using the input bits. If there were no XOR operation or if an XOR were applied symmetrically to the two halves, the parity of the outputs would be straightforward, but because of the XOR operation, a module for parity calculation was needed. If we denote a_r and a_l the two halves of the input to the orthomorphism and b_l and b_r the respective output halves, then the parity bit of this operation, denoted a_p , can be calculated as

$$\begin{aligned}
 a_p &= \text{Parity}(\text{ORTHO}(a_l, a_r)) = \text{Parity}(a_r \text{ XOR } (a_r \text{ XOR } a_l)) \\
 &= \text{Parity}(a_r) \text{ XOR } \text{Parity}(a_l) \text{ XOR } \text{Parity}(a_r) = \text{Parity}(a_l)
 \end{aligned}
 \tag{4}$$

4.2 Error-Detection Mechanism for the Key Scheduler

IDEA NXT's key scheduler is mostly composed of the same operations as the datapath, this is why the general testing architecture is very similar to the one we constructed for the datapath, as can be seen by analysing comparatively Figs. 2 and 4.

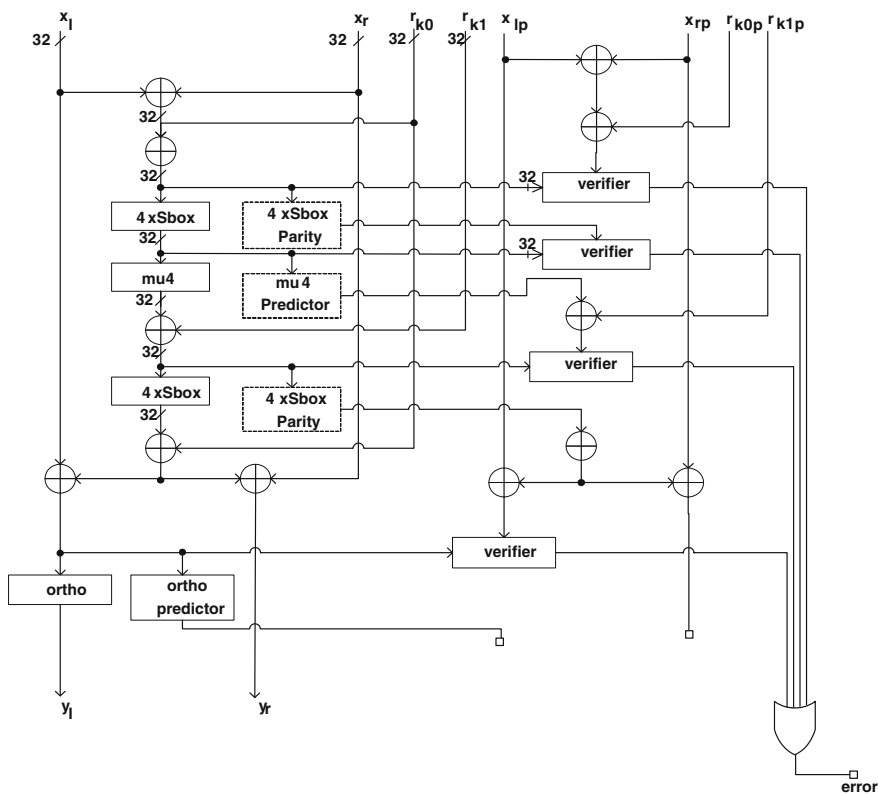


Fig. 4 Parity-based test architecture for IDEA NXT's *lmr64*, part of datapath and key scheduler

When using one parity bit for each for bytes we will associate two parity bits for the round key, r_{k0p} and r_{k1p} , and only one parity bit for the data, denoted x_p , where $x_p = \Sigma x_i$ (x_l, x_r denoting the two input halves for the Key Scheduler). The first parity bit of the error-detection scheme is calculated by doing an XOR between the two halves of the input data bytes and summing up the results of this for each round

$$x_p = \Sigma a = \Sigma(x_l \text{ XOR } x_r) \quad (5)$$

The output is furthered XOR-ed with r_{k0} and so the new intermediate parity bit will be the sum of these results

$$\Sigma b = \Sigma a \text{ XOR } \Sigma r_{k0p} = x_p \text{ XOR } r_{k0p} \quad (6)$$

For the *sigma4* and *mu4* operations we can use the *sbox* and *mu4* parity predictors which we already developed for the datapath error-detection scheme. After a parity bit is calculated for each of them, we must check for correctness with a *verifier* module to see if the parity data is correct. Three verifiers are used in the scheme. For the complementation operation, which takes place during key generation process, the parity bit doesn't change its value.

An element which appears in the key scheduler but not in the datapath is the LFSR. Calculating the parity for the series of pseudo-random number generators is not a trivial task, and in consequence also a parity predictor has to be constructed. A parity bit is generated for each group of 8 bits generated by each of the six 24-bit LFSRs and they are combined correspondingly to assure the necessary parity data bits. Mention should be made that only 8 bits of the final LFSR are used. For the case of one parity bit associated to 32 data bits, out of all 128 bits generated through LFSRs, four parity bits are generated whereas for a redundancy level of one parity bit associated to one data byte, 16 parity bits are generated for the LFSR output.

5 Experimental Results

This chapter presents the experimental results obtained by synthesizing the proposed on-line test architecture designed for the IDEA-NXT64 algorithm. Apart from the parity-based error-detection approach that associates one parity bit to each group of 4 bytes of the encryption process, we also evaluated the performance of the constructed architecture when using more redundancy bits. More precisely, we investigated the effect of using one parity bytes for each pair of 2 bytes as well as using one parity bit associated with each byte of the datapath and key scheduler.

Besides the increased error-detection capability associated with higher redundancy levels, because of the particular aspects of the IDEA-NXT64 algorithm as well as of the concurrent error-detection architecture, the higher the redundancy level of the architectures the faster it performs, at the expense of a larger design, as the experimental results reveal.

Table 1 IDEA-NXT64 parity-based architectures synthesis results

IDEA-NXT architecture	Max frequency (MHz)	Area (slices)	Throughput (Mbps)	Throughput/area (Mbps/slices)
Base	37.517	5189	150.068	0.029
Parity checked 1 bit	34.732	6045	138.928	0.023
Parity checked 2 bit	37.368	6064	149.472	0.025
Parity checked 4 bit	37.474	6070	149.896	0.025

The architecture employing 1 bit of parity for each group of 4 bytes has the largest critical path compared with the solution employing 4 bits of parity for the same data size, as evident from Table 1. The reason for the degradation of device's performance with reduction in the redundancy level is partly due to the complexity associated with the *verifier* modules, and for the case of one parity bit, because of the parity prediction for the *ortho* module, depicted in Fig. 7. More precisely, for all implementations involving more than one parity bit associated to the 32 bits processed by *ortho*, as evident from Eq. (1), the parity of module's output can be directly predicted based solely on input's parity. In consequence, the implementations using 2 and 4 bits of parity for the 32 bits processed by the *ortho* module, the final *verifier* unit checking the correctness of parity bits is not required.

Apart from this, the higher the number of parity bits, the smaller the height of the XOR tree used inside the *verifier* module and thus the faster the parity verification. More precisely, when using a single bit of parity for a group of 32 bits, the *verifier* unit contains an XOR tree of height 5, whereas when a parity bit is associated with a byte, the XOR tree has a height of only three logic levels. The latency associated with the *verifier* modules justify also the faster performance of the four parity bit design compared to the two parity bit solution.

As can be seen from Table 1, the effect of increasing the redundancy level over the area of the design is consistent. With respect to the combined metric throughput/area, the two parity bit and four parity bit architectures have similar scores, also higher than the score for single parity bit design. This is the reason that IDEA-NXT64 is better verified concurrently for errors by employing either two or four parity bits associated with each group of 4 bytes processed by the algorithm.

6 Conclusions

In this paper we have addressed the problem of including error-detection capabilities into a crypto-chip hardware implementation for the new family of crypto-algorithms, IDEA NXT. To the best of our knowledge little work has been done in the field of concurrent error-detection mechanisms for IDEA NXT so far. In this sense we designed a parity-based testing architecture, which is completely independent from the algorithm itself, and which works for all versions of the algorithm, independent of the key and text length. It mainly consists of generating

and processing a series of parity bits for the datapath and the key scheduler and checking their value at every step of the algorithm, by verifying the outputs of the parity-predictor modules (built for complex operations where the output parity cannot be determined based on module's input parity) against a checker scheme—if the parity bit was incorrect, an error had been introduced at that stage.

After constructing the design, we proceeded to verifying and synthesizing the error-detection architecture for three different redundancy levels, and demonstrated the efficiency of the proposed solution.

Acknowledgments This work was partially supported by the strategic grant POSDRU/159/1.5/S/137070 (2014) of the Ministry of National Education Protection, Romania, co-financed by the European Social Fund—Investing in People, within the Sectoral Operational Programme Human resources Development 2007–2013.

References

1. Junod P, Vaudenay S (2005) FOX specifications version 1.2, pp 5–40
2. Junod P, Vaudenay S (2005) Perfect diffusion primitives for block ciphers. In: Handschuh H, Hasan MA (eds) Selected areas in cryptography, lecture notes in computer science. Springer Berlin Heidelberg, pp 84–99
3. Opritoiu F, Vladutiu M, Udrescu M, Prodan L (2009) Round-level concurrent error detection applied to advanced encryption standard. Design and diagnostics of electronic circuits & systems, 2009. DDECS '09. In: 12th international symposium on, pp 270, 275
4. Chong Hee K, Quisquater JJ (2007) Faults, injection methods, and fault attacks. IEEE Design Test Comput 24(6):544–545
5. Bozesan A, Opritoiu F, Vladutiu M (2013) Hardware implementation of the IDEA NXT cryptoalgorithm. In: Design and technology in electronic packaging (SIITME), 2013 IEEE 19th international symposium for, pp 35, 38
6. Rao TRN, Fujiwara E (1989) Error-control coding for computer systems. Prentice-Hall International
7. Daemen J, Rijmen V (2002) The design of Rijndael. Springer, New York
8. Courtois N, Pieprzyk J (2002) Cryptanalysis of block ciphers with over defined systems of equations. In: Advances in cryptology—ASIACRYPT'02, vol 2501 of lecture notes in computer science. Springer, pp 267–287
9. Avizienis A, Laprie J-C, Rendall B (2004) Basic concepts and taxonomy of dependable and secure computing. IEEE Trans Dependable Secure Comput
10. Security Requirements for Cryptographic Modules (2002) Federal information, processing standards publication 140–2
11. Burton Kaliski S Jr, Robshaw MJB (1994) Linear cryptanalysis using multiple approximations
12. Meier W (1996) On the security of the IDEA block cipher. Adv Cryptol
13. Coron JS, Goubin L (2000) On boolean and arithmetic masking against differential power analysis. In: Proceedings of workshop on cryptographic hardware and embedded systems—CHES 2000. Springer, pp 231–237
14. Moradi A, Mischke O, Paar C (2013) One attack to rule them all: collision timing attack versus 42 AES ASIC cores. IEEE Trans Comput 62(9):1786–1798
15. Tarnick S (1994) Bounding error masking in linear output space compression schemes. Test symposium, 1994. In: Proceedings of the third Asian, pp 27, 32. Almukhaizim S, Makris Y (eds) Fault tolerant design of random logic based on a parity check code. Electrical Engineering Department Yale University

16. Karpovsky M, Kulikowski KJ, Taubin A (2004) Differential fault analysis attack resistant architectures for the advanced encryption standard. Quisquater J-J, Paradinas P, Deswarte Y et al (eds) Smart card technologies and applications. Springer, pp 177–192
17. Cachin C, Camenisch J, Deswarte Y, Dobson J, Horne D, Kursawe K, Laprie, JC, Lebraud JC, Long D, McCucheon T, Muller J, Petzold F, Pfitzmann B, D
18. Daemon J, Govaerts R, Vandervale J (1994) Weak keys of IDEA. In: Advances in cryptology, CRYPTO 93 proceedings, lecture notes in computer science, vol 773. pp 224–231
19. Kitsos P, Sklavos N, Galanis MD, Koufopavlou O (2004) 64-bit block ciphers: hardware implementations and comparison analysis. In: VLSI Design Lab, Electr Comput Eng Dept 30 (8). University of Patras, Greece
20. Mozaffari-Kermani M, Reyhani-Masoleh A (2010) Concurrent structure-independent fault detection schemes for the advanced encryption standard. *IEEE Trans Comput* 59(5):608–622